TDFD
TÜRK DOĞA ve FEN DERGİSİ

TURKISH JOURNAL OF NATURE AND SCIENCE

TJNS
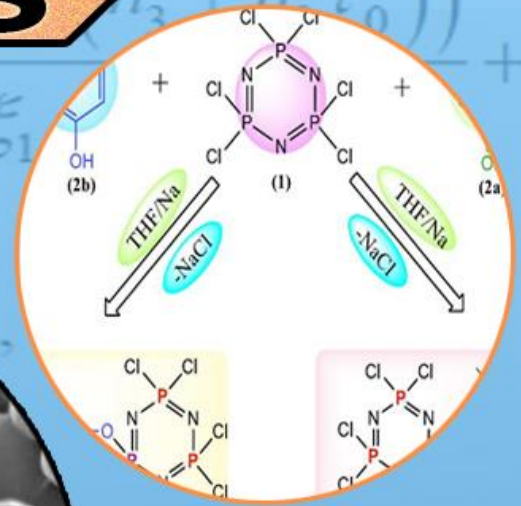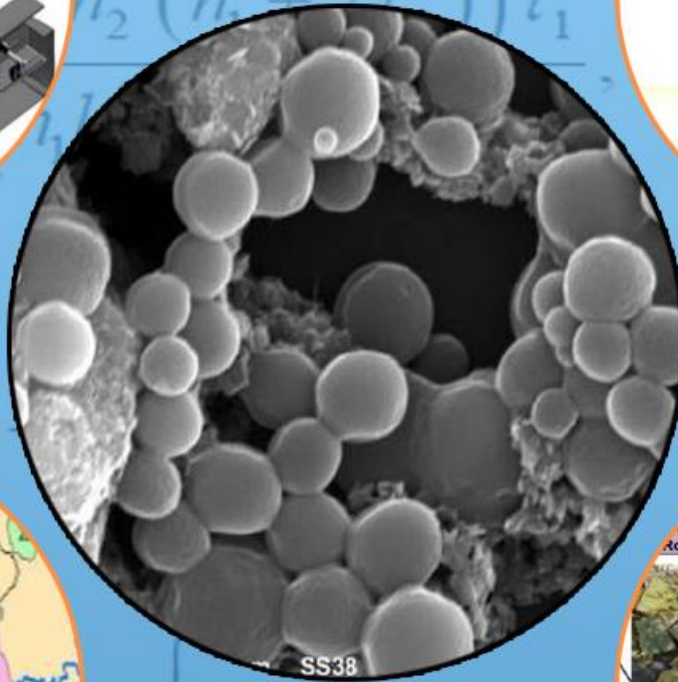
TÜRK DOĞA VE FEN DERGİSİ

Amaç

Türk Doğa ve Fen Dergisi, Dergipark tarafından yayınlanan Bingöl Üniversitesi Fen Bilimleri Enstitüsüne ait ulusal ve hakemli bir dergidir. Türk Doğa ve Fen Dergisi, Türkiye ve dünyanın her yerinden gelen doğa ve fen bilimlerinin her alanında özgün, yayımlanmamış, yayımlanmak üzere başka yere gönderilmemiş makale, derleme ve sempozyum değerlendirmesi gibi çalışmaların bilim alemine sunulması amacıyla kurulmuştur.

Kapsam

Türk Doğa ve Fen Dergisinde Mühendislik, Ziraat, Veterinerlik, Fen ve Doğa Bilimleri alanlarından olmak üzere Türkçe ve İngilizce hazırlanmış orijinal makale, derleme ve sempozyum değerlendirmesi gibi çalışmalar yayımlanır. Türk Doğa ve Fen Dergisi sadece online sistemde yayınlanmakta olup ayrıca kağıt baskısı bulunmamaktadır.

Merhaba…

Türk Doğa ve Fen Dergisi, Dergipark tarafından yayınlanmakta olup Bingöl Üniversitesi Fen Bilimleri Enstitüsüne aittir. Bahar ve güz dönemi olmak üzere yılda iki defa çıkarılan ulusal hakemli bir dergi olarak ilk sayısını 2012 bahar döneminde yayımlamıştır. Türk Doğa ve Fen Dergisi, Türkiye ve dünyanın her yerinden gelen doğa ve fen bilimlerinin her alanında özgün, yayımlanmamış, yayımlanmak üzere başka yere gönderilmemiş makale, derleme ve sempozyum değerlendirmesi gibi çalışmaların bilim alemine sunulması amacıyla kurulmuştur. İlk sayısından bugüne kesintisiz olarak faaliyetlerini sürdürmektedir.

Türk Doğa ve Fen Dergisi sadece online sistemde yayınlanmakta olup ayrıca kağıt baskısı bulunmamaktadır. Dergimize gelen her çalışma öncelikle Turnitin intihal programında taranmaktadır. Dergimizde editörlerin, hakemlerin ve yazarların, uluslararası yayım etik kurallarına uyması ve makalelerin yazım kurallarına uyumlu olması zorunluluğu vardır.

Yazarlar yayımlanmak üzere dergimize gönderdikleri çalışmaları ile ilgili telif haklarını zorunlu olarak Bingöl Üniversitesi Türk Doğa ve Fen Dergisi'ne devretmiş sayılırlar. Yazarlardan herhangi bir ücret talep edilmemektedir. Yazarların değerlendirmeleri, dergimizin resmi görüşü olarak kabul edilemez. Çalışmaların her türlü sorumluluğu yazarlarına aittir. Araştırma ürünleri için etik kurul raporu gerekli ise, çalışma üzerinde bu raporun alınmış olduğu belirtilmeli ve kurul raporu sisteme kaydedilmelidir. Araştırma ile ilgili intihal, atıf manipülasyonu, sahte veri uydurma vb. suistimallerin tespit edilmesi halinde yayım ve etik ilkelerine göre davranılır. Bu durumda çalışmanın yayımlanmasını önlemek, yayımdan kaldırmak ya da başka işlemler yapmak için gerekli işlemler takip edilmektedir.

Dergimizde, kaynak gösteriminde uluslararası Vancouver sistemine geçilmiştir. Ayrıca dergimiz, Creative Commons ile lisanslanmak suretiyle dergimizde yayımlanan makalelerin paylaşımı, kaynak gösterimi ve yayımlanmasında dergi ve yazar haklarını korumaya almıştır. 2018 yılı güz döneminden itibaren makaleler, uluslararası yazar kimlik numarası ORCID No'su ile yayımlanmaktadır.

Dergi ekibi, dergimizin ulusal ve uluslararası indekslerce taranan bir dergi olması yönünde çalışmalarını titizlikle sürdürmektedir. Dergimize gösterilen ilgi bu yönde bizleri teşvik etmeye devam edecektir.

Prof. Dr. Zafer ŞİAR

Bingöl Üniversitesi, Fen-Edebiyat Fakültesi, Matematik Bölümü
E-Mail: zsiar@bingol.edu.tr

Prof. Dr. Uğur ÇAKILCIOĞLU

Munzur Üniversitesi, Pertek Sakine Genç Meslek Yüksekokulu, Bitki Morfolojisi
ve Anatomisi Bölümü
E-Mail: ucakilcioglu@yahoo.com

Doç. Dr. Kamuran DİLSİZ

Bingöl Üniversitesi, Fen-Edebiyat Fakültesi, Fizik Bölümü
E-Mail: kdilsiz@bingol.edu.tr

Doç. Dr. Şükran KONCA

Bakırçay Üniversitesi, Mühendislik ve Mimarlık Fakültesi, Temel Bilimler,
Matematik Bölümü
E-Mail: sukran.konca@bakircay.edu.tr

Doç. Dr. İdris YAZGAN

Kastamonu Üniversitesi, Fen Edebiyat Fakültesi, Biyoloji

E-Mail: idrisyazgan@gmail.com

Doç. Dr. Abdulcabbar YAVUZ

Gaziantep Üniversitesi, Mühendislik Fakültesi, Metalurji ve Malzeme Mühendisliği
E-Mail: ayavuz@gantep.edu.tr

Doç. Dr. Bünyamin ALIM

Bayburt Üniversitesi, Teknik Bilimler Meslek Yüksekokulu, Elektrik ve Enerji
Bölümü
E-Mail: balim@bayburt.edu.tr

Doç. Dr. Mustafa Şükrü KURT

Erzurum Teknik Üniversitesi, Fen Fakültesi, Temel Bilimler
E-Mail: mustafa.kurt@erzurum.edu.tr

Doç. Dr. Sinan SAĞIR

Karamanoğlu Mehmetbey Üniversitesi, Fizik

E-Mail: sinansagir@kmu.edu.tr / sinan.sagir@cern.ch

Doç. Dr. Murat AYDEMİR

Erzurum Teknik Üniversitesi, Fen Fakültesi, Temel Bilimler

E-Mail: murat.aydemir@erzurum.edu.tr

Mühendislik Bilimleri

Prof. Dr. Figen KOREL

İzmir Yüksek Teknoloji Enstitüsü, Gıda Mühendisliği Bölümü
E-Mail: figenkorel@iyte.edu.tr

Prof. Dr. Kubilay ASLANTAŞ

Afyon Kocatepe Üniversitesi, Teknoloji Fakültesi, Makine Mühendisliği Bölümü
E-Mail: aslantas@aku.edu.tr

Prof. Dr. Hamit Özkan GÜLSOY

Marmara Üniversitesi, Teknoloji Fakültesi, Metalurji ve Malzeme Mühendisliği Bölümü
E-Mail: ogulsoy@marmara.edu.tr

Prof. Dr. Ali Adnan HAYALOĞLU

İnönü Üniversitesi, Mühendislik Fakültesi, Gıda Mühendisliği Bölümü
E-Mail: adnan.hayaloglu@inonu.edu.tr

Prof. Dr. Barbara SAWICKA

University of Life Sciences in Lublin, Department of Plant Production Technology and Commodities Sciences
E-Mail: barbara.sawicka@gmail.com

Prof. Dr. İbrahim GÜNEŞ

Giresun Üniversitesi, Mühendislik Fakültesi, İnşaat Mühendisliği Bölümü
E-Mail: ibrahim.gunes@giresun.edu.tr

Doç. Dr. Serhat ŞAP

Bingöl Üniversitesi, Teknik Bilimler Meslek Yüksekokulu, Elektrik ve Enerji Bölümü
E-Mail: ssap@bingol.edu.tr

Doç. Dr. Sırma YEĞİN

Ege Üniversitesi, Mühendislik Fakültesi, Gıda Mühendisliği Bölümü
E-Mail: sirma.yegin@ege.edu.tr

Doç. Dr. Hasan OĞUL

Sinop Üniversitesi, Mimarlık ve Mühendislik Fakültesi, Nükleer Enerji
Mühendisliği
E-Mail: hogul@sinop.edu.tr

Doç. Dr. Murat YILMAZTEKİN

İnönü Üniversitesi, Mühendislik Fakültesi, Gıda Mühendisliği Bölümü
E-Mail: murat.yilmaztekin@inonu.edu.tr

Doç. Dr. Ferhat AYDIN

Sakarya Uygulamalı Bilimler Üniversitesi, Teknoloji Fakültesi, İnşaat
Mühendisliği Bölümü
E-Mail: ferhata@subu.edu.tr

Dr. Öğr. Üyesi Nurullah DEMİR

Bingöl Üniversitesi, Mühendislik ve Mimarlık Fakültesi, Gıda Mühendisliği
Bölümü
E-Mail: ndemir@bingol.edu.tr

Doç. Dr. Ahmet GÜNER

Bingöl Üniversitesi, Mühendislik ve Mimarlık Fakültesi, Elektrik ve Elektronik
Mühendisliği Bölümü
E-Mail: aguner@bingol.edu.tr

Dr. Öğr. Üyesi Tahir AKGÜL

Sakarya Uygulamalı Bilimler Üniversitesi, Teknoloji Fakültesi, İnşaat
Mühendisliği Bölümü
E-Mail: tahirakgul@subu.edu.tr

Dr. Erhan Sulejmani

University of Tetova, Faculty of Food Technology and Nutrition
E-Mail: erhan.sulejmani@unite.edu.mk

Dr. Hacène Medjoudj

Larbi Ben M'Hidi University of Oum El Bouaghi, Food Science Department
E-Mail: medjoudjh@yahoo.com

Dr. Avinash Lakshmikanthan

Nitte Meenakshi Institute of Technology, Department of Mechanical Engineering,
Karnataka, India
E-Mail: avinash.laks01@gmail.com

Dr. Manjunath Patel GC

PES Institute of Technology and Management, Department of Mechanical
Engineering, Karnataka, India
E-Mail: manju09mpm05@gmail.com

Sağlık Bilimleri

Doç. Dr. Aydın Şükrü BENGÜ

Bingöl Üniversitesi, Sağlık Hizmetleri Meslek Yüksekokulu, Tıbbi Hizmetler ve
Teknikler
E-Mail: abengu@bingol.edu.tr

Dr. Öğr. Üyesi Dilhun Keriman ARSERİM UÇAR

Bingöl Üniversitesi, Sağlık Bilimleri Fakültesi, Beslenme ve Diyetetik Bölümü
E-Mail: dkucar@bingol.edu.tr

Dr. Öğr. Üyesi Abdullah TUNÇ

Bingöl Üniversitesi, Sağlık Bilimleri Fakültesi, İş Sağlığı ve Güvenliği Bölümü
E-Mail: atunc@bingol.edu.tr

Dr. Öğr. Üyesi Ramazan GÜNDOĞDU

Bingöl Üniversitesi, Sağlık Hizmetleri Meslek Yüksekokulu, Eczane Hizmetleri
E-Mail: rgundogdu@bingol.edu.tr

Dr. Alexander HERGOVICH

UCL Cancer Institute, Faculty of Medical Sciences, Department of Cancer Biology,
UCL, London, UK
E-Mail: a.hergovich@uc.ac.uk

Dr. Valenti GOMEZ

UCL Cancer Institute, Faculty of Medical Sciences, Department of Oncology, UCL, London, UK
E-Mail: valentin.gomez@ucl.ac.uk

Veterinerlik Bilimleri

Prof. Dr. Fatih Mehmet KANDEMİR

Atatürk Üniversitesi, Veteriner Fakültesi, Veteriner Hekimliği Temel Bilimler
E-Mail: fmehmet.kandemir@atauni.edu.tr

Doç. Dr. Akın KIRBAŞ

Bozok Üniversitesi, Veteriner Fakültesi, Klinik Bilimler Bölümü
E-Mail: akindahiliye55@yahoo.com

Doç. Dr. Emrah Hicazi AKSU

Atatürk Üniversitesi, Veteriner Fakültesi, Klinik Bilimler Bölümü
E-Mail: emrahaksu@atauni.edu.tr

Ziraat Bilimleri

Doç. Dr. Zeynep DUMANOĞLU

Bingöl Üniversitesi, Ziraat Fakültesi, Biyosistem Mühendisliği Bölümü
E-Mail: zdumanoglu@bingol.edu.tr

Prof. Dr. Kağan KÖKTEN

Bingöl Üniversitesi, Ziraat Fakültesi, Tarla Bitkileri Bölümü
E-Mail: kahafe1974@yahoo.com

Prof. Dr. Mustafa SÜRMEN

Adnan Menderes Üniversitesi, Ziraat Fakültesi, Tarla Bitkileri Bölümü
E-Mail: mustafa.surmen@adu.edu.tr

Prof. Dr. Banu YÜCEL

Ege Üniversitesi, Ziraat Fakültesi, Hayvan Yetiştirme Anabilim Dalı, Zootekni Bölümü
E-Mail: banu.yucel@ege.edu.tr

Prof. Dr. Hakan İNCİ

Bingöl Üniversitesi, Ziraat Fakültesi, Zootekni Bölümü
E-Mail: hinci@bingol.edu.tr

TEKNİK EDİTÖRLER

Dr. Nimetullah KORKUT

Bingöl Üniversitesi, BİNUZEM, Bilgisayar Teknolojileri
E-Mail: nkorkut@bingol.edu.tr

DİL EDİTÖRÜ

Dr. Öğr. Üyesi Ahmet KESMEZ
Bingöl Üniversitesi, Yabancı Diller Yüksekokulu, İngilizce Bölümü
E-Mail: akesmez@bingol.edu.tr

Türk Doğa ve Fen Dergisi
Turkish Journal of Nature and Scienc

İÇİNDEKİLER/CONTENTS

AW(k) -Type Curves in Modified Orthogonal Frame

Esra DAMAR[1]* iD , **Burçin SALTIK BAEK**[2] iD , **Nural YÜKSEL**[2] iD , **Nurdan OĞRAŞ**[2] iD

[1] Hitit University, Vocational School of Technical Sciences, Motor Vehicles and Transportation Technologies Department, Çorum, Türkiye
[2] Erciyes University, Faculty of Science, Department of Mathematics, Kayseri, Türkiye
Esra DAMAR ORCID No: 0000-0002-0743-8545
Burçin SALTIK BAEK ORCID No: 0000-0001-5174-6484
Nural YÜKSEL ORCID No: 0000-0003-3360-5148
Nurdan OĞRAŞ ORCID No: 0000-0002-5539-4890

Corresponding author: esradamar@hitit.edu.tr

33

Weldability of Dissimilar 316L and A106 Steels with GTAW and SMAW Using 309L and Inconel 82 Electrodes

Esin Tuğba ŞİMŞEK ÇELİK[1]* iD , **Başar Ersegün ÇELİK**[2] iD , **Şükrü TALAŞ**[3] iD

[1] Sivas Cumhuriyet University, Hafik Kamer Ornek Vocational School of Higher Education, Department of Transportation Services, Rail Systems Management Program, Sivas, Türkiye
[2] Afyon Kocatepe University, Institute of Natural Sciences, Afyonkarahisar, Türkiye
[3] Afyon Kocatepe University, Faculty of Technology, Department of Metallurgical and Materials Engineering, Afyonkarahisar, Türkiye
Esin Tuğba ŞİMŞEK ÇELİK ORCID No: 0000-0003-2063-7802
Başar Ersegün ÇELİK ORCID No: 0000-0002-3015-2553
Şükrü TALAŞ ORCID No: 0000-0002-4721-0844

Corresponding author: esimsek@cumhuriyet.edu.tr

41

Comparison of the Views of Local People Who Directly Benefited and Did Not Benefit from the Murat River Rehabilitation Projects

Alaaddin YÜKSEL[1] iD , **Ahmet USLU**[2] iD , **Bayram HOPUR**[3] iD , **Ersin KARAKAYA**[4] iD , **Semra ÇAMUKA**[5] iD , **Şenol ÇELİK**[6] iD , **Mahmut YILMAZ**[7] iD

[1] Alaaddin YÜKSEL, Bingöl University Faculty of Agriculture, Soil Science and Plant Nutrition, Türkiye
[2] Ahmet USLU, Bingöl Vocational School of Social Sciences / Office Services and Secretariat, Türkiye
[3] Bayram HOPUR, General Directorate of Combating Desertification and Erosion, Türkiye
[4] Ersin KARAKAYA, Bingöl University Faculty of Agriculture, Türkiye
[5] Semra ÇAMUKA, Bingöl University International Relations Office, Türkiye
[6] Şenol ÇELİK, Bingöl University Faculty of Agriculture, Bingöl, Türkiye
[7] Mahmut Yılmaz, Forest General Directorate Tulip Monitoring and Evaluation Specialist,
Alaaddin YÜKSEL ORCID No: 0000-0003-4760-1092
Ahmet USLU ORCID No: 0000-0003-0273-0069

49

Bayram HOPUR ORCID No: 0000-0002-7443-8051
Ersin KARAKAYA ORCID No: 0000-0002-6734-4962
Semra ÇAMUKA ORCID No: 0000-0002-4966-9296
Şenol ÇELİK ORCID No: 0000-0001-5894-8986
Mahmut Yılmaz ORCID No: 0009-0008-9481-1950

*Corresponding Author: karakayaersin@hotmail.com

Investigation of the Catalytic Effect of ZnO Produced by Green Synthesis on NaBH₄ Hydrolysis

Mehmet Erman MERT[1*] , **Başak DOĞRU MERT[2]**

[1] Adana Alparslan Türkeş Science and Technology University, Advanced Technology Research and Application Center, Adana, Türkiye
[2] Adana Alparslan Türkeş Science and Technology University, Engineering Faculty, Energy Systems Engineering Department, Adana, Türkiye
Mehmet Erman MERT ORCID No: 0000-0002-0114-8707
Başak DOĞRU MERT ORCID No: 0000-0002-2270-9032

*Corresponding author: memert@atu.edu.tr

58

Design and Mechanical Analyses of Autonomous Mobile Robot with Swerve Driving System

Oğuz MISIR[1*] , **Melike BEYAZLI [1]** , **Sümeyye ALP [1]** ,
Görkem Burak TAŞKIN [1] , **Zeynep IŞIK[1]**

[1]Bursa Teknik Üniversitesi, Mühendislik ve Doğa Bilimleri Fakültesi, Mekatronik Mühendisliği, Bursa, Türkiye
Oğuz MISIR ORCID No: 0000-0002-3785-1795
Melike BEYAZLI ORCID No: 0009-0005-6315-794X
Sümeyye ALP ORCID No: 0009-0006-5922-8706
Görkem Burak TAŞKIN ORCID No: 0009-0004-0483-0404
Zeynep IŞIK ORCID No: 0009-0005-1388-7194

*Corresponding author: oguz.misir@btu.edu.tr

66

Synthesis and Characterization of 2,4-*di*-methyl-, and 3,4-*di*-methyl-phenol Derivatives of Hexachlorocyclotriphosphazatriene

Saliha BEGEÇ[1*]

[1] İnönü University, Arts and Sciences Faculty, Chemistry Department, Malatya, Türkiye
Saliha BEGEÇ ORCID No: 0000-0001-5331-6736

*Corresponding author: saliha.begec@inonu.edu.tr

85

Optimizing Weight in Gear Wheels with Different Filling Geometries

Hanife KARA[1]* , Mahir UZUN

[1]Inonu University, Engineering Faculty, Mechanical Engineering Department,
Malatya, Türkiye
[2] Inonu University, Engineering Faculty, Mechanical Engineering Department,
Malatya, Türkiye
Hanife KARA ORCID No: 0000-0003-3087-748X
Mahir UZUN ORCID No 0000-0002-0907-6875

Corresponding author: mahir.uzun@inonu.edu.tr

135

Color Response of Turfgrass Cultivars to Gibberellic Acid under Mediterranean Climate Conditions

Emre KARA[1]* , Mustafa SÜRMEN[1] , Türkan METİN[1] Bekir Sami GÜNGÖR[1]

[1] Aydın Adnan Menderes University, Faculty of Agriculture, Department of Field
Crops, Aydın, Türkiye
Emre KARA ORCID No: 0000-0002-5535-8398
Mustafa SÜRMEN ORCID No: 0000-0001-9748-618X
Türkan METİN ORCID No: 0009-0000-0073-3990
Bekri Sami GÜNGÖR ORCID No: 0009-0005-6597-1937

Corresponding author: emre.kara@adu.edu.tr

141

Retrospective Analysis of Extremity Fractures in Cats: 288 Cases (2018-2023)

Ali GÜLAYDIN[1]* , Nihat ŞINDAK[1] , Mustafa Barış AKGÜL[1] , Müzzemil Hattap SOYSAL[2] ,
Onur YILDIRIM[1] , Sevdet KILIÇ[1] , Maruf YILMAZ[1] , Bahar ERDEN[1]

[1] Siirt University, Faculty of Veterinary Medicine, Department of Surgery, Siirt,
Türkiye
[2] Siirt University, Institute of Health Sciences, Department of Veterinary Surgery,
Siirt, Türkiye
Ali GÜLAYDIN ORCID No: 0000-0002-7200-1040
Nihat ŞINDAK ORCID No: 0000-0003-0431-8940
Mustafa Barış AKGÜL ORCID No: 0000-0002-9365-9925
Müzzemil Hattap SOYSAL ORCID No: 0009-0002-6760-8494
Onur YILDIRIM ORCID No: 0000-0002-5462-6100
Sevdet KILIÇ ORCID No: 0000-0003-1033-658X
Maruf YILMAZ ORCID No: 0009-0009-6757-7457
Bahar ERDEN ORCID No: 0000-0002-8775-6673

Corresponding author: a.gulaydin@siirt.edu.tr

148

Ensemble and Non-Ensemble Machine Learning-Based Classification of Liver Cirrhosis Stages

Zeinab Mahdi MOUMIN[1] , **İrem Nur ECEMİŞ[2*]** , **Mustafa KARHAN[3]**

[1]Çankırı Karatekin University, Institute of Science, Department of Electronics and Computer Science, Çankırı, Türkiye
[2*]Çankırı Karatekin University, Faculty of Engineering, Department of Computer Engineering, Çankırı, Türkiye
[3]Çankırı Karatekin University, Institute of Science, Department of Electronics and Computer Science, Çankırı, Türkiye
Zeinab Mahdi MOUMIN ORCID No: 0009-0003-8889-9160
İrem Nur ECEMİŞ ORCID No: 0000-0001-9535-2209
Mustafa KARHAN ORCID No: 0000-0001-6747-8971

Corresponding author: iremnurecemis@karatekin.edu.tr

153

Investigation of the Effects of Acetylsalicylic Acid Administration at Different Doses on Behavioral Disorders in Rats

Hasan ŞİMŞEK[1*] , **Özge KANDEMİR[2]** , **Nurhan AKARAS[3]**

[1] Aksaray University, Faculty of Medicine, Department of Physiology, Aksaray, Türkiye
[2] Aksaray University, Vocational School of Technical Sciences, Department of Food Processing, Aksaray, Türkiye
[3] Aksaray University, Faculty of Medicine, Department of Histology and Embryology, Aksaray, Türkiye
Hasan ŞİMŞEK ORCID No: 0000-0001-5573-4923
Özge KANDEMİR ORCID No: 0000-0001-8884-4168
Nurhan AKARAS ORCID No: 0000-0002-8457-9448

Corresponding author: hasansimsek@aksaray.edu.tr

162

The Effect of Sodıum Hypochlorite and Hydrogen Peroxide on the Vase life of Cut Rose Flowers

Ezgi DOĞAN MERAL[1*] , **Çiçek ARMAN[2]** **Zahide SÜSLÜOĞLU[3]**, **Serda ARSLAN[4]**

[1,3]Bingöl University, Agriculture Faculty, Horticulture Department, Bingöl, Türkiye
[2,4] Bingöl University, Agriculture Faculty, Landscape Architecture Department, Bingöl, Türkiye
Ezgi DOĞAN MERAL ORCID No: 0000-0003-0854-7134
Çiçek ARMAN ORCID No: 0009-0008-5304-8290
Zahide SÜSLÜOĞLU ORCID No: 0000-0002-3958-6374
Serda ARSLAN ORCID No: 0009-0008-8792-2847

Corresponding Author: ezgidgn23@gmail.com

173

Carvacrol Ameliorates Cisplatin-Induced Cardiotoxicity By Regulating Notch/Hes1 Signaling Pathway, Oxidative Stress and Cell Death In Rat Cardiac Tissue

Nurhan AKARAS[1*] , **Özge KANDEMİR[2]** , **Hasan ŞİMŞEK[3]**

[1] Aksaray University, Faculty of Medicine, Department of Histology and Embryology, Aksaray, Türkiye

[2] Aksaray University, Vocational School of Technical Sciences, Department of Food Processing, Aksaray, Türkiye

[3] Aksaray University, Faculty of Medicine, Department of Physiology, Aksaray, Türkiye

Nurhan AKARAS ORCID No: 0000-0002-8457-9448
Özge KANDEMİR ORCID No: 0000-0001-8884-4168
Hasan ŞİMŞEK ORCID No: 0000-0001-5573-4923

Corresponding author: nurhanakaras@aksaray.edu.tr

Investigation of Waste Mineral Wool in Geopolymer Production

Mehrzad MOHABBI[1*] , **Mehmet Nuri KOLAK[2]**

[1] Bingöl University, Faculty of Engineering and Architecture, Civil Engineering Department, Bingöl, Türkiye

[2] Bingöl University, Vocational School of Technical Sciences, Department of Construction, Bingöl, Türkiye

Mehrzad MOHABBI ORCID No: 0000-0001-8584-1658
Mehmet Nuri KOLAK ORCID No: 0000-0003-3533-3422

Corresponding author: mnkolak@bingol.edu.tr

Investigation of Leishmaniasis Seroprevalence in Dogs in Bingöl Province of Turkey

Murat UZTİMÜR [1*] , **Hakan KEÇECİ [1]** , **Taylan TURAN [2]** , **Cennet Nur ÜNAL [1]**

[1] Bingöl University, Faculty of Veterinary Medicine, Department of Internal Medicine, 12000, Bingöl, Turkey

[2] Gazi University, Faculty of Pharmacy, Department of Biochemistry, 06330, Ankara, Turkey.

Murat UZTİMÜR, ORCID No:0000-0001-9294-1825
Hakan KEÇECİ, ORCID No: 0000-0001-5654-0581
Taylan TURAN, ORCID No:0000-0001-7335-1213
Cennet Nur ÜNAL, ORCID No:0000-0002-8676-6490

Corresponding author: cnaltunboga@gmail.com

Silent Treasures of Nature: The Awakening of Bingöl Lakes With Ecotourism

Alperen MERAL[1*] , **Yeşim KABAY[1]** , **Sefa BAYRAM[1]** , **Rozelin KAYALI[1]** ,
Ahmet USLU[2]

[1] Bingöl University, Agriculture Faculty, Landscape Architecture Department, Bingöl, Türkiye

[2] Bingol University, Vocational School of Social Sciences, Office Services and Secretarial Department, Bingöl, Türkiye

Alperen MERAL ORCID No: 0000-0001-6714-7187
Yeşim KABAY ORCID No: 0009-0006-3403-7671
Sefa Bayram ORCID No: 0009-0007-7282-557X
Rozelin KAYALI ORCID No: 0009-0000-5852-266X
Ahmet USLU ORCID No: 0000-0001-8745-423X

Corresponding author: alperenmeral@bingol.edu.tr

Türk Doğa ve Fen Dergisi
Turkish Journal of Nature and Science
www.dergipark.gov.tr/tdfd

Exceptional Winter Activity Record from Blunt-nosed Viper (*Macrovipera lebetinus*) in Türkiye

Muammer KURNAZ [1] (ID), Mehmet Kürşat ŞAHİN [2]* (ID)

[1] Gümüşhane University, Kelkit Sema Doğan Vocational School of Health Services, Department of Medical Services and Techniques, Kelkit, Gümüşhane, Türkiye
[2] Hacettepe University, Faculty of Science, Department of Science, Ankaral, Türkiye
Muammer KURNAZ ORCID No: 0000-0002-0498-0208
Mehmet Kürşat ŞAHİN ORCID No: 0000-0003-0834-5081

Corresponding author: : yasambilimci.kursat@gmail.com

Abstract: The seasonal dynamics of reptile species, particularly their responses to temperature fluctuations, play a crucial role in their ecological functioning. Here we report the winter activity of the Blunt-nosed Viper (*Macrovipera lebetinus*), a reptilian species primarily distributed across the Middle East for the first time. While extensive research exists on various aspects of this species, including taxonomy and distribution, there remains a notable gap in the understanding of its winter behaviors. By conducting field observations in the Direktaşı-Bitlis province of Türkiye, present study offers novel insights into the winter activity of *M. lebetinus*. The study identifies a juvenile specimen of *M. lebetinus* exhibiting activity during December, a period typically associated with hibernation in reptiles. The observed air temperature of approximately 15.1°C is noteworthy as an unusual value. This anomaly prompts an exploration into the potential influences of climate change on reptilian hibernation patterns. The findings highlight the vulnerability of ectothermic creatures to temperature fluctuations induced by climate change, which can disrupt their hibernation cycles and lead to untimely activity. Since this study represents the first time the winter activity of *M. lebetinus* has been documented. Moreover, the study underscores the critical implications of disrupted hibernation for reptilian populations, potentially jeopardizing their survival and reproductive success. The unforeseen activity observed in *M. lebetinus* serves as a poignant example of how climate-induced temperature shifts can disrupt established ecological rhythms, posing significant threats to species viability.

1

Koca engereğin (*Macrovipera lebetinus*) Türkiye'deki Olağandışı Kış Aktivitesi Kaydı

Öz: Sürüngen türlerinin mevsimsel dinamikleri, özellikle de sıcaklık dalgalanmalarına verdikleri tepkiler, ekolojik işlevlerinde önemli bir rol oynar. Bu çalışmada *Macrovipera lebetinus* (Koca Engerek)in kış aktivitesi ilk kez rapor edilmiştir. Bu türle ilgili taksonomi ve dağılım dahil olmak üzere çeşitli yönlerde geniş kapsamlı araştırmalar mevcut olmasına rağmen, kış davranışlarını anlama konusunda önemli bir boşluk bulunmaktadır. Türkiye'nin Direktaşı-Bitlis ilinde yapılan saha gözlemleri ile bu çalışma, Aralık ayında aktivite gösteren *M. lebetinus*'un kış aktivitesi hakkında yeni veriler sunmaktadır. Yaklaşık 15.1°C olarak tespit edilen gözlem hava sıcaklığı olağandışı bir değer olarak dikkat çekicidir. Bu anormallik, iklim değişikliğinin sürüngen kış uykusu desenleri üzerindeki potansiyel etkilerini araştırmaya yol açmaktadır. Zira bu çalışma ile *M. lebetinus*'un kış aktivitesi ilk kez gözlenmiştir. Haliyle bu çalışma, iklim değişikliği tarafından tetiklenen sıcaklık dalgalanmalarının, sürüngenlerin hibernasyon döngülerini bozabileceğini ve aktiviteye yol açabileceğini vurgulamaktadır. Dahası, bu çalışma hibernasyondan erken uyanma, sürüngen popülasyonları için kritik sonuçlara yol açabileceğini ve bunun potansiyel olarak hayatta kalma ve üreme başarısını tehlikeye atabileceğini göstermektedir. *M. lebetinus*'ta gözlenen beklenmedik aktivite, iklim tarafından tetiklenen sıcaklık değişikliklerinin mevcut ekolojik ritimleri nasıl bozabileceğine dair etkileyici bir örnek oluşturmakta olup, türlerin yaşamsallığı için önemli tehditlere örnek olmaktadır.

1. INTRODUCTION

A considerable number of organisms, including reptile species, rely heavily on seasonal temperature fluctuations to perform their daily functions, as their body temperatures are highly sensitive to variations in the surrounding environment [1]. For instance, during the warm seasons, these organisms engage in reproduction, nutrition, biological activity, food capturing, and predator evasion. However, during the cold seasons, their physiological processes become impeded by the low temperature, rendering them incapable of carrying out these activities [1,2-7]. As a result, they restrict their physiological endeavors and exhibit a preference for specialized biological processes like hibernation or brumation [8]. These inclinations enable them to maintain optimal health, dormancy, and shelter beneath the ground or in a nest, thereby consuming minimal energy until the subsequent mild season [8].

Nonetheless, meteorological conditions can occasionally cause atypical fluctuations in temperature. Elevated temperatures that occur in the winter months have the potential to induce transient awakenings and atypical behavior in these organisms [1,9].

The Blunt-nosed Viper (*Macrovipera lebetinus*) is one of two *Macrovipera* species, that inhabits in this region [10]. It is a species that has a very wide distribution in the Middle East and is generally distributed in the south, southeast, east, and northeast of Türkiye [11]. *Macrovipera lebetinus* is listed as Least Concern (LC) on the IUCN Red List. In fact the species is locally threatened in some regions due to habitat loss and persecution, its overall population has a declining trend. Their habitat preferences are generally steppe-like semi-arid areas such as forests, shrubs, rocky areas, and deserts [11,12]. Its vertical distribution generally reaches up to 2500 meters above sea level [11]. However, this altitude preference is between sea level and 1700 m for the Mediterranean region [12].

Although various taxonomic, systematic, phylogenetic, and distributional studies have been conducted on *M. lebetinus* [13-15], ecological studies are quite lacking [12]. For instance, research on the spring activities of males of this species in Türkiye and Cyprus has been conducted; however, information regarding their winter activities is currently unavailable. In this context this study provides novel insights into the winter activity of species of blunt-nosed vipers for the scientific community as a case study.

2. MATERIAL AND METHOD

The *M. lebetinus* specimen was detected during a field study between 13:30 and 14:30 in Direktaşı-Bitlis province (Figure 1) (GPS data: 38.30 N; 41.97 E; elevation about 1500 m asl.). The air temperature and humidity in the observation area were taken with a digital thermometer (HTC 288-ATH ®) and was 15.1°C. The soil surface and under 10 cm temperatures were measured by Fluke Type K Thermocouple Probes. The wind speed

was measured by Multicomp Pro Anemometer. The specimen was diagnosed by direct observation and no treatment was performed. Despite this, the specimen's size suggested that it was a juvenile. The photographs of the specimen were captured in the field, and it was subsequently relocated from the location where the specimen was found.
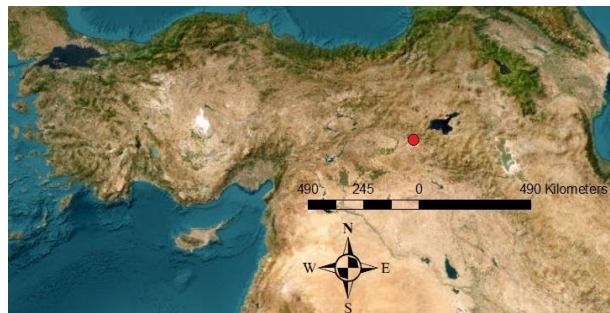
Figure 1. The map shows observed activity locality of *M. lebetinus* species (red circle).

3. RESULTS

The juvenile individual of the Blunt-nosed viper was observed on December 4, 2023 (Figure 2). The sample was detected in the area where pistachio trees were located during pistachio pruning. While the soil surface temperature in the observation area was measured as 17.6°C and the temperature 10 cm below the soil was measured as 20.1°C, the wind in the observation area was calculated as 2m/sec and the humidity was 86.9%.

Figure 2. A juvenile specimen *M. lebetinus*, observed from Direktaşı, Bitlis province (Türkiye) during the winter period (4 December 2023).

4. DISCUSSION AND CONCLUSION

Since *M. lebetinus* is an ectothermic creature like other reptiles, it has to spend the winter months in hibernation. Otherwise, since their physiological activities, which depend on the temperature of the environment, will decrease, it will be difficult for them to reach prey to escape from predators. It may cause both the death of the viper species and a decrease in its body mass due to a lack of calories [1,9,16].

No winter activity investigation on *M. lebetinus* has been documented in the literature up to date. Therefore, this study is the first and an important study showing the activity of this species in December. The fact that the air temperature of the area where the snake was observed is approximately 15°C is perhaps one of the important

2

reasons for this winter activity. Because it has been reported that the activity temperature of the environment for many snake species is between 10-25°C [7].

The reason why the viper species reported in the present study showed winter activity may be that daily temperature changes are very fluctuating. Otherwise, according to seasonal norms, the air temperature is expected to be lower since the altitude of the area where the viper species is observed is 1500 m above sea level. Therefore, this is not a common occurrence and seems to be very rare for reptile species during the winter months.

Global climate change seems to be one of the important factors affecting the hibernation period of all ectothermic creatures in the near future [12]. This will cause daily temperature activities in the winter months to be unbalanced and reptile species to be warm enough to be active. In addition, reptile species can wake up from hibernation early and exhibit reproductive behavior due to these temperature changes [17-19].

Ultimately, species that are deceived by untimely temperatures and start breeding activities will have to enter hibernation again as a result of the deterioration of air temperatures and decrease in air temperatures. This may cause the extinction of the generation of these reptile species in the year in which winter activity is observed and their offspring not being able to develop [20]. Stűmpel et al. (2019) report that March seems to be the earliest month in which *M. lebetinus* exhibits activity. A four-month interval separates the months of activity that are documented in this research.

The majority of reptile species are sensitive to temperature changes. The reason for this is that these creatures carry out all their biological activities between certain temperatures. When temperatures decrease, they go into hibernation or brumation processes, ensuring the continuity of their lives and minimizing energy losses. Although the *M. lebetinus* specimen observed in this study is normally active after March, this is the first time such a situation has been encountered. This situation is probably a result of daily temperature changes in the winter months caused by climate change.

According to the temperature data provided by the Turkish State Meteorological Service, it is seen that the temperature changes in the area where the species is observed, have decreased significantly in the approximately 2.5-month period since December 4, 2023. This shows that hibernation activity is believed to be continued for all reptile species living in that region. As a result, disruption of hibernation activities in reptile species are important factor that can affect their lives. These temperature fluctuations could put species at risk of extinction in the future.

Acknowledgement

REFERENCES

[1] Zuffi MAL, Macchia M, Ioalè P, & Giudici F. Winter activity in a coastal population of *Vipera aspis* (Reptilia, Viperidae). Revue d'Ecologie, Terre et Vie. 1999; 54(4): 365-374.

[2] Huey RB. Temperature, physiology, and the ecology of reptiles. Pp. 25–91 In C. Gans and P. H. Pough (Eds.), Biology of the Reptilia, 1982: Vol. 12. Academic Press, London.

[3] Naulleau G. The effects of temperature on digestion in *Vipera aspis*. J. Herpetol. 1983; 17:166–170.

[4] Stevenson RD, Peterson CR, Tsuji JS. The thermal dependence of locomotion, tongue flicking, digestion, and oxygen consumption in the wandering garter snake. Physiol. Zool. 1985; 58:46–57.

[5] Lillywhite HB. Temperature, energetics, and physiological ecology. Pp. 422–477 In R. A. Seigel, J. T. Collins, and S. S. Novak (Eds.), Snakes: Ecology and Evolutionary Biology. 1987. Macmillan, New York

[6] Peterson CR. Daily variation in the body temperatures of free-ranging garter snakes. Ecology. 1987; 68:160–169

[7] Mori A, Toda M, Ota H. Winter activity of the Hime-Habu (*Ovophis okinavensis*) in the humid subtropics: Foraging on breeding anurans at low temperatures. Biology of the Vipers. Eagle Mountain Publishing LC., Eagle Mountain. 2002; 329-344.

[8] Nordberg EJ, Cobb VA. Body temperatures and winter activity in overwintering timber rattlesnakes (*Crotalus horridus*) in Tennessee, USA. Herpetological Conservation and Biology. 2017; 12(3): 606-615.

[9] Duguy R. Biologie de la latence hivernale chez *Vipera aspis* L. Vie et Milieu. 1963;14(3) 1-443.

[10] Uetz P, Freed P, Hosek J. The Reptile database 2024. Available at http://www.reptile-database.org Accessed on 11 February 2024.

[11] Aghasyan A, Ananjeva NB, Böhme W, Cogălniceanu D, Hraoui-Bloquet S, Lymberakis P, Orlov NL, Sadek R, Sevinç M, Tok CV, Tuniyev B, Ugurtas IH, Werner YL, Wilkinson J, Borkin L, Milto K, Golynsky E, Rustamov A, Nuridjanov D, Munkhbayar K & Giri V 2021. *Macrovipera lebetina*. The IUCN Red List of Threatened Species 2021: e.T157295A750117. https://dx.doi.org/10.2305/IUCN.UK.2021-3.RLTS.T157295A750117.en. Accessed on 11 February 2024.

[12] Stüempel N, Zinenko O, & Mebert K. On elevation-related shifts of spring activity in male vipers of the genera *Montivipera* and *Macrovipera* in Turkey and Cyprus. Herpetozoa. 2019; 31(3-4): 125-132.

[13] Joger U. The venomous snakes of the Near and Middle East. Tübinger Atlas des Vorderen orients, beihefte, Wiesbaden (Reihe A). 1984; 12: 1-115.

[14] Stüempel N, Joger U. Recent advances in phylogeny and taxonomy of Near and Middle Eastern Vipers –

an update. Zookeys, Washington [electronic resource]. 2009; 31: 179-191.

[15] Mebert K, Göçmen B, İğci N, Oğuz MA, Karış M, & Ursenbacher S. New records and search for contact zones among parapatric vipers in the genus *Vipera* (*barani*, *kaznakovi*, *darevskii*, *eriwanensis*), *Montivipera* (*wagneri*, *raddei*), and *Macrovipera* (*lebetina*) in northeastern Anatolia. Herpetol. Bull. 2015; 133: 13-22.

[16] Aleksiuk M. Reptilian hibernation: evidence of adaptive strategies in *Thamnophis sirtalis parietalis*. Copeia. 1976; 170-178.

[17] Sahin MK. Unusual mating behavior of Apathya cappadocica in the winter season from southeastern Anatolia. SLRS. 2021; *2*(2): 49-53.

[18] Özkan H, Bülbül U. The winter activity of the endemic lizard species, Anatololacerta danfordi (Günther, 1876). JIST. 2021; *11*(1): 99-105.

[19] Özgül CN, Kurtul D, Gül Ç, & Tosunoğlu M. Unusual winter activity of some amphibian and reptile species living in Bozcaada (Çanakkale, Turkey). JAES. 2022; *7*(3): 244-250.

[20] Huey RB, Ma L, Levy O, & Kearney MR. Three questions about the eco-physiology of overwintering underground. Ecol. Lett. 2021; *24*(2): 170-185.

Türk Doğa ve Fen Dergisi
Turkish Journal of Nature and Science
www.dergipark.gov.tr/tdfd

BINGÖL UNIVERSITY

Statistical Analysis of Wind Speed Data with Different Distributions: Bitlis, Türkiye

Asuman YILMAZ [1*] iD , Mahmut KARA [1] iD

[1,2] Van Yüzüncü Yıl University, Faculty of Economics and Administrative Sciences, Department of Econometrics, Van, Türkiye
Asuman YILMAZ ORCID No: 0000-0002-8653-6900
Mahmut KARA ORCID No: 0000-0001-7678-8824

Corresponding author: asumanduva@yyu.edu.tr

Abstract: Accurately modeling wind speed is important in estimating the wind energy potential of a specified region. Two- parameter Weibull distribution is the most widely used and accepted distribution in the energy literature. However, it does not model the all wind speed data encountered in nature. Therefore, in this study, different distributions are used for modeling wind energy, such as Gamma, lognormal, Generalized Rayleigh. The estimators of the unknown parameters of these distributions are found by using maximum likelihood estimators.

Rüzgar Hızı Verilerinin Farklı Dağılımlara Göre İstatistiksel Analizi: Bitlis, Türkiye

Öz: Rüzgâr hızının doğru bir şekilde modellenmesi, belirli bir bölgenin rüzgâr enerjisi potansiyelinin tahmin edilmesi açısından önemlidir. İki parametreli Weibull dağılımı enerji literatüründe en yaygın kullanılan ve kabul edilen dağılımdır. Ancak doğada karşılaşılan tüm rüzgâr hızı verilerini modellemez. Bu nedenle bu çalışmada rüzgâr enerjisinin modellenmesinde Gamma, log-normal, Genelleştirilmiş Rayleigh gibi farklı dağılımlar kullanılmıştır. Bu dağılımların bilinmeyen parametrelerinin tahmin edicileri, maksimum olabilirlik tahmin edicileri kullanılarak bulunur.

1. INTRODUCTION

Energy consumption is rising substantially as a result of both population growth and advancements in technology. One of the most crucial elements in the growth of a country is its energy needs [1,2]. These days, fossil fuels are used extensively in practically every aspect of daily life, such as production, logistics, and heating. However, continued consumption of fossil fuels endangers both people and the world in the long run due to carbon emissions, air pollution, and climate change [3]. To solve these problems, it is recommended to use environmentally friendly alternative energy sources including geothermal, solar, and wind power. Therefore, renewable energy sources have attracted attention in recent decades, particularly in developed countries [4, 5].

A promising renewable energy source, wind power can be used for stand-alone, remote, and grid-connected applications in addition to direct energy delivery [6]. Over the past 20 years, wind power generation has grown amazingly rapidly, and it is now a mature, reliable, and efficient technology for producing electricity [3]. It has been used as an essential renewable energy source in electricity production in many developed countries.

To effectively and economically obtain wind energy, there are two key components. The first of these is where the wind system will be built. The second is to decide on the statistical distributions to be used to determine wind speed characteristics. Accurately determining the wind speed distribution has an important impact on wind power calculations [7]. Because small errors in the modeling of the wind speed data lead to significantly larger errors in the energy outcome computation [8]. The Weibull distribution is frequently used in literature to model wind speed data. However, it is not suitable for all wind regimes [9-10]. Therefore, different distributions including

Gamma, inverse Weibull, Inverted Kumaraswamy, lognormal, and inverse Gaussian are used for modelling the wind speed, see [8,11-15]. Considering all these points, Weibull, Gamma, log-normal, and Generalized Rayleigh distributions are used in modeling wind energy in this study. The estimators of the unknown parameters of these distributions are found by using maximum likelihood estimators (MLEs). The originality of this study comes from the fact that it considers different statistical distributions to model wind speed data.

The rest of the study is organized as follows. In section 2, the distributions used in the study are given along with the ML method for estimating parameters of the Weibull, Gamma, inverse Gauss, and lognormal distributions. In section 3, application results are presented and modeling performances of the given distributions are compared. In section 4, the study is finalized with some concluding remarks.

2. MATERIAL AND METHOD

This section provides parameter estimations and the probability distribution functions (pdf), the cumulative density function (cdf) for the Weibull, and gamma, lognormal, and generalized Rayleigh distributions.

2.1. Weibull Distribution

Among lifetime distributions, the Weibull distribution is one of the most often used. W. Weibull first proposed the Weibull distribution and used it to describe the distribution of a materials breaking strength. The reliability theory, numerous environmental science fields, and renewable energy have all benefited greatly from the distribution; see [16–18]. The probability density function (pdf) and the pdf cumulative density function (cdf) and of the Weibull distribution are:

$$f(x; \alpha, \beta) = \frac{\alpha}{\beta^\alpha} x^{\alpha-1} e^{\left(\frac{-x}{\beta}\right)^\alpha} < x < \infty; \ \alpha > 0, \beta > 0 \quad (1)$$

and

$$F(x; \alpha, \beta) = 1 - e^{\left(\frac{x}{\beta}\right)^{-\alpha}} \ 0 < x < \infty; \ \alpha > 0, \beta > 0. \quad (2)$$

Here, α is the shape parameter and β is the scale parameter.

2.1.1 Parameter estimation of Weibull distribution

Let $X_1, X_2, \ldots, X_n$ be a random sample from Weibull distribution. The likelihood function is given by:

$$L(x; \alpha, \beta) = \frac{\alpha^n}{\beta^{n\alpha}} \prod_{i=1}^{n} x_i^{(\alpha-1)} e^{-\left(\frac{x_i}{\beta}\right)^\alpha} \quad (3)$$

Following that, the logarithm of $L(x; \alpha, \beta)$ is defined as follows to define the log-likelihood function:

$$lnL = nln\alpha - n\alpha ln\beta + (\alpha - 1) \sum_{i=1}^{n} lnx_i - \sum_{i=1}^{n} \left(\frac{x_i}{\beta}\right)^\alpha. \quad (4)$$

By taking the partial derivative of (4) with respect to α and β, and equating them to zero, we obtain the following log-likelihood equations:

$$\frac{\partial lnL}{\alpha} = \frac{n}{\alpha} - nln\beta + \sum_{i=1}^{n} lnx_i - \sum_{i=1}^{n} \left(\frac{x_i}{\beta}\right)^\alpha ln\left(\frac{x_i}{\beta}\right) = 0 \quad (5)$$

$$\frac{\partial lnL}{\beta} = \frac{-n\alpha}{\beta} + \frac{\alpha \sum_{i=1}^{n} x_i^\alpha}{\beta^{\alpha+1}} = 0. \quad (6)$$

Then, from the solution of equation (6), the parameter β is obtained as

$$\beta = \left(\frac{\sum_{i=1}^{n} x_i^\alpha}{n}\right)^{\frac{1}{\alpha}}$$

By substituting the solution of β into equation (5), we have

$$\frac{\sum_{i=1}^{n} x_i^\alpha lnx_i}{\sum_{i=1}^{n} x_i^\alpha} - \frac{1}{\alpha} - \frac{\sum_{i=1}^{n} lnx_i}{n} = 0.$$

The equation $g(\alpha)=0$ cannot be solved explicitly, but a numerical method should be used to solve this equation. The $\hat{\alpha}$ can be obtained by using the following well-known Newton-Raphson formula

$$\hat{a}_{m+1=\hat{a}_m} - \frac{g(\hat{a}_m)}{g'(\hat{a}_m)} \ m = 1,2,3, \ldots$$

where $\hat{\alpha}_1$ is as initial value and $g'(\hat{\alpha})$ is the derivative of $g(\alpha)$. Then the ML estimator of β is given as follows:

$$\hat{\beta} = \left(\frac{\sum_{i=1}^{n} x_i^{\hat{\alpha}}}{n}\right)^{\frac{1}{\hat{\alpha}}}.$$

2.2. Gamma Distribution

Because of its flexible shape, the positively skewed gamma distribution has numerous applications in a variety of industries, including hydrology, engineering, medicine, seismology, and reliability. The works of Aksoy [19], Shapiro and Chen [20], and Hristopulos et al. [21] provide a thorough summary of the literature's study on the application of gamma distribution.

The pdf and the cdf of the Gamma distribution are given by:

$$f(x) = \frac{1}{\Gamma(\alpha)\beta^\alpha} x^{\alpha-1} e^{\frac{-x}{\beta}}, x > 0; \alpha, \beta > 0, \quad (7)$$

and

$$F(x) = \int_0^x \frac{1}{\Gamma(\alpha)\beta^\alpha} x^{\alpha-1} e^{\frac{-x}{\beta}} dx \ x > 0; \alpha, \beta > 0, \quad (8)$$

respectively.

2.2.1. Parameter estimation of Gamma distribution

Let $X_1, X_2, \ldots, X_n$ be a random sample of size n from Gamma (α, β) distribution. The likelihood function for $X_i \ i = 1,2, \ldots, n$ is written as follows:

$$L(x; \alpha, \beta) = \prod_{i=1}^{n} \frac{1}{\Gamma(\alpha)\beta^{\alpha}} x_i^{(\alpha-1)} e^{-\frac{x_i}{\beta}} \qquad (9)$$

Then the log-likelihood function is defined as the logarithm of $L(x; \alpha, \beta)$ is given by:

$$lnL(x; \alpha, \beta) =$$

$$-nln\Gamma(\alpha) - n\alpha ln(\beta) + (\alpha - 1)\sum_{i=1}^{n} lnx_i - \frac{1}{\beta}\sum_{i=1}^{n} x_i. \quad (10)$$

The likelihood equations are found by equating the first partial derivatives of $lnL(x; \alpha, \beta)$ with respect to the α and β parameters to zero. The α and β parameters are shown as follows:

$$\frac{\partial lnL}{\partial \alpha} = -n\Psi(\alpha) - nln\beta + \sum_{i=1}^{n} \ln x_i = 0 \quad (11)$$

and

$$\frac{\partial lnL}{\partial \beta} = \frac{-n\alpha}{\beta} + \frac{1}{\beta^2}\sum_{i=}^{n} x_i = 0. \qquad (12)$$

Here $\Psi(\alpha) = \frac{\partial ln\Gamma(\alpha)}{\partial \alpha}$ is the digamma function. Then, by solving equation (11), the parameter β is found as:

$$\beta = \frac{1}{n\alpha}\sum_{i=1}^{n} x_i.$$

Substitution of β into equation (12), the resulting equation in α becomes

$$-n\Psi(\alpha) - nln\left(\frac{1}{n\alpha}\sum_{i=1}^{n} x_i\right) + \sum_{i=1}^{n} \ln x_i = 0 .$$

This equation does not yield an explicit estimator for the α; therefore, we resort to iterative methods. Hence, approximate solutions for the parameters are found using iterative numerical methods. In this study, we used the Newton Raphson method.

2.3.   Lognormal Distribution

The lognormal distribution, a long-tailed, positively skewed distribution, is a suitable model for reliability and life span study. Furthermore, Johnson et al. [22] mention that it can be used as a model for several applications in engineering and medical.

The pdf of the log-normal distribution is given by:

$$f(x) = \frac{1}{x\tau\sqrt{2\pi}} e^{\frac{-1}{2}\left(\frac{lnx-\mu}{\tau}\right)^2}, x > 0, \mu \in \mathbb{R}, \tau > 0, \qquad (13)$$

where $\frac{1}{\tau}$ is the shape parameter and μ is the scale parameter.

2.3.1. Parameter estimation of lognormal distribution

The likelihood function based on the observed values of a random sample from the lognormal distribution with pdf (13) is given by

$$L(x; \mu, \tau) = \frac{1}{\sigma^n (2\pi)^{n/2}} \prod_{i=1}^{n} \frac{1}{x_i} e^{\frac{-1}{2\sigma^2}\sum_{i=1}^{n}(lnx_i - \mu)^2} \qquad (14)$$

Then the log likelihood function is

$$lnL(x; \mu, \tau) =$$

$$-nln\tau - \frac{n}{2} ln(2\pi) - \sum_{i=1}^{n} lnX_i - \frac{1}{2}\sum_{i=1}^{n} \left(\frac{(lnX_i - \mu)}{\tau}\right)^2 \qquad (15)$$

By taking the derivatives of lnL with respect to these parameters and equating them to zero, the following likelihood equations are obtained

$$\frac{\partial lnL}{\partial \mu} = \frac{\sum_{i=1}^{n} lnx_i}{\tau^2} - \frac{2n\mu}{2\tau^2} = 0 \quad (16)$$

and

$$\frac{\partial lnL}{\tau^2} = \frac{-n}{2\tau^2} + \sum_{i=1}^{n} \frac{(lnX_i - \mu)^2}{2\tau^4} = 0. \qquad (17)$$

Thus, the MLs are

$$\hat{\mu} = \frac{\sum_{i=1}^{n} lnx_i}{n} \text{ and } \hat{\tau}^2 = \frac{1}{n}\sum_{i=1}^{n} \left(lnx_i - \frac{\sum_{i=1}^{n} lnx_i}{n}\right)^2,$$

respectively.

2.4.   Generalized Rayleigh Distribution

For data modeling, Burr [23] provided twelve distinct kinds of cumulative distribution functions. Out of the twelve, Burr-Type X and Burr-Type XII were the two distribution functions that attracted the greatest attention. The generalized Rayleigh distribution was appropriately termed and the two parameter Burr Type X distribution was recently presented by Surles and Padgett [24]. Keep in mind that the exponentiated Weibull distribution, which was first put forth by Mudholkar and Srivastava [25], includes the two-parameter generalized Rayleigh distribution as one of its members. Both general lifetime modeling and the modeling of strength data can benefit greatly from the application of this distribution.

The pdf of the two-parameter generalized Rayleigh distribution is:

$$f(x; \alpha, \lambda) =$$

$$2\alpha\lambda^2 x e^{-(\lambda x)^2}\left(1 - e^{-(\lambda x)^2}\right)^{\alpha-1}, x > 0, \alpha, \lambda > 0. \qquad (18)$$

2.4.1. Parameter estimation of generalized Rayleigh distribution

Let $X_1, X_2, ..., X_n$ be random sample of size n from generalized Rayleigh distribution with α and λ parameters, then the likelihood function can be written as:

$$L(x; \alpha, \lambda) = 2^n \alpha^n \lambda^{2n} \prod_{i=1}^{n} x_i e^{-(\lambda x_i)^2}\left(1 - e^{-(\lambda x_i)^2}\right)^{\alpha-1}. \quad (19)$$

Then, the log-likelihood function $lnL(x; \alpha, \lambda)$ as follows:

$$lnL(x; \alpha, \lambda) = nln2 + nln\alpha + 2nl$$

$$+ \sum_{i=1}^{n} lnx_i - \lambda^2 \sum_{i=1}^{n} x_i^2$$

$$+(\alpha - 1) \sum_{i=1}^{n} ln\big(1 - e^{-(\lambda x)^2}\big).$$

When we take the derivatives with respect to parameters normal equations become:

$$\frac{\partial lnL}{\partial \alpha} = \frac{n}{\alpha} + \sum_{i=1}^{n} ln\big(1 - e^{-(\lambda x)^2}\big) = 0 \qquad (20)$$

and

$$\frac{\partial lnL}{\partial \lambda} = \frac{2n}{\lambda} - 2\lambda \sum_{i=1}^{n} x_i^2 + 2\lambda(\alpha - 1) \sum_{i=1}^{n} \frac{x_i^2 e^{-(\lambda x)^2}}{1 - e^{-(\lambda x)^2}} = 0 \quad (21)$$

Note that $\hat{\alpha}$ and $\hat{\lambda}$ are not in explicit form and hence, numerical methods, such as fixed-point solution. The ML estimators of generalized Rayleigh distribution can be seen from Esemen and Gürler [26].

3. DATA AND APPLICATION

In this section, the data set introduced and the Weibull, Gamma, lognormal, and generalized Rayleigh distributions are applied to the hourly wind speed data (m/s). The performances of the distributions are compared using several well-known criteria, such as the AIC, R^2 and RMSE. For analyzing MatlabR2021 software is used.

3.1. The Data Set

In this section, hourly wind speed data (m/s), measured hourly at 10m from Bitlis, Turkey during January, February, March, and April 2017 is used. There are 2978 observations recorded. The data is taken with official permission from the Turkish State Meteorological Service. For the hourly wind speed data (m/s), estimates of the parameters of above mentioned distributions are obtained as reported in Table 1. To determine the distribution providing better determination (R^2) and Akaike information criteria (AIC) values for each distribution, as shown in Table 2. In addition to these statistical criteria, the cumulative density function of the given distributions is presented in Figure 1 for wind speed data.

Table 2 gives the values of the evaluation criteria for the generalized Rayleigh, Gamma, Weibull, and lognormal distributions. It is well-known that a better fit is indicated by lower values of the AIC and RMSE and higher values of the R^2.

Table 1. ML estimators of the parameters for the given distributions

Month	Weibull		Gamma		Lognormal		G.Rayleigh	
	$\hat{\alpha}$	$\hat{\beta}$	$\hat{\alpha}$	$\hat{\beta}$	$\hat{\mu}$	$\hat{\tau}$	$\hat{\alpha}$	$\hat{\lambda}$
January	1.207	2.796	1.477	1.767	0.895	0.585	1.567	0.706
February	1.432	2.364	1.999	1.067	0.488	0.781	2.292	0.906
March	1.853	3.064	2.827	0.961	0.813	0.679	3.175	0.725
April	1.639	3.643	2.220	1.467	0.939	0.776	2.299	0.588

Table 2. Modeling performances of the given distribution for wind speed data

Month	Weibull			Gamma			Lognormal			G. Rayleigh		
	R^2	RMSE	AIC	R^2	RMSE	AIC	R^2	RMSE	AIC	R^2	RMSE	AIC
January	0.9675	0.0513	2739.63	0.9969	0.0498	2706.23	0.9932	0.0242	2546.33	0.9527	0.1534	2765.87
February	0.9778	0.0401	2134.90	0.9989	0.0309	2109.78	0.9829	00363	2194.20	0.9193	0.2145	0.2180.32
March	0.9968	0.0160	2625.55	0.9998	0.0132	2635.83	0.9717	0.0471	2725.20	0.9085	0.2338	2778.88
April	0.9990	0.0094	2907.13	0.9995	0.0203	2905.42	0.9715	0.0477	2990.68	0.9049	0.2391	2986.68
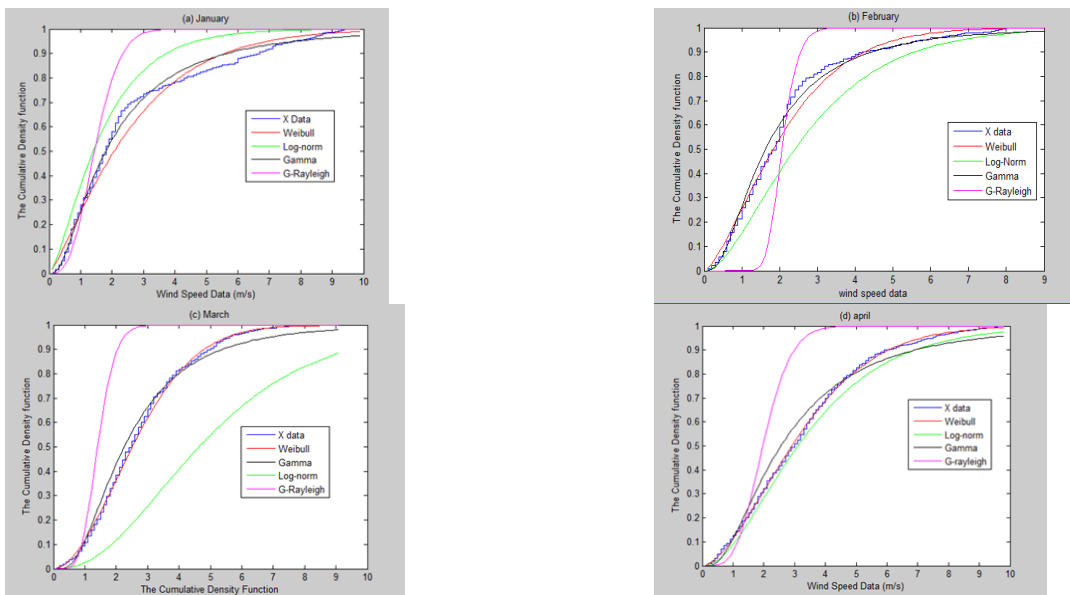
Figure 1. Cumulative density functions of Weibull, Gamma, lognormal, and generalized Rayleigh distributions, along with observed data (X Data), for wind speed measurements in Bitlis, Turkey, during (a) January, (b) February, (c) March, and (d) April (2017)

It can be seen from Table 1 that the Gamma distribution provided the smallest values for the AIC, and RMSE and the largest values for the R^2 . In other words, the Gamma distribution performed better than the other three distributions in modeling the first months of 2017 of Bitlis province. Furthermore, in Figure 1 are consistent with Table 2.

4. CONCLUSION

In this study, the Weibull, Gamma, lognormal, and generalized Rayleigh are used in modelling the wind speed data of Bitlis in Turkey for the first four months of 2017. In parameter estimation, the ML estimation methods are considered. The results summarized in both Figure 1 and Table 2 show that the Gamma distribution described wind speed data in Bitlis during January, February, March, and April 2017 better than Weibull, lognormal, and generalized Rayleigh distributions.

Acknowledgement

REFERENCES

[1] Keyhani, A., Ghasemi-Varnamkhasti, M., Khanali, M., Abbaszadeh, R. An assessment of wind energy potential as a power generation source in the capital of Iran, Tehran. Energy,2010; 35(1), 188-201.

[2] Akpinar, E. K., Akpinar, S. An assessment on seasonal analysis of wind energy characteristics and wind turbine characteristics. Energy conversion and management, 2005; 46(11-12), 1848-1867.

[3] Fyrippis, I., Axaopoulos, P. J., Panayiotou, G. Wind energy potential assessment in Naxos Island, Greece. Applied Energy, 2010; 87(2), 577-586.

[4] Köse, R. An evaluation of wind energy potential as a power generation source in Kütahya, Turkey. Energy conversion and management, 2004; 45(11-12), 1631-1641.

[5] Kaplan, Y. A. Overview of wind energy in the world and assessment of current wind energy policies in Turkey. Renewable and Sustainable Energy Reviews, 2015; 43, 562-568.

[6] Mabel, M. C., Fernandez, E. Growth and future trends of wind energy in India. Renewable and Sustainable Energy Reviews, 2008;12(6), 1745-1757.

[7] Mohammadi, K., Alavi, O., Mostafaeipour, A., Goudarzi, N., & Jalilvand, M. Assessing different parameters estimation methods of Weibull distribution to compute wind power density. Energy Conversion and Management, 2016; 108, 322-335.

[8] Akgül, F. G., Şenoğlu, B., Arslan, T.. An alternative distribution to Weibull for modeling the wind speed data: Inverse Weibull distribution. Energy Conversion and Management, 2016; 114, 234-240.

[9] Akdağ, S. A., Dinler, A. A new method to estimate Weibull parameters for wind energy applications. Energy conversion and management, 2009; 50(7), 1761-1766.

[10] Kusiak, A., Zheng, H., Song, Z. On-line monitoring of power curves. Renewable Energy, 2009; 34(6), 1487-1493.

[11] Brano, V. L., Orioli, A., Ciulla, G., Culotta, S. Quality of wind speed fitting distributions for the urban area of Palermo, Italy. Renewable Energy, 2011; 36(3), 1026-1039.

[12] Carta, J. A., Ramírez, P., Velázquez, S. Influence of the level of fit of a density probability function to wind-speed data on the WECS mean power output estimation. Energy Conversion and Management, 2008; 49(10), 2647-2655.

[13] Morgan, E. C., Lackner, M., Vogel, R. M., Baise, L. G. Probability distributions for offshore wind speeds. Energy Conversion and Management, 2011; 52(1), 15-26.

[14] Sohoni, V., Gupta, S., Nema, R. A comparative analysis of wind speed probability distributions for wind power assessment of four sites. Turkish Journal of Electrical Engineering and Computer Sciences, 2016; 24(6), 4724-4735.

[15] Bagci, K., Arslan, T., Celik, H. E. Inverted Kumarswamy distribution for modeling the wind speed data: Lake Van, Turkey. Renewable and Sustainable Energy Reviews, 2021;135, 110110

[16] Raghunathan, K., Subramaniam, V., Srinivasamoorthy, V. R. Studies on the tensile characteristics of ring and rotor yarns using modified Weibull distribution, 2002.

[17] Chiang, Y. J., Shih, C. D., Lin, C. C., Tseng, Y. Y. Examination of tyre rubber cure by Weibull distribution functions. International Journal of Materials and Product Technology, 2004; 20(1-3), 210-219.

[18] Wood, M. A., Gunderson, B., Xia, A., Zhou, X., Padmanabhan, V., Ellenbogen, K. A. Temporal patterns of ventricular tachyarrhythmia recurrences follow a Weibull distribution. Journal of cardiovascular electrophysiology, 2005;16(2), 181-185.

[19] Aksoy, H. Use of gamma distribution in hydrological analysis. Turkish Journal of Engineering and Environmental Sciences, 2000; 24(6), 419-428.

[20] Shapiro, S. S., Chen, L. Composite tests for the gamma distribution. Journal of Quality Technology, 2001;33(1), 47-59.

[21] Hristopulos, D. T., Petrakis, M. P., Kaniadakis, G. Weakest-link scaling and extreme events in finite-sized systems. Entropy, 2015;17(3), 1103-1122.

[22] Johnson, N. L., Kotz, S., Balakrishnan, N. Continuous univariate distributions, volume 2 (Vol. 289). John wiley & sons;1995.

[23] Burr, I. W. Cumulative frequency functions. The Annals of mathematical statistics, 1942; 13(2), 215-232.

[24] Surles, J. G., Padgett, W. J. Inference for reliability and stress-strength for a scaled Burr type X distribution. Lifetime data analysis, 2001; 7, 187-200.

[25] Mudholkar, G. S., Srivastava, D. K. Exponentiated Weibull family for analyzing bathtub failure-rate data. IEEE transactions on reliability, 1993;42(2), 299-302.

[26] Esemen, M., Gürler, S. Parameter estimation of generalized Rayleigh distribution based on ranked set sample. Journal of Statistical Computation and Simulation, 2018; 88(4), 615-628.

Türk Doğa ve Fen Dergisi
Turkish Journal of Nature and Science
www.dergipark.gov.tr/tdfd

Calculation of Standard Working Hours According to Production Activities in Agricultural Enterprises

Merve BOZDEMİR AKÇİL[1]* , Zeki BAYRAMOĞLU[2] , Kemalettin AĞIZAN[3] ,
Süheyla AĞIZAN[4] , Orhan EROĞLU[5]

[1]Selcuk University, Agricultural Faculty, Agricultural Economics Department, Konya, Türkiye
[2]Selcuk University, Agricultural Faculty, Agricultural Economics Department, Konya, Türkiye
[3]Aydın Adnan Menderes University, Cine Vocational School, Aydın, Turkey
[4]Selcuk University, School of Applied Sciences, Çumra, Turkey
[5]Selcuk University, Agricultural Faculty, Agricultural Economics Department, Konya, Türkiye

Merve BOZDEMİR AKÇİL ORCID No: 0000-0002-5323-2265
Zeki BAYRAMOĞLU ORCID No: 0000-0003-3258-3848
Kemalettin AĞIZAN ORCID No: 0000-0002-2340-2614
Süheyla AĞIZAN ORCID No: 0000-0002-9210-1671
Orhan EROĞLU ORCID No: 0000-0003-4633-8042
Corresponding author: mbozdemir.akademi@gmail.com

Abstract: This study was conducted to analyze the labor in the agricultural sector and determine the employment structure according to production activities for a micro-scale structure. Within the scope of this study, according to the production patterns of agricultural enterprises, the working time realized during the season on 1 decare area was calculated. Although many components are effective on the working time of the labor, technological changes, qualifications, and skills of the labor have been ignored. In this study, agro-ecological areas were taken into consideration to make an evaluation by considering ecological, geological, and topographical conditions. The findings showed that these variables were effective on working hours. The calculated working hours were based on 1 male labor unit for 1 decare. For all regions, tomato was the crop that required the most time in production, and the average working time per decare was 127 hours 41 minutes. After tomato, apple with 119 hours 55 minutes and cherry with 111 hours 16 minutes were the crops requiring the longest working hours in Konya province. It is expected that the products grown in the research region will be a reference for standardized working hours and contribute to the studies to be conducted for planning the workforce and increasing the agricultural employment potential in the region.

Tarım İşletmelerinde Üretim Faaliyetlerine Göre Standart Çalışma Sürelerinin Hesaplaması

Öz: Tarım sektöründeki işgücü varlığının analiz edilebilmesi ve mikro ölçekte bir yapı için üretim faaliyetlerine göre istihdam yapısının belirlenebilmesi amacıyla bu çalışma gerçekleştirilmiştir. Çalışma kapsamında tarım işletmelerinin üretim desenlerine göre 1 dekar alanda sezon boyunca gerçekleştirilen çalışma zamanları hesaplanmıştır. İşgücünün çalışma zamanına yönelik olarak birçok bileşen etkili olsa da teknolojik değişimler, işgücünün sahip olduğu nitelik ve yetenekler göz ardı edilmiştir. Çalışmada ekolojik, jeolojik ve topografik koşulların dikkate alınarak bir değerlendirme yapılabilmesi amacıyla agro-ekolojik alanlar dikkate alınmıştır. Söz konusu değişkenlerin çalışma süreleri üzerinde etkili olduğu belirlenmiştir. Hesaplanan çalışma süreleri 1 dekar için 1 erkek işgücü birimi üzerinden gerçekleştirilmiştir. Tüm bölgeler için üretiminde en çok zamana ihtiyaç duyulan ürün domates olup, dekarda çalışma süresi ortalama 127 saat 41 dakikadır. Domatesten sonra 119 saat 55 dakika ile elma ve 111 saat 16 dakika ile kiraz Konya ilinde en uzun çalışma sürelerini gerektiren ürünlerdir. Araştırma bölgesinde yetiştirilen ürünlerin standartlaşmış çalışma süreleri için referans olması, işgücünün planlaması ve bölgedeki tarımsal istihdam potansiyelinin artırılması için yapılacak çalışmalara katkı sağlaması beklenmektedir.

1. INTRODUCTION

In all global markets and economies, the focus is on increasing productive capacity and production volume; in short, economic growth is targeted. Within the framework of these targets, it is necessary to determine the contribution of cultural, scientific, institutional, and technological factors to economic growth [1]. The analysis of sectoral contributions is critical in economic growth processes, and it is necessary to determine partial productivity increases in agricultural and non-agricultural sectors [2]. Standardized and scientifically accepted data are needed for the theoretically accurate calculation of productivity and for comparisons at regional, national, and international levels. These data will be a reference for comparison and evaluation processes. However, it should not be ignored that this is a theoretical assumption. Structural changes in the economy make it difficult to set and manage standards, particularly for labor markets. The emergence of labor-intensive services that require less capital in the market, the restructuring of firms by taking into account numerical flexibility as a result of increased competition, the reduction of costs by firms through technological innovation, the emergence of new markets, the facilitation of employers' hiring and firing of workers through flexibility provisions in labor laws, the visibility of women in the labor market and employers' search for flexibility have increased non-standard forms of work [3-4]. In line with these effects, there has been a change in the organic structure of employment relations, and the agricultural sector has also been part of this change. Organizational units, the conditions that will arise for work areas, and the use of many inputs that can be measured in different units will produce many different outputs [5-6]. In addition, in labor-intensive sectors, such as agriculture, the qualifications and competencies of the labor will also cause productivity to change. Standardizing the working conditions of the agricultural labor is significant in increasing efficient production and quality. While standards pave the way for planned production, production processes should also be developed on this basis. In the agricultural sector, it is necessary to establish specific working standards to improve the performance of the labor working outside the enterprise and to create efficient work by combining work and knowledge.

Seasonal working conditions in the agricultural sector, especially in crop production, prevent the standardization of the workforce, which is reflected in contractual, wage and social security conditions. Non-standardized employment leads to much lower incomes than standard jobs. For example, in EU countries, temporary jobs are paid on average 20% less than permanent jobs [7-8]. Short-term work allows employers to avoid redundancy costs and offers numerical flexibility with easy hiring and firing [9]. Non-standardized forms of work are usually characterized by fixed-term or short-term work [10-11].

Setting standards for working hours in agricultural enterprises is crucial for the sustainability of the enterprise. In terms of accounting for the activities in the enterprise and determining product prices, the reference prices in the agricultural sector constitute the labor given to the product. The wages of the people who work in agricultural production units and carry out production are expressed in labor expenses. Since these expenses can be directly associated with the cost of the product, they are directly charged to the cost of the product. Apart from the main labor expenses, wages, such as overtime work and product premiums, are also included in direct labor expenses [12-13]. Considering the time worked by the entrepreneur and his family members as labor in the cost calculation, "if the entrepreneur and his family members did not work, the work done by them would be done by foreign labor for a fee" and secondly," it should provide the opportunity to compare with enterprises employing foreign labor" [14]. The labor and time spent on agricultural work are usually calculated in real prices. For example, if hoeing is done by unpaid family labor, the total working time spent on hoeing should be considered, as well as the prevailing labor wages in the region [14].

Agricultural labor and labour practices play a central role in the sustainability of enterprises [15-16] and are one of the main components of social sustainability [17-18]. Therefore, planning for agricultural enterprises is likely to contribute to the effective and efficient use of resources. However, it is necessary to regulate the labor and working conditions within the enterprise. Since the agricultural sector constitutes the basis of economic activities, the successful implementation of planning in the sector will directly contribute to the management and planning of other sectors. Given the changing conditions for agricultural production and the constraints specific to agricultural production, it is necessary to calculate product-based standard working hours in rural areas. Within the scope of this study, working hours were calculated by considering agro-ecological regions and product pattern with a micro-scale application.

2. MATERIAL AND METHOD

The study was conducted with the permission of Selcuk University, Agricultural Faculty, Scientific Ethics Committee, decision numbered 528366 dated 01.06.2023.

Agro-ecological zones refer to regions divided into sub-areas with similar environmental characteristics, potential yield, and land suitability [19]. Konya is among the provinces with high agricultural production potential in Türkiye. The province stands out in terms of its high product diversity and agricultural employment diversity. Agro-ecological zones of Konya province is provided in Table 1 below.

Table 1. Agro-Ecological Zones of Konya Province

Region	Districts in the Region	Area (ha)	Percentage (%)	Annual (mm)
Region 1	Çumra, Karatay, Meram, Selçuklu	704.649	16.90	<400
Region 2	Akören, Ahırlı, Bozkır, Güneysınır, Hadim, Taşkent, Yalıhüyük	525.234	12.60	>400
Region 3	Akşehir, Ereğli, Halkapınar, Ilgın, Tuzlukçu	597.982	14.30	>400
Region 4	Beyşehir, Derbent, Derebucak, Doğanhisar, Hüyük, Seydişehir	589.385	14.20	<400
Region 5	Altınekin, Cihanbeyli, Çeltik, Emirgazi, Kadınhanı, Karapınar, Kulu, Sarayönü, Yunak	1.752.150	42.00	<400
Total	31 District	4.169.400	100.00	-

Source: [20-21]

There were more than 120,000 agricultural workers employed only in the livestock sector in Konya. This study was carried out to determine the perspective towards the labor employed permanently and seasonally in various jobs. A stratified random sampling method was used to determine the number of enterprises to be surveyed; 5% error and 90% confidence limits were used. As in determining the number of surveys, Yamane's [22] formula was used to determine the stratum distribution. In line with the results obtained, 375 surveys were conducted in 2022. The questionnaires were obtained from face-to-face data. Accordingly, the distribution of the number of enterprises to be surveyed according to districts and strata was determined by proportioning the number of enterprises of each district to the "k" value of the strata (number of enterprises/k).

Table 2. 1st Region Distribution of Survey Numbers by Districts

Region 1	Total Number of Enterprises	1st Layer	2nd Layer	3rd Layer
	Sample Number	3	25	49
	k value	5.076	609	311
Çumra	5.548	1	9	18
Karatay	5.621	1	9	18
Meram	2.126	0	3	7
Selçuklu	1932	0	3	6
Toplam	15.227	3	25	49

Table 3. 2nd Region Distribution of Survey Numbers by Districts

Region 2	Total Number of Enterprises	1st Layer	2nd Layer	3rd Layer	4th Layer
	Sample Number	3	14	23	10
	k value	1.363	292	178	409
Akören	630	0	2	4	2
Ahırlı	386	0	1	2	1
Bozkır	780	1	3	4	2
Güneysınır	980	1	3	6	2
Hadim	1.024	1	4	6	3
Taşkent	171	0	1	1	0
Yalıhüyük	118	0	0	1	0
Toplam	4.089	3	13	23	10

Table 4. 3rd Region Distribution of Survey Numbers by Districts

Region 3	Total Number of Enterprises	1st Layer	2nd Layer	3rd Layer	4th Layer
	Sample Number	2	18	49	19
	k value	8.700	967	405	916
Akşehir	4.215	0	4	10	5
Ereğli	5.585	1	6	14	6
Halkapınar	499	0	1	1	1
Ilgın	5270	1	5	13	6
Tuzlukçu	1.830	0	2	5	2
Toplam	17.399	2	18	43	19

Table 5. 4th Region Distribution of Survey Numbers by Districts

Region 4	Total Number of Enterprises	1st Layer	2nd Layer	3rd Layer
	Sample Number	6	30	47
	k value	1.663	333	212
Beyşehir	2.895	2	9	14
Derbent	824	1	2	4
Derebucak	128	0	0	1
Doğanhisar	2098	1	6	10
Hüyük	1.571	1	5	7
Seydişehir	2.460	1	7	12
Toplam	9.976	6	30	48

Table 6. 5th Region Distribution of Survey Numbers by Districts

Region 5	Total Number of Enterprises	1st Layer	2nd Layer	3rd Layer
	Sample Number	3	28	52
	k value	12.001	1.286	692
Altınekin	3.085	0	2	4
Cihanbeyli	6.215	1	5	9
Çeltik	1.677	0	1	2
Emirgazi	1905	0	1	3
Kadınhanı	4.758	0	4	7
Karapınar	5.263	0	4	8
Kulu	4.856	1	4	7
Sarayönü	3.622	0	3	5
Yunak	4.621	1	4	7
Toplam	36.002	3	28	52

The total amount of labor that agricultural enterprises have is a factor that restricts production processes. To calculate the amount of labor used in agricultural production, a standard male labor unit is needed. "Standard Male Labor Unit" (SMLU) is the value of an average labor working at most 8 hours a day [23]. In this study, the working hours of an ESU (between the ages of 15-49) needed based on crops on one decare of land according to the agro-ecological regions of Konya province were calculated. Regarding the use of labor, the unit of time measurement (hours, minutes) is the most appropriate distribution method. For example, it is a very healthy measure since the hours of machine and labor used in tillage activities overlap [13]. Thus, the hour unit was used to express the labor within the scope of this study.

3. RESULTS

Working hours by crop differ according to the climatic and topographical characteristics of agro-ecological regions. For example, Akören, Ahırlı, Bozkır, Güneysınır, Hadim, Taşkent, and Yalıhüyük districts are in the second region. These districts are generally mountainous, and their land structures are small and fragmented. This situation causes the working time of the enterprises to be prolonged due to their land structures, even if the tractor-pulling power and machinery and equipment features are similar. The level of specialization of the workforce in the study area was ignored to determine a standard working time. Because, although the labor does not have similar physical characteristics in every enterprise, the practices acquired for the work, the techniques used and the way the work is done are the features that directly affect the change in working hours.

In addition to climatic and topographical characteristics, the environmental and economic opportunities of the enterprises may also cause changes in the duration of work. In crops, such as wheat, barley, and chickpea, which are both irrigated and dry farmed, working hours vary according to irrigation activities. For example, in the first region where Çumra, Karatay, Meram and Selçuklu districts are located, the same procedures are applied for irrigated barley and wheat and three hours and 28 minutes of work is needed for all operations from planting to harvesting in one decare. For wheat and barley produced in the dry, 52 minutes of working time is sufficient. Therefore, in irrigated areas where sprinkler irrigation is used, separate working time is needed for laying, transporting, and collecting the pipes and working times differ.

Tomato is the crop that requires the most working time on average across all regions. In the third region, which includes the districts of Akşehir, Ereğli, Halkapınar, Ilgın and Tuzlukçu, the working time required for tomato, which is cultivated mainly in Ereğli, is 127 hours and 41 minutes for a male laborer. Intensive labor is needed for tomatoes, especially during irrigation, top rowing, hoeing, and harvesting periods. After tomatoes, apple is the crop that requires the most working time. For apples, 119 hours, and 55 minutes of working time is needed for a male labor in one decare of land in the regions' average. Although the working time varies according to the variety and yield in apple production, considering that there are approximately 200 trees and an average yield of 100 kg per tree in semi-dwarf varieties grown throughout Konya, the average working time required in the harvest period for one decare is 63 hours and 39 minutes. In addition, acting precisely in apple harvesting is significant for the preservation and trade of the fruit and is effective in extending the working time. The third product that requires the longest working time is cherry. The average working time of cherries in the regions is 111 hours and 16 minutes. In cherry production, harvesting accounts for approximately 50.00% of the working time.

14

Table 7. Standard Working Hours in the Agricultural Enterprises Investigated are Presented

Regions	Region 1	Region 2	Region 3	Region 4	Region 5	RegionAverage
Wheat (Irrigated)	3.28	4.21	3.43	4.07	3.44	3.52
Barley (Irrigated)	3.28	4.21	3.43	4.07	3.44	3.52
Wheat (Dry)	0.52	1.31	1.03	1.22	1.02	1.10
Barley (Dry)	0.52	1.31	1.03	1.22	1.02	1.10
Grain Maize	4.45	5.51	5.21	5.36	4.55	5.17
Silage Maize	4.45	5.51	5.21	5.36	4.55	5.17
Sunflower (Oil)	3.21	0.00	3.55	0.00	3.29	3.35
Sunflower (Snack)	6.20	7.06	6.27	0.00	6.11	6.31
Clover	3.25	0.00	3.50	4.20	3.48	3.51
Sugar Beet	20.45	0.00	21.26	22.24	21.30	21.25

Chickpea	6.17	9.38	6.22	9.48	6.09	7.39
Beans (Dry)	13.19	14.08	0.00	14.23	13.30	13.43
Potato	25.26	0.00	26.45	27.43	0.00	26.38
Hungarian Vetch	2.41	3.25	3.00	3.16	2.48	3.02
Oats	3.42	1.49	0.00	1.41	3.48	2.45
Zucchini (Snack)	11.04	12.25	11.33	12.08	11.17	11.41
Onion (Dry)	13.21	0.00	0.00	0.00	13.34	13.28
Grape	0.00	44.41	0.00	42.19	0.00	43.30
Lavender	0.00	29.41	0.00	28.10	0.00	28.56
Peach	0.00	38.46	0.00	0.00	0.00	38.46
Walnut	0.00	55.23	0.00	0.00	0.00	55.23
Cherry	0.00	113.16	109.15	0.00	0.00	111.16
Pear	0.00	74.07	0.00	0.00	0.00	74.07
Apple	0.00	124.36	115.13	0.00	0.00	119.55
Strawberry	0.00	83.43	0.00	81.05	0.00	82.24
Rye	0.00	0.00	1.49	0.00	1.39	1.44
Poppy	0.00	0.00	25.45	27.16	25.49	26.17
Tomato	0.00	0.00	127.41	0.00	0.00	127.41
Sour Cherry	0.00	0.00	109.00	0.00	0.00	109.00
Plum	0.00	0.00	65.40	0.00	0.00	65.40
Lentil	0.00	0.00	0.00	34.25	31.53	33.09
Safflower	0.00	0.00	0.00	3.01	0.00	3.01
Melon	0.00	0.00	0.00	27.34	0.00	27.34
Canola	0.00	0.00	0.00	0.00	3.18	3.18
Cumin	0.00	0.00	0.00	0.00	3.33	3.33
Millet	0.00	0.00	0.00	0.00	4.03	4.03
Grass	0.00	0.00	0.00	0.00	3.22	3.22
Fallow	0.12	0.20	0.15	0.18	0.15	0.16

4. DISCUSSION AND CONCLUSION

This study was carried out to determine working time and standard labor units in the agricultural sector. The labor requirements for different crops, especially in agro-ecological regions, were examined as crop production is generally carried out in open areas and varies according to seasonal conditions. Within the product group, cherry has the highest SMLU value. Since the maintenance processes of cherry are sensitive and require intensive labor during harvest periods, its value in the regions' average was 2.259. In addition, there is a need for a labor that is advanced regarding qualifications in the harvesting processes of cherries and that will contribute to reducing the wastage rate without damaging the product. After cherries, sugar beet was determined as the crop with the highest SMLU requirement in the regions' average. The SMLU value of sugar beet is 1,652. As a result of the need for intensive use of labor, especially during the hoeing periods of the product, the SMLU value was high. Wheat, frequently preferred in the production processes in the research region and the enterprises examined, has an SMLU value of 0.734. According to the regions' average, the enterprises in the 5th region had the highest value in the SMLU in irrigated wheat production. In the 5th region where Altınekin, Cihanbeyli, Çeltik, Emirgazi, Kadınhanı, Karapınar, Kulu, Sarayönü, and Yunak districts are located, the SIB used in the production process is 1.145. The use of standard labor is an important data for calculating labor needs and planning areas where employment opportunities can be provided according to the production pattern. Standard labor needs may decrease due to the participation of specialized labor in employment or the widespread use of technology. Therefore, there is a need for controlled development in the agricultural sector, which contributes to the employment of many people.

The definition of standard work units is important for increasing productivity and optimizing the use of labor on farms. Standards ensure the planning of business processes and the efficient use of resources, while creating a competitive advantage for businesses. However, the applicability of these standards may vary depending on the geographical and climatic conditions of farms. For example, long working hours in regions with mountainous and fragmented terrain may make it difficult to set standards. For this reason, it is necessary to define standard working units in the agricultural sector and to evaluate the specific conditions of each region and each product when planning production at both micro and macro levels.

As in all sectors, the aim is to create sustainable production processes and optimize the use of resources in the agricultural sector, and existing policies are being renewed with these objectives in mind. Determining the standard labor force in the agricultural sector makes it possible to measure and improve labor productivity over a given period. This will help to reduce energy consumption and therefore the carbon footprint, while increasing the accuracy of reporting by providing reference values for the calculation of labor-related emissions. In addition to environmental contributions, a mechanism can be established to ensure social sustainability. Standardized labor is critical to ensuring decent working conditions. Standardization of labor in the agricultural sector helps to ensure the protection of workers' social rights, fair remuneration and healthy working conditions.

It is necessary to collect standardized, gender-disaggregated and more detailed data on time use and to formulate specific policies for agricultural employment. To this end, special funding should be allocated to project/program designs and activities that can provide

15

information on this issue. A map of working hours should be prepared, considering the technologies used in all agricultural activity areas. Develop and test specific indicators, methodologies, and tools (e.g., surveys and censuses) to measure agricultural workload. In this way, it will be possible to identify alternative working areas and income-generating activities for both on-farm and off-farm labor. It is important to identify and manage working hours to increase income-generating activities, especially for seasonal labor.

Acknowledgement

REFERENCES

[1] Uyan B. Ekonomik Büyüme Kuramlarının Bölgesel Ekonomik Gelişme Açısından Incelenmesi ve Türkiye'de Bölgesel Ekonomik Gelişme. İktisadi Yenilik Dergisi. 2009;6(2):129-142.

[2] Blanco C, Raurich X. Agricultural Composition and Labor Productivity. Journal of Development Economics. 2022;158.

[3] Stone KVW. From Widgets to Digits Employment Regulation for Changing Workplace, Cambridge; 2004.

[4] Arısoy B, Parlak Z. Standart Dışı Çalışma ve Diğer Çalışma Şekilleri. Sosyal, Beşerî ve İdari Bilimler Dergisi. 2022;5(5):657-669.

[5] Ulucan A. İSO 500 Şirketlerinin Etkinliklerinin Ölçülmesinde Veri Zarflama Analizi Yaklaşımı, Farklı Girdi Çıktı Bileşenleri ve Ölçeğe Göre Getiri Yaklaşımları Ile Değerlendirmeler. Ankara Üniversitesi Siyasal Bilgiler Fakültesi Dergisi. 2002;5(72):185-202.

[6] Sezen B, Doğan E. Askeri Bir Tersaneye Bağlı Atölyelerin Karşılaştırmalı Verimlilik Değerlendirmesi: Bir Veri Zarflama Yöntemi Uygulaması. Havacılık ve Uzay Teknolojileri Dergisi. 2005;2(2):77-87.

[7] International Labour Organization (ILO). World of Work Report 2008, Income Inequalities in The Age of Financial Globalization, Geneva.

[8] Çaşkurlu S. Küreselleşen Işgücünün Krizi ve Küresel Eşitsizlik. Ekonomik Yaklaşım. 2010;21(77):49-100.

[9] Schmid G. The Transitional Labour Market and Employment Services. Seoul Job Centre, Seoul, Korea, August 26-27, 2010.

[10] Rani U. Impact of Changing Work Patterns on Income Inequality. ILO Discussion Paper; 2008. DP/193/2008.

[11] Serrano MR. Regulating Non-Standart Employment in Asia and East Asia: a comparative survey of labour laws and union strategies (2015). [cited 2018 October 13]. Available from: http://www.rdw2015.org/uploads/submission/full_paper/42/Regulating_nonstandard_employment_in_ ASEAN___East_Asia_Final_RDW_2015_MRSerrano.pdf

[12] Yükçü S. Yönetim Açısından Maliyet Muhasebesi. İzmir; 1999.

[13] Büyükarıkan U. Türkiye Muhasebe Standardı 41 Tarımsal Faaliyetler Standardına Göre Tarım Muhasebesi: Elma Üretimi Yapan Bir Tarım İşletmesi Uygulaması. Konya: Selçuk Üniversitesi; 2018.

[14] Kıral T, Kasnakoğlu H. Tarımsal Ürünler İçin Maliyet Hesaplama Metodolojisi Ve Veri Tabanı Rehberi. Ankara: Tarımsal Ekonomi Araştırma Enstitüsü. [cited 2023 April 19]. Available from: https://arastirma.tarimorman.gov.tr/tepge/Belgeler/Yay%C4%B1n%20Ar %C5%9Fivi/1997-2005%20Yay%C4%B1n%20Ar%C5%9Fivi/Yay%C4%B1nNo37.pdf

[15] Minkoff-Zern L. The Case for Taking Account of Labor in Sustainable Food Systems in The United States. Renewable Agriculture and Food Systems. 2017;32(6):576-578.

[16] Shreck A, Christy G, Gail F. Social Sustainability, Farm Labor, And Organic Agriculture: Findings from An Exploratory Analysis. Agriculture and Human Values. 2006;23(4):439-449.

[17] Guptill A. SARE Brief: Understanding and Measuring Social Sustainability SARE: Sustainable Agriculture Research & Education (2021). [cited 2023 October 13]. Available from: https://www.sare.org/resources/understanding-and-measuring-social-sustainability/

[18] Ranawera K, Schewe R. Labor and Sustainability: The Role of Farm Labor Practices in Shaping Antibiotic Use. Rural Sociology. 2023;88(3):625-656.

[19] Soylu S. Konya Ilinin Bitkisel Üretimdeki Yeri ve Önemi. I. Konya Kent Sempozyumu; 2011; 385-395.

[20] Anonym. Konya Tarım Master Planı. T.C. Tarım ve Köyişleri Bakanlığı ve Konya Tarım İl Müdürlüğü, Konya; 2004.

[21] Çelik Y, Bayramoğlu Z, Gündüz O, Karakayacı Z. Konya İlinde Farklı İşletme Tipleri ve Agro-Ekolojik Bölgelere Göre Çiftçilerin Sosyal Güvenlik Durumu. Türk Tarım ve Doğa Bilimleri Dergisi. 2015;2(1):60-68.

[22] Yamane T. Statistics: An Introductory Analysis. 2nd Edition. Harper and Row; 1967.

[23] İnan İH. Tarım Ekonomisi ve İşletmeciliği. 9. Baskı. İdeal Kültür Yayıncılık; 2016.

16

Türk Doğa ve Fen Dergisi
Turkish Journal of Nature and Science
www.dergipark.gov.tr/tdfd

In Vitro Effects Of Some Chemotherapeutic Drugs On Rat Erythrocytes Glutathione S-Transferase (GST) Enzyme

Barzan Mirza AHMED [1*] iD, Yusuf TEMEL [2] iD, Mehmet ÇİFTCİ [3] iD

[1*] Sulaimani Polytechnic University, Halabja Technical Institute, Department of Medical Laboratory Technique, Sulaymaniyah, IRAQ
[2] Bingöl University, Solhan Healty Services Vocational School/Medical Services and Techniques, Bingöl, Türkiye
[3] Bingol University, Faculty of Veterinary, Basic Sciences, Bingöl, Türkiye
Barzan Mirza AHMED ORCID No: 0000-0002-0088-6900
Yusuf TEMEL ORCID No: 0000-0001-8148-3718
Mehmet ÇİFTCİ ORCID No: 0000-0003-1098-4413

Corresponding author: barzan.mirza@spu.edu.iq

Abstract: Cancer is the leading cause of death worldwide after heart disease. Currently, breast, lung, bowel, and prostate cancer are the most common cancers in the worldwide. By stopping cancer cells from dividing, spreading, growing, making more cells, and then destroying them, chemotherapy drugs are used to treat diseases caused by cancer. The glutathione S-transferase enzyme is responsible for the detoxification of xenobiotic molecules produced by the body during cancer treatment. In this study, glutathione S-transferase enzyme (GST) was purified from the erythrocytes of rats by affinity column chromatography in one step. The SDS-PAGE (gel electrophoresis) was used to verify the GST enzyme's purity, A single protein band was obtained. The GST enzyme was purified with 22.5 EU/mg specific activity, 237.14 purification-fold, and 48.98% purification yield. Then, the *in vitro* effects of chemotherapy drugs 5-fluorouracil (5-FU) and cyclophosphamide (CP) on purified GST enzyme activity were investigated. The research results showed that both 5-fluorouracil and cyclophosphamide increased GST activity in the concentration ranges of (0.385 to 15.4 mM) and (19.15 to 191.5 mM), respectively.

17

Bazı Kemoterapötik İlaçların Sıçan Eritrositleri Glutatyon S-transferaz (GST) Enzimi Üzerine İn Vitro Etkileri

Öz: Kanser dünya çapındaki ölümlerin kalp hastalıklarından sonra önde gelen nedenidir. Günümüzde meme, akciğer, bağırsak ve prostat kanseri dünya çapında en sık görülen kanserlerdir. Kemoterapi ilaçları, kanser hastalığının tedavisinde kullanılan ve kanser hücrelerinin bölünmesini, yayılmasını, büyümesini ve daha fazla hücre oluşturmasını durduran ilaçlardır. Glutatyon S-transferaz enzimi, kanser tedavisi sırasında vücudun ürettiği ksenobiyotik moleküllerin detoksifikasyonundan sorumludur. Bu çalışmada sıçan eritrositlerinden glutatyon S-transferaz enzimi (GST, EC: 2.5.1.18) afinite kolon kromatografisi ile tek adımda saflaştırıldı. GST enziminin saflığını control etmek için SDS-PAGE (jel elektroforezi) kullanıldı. Jelde tek bant elde edildi. Saflaştırma işlemi sonucunda GST enzimi 22,5 EU/mg spesifik aktiviteyle ve %48,98 verimle 237,14 kat ile saflıkta elde edildi. Daha sonra 5-florourasil (5-FU) ve siklofosfamid (CP) kemoterapi ilaçlarının saflaştırılan GST enzim aktivitesi üzerindeki *in vitro* etkileri araştırıldı. Araştırma sonuçları, hem 5-florourasil hem de siklofosfamidin sırasıyla (0,385 ila 15,4 mM) ve (19,15 ila 191,5 mM) konsantrasyon aralığında GST aktivitesini arttırdığı belirlendi.

1. INTRODUCTION

Cancer is a large category of illnesses that includes the unnatural growth and division of cells, Cancer is one of the most prevalent diseases, and it causes a lot of deadliness. Advances in cancer prevention and treatment have resulted in longer lifespans or even healing for some patients who have cancer diseases. However, chemotherapy drugs are still required for most patients, and they often cause severe side effects [1]. There are many different chemotherapy drugs used to treat various kinds of cancer diseases, 5-fluorouracil (5-FU) is an anticancer drug used to treat several types of cancer such as breast, lung, skin, and head [2]. 5-FU can enter cells through the uracil transport system, inhibiting thymidylate synthase enzymes and RNA synthesis function, and acts on the S-phase of the cell cycle to cause DNA damage [3]. Cyclophosphamide (CYP) is a chemotherapy drug widely used to treatment of various neoplastic diseases and chronic autoimmune diseases. Cyclophosphamide chemotherapy can damage normal cells in the body, such as the heart, bladder, and testicle. This can lead to multiple organ toxicity [4,5].

Glutathione molecule is a natural antioxidant that plays a major role in neutralizing xenobiotic compounds, this impact is attributable to the capacity of the sulfhydryl (-SH) group on cystine amino acid by donating more electrons and preventing tissue cells from being damaged as associated with the defense of cellular against toxicity. There are two main sources formation of xenobiotic molecules. First, endogenous factors of normal cellular metabolism such as endoplasmic reticulum oxidation, electron transport chain, and most enzymatic activity. Second, exogenous factors such as chemotherapy, radiation, cigarette, and oxygen themselves. The body detoxification process works to out most of the xenobiotic molecules produced by both above sources through the use of group enzymes [6-9]. Glutathione S-transferases (GSTs) are a multigene family of enzymes with about 223 amino acids in total. They are categorized, as alpha, zeta, theta, kappa, mu, pi, sigma, and omega GST isoforms based on their amino acid sequence and specificity of substrates [10]. Glutathione S-transferase can be detected in both eukaryotic and prokaryotes, and work to detoxify xenobiotic compounds from exogenous and endogenous living cells by catalyzing glutathione natural anti-oxidant molecule reactions with xenobiotics, changing toxic molecules to non-toxic metabolizable molecules and excretion from the body. Glutathione S-transferase is an important enzyme that helps to detoxify harmful compounds by catalyzing the conversion of glutathione-toxic compounds into non-harmful substances [8,11–13].

The purpose of this study is to purify glutathione S-transferase (GST) enzyme from rat erythrocytes and investigate the effects of 5-fluorouracil and cyclophosphamide chemotherapy drugs on enzyme activity from in vitro, possibly the results of this study could help improve the treatment of cancer disease and have benefits in toxicology systems, the clinical cancer research community must collaborate and focus on new research that uses comprehensive results to determine the best way to treat cancer diseases.

2. MATERIAL AND METHOD

2.1 Materials

Reduced glutathione (GSH), 5-FU (5-Fluorouracil), ethylene diamine tetra acetic acid (EDTA), β-mercaptoethanol, 1-chloro-2,4-dinitrobenzene (CDNB), TEMED (N, N, N, N-tetramethyl-ethylenediamine), acrylamide, Tris (Trihydroxy methyl amino methane), and glutathione-agarose affinity gel got from Sigma-Aldrich (Sigma-Aldrich and MERCK, Darmstadt, Germany). Ammonium persulfate (Chem Solute Bio). CYP (Endoxan) was purchased from a pharmacy (Istanbul, Turkiye). Glycerol, isopropanol, Ammonium sulfate, stacking gel, separation gel, separation buffer, Coomassie Brilliant Blue R-250, paint solution, and fixing solution (Fishcer Scientific).

2.2 Methods

2.2.1 Preparation of homogenate

The blood sample of the rat was obtained from the Bingöl University Experimental Research Center and brought the sample to the biochemistry laboratory in anticoagulant tubes, it was centrifuged at (4 oC, 2,500 Xg, for 15 min), discarded plasma and saved rat erythrocytes were in the refrigerator at -20 °C according to the cold chain rule. The rat erythrocyte sample was washed with KCl solution (0.16 M) and centrifuged at (4 °C in 2,500 Xg for 15 min) three times repeating this step, and the erythrocyte cells were hemolyzed with ice water in the ratio of (1: 5 = erythrocyte: ice water), then centrifuged at (4oC in 10,000 Xg for 60 min), finally, 3.5 mL supernatant was saved for purification of GST and the precipitate was discarded [14–16]. The study was designed and conducted according to ethical norms approved by the Animal Experimentation Ethics Committee of the Bingol University (Bingol, Turkiye) (Protocol No. 2019-85680299/020).

2.2.2 GST enzyme activity determination

The activity of glutathione S-transferase enzyme was measured by monitoring the absorbance of 2,4-dinitrophenyl glutathione product of a reaction between 1,2-dichloro-4-nitrobenzene (CDNB) and reduced glutathione (GSH) at 340 nm in a spectrophotometer (Shimadzu UV-1601, Australia) [17–19].

2.2.3 Applied glutathione-agarose affinity chromatography for Purification of GST enzyme

The affinity column chromatography of glutathione-agarose was prepared and the flow rate of the column was adjusted by using a peristaltic pump to 20 mL/h. Next using (10 mM KH_2PO_4 and 150 mM NaCl) equilibration solution to adjust the pH = 7.4 of the column. Then the hemolytic erythrocyte sample was placed on the column and washed column with (10 mM KH_2PO_4 and 0.1M KCl,

18

pH = 8.0) buffer solution. Then, continued washing process until the absorbance of the column eluate at 280 nm was 0.05. Finally, using gradient elution purifies the GST enzyme. The gradient elution solution consists of (1.25-10 mM GSH and 50 mM Tris-HCl, pH = 9.5) and using Eppendorf tubes (1.5 mL) to collect eluates and, absorbance was measured spectrophotometrically at 340 nm [13, 18, 20].

2.2.4 Protein assay

The qualitative protein was tested by measuring the absorbance of tyrosine and tryptophan amino acids in the protein structure at 280 nm. standard bovine serum albumin was used to determine quantitative protein by measuring absorbance spectrophotometrically at 595 nm based on the Bradford method [21, 22].

2.2.5 Applied SDS-PAGE to control enzyme purity

The pure glutathione S-transferase enzyme was examined by gel electrophoresis (SDS-PAGE) method, and the purified GST enzyme was seen as a single band of protein on the SDS-PAGE, according to the Laemmle procedure [23].

2.2.6 *In vitro* investigation of chemotherapeutic drugs

The *in vitro* effect of chemotherapy drugs on the Glutathione S-transferase enzyme activity in rat erythrocytes was determined by adding different concentrations of 5-fluorouracil (0.385 to 15.4 mM) respectively and different concentrations of Cyclophosphamide (19.15 to 191.5 mM) respectively into the reaction medium in the cuvette and measured absorbance spectrophotometrically at 340 nm. The absorbance of absence drugs used as control (%100 activity). Graphs of % activity against drug concentrations were drawn using MS Excel program.

3. RESULTS

Glutathione S-transferase (GSTs) enzyme of phase II detoxification process that works to protect cellular organs from attack xenobiotic reactive molecule, It acts as a catalyst for the conjugation of the glutathione (GSH)

molecule to numerous electrophilic molecules, both endogenous and exogenous, the conjugation reaction of glutathione involve in the first step of the mercapturic acid pathway causes the elimination of the toxic compound [24].

The G6PD enzyme functions in the pentose phosphate pathway and produces NADPH [25,26]. NADPH ensures that GSH in the cell remains in its reduced form [27]. Glutathione is linked to defense against some cancer etiology as it is the principal intracellular antioxidant, detoxifies several carcinogens through phase II conjugation, and maintains immunological function by controlling the mitogenic response and lymphocyte proliferation [28]. Among the enzymes that shield organ cellular structures from damage caused by carcinogens and toxic chemicals, glutathione S-transferase is the most significant enzyme, It is important for detoxifying endogenous and exogenous toxic substances. GST enzyme catalyzes the reaction between glutathione and electrophile toxic molecules to form glutathione S-conjugates, which are crucial for the deactivation and subsequent excretion of xenobiotic molecules [29].

The purification process of the Glutathione S-transferase enzyme from rat erythrocytes was carried out by applying the GSH-agarose affinity column chromatography method. It is a one-step process that is powerful, simple to perform, inexpensive, and takes less time. Portable and very effective for large quantities of enzymes that have been purified. The same method was applied to purify GST enzyme from human hepatoma [29], catfish intestinal mucosa [30], rainbow trout liver [31], and the freshwater fish Monopterus albus's liver [32], erythrocytes of children with Down syndrome (DS) and healthy children [33], from rat liver [34], Van Lake fish muscle tissue [23], and the human erythrocyte [12]. GST Enzyme activity measured during the purification process is a significant key and helps to continue the study.

In this study, purification of rat erythrocyte glutathione S-transferase (GST) enzyme was carried out with 22.5 EU/mg specific activity, 237.14 purification-fold, and 48.98% purification yield, by a one-step of GSH-agarose affinity column chromatography (Table 1).

Table 1. Purification table of GST enzyme in the rat erythrocyte

Purification Steps	Total Volum (mL)	Activity (EU/mL)	Protein (mg/mL)	Total Activity (EU)	Total Protein (mg)	Specific Activity (EU/mg)	Yield %	Purification Fold
Hemolaysate	3.5	0.315	3.32	1.105	11.62	0.095	100	1
Glutathione agarose affinity chromatography	2	0.27	0.012	0.541	0.024	22.569	48.98	237.142

The results were compared with GST purification from the human placenta tissues with 23.7 EU/mg specific activity, 11% yield, and 1107 folds [35], from the turkey liver 164.31 U/mg specific activity, 45% yield and 252.7-folds [36] and human erythrocytes 16.2 EU/mg specific activity, 35% yield and 265.97-folds [12]. The result of this study is near to the result of the human erythrocytes study it is a significant point.

The SDS-PAGE method was used to verify the GST enzyme's purity. A single protein band of the purified GST enzyme appeared on the SDS-PAGE, which revealed the enzyme was successfully purified and allowed the study to continue (Figure 1).
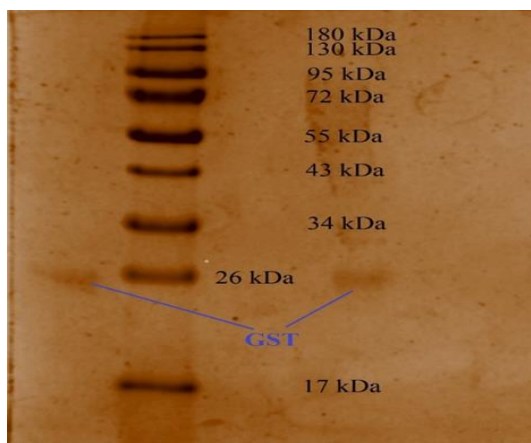
Figure 1. SDS-PAGE of rat erythrocytes GST enzyme.

The same way is used in the human erythrocytes [12], human hepatoma [29], rat liver [34] and brain cytosol of rats [37]. The study's findings demonstrate that GST enzymes in rat erythrocytes have been successfully separated from other enzymes, which is a positive result that should encourage researchers to continue with additional research steps.

In vitro, study to investigate the chemotherapy drug effects on the purified GST enzyme activity from the rat erythrocyte was performed, and the results show both 5-Fluroruracil and Cyclophosphamide chemotherapy drugs increased the GST enzyme activity from the concentration range 0.385 to 15.4 mM (Figure 2) and 19.15 to 191.5 mM (Figure 3) respectively.
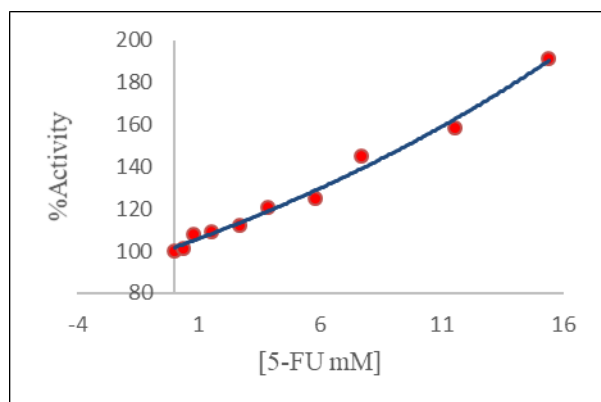
Figure 2. In vitro effect of 5-Fluorouracil on GST enzyme activity
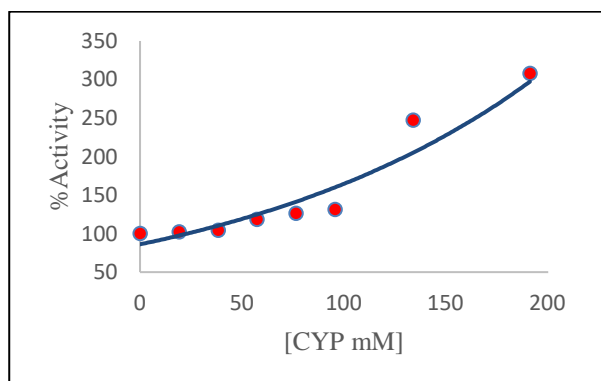
Figure 3. *In vitro* effect of cyclophosphamide on GST enzyme activity

4. DISCUSSION AND CONCLUSION

The results indicated that both drugs have a positive effect by increasing GST enzyme activity when the concentration of the drugs is increased. This is crucial to the field of pharmacology because it helps scientists to understand how drugs affect the biological system in living cells and how the body's living cells react particularly chemotherapy drugs, which have a long list of side effects when used to treat cancer. These side effects make patients more likely to experience complications and eventually destroy their bodies. Researchers must work with utmost sincerity, patience, and honesty to get information about drugs and treatment ways to improve pharmacologist science. Comparing this study's findings to those of other studies, it was found both 5-FU and tamoxifen chemotherapy drugs increase the GST enzyme activity that is purified from erythrocytes of humans [12]. 5-FU and tamoxifen chemotherapy drugs increase the activities of 6PGD and G6PD enzymes [38]; the GST enzyme from human erythrocytes was found to be inhibited by the effects of paclitaxel, cyclophosphamide, and gemcitabine [39].

Glutathione S-transferase enzyme purification was carried out in the rat erythrocytes in one step by using GSH-agarose affinity column chromatography. The purified enzyme was examined using SDS-PAGE. In the second phase, the effects of 5-fluorouracil and cyclophosphamide chemotherapeutic drugs on enzyme activity were investigated. The findings indicate that both drugs increase GST enzyme activity. This study results may be a guide for purification studies on the GST enzyme and chemotherapy approaches whose target is the GST enzyme.

Acknowledgement

REFERENCES

[1] Rasul MF, Hussen BM, Salihi A, Ismael BS, Jalal PJ, Zanichelli A, Jamali E, Baniahmad A, Ghafouri-Fard S, Basiri A, Taheri M. Strategies to overcome the main challenges of the use of CRISPR/Cas9 as a replacement for cancer therapy. Mol Cancer. 2022; 21(1) 64: 2-30.

[2] Focaccetti C, Bruno A, Magnani E, Bartolini D, Principi E, Dallaglio K, Bucci EO, Finzi G, Sessa F., Noonan DM, Albini A. Effects of 5-fluorouracil on morphology, cell cycle, proliferation, apoptosis, autophagy and ROS production in endothelial cells and cardiomyocytes. PloS one. 2015; 10(2): 0115686.

[3] Jahani M, Azadbakht M, Norooznezhad F, Mansouri K. L-arginine alters the effect of 5-fluorouracil on breast cancer cells in favor of apoptosis. Biomed Pharmacother. 2017; 88: 114-123.

[4]	Ince S, Kucukkurt I, Demirel HH, Acaroz DA, Akbel E, Cigerci IH, Protective effects of boron on cyclophosphamide induced lipid peroxidation and genotoxicity in rats. Chemosphere. 2014; 108:197-204.

[5]	Temel Y, Çağlayan C, Ahmed BM, Kandemir FM, Çiftci M., The effects of chrysin and naringin on cyclophosphamide-induced erythrocyte damage in rats: biochemical evaluation of some enzyme activities in vivo and in vitro. Naunyn Schmiedebergs Arch. 2021; 394: 645-654.

[6]	Orhan H, Şahin G, Glutatyon S-Transferazların klinik ve toksikolojik önemi. Türkiye Klinikleri Tıp Bilimleri. 1995; 15: 303-15.

[7]	Ballatori N, Krance SM, Notenboom S, Shi S, Tieu K, Hammond CL. Glutathione dysregulation and the etiology and progression of human diseases. Biol. Chem. 2009; 390: 191-214.

[8]	Kaur G, Gupta SK, Singh P, Ali V, Kumar V, Verma M. Drug-metabolizing enzymes: role in drug resistance in cancer. Clin Transl Oncol. 2020; 22: 1667-1680.

[9]	Lu J, Holmgren A, The thioredoxin antioxidant system. Free Radic Biol Med. 2014; 66: 75-87.

[10]	Singh RR, Reindl KM. Glutathione S-transferases in cancer. Antioxid. 2021; 10(5): 701-710.

[11]	Temel Y, Taysi MŞ, The effect of mercury chloride and boric acid on rat erythrocyte enzymes. Biol. Trace Elem. Res. 2019; 191(1): 177-182.

[12]	Aybek H, Temel Y, Ahmed BM, Ağca CA, Çiftci M. Deciphering of the effect of chemotherapeutic agents on human glutathione S-transferase enzyme and MCF-7 cell line. Protein Peptide Lett. 2020; 27(9): 888-894.

[13]	Taysi MŞ, Temel Y. Glutathione S-transferase: Purification and characterization from quail (Coturnix coturnix japonica) liver and the impact of some metal ions on enzyme activity. Bionanosci. 2021; 11: 91-98.

[14]	Ayna A, Khosnaw L, Temel Y, Ciftci M. Antibiotics as inhibitor of glutathione S-transferase: biological evaluation and molecular structure studies. Curr. Drug Metab. 2021; 22(4): 308-314.

[15]	Temel Y, Kocyigit UM. Purification of glucose-6-phosphate dehydrogenase from rat (Rattus norvegicus) erythrocytes and inhibition effects of some metal ions on enzyme activity. J Biochem Mol Toxicol. 2017; 31(9): e21927.

[16]	Habig WH, Pabst MJ, Jakoby WB. Glutathione S-transferases: the first enzymatic step in mercapturic acid formation. J. Biol. Chem. 1974; 249(22): 7130-7139.

[17]	Türkan F, Huyut Z, Taslimi P, Gülçin, İ. Investigation of the effects of cephalosporin antibiotics on glutathione S-transferase activity in different tissues of rats in vivo conditions in order to drug development research. Drug Chem. Toxicol. 2020; 43(4): 423-428.

[18]	Temel Y, Koçyigit UM, Taysı MŞ, Gökalp F, Gürdere MB, Budak Y, Ceylan M, Gülçin İ, Çiftci, M. Purification of glutathione S-transferase enzyme from quail liver tissue and inhibition effects of (3aR, 4S, 7R, 7aS)-2-(4-((E)-3-(aryl) acryloyl) phenyl)-3a, 4, 7, 7a-tetrahydro-1H-4, 7-methanoisoindole-1, 3 (2H)-dione derivatives on the enzyme activity. Biochem Mol Toxicol. 2018; 32(3); e22034.

[19]	Aksoy M, Ozaslan MS, Kufrevioglu OI, Purification of glutathione S-transferase from Van Lake fish (Chalcalburnus tarichii Pallas) muscle and investigation of some metal ions effect on enzyme activity. J. Enzyme Inhib. Med. Chem. 2016; 31(4): 546-550.

[20]	Kruger NJ. The Bradford method for protein quantitation. The protein protocols handbook. Springer; 2009. P. 17-24.

[21]	Bradford MM. A rapid and sensitive method for the quantition of microgram quantities of protein utilizing the principle of protein-dye binding. Anal Biochem. 1976; 72 (1–2): 248–251.

[22]	Laemmli UK. Cleavage of structural proteins during the assembly of the head of bacteriophage T4. Nature. 1970; 227(5259): 680-685.

[23]	Townsend DM, Tew KD. The role of glutathione-S-transferase in anti-cancer drug resistance. Oncogene. 2003; 22(47);7369-7375.

[24]	Batt AM, Magdalou J, Vincent-Viry M, Ouzzine M, Fournel-Gigleux S, Galteau MM, Siest G. Drug metabolizing enzymes related to laboratory medicine: Cytochromes P-450 and UDP-glcuronosyltransferases. Clin Chim Acta. 1994;226(2): 171-190.

[25]	Temel Y, Ayna A, Hamdi Shafeeq I, Ciftci M. In vitro effects of some antibiotics on glucose-6-phosphate dehydrogenase from rat (Rattus norvegicus) erythrocyte. Drug Chem. Toxicol. 2020; 43(2): 219-223.

[26]	Bayindir S, Ayna A, Temel Y, Ciftci M. The synthesis of new oxindoles as analogs of natural product 3, 3′-bis (indolyl) oxindole and in vitro evaluation of the enzyme activity of G6PD and 6PGD. Turk. J. Chem. 2018; 42(2): 332-345.

[27]	Bayindir S, Temel Y, Ayna A, Ciftci M. The synthesis of N-benzoylindoles as inhibitors of rat erythrocyte glucose-6-phosphate dehydrogenase and 6-phosphogluconate dehydrogenase. J Biochem Mol Toxicol. 2018; 32(9): e22193.

[28]	Pljesa-Ercegovac, M., Savic-Radojevic, A., Matic, M., Coric, V., Djukic, T., Radic, T. and Simic, T. Glutathione transferases: potential targets to overcome chemoresistance in solid tumors. International J Molecular Sci. 2018; 19(12): 3785.

[29]	Dierickx PJ. Purification and characterization of glutathione S-transferase from the human hepatoma derived PLC/PRF/5 cell line. Biomed res. 1989; 10(4); 301-306.

[30]	Gadagbui, B.K. and James, M.O. Activities of affinity-isolated glutathione S-transferase (GST) from channel catfish whole intestine. Aquat Toxicol. 2000; 49(1-2): 27-37.

21

[31] Riol MM, Valinas MN, Fernandez MG, Lopez MP. Glutathione S-transferases from rainbow trout liver and freshly isolated hepatocytes: purification and characterization. Comp Biochem Physiol C Toxicol Pharmacol. 2001; 128(2): 227-235.

[32] Huang Q, Liang L, Wei T, Zhang D, Zeng QY. Purification and partial characterization of glutathione transferase from the teleost Monopterus albus. Comp Biochem Physiol C Toxicol Pharmacol. 2008; 147(1): 96-100.

[33] Hamed RR, Maharem TM, Abdel-Meguid N, Sabry GM, Abdalla AM, Guneidy RA. Purification and biochemical characterization of glutathione S-transferase from Down syndrome and normal children erythrocytes: A comparative study. Res. Dev. Disabil. 2011; 32(5): 1470-1482.

[34] Lebda M, Taha N, Noeman S, Korshom M, El-Wahab Mandour A. Purification and Characterization of Glutathione-S-Transferase from Rat′s Liver: Effect of Carbon Tetrachloride and Camel′s Milk. J Chromat. Separation Techniq. 2012; 3(4): 2-8.

[35] Howie AF, Hayes JD, Beckett GJ. Purification of acidic glutathione S-transferases from human lung, placenta and erythrocyte and the development of a specific radioimmunoassay for their measurement. Clinica chimica acta. 1988; 177(1): 65-75.

[36] Akkemik E, Taser P, Bayindir A, Budak H, Ciftci M. Purification and characterization of glutathione S-transferase from turkey liver and inhibition effects of some metal ions on enzyme activity. Environ Toxicol Pharmacol. 2012; 34(3): 888-894.

[37] Senjo M, Ishibashi T. Purification and characterization of glutathione S-transferase from rat brain cytosol: identification of four isozymes and evidence for absence of the Ya subunit. Biomed Res. 1986; 7(1): 19-26.

[38] Temel Y. The in vitro effect of 5-FU and Tamoxifen Chemotherapeutics on penthose phosphate pathway enzymes. Cumhuriyet Sci J. 2021; 42(2): 245-251.

[39] Erat M, Şakiroğlu H. The effect of some antineoplastic agents on glutathione S-transferase from human erythrocytes. J Enzyme Inhib Med Chem. 2013; 28(4): 711-716.

22

BİNGÖL UNIVERSITY

Phytochemical Analysis and Determination of Antioxidative, Antimicrobial And *In Vitro* Cytotoxic Properties of Black Rosehip (*Rosa Pimpinellifolia* L.) Fruits Growing in The Northeast of Türkiye

Büşra KICIK[1] , **Hamit Emre KIZIL[2*]** , **Sinan BAYRAM[2]**

[1] Bayburt University, Engineering Faculty, Food Engineering Department, Bayburt, Türkiye
[2] Bayburt University, Vocational School of Health Services, Department of Medical Services and Techniques, Bayburt, Türkiye
Büşra KICIK ORCID No: 0000-0002-2053-2229
Hamit Emre KIZIL ORCID No: 0000-0001-6193-3734
Sinan BAYRAM ORCID No: 0000-0002-2156-1566

Corresponding author: ekizil@bayburt.edu.tr

Abstract: The aim of this study was to determine the phenolic content of *Rosa pimpinellifolia* (L.) fruit extract and antibacterial, antioxidant activity and show the cytotoxic effects of different concentrations of *Rosa pimpinellifolia* L. fruit extract obtained by ultrasonic assisted method on MCF-7 cell line by WST-8 assay. Antibacterial effects analyzed by disk diffusion method and determined that there was no antibacterial effect in 500 µg/mL *Rosa pimpinellifolia* L. fruit extract dose. In addition, the total phenolic content was determined by the Folin-Ciocalteu method and found that total phenolic content is 37.5±0.2 mg GA/g. Antioxidant activity value was determined as 32.06±1.1 mg TE/g by ABTS method and 23.47±1.6 mg TE/g by DPPH method. The highest cytotoxic effect of *Rosa pimpinellifolia* L. fruit extract was determined in dose of 40 µg/mL on MCF-7 cell.

23

Türkiye'nin Kuzeydoğusunda Yetişen Siyah Kuşburnu (*Rosa Pimpinellifolia* L.) Meyvelerinin Fitokimyasal Analizi ve Antioksidatif, Antimikrobiyal ve *In Vitro* Sitotoksik Özelliklerinin Belirlenmesi

Öz: Bu çalışmanın amacı, *Rosa pimpinellifolia* (L.) meyve ekstraktının fenolik içeriğini ve antibakteriyel, antioksidan aktivitesini belirlemek ve ultrasonik destekli yöntemle elde edilen farklı konsantrasyonlarda *Rosa pimpinellifolia* (L.) meyve ekstraktının MCF-7 hücre dizisi üzerindeki sitotoksik etkilerini WST-8 analizi ile göstermektir Antibakteriyel etkiler disk difüzyon yöntemiyle analiz edilmiş ve 500 µg/mL *Rosa pimpinellifolia* (L.) meyve ekstraktı dozunda antibakteriyel etkinin olmadığı belirlenmiştir. Ayrıca toplam fenolik içerik Folin-Ciocalteu yöntemiyle belirlenmiş ve toplam fenolik içeriğin 37.5±0,2 mg GA/g olduğu bulunmuştur. Antioksidan aktivite değeri ABTS yöntemiyle 32.06±1,1 mg TE/g, DPPH yöntemiyle ise 23.47±1.6 mg TE/g olarak belirlenmiştir. *Rosa pimpinellifolia* (L.) meyve ekstraktının MCF-7 hücresi üzerindeki en yüksek sitotoksik etkisi 40 µg/mL olarak belirlenmiştir.

1. INTRODUCTION

Cancer, characterized by the uncontrolled growth and spread of cells in the body, poses a significant global public health concern, with its prevalence on the rise [1-3]. According to data from the World Health Organization (WHO) on cancer statistics, breast cancer accounts for 12%, lung cancer 12%, colorectal cancer 11%, prostate cancer 8%, stomach cancer 6%, liver cancer 3%, with the remaining 48% encompassing other types of cancer. Among these, breast cancer is the most frequently diagnosed cancer in women, with projections indicating a doubling of the 8.1 million deaths recorded in 2012 by the year 2040. Particularly alarming is the diagnosis of breast

cancer in young women aged 20-59, who face an increased risk of mortality within this demographic [4, 5]. Various risk factors contribute to the etiology of breast cancer, including certain medical conditions, sedentary lifestyles, obesity, exposure to environmental toxins and trauma to breast tissue, and prolonged use of exogenous hormones [6]. Breast cancer presents a complex phenotype, encompassing both carcinoma in situ and invasive carcinoma, with diverse histological subtypes [7].

One promising avenue in cancer treatment lies in the use of medicinal aromatic plants. In this regard, rosehip fruit emerges as a potential alternative remedy. Belonging to the genus *Rosa* within the Rosaceae family, rosehip is characterized by its erect or shrubby stature, ranging in height from 1.5 to 3.5 meters, depending on the variety. The fruit typically exhibits an elliptical shape and is found in hues of yellow, red, and orange [8]. Rosehip boasts a spectrum of health-promoting properties, including anti-inflammatory, antioxidant, immunomodulatory, cardioprotective, anticancer, antidiabetic, neuroprotective, and antibacterial effects. Rosehip is renowned for its rich phytochemical composition, comprising phenolics, flavonoids, folic acid [9], vitamins such as α-tocopherol (Vitamin E) and γ-tocopherol [10], terpenes, carotenoids, galactolipids, minerals, and tannins [11]. Furthermore, it contains essential fatty acids such as oleic, linoleic [12], alongside catechin, chlorogenic acid, caffeic acid, and apigenin 7-O-glucoside [13].

Our study is conducted in the province of Bayburt, an area characterized by its natural landscape, nestled within the inner region of the Upper Coruh Basin, within the widened portion of the valley carved by the Coruh River. There is limited research on the biological activity of *Rosa pimpinellifolia* (L.) extracts naturally occurring in Bayburt province. This research aims to determine the phenolic content, antibacterial and antioxidant activity of *Rosa pimpinellifolia* (L.) fruit extract at varying concentrations, as well as its cytotoxicity on breast cancer cells.

2. MATERIAL AND METHOD

This study was conducted using the data of Büşra KICIK's master's thesis (YÖK ID: 701041).

2.1. The Methanolic Fruit Extract Preperation

Black fruit rosehip (*Rosa pimpinellifolia* L.) was gathered from the same plants and location in Bayburt Province, Central District Gümüşsu Village, at an altitude of 1.817 m. A portion of the collected *R. pimpinellifolia* (L.) plant was dried in a dark environment away from sunlight exposure for extraction processes. The completely dried 1 g fruit sample was pulverized, and added 10 mL of 80% methanol. The mixture was then subjected to an ultrasonic water bath at 40 ºC for 60 minutes. Then, it was centrifuged at 5000 rpm for 30 min, and transferred into a glass tube. The extraction process was conducted twice, and the resulting supernatants were pooled together to

attain a total volume of 25 mL using methanol. The mixture was then passed through a 0.45 μm membrane filter and subsequently transferred to an amber bottle. The extract was stored at -20°C for further analysis, while the remainder was dried using a vacuum evaporator, lyophilized.

2.1.1. Evaluation of total phenolic content

The total phenolic content was determined following the Folin-Ciocalteu method as outlined by Magalhães et al. (2010), with gallic acid employed as the reference standard. In summary, 50 μL of fruit extract was combined with 50 μL of Folin-Ciocalteu reagent (1:5, v/v) and 100 μL of sodium carbonate (Na_2CO_3) solution (0.35 M) in a microplate well. The mixture was allowed to react for 3 minutes, after which the absorbance was measured at 760 nm using a spectrophotometer (Multiskan GO Thermo). All measurements were conducted in triplicate. The outcomes were quantified and expressed as gallic acid equivalent (mg GAE/g).

2.1.2. Determination of *in vitro* antibacterial effect

For the assessment of antibacterial activity, 24-hour-old cultures were employed. Pathogenic strains, preserved as stock cultures at -20°C, were introduced into tryptic soy agar (TSA) medium using the streak plate inoculation technique. After inoculation, single colonies were selected from the strains and incubated at 37°C for 24 hours. These colonies were then transferred to sterile tryptic soy broth medium in 15 mL Falcons and incubated for 18 hours. The resulting strains were adjusted to 0.5 McFarland standard turbidity and used as the inoculum [14]. The in vitro antibacterial activities of *Rosa pimpinellifolia* (L.) extracts were evaluated using the disc diffusion method. The solvent was evaporated from the methanol extract, previously prepared using ultrasonic extraction, using a nitrogen volatilization device. After quantifying the obtained active substance, dimethyl sulfoxide (DMSO) was added to achieve a dose of 500 μg/mL. Subsequently, 10 μL of this extract was taken and impregnated into 6 mm diameter blank antimicrobial susceptibility discs (OXOID). The impregnated discs were then allowed to dry in a sterile cabinet for two hours. Following this drying period, pathogenic microorganisms were inoculated onto TSA media using sterile cotton-tipped swabs. Immediately after inoculation, the discs impregnated with water and methanol extracts, prepared using microwave and ultrasonic extraction methods, were carefully positioned in the petri dishes [15, 16].

2.1.3. Determination of antioxidant activity

For the 2,2-azino-bis 3-ethylbenzthiazoline-6-sulphonic acid (ABTS) test, the ABTS reagent was prepared at a concentration of 7 mM by dissolving it in water. The solution was subsequently mixed with 2.45 mM potassium persulfate, and the resulting mixture was kept in the dark at room temperature for 12-16 hours prior to utilization. To perform the test, 1 mL of methanolic fruit extract and 1 mL of ABTS solution were diluted with methanol (80%) to a total volume of 4 mL. After sealing

24

the tubes, they were left at 25 C for 6 minutes. Following this incubation period, the absorbance was measured at 734 nm. All measurements were conducted in triplicate, and the results were expressed as trolox equivalent (TE mg/g). For the 1,1-diphenyl-2-picrylhydrazyl (DPPH) test, DPPH solution was prepared by dissolving it in 185 μL methanol, to which 15 μL of fruit extract was added and vortexed for 10 seconds. This mixture was then kept at room temperature in the dark for 45 minutes. After the incubation period, the absorbance was measured at 515 nm using a microplate reader (Multiskan Go, Thermo). All measurements were performed in triplicate, and the results were expressed as trolox equivalent (TE mg/g) [17,18].

2.1.4. Cell culture and viability analysis

Black rosehip extract was dissolved in DMSO at 20 mg/mL and concentrations of 400, 300, 200, 100, and 40 μg/mL were prepared by serial dilution. The breast cancer cell line MCF-7 was cultured in RPMI 1640 medium supplemented with 10% fetal bovine serum (FBS) in 25 mL flasks to support cell proliferation. Cell transfer was carried out using trypsin-Ethylenediaminetetraacetic acid (EDTA) solution after rinsing with phosphate buffered saline (PBS) buffer to ensure viable cells at the flask base. Subsequently, flasks were incubated for 24-48 hours in a 5% CO_2 incubator at 37°C. Cell viability was assessed before each passage using trypan blue dye. After centrifugation, the cell suspension was quantified on a Thoma slide stained with trypan blue dye. Tetrazolium salts, which are organic compounds with a heterocyclic structure, undergo reduction by gaining electrons and transform into a formazan structure, resulting in a color change [19] due to active mitochondria breaking the tetrazolium rings [20]. This color change is absent in dead cells, leading to no formation of color. Therefore, the quantity of formazan dye produced is directly proportional to the number of living cells. Water-soluble tetrazolium-8 (WST-8) is reduced by dehydrogenases in cells to yield an orange-colored product soluble in cell culture medium. MCF-7 cells were seeded into 96-well plates and incubated at 37°C for 24 hours to allow for proper adherence to the well surfaces. Following the incubation period, the medium was aspirated from the wells. The cells were then exposed to varying concentrations of black rosehip extract (400, 300, 200, 100, and 40 μg/mL) in triplicate. A DMSO-treated group served as the negative control, while a group treated with medium containing 10% DMSO functioned as the positive control. Upon completion of the optimized incubation periods, cell viability was assessed using the Cell Viability Detection Kit-8 (CVDK-8, EcoTech Biotechnology) following the manufacturer's instructions. In brief, the culture medium from the treated cells was replaced with fresh medium containing 10% CVDK-8 solution, and changes in cell viability were quantified by measuring the optical density at 590 nm. [21].

2.1.5. Statistical analysis

The cytotoxicity investigation was performed with three repetitions, and the data were presented as mean ±

standard deviation. Statistical analysis was conducted utilizing Student's t-test through GraphPad Prism software. A significance level of $p \leq 0.05$ was considered statistically significant.

3. RESULTS

In this study, the methanol extract prepared using *Rosa pimpinellifolia* (L.) fruit sample exhibited a total phenolic content of 37.5 ± 0.2 mg/g GA/g. However, when tested against 10 different pathogenic bacteria at a concentration of 500 μg/mL (Table 1), the extract showed no antibacterial effects, as evidenced by the absence of inhibition zones around the antimicrobial test discs.

Table 1. Antimicrobial effect of *R. pimpinellifolia* (L.) fruit methanolic extract depending on 500 μg/mL dose application

	No	Microorganisms	IZD	GEN	20%DMSO
GRAM (+)	P1	*Bacillus cereus* BC 6830	-	20	-
	P2	*Enterococcus faecalis* NCTC 12697	-	17	-
	P3	*Staphylococcus aureus* NCTC 10788	-	19	-
	P4	*Staphylococcus aureus* BC 7231	-	18	-
	P5	*Staphylococcus aureus* ATCC25923	-	17	-
GRAM (-)	P6	*Escherichia coli* NCTC 9001	-	15	-
	P7	*Escherichia coli* BC 1402	-	14	-
	P8	*Pseudomonas aeruginosa* NCTC 12924	-	13	-
	P9	*Salmonella* Typhimurium RSSK 95091	-	16	-
	P10	*Yersinia enterocolitica* ATCC 27729	-	19	-

IZD : Inhibition zone diameter (mm); GEN: Gentamicin = positive control; 20%DMSO = negative control

Furthermore, the antioxidant capacity of the *Rosa pimpinellifolia* (L.) fruit extract was assessed using the ABTS and DPPH test methods. The results showed an antioxidant capacity of 32.06 ± 1.1 mg TE/g by the ABTS test and 23.47 ± 1.6 mg TR/g by the DPPH test (Table 2).

Table 2. Antioxidant activity (ABTS, DPPH) and total phenolic compounds assays results of *R. pimpinellifolia* (L.) methanolic fruit extract

R. pimpinellifolia L. Methanolic Fruit Extract	ABTS (mg TE/g)	DPPH (mg TE/g)	TPC (mg GA/g)
	32,0±1.1	23,4±1.6	37,5 ±0.2

Regarding cytotoxicity, different doses (400 μg/ml, 300 μg/ml, 200 μg/ml, 100 μg/ml, 40 μg/ml) of the methanol extract of *Rosa pimpinellifolia* (L.) fruit were evaluated for their effects on the breast cancer cell line (MCF-7) over a 72-hour period. All doses of the fruit extracts exhibited antiproliferative properties in MCF-7 cells. Notably, doses of 100 μg/ml and 40 μg/ml demonstrated higher antiproliferative effects compared to doses of 400

µg/ml, 300 µg/ml, and 200 µg/ml. Specifically, the highest cytotoxic effect was observed at a concentration of 40 µg/ml, while the lowest was found at 400 µg/ml. The cytotoxic effect was statistically significant at concentrations of 200 µg/ml, 100 µg/ml, and 40 µg/ml (Fig. 1) ($p < 0.05$).
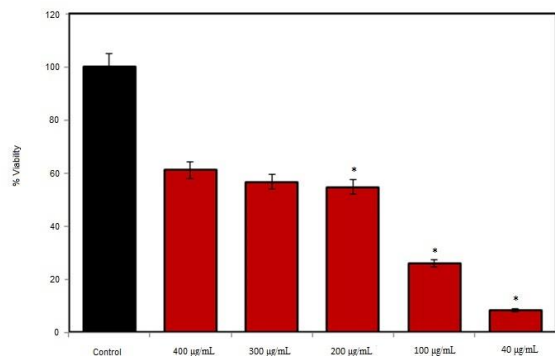
Figure 1. % Viability results of *R. pimpinellifolia* (L.) fruit extract on MCF-7 cells (*<0.05)

4. DISCUSSION AND CONCLUSION

The discrepancy between the findings of the study conducted by Öz et al. [22] and the current study regarding the antimicrobial activity of essential oils from *Rosa canina* (L.) and *R. pimpinellifolia* (L.) plants, particularly in relation to different plant parts, underscores the variability in antimicrobial properties within and between different plant species. While they observed limited and low-level antimicrobial activity in essential oils extracted from flower, leaf, and stem samples of *Rosa canina* (L.) and *R. pimpinellifolia* (L.) plants, no antimicrobial activity was detected in essential oils obtained from fruits. On the other hand, Gidik et al. [23] evaluated the antimicrobial activity of rosehip samples against various microorganisms and found antimicrobial effects at a concentration of 40 mg/mL. This contrasts with the current study's findings, where the extracts of *R. pimpinellifolia* (L.) fruit samples prepared using ultrasonic and microwave-assisted extraction methods showed no antibacterial effect against the selected target pathogens at a concentration of 500 µg/mL. The discrepancy between these studies could be attributed to several factors, including differences in the extraction methods, concentrations tested, variations in microbial strains used, and inherent differences in the chemical composition of the plant materials. Additionally, the specific antimicrobial assays employed in each study may have different sensitivities and specificities, leading to variations in the observed results. Overall, these findings highlight the importance of considering various factors when assessing the antimicrobial activity of plant extracts and emphasize the need for further research to elucidate the mechanisms underlying these activities and their potential applications. The comparison of the findings from our study with those of other research efforts sheds light on the variability in phenolic content and antioxidant activity across different *Rosa* species and extraction methods. The total phenolic content of *R. pimpinellifolia* (L.) fruit extract was determined to be 37.5 ± 0.2 mg/g, which is notably higher than the values reported by Shameh et al. [24] for various *Rosa* species, including *R. canina*. Additionally, the antioxidant activity of *R. pimpinellifolia* (L.) extract, as measured by ABTS and DPPH assays, was found to be 32.06 mg TE/g and 23.47 mg TE/g, respectively, demonstrating a substantial antioxidant effect and reported lower total phenolic content and antioxidant activity values for *Rosa* species, including *R. canina*, suggesting potential species-specific variations or differences in extraction methods and conditions. Similarly, Tahirović, Bašić [25] found varying phenolic content and antioxidant activity in *R. canina* extracts prepared using different solvents, with 80% methanol yielding lower phenolic content compared to 50% methanol. This indicates that the choice of solvent and its concentration can influence the extraction efficiency of phenolic compounds. Furthermore, Demir et al. [26] observed similar DPPH values for different *Rosa* fruit samples compared to our study's findings, indicating consistency in antioxidant activity within the genus *Rosa*. Overall, the discrepancies in phenolic content and antioxidant activity observed across different studies could stem from various factors, including genetic variability among *Rosa* species, environmental conditions, extraction methods, and analytical techniques used for assessment. Further research exploring these factors is necessary to better understand the composition and bioactivity of *Rosa* species extracts. The comparison of our study's findings with those of other research endeavors highlights the variability in total phenolic content and antioxidant activity among different *Rosa* species, as well as the influence of various extraction parameters. In our study, the antioxidant activity of *R. pimpinellifolia* (L.) fruit extract, determined by the ABTS method, was found to be 32.06 mg TE/g, which is substantially higher than the values reported by Gidik et al. [23] for different *Rosa* species collected from Bayburt, Türkiye. Similarly, they reported the total phenolic content reported for these *Rosa* species was higher compared to the values obtained in our study, indicating potential differences in phenolic composition among *Rosa* species from different regions. Moreover, the total phenolic content determined in the methanol extract of *R. pimpinellifolia* fruit in our study was lower than that reported by Güven [27] and Fattahi et al. [11] for the same species, suggesting variations in phenolic composition even within the same species. The discrepancy in antioxidant activity and total phenolic content among different studies can be attributed to several factors, including genetic variability among *Rosa* species, environmental conditions, harvesting time, extraction solvent type and ratio, as well as extraction methods and procedures. Additionally, variations in analytical techniques and assay conditions may contribute to differences in reported values. Furthermore, Öz et al. [22] highlighted the variability in antioxidant activities of essential oils obtained from different plant parts of *R. pimpinellifolia* (L.) and *R. canina* (L.), with higher antioxidant activities observed in essential oils from *R. pimpinellifolia* (L.). They also noted differences in total phenolic content between different harvest years,

26

underscoring the impact of temporal variations on chemical composition and biological activities. Overall, these findings emphasize the need for standardized methods and careful consideration of extraction parameters when evaluating the chemical composition and biological activities of *Rosa* species extracts. Additionally, further research exploring the effects of environmental factors and harvesting time on the bioactivity of *Rosa* species is warranted to better understand and harness their therapeutic potential. The literature on the anticancer and cytotoxic properties of black rose hips (*Rosa pimpinellifolia*) is relatively sparse. However, a notable study by Demir et al. in 2021 investigated the antioxidant potential and cytotoxic effects of *R. pimpinellifolia* extract on human colon (WiDr), liver (HepG2), and lung (A549) cancer cell lines, in comparison to normal fibroblast (BJ) cells. The researchers quantified the extract's total phenolic content as 16.4±0.4 mg gallic acid equivalent, total flavonoid content as 5.2±0.2 mg quercetin equivalent, and reducing power as 34.3±2.4 mg trolox equivalent per gram of sample. Their findings revealed that the extract exerted a selective cytotoxic effect on all three cancer cell lines in a dose-dependent manner, underscoring its potential therapeutic applications [28]. In our study, it was observed that cytotoxicity decreased as the concentration increased, confirming the need to use low concentrations of active substances in cytotoxicity studies. This is because the administration of high concentrations of the substance may have a nutritive effect on cancer cells or may have an unreasonably high cytotoxic effect. Therefore, when calculating the concentration, it is important to conduct preliminary trials and observe the effects at low concentrations.

In summary, the results of this study suggest that *R. pimpinellifolia* (L.) fruits hold promise for applications in various industries, including food and pharmaceuticals, owing to their notable antioxidant capacity and total phenolic content. However, further research is necessary to delve into the specific phenolic compounds present in the plant and their roles in conferring antioxidant and antiproliferative effects. Understanding the individual phenolic profiles of *R. pimpinellifolia* (L.) fruits could provide insights into their potential health benefits and aid in the development of novel products with enhanced bioactivity. Additionally, elucidating the mechanisms underlying the antioxidant and antiproliferative properties of these fruits could pave the way for the development of targeted therapies for various ailments, including cancer. Moreover, exploring the variability in phenolic composition among different harvests and geographical locations may uncover factors influencing the bioactivity of *R. pimpinellifolia* (L.) fruits, thereby facilitating optimized cultivation and harvesting practices to maximize their therapeutic potential. In conclusion, while this study sheds light on the promising attributes of *R. pimpinellifolia* (L.) fruits, further research is warranted to unlock their full potential and capitalize on their valuable bioactive compounds for the benefit of human health and well-being. Moreover, it is crucial to perform additional molecular biology experiments on the extract that demonstrated cytotoxic effects in cell culture studies.

Specifically, it is important to ascertain the mechanism of cell death, particularly by identifying whether it occurs through apoptotic pathways. In this regard, the expression levels of genes associated with apoptosis can be analyzed to provide a deeper understanding of the underlying processes. Furthermore, positive outcomes from *in vitro* studies must be proven *in vivo* animal experiments to confirm the therapeutic potential and biological relevance of the findings.

Acknowledgement

Conflicts of Interest

The authors declare that there is no conflict of interest.

REFERENCES

[1] Rozenblatt-Rosen O, Regev A, Oberdoerffer P, Nawy T, Hupalowska A, Rood JE, et al. The human tumor atlas network: charting tumor transitions across space and time at single-cell resolution. Cell. 2020;181(2):236-49.

[2] Feinberg AP, Levchenko A. Epigenetics as a mediator of plasticity in cancer. Science. 2023;379(6632):eaaw3835.

[3] Bayraktar B. Investigation of The Synthesis of Cyrinary Thyradyen Ritim and Cortizol Thycradium In Cancer. In: Sebahattin Çiftçi MU, Erdal Hamarta, Coşkun Arslan, editor. Bilim ve Teknoloji Araştırmaları 2019. Konya: Çizgi Kitabevi; 2019.

[4] Brenner DR, Brockton NT, Kotsopoulos J, Cotterchio M, Boucher BA, Courneya KS, et al. Breast cancer survival among young women: a review of the role of modifiable lifestyle factors. Cancer causes & control. 2016;27:459-72.

[5] Cuthrell KM, Tzenios N. Breast Cancer: Updated and Deep Insights. International Research Journal of Oncology. 2023;6(1):104-18.

[6] Tomasetti C, Li L, Vogelstein B. Stem cell divisions, somatic mutations, cancer etiology, and cancer prevention. Science. 2017;355(6331):1330-4.

[7] Cecil KM, Schnall MD, Siegelman ES, Lenkinski RE. The evaluation of human breast lesions with magnetic resonance imaging and proton magnetic resonance spectroscopy. Breast cancer research and treatment. 2001;68:45-54.

[8] Mulligan B. Manual of cultivated trees and shrubs hardy in North America. Nature Publishing Group UK London; 1941.

[9] Strålsjö L, Alklint C, Olsson ME, Sjöholm I. Total folate content and retention in rosehips (*Rosa* ssp.) after drying. Journal of agricultural and food chemistry. 2003;51(15):4291-5.

[10] Guimarães R, Barros L, Calhelha RC, Carvalho AM, Queiroz MJR, Ferreira IC. Bioactivity of different enriched phenolic extracts of wild fruits from Northeastern Portugal: A comparative study. Plant Foods for Human Nutrition. 2014;69:37-42.

[11] Fattahi S, Jamei R, Hosseini SS. Antioxidant and antiradical activities of *Rosa canina* and *Rosa pimpinellifolia* fruits from West Azerbaijan. 2012.

[12] Nowak R. Fatty acids composition in fruits of wild rose species. Acta Societatis Botanicorum Poloniae. 2005;74(3).

[13] Özçelik H, Gül A, Özgökçe F, Ünal M, Özkan G, Fakir H, et al. Türkiye *Rosa* L. (Gül) taksonlarının genetik çeşitliliğinin tespiti, ekonomiye kazandırılma olanaklarının araştırılması ve Süleyman Demirel Üniversitesi bünyesinde Rosaryum (Gülistan) tesisi. 2009.

[14] Ecem Bayram N, Gerçek YC, Bayram S, Toğar B. Effects of processing methods and extraction solvents on the chemical content and bioactive properties of propolis. Journal of Food Measurement and Characterization. 2020;14:905-16.

[15] Dhanasekaran S, Rajesh A, Mathimani T, Samuel SM, Shanmuganathan R, Brindhadevi K. Efficacy of crude extracts of *Clitoria ternatea* for antibacterial activity against gram negative bacterium (*Proteus mirabilis*). Biocatalysis and Agricultural Biotechnology. 2019;21:101328.

[16] qbal M, Bakht J, Shafi M. Phytochemical screening and antibacterial activity of different solvent extracted samples of *Arisaema jacquemontii*. Pakistan journal of pharmaceutical sciences. 2018;31(1).

[17] Herald TJ, Gadgil P, Tilley M. High-throughput micro plate assays for screening flavonoid content and DPPH-scavenging activity in sorghum bran and flour. J. Sci. Food Agric. 2012;92(11), 2326–2331.

[18] Re R, Pellegrini N, Proteggente A, Pannala A, Yang M, Rice-Evans C. Antioxidant activity applying an improved ABTS radical cation decolorization assay. Free Radic. Biol. Med. 1999;26(9–10), 1231–1237.

[19] Riss TL, Moravec RA. Use of multiple assay endpoints to investigate the effects of incubation time, dose of toxin, and plating density in cell-based cytotoxicity assays. Assay and drug development technologies. 2004;2(1):51-62.

[20] Mosmann T. Rapid colorimetric assay for cellular growth and survival: application to proliferation and cytotoxicity assays. Journal of immunological methods. 1983;65(1-2):55-63.

[21] Karataş, EA, Bayındırlı K. Enhanced Antıcancer Potency Of Gemcıtabıne In Combınatıon Wıth Propofol In Prostate Cancer. Hacettepe Journal of Biology and Chemistry. 2022; 50(1), 1-12.

[22] Öz M, Deniz I, Okan OT, Baltaci C, Karatas SM. Determination of the chemical composition, antioxidant and antimicrobial activities of different parts of *Rosa canina* L. and *Rosa pimpinellifolia* L. essential oils. Journal of Essential Oil-Bearing Plants. 2021;24(3):519-37.

[23] Gidik B, Akar Z, Can Z, Sefali A, Erturk O. Determination of antioxidant, antimicrobial activities, phenolic compounds of wild *Rosa* L. species Bayburt Turkey. Fresenius Environmental Bulletin. 2019;28(12A):9973-82.

[24] Shameh S, Alirezalu A, Hosseini B, Maleki R. Fruit phytochemical composition and color parameters of 21 accessions of five *Rosa* species grown in North West Iran. Journal of the Science of Food and Agriculture. 2019;99(13):5740-51.

[25] Tahirović A, Bašić N. Determination of phenolic content and antioxidant activity of *Rosa canina* L. fruits in different extraction systems. Radovi Šumarskog Fakulteta Univerziteta u Sarajevu. 2017;47(1):47-59.

[26] Demir N, Yildiz O, Alpaslan M, Hayaloglu A. Evaluation of volatiles, phenolic compounds and antioxidant activities of rose hip (*Rosa* L.) fruits in Turkey. Lwt-food science and technology. 2014;57(1):126-33.

[27] Güven L. *Rosa pimpinellifolia* yalancı meyve meyve ve köklerinde fitokimyasal ve biyolojik aktivite çalışmaları. health Sciences Institute. Erzurum: Ataturk University; 2016. p. 288.

[28] Demir EA, Demir S, Türkmen N, Turan, İ. The effect of *Rosa pimpinellifolia* extract on the proliferation of human tumor cells. KSU Journal of Agriculture and Nature. 2021; 24(6): 1170-1176.

28

Türk Doğa ve Fen Dergisi
Turkish Journal of Nature and Science

www.dergipark.gov.tr/tdfd

The Detailed Karyotype Analysis, Karyotype Asymmetry and Polyploidy in Hemp (*Cannabis sativa* L.)

Halil Erhan EROĞLU[1*] (iD), **Nisa GÜMÜŞ[2]** (iD), **Güngör YILMAZ[3]** (iD), **Levent YAZICI[3]** (iD)

[1] Yozgat Bozok University, Faculty of Science and Art, Department of Biology, Yozgat, Türkiye
[2] Yozgat Bozok University, Institute of Graduate Education, Department of Biology, Yozgat, Türkiye
[3] Yozgat Bozok University, Faculty of Agriculture, Department of Field Crops, Yozgat, Türkiye
HALİL ERHAN EROĞLU ORCID NO: 0000-0002-4509-4712
NİSA GÜMÜŞ ORCID NO: 0000-0002-5067-3874
GÜNGÖR YILMAZ ORCID NO: 0000-0003-0070-5484
LEVENT YAZICI ORCID NO: 0000-0002-6839-5366

Corresponding author: herhan.eroglu@bozok.edu.tr

Abstract: Hemp (*Cannabis sativa* L.) is an economical plant with a diploid chromosome number of $2n = 20$ and used in many areas, especially in industry. The aim of this study is to perform detailed karyotype analysis and detailed chromosomal measurements using five different genotypes of the plant known as diploid chromosome number $2n = 20$, to determine the karyotype asymmetry for the first time, and to investigate the polyploidy variations. The diploid chromosome number and karyotype formula were $2n = 2x = 20 = 18m + 2sm$. The karyotype had small metacentric and submetacentric chromosomes. The smallest chromosome length, largest chromosome length, total haploid chromosome length, and average haploid chromosome length were 2.41, 3.55, 29.87, and 2.99 μm, respectively. Intrachromosomal and interchromosomal karyotype asymmetries were calculated using many different parameters, mainly M_{CA} (mean centromeric asymmetry) and CV_{CL} (variation coefficient of chromosome length). According to the asymmetry values, the species had quite symmetrical karyotype. Although the diploid chromosome number was known as $2n = 20$, detailed karyotype analysis and asymmetry data were presented for the first time by this study. In addition, in the study carried out on five different genotypes, polyploidy variation was detected in one genotype.

Kenevirde (*Cannabis sativa* L.) Detaylı Karyotip Analizi, Karyotip Asimetrisi ve Poliploidi

Öz: Kenevir (*Cannabis sativa* L.), diploid kromozom sayısı $2n = 20$ olan ve sanayi başta olmak üzere birçok alanda kullanılan ekonomik bir bitkidir. Bu çalışmanın amacı, diploid kromozom sayısı $2n = 20$ olarak bilinen bitkinin beş farklı genotipini kullanarak detaylı karyotip analizini ve detaylı kromozomal ölçümlerini yapmak, karyotip asimetrisini ilk kez belirlemek ve poliploidi varyasyonlarını araştırmaktır. Diploid kromozom sayısı ve karyotip formülü, $2n = 2x = 20 = 18m + 2sm$'dir. Karyotip, küçük metasentrik ve submetasentrik kromozomlara sahiptir. En küçük kromozom uzunluğu, en büyük kromozom uzunluğu, toplam haploid kromozom uzunluğu ve ortalama haploid kromozom uzunluğu sırasıyla 2.41, 3.55, 29.87 ve 2.99 μm'dir. İntrakromozomal ve interkromozomal karyotip asimetrileri, M_{CA} (ortalama sentromerik asimetri) ve CV_{CL} (kromozom uzunluğunun varyasyon katsayısı) parametreleri kullanılarak hesaplandı. Asimetri değerlerine göre tür oldukça simetrik karyotipe sahiptir. Diploid kromozom sayısı $2n = 20$ olarak bilinmesine rağmen detaylı karyotip analizi ve asimetri verileri ilk kez bu çalışma ile ortaya konmuştur. Ayrıca beş farklı genotip üzerinde yapılan çalışmada bir genotipte poliploidi varyasyonu tespit edilmiştir.

29

1. INTRODUCTION

Hemp (*Cannabis sativa* L.) is an economical plant with a diploid chromosome number of $2n = 20$ and used in many areas, especially in industry. Its fibers, stems and seeds are used in many different areas such as energy, construction, medicine, and food. In archaeological studies, the remains of fabric made from hemp were found in 8000 BC and the hemp was the first plant used to make rope. It is a plant originating from a very wide distribution area extending from the Caspian Sea and the Himalayan mountains to China and Siberia. It is known that it was found in Anatolia in 700-800 BC [1, 2]. Today, it is classified as drug type (medicinal cannabis or marijuana) and fibre type (industrial hemp), depending on its cannabinoid content and use [3].

Modern phylogenetic research mainly relies on morphological and molecular characters, but chromosomal characters and karyotype evolution play an important role to evaluate origin of the plants and interspecific relationships [4, 5]. The fundamental characters of chromosomal data are basic number (*x*), diploid number (*2n*), and chromosome lengths, which are total length, long arm length, short arm length, and relative length. These basic characters can be changed numerically by aneuploidy and polyploidy mechanisms, or structurally by rearrangements such as deletions, inversions, duplications, and translocations. All these mechanisms produce the intrachromosomal and interchromosomal variations in karyotypes by changing centromere position and chromosome morphology [6, 7].

In *Cannabis sativa*, the diploid chromosome number is $2n = 20$ consisting of eighteen autosomal chromosomes and one pair sex chromosomes [8-12]. The aim of this study is to perform detailed karyotype analysis and detailed chromosomal measurements using five different genotypes of the plant known as diploid chromosome number $2n = 20$, to determine the karyotype asymmetry (intrachromosomal and interchromosomal asymmetry) for the first time, and to investigate the polyploidy variations.

2. MATERIAL AND METHOD

2.1. Plant Material

Within the scope of the study, five different hemp genotypes were used as material. They were Eminönü, Kavacık, Maltepe, Spice bazaar, and Van genotypes. The hemp seeds were obtained from the Institute of Hemp Research.

2.2. Cytogenetic Procedure

(i) Germination; the hemp seeds were germinated between moist filter papers in petri dishes at room temperature. (ii) Pretreatment; the germinated seeds were pretreated in alpha-monobromonaphthalene solution at 4°C for 16 h. (iii) Fixation; then the materials were fixed in fixative solution containing ethanol:glacial acetic acid (3:1, v:v) at 4°C for 24 h. (iv) Hydrolysis; the materials were hydrolyzed in 1 N HCl at 60°C for 12 min. (v) Staining; the materials were stained in acetoorcein (2%) for 2 h. (vi) Preparation; the preparations were made by the squash method [13].

2.3. Karyotype Analysis

At least 10 well-spread metaphase plates were used for chromosomal measurements. The chromosomal measurements were performed by the KaryoType 2.0 software using well-spread metaphase plates. The following parameters were used to karyotype analysis: short arm length (p), long arm length (q), total chromosome length (CL = p + q), total haploid length (THL = CL_1 + CL_2 + CL_3 + …………. CL_n), relative length (RL) = [(p + q)/THL] × 100, mean chromosome length (MCL = THL/n), and centromeric index (CI) = [(p)/(p + q)] × 100. The karyotype formulae were detected based on arm rates (r = q/p) as described by Levan et al. [14]. The monoploid ideograms were drawn by the ChemDraw Professional software depending on short arm and long arm lengths.

Karyotype asymmetries were estimated by intrachromosomal asymmetry (M_{CA} = mean [(Σq − Σp) / (Σq + Σp)] × 100) and interchromosomal asymmetry (CV_{CL} = [SD (standard deviation) / MCL] × 100). M_{CA} and CV_{CL} refer to the mean centromeric asymmetry and variation coefficient of chromosome length, respectively [15, 16].

3. RESULTS AND DISCUSSION

The somatic metaphase chromosomes and monoploid ideogram of *Cannabis sativa* were represented in Figure 1 and Figure 2. In *Cannabis sativa*, the diploid chromosome number was determined as $2n = 20$ in all genotypes and $2n = 20, 40$ in Eminönü genotype. No satellites and seconder construction were observed in *Cannabis sativa* karyotype measurements. Srivastava et al. [8] reported the secondary constriction in chromosome 3.

The chromosomes were type of metacentric and submetacentric and the karyotype formulae were $2n = 2x = 20 = 18m + 2sm$ in all genotypes and $2n = 4x = 36m + 4sm$ in Eminönü genotype (Table 1). It was reported that the diploid chromosome number of *Cannabis sativa* was $2n = 20$ [10-12] and the karyotype formula was 18m + 2sm [8, 9]. These data were compatible with our study results.

Eminönü genotype showed polyploidy variation with ploidy level of $4x$. There was only one report in the literature regarding the polyploidy variation of *Cannabis sativa*. Moteg [17] reported that the chromosome number and ploidy level were $2n = 20, 40, 80$ and $2x, 4x, 8x$, respectively. Since our country has very different climate, soil, and geographical characteristics, it has a suitable environment for plant karyological variations. Plant communities can also show morphological and genetic variations at various levels by adapting themselves to their environment.
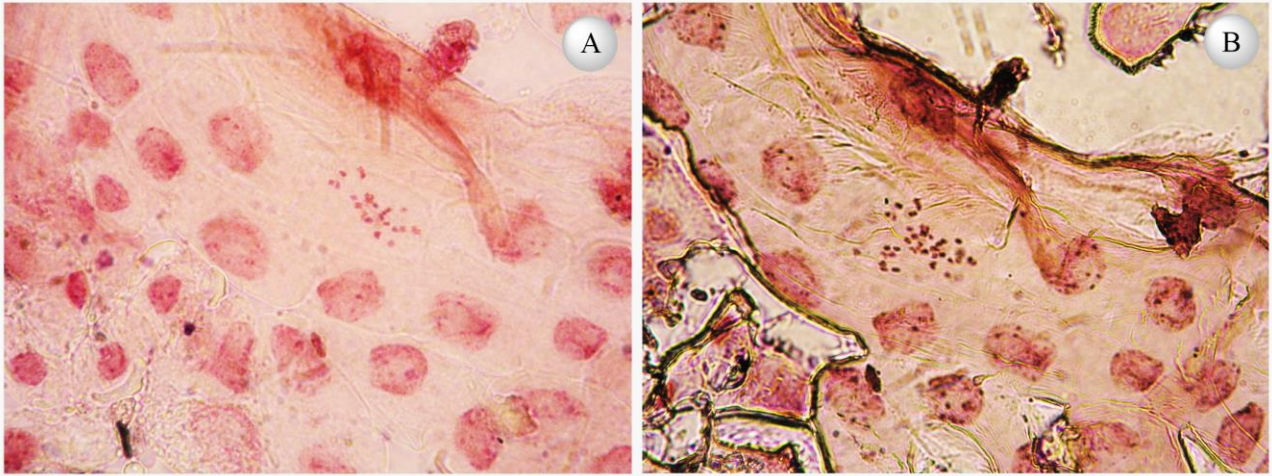
Figure 1. Metaphase chromosomes (2n = 20) of the spice bazaar genotype (A). Polyploidy variation observed in Eminönü genotype (2n = 40) (B).
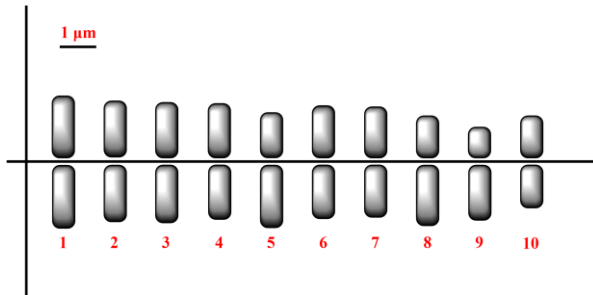
Figure 2. The monoploid ideogram of *Cannabis sativa*.

Table 1. The diploid chromosome numbers and karyotype formulae of hemp genotypes.

Genotype	2n	Karyotype formula
Eminönü	20	18m + 2sm
	40	36m + 4sm
Kavacık	20	18m + 2sm
Maltepe	20	18m + 2sm
Spice bazaar	20	18m + 2sm
Van	20	18m + 2sm

The smallest chromosome length, the largest chromosome length, total haploid chromosome length was average chromosome length were 2.41 μm, 3.55 μm, 29.87 μm, and 2.98 μm, respectively. The values of relative length and centromeric index ranged from 8.06-11.88% and 35.77-50.00%, respectively (Table 2). The low centromeric index indicated movement away from the median region. The chromosome 9 was an asymmetric chromosome with the lowest centromeric index and the highest arm ratio.

Karyotype asymmetries were calculated with CV_{CL} and M_{CA} values, which were considered the most reliable interchromosomal and intrachromosomal parameters. CV_{CL} and M_{CA} values were 11.50 and 7.07, respectively. According to these values, the karyotype of *Cannabis sativa* was quite symmetrical.

31

Table 2. Detailed chromosome measurements of *Cannabis sativa*.

Chromosome pair	Length (μm)	Long arm (μm)	Short arm (μm)	Arm ratio	Relative length (%)	Centromeric index (%)	Chromosome type
1	3.55	1.80	1.75	1.03	11.88	49.30	metacentric
2	3.25	1.65	1.60	1.03	10.87	49.23	metacentric
3	3.20	1.63	1.57	1.04	10.71	49.06	metacentric
4	3.08	1.54	1.54	1.00	10.30	50.00	metacentric
5	3.06	1.78	1.28	1.39	10.24	41.83	metacentric
6	3.02	1.52	1.50	1.01	10.10	49.67	metacentric
7	2.94	1.49	1.45	1.03	9.84	49.32	metacentric
8	2.92	1.72	1.20	1.43	9.77	41.10	metacentric
9	2.46	1.58	0.88	1.80	8.23	35.77	submetacentric
10	2.41	1.22	1.19	1.03	8.06	49.38	metacentric

4. CONCLUSION

In the present study, it was recorded only one chromosome number (2n = 20) in all genotypes excluding polyploidy (2n = 40) in Eminönü genotype. The polyploidy was not very common in *Cannabis sativa* and in this respect, it was an important variation. In addition, the karyotype asymmetry was reported for the first time. The results made a significant contribution to *Cannabis* cytotaxonomy.

REFERENCES

[1] İncekara F. Endüstri bitkileri ve ıslahı. İzmir: Ege Üniversitesi, Ziraat Fakültesi Yayınları; 1971.
[2] Atakişi İK. Lif bitkileri yetiştirme ve ıslahı. Tekirdağ: Trakya Üniversitesi, Ziraat Fakültesi Yayınları; 1999.

[3] Hurgobin B, Tamiru-Oli M, Welling MT, Doblin MS, Bacic A, Whelan J, et al. Recent advances in Cannabis sativa genomics research. New Phytol. 2021;230(1):73-89.

[4] Stebbins GL. Chromosomal evolution in higher plants. London: Edward Arnold Publisher Ltd; 1971.

[5] Eroğlu HE, Şimşek N, Koç M, Hamzaoğlu E. Karyotype analysis of some Minuartia L. (Caryophyllaceae) taxa. Plant Syst Evol. 2013;299:67-73.

[6] Martin E, Kahraman A, Dirmenci T, Bozkurt H, Eroğlu HE. Karyotype evolution and new chromosomal data in Erodium: chromosome alteration, polyploidy, dysploidy, and symmetrical karyotypes. Turk J Bot. 2020;44(3):255-68.

[7] Martin E, Celep F, Eroğlu HE. Comparative chromosomal features and new karyological data in Salvia: B-chromosomes, polyploidy, dysploidy and symmetric karyotypes. Braz J Bot. 2022;45:625-34.

[8] Srivastava P, Srivastava S, Verma MK, Mishra SK. Karyological studies in root-tip cells of Cannabis sativa var. indica. Cytologia. 1999;64:435-40.

[9] Divashuk MG, Alexandrov OS, Razumova OV, Kirov IV, Karlov GI. Molecular cytogenetic characterization of the dioecious Cannabis sativa with an XY chromosome sex determination system. PLoS One. 2014;9(1):e85118.

[10] Razumova OV, Alexandrov OS, Divashuk MG, Sukhorada TI, Karlov GI. Molecular cytogenetic analysis of monoecious hemp (Cannabis sativa L.) cultivars reveals its karyotype variations and sex chromosomes constitution. Protoplasma. 2016;253(3):895-901.

[11] Braich S, Baillie RC, Jewell LS, Spangenberg GC, Cogan NOI. Generation of a comprehensive transcriptome atlas and transcriptome dynamics in medicinal Cannabis. Sci Rep-UK. 2019;9:1-12.

[12] CCDB [Internet]. Chromosome Count Database; 2024 [cited 2024 Apr 1]. Available from: https://taux.evolseq.net/CCDB_web/home

[13] Martin E, Kahraman A, Dirmenci T, Bozkurt H, Eroğlu HE. New chromosomal data and karyological relationships in Geranium: basic number alterations, dysploidy, polyploidy, and karyotype asymmetry. Braz Arch Biol Techn. 2022;65:e22210354.

[14] Levan AK, Fredga K, Sandberg AA. Nomenclature for centromeric position on chromosomes. Hereditas. 1964;52:201-20.

[15] Paszko B. A critical review and a new proposal of karyotype asymmetry indices. Plant Syst Evol. 2006;258:39-48.

[16] Peruzzi L, Eroğlu HE. Karyotype asymmetry: again, how to measure and what to measure? Comp Cytogenet. 2013;7:1-9.

[17] Moteg IT. On the culture of leaf callus tissue of Cannabis sativa. Kromosomo. 1968;74: 2406-14.

Türk Doğa ve Fen Dergisi
Turkish Journal of Nature and Science
www.dergipark.gov.tr/tdfd

AW(k) -Type Curves in Modified Orthogonal Frame

Esra DAMAR[1]* , Burçin SALTIK BAEK[2] , Nural YÜKSEL[2] ,Nurdan OĞRAŞ[2]

[1] Hitit University, Vocational School of Technical Sciences, Motor Vehicles and Transportation Technologies Department, Çorum, Türkiye
[2] Erciyes University, Faculty of Science, Department of Mathematics, Kayseri, Türkiye
Esra DAMAR ORCID No: 0000-0002-0743-8545
Burçin SALTIK BAEK ORCID No: 0000-0001-5174-6484
Nural YÜKSEL ORCID No: 0000-0003-3360-5148
Nurdan OĞRAŞ ORCID No: 0000-0002-5539-4890

Corresponding author: esradamar@hitit.edu.tr

Abstract: The goal of this article is to examine $AW(k)$ -type curves in Euclidean 3-space according to a modified orthogonal frame with non-zero curvature. Firstly, the relations between the curvatures κ, τ for $AW(k)$ -type curves in the modified orthogonal frame are given. Also, the harmonic curvatures of $AW(k)$ -type curves according to this frame are obtained. The results are illustrated in examples. Finally, slant helices are analyzed for the modified orthogonal frame and some relations are obtained for the curvatures of the curve to be of $AW(1)$ and $AW(2)$ type in case the curve is a slant helix.

33

Modifiye Ortogonal Çatıda *AW(k)* -Tipinde Eğriler

Öz: Bu çalışmanın amacı 3-boyutlu Öklid uzayı E^3 de $AW(k)$ -tipinde eğrileri, eğrilik ile modifiye edilmiş ortogonal çatıya göre analiz etmektir. İlk olarak modifiye ortogonal çatıya göre $AW(k)$ -tipinde eğriler için κ, τ eğrilikleri arasındaki bağıntılar verilmiştir. Ayrıca bu çatıya göre $AW(k)$ -tipinde eğrilerin harmonik eğrilikleri elde edilmiştir. Bulunan sonuçlar örnekler üzerinde gösterilmiştir. Son olarak, slant helisler modifiye ortogonal çatıya göre incelenmiş ve eğrinin slant helis olması durumunda eğrinin eğriliklerinin $AW(1)$ ve $AW(2)$ tipinde olması için bazı bağıntılar elde edilmiştir.

1. INTRODUCTION

Arslan et al. [1] explored the concept of $AW(k)$ -type submanifolds, and many subsequent studies have focused on $AW(k)$ -type curves. For example, the authors in [2, 3] provided detailed characteristics and curvature criteria for these curves in E^m. In [4], $AW(k)(k = 1, 2 \ or \ 3)$ -type curves and surfaces were considered. $AW(k)$ -type curves in Euclidean, Lorentz, and Galilean spaces have yielded several intriguing findings in [5-7]. In Euclidean 3-space, a moving frame at a particular point on any regular curve is known as a Frenet frame. The tangent, normal, and binormal vectors

of the curve, which are the curve's Serret-Frenet vectors, combine to form the orthonormal Frenet frame of the curve. With this frame, the curve's curvature and torsion functions can be determined. In this regard, there are numerous sources of research on the Frenet frame of the regular curve [8–10].

A regular curve is defined as having functions (torsion and curvature) that can be differentiated at every point on the curve, in accordance with the basic theorem of regular curves [11]. On the analytical curves, the curvature function might, nevertheless, be zero at certain locations. It is evident that the curvature function κ isn't always differentiable since the principal normal and binormal vectors of the curves are typically

discontinuous at the curvature's zero point. In this instance as well, an analytical curve's Frenet derivative equations lead to uncertainty at the point where the curvature disappears. Various substitute frames have been constructed to eliminate these uncertain situations [12, 13]. Many researchers have examined curves and surfaces using these different frameworks [14–16]. After considering this issue, Hord [17] and Sasai [18] engaged in a different frame that is effective on these issues. Sasai [19] presented an orthogonal frame for unit speed analytical curves in a straightforward but practical method. Even though the curvature function κ multiplies each Frenet vector to get these modified orthogonal frame vectors, they enable the application of a new formula that corresponds to the Frenet derivative equations for the aforementioned situation. With its help, analytical curves with singular points can be explored efficiently.

Subsequently, Bükçü et al. [20] expanded Sasai's [21] investigation and got the newly modified frame by using the Frenet vectors and the torsion. The modified orthogonal frame of a curve in Lorentzian or Euclidean 3-space has been the area of several searches [22-27].

The arrangement of the paper is as follows. The 2nd section gives some basic concepts on modified orthogonal frames with non-zero curvature over the curves. Curves of type $AW(k)$ are given in the 3rd section using the modified orthogonal frame in E^3. In the 4th section, the findings regarding the harmonic curvatures of the $AW(k)$ curves in the modified orthogonal frames and their status as general helix, slant helix, and circular helix are discussed.

2. MATERIAL AND METHOD

Let α be a space curve in Euclidean 3-space according to the arclenght s. At each point $\alpha(s)$ on a curve α, there are vectors the tangent t, principal normal n, and binormal b respectively. The Serret-Frenet equations are given by

$$t' = \kappa n,$$
$$n' = -\kappa t + \tau b,$$
$$b' = -\tau n,$$

where κ, τ represent the first and second curvature of the curve, respectively.

Let $\alpha : I \to E^3$ be a space curve. We assume that the curvature κ of α is not identically zero. As a result, the modified orthogonal frame $\{T, N, B\}$ with the curvature κ of the curve α can be defined. Now we define the modified orthogonal frame $\{T, N, B\}$ as follows:

$$T = \frac{d\alpha}{ds}, \quad N = \frac{dT}{ds}, \quad B = T \wedge N.$$

The following represents the relationships between the modified orthogonal frame $\{T, N, B\}$ and Frenet frame $\{t, n, b\}$ at non-zero positions of κ

$$\begin{aligned} T &= t, \\ N &= \kappa n, \\ B &= \kappa b. \end{aligned} \tag{1}$$

The modified orthogonal frame $\{T, N, B\}$ satisfies the below relations,

$$\begin{aligned} &<T,T> = 1, \\ &<N,N> = <B,B> = \kappa^2, \\ &<N,T> = <B,T> = <B,N> = 0, \end{aligned} \tag{2}$$

where $\langle , \rangle$ is the inner product.
Due to these equations, the derivative equations of the modified orthogonal frame $\{T, N, B\}$ are given as

$$T' = N,$$
$$N' = -\kappa^2 T + \frac{\kappa'}{\kappa} N + \tau B,$$
$$B' = -\tau N + \frac{\kappa'}{\kappa} B, \tag{3}$$

where, $\tau = \dfrac{det(\alpha', \alpha'', \alpha''')}{\kappa^2}$ is the torsion of α. The frame denoted by equations (1) and (3) is called a modified orthogonal frame with curvature [20].

Proposition 2.1 [2] Let γ be a Frenet curve of E^3 osculating order 3. Then we have

$$\gamma' = t,$$
$$\gamma'' = t' = \kappa n,$$
$$\gamma''' = -\kappa^2 t + \kappa' n + \kappa \tau b,$$
$$\gamma^{(iv)} = -3\kappa\kappa' t + (\kappa'' - \kappa^3 - \kappa\tau^2)n + (2\kappa'\tau + \kappa\tau')b,$$

where, $\kappa = \kappa(s)$, $\tau = \tau(s)$ are the curve's curvature and torsion of the curve γ and $\gamma' = \dfrac{d\gamma}{ds}$.

Let γ be a Frenet curve of osculating order in E^3, then we have

$$N_1 = \kappa \boldsymbol{n},$$

$$N_2 = \kappa' \boldsymbol{n} + \kappa \tau \boldsymbol{b},$$

$$N_3 = (\kappa'' - \kappa^3 - \kappa \tau^2)\boldsymbol{n} + (2\kappa' \tau + \kappa \tau')\boldsymbol{b},$$

where the curve's curvature and torsion are represented by the values of $\kappa = \kappa(s)$, $\tau = \tau(s)$ of the curve γ [2].

Definition 2.1 [2] For the Frenet curves,
i) of type weak $AW(2)$ if they satisfy;

$$N_3 = < N_3, N_2^* > N_2^*,$$

ii) of type weak $AW(3)$ if they satisfy;

$$N_3 = < N_3, N_1^* > N_1^*,$$

where,

$$N_1^* = \frac{N_1}{\parallel N_1 \parallel}, \quad N_2^* = \frac{N_2 - < N_2, N_1^* > N_1^*}{\parallel N_2 - < N_2, N_1^* > N_1^* \parallel}.$$

Definition 2.2 [2] Frenet curves are,

i) of type $AW(1)$ if they satisfy;

$$N_3 = 0,$$

ii) of type $AW(2)$ if they satisfy;

$$\parallel N_2 \parallel^2 N_3 = \langle N_3, N_2 \rangle N_2,$$

iii) of type $AW(3)$ if they satisfy;

$$\parallel N_1 \parallel^2 N_3 = \langle N_3, N_1 \rangle N_1.$$

Definition 2.3 [28] Let γ be a unit speed curve of osculating order d. The functions

$$H_j : I \to E, 1 \le j \le d-2 \quad \text{defined by}$$

$$H_1(s) = \frac{\kappa_1(s)}{\kappa_2(s)}, \quad H_k = \{D_{v1}H_{k-1} + H_{k-2}\kappa_k\}\frac{1}{\kappa_{k+1}},$$

$$2 \le j \le d-2,$$

are called the harmonic curvatures of γ, where $v1 = \gamma'$ and $\kappa_1(s), \kappa_2(s), \ldots, \kappa_{d-1}$ Frenet curvatures γ which are not necessarily constant.

Definition 2.4 [29] A curve γ with $\kappa_1 \ne 0$ is called a slant helix if the principal normal lines of the curve γ make a constant angle in a fixed direction.

Theorem 2.1 [23] Let $\gamma : I \to E^3$ be a unit speed curve in E^3. Then γ is a slant helix determined by the modified orthogonal frame if and only if

$$\frac{\tau'}{(\kappa^2 + \tau^2)^{\frac{3}{2}}}$$

is constant.

3. RESULTS

3.1. Curves in the Modified Orthogonal Frame

$AW(k)$-type curves in the modified orthogonal frame in E^3 are introduced in this section, along with some results and examples.

Proposition 3.1 Let γ be a curve with arclenght parameter s and belonging to osculating order 3 in E^3 and $\{T, N, B\}$ be a modified orthogonal frame. We have

$$\gamma' = T_\gamma,$$

$$\gamma'' = T_\gamma' = N_\gamma,$$

$$\gamma''' = -\kappa^2 T_\gamma + \frac{\kappa'}{\kappa}N_\gamma + \tau B_\gamma,$$

$$\gamma^{(iv)} = -3\kappa\kappa' T_\gamma + \left(\frac{\kappa''}{\kappa} - \kappa^2 - \tau^2\right)N_\gamma + \left(\frac{2\tau\kappa'}{\kappa} + \tau'\right)B_\gamma.$$

We will use some notations for defining $AW(k)$-type curves determined by the modified orthogonal frame like as follow

$$A_{\gamma 1} = N_\gamma, \tag{4}$$

$$A_{\gamma 2} = \frac{\kappa'}{\kappa}N_\gamma + \tau B_\gamma, \tag{5}$$

$$A_{\gamma 3} = \left(\frac{\kappa''}{\kappa} - \kappa^2 - \tau^2\right)N_\gamma + \left(\frac{2\tau\kappa'}{\kappa} + \tau'\right)B_\gamma. \tag{6}$$

Corollary 3.1 $\gamma', \gamma'', \gamma'''$ and $\gamma^{(iv)}$ are linearly dependent if and only if $A_{\gamma 1}, A_{\gamma 2}$ and $A_{\gamma 3}$ are linearly dependent.

Definition 3.1 Frenet curves are,
i) of type modified $AW(1)$ if they satisfy;

$$A_{\gamma 3} = 0, \tag{7}$$

ii) of type modified $AW(2)$ if they satisfy;

35

$$\| A_{\gamma_2} \|^2 A_{\gamma 3} = \langle A_{\gamma_3}, A_{\gamma_2} \rangle A_{\gamma_2}, \tag{8}$$

iii) of type modified $AW(3)$ if they satisfy,

$$\|\widetilde{A_{\gamma_1}}\|^2 \widetilde{A_{\gamma_3}} = \langle \widetilde{A_{\gamma_3}}, \widetilde{A_{\gamma_1}} \rangle \widetilde{A_{\gamma_1}}. \tag{9}$$

Definition 3.2 The unit speed curves of order 3 are

i) of type weak modified $AW(2)$ if they hold;

$$\widetilde{A_{\gamma_3}} = < \widetilde{A_{\gamma_3}}, \widetilde{A_{\gamma_2}}^* > \widetilde{A_{\gamma_2}}^*, \tag{10}$$

ii) of type weak modified $AW(3)$ if they hold;

$$\widetilde{A_{\gamma_3}} = < \widetilde{A_{\gamma_3}}, \widetilde{A_{\gamma_1}}^* > \widetilde{A_{\gamma_1}}^*, \tag{11}$$

where,

$$\widetilde{A_{\gamma_1}}^* = \frac{\widetilde{A_{\gamma_1}}}{\|\widetilde{A_{\gamma_1}}\|},$$

$$\widetilde{A_{\gamma_2}}^* = \frac{\widetilde{A_{\gamma_2}} - < \widetilde{A_{\gamma_2}}, \widetilde{A_{\gamma_1}}^* > \widetilde{A_{\gamma_1}}^*}{\|\widetilde{A_{\gamma_2}} - < \widetilde{A_{\gamma_2}}, \widetilde{A_{\gamma_1}}^* > \widetilde{A_{\gamma_1}}^*\|}.$$

Theorem 3.1 Let γ be a curve with arc-length parameter s and belonging to osculating order 3. If γ is of type modified $AW(1)$, then the curvature equations are given by

$$\frac{\kappa''}{\kappa} - \kappa^2 - \tau^2 = 0 \tag{12}$$

and

$$\tau = \frac{c}{\kappa^2}. \ c \in \mathbb{R}, (\kappa \neq 0) \tag{13}$$

Proof. We can easily obtain from equation (6) and (7)
Corollary 3.2 Every plane curve of $AW(1)$ type is also weak $AW(2)$ type.

Theorem 3.2 Let the curve γ be a unit speed curve of order 3. If the curve γ is of type modified $AW(2)$, then the curvature relations of the curve is given by

$$2\tau\kappa'^2 + \tau' \kappa \kappa' + \tau\kappa^4 - \tau\kappa \kappa'' + \tau^3\kappa^2 = 0. \tag{14}$$

Proof If equation (5) and equation (6) are substituted into equation (8), then we get equation (14).

Theorem 3.3 Let the curve γ be a unit speed curve of order 3. If the curve γ is of type modified $AW(3)$, then there is a relation between curvatures as follows

$$2\tau\kappa' + \tau' \kappa = 0 \tag{15}$$

and

$$\tau = \frac{c}{\kappa^2}, \quad c \in \mathbb{R}, \quad (\kappa \neq 0). \tag{16}$$

Proof If equation (4) and equation (6) substitute into equation (9) we get equations (15) and (16).

Theorem 3.4 Let the curve γ be a unit speed curve of order 3. If the curve γ is of type weak modified $AW(2)$ then the curvature relation is provided by

$$-\kappa^2 + \frac{\kappa''}{\kappa} - \tau^2 = 0. \tag{17}$$

Proof By the below equation

$$\tilde{A}_2^* = \frac{1}{\kappa} B \tag{18}$$

if we equations (6) and (18) substitute into equation (10), then we have equation (17).

Theorem 3.5 Let the curve γ be a unit speed curve of order 3. If the curve γ is of type weak modified $AW(3)$ then the curvature equations is given by

$$2\tau\kappa' + \tau' \kappa = 0. \tag{19}$$

Proof By the below equation

$$\tilde{A}_1^* = \frac{1}{\kappa} N, \tag{20}$$

if equations (6) and (20) are substituted into equation (11), then we have equation (19).

Example 3.1 Let us consider the curve $c_1(s)$ which is given by

$$c_1(s) = (\cos \frac{s}{\sqrt{2}}, \sin \frac{s}{\sqrt{2}}, \frac{s}{\sqrt{2}}).$$

The curve c_1 satisfies modified $AW(2), AW(3)$ - type curves conditions, for $\kappa(s) = \frac{1}{2}$ and $\tau(s) = \frac{1}{2}$.

Example 3.2 Let us consider the curve $c_2(s)$ which is given by

$$c_2 = \begin{pmatrix} s, \dfrac{s}{6}(2\sinh(2\ln s) - \cosh(2\ln s), \\ \dfrac{s}{6}(2\cosh(2\ln s) - \sinh(2\ln s) \end{pmatrix}.$$

The curve $c_2(s)$ satisfies modified $AW(3)$ type curve condition, for $\kappa = 1$ and $\tau = -2$, see Figure 1.
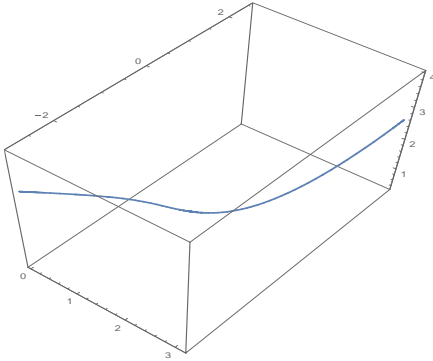
Figure 1. The curve of c_2.

3.2. Curves with Harmonic Curvatures in the Modified Orthogonal Frame

Theorem 3.6 $\gamma'', \gamma''', \gamma^{(iv)}$ are linearly dependent if and only if γ is a general helix.

Proof If γ'', γ''' and $\gamma^{(iv)}$ are linearly dependent, then the following equation is valid:

$$\begin{vmatrix} 0 & 1 & 0 \\ -\kappa^2 & \dfrac{\kappa'}{\kappa} & \tau \\ -3\kappa\kappa' & \left(\dfrac{\kappa''}{\kappa} - \kappa^2 - \tau^2\right) & \left(\dfrac{2\tau\kappa'}{\kappa} + \tau'\right) \end{vmatrix} = 0.$$

We have $\dfrac{\kappa'}{\tau} = \dfrac{\kappa}{\tau}$ and $\dfrac{d}{ds}(\dfrac{\kappa(s)}{\tau(s)}) = 0$. Thus

$\dfrac{\kappa}{\tau} = $ constant and γ is a general helix. In reverse γ is

a general helix, thus $\dfrac{\kappa}{\tau} = $ constant and $\gamma'', \gamma''', \gamma^{(iv)}$

are linearly dependent.
We will use some notations for defining $AW(k)$-type curves determined by the modified orthogonal with harmonic curvatures like the following

$$A_{\gamma_1} = N_\gamma , \tag{21}$$

$$A_{\gamma_2} = \dfrac{\kappa'}{\kappa} N_\gamma + \dfrac{\kappa}{H} B_{\gamma'} , , \tag{22}$$

$$\widetilde{A_{\gamma_3}} = \left(\dfrac{\kappa''}{\kappa} - \kappa^2 (1 + \dfrac{1}{H^2})\right) N_\gamma + \left(\dfrac{3H\kappa' - \kappa H'}{H^2}\right) B_{\gamma'}, \tag{23}$$

where κ, τ, H are curvature, torsion, and harmonic curvature of $AW(k)$-type curves respectively. Also

$$\tau = \dfrac{\kappa}{H} \text{ and } \tau' = \dfrac{\kappa'H - \kappa H'}{H^2}.$$

Theorem 3.7 If γ is a weak harmonic curve of the modified $AW(2)$-type, then the equation is provided by

$$\dfrac{\kappa''}{\kappa} - \kappa^2 \left(1 + \dfrac{1}{H^2}\right) = 0. \tag{24}$$

Proof By the below equation

$$A_{\gamma_2}{}^* = \dfrac{1}{\kappa} B_\gamma , \tag{25}$$

if equations (23) and (25) are substituted into equation (10), then we have equation (24).

Theorem 3.8 Let the curve γ be a unit speed curve of order 3. The modified $AW(1)$-type with harmonic curvature has no general, circular helix.

Proof Let the curve γ be a helix. Thus H is constant, $H' = 0$. Since γ is a modified $AW(1)$-type with harmonic curvature we get

$$\begin{cases} \left[\left(\dfrac{\kappa''}{\kappa} - \kappa^2(1 + \dfrac{1}{H^2})\right)N\right] \\ + \left(\dfrac{3H\kappa' - \kappa H'}{H^2}\right)B \end{cases} = 0,$$

$$-\kappa^2(1 + \dfrac{1}{H^2}) \neq 0 . \tag{26}$$

Since there are no solutions of the differential equations in equation (26), the proof is completed.

Theorem 3.9 If the curve γ is a weak harmonic curve of the modified $AW(3)$-type, then the equation is given by

$$\frac{3H\,\kappa' - \kappa\,H'}{H^2} = 0. \tag{27}$$

Proof By the below equation

$$A_{\gamma_1}^* = \frac{1}{\kappa} N_\gamma, \tag{28}$$

if equations (23) and (28) are substituted into equation (11), then we get equation (27) .

Theorem 3.10 If the curve γ is a harmonic curve of the modified $AW(1)$ -type, then the equation is provided by

$$\left(\frac{\kappa''}{\kappa} - \kappa^2(1 + \frac{1}{H^2})\right) = 0 \, , \, \left(\frac{3H\kappa' - \kappa H'}{H^2}\right) = 0.$$

Proof From equations (7) and (23) , the proof is obvious.

Theorem 3.11 If the curve γ is a harmonic curve of the modified $AW(2)$ -type, then the equation is given by

$$\frac{\left\{ \begin{array}{l} 3H\,\kappa'^2 - \kappa\kappa'\,H' \\ -H\kappa\kappa'' + \kappa^4 H(1 + \frac{1}{H^2}) \end{array} \right\}}{\kappa H^2} = 0. \tag{29}$$

Proof If equations (22) and (23)substitute into equation (8), then we get equation(29).

Corollary 3.3 If the curve γ is the general helix of the modified $AW(2)$ -type with harmonic curvature, then the equation is given by

$$3\kappa'^2 - \kappa\,\kappa'' + \kappa^4(1 + \frac{1}{H^2}) = 0.$$

Theorem 3.12 If the curve γ is a harmonic curve of the modified $AW(3)$ -type, then the equation is given by

$$3H\kappa' - \kappa\,H' = 0. \tag{30}$$

Proof If equations (21) and (23) are substituted into equation (9), then we get equation (30).

Corollary 3.4 Let the curve γ be a harmonic curve of the modified $AW(3)$ -type curve. If γ is a general helix, then γ is a circular helix.

Proof As the curve γ be a helix, H is constant and $H' = 0$. By equation (30), we have

$3H\kappa' = 0$. Since $H \neq 0$, $\kappa' = 0$ and $\tau = $ constant, thus γ is a circular helix.

3.3 Slant Helices in the Modified Orthogonal Frame

Corollary 3.5 If the curve γ is a slant helix belonging to the osculating order 3 in E^3 , then the curvature equation is provided by

$$\tau' = c(\kappa^2 + \tau^2)^{\frac{3}{2}}, \quad c \in \mathbb{R}. \tag{31}$$

Theorem 3.13 Let the curve γ be a slant helix belonging to the osculating order 3 in E^3 . If the curve γ is of the $AW(1)$ -type, then the formula is provided by

$$\kappa'' = \left(\begin{array}{l} \frac{3}{2}\frac{c_1}{c}\left\{ \frac{\kappa'}{\kappa^4}(\kappa^6 + c^2)^{\frac{3}{2}} - 9\kappa^5\kappa'(\kappa^6 + c^2)^{\frac{1}{2}} \right\} \\ -\kappa^3 - \frac{c^2}{\kappa^3} = 0. \end{array} \right).$$

Proof From derivated equation (13),

$$\tau' = -\frac{2c\kappa'}{\kappa^3}$$

is obtained. If we substitute equation (13) into equation (14), then we get the proof.

Theorem 3.14 Let γ be a slant helix belonging to the osculating order 3 in E^3 . If γ is of the $AW(2)$ - type, then the equation is provided by

$$2\tau\left(\kappa'\right)^2 + c_1\left(\kappa^2 + \tau^2\right)^{3/2}\kappa'\kappa - \kappa^4\tau - \tau\kappa\kappa'' + \tau^3\kappa^2 = 0. \tag{32}$$

Proof Using equation $\left(31\right)$ and equation $\left(14\right)$ we obtain equation $\left(32\right)$.

Theorem 3.15 Let the curve γ be a slant helix belonging to an osculating order 3 in E^3 . If γ is of the $AW(3)$ - type, then the formula is provided by

$$2c\kappa^3\kappa' + c_1(\kappa^6 + c^2)^{3/2} = 0.$$

Proof Since the curve γ is a slant helix of $AW(3)$ - type equations $\left(15\right)$, $\left(16\right)$ and $\left(31\right)$ hold.

38

4. DISCUSSION AND CONCLUSION

In 1999, Arslan et al. [2] reduced the notion of a submanifold of type $AW(k)$ to a curve of type $AW(k)$ and showed the relations between the first and second curvatures of such curves with respect to the Frenet frame.

In this study, we first define $AW(k)$-type curves determined by the modified orthogonal frame in 3-dimensional Euclidean space and obtain some relations between their curvatures that the curve is $AW(k)$-type curves. Then, the first harmonic curvature of this curve according to the modified orthogonal frame is found and the condition needed that is both sufficient and necessary for the curve to be a general helix is given. In addition, the curve is $AW(k)$-type curves, the first harmonic curvature, and some relations between the curvatures are found and a conclusion is given about the general helix and circular helix.

Finally, slant helices according to the modified orthogonal frame are analyzed and some relations are obtained for the curvatures of the curve to be $AW(1)$-type curve and $AW(2)$-type curve in case the curve is a slant helix.

This study will shed light on the characterization of $AW(k)$-type curves for different frames for researchers working in this field.

REFERENCES

[1] Arslan K, West A. Product submanifolds with point-wise 3-planar normal sections. Glasgow Mathematical Journal. 1995; 37(1):73–81.

[2] Arslan K, Özgür C. Curves and surfaces of AW (k) type. In Geometry and Topology of SubmanifoldsIX. 1999; 21–26.

[3] Özgür C, Gezgin F. On some curves of AW(k)-type. Differential Geometry Dynamical Systems. 2005; 7:74.

[4] Kılıç B, Arslan K. On curves and surfaces of AW(k)-type. Journal of the Institute of Science and Technology of Balıkesir University. 2004; 6(1):52-61.

[5] Kişi İ, Öztürk G. Bishop Çatısına Göre AW (k)-Tipinden Eğriler. Afyon Kocatepe University Journal of Science and Engineering. 2019; 19(3):620-625.

[6] Külahcı M, Öğrenmiş AO, Ergüt M. New characterizations of curves in the Galilean space G^3. International Journal of Physical and Mathematical Sciences. 2010; 1(1).

[7] Sun J, Pei D. Null Cartan Bertrand curves of AW (k)-type in Minkowski 4-space. Physics Letters A. 2012; 376(33):2230-2233.

[8] Gür S, Şenyurt S. Frenet vectors and geodesic curvatures of spheric indicators of Salkowski curve in E^3. Hadronic Journal. 2010; 33(5):485.

[9] Hacisalihoğlu HH. Differential geometry. Ankara University Faculty of Science Press. Ankara; 2000.

[10] Şenyurt S, Çalışkan A. Smarandache curves of Mannheim curve couple according to Frenet frame. Mathematical Sciences and Applications E-Notes. 2017; 5(1):122-136.

[11] Do Carmo MP. Differential geometry of curves and surfaces: revised and updated second edition. Courier Dover Publications; 2016.

[12] Bishop RL. There is more than one way to frame a curve. The American Mathematical Monthly. 1975; 82(3):246–251.

[13] Yılmaz S, Turgut M. A new version of Bishop frame and an application to spherical images. Journal of Mathematical Analysis and Applications. 2010; 371(2):764-776.

[14] Damar E, Yüksel N, Vanlı AT. The ruled surfaces according to type-2 Bishop frame in E^3. In International Mathematical Forum 2017; 12(3):133-143.

[15] Damar E, Yüksel N, Karacan MK. Ruled surfaces according to parallel trasport frame in E^3. Mathematical Combinatorics.2020; 20.

[16] Yüksel N. The ruled surfaces according to Bishop frame in Minkowski 3-space. In Abstract and Applied Analysis.2013; (2013): 810640

[17] Hord RA. Torsion at an inflection point of a space curve. The American Mathematical Monthly.1972; 79(4):371-374.

[18] Sasai T. The fundamental theorem of analytic space curves and apparent singularities of Fuchsian differential equations. Tohoku Mathematical Journal, Second Series.1984; 36(1):17-24.

[19] Sasai T. Geometry of analytic space curves with singularities and regular singularities of differential equations. Funkcial. Ekvac.1987; 30, 283-303.

[20] Bükçü B, Karacan MK. On the modified orthogonal frame with curvature and torsion in 3-Space. Mathematical Sciences and Applications E-Notes. 2016; 4(1):184-188.

[21] Bükçü B, Karacan MK. Spherical curves with modified orthogonal frame. Journal of New Results in Science.2016; 5(10):60-68.

[22] Gür S, Bektaş M. On the modified orthogonal frames of the non-unit speed curves in Euclidean Space E^3. Turkish Journal of Science.2022; 7(2):58-74.

[23] Lone MS, Es H, Karacan MK, Bükçü B. On some curves with modified orthogonal frame in Euclidean 3-space. Iranian Journal of Science and Technology, Transactions A: Science.2019; 43:1905-1916.

[24] Uddin S, Stankovi´c MS, Iqbal M, Yadav SK, Aslam M. Slant helices in Minkowski 3-space E_1^3 with Sasai's modified frame fields. Filomat.2022; 36(1):151-164.

[25] Yüksel N, Karacan MK, Demirkıran T. Spherical curves with modified orthogonal frame with torsion. Turkish Journal of Science.2022; 7(3):177-184.

[26] Yüksel N, Ogras N. Canal surfaces with modified orthogonal frame in Minkowski 3-Space. Acta

Universitatis Apulensis Mathematics-Informatics.2022;70.

[27] Gür Mazlum S, Şenyurt S, Bektaş, M. Salkowski curves and their modified orthogonal frames in E3. *Journal of New theory*. 2022; *40*, 12-26.

[28] Arslan K, Çelik Y, Hacısalihoglu HH. On harmonic curvatures of Frenet curve. Commum. Fac. Sci. Univ. Ank. Series A1.2000; 49:15-23.

[29] Izumiya S, Takeuchi N. New special curves and developable surfaces. Turkish Journal of Mathematics.2004; 28(2):153-164.

Türk Doğa ve Fen Dergisi
Turkish Journal of Nature and Science

www.dergipark.gov.tr/tdfd

BINGÖL UNIVERSITY

Weldability of Dissimilar 316L and A106 Steels with GTAW and SMAW Using 309L and Inconel 82 Electrodes

Esin Tuğba ŞİMŞEK ÇELİK[1]* iD , Başar Ersegün ÇELİK[2] iD , Şükrü TALAŞ[3] iD

[1] Sivas Cumhuriyet University, Hafik Kamer Ornek Vocational School of Higher Education, Department of Transportation Services, Rail Systems Management Program, Sivas, Türkiye
[2] Afyon Kocatepe University, Institute of Natural Sciences, Afyonkarahisar, Türkiye
[3] Afyon Kocatepe University, Faculty of Technology, Department of Metallurgical and Materials Engineering, Afyonkarahisar, Türkiye
Esin Tuğba ŞİMŞEK ÇELİK ORCID No: 0000-0003-2063-7802
Başar Ersegün ÇELİK ORCID No: 0000-0002-3015-2553
Şükrü TALAŞ ORCID No: 0000-0002-4721-0844

Corresponding author: esimsek@cumhuriyet.edu.tr

(Received: 06.06.2024, Accepted: 22.10.2024, Online Publication: 30.12.2024)

Keywords	**Abstract:** The mechanical properties of steel welds of different compositions are affected by the mechanical properties of the filler wires used, and it is important for practitioners to analyze the results in situ without detailed metallographic studies. In this study, the joining of the material pair A 312 TP 316L stainless steel and A106 Gr.B carbon steel was investigated by Tungsten Inert Gas (TIG) and Shielded Metal Electrode Welding (SMAW) using different welding wires and different welding parameters. In the first welding process, A 312 TP 316L stainless steel and A106 Gr.B carbon steel materials were welded by GTAW (Gas Tungsten Arc Welding) method using 2.4 mm ER309L electrode for root and hot passes and by SMAW (Shielded Metal Arc Welding) method using 2.5 mm E309L-15 electrode for filler and cover passes. In the second welding process, A 312 TP 316L stainless steel and A106 Gr.B carbon steel materials were welded by GTAW method using 2.4 mm INCONEL 82 (ER NiCr-3) electrode for root and hot passes and by SMAW method using 2.5 mm INCONEL 182 (E NiCrFe-3) electrode for filler and cover passes. Tensile test, bending test, hardness test, PMI (Positive Material Identification) test carried out and macro images of the welded parts were taken and compared. As a result, the weldability of stainless and carbon steels with different filler metals and their effects on mechanical properties were investigated. The results show that welding with E309L stainless steel gives better results than welding with Inconel 182.
Weldability, Inconel Electrodes, 316L, A106, GTAW, SMAW	

41

Benzer Olmayan 316L ve A106 Çeliklerin, GTAW ve SMAW ile 309L ve Inconel 82 Elektrotlar Kullanılarak Kaynaklanabilirliği

Anahtar Kelimeler	**Öz:** Farklı bileşimlere sahip çelik kaynaklarının mekanik özellikleri, kullanılan dolgu tellerinin mekanik özelliklerinden etkilenmektedir ve uygulayıcılar için detaylı metalografik çalışmalar yapmadan sonuçları yerinde analiz etmek önemlidir. Bu çalışmada, A 312 TP 316L paslanmaz çelik ve A106 Gr.B karbon çeliği malzeme çiftinin birleştirilmesi, farklı kaynak telleri ve farklı kaynak parametreleri kullanılarak Tungsten İnert Gaz (TIG) ve Korumalı Metal Elektrot Kaynağı (SMAW) ile incelenmiştir. İlk kaynak işleminde, A 312 TP 316L paslanmaz çelik ve A106 Gr.B karbon çelik malzemeler kök ve sıcak pasolar için 2.4 mm ER309L elektrot kullanılarak GTAW (Gaz Tungsten Ark Kaynağı) yöntemiyle ve dolgu ve örtü pasoları için 2.5 mm E309L-15 elektrot kullanılarak SMAW (Korumalı Metal Ark Kaynağı) yöntemiyle kaynaklanmıştır. İkinci kaynak işleminde, A 312 TP 316L paslanmaz çelik ve A106 Gr.B karbon çelik malzemeler, kök ve sıcak pasolar için 2,4 mm INCONEL 82 (ER NiCr-3) elektrot kullanılarak GTAW yöntemiyle ve dolgu ve örtü pasoları için 2,5 mm INCONEL 182 (E NiCrFe-3) elektrot kullanılarak SMAW yöntemiyle kaynaklanmıştır. Çekme testi, eğme testi, sertlik testi, PMI (Positive Material Identification) testi yapılmıştır ve makro görüntüleri alınmış ve karşılaştırılmıştır. Sonuç olarak, paslanmaz ve karbon çeliklerin farklı dolgu metalleri ile kaynaklanabilirliği ve mekanik özellikler üzerindeki etkileri araştırılmıştır. Sonuçlar paslanmaz çelik E309L kullanılarak yapılan kaynakların Inconel 182 ile yapılan elektrodlara göre daha iyi sonuçlar verdiğini göstermektedir.
Kaynak Kabiliyeti, Inconel Elektrotlar, 316L, A106, GTAW, SMAW	

1. INTRODUCTION

Austenitic stainless steels (ASSs) are extensively employed due to their superior mechanical properties and excellent corrosion resistance [1,2]. The microstructure of ASSs is primarily influenced by alloying elements like Ni and Cr, which contribute to a fully-austenitic structure, ensuring weldability, strength at room and high temperatures, oxidation resistance, and corrosion resistance [3]. These steels are often preferred for the use in seawater and various chemical environments, but the choice of a specific steel grade with an appropriate chemical composition is crucial, depending on the environmental conditions [4-6]. A 312 TP 316L steels provide, among the most commonly used ASSs, significantly enhanced strength, creep resistance, and notably, corrosion resistance, especially in highly-corrosive settings such as chloride-containing environments, seawater, chemical environments, and sub-zero temperatures [6,7]. Carbon steel alloy pipes of grade A106-Gr.B are typically employed in power plants, boilers, oil and gas refineries, as well as in ship manufacturing applications, under conditions of elevated pressures and temperatures. In the petroleum refineries, these steel pipelines play a crucial role in conveying gas, oil, and their derivatives from the production area to local markets or for export [12]. Fusion welding of A 312 TP 316L and A106 Gr.B is essential due to its widespread applications across various industries. Several fusion welding processes, including Gas Tungsten Arc Welding (GTAW) [8,9], Shielded Metal Arc Welding (SMAW) [10] have been utilized for fabricating A 312 TP 316L joints and A106 Gr.B joints. The mechanical properties and corrosion resistance of these joints are influenced by the chemical composition and solidification of the weld metal during fusion welding processes [8-11]. SMAW is a metal joining process that holds a predominant position in small-scale industries and remains extensively employed in domestic, maintenance, fabrication, and offshore applications [13], which can efficiently operate with both alternating and direct current power sources, depending on specific requirements [14,15]. On the other hand, GTAW process is an electric arc welding technique that utilizes non-consumable tungsten electrodes with filler metal is introduced through a separate filler rod using commonly used shielding gases that include argon, helium, nitrogen, hydrogen, or a mixture thereof [16]. In their study, Pahlawan et al. [17] analyzed the effect of the welding electrode on the tensile strength, macrostructure and microstructure of steel ST41 and 316L stainless steel weld metal. The two electrode types used in the study were E309-L and E6013 with SMAW process. Tensile test results showed that the welding process produced the maximum tensile strength greater than the parent material strength level. It has been found that welding with E6013 tends to have a lower corrosion resistance. In their study, Sirohi et al. [18] prepared a different welded joint from Inconel 718 and 304L austenitic stainless steel using a combined procedure with GTAW and SMAW processes using Ni-based fillers: ERNiCr-3 and ENiCrFe-3. Welded joints were investigated in terms of metallographic tests and mechanical properties, and a relationship between the microstructure and the resulting mechanical properties

was established. Room temperature tensile test results showed that damage to the weld metal could result from the partition of alloying elements along the dendritic gaps. It was observed that the impact resistance of the weld metal was quite low compared to the base metals, and it was thought that this may be due to the formation of the NbC phase along the dendritic gaps. Ni-based super alloy Inconel 625 and stainless steel AISI 304L base materials were joined by TIG (Tungsten Inert Gas) method using ER310 and ERNiCrMo3 filler metals Tümer & Kerimak [19]. Due to Ni content of filler metals, all notch impact test samples displayed ductile nature after fracture. Additionally, ERNiCrMo3 filler metal displayed improved notch impact toughness results in comparison to other filler metals.

In this study, two separate welding processes were used to investigate the compatibility of Inconel 82/Inconel 182 and 309L filler metals for joining 316L and A106 carbon steels, and to observe whether sufficient mechanical properties were provided by dissimilar welds deposited by two different welding processes. Tensile tests, hardness tests, bend tests and PMI tests were carried out on the welds and their effects on weld quality were discussed.

2. MATERIAL AND METHOD

2.1. Preparation and Assembly of Test Samples for Welding Process

It is well known that increasing the carbon content of steel leads to reduced weldability due to cracking as a result of thermal stresses and the presence of hard phases such as martensite during the cooling stage. However, the situation becomes more complicated when ferrite-promoting alloying elements such as Cr are introduced during welding; the weld metal is at risk of containing carbides, reducing the mechanical properties of the weld metal. To prevent the formation of chromium carbides, Ni-containing alloys are effectively used, as was the idea behind this research. The chemical composition of the 7.11 mm thick 316L stainless steel and A106 Gr.B carbon steel used in this study is shown in Table 1. In the first welding process, A 312 TP 316L and A106 Gr.B materials were joined by GTAW method using 2.4 mm ER309L electrode, and SMAW method using 2.5 mm E309L-15 electrode. The first welding process was given the code W-309. In the second welding process, A 312 TP 316L and A106 Gr.B materials were joined by GTAW process using 2.4 mm INCONEL 82 (ER NiCr-3) electrode, and SMAW welding method using 2.5 mm INCONEL 182 (E NiCrFe-3) electrode. The second welding process was given the code of W-INC.

The base metal, electrodes, welding processes and passes used in the W-309 coded welding process and W-INC coded welding process are shown in Figure 1. The chemical compositions of the electrodes are given in Table 2.

In the W-309 coded welding process, root pass and hot pass were made by the GTAW method, filler pass and two cover passes were made by the SMAW method, whereas

in the W-INC coded welding process, the root pass and the hot pass were made by the GTAW method and filler pass and two cover passes were made by the SMAW method. The weld groove and weld passes for the W-309 and W-INC coded welding process are shown in Figure 2.

The design of weld passes, operating parameters of weld deposition i.e. the welding current and voltage, weld/electrode travel speed and the total heat input values of the W-309 and W-INC welding processes are given in Table 3 and Table 4.
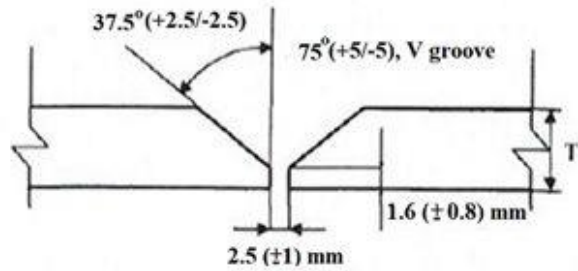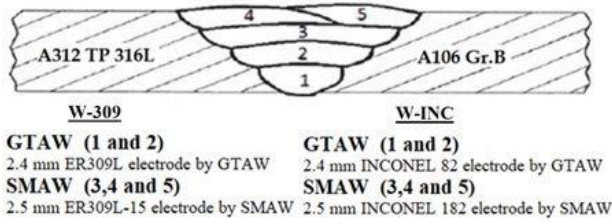
Figure 1. Base metals, electrodes, welding methods and welding passes used in W-309 and W-INC coded welding processes

Figure 2. Weld groove measurements

Table 1. Chemical compositions of A 312 TP 316L and A106 Gr.B base metals (Fe: Bal. and in wt. %)

	C	Si	Mn	P	S	Cr	V	Mo	Ni	Cu	B	Nb	Ti	N
A106 Gr B	0.12	0.27	1.07	0.012	0.003	0.03	0.01	0.01	0.03	0.04	0.0004	0.001	0.02	-
316L	0.013	0.38	1.41	0.026	0.001	16.75	-	2.11	11.4	0.36	-	-	-	0.065

Table 2. Chemical compositions of the electrodes (wt. %)

	C	Si	Mn	P	S	Cr	Mo	Ni	Cu	Nb	Ti	Fe
ER309LSİ	0.01	0.7	2	0.01	0.01	23	0.13	13.9	0.1	-	-	-
E309L-15	0.04	0.34	2.1	0.013	0.003	23.5	0.17	13	0.05	-	-	-
ERNiCr-3 (INCONEL 82)	0.03	0.08	3.1	0.01	0.001	20.1	-	72.3	0.01	2.4	0.3	1.3
ENiCrFe-3 (INCONEL 182)	0.04	0.8	5.8	0.01	0.014	16	-	69.2	-	1.8	0.1	5.9

43

Table 3. Weld passes, weld current, weld voltage, weld/electrode travel speed and overall heat input values in the W-309 coded welding process

Weld Layers	Welding Process	Class	Diameter (mm)	Polarity	Weld Current Range (A)	Weld Voltage Range (V)	Travel Speed (mm min^{-1})	Heat input (KJ mm^{-1})
Root	GTAW	ER309L	2.40	DC(-)	107-111	10-12	36.00	2.22
Hot	GTAW	ER309L	2.40	DC(-)	145-150	11-13	87.00	1.34
Fill	SMAW	ER309L-15	2.50	DC(+)	70-75	24-26	84.00	1.39
Cover	SMAW	ER309L-15	2.50	DC(+)	85-90	22-23	94.00	1.32
Cover	SMAW	ER309L-15	2.50	DC(+)	85-90	22-23	93.00	1.33

Table 4. Weld passes, weld current, weld voltage, weld/electrode travel speed and overall heat input values in the W-INC coded welding process

Weld Layers	Process	Class	Diameter (mm)	Polarity	Weld Current Range (A)	Weld Voltage Range (V)	Travel Speed (mm min^{-1})	Heat input (KJ mm^{-1})
Root	GTAW	INCONEL 82	2.40	DC(-)	100-110	10-11	32.64	2.02
Hot	GTAW	INCONEL 82	2.40	DC(-)	150-160	13-14	77.63	1.61
Fill	SMAW	INCONEL 182	3.25	DC(+)	90-95	19-20	110.48	0.97
Cover	SMAW	INCONEL 182	3.25	DC(+)	80-85	18-19	114.90	0.79
Cover	SMAW	INCONEL 182	3.25	DC(+)	80-85	18-19	112.65	0.81

During the execution of GTAW, pure argon gas was used as shielding gas with flow rate of 12-16 lt min-1. ESAB

TIG 3001i make and model welding machine was used for GTAW passes.

2.2. Mechanical and Hardness Tests Applied to Welded Parts

Mechanical tests, i.e. tensile test (DIN EN ISO 6892-1), bending (ASTM E290) and hardness tests were performed on welded parts and macro images were taken after metallographic preparation. In addition, PMI (Positive Material Identification) tests were also carried out. The

hardness tests were carried out using Qness brand hardness tester device with a setting of HV10 (10kgf) using Vickers tip. Instron-5989 was used as the tensile test device and a cross-head speed of 3 mm min-1 was used. In the bending tests, 4 bending test specimens (BT) from the W-309 and the W-INC coded welding processes were used. The parameters and conditions employed in the bending tests are given in Table 5.

Table 5. Parameters used for bending test

Sample	Distance Between Rollers (mm)	Diameter of Mandrel (mm)	Bending Angle
W-309-BT1			
W-309-BT2			
W-309-BT3			
W-309-BT4	51	30	180°
W-INC-BT1			
W-INC-BT2			
W-INC-BT3			
W-INC-BT4			

Hardness values were obtained from welds coded with W-309 and the W-INC welding process, on 15 points along the line for the cover pass and at 15 points along the line for the root pass.

3. RESULTS AND DISCUSSION

3.1. Microhardness Test Results

The microhardness distribution values for the W-309 coded weld are shown in Figure 3 and the hardness distribution values for the W-INC coded weld are shown in Figure 4. Microhardness values were obtained from the W-309 and W-INC coded welds at 15 points along the cover pass line and 15 points along the root pass line. The distribution of 15 points taken from the root and cover pass is as follows. Hardness measurement points 1, 2, 3 are from 316 stainless steel base material; points numbered 4, 5, 6 are from 316 stainless steel HAZ (Heat Affected Zone), points numbered 7, 8, 9 are from weld filler metal; points 10, 11, 12 are taken from A 106 Gr.B carbon steel HAZ and points 13, 14, 15 are taken from A 106 Gr.B carbon steel base material.
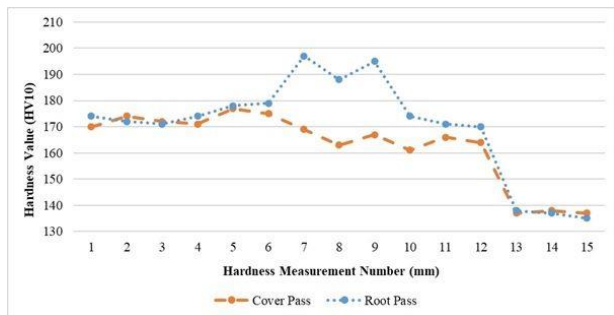
Figure 3. Hardness distribution for base metals, heat affected zones and weld metal in W-309 series
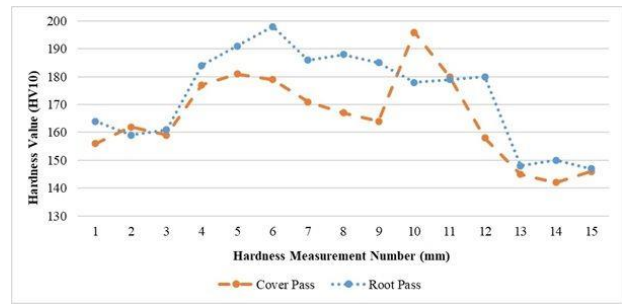
Figure 4. Hardness distribution for base metals, heat affected zones and weld metal of W-INC series

Figures 3 and Figure 4 show the microhardness values for the cover pass and root pass for W-309 and W-INC coded welds, respectively; it can be seen that the average root pass microhardness value is higher than the average cover pass microhardness value in the weld metal. The lowest hardness value is 135HV measured in the A106 Gr.B base metal zone and the highest hardness value is 197HV, which is the value in the root pass weld metal zone. Considering the average hardness values, the average hardness values for the W-INC coded welds are slightly higher. Although the base metals and number of passes are the same for both welding processes, the electrodes used are different. For W-INC, welding using INCONEL 82 (ER NiCr-3) and INCONEL 182 (E NiCrFe-3) electrodes produced higher hardness than welding with ER309L and E309L-15 electrodes. It can be assumed that the reason for such variation could be related to the matrix hardness, which caused such a small variation in hardness despite the fact that the root weld metal contains less Si. Higher Si content increases the strength and hardness of stainless steels. Si addition leads to the formation of high amount of γ phase precipitated in eutectic nodules and significantly promotes a $Mo(Ni,Si)_2$ Laves phase in the alloys containing Mo [20,21]. Interestingly, the W-309 welds should contain a higher amount of Si, but the effect is not obviously observed as their hardness is lower on average, which may be due to Si loss or weld tempering and redistribution of elements during high heat input deposition of the cover pass. However, the W-INC series also suffers from the same effect, so it can be argued that the top layer depositions are inherently less hard due to factors such as highly tempered and reduced microstructural content and also internal stresses. The root passes and other passes are always tempered with the subsequent weld pass deposited on top of each other and therefore the grain sizes in the heat affected zone and the weld zone can be altered to a limited extent due to the heat input effect both in the base metal and in the vicinity of the weld zone [22]. The root pass weld is also annealed with the hot pass weld, but the stress development may not be as effective for surface-facing passes such as root welds, which may result in higher residual stresses in the weld and higher microhardness results. Another factor by which the hardness may increase is that the formation of intermetallics in superalloy welds [23,24], however, it is not always desirable to have intermetallics phases as they may lead to the formation of stresses leading to cracks or resulting in the excessive hardness of matrix [25,26]. In Figure 4, the cover pass and root pass hardness values are given for the W-INC coded welding joint, and it is seen that the root pass hardness value has a slightly higher

hardness than the cover pass hardness value in the weld filler. The highest hardness value is 198HV, which is the Heat Affected Zone value of the root pass. The presence of higher amounts of Ni, Cr and Mo in electrode for root weld may have led to the formation of harder phases which may have increased the hardness of this zone. The lowest hardness value is 147HV in the A106 Gr.B base metal region.

3.2. Macro Image Interpretation and PMI Test Results

The macro images of the W-309 coded and the W-INC coded welding processes are shown in Figure 5a and b. It was determined that the welding method coded W-309 which involves the electrodes of ER309L and E309L-15 that are frequently used in the industrial applications in the joining of A 312 TP 316L and A106 Gr.B materials have good weld penetration property and that there is no observed discontinuity or defect on the weld surface and on base metal.
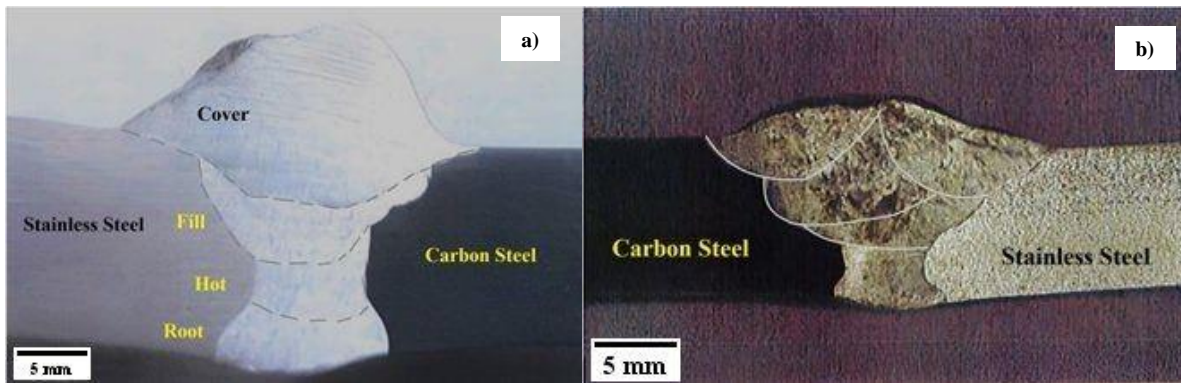
Figure 5. Macro images of **a)** W-309 coded welding process and **b)** W-INC coded welding process

As shown in Figure 5b, a discontinuity type structure was encountered in the sample welded with INCONEL 82 (ER NiCr-3) and INCONEL 182 (E NiCrFe-3) electrodes, specifically on the 316L side. In addition, the appearance of different microstructures can also be seen in the weld metal produced with INCONEL electrodes.

3.3. PMI Values After Welding Processes

PMI values for the W-309 and W-INC coded welding process were measured after each welding process and are given in Table 6.

Table 6. Positive Material Identification (PMI) values for W-309 and W-INC coded welding process

	Positive Material Identification (PMI)						
	W-309	**Cr**	**Ni**	**Mn**	**Mo**	**Ti**	**Fe**
316L	(Base Metal) BM1	16.81	11.6	-	2.08	-	Bal.
309L	(Weld Metal) WM1	22.94	13.05	-	-	-	Bal.
A106	(Base Metal) BM2	0.03	0.06	1.16	-	-	Bal.
	W-INC	**Cr**	**Ni**	**Mn**	**Mo**	**Ti**	**Fe**
316L	(Base Metal) BM1	16.51	10.29	-	2.14	-	Bal.
Inconel	(Weld Metal) WM1	16.52	61.14	-	0.073	1.02	Bal.
A106	(Base Metal) BM2	0.024	0.039	1.16	-	-	Bal.

As can be observed from Table 6 that there is a little variation in base metal compositions regarding Mn, C, Cr, N, and Mo, however, the Cr and Ni contents of weld metals in both weld processes are different with respect to electrode compositions. This may be due to the fact that the electrodes used in welding are different even though the base metals are the same. This is expected when base metals and electrode compositions are dissimilar and a mixing of base metal and electrode at a ratio of, for example, 50% is assumed to occur. This dilution is more apparent when two distinctive compositions are used for welding [26,27]. The calculations based on the Creq and Nieq values show that, 316L base steel falls within austenite or right at the border of Austenite 5% ferrite zone (Creq: 19.43, Nieq: 12.5) according to Schaffler diagram whereas the electrode materials i.e. ER309LSi and ER309L15 fall in Austenite+10% ferrite zone (Creq:24.18 + Nieq:15.25). On the other hand, weld metal

composition of W-309 weld process based on Cr and Ni values shows that W-309 weld metal is fully austenitic, which can be understood from the featureless appearance of weld metal cross section, too. Elements from the electrode chemical content have a strong effect on the final composition of weld metal [28]. It is such that in the W-309 coded welding process, the weld metal has a higher Cr content (from 16.75 to 22.94 wt%) and higher Ni content (from 11 to 13 wt%) whereas the W-INC coded welding process weld metal has produced lower Ni percentages (from 69 to 61 wt%) and higher Ti content (from 0.1 to 1.02 wt%). It is interesting note that the increase in Ti content is very high compared to filler metals and base metal contents of Ti. Some losses of alloying elements apart from Ti may have occurred due to evaporation as a result of high heat released during welding process, increasing the amount of Ti in the weld metal.

3.4. Tensile Test and Bending Test Results

The samples for which tensile and bending tests were performed are shown in Figure 6. A 3-point 180° bending test was applied to the test piece samples. The samples showed successful performance in the 180° bending test, and although the materials were bent 180°, they did not break. There was no tearing was observed, and no visible discontinuity or defect was detected along the bent surface. The successful results of the samples that were exposed to 180° three point bending test showed that the welding process was carried out correctly and the selected filler metals were suitable for material combination selected for this process.

Figure 6. Tensile and 180° three point bending tested samples

Tensile test results on samples obtained from the welding process coded W-309 and coded W-INC are given in Table 7. The tensile test results are given in Figure 7.

Table 7. Cross sectional area, flow stress, Fmax, elongation and maximum tensile strength values obtained from specimen the welding process coded W-309 and W-INC

Sample	Cross-sectional area (mm^2)	$R_{0,2}$ (N mm^{-2})	Fmax (kN)	Rm (N mm^{-2})	Elongation (%)
W-309-1	138	462	77.7	563	28.33
W-309-2	138	451	76.45	554	27.33
W-INC-1	189.05	286	96.2	50884	29.9
W-INC-2	190	286.37	97.86	515.07	29.83
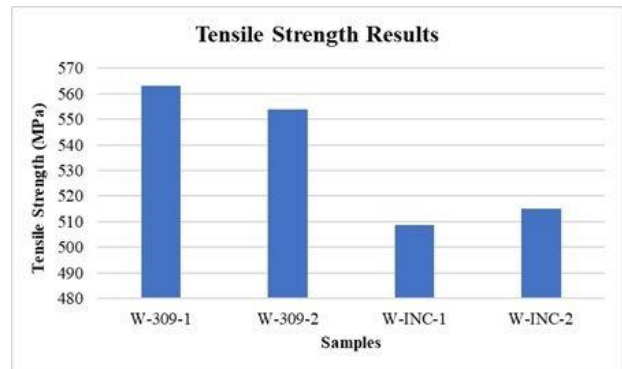
Figure 7. Comparative table for tensile strengths of W-309-1, W-309-2, W-INC-1, W-INC-2

As a general requirement for the successful joint, the tensile strength of the weld zone of the welded samples should be higher than the tensile strength of the base metal. Dissimilar joints can be, on the other hand, may differ depending on the amount and type of filler metal compositions. In this study, high amount of Ni, Cr and Nb in INCONEL filler metals results in the hardening of weld metals in W-INC series but bending tests indicate that both weld metals do not fail and but deforms in ductile manner owing to high amount of Ni present in the weld metal and stainless steel, which can be also be observed in some dissimilar steel produced with stainless steel and carbon steels [28-30]. In the test samples (Figure 6), the appearance of cracking of bent surfaces followed by the rupture occurred on A106Gr.B carbon steel side, one of the base metals. Yield and ultimate tensile strength values of welds made with ER309L and E309L-15 filler metals, are slightly higher than those of samples made with INCONEL 82 (ER NiCr-3) and INCONEL 182 (E NiCrFe-3) filler metals, as a result of high amount of austenite or Ni in microstructures of INCONEL containing welds. However, there is almost no difference in tensile strength values within the groups of welds tested for different zones of the welds.

4. CONCLUSION

Following conclusions can be drawn from this study:

1. Bending test results showed that the samples failed in base metal, namely A106Gr.B carbon steel, and no visible discontinuity or error was detected in weld metal.
2. It was concluded that yield and tensile strength values of welds made with ER309L and E309L-15 filler metals are higher than the welds made with INCONEL 82 (ER NiCr-3) and INCONEL 182 (E NiCrFe-3) filler electrodes.
3. The root pass hardness value for W-309 coded weld metal has a higher hardness than the cover pass hardness value of the weld filler metal. The root pass hardness value for the W-INC coded weld metal has a higher hardness than the cover pass hardness value in the weld filler.
4. Considering the average hardness values, the average hardness values for the W-INC coded welding process are higher; INCONEL 82 (ER NiCr-3) and INCONEL 182 (E NiCrFe-3) electrodes produced

higher matrix hardness than ER309L and E309L-15 electrodes.

5. It was determined that ER309L and E309L-15 electrodes used in the joining of A 312 TP 316L and A106 Gr.B produced good weld penetration with no discontinuity or defects in the weld surface and base metal. However, INCONEL 82 (ER NiCr-3) and INCONEL 182 (E NiCrFe-3) electrodes produced a slightly less penetration, especially on the 316L side of the welds.

6. Some changes in the compositions of weld metals have been observed after welding processes, which may be due possibly to the fact that the electrodes used in welding passes are different compared to base metals.

REFERENCES

[1] Chuaiphan W, Srijaroenpramong L. Effect of hydrogen in argon shielding gas for welding stainless steel grade SUS 201 by GTA welding process. Journal of Advanced Joining Processes. 2020;1:100016.

[2] Zhu Z, Ma X, Wang C, Mi G, Zheng S. The metallurgical behaviors and crystallographic characteristic on macro deformation mechanism of 316 L laser-MIG hybrid welded joint. Materials & Design. 2020;194:108893.

[3] Sirohi S, Pandey C, Goyal A. Role of heat-treatment and filler on structure-property relationship of dissimilar welded joint of P22 and F69 steel. Fusion Engineering and Design. 2020;159:111935.

[4] Sharma P, Dwivedi DK. A-TIG welding of dissimilar P92 steel and 304H austenitic stainless steel: Mechanisms, microstructure and mechanical properties. Journal of Manufacturing Processes. 2019;44:166-178.

[5] Malhotra D, Shahi AS. Metallurgical, fatigue and pitting corrosion behavior of AISI 316 joints welded with Nb-based stabilized steel filler. Metallurgical and Materials Transactions A. 2020;51:1647-1664.

[6] Yu D, Tian J, Dai J, Wang X. Corrosion resistance of three-layer superhydrophobic composite coating on carbon steel in seawater. Electrochimica Acta. 2013;97:409-419.

[7] Sajjadnejad S, Saleh Haghshenas SM, Tavangar M, Ghani Kolahloo A. Creep behavior of 316 austenitic stainless steel under variant operating conditions. Asian Journal of Nanoscience and Materials. 2021;3:266-279.

[8] Kant R, Mittal R, Kumar C, Rana BS, Kumar M, Kumar, R. Fabrication and characterization of weldments AISI 304 and AISI 316 used in industrial applications. Materials Today: Proceedings. 2018;5(9):18475-18481.

[9] Venkatesu S, Gangaraju M, Bhaskar S, Naidu BVV. A study of laser beam welding, gas tungsten arc welding and high temperature brazing processes on micro hardness and tensile strength of AISI Type 316 stainless steel. Procedia Computer Science. 2018;133:10-18.

[10] Cui Y, Lundin CD. Austenite-preferential corrosion attack in 316 austenitic stainless steel weld metals. Materials & Design. 2007;28(1):324-328.

[11] Pujar MG, Dayal RK, Gill TPS, Malhotra SN. Evaluation of microstructure and electrochemical corrosion behavior of austenitic 316 stainless steel weld metals with varying chemical compositions. Journal of Materials Engineering and Performance. 2005;14:327-342.

[12] Cramer SD, Covino Jr BS. Corrosion: Fundamentals, Testing, and Protection, Volume 13A, ASM Handbook. Journal of Thermal Spray Technology. 2003;12(4):459.

[13] Bodude MA, Momohjimoh I. Studies on effects of welding parameters on the mechanical properties of welded low-carbon steel. Journal of Minerals and Materials Characterization and Engineering. 2015;3(03):142.

[14] Pathak D, Singh RP, Gaur S, Balu V. Experimental investigation of effects of welding current and electrode angle on tensile strength of shielded metal arc welded low carbon steel plates. Materials Today: Proceedings. 2020;26:929-931.

[15] Weerasekralage LSSK, Karunaratne MSA, Pathirana SD. Technical Papers; 2020.

[16] Magalhaes EDS, Lima e Silva ALFD, Lima e Silva SMM. A GTA welding cooling rate analysis on stainless steel and aluminum using inverse problems. Applied Sciences. 2017;7(2):122.

[17] Pahlawan IA, Arifin AA, Marliana E, Irawan H. Effect of welding electrode variation on dissimilar metal weld of 316l stainless steel and steel ST41. In IOP Conference Series: Materials Science and Engineering. 2021;1010(1):012001.

[18] Sirohi S, Pandey SM, Świerczyńska A, Rogalski G, Kumar N, Landowski M, et al. Microstructure and mechanical properties of combined GTAW and SMAW dissimilar welded joints between Inconel 718 and 304L austenitic stainless steel. Metals. 2022);13(1):14.

[19] Tümer M, Kerimak MZ. The effects of different filler metals on the toughness and microstructure properties of dissimilar welding of Nickel Base Super Alloy, Inconel 625 and Stainless Steel, AISI 304L. El-Cezerî Journal of Science and Engineering. 2017;4(1):116-126.

[20] Zhu HQ, Guo SR, Guan HR, Zhu VX, Hu ZQ, Murata V, et al. The effect of silicon on the microstructure and segregation of directionally solidified IN738 superalloy. Materials at High Temperatures. 1994;12(4):285–291.

[21] Xiong W, Zhou S, Zhang D, Huang Z, Wang Z, Wu H, et al. Effect of Si addition on the creep performance of a Ni-based superalloy. Materials Science and Technology. 2021);37(3): 292-300.

[22] Gao H, Dutta RK, Huizenga RM, Amirthalingam M, Hermans MJM, Buslaps T, et al. Pass-by-pass stress evolution in multipass welds, Science and Technology of Welding and Joining. 2014;19(3):256-264.

[23] Nohutçu S, Kaçar R, Ertek HE. Weldability of haynes 188 cobalt based superalloy and AISI 316L

47

austenitic stainless steel. Journal of Polytechnic. 2023;1:1.

[24] Sonar T, Balasubramanian V, Venkateswaran T, Xavier V, Agilan M, Manjunath A, et al. Minimizing intermetallic Laves phase evolution and enhancing precipitation strengthening of Superalloy-718 joints using InterPulse magnetic arc constriction and high frequency pulsation. Materials Science and Engineering: A. 2023;880:145323.

[25] Radhakrishna C, Prasad Rao K. The formation and control of Laves phase in superalloy 718 welds. Journal of Materials Science. 1997;32:1977-1984.

[26] Sun YL, Obasi G, Hamelin CJ, Vasileiou AN, Flint TF, Balakrishnan J, et al. Effects of Dilution on Alloy Content and Microstructure in Multi-Pass Steel Welds. J. Mater. Process. Technol. 2019;265:71-86.

[27] DuPont JN, Marder AR. Dilution in Single Pass Arc Welds. Metall. Mater. Trans. B. 1996;27(3):481-489.

[28] Taban E, Deleu E, Dhooge A, Kaluc E. Evaluation of dissimilar welds between ferritic stingless steels modified 12%Cr and carbon steel. Welding Journal. 2008;291-297.

[29] Kim JK, Hong SG, Kang KB, Kang CY. Microstructure and high temperature properties of the dissimilar weld between ferritic stainless steel and carbon steel. Met. Mater. Int. 2009;15:843-849.

[30] Chuaiphan W, Somrerk CA, Niltawach S, Sornil, B. Dissimilar welding between AISI 304 stainless steel and AISI 1020 carbon steel plates. Applied Mechanics and Materials. 2013;268:283-290.

Türk Doğa ve Fen Dergisi
Turkish Journal of Nature and Science
www.dergipark.gov.tr/tdfd

BINGÖL UNIVERSITY

Comparison of the Views of Local People Who Directly Benefited and Did Not Benefit from the Murat River Rehabilitation Projects

Alaaddin YÜKSEL[1] , Ahmet USLU[2] , Bayram HOPUR[3] , Ersin KARAKAYA[4] , Semra ÇAMUKA[5] , Şenol ÇELİK[6] , Mahmut YILMAZ[7]

[1] Alaaddin YÜKSEL, Bingöl University Faculty of Agriculture, Soil Science and Plant Nutrition, Türkiye
[2] Ahmet USLU, Bingöl Vocational School of Social Sciences / Office Services and Secretariat, Türkiye
[3] Bayram HOPUR, General Directorate of Combating Desertification and Erosion, Türkiye
[4] Ersin KARAKAYA, Bingöl University Faculty of Agriculture, Türkiye
[5] Semra ÇAMUKA, Bingöl University International Relations Office, Türkiye
[6] Şenol ÇELİK, Bingöl University Faculty of Agriculture, Bingöl, Türkiye
[7] Mahmut Yılmaz, Forest General Directorate Tulip Monitoring and Evaluation Specialist,
Alaaddin YÜKSEL ORCID No: 0000-0003-4760-1092
Ahmet USLU ORCID No: 0000-0003-0273-0069
Bayram HOPUR ORCID No: 0000-0002-7443-8051
Ersin KARAKAYA ORCID No: 0000-0002-6734-4962
Semra ÇAMUKA ORCID No: 0000-0002-4966-9296
Şenol ÇELİK ORCID No: 0000-0001-5894-8986
Mahmut Yılmaz ORCID No: 0009-0008-9481-1950

Corresponding Author: karakayaersin@hotmail.com

(Received: 10.06.2024, Accepted: 26.11.2024, Online Publication: 30.12.2024)

49

Abstract: This research was carried out to compare the perspectives and satisfaction of local people who benefited and did not benefit from projects implemented in micro-catchments in the provinces of Bingöl, Elâzığ, and Muş. The survey, focus group (FG) interviews, and key informative (KB) interviews were conducted in selected villages between the 16th and 25th of August, 2021. The "Chi-square independence test" was used to compare beneficiary and non-beneficiary responses to some questions. It was determined that the participants were generally satisfied with the project activities from which they benefited. Furthermore, the majority of people agreed that such projects should be continued. When individuals who didnt benefit from the project were statistically compared, it was determined that there were significant positive developments such as the use of new agricultural technology, increased production area, increased irrigated land, and increased use of forests and pastures. Within the context of all of this information, it is thought that the project is an important source of development opportunity for the region and that this level of development will emerge more clearly in the coming years.

Murat Nehri Rehabilitasyon Projelerinden Doğrudan Faydalanan ve Faydalanmayan Yöre Halkının Görüşlerinin Karşılaştırılması

Öz: Bu çalışma; Bingöl, Elâzığ ve Muş illerinde yer alan mikro havzalarda uygulanan projelerden faydalanan ve faydalanmayan yöre halkının proje hakkındaki görüş ve memnuniyetlerinin karşılaştırılması amacıyla yapılmıştır. Araştırmada; 16-25 Ağustos 2021 tarihleri arasında seçilen köylerde yapılan anket çalışması, odak grup (OG) görüşmeleri ve kilit bilgilendirici (KB) görüşmeler birincil verileri oluşturmuştur. Projeden doğrudan faydalanan ve faydalanmayan bireylerin bazı sorulara verdiği cevapların karşılaştırılmasında "Ki kare bağımsızlık testi" kullanılmıştır. Katılımcıların genel olarak yararlandıkları proje faaliyetlerinden memnun olduğu sonucuna varılmıştır. Ayrıca bireylerin çoğunluğu bu tür projelerin devam etmesi gerektiği şeklinde görüşlerini ifade etmişlerdir. Projeden

| faydalanan bireyler, projeden faydalanmayan bireyler | faydalanmayan bireyler ile faydalanan bireyler istatistiki olarak karşılaştırıldığında; yeni tarımsal teknoloji kullanma, üretim sahasını çoğaltma, sulanan araziyi arttırma, ormanlardan ve meralardan daha çok faydalanma gibi önemli olumlu gelişmelerin olduğu belirlenmiştir. Bütün bu bilgiler çerçevesinde projenin bölge için kalkınma açısından önemli bir fırsat kaynağı olduğu ve bu kalkınma düzeyinin gelecek yıllarda daha net bir şekilde ortaya çıkacağı düşünülmektedir. |

1. INTRODUCTION

The Murat River Basin Rehabilitation Project (MRWRP) aims to ensure sustainable use of vegetation, soil, and water resources, natural resource rehabilitation, sustainable land management, increasing the welfare of the region's people, providing employment, reducing migration from rural to urban areas, landslide and flood control, and improving transportation [1,2,3,4]. The General Directorate of Forestry is the MRWRP's main executive, and the General Directorate of Combating Desertification and Erosion is in charge of monitoring and evaluation. Within the scope of the project, which was planned to be implemented in 25 micro-catchments in the provinces of Bingöl, Elazığ, and Muş, 36 basins, 292 villages, 20 thousand 850 households, and 131 thousand 52 citizens benefited directly or indirectly.
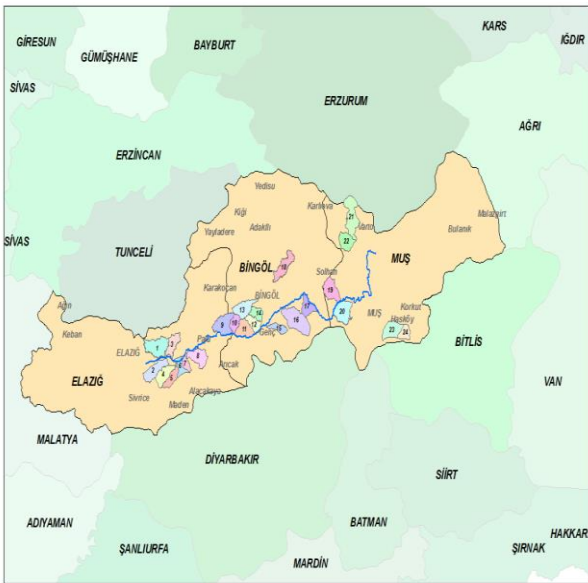
Figure 1. Provinces where MRWRP is implemented

Activities Performed Under the Project

Investments for the improvement of natural resources

It has been used for afforestation, soil conservation and erosion control, rehabilitation of degraded oak forests, and improvement of pasture and grazing areas.

Investments to Increase Income and Improve Living Conditions

Improvement of wheat and barley yield, improvement of animal production (forage crop production in wet and dry areas, improvement of animal shelters (barn), improvement of plant production (establishment of indoor orchard, field vegetable production, greenhouse vegetable production), small-scale irrigation sub-investments (water storage ponds, improvement of soil irrigation channels, in-field drip irrigation, village fountain for common use), the development of beekeeping and the introduction and dissemination of energy-efficient technologies (solar water heating units, house insulation (building insulation), energy-efficient (cooker) stoves, stone bread ovens for general use).

Education And Awareness Activities

To protect natural resources and raise the income level of the local people, training and awareness raising activities were carried out on the subjects of natural resource protection, use, and development, increasing agricultural productivity, improving animal and plant production, promoting environmentally friendly practices, organic agriculture, contracted sapling production, and product marketing.

Strengthening Institutional Capacity

Project; through experience gained in project construction techniques, project approach, logical framework, soil conservation techniques, monitoring and evaluation, and evaluation of non-wood product opportunities, institutions' capacity is increased and inter-institutional cooperation is developed.

Studies were conducted to determine the satisfaction level of local people who benefited from the projects implemented in micro-basins located in Bingöl, Elâzığ and Muş provinces by [5], and to determine the opinions of local people who did not benefit from the Murat River Rehabilitation Projects by [6]. This research was carried out to compare the perspectives and satisfaction of local people who directly benefited and did not benefit from projects implemented in micro-catchments in the provinces of Bingöl, Elâzığ, and Muş.

2. MATERIAL AND METHOD

The standard, beneficiary and non-beneficiary questionnaire prepared for the International Fund for Agricultural Development (IFAD) Annual Results Surveys was finalized in agreement with the Administration regarding objectives of the project. This survey was applied in the selected villages between 16-25 August 2021. In addition, the research team conducted focus group (FG) interviews and key informative (KB) interviews as well in the selected villages. Within the scope of the project, 241 villages and in 34 micro-catchments in question were specified in the technical specifications for the study to be sampled. Survey study and other studies were carried out by systematic random

50

sampling method in 30 villages where project activities were implemented and selected in consultation with local authorities. Considering the number of villages within the scope of the project in the provinces, 12 villages from Elazığ, 11 from Bingöl and 7 from Muş were determined. For this, the village names sent from the project area were listed alphabetically; the systematic random sampling coefficient was determined by dividing the total number of villages by the number of villages to be studied. By starting from the first village and skipping with the determined coefficients, the randomly selected villages were determined as the villages to be studied. In this context, a survey was conducted with 336 beneficiaries. 37.3% of the surveys were carried out in the villages of Bingol, 34.8% in the villages of Elâzıg and 27.9% in the villages of Muş (Table 1). When comparing the answers of beneficiaries and non-beneficiaries to some questions, whether there is a relationship between the two questions was anaishallysed by cross-tables and the *chi-square* independence test for these tables. The chi-square independence test has been used in many studies [7,8,9,10,11,12,13,14).

Table 1. Number of villages surveyed on provincial basis

Provinces	Number of villages	Number of surveys	Ratio
Bingöl	11	125	37.3
Elazığ	12	117	34.8
Muş	7	94	27.9
Total	30	336	100

3. RESULTS

The relationship between the availability of cash income sources and beneficiaries and non-beneficiaries is given in Table 2. It was determined that 61% of the individuals who answered this question had a cash income source on the general average, and 39% did not have a cash income source. While the rate of having a source of cash income for individuals benefiting from the project was 59.1%, this rate was determined as 64.9% for those who did not benefit from the project. It has been determined that there is no statistically significant relationship between having a cash income source and being a project beneficiary. In the study conducted by [15] this article evaluates the impact of the Livelihood Empowerment Against Poverty (LEAP) program on reducing rural poverty in the Karaga district of Northern Ghana. Utilizing a mixed-methods research design, the study compares the livelihoods of LEAP beneficiaries with those of non-beneficiaries. The findings indicate that the program significantly contributes to poverty reduction among the poor and vulnerable populations. The article recommends that school children benefiting from LEAP should be exempt from paying additional costs such as examination and PTA fees. Additionally, it suggests establishing a subsidy system for agricultural inputs to empower beneficiaries to engage in farming, thereby fostering long-term poverty alleviation. The study which was carried out by [16] aimed at determining variations in access to basic livelihoods between programme beneficiaries and non-beneficiaries. The results indicate that program beneficiaries were approximately 4.5 times more likely to access at least three meals per day compared to non-beneficiaries. Additionally, beneficiaries were about 3.9 times more likely to achieve an average dietary diversity score of 4.0 compared to non-beneficiaries. Furthermore, beneficiaries had roughly 3.3 times the odds of establishing an income-generating activity to enhance their income compared to non-beneficiaries. These results suggest that the program's impact was statistically significant across all five indicators examined in the study. In a previous study conducted in Nigeria the results indicated that socio-economic characteristics significantly influence the income and productivity of respondents in the study area. The findings showed a male dominance among both beneficiary and non-beneficiary farmers. Most respondents, both beneficiaries and non-beneficiaries, had farm sizes between 0.5 and 1.0 hectares before and after the NSPFS project, respectively. Statistical analysis revealed a significant difference between the socio-economic characteristics of NSPFS project beneficiaries and non-beneficiaries. The regression result showed that NSPFS project has positive impact on crop productivity of beneficiary farmers in the study area. The net farm income realized by the responder is indicates an increase in the net farm income of both beneficiaries and non-beneficiaries. NSPFS had impact on crop productivity of beneficiaries. Other reasons by the non-beneficiaries for not participating include lack of capital, not being a member of any farmer's cooperative society and also bad experience from other agricultural projects [17].

51

Table 2. The relationship between the availability of cash income sources and beneficiaries and non-beneficiaries

The status of having a cash income source or not		Groups		Overall average/Total
		Non-beneficiaries	Beneficiaries	
Yes	Number	109	195	304
	Ratio (%)	64.9	59.1	61
No	Number	59	135	194
	Ratio (%)	35.1	40.9	39
Total	Number	168	330	498
	Ratio (%)	100.0	100.0	100
Chi square and p value		**1.569 and 0.210**		

The relationship between the main income source of the household and beneficiary and non-beneficiary individuals was found statistically significant.

Considering the general averages of the individuals who answered this research question, the rate of agricultural production and sales as the main income source of the

households is 22.2%, the rate of animal production and sales is 30.7%, the rate of unqualified labor is 6.4%, the rate of salaries and wages is 25.5%, the rate of state support is determined as 5.6% and the rate of other income sources is determined as 8.6% (Table 3). The rate of the project beneficiaries having agricultural production and sales, animal production and sales income sources was found higher than the rate of individuals who were not beneficiaries. It has been determined that the household income sources of non-beneficiary individuals are salaries and wages at a high rate. The present study aimed to examine the impact of family income and conditional cash transfers on changes in household food insecurity (FI) status in a highly vulnerable municipality in Northeast Brazil. There was a 17.5% reduction in food insecurity

(FI) prevalence over time, with 24.5% of families who were food insecure in 2011 becoming food secure by 2014. After adjustments, it was found that families who did not see an increase in their total household income or experienced a reduction in their cash transfer amount were at a higher risk of persistent FI over time. Without the cash transfer program, approximately 10% of the families that transitioned from food insecure to food secure would have remained food insecure. The decrease in food insecurity (FI) occurred in an area of extreme climatic and social vulnerability. These changes were more closely associated with the cash transfer program than with the increase in family income over time [18].

Table 3. The relationship between the main source of income of the household and beneficiaries and non-beneficiaries

Main source of income of the household		Groups		Overall average/Total
		Non-beneficiaries	Beneficiaries	
Agricultural production and sale	Number	13	95	108
	Ratio (%)	7.8	29.8	22.2
Animal production and sale	Number	33	116	149
	Ratio (%)	19.8	36.4	30.7
unqualified labor force	Number	17	14	31
	Ratio (%)	10.2	4.4	6.4
Salaries wages	Number	67	57	124
	Ratio (%)	40.1	17.9	25.5
State support	Number	9	18	27
	Ratio (%)	5.4	5.6	5.6
Other	Number	25	17	42
	Ratio (%)	15.0	5.3	8.6
Total	Number	167	319	486
	Ratio (%)	100.0	100.0	100.0
Chi square and p value		74.902 and 0.000***		

***: p≤0.01

Individuals who answered the questions of his survey generally, 91.9% stated that they had no other source of income, and 8.1% stated that they had another source of income. The rate of the beneficiaries having other income sources was calculated as 3.7%, while the rate of those who did not benefit from the project was found as 16.1% (Table 4). The relationship between having another source of income and beneficiary and non-beneficiary individuals was found statistically significant. Micro watershed projects abroad have yielded a range of impactful results, showcasing the effectiveness of integrated land, water, and vegetation management. For instance, in Mexico, the *Strengthening Project for the National Micro-Watershed Programme* faced challenges with budget allocation and government support, but it still managed to implement numerous conservation

workshops and small community-based projects for soil and water management [19]. Meanwhile, in India, the *Karnataka Watershed Development Project* (Sujala) made extensive use of satellite imagery and GIS technologies to plan and monitor interventions, helping to rejuvenate rural landscapes and boost agricultural productivity in semi-arid regions. This project highlighted the role of technology in watershed management and earned several prestigious awards [20]. Another study in Gujarat examined the impact of watershed programs on soil erosion, groundwater levels, and socio-economic indicators, finding notable improvements. These projects used a Watershed Performance Benchmarking Index (WPBI) to evaluate success across various metrics, such as crop productivity, income generation, and migration reduction [21].

Table 4. The relationship between having another source of income and beneficiaries and non-beneficiaries

Groups		The status of having another source of income		Total
		Yes	No	
Non-beneficiaries	Number	27	141	168
	Ratio (%)	16.1	83.9	100.0
Beneficiaries	Number	11	288	299
	Ratio (%)	3.7	96.3	100.0
Overall average/Total	Number	38	429	467
	Ratio (%)	8.1	91.9	100.0
Chi square and p value	22.099 and 0.000***			

The relationship between ownership of agricultural land and beneficiary and non-beneficiary individuals is given in Table 5. It was determined that half of the individuals who answered this research question generally owned agricultural land and half of them did not. Ownership rate of individuals benefiting from the project was determined as 50.6%, and ownership rate of individuals not benefiting from the project was determined as 48.8%. One example is the "Wellness and Agriculture for Life Advancement" (WALA) project in Malawi. This project, which focused on improving watershed management and livelihoods, demonstrated substantial benefits in terms of crop yields, soil quality, and resilience to climate shocks [23].

Table 5. The relationship between ownership of agricultural land and beneficiary and non-beneficiary individuals

Groups		Ownership status of agricultural land		Total
		Yes	No	
Non-beneficiaries	Number	82	86	168
	Ratio (%)	48.8	51.2	100.0
Beneficiaries	Number	165	161	326
	Ratio (%)	50.6	49.4	100.0
Overall average/Total	Number	247	247	494
	Ratio (%)	50.0	50.0	100.0
Chi square and p value	0.144 and 0.704			

Considering the relationship between the increase in the production area compared to the previous year and the beneficiary and non-beneficiary individuals, it has been concluded that there is a statistically significant relationship between the production area situation, which is determined to be dependent on the beneficiaries of the project and those who do not benefit from the project, and benefiting or not benefiting from the project. While the rate of individuals expressing that the production area has increased compared to the previous year is 11.3%, this rate was found as 10.4% for individuals who are project beneficiaries and 50% for individuals not benefitting from the project. Half of the individuals who did not benefit from the project stated that the production area increased compared to the previous year (Table 6). One example is the "Wellness and Agriculture for Life Advancement" (WALA) project in Malawi. This project, which focused on improving watershed management and livelihoods, demonstrated substantial benefits in terms of crop yields, soil quality, and resilience to climate shocks [23]

Table 6. The relationship between the increase in the production area compared to the previous year and the beneficiary and non-beneficiary individuals

Groups		The increase in the production are compared to last year		Total
		Yes	No	
Non-beneficiaries	Number	3	3	6
	Ratio (%)	50.0	50.0	100.0
Beneficiaries	Number	27	232	259
	Ratio (%)	10.4	89.6	100.0
Overall average/Total	Number	30	235	265
	Ratio (%)	11.3	88.7	100.0
Chi square and p value	9.149 and 0.002**			

**: $p \leq 0.05$

Individuals who answered this survey question stated that 53.8% of them do animal husbandry in general and 46.2% of them do not. The rate of animal husbandry was found as 57.8% for the project beneficiaries and 45.8% for the individuals who did not benefit from the project. These two situations on whether the status of doing animal husbandry depends on being a project beneficiary or not has been determined as a statistically significant relationship. It was concluded that individuals who are project beneficiaries have a higher rate of animal husbandry (Table 7). One example is the "Wellness and Agriculture for Life Advancement" (WALA) project in Malawi. This project, which focused on improving watershed management and livelihoods, demonstrated substantial benefits in terms of crop yields, soil quality, and resilience to climate shocks [23].

Table 2. The relationship between the status of animal husbandry and beneficiary and non-beneficiary individuals

Groups		The status of animal husbandry		Total
		Yes	No	
Non-beneficiaries	Number	77	91	168
	Ratio (%)	45.8	54.2	100.0
Beneficiaries	Number	192	140	332
	Ratio (%)	57.8	42.2	100.0
Overall average/Total	Number	269	231	500
	Ratio (%)	53.8	46.2	100.0
Chi square and p value	**6.461 and 0.011****			

The relationship between the status of earning income from agricultural and animal production and the beneficiary and non-beneficiary individuals is given in Table 8. While the overall rate of individuals earning income from agricultural and animal production is 33.7%, this rate is determined as 34.5% for individuals benefiting from the project and 32.1% for those who do not benefit

from the project. One example is the "Wellness and Agriculture for Life Advancement" (WALA) project in Malawi. This project, which focused on improving watershed management and livelihoods, demonstrated substantial benefits in terms of crop yields, soil quality, and resilience to climate shocks [23].

Table 8. The relationship between the status of earning income from agricultural and animal production, and beneficiary and non-beneficiary individuals

Groups		The status of earning income from agricultural and animal production		Total
		Yes	No	
Non-beneficiaries	Number	54	114	168
	Ratio (%)	32.1	67.9	100.0
Beneficiaries	Number	114	216	330
	Ratio (%)	34.5	65.5	100.0
Overall average/Total	Number	168	330	498
	Ratio (%)	33.7	66.3	100.0
Chi square and p value	**0.287 and 0.597**			

Considering the relationship between borrowing status and beneficiary and non-beneficiary individuals, it was determined that 33.9% of the individuals benefiting from the project borrowed money, and 27.8% of the individuals who did not benefit from the project borrowed money. It was determined that 33.6% of the individuals who replied this question, on general average, borrowed (Table 9).

One example is the "Wellness and Agriculture for Life Advancement" (WALA) project in Malawi. This project, which focused on improving watershed management and livelihoods, demonstrated substantial benefits in terms of crop yields, soil quality, and resilience to climate shocks [23].

Table 9. The relationship between borrowing status and beneficiary and non-beneficiary individuals

Groups		Borrowing status		Total
		Yes	No	
Non-beneficiaries	Number	5	13	18
	Ratio (%)	27.8	72.2	100.0
Beneficiaries	Number	113	220	333
	Ratio (%)	33.9	66.1	100.0
Overall average/Total	Number	118	233	351
	Ratio (%)	33.6	66.4	100.0
Chi square and p value	**0.290 and 0.590**			

In general, 25.9% of the individuals who answered this question stated that their household income level has improved. The rate of stating that the household income has improved for the individuals who benefited from the project was 23.6%, while the rate of the ones stating that the household income has improved for the individuals who did not benefit from the project was found as 30.4% (Table 10). In a previous study conducted in Nigeria the results indicated that socio-economic characteristics significantly influence the income and productivity of respondents in the study area. The findings showed a male dominance among both beneficiary and non-beneficiary

farmers. Most respondents, both beneficiaries and non-beneficiaries, had farm sizes between 0.5 and 1.0 hectares before and after the NSPFS project, respectively. Statistical analysis revealed a significant difference between the socio-economic characteristics of NSPFS project beneficiaries and non-beneficiaries. The regression result showed that NSPFS project has positive impact on crop productivity of beneficiary farmers in the study area. The net farm income realized by the responder is indicates an increase in the net farm income of both beneficiaries and non-beneficiaries. NSPFS had impact on crop productivity of beneficiaries. Other reasons by the

non-beneficiaries for not participating include lack of capital, not being a member of any farmer's cooperative society and also bad experience from other agricultural projects [15].

Table 10. The relationship between the improvement in household income level and beneficiaries and non-beneficiaries

| Groups | | The improvement in household income level | | Total |
		Yes	No	
Non-beneficiaries	Number	8	160	168
	Ratio (%)	4.8	95.2	100.0
Beneficiaries	Number	78	252	330
	Ratio (%)	23.6	76.4	100.0
Overall average/Total	Number	129	369	498
	Ratio (%)	25.9	74.1	100.0
Chi square and p value	2.620 and 0.106			

The relationship between the project's job finding or improving working conditions and the relationship between beneficiary and non-beneficiary individuals was statistically significant. When the distribution of the opinions of the individuals who answered this question is examined, 63.1% of the individuals who benefited from the project thought that the project had an effect on finding a job or improving their working conditions. On the other hand, the rate of individuals not being project beneficiaries but thinking positively about the issue was determined as 4.8%. The impact of the project on finding a job or improving working conditions was determined as 41.3% in general average. It has been concluded that a high percentage of the individuals benefiting from the project think that the project has a positive effect on finding a job or improving working conditions (Table 11). The study revealed that the dependency ratio to total workers was 0.40 for beneficiary families and 0.26 for non-beneficiary families. It was found that there was a significant change in the area of major crops, increase in productivity and increase in net returns of beneficiary farms due to the interventions of the project. Return per investment of agricultural and horticultural products was higher in beneficiary farms than in non-beneficiary farms [22].

Table 11. The relationship between the project's ability to find a job or improve working conditions and beneficiary and non-beneficiary individuals

| Groups | | The project's ability to find a job or improve working conditions | | Total |
		Yes	No	
Non-beneficiaries	Number	8	160	168
	Ratio (%)	4.8	95.2	100.0
Beneficiaries	Number	178	104	282
	Ratio (%)	63.1	36.9	100.0
Overall average/Total	Number	186	264	450
	Ratio (%)	41.3	58.7	100.0
Chi square and p value	147.86 and 0.000***			

The relationship between the forest utilization status and beneficiary and non-beneficiary individuals is given in Table 12. When the distribution of the opinions of the individuals who answered this question is examined, the overall average rate of the individuals benefiting from the forest is 37.3%, while this ratio is determined as 50.3% for the individuals benefiting from the project and as 3.8% for the non-beneficiaries. The relationship between forest utilization and beneficiary and non-beneficiary individuals was statistically significant. It has been determined that individuals benefiting from the project benefit from forests at a higher rate. One example is the "Wellness and Agriculture for Life Advancement" (WALA) project in Malawi. This project, which focused on improving watershed management and livelihoods, demonstrated substantial benefits in terms of crop yields, soil quality, and resilience to climate shocks [23]. In Bolivia, the concept of "watershed agreements" has been applied as a locally-driven, adaptive model for managing water resources and mitigating climate change. These agreements incentivize upstream landowners to conserve forests in exchange for benefits such as training in sustainable practices. This model has expanded significantly, with thousands of families now involved in watershed conservation efforts, covering vast areas of land. The success of this project highlights the importance of community engagement, reciprocal benefits, and local design flexibility in fostering sustainable environmental governance [24].

Table 12. The relationship between forest utilization and beneficiary and non-beneficiary individuals

Groups		Status of forest utilization		Total
		Yes	No	
Non-beneficiaries	Number	5	125	130
	Ratio (%)	3.8	96.2	100.0
Beneficiaries	Number	168	166	334
	Ratio (%)	50.3	49.7	100.0
Overall average/Total	Number	173	291	464
	Ratio (%)	37.3	62.7	100.0
Chi square and p value	86.358 and 0.000***			

The relationship between the benefiting status of the common pasture land and the beneficiary and non-beneficiary individuals was statistically significant. When the distribution of the opinions of the individuals who answered this question is examined, it is determined that 53% of the individuals benefit from the pasture lands on the general average, while this rate is determined as 60.7% for the individuals who are project beneficiaries and 38.1% for the individuals who are not project beneficiaries (Table 13). It was determined that

individuals benefiting from the project benefited from the common pasture land at a higher rate. The study revealed that the dependency ratio to total workers was 0.40 for beneficiary families and 0.26 for non-beneficiary families. It was found that there was a significant change in the area of major crops, increase in productivity and increase in net returns of beneficiary farms due to the interventions of the project. Return per investment of agricultural and horticultural products was higher in beneficiary farms than in non-beneficiary farms [22]

Table 13. The relationship between the status of benefiting from common pasture land and beneficiary and non-beneficiary individuals

Groups		Status of benefiting from common pasture land*		Total
		Yes	No	
Non-beneficiaries	Number	64	104	168
	Ratio (%)	38.1	61.9	100.0
Beneficiaries	Number	199	129	328
	Ratio (%)	60.7	39.3	100.0
Overall average/Total	Number	263	233	496
	Ratio (%)	53.0	47.0	100.0
Chi square and p value	22.731 and 0.000***			

4. DISCUSSION AND CONCLUSION

The percentage of project beneficiaries with agricultural production and sales, animal production and sales, and other sources of income was found to be higher than the percentage of non-beneficiaries. Individuals who benefited from the project had a lower rate of having other sources of income than those who did not benefit from the project. It was discovered that project beneficiaries have a higher rate of animal husbandry. It has been determined that a high percentage of those who benefit from the project believe that the project helps them find work or improves their working conditions. It has been determined that individuals who benefit from the project benefit more from forests and common pasture land.

In general, based on the information gathered from the participants, it is possible to conclude that the project activities resulted in positive developments in the villages and made a significant contribution to rural development. Furthermore, with the assistance of project activities, income-generating activities have increased in the villages. It has been concluded that the MRWRP activities have reduced the pressure on forest vegetation, and the improvements made in pasture areas have made significant contributions to animal husbandry. It was determined that the participants were generally pleased with the project activities from which they benefited. Furthermore, the majority of people agreed that such

projects should be continued. When the individuals who do not benefit from the project are statistically compared to the beneficiaries, it has been determined that there are significant positive developments such as the use of new agricultural technology, increased production area, increased irrigated land, and increased use of forests and pastures. Within the context of all of this information, it is believed that the project is a significant source of development for the region, and that this level of development will become clearer in the coming years.

REFERENCES

[1] Yüksel A, Eraslan İH. Rural Development General Approach and Watershed Management Practices, 2015 Ankara.

[2] Bilinmiş A.) Çapakçur, Göynük, Lediz ve Vahkin çanakçı havzaları yüksek lisans tezi Orman Genel Müdürlüğü (OGM) Bingöl (2016).

[3] Baydas, A., Demirkiran, A.R. Bilinmiş, M. M.. Determining the satisfaction level of local people from Murat river rehabilitation projects: Example of Bingöl (lediz, vahkin-canakçı, Göynük stream and Çapakçur micro-catchments). JOEEP: Journal of Emerging Economies and Policy, 3 (1), 2018 31-57.

[4] Danış, H. Murat nehri havzası rehabilitasyon projesi kapsamında Bingöl ili Genç ilçeside bulunan mikrohavza projelerinin verimliliği ve sürdürebilirliğinin araştırılması, Bingöl

Üniversitesi, Fen Bilimleri Enstitüsü Yüksek Lisans Tezi 2019 s. 73.

[5] Uslu, A., Yuksel, A., Karakaya, E., Çamuka, S., et al. (2024). Determination of the Satisfaction Level of the Local People Benefiting from Murat River Rehabilitation Project (Bingöl, Elâzığ, and Muş Microcatchment Sample). Türk Tarım Ve Doğa Bilimleri Dergisi, 11(4), 959-973. https://doi.org/10.30910/turkjans.1487427

[6] Karakaya, E., Çamuka, S., Uslu, A., Yuksel, A., et al. (2024). Local People's View of Non-Benefiting from Murat River Projects: Examples of Bingöl, Elazığ and Muş Basins. Tekirdağ Ziraat Fakültesi Dergisi, 21(4), 1045-1057. https://doi.org/10.33462/jotaf.1436505

[7] MacDonald, P. L., & Gardner, R. C. Type I error rate comparisons of post-hoc procedures for I J chi-square tables. Educational and Psychological Measurement, (2000). 60(5), 735-754.

[8] Güngör M, Bulut Y. Ki-kare Testi Üzerine. Doğu Anadolu Bölgesi Araştırmaları. 2008;84-9.

[9] Yılmaz, H., Demircan, V., Gül, M. Üreticilerin Kimyasal Gübre Kullanımında Bilgi Kaynaklarının Belirlenmesi ve Tarımsal Yayım Açısından Değerlendirilmesi. Ziraat Fakültesi Dergisi, (2009). 4(1), 31-44.

[10] Ludbrook, J. Is there still a place for Pearson's chi-squared test and Fisher's exact test in surgical research?. Australia and New Zealand Journal of Surgery, (2011). 81, 923- 926.

[11] Franke, T. M., Ho, T., & Christie, C. A. The Chi-square test: Often used and more often misinterpreted. American Journal of Evaluation, (2012). 33(3), 448–458.

[12] Sharpe, D.E. Your Chi-Square Test Is Statistically Significant: Now What?. Practical Assessment, Research & Evaluation, (2015). 20(8), 1-10.

[13] Doğan, B. Üreticilerin iyi tarım uygulamaları istekliliklerini etkileyen faktörlerin analizi: Kahramanmaraş ili örneği. T.C. Kahramanmaraş Sütçü İmam Üniversitesi Fen Bilimleri Enstitüsü Yüksek Lisans Tezi Tarım Ekonomisi Anabilim Dalı, Kahramanmaraş 2017, s. 85.

[14] Terzi, C., Şahin, M., & Yurdugül, H. İki-Yönlü Olumsallık Çizelgelerinde Gözenek Artık Testi: Ki-Kare Analizi İçin Post-Hoc Testleri. Eğitim Teknolojisi Kuram Ve Uygulama, (2023). 13(1), 304-328. https://doi.org/10.17943/etku.1075830

[15] Sulemana, M., Malongza, B. F. I., & Abdulai, M. Assessment of the Livelihood Empowerment Against Poverty programme in Karaga district, Ghana. Development in Practice, (2018). 29(4), 437–447. https://doi.org/10.1080/09614524.2018.1551859

[16] Rambo CM. Effect Of The Natıonal Cash Transfer Programme For Older Persons On Access To Basıc Lıvelıhoods: A Comparatıve Analysıs Of Beneficıarıes And Nonbeneficıarıes In Sıaya County, Kenya European Journal of Business, Economics and Accountancy Vol. 6, No. 5, 2018 ISSN 2056-6018.

[17] Ephraim Panwal F and Arene C.J. Assessment of National Special Programme for Food Security (NSPPS) Project on Productivity and Income of Beneficiary Farmers in Plateau State, Nigeria, Journal of Agriculture and Sustainability ISSN 2201-4357 Volume 8, Number 2, 2015, 43-60

[18] Palmeira PA, Salles-Costa R, Pérez-Escamilla. Effects of family income and conditional cash transfers on household food insecurity: evidence from a longitudinal study in Northeast Brazil. Public Health Nutr. 2020 Mar;23(4):756-767. doi: 10.1017/S1368980019003136. Epub 2019 Nov 5. PMID: 31685079; PMCID: PMC10200439.

[19] IFAD https://www.ifad.org/documents/d/new-ifad.org/project-completion-report-digest_108, 2012.

[20] Worldbank https://www.worldbank.org/en/news/feature/2012/02/28/karnataka-watershed-development-project. 2012

[21] Vishalkumar R. Gor, Vinodkumar M. Patel. Benchmarking the Impact of Micro Watersheds of Sabarkantha and Aravalli Districts of Gujarat, India, 2022 https://arccjournals.com/journal/agricultural-science-digest/D-5618

[22] Kapil Dev, Ravinder Sharma, Amit Guleria and Dev Raj. 2017. Impact Analysis of Mid-Himalayan Watershed Development Project on Socio-Economic and Agricultural Status of Beneficiary Farms in Ani Tehsil of Kullu District in Himachal Pradesh.Int.J.Curr.Microbiol.App.Sci. 6(7): 2244-2255. https://doi.org/10.20546/ijcmas.2017.607.325

[23] Anonymous Scaling and Replicating Sustainable Watershed Management: A Malawi Case Study https://www.crs.org/our-work-overseas/research-publications/scaling-and-replicating-sustainable-watershed-management, 2024.

[24] Anonymous https://www.iucn.nl/en/story/bolivias-watershed-agreements-a-case-study-of-locally-led-adaptation-for-climate-resilience/

57

Türk Doğa ve Fen Dergisi
Turkish Journal of Nature and Science
www.dergipark.gov.tr/tdfd

BINGÖL UNIVERSITY

Investigation of the Catalytic Effect of ZnO Produced by Green Synthesis on NaBH₄ Hydrolysis

Mehmet Erman MERT[1*] (iD) **, Başak DOĞRU MERT[2]** (iD)

[1] Adana Alparslan Türkeş Science and Technology University, Advanced Technology Research and Application Center, Adana, Türkiye
[2] Adana Alparslan Türkeş Science and Technology University, Engineering Faculty, Energy Systems Engineering Department, Adana, Türkiye
Mehmet Erman MERT ORCID No: 0000-0002-0114-8707
Başak DOĞRU MERT ORCID No: 0000-0002-2270-9032

Corresponding author: memert@atu.edu.tr

Abstract: This study investigates the catalytic performance of ZnO nanoparticles (NPs) synthesized using ethanolic turmeric extract for the hydrolysis of NaBH₄. The ZnO NPs were characterized using scanning electron microscopy (SEM), energy dispersive X-ray analysis (EDX), and transmission electron microscopy (TEM) to determine their morphology and elemental composition. Ultraviolet (UV) spectroscopy and zeta potential measurements were also conducted to evaluate optical properties and colloidal stability. The ZnO NPs exhibited granular morphology with an average diameter of 0.6 μm and a Zn-to-O weight ratio of 57:43. Particle size distribution ranged from 30 nm to 70 nm, enhancing catalytic efficiency by increasing the surface area-to-volume ratio and active sites for the hydrolysis reaction. UV spectra revealed absorption peaks at 253 nm, 513 nm, and 977 nm, indicating intrinsic bandgap absorption and surface-related states. The zeta potential of -5.78 mV suggested moderate stability, with some agglomeration observed in solution. The ZnO NPs significantly improved hydrogen generation, increasing the hydrogen volume from 29.4 mL to 383.4 mL, achieving nearly a 13-fold enhancement in NaBH₄ hydrolysis.

58

Yeşil Sentez ile Üretilen ZnO'nun NaBH₄ Hidrolizi Üzerindeki Katalitik Etkisinin İncelenmesi

Öz: Bu çalışma, NaBH₄'ün hidroliz reaksiyonu için etanolik zerdeçal özütü kullanılarak sentezlenen ZnO nanopartiküllerinin (NP'ler) katalitik performansını araştırmaktadır. ZnO NP'lerin morfolojisi ve elementel bileşimini belirlemek amacıyla taramalı elektron mikroskobu (SEM), enerjı dağılımlı X-ışını analizi (EDX) ve transmisyon elektron mikroskobu (TEM) ile karakterizasyon yapılmıştır. Optik özellikleri ve kolloidal kararlılığı değerlendirmek için ultraviyole (UV) spektroskopisi ve zeta potansiyel ölçümleri de gerçekleştirilmiştir. ZnO NP'lerin ortalama 0,6 μm çapında granüler bir morfolojiye ve %57 Zn ile %43 O ağırlık oranına sahip olduğu belirlenmiştir. Parçacık boyutu dağılımının 30 nm ile 70 nm arasında değişmesi, yüzey alanı/hacim oranını ve reaksiyon için aktif alanları artırarak katalitik verimliliği artırmıştır. UV spektrumları, 253 nm, 513 nm ve 977 nm'de doruklar göstermiş ve bu doruklar, içsel bant aralığı soğurması ve yüzeyle ilişkili durumlarla ilişkilendirilmiştir. -5,78 mV olarak ölçülen zeta potansiyeli, çözeltide bir miktar aglomerasyon gözlenmesine rağmen, orta derecede bir kararlılık önermiştir. ZnO NP'ler, NaBH₄ hidrolizinde üretilen hidrojen miktarını 29,4 mL'den 383,4 mL'ye çıkararak hidrojen üretiminde yaklaşık 13 katlık bir artış sağlamıştır.

1. INTRODUCTION

Hydrogen is a important energy carrier in the global transition towards clean and sustainable energy systems. Its significance arises from its ability to function as both a clean fuel and a key enabler for reducing greenhouse gas emissions, offering practical solutions to the growing demand for sustainable energy alternatives. Due to its role in mitigating environmental challenges, hydrogen has become central to various national and international strategies focused on achieving net-zero emissions. In addition to its environmental benefits, hydrogen plays a significant role in industrial processes, including the synthesis of chemical compounds, petroleum refining, and the production of ammonia for fertilizers [1-3]. An essential application of hydrogen lies in the development of fuel cells, which provide a promising alternative to conventional fossil fuel-based energy sources. Fuel cells convert hydrogen into electricity with high efficiency, offering a low-carbon solution for power generation and transportation. However, efficient storage and transport remain challenges due to hydrogen's low density, high diffusivity, and flammable nature, necessitating the development of practical hydrogen storage technologies. Among the various methods, $NaBH_4$ has emerged as a viable hydrogen storage material because of its stability and ability to release hydrogen gas upon hydrolysis [4-6]. The use of $NaBH_4$ for hydrogen storage offers several advantages. It allows for safe, compact, and efficient hydrogen storage and transport, addressing key challenges associated with conventional hydrogen storage. $NaBH_4$ is particularly advantageous due to its solid form, which simplifies handling and minimizes safety risks. Furthermore, it provides a high hydrogen content by weight, making it attractive for applications requiring high energy density [7-9]. The hydrolysis of $NaBH_4$ is a straightforward, low-cost process that generates hydrogen gas under mild conditions, ensuring high-purity hydrogen without the risk of contamination or undesirable side reactions [10, 11]. The effectiveness of $NaBH_4$ hydrolysis depends significantly on the catalysts used to promote the reaction. Transition metal oxides and other nanomaterials have been widely explored as catalysts for this purpose, aiming to enhance hydrogen production rates and reduce activation energy barriers [5, 7, 12]. Notable studies in the field include the work of Changwoo Kim et al. [13] who synthesized cobalt oxide nanorods (wz-CoO-NRs) via the thermal decomposition of cobalt oleate and cobalt stearate. Their study demonstrated that wz-CoO-NRs achieved a hydrogen production rate of 10,367 mL min^{-1} g^{-1} at 293 K with an activation energy of 27.4 kJ mol^{-1}, highlighting the importance of morphology and surface characteristics for catalytic efficiency. Similarly, Guo et al. [14], developed NiCoB hollow nanospheres using galvanic replacement. These nanospheres exhibited superior catalytic activity with a hydrogen production rate of 6400 mL H_2 min^{-1} g^{-1} at 303 K and an activation energy of 33.1 kJ mol^{-1}, attributed to their large surface area and electronic effects. In another study, Kılınç and Şahin [15], synthesized a Zn complex of *4,4'-methylenebis(2,6-diethyl)aniline-3,5-di-tert-butylsalicylaldimine* and characterized its catalytic

performance for $NaBH_4$ hydrolysis. Their results indicated activation energy of 22.978 kJ mol^{-1}, with hydrogen generation rates of 952.5 mmol H_2 g^{-1} min^{-1} at 50°C and 614.4 mmol H_2 g^{-1} min^{-1} at 30°C, demonstrating the critical role of synthesis parameters in determining catalytic efficiency.

Given the growing demand for environmentally friendly hydrogen production, the exploration of green synthesis methods for catalysts has gained momentum. Green synthesis techniques, which employ environmentally benign solvents, plant extracts, and renewable precursors, offer a sustainable approach to catalyst development. In the study achieved by Boro et al., they investigated the green synthesis of ZnO nanoparticles using ethanolic leaf extract of Xanthium indicum, a plant native to North East India with pharmaceutical applications. The ZnO nanoparticles were characterized by DLS, TEM, FTIR, UV-Vis and XRD and showed high antioxidant, antimicrobial, antifungal and photocatalytic activities compared to their chemically synthesized counterparts. This eco-friendly approach offers a cost-effective alternative by reducing the need for toxic reagents and energy-intensive processes. The findings highlight the potential of green ZnO nanoparticles for applications in nanodevices, energy storage and healthcare [16]. Naiel et al. synthesized zinc oxide (ZnO) nanoparticles using the aqueous extract of Limonium pruinosum (sea lavender). The ZnO NPs exhibited an average size of ~41 nm and a hexagonal/cubic crystal structure. The findings highlight the biocompatibility, environmental friendliness, and cost-effectiveness of these ZnO NPs, making them promising candidates for biomedical and therapeutic applications [17]. ZnO is known for its high surface area, chemical stability, and catalytic versatility, making it suitable for various industrial applications, including hydrogen production [18, 19]. Furthermore, ZnO's non-toxic nature aligns with sustainability goals, ensuring safer handling and reduced environmental impact compared to other catalytic materials [20, 21]. In this context, zinc oxide (ZnO) synthesized via green chemistry principles presents an attractive candidate for $NaBH_4$ hydrolysis reactions.

This study aims to investigate the catalytic performance of green-synthesized ZnO in $NaBH_4$ hydrolysis reactions. By using a sustainable synthesis route, this research contributes to the development of eco-friendly catalysts while addressing key challenges in hydrogen storage and production. The findings are expected to advance the practical application of $NaBH_4$ as a hydrogen carrier and promote the integration of green chemistry principles in catalytic material design.

2. MATERIAL AND METHOD

The ZnO nanoparticles were synthesized through an environmentally friendly method using turmeric extract without any toxic reducing chemicals. To prepare the turmeric extract, 10 grams of turmeric powder were weighed and mixed with 100 mL of 70% ethanol. The mixture was shaken well for 5 minutes and then allowed

to soak for two days at room temperature (approximately 25-30°C). The resulting ethanol extract was filtered using qualitative Whatman filter paper no.1 (125 mm) and stored at 4°C. For the synthesis of ZnO nanoparticles, a zinc (II) nitrate solution at a concentration of 10 mM was combined with 50 mL of the turmeric ethanolic extract and incubated at 60°C for 60 minutes in a dark room. Afterward, the mixture was cooled to 25°C for 24 hours, followed by centrifugation at 3600 rpm for 30 minutes. The product was then washed several times with distilled water and ethanol. Finally, a dark brown precipitate was formed, which was dried at 90°C for 1 hour. The synthesized ZnO nanoparticles (NPs) were analyzed using various techniques. Scanning electron microscopy (SEM) was performed on a JEOL JSM-5500LV. Energy dispersive X-ray analysis (EDX) was conducted with an X-ray micro-analyzer (Oxford *6587*, INCA) attached to the SEM, operating at 20 kV. Transmission electron microscopy (TEM) was carried out on a Thermo Scientific Talos F200i using carbon-coated grids (Type G 200, 3.05 μm diameter). The zeta potential of the NPs was measured using a Malvern Panalytical instrument with ethanol as the dispersant. UV-Visible absorption spectroscopy was performed using a Unicam UV-VIS spectrophotometer UV2. To determine the rate of hydrogen generation, a hydrolysis reaction was conducted using a continuous system. Initially, 0.15 g of $NaBH_4$ was added to the reaction vessel in the absence of a catalyst, and the volume of hydrogen gas produced was measured over a period of 900 seconds. Subsequently, the experiment was repeated under the same conditions with the addition of 0.15 g of ZnO catalyst to the reaction mixture. Both were introduced into a two-neck flask, and the resulting hydrogen gas was captured and measured using an inverted, solution-immersed graduated cylinder. The volume of hydrogen gas collected in the graduated cylinder was carefully recorded, and adjustments were made to account for the volume changes due to the evaporation of water at the reaction temperature. This method ensured accurate measurement of the hydrogen gas produced, allowing for a precise determination of the catalytic activity of ZnO in the hydrolysis reaction of $NaBH_4$. The presence of ZnO catalyst enhanced the hydrogen generation rate, which was systematically compared to the control reaction without the catalyst.

3. RESULTS

In this study, we aimed to synthesize ZnO nanoparticles through an environmentally friendly method using ethanolic extract of turmeric. Turmeric is a commonly used spice in India and other Asian countries. The main active ingredient in turmeric is curcumin, chemically known as "*(1E,6E)-1,7-bis(4-hydroxy-3-methoxyphenyl)hepta-1,6-diene-3,5-dione*" (Figure 1).
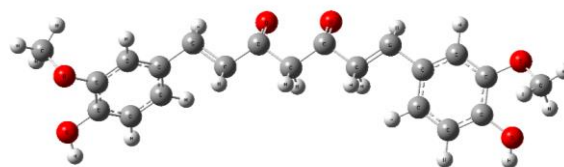
Figure 1. The molecular structure of curcumin

As illustrated in Figure 1, curcumin features two hydroxy groups (-OH) and two methoxy groups ($-OCH_3$) on its aromatic phenyl rings. These rings are connected by a heptadiene chain with two conjugated double bonds (C=C), creating a rigid and planar structure [22, 23]. Curcumin appears as a yellow to orange solid, with limited solubility in water but good solubility in organic solvents such as ethanol, methanol, and acetone. Its phenolic groups contribute to its well-documented antioxidant and anti-inflammatory properties [24-26].

The synthesized ZnO NPs were analyzed by SEM-EDX and related results were given in Figure 2. SEM-EDX analysis is a very useful method for morphological and compositional data for analyzing NPs. The granular shaped ZnO NPs were detected in SEM image with 0.791 μm average diameter. The precision with which the elemental composition of ZnO may be obtained makes these methods very useful for their analysis. The ZnO NPs EDX spectrum was shown in Figure 2, where zinc (Zn) and oxygen (O) are represented by separate peaks. The successful production of zinc oxide is confirmed by the presence of these Zn and O peaks in the EDX spectrum. The weight% values of Zn and O were 57 and 43%, respectively.
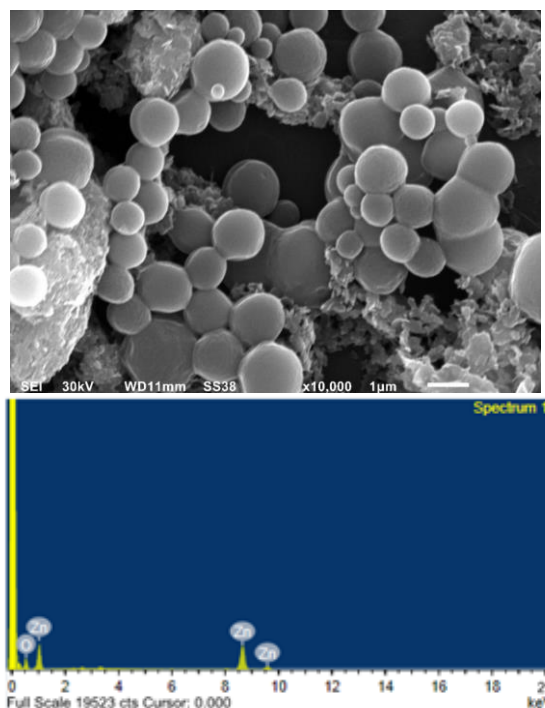
Figure 2. SEM-EDX anaysis of ZnO

Sadiya Samar et al. [27] synthesized ZnO via extract of Chenopodium album leaf, agglomeration was detected as the similar situation in Figure 2. Production of ZnO using green synthetic route was achieved by Boro et al.

[16] via ethanolic leaf extract of Xanthium indicum plant which is available only in North-East India. According to morphological analysis results, same structural view was detected.

TEM study was carried out after SEM-EDX investigation to obtain a more complete understanding of the ZnO structure. While the following TEM examination revealed higher resolution imaging and deeper insights into the crystalline structure of the ZnO samples, the SEM-EDX initially provided surface morphology and elemental composition data.
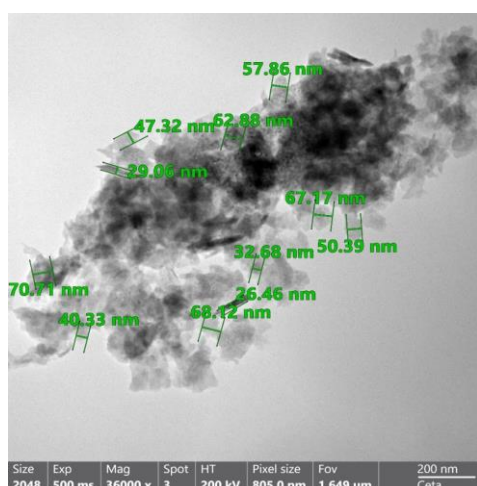

Figure 3. TEM anaysis of ZnO

As seen from Figure 3, the partice size was ranged between 30 nm and 70 nm. The distribution of sizes at the nanoscale is highly useful for catalytic processes, like the hydrolysis of $NaBH_4$. Because smaller particles have a larger surface area to volume ratio, there are more active sites available for catalytic reactions. The efficiency and rate of the hydrolysis process can be greatly enhanced by this greater surface area, resulting in more efficient production of hydrogen. Catalytic performance can be achieved by exact control over particle size and distribution, as demonstrated by TEM investigation. These characteristics together demonstrate ZnO nanoparticles' potential as an efficient catalyst in a range of chemical reactions, including the efficient and sustainable hydrolysis of $NaBH_4$ to produce hydrogen. According to literature the synhesis mechanism can be clarifed, for this purpose UV analysis should be helpful. The obtained results were given in Figure 4.

Curcumin is a beta-diketone characterized by the replacement of two hydrogen atoms with feruloyl groups, existing in two tautomeric forms: keto and enol [28, 29]. The keto form predominates in acidic and neutral pH environments, while the enol form is stable in alkaline conditions. Structurally, curcumin comprises a seven-carbon linker and three key functional groups: an α, β-unsaturated β-diketone moiety, an aromatic O-methoxy-phenolic group, and a seven-carbon chain. The α, β-unsaturated carbonyl groups bridge the aromatic rings, and the diketones can deprotonate to form enolates, with the α, β-unsaturated carbonyl acting as a acceptor for nucleophilic addition. The antioxidant properties of curcumin are due to its phenolic groups,

while its hydrophobic character stems from the carbon linker. To enhance its biological activity, curcumin has been modified, taking advantage of its strong metal-chelating properties via the α, β-unsaturated β-diketo moiety [30, 31].
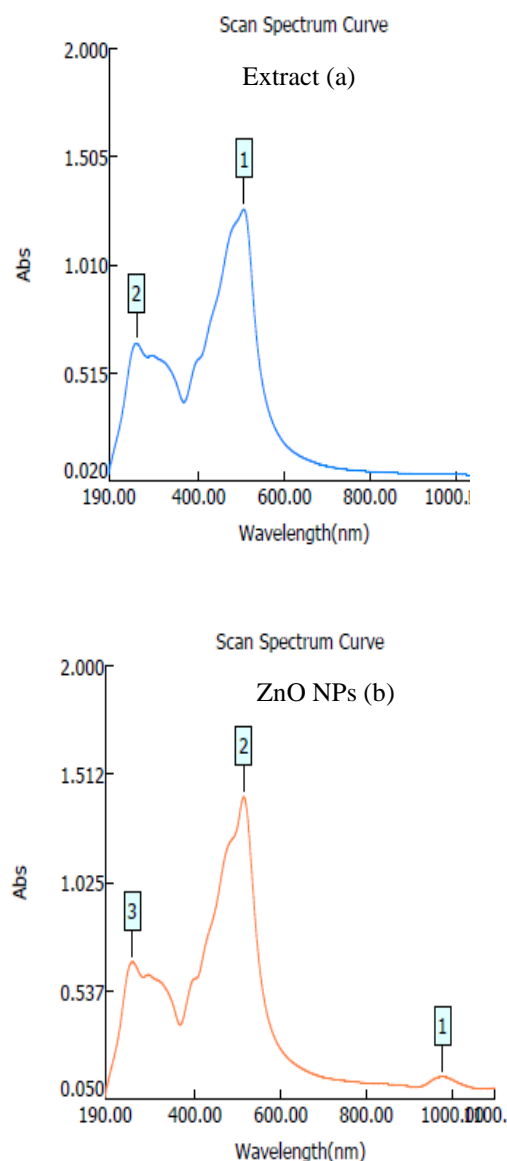
Figure 4. The UV sprectra of extract (a) and ZnO (b)

UV-vis spectroscopy was employed to study metal binding to curcumin, which typically occurs through the β-diketone group via chelation. This process involves the formation of dative covalent bonds, where one atom provides both electrons for the bond, introducing semipolar characteristics [32]. Metal coordination often involves one or two curcumin molecules, occasionally three, as seen in some complexes like the hexagonal structure. Metal-curcumin binding through the enolic group induces structural changes, with variations in metal-oxygen bond lengths and coordination geometries depending on the metal-to-curcumin ratio [32]. ZnO exhibited absorption peaks in its UV spectra at 253 nm, 513 nm, and 977 nm. The ZnO material's structural features and several electronic transitions are responsible for these peaks. The intrinsic bandgap absorption of

61

ZnO, which correlated to the electrical transition from the valence band to the conduction band, was most likely the cause of the absorption peak at 253 nm. This peak is associated with the excitonic absorption typical of ZnO nanostructures, and ZnO has a wide bandgap of about 3.37 eV. The ZnO lattice's defect states or impurities could be related to the peak at 513 nm. Defect states like oxygen vacancies or zinc interstitials can produce additional absorption features in the visible spectrum by generating localized energy levels within the bandgap. Surface states or deep-level imperfections may be the cause of the absorption peak at 977 nm. These deep-level flaws have the ability to trap electrons and aid in near-infrared absorption. Surface states or plasmonic phenomena resulting from ZnO's contact with its surroundings may possibly play a role in this absorption property [33-35]

Figure 5. The zeta potential of ZnO

Figure 5 showed the zeta potential measurements for ZnO nanoparticles (NPs). Typically, ZnO NPs with a size of approximately 5 nm exhibit zeta potential values ranging from -20 mV to +20 mV Ateş [36] Generally, ZnO NPs possessing a zeta potential less than -10 mV demonstrate increased stability in aqueous solutions due to electrostatic repulsion, which prevents particle aggregation. In the current study, the measured zeta potential value was -5.78 mV. Accord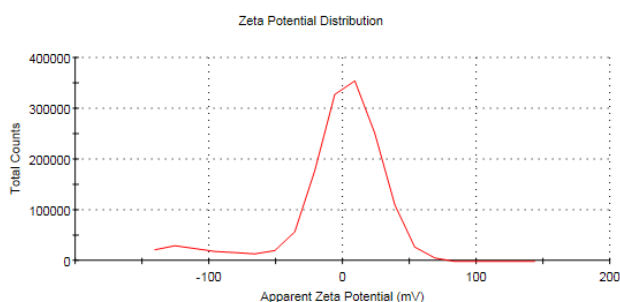ing to the literature, zeta potential values closer to zero indicate a propensity for particle agglomeration due to reduced electrostatic repulsion. Zeta potential is a critical parameter in evaluating the colloidal stability of nanoparticle suspensions. Higher absolute values of zeta potential (either positive or negative) suggest stronger repulsive forces between particles, thereby enhancing

stability [37]. Conversely, lower absolute values, as observed here, suggest weaker repulsive interactions and a higher likelihood of aggregation. The measured zeta potential of -5.78 mV for ZnO NPs indicates that while there is some repulsion, it is insufficient to prevent agglomeration entirely [38]. Thus, the ZnO NPs in this study were prone to agglomeration (as seen in SEM micropgraph)

The catalytic behavior of ZnO was investigated and related results were presented in Figure 6.
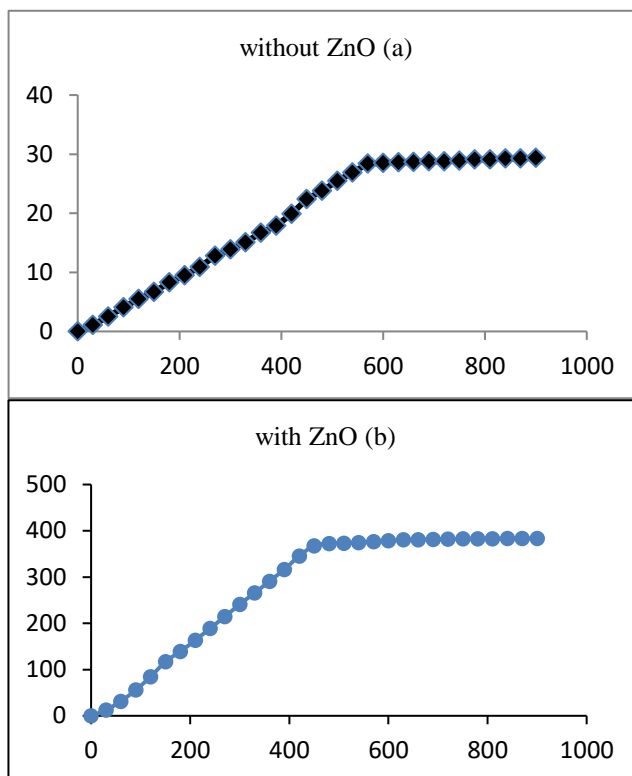
Figure 6. The hydrogen gas volume in the absence (a) and presence (b) of ZnO NPs catalyst

According to obtained result the produced hydrogen gas was 29.4 mL after 560 s, in the absence of ZnO but the value was increased almost 13 times in presence of ZnO NPs. The obtained hdrogen gas was almost 383.4 mL in the presence of ZnO after 430 s.

Table 1. Comparative analysis of catalysts for hydrogen generation from NaBH$_4$ under various conditions

Catalysts	Size (nm)	Catalyst (mg)	Conditions	HGR (mLH$_2$ g^{-1} min^{-1})	References
Ni-B	-	Foam	20 wt% NaBH$_4$, 5 wt% NaOH, 60 ^{0}C	130	[39]
CuFe$_2$O$_4$/RGO	5	30	40 mg NaBH$_4$	622	[40]
Ni	-	75 wt%	14 wt% NaBH$_4$, 30 ^{0}C	96.3	[41]
Ni-Ru/50WX8	20-60	200	10 wt% NaBH$_4$, 5 wt% NaOH, 35 ^{0}C	400	[42]
G-CoB	15-100	100	568 mg NaBH$_4$, 20 ^{0}C	258	[43]
Ru-Ni/Ni	-	-	20 wt% NaBH$_4$, 1 wt% NaOH, 30 ^{0}C	360	[44]
Pt/Co$_3$O$_4$	39.8	10	100 mg NaBH$_4$	120	[45]
ZnO NPs	30-70	150	150 mg NaBH$_4$, 25 ^{0}C	356.5	In this study

A comparative analysis of catalysts for producing hydrogen from NaBH$_4$ under various circumstances was shown in Table 1, using 150 mg of NaBH$_4$ at 25°C, our work showed hydrogen generation rate (HGR) of 356.5 mLH$_2$ g^{-1} min^{-1} using ZnO nanoparticles (NPs) with a size range of 30–70 nm. Because of this performance,

ZnO NPs can compete with other catalysts. CuFe$_2$O$_4$/RGO, for example, demands a greater NaBH$_4$ load (40 mg) and smaller particle sizes (5 nm), although achieving a HGR of 622 mLH$_2$ g^{-1} min^{-1}. This suggests that material synthesis needs to be tightly controlled. In this study, ZnO NPs perform better than some catalysts

that use more material and complex compositions. For instance, Ni-B foam achieves 130 mLH$_2$ g^{-1} min^{-1} at 60°C, whereas Pt/Co$_3$O$_4$ only reaches 120 mLH$_2$ g^{-1} min^{-1} with 10 mg of catalyst. Additionally, Ni-Ru/50WX8 shows a higher HGR of 400 mLH$_2$ g^{-1} min^{-1} but requires 200 mg of catalyst and operates at 35°C, demonstrating that ZnO NPs offer a simpler, scalable option under this condition. ZnO NPs are effective and useful catalyst that offers a high rate of hydrogen generation under comparatively simple circumstances. Higher HGRs are produced by some catalysts, although they frequently require greater amounts of material, intricate compositions, or higher temperatures. This study showcases the scalability and simplicity of ZnO NPs for sustainable hydrogen generation, with opportunities for future work focused on optimizing reagent concentrations and exploring synergistic catalyst combinations.

4. DISCUSSION AND CONCLUSION

The synthesized ZnO NPs demonstrated high potential for catalytic applications, particularly in the hydrolysis of NaBH$_4$ for hydrogen generation. SEM-EDX analysis confirmed the granular morphology of the ZnO NPs with an average diameter of 0.6 µm and provided precise compositional data, indicating a Zn to O weight ratio of 57% to 43%. The particle size distribution ranged from 30 nm to 70 nm, enhancing catalytic efficiency due to the increased surface area-to-volume ratio, which provides more active sites for reactions. UV spectroscopy revealed absorption peaks at 253 nm, 513 nm, and 977 nm, attributed to intrinsic bandgap absorption, defect states, and surface states, respectively. The zeta potential measurement of -5.78 mV indicated moderate stability in aqueous solutions, although some agglomeration was seen. Despite this, the ZnO NPs significantly improved hydrogen production in the NaBH$_4$ hydrolysis reaction, increasing the volume of hydrogen generated from 29.4 mL to 383.4 mL, demonstrating a nearly 13-fold enhancement. These findings highlight the importance of particle size control and surface characteristics in optimizing the catalytic performance of ZnO NPs, making them a promising material for efficient hydrogen generation.

Acknowledgement

Conflict of Interest

There are no conflicts of interest declared by any of the writers.

REFERENCES

[1] Şahin Ö, Baytar O, Kutluay S, Ekinci A. Potential of nickel oxide catalyst from banana peel extract via green synthesis method in both photocatalytic reduction of methylene blue and generation of hydrogen from sodium borohydride hydrolysis. Journal of Photochemistry and Photobiology A: Chemistry. 2024;448:115301.

[2] Onat E. Synthesis of a cobalt catalyst supported by graphene oxide modified perlite and its application on the hydrolysis of sodium borohydride. Synthetic Metals. 2024;306:117621.

[3] Li Q, Wang F, Zhou X, Chen J, Tang C, Zhang L. Synergistical photo-thermal-catalysis of Zn2GeO4:xFe3+ for H2 evolution in NaBH4 hydrolysis reaction. Catalysis communications. 2021;156:106321.

[4] Abdelhamid HN. A review on hydrogen generation from the hydrolysis of sodium borohydride. International Journal of Hydrogen Energy. 2021;46(1):726-65.

[5] Prasad D, Patil KN, Sandhya N, Chaitra CR, Bhanushali JT, Samal AK, et al. Highly efficient hydrogen production by hydrolysis of NaBH4 using eminently competent recyclable Fe2O3 decorated oxidized MWCNTs robust catalyst. Applied Surface Science. 2019;489:538-51.

[6] Zou Y, Yin Y, Gao Y, Xiang C, Chu H, Qiu S, et al. Chitosan-mediated Co–Ce–B nanoparticles for catalyzing the hydrolysis of sodium borohydride. International Journal of Hydrogen Energy. 2018;43(10):4912-21.

[7] Kılınç D, Şahin Ö. Effective TiO2 supported Cu-Complex catalyst in NaBH4 hydrolysis reaction to hydrogen generation. International Journal of Hydrogen Energy. 2019;44(34):18858-65.

[8] Wei Y, Meng W, Wang Y, Gao Y, Qi K, Zhang K. Fast hydrogen generation from NaBH4 hydrolysis catalyzed by nanostructured Co–Ni–B catalysts. International Journal of Hydrogen Energy. 2017;42(9):6072-9.

[9] Wang L, Li Z, Zhang Y, Zhang T, Xie G. Hydrogen generation from alkaline NaBH4 solution using electroless-deposited Co–Ni–W–P/γ-Al2O3 as catalysts. Journal of Alloys and Compounds. 2017;702:649-58.

[10] Lin K-YA, Chang H-A. Efficient hydrogen production from NaBH4 hydrolysis catalyzed by a magnetic cobalt/carbon composite derived from a zeolitic imidazolate framework. Chemical Engineering Journal. 2016;296:243-51.

[11] Chou C-C, Hsieh C-H, Chen B-H. Hydrogen generation from catalytic hydrolysis of sodium borohydride using bimetallic Ni–Co nanoparticles on reduced graphene oxide as catalysts. Energy. 2015;90:1973-82.

[12] Aman D, Alkahlawy AA, Zaki T. Hydrolysis of NaBH4 using ZVI/Fe2(MoO4)3 nanocatalyst. International Journal of Hydrogen Energy. 2018;43(39):18289-95.

[13] Kim C, Lee SS, Li W, Fortner JD. Towards optimizing cobalt based metal oxide nanocrystals

for hydrogen generation via NaBH4 hydrolysis. Applied Catalysis A: General. 2020;589:117303.

[14] Guo J, Hou Y, Li B, Liu Y. Novel Ni–Co–B hollow nanospheres promote hydrogen generation from the hydrolysis of sodium borohydride. International Journal of Hydrogen Energy. 2018;43(32):15245-54.

[15] Kılınç D, Şahin Ö. Performance of Zn-Schiff Base complex catalyst in NaBH4 hydrolysis reaction. International Journal of Hydrogen Energy. 2020;45(60):34783-92.

[16] Boro B, Boruah JS, Devi C, Alemtoshi, Gogoi B, Bharali P, et al. A novel route to fabricate ZnO nanoparticles using Xanthium indicum ethanolic leaf extract: Green nanosynthesis perspective towards photocatalytic and biological applications. Journal of Molecular Structure. 2024;1300:137227.

[17] Naiel B, Fawzy M, Halmy MWA, Mahmoud AED. Green synthesis of zinc oxide nanoparticles using Sea Lavender (Limonium pruinosum L. Chaz.) extract: characterization, evaluation of anti-skin cancer, antimicrobial and antioxidant potentials. Scientific Reports. 2022;12(1):20370.

[18] Goswami S, Bishnoi A, Tank D, Patel P, Chahar M, Khaturia S, Modi N, Khalid M, Alam MW, Kumar Yadav V, Alreshidi MA, Yadav KK. Recent trends in the synthesis, characterization and commercial applications of zinc oxide nanoparticles- a review. Inorganica Chimica Acta. 2024;573:122350.

[19] Bakranova D, Nagel D. ZnO for Photoelectrochemical Hydrogen Generation. Clean Technologies. 2023;5(4):1248-68.

[20] Gadewar M, Prashanth GK, Ravindra Babu M, Dileep MS, Prashanth PA, Rao S, Mahadevaswamy M, Kumar Ghosh M, Singh N, Mandotra SK, Chauhan A, Rustagi S, Yogi R, Chinnam S, Ali B, Ercisli S, Orhan E. Unlocking nature's potential: Green synthesis of ZnO nanoparticles and their multifaceted applications – A concise overview. Journal of Saudi Chemical Society. 2024;28(1):101774.

[21] Zhou X-Q, Hayat Z, Zhang D-D, Li M-Y, Hu S, Wu Q, Cao Y-F, Yuan Y. Zinc Oxide Nanoparticles: Synthesis, Characterization, Modification, and Applications in Food and Agriculture. Processes. 2023;11(4):1193.

[22] Zhai K, Brockmüller A, Kubatka P, Shakibaei M, Büsselberg D. Curcumin's Beneficial Effects on Neuroblastoma: Mechanisms, Challenges, and Potential Solutions. Biomolecules. 2020;10(11):1469.

[23] Badmanaban R, Dhananjoy S, Dhrubo JS, Arpita B, Supradip M, Susmita B. Turmeric: A holistic Solution for Biochemical malfunction. Research Journal of Pharmacy and Technology. 2021; 14(10):5540-0.

[24] Hani U, Shivakumar HG. Solubility enhancement and delivery systems of curcumin a herbal medicine: a review. Current Drug Delivery. 2014;11(6):792-804.

[25] Ipar VS, Dsouza A, Devarajan PV. Enhancing Curcumin Oral Bioavailability Through Nanoformulations. European Journal of Drug Metabolism and Pharmacokinetics. 2019;44(4):459-80.

[26] Sharifi-Rad J, Rayess YE, Rizk AA, Sadaka C, Zgheib R, Zam W, Sestito S, Rapposelli S, Neffe-Skocińska K, Zielińska D, Salehi B, Setzer WN, Dosoky NS, Taheri Y, El Beyrouthy M, Martorell M, Ostrander EA, Suleria HAR, Cho WC, Maroyi A, Martins N. Turmeric and Its Major Compound Curcumin on Health: Bioactive Effects and Safety Profiles for Food, Pharmaceutical, Biotechnological and Medicinal Applications. Frontiers in Pharmacology. 2020;11:01021.

[27] Samar S, Kumar A, Kumar P. Green synthesis of ZnO nano-crystals using Chenopodium album L. Leaf extract, their characterizations and antibacterial activities. Materials Science and Engineering: B. 2024;299:117005.

[28] Lee WH, Loo CY, Bebawy M, Luk F, Mason RS, Rohanizadeh R. Curcumin and its derivatives: their application in neuropharmacology and neuroscience in the 21st century. Current Neuropharmacology. 2013;11(4):338-78.

[29] Cornago P, Claramunt RM, Bouissane L, Alkorta I, Elguero J. A study of the tautomerism of β-dicarbonyl compounds with special emphasis on curcuminoids. Tetrahedron. 2008;64(35):8089-94.

[30] Ciuca MD, Racovita RC. Curcumin: Overview of Extraction Methods, Health Benefits, and Encapsulation and Delivery Using Microemulsions and Nanoemulsions. International Journal of Molecular Sciences. 2023;24(10).

[31] Kawano S-i, Inohana Y, Hashi Y, Lin J-M. Analysis of keto-enol tautomers of curcumin by liquid chromatography/mass spectrometry. Chinese Chemical Letters. 2013;24(8):685-7.

[32] Prasad S, DuBourdieu D, Srivastava A, Kumar P, Lall R. Metal-Curcumin Complexes in Therapeutics: An Approach to Enhance Pharmacological Effects of Curcumin. International Journal of Molecular Sciences. 2021;22(13):7094.

[33] Song Z, Timothy A. Kelf, Washington H. Sanchez, Michael S. Roberts, Jaro Rička, Martin Frenz, et al. Characterization of optical properties of ZnO nanoparticles for quantitative imaging of transdermal transport. Biomedical Optics Express. 2011;2(12):3321-33.

[34] Singh S, Gade JV, Verma DK, Elyor B, Jain B. Exploring ZnO nanoparticles: UV–visible analysis and different size estimation methods. Optical Materials. 2024;152:115422.

[35] Singh DK, Pandey DK, Yadav RR, Singh D. A study of nanosized zinc oxide and its nanofluid. Prama. 2012;78(5):759-66.

[36] Ateş M. Nanoparçacıkların Ölçme ve İnceleme Teknikleri. Turkish Journal of Scientific Reviews. 2018;11(1):63-9.

[37] Marsalek R. Particle Size and Zeta Potential of ZnO. APCBEE Procedia. 2014;9:13-7.

[38] Günay K, Leblebici Z, Koca FD. Çinko Nanopartiküllerinin (ZnO NP) Biyosentezi, Karakterizasyonu ve Anti- Bakteriyel Etkisinin İncelenmesi. Nevşehir Bilim Teknoloji Dergisi. 2021;10(1):56-66.

[39] Lee JK, Ann H-h, Yi Y, Lee KW, Uhm S, Lee J. A stable Ni–B catalyst in hydrogen generation via NaBH4 hydrolysis. Catalysis Communications. 2011;16(1):120-3.

[40] Tang M, Xia F, Gao C, Qiu H. Preparation of magnetically recyclable CuFe2O4/RGO for catalytic hydrolysis of sodium borohydride. International Journal of Hydrogen Energy. 2016;41(30):13058-68.

[41] Kim J-H, Kim K-T, Kang Y-M, Kim H-S, Song M-S, Lee Y-J, Lee PS, Lee J-Y. Study on degradation of filamentary Ni catalyst on hydrolysis of sodium borohydride. Journal of Alloys and Compounds. 2004;379(1):222-7.

[42] Liu C-H, Chen B-H, Hsueh C-L, Ku J-R, Jeng M-S, Tsau F. Hydrogen generation from hydrolysis of sodium borohydride using Ni–Ru nanocomposite as catalysts. International Journal of Hydrogen Energy. 2009;34(5):2153-63.

[43] Zhang F, Hou C, Zhang Q, Wang H, Li Y. Graphene sheets/cobalt nanocomposites as low-cost/high-performance catalysts for hydrogen generation. Materials Chemistry and Physics. 2012;135(2):826-31.

[44] Wang F, Luo Y, Wang Y, Zhu H. The preparation and performance of a novel spherical spider web-like structure RuNi / Ni foam catalyst for NaBH4 methanolysis. International Journal of Hydrogen Energy. 2019;44(26):13185-94.

[45] Hung T-F, Kuo H-C, Tsai C-W, Chen HM, Liu R-S, Weng B-J, Lee J-F. An alternative cobalt oxide-supported platinum catalyst for efficient hydrolysis of sodium borohydride. Journal of Materials Chemistry. 2011;21(32):11754-9.

Türk Doğa ve Fen Dergisi
Turkish Journal of Nature and Science
www.dergipark.gov.tr/tdfd

Design and Mechanical Analyses of Autonomous Mobile Robot with Swerve Driving System

Oğuz MISIR[1*] ID, Melike BEYAZLI [1] ID, Sümeyye ALP [1] ID,

Görkem Burak TAŞKIN [1] ID, Zeynep IŞIK[1] ID

[1]Bursa Teknik Üniversitesi, Mühendislik ve Doğa Bilimleri Fakültesi, Mekatronik Mühendisliği, Bursa, Türkiye
Oğuz MISIR ORCID No: 0000-0002-3785-1795
Melike BEYAZLI ORCID No: 0009-0005-6315-794X
Sümeyye ALP ORCID No: 0009-0006-5922-8706
Görkem Burak TAŞKIN ORCID No: 0009-0004-0483-0404
Zeynep IŞIK ORCID No: 0009-0005-1388-7194

*Corresponding author: oguz.misir@btu.edu.tr

Abstract: The use of mobile robots has become increasingly prevalent in various sectors, including industry, healthcare, logistics, and services. One of the most crucial attributes of these robots for their intended applications is their capacity to transport payloads. Autonomous mobile vehicles capable of carrying payloads are robots that process data received from their environment through electronic components. They contain and deliver the load to the target location in accordance with the data. This study presents the design of a mobile robot with scissor lift and swerve driving systems. Finite element analysis was employed to investigate the stress and deformation behavior of the designed vehicle under a load. The suitability of the materials used for the design was verified as a result of the analyses. Subsequently, the ability of the real-time driving algorithms to act in possible scenarios is tested in a simulation environment.

Swerve Sürüş Sistemine Sahip Otonom Mobil Robotun Tasarımı ve Mekanik Analizleri

Anahtar Kelimeler:
Sonlu
elemanlar
analizi,
Mobil robot,
Otonom

Öz: Mobil robotlar, endüstride, sağlık sektöründe, lojistik sektöründe ve servis hizmetlerinde kullanımıyla giderek artan popülerlik kazanmıştır. Bu robotların kullanım amaçları arasındaki en önemli özellikleri arasında faydalı yük taşıyabilme kabiliyetleridir. Bu maksatla mobil robotun yük taşıma kabiliyetinin kazandırılmasında tasarım ve donanım önem kazanmaktadır. Bu çalışmada, makaslı kaldıraç sistemine sahip olan ve "swerve" sürüş sistemiyle hareket eden mobil robotun tasarımı sunulmaktadır. Tasarlanan aracın yük altındaki gerilim ve deformasyon değişimlerini incelemek için sonlu elemanlar kullanılmıştır. Analizler sonucunda kullanılan malzemelerin tasarıma uygunluğu kontrol edilmiştir. Yapısal analizi tamamlanan aracın gerçek zamanlı sürüş algoritmalarının olası senaryolar karşısındaki hareket kabiliyeti simülasyon ortamında test edilmiştir.

1. INTRODUCTION

In a world characterized by constant change, the capacity to adapt to novel situations and acquire new skills and abilities is essential. Within this context, robots capable of

multidirectional movement in time and space are utilized [1]. Robots are technological systems that perceive their environment for specific purposes and generate motion plans by evaluating the information they obtain [2]. They have a wide range of applications, including industrial

manufacturing, healthcare, space exploration, and domestic use [3]. Consequently, robotics has become a pervasive feature of the contemporary world, including roles directly oriented towards humans, and is employed in numerous contexts. The human need for technological solutions, which has consistently influenced the evolution of technology, has led to the development of mobile robots, as stationary robots are no longer sufficient.

Autonomous robotic systems are increasingly being employed to develop innovative tools to enhance work efficiency and perform multiple operations in diverse environments, as well as a potential countermeasure to the impending issue of labor shortages [4]. Autonomous mobile robots (AMR) are defined as robots that operate in accordance with environmental information obtained by sensors, cameras, artificial intelligence applications, and other means. They autonomously perform assigned tasks [5]. In contrast to many industrial robots, mobile robots are capable of navigating to their task locations without human intervention, possess expansive movement areas, and complete their tasks by reaching the desired location while avoiding obstacles under varying conditions [6]. Mobile robots are increasingly utilized in numerous industrial and specialized applications. They can be designed according to the specific requirements of their intended use. Mobile robots, which are equipped with various components for different purposes and controlled by diverse software algorithms, are capable of detecting environmental data such as lines, light, and sound autonomously and moving automatically. Alternatively, they can be controlled manually with the assistance of a user interface. The motion mechanisms of mobile robots represent a crucial aspect. Although the motion mechanisms in the vehicle affect numerous parameters, the selection of an appropriate wheel for the vehicle and the creation of wheel configurations on the chassis result in the vehicle being used with high efficiency [7]. Mobile robots are categorized into three types according to their motion mechanism: wheeled, tracked, and legged systems.

The wheel is the most commonly used motion mechanism in mobile robots. Wheeled robots have been the most prevalent locomotion mechanism due to their simple structure, high acceleration, and ease of control. One of the most widely used wheeled mobile robots in industry is the autonomous mobile robot for load handling [8].

The designs of robots used for load-carrying vary according to the manner in which they lift and carry the load. In this context, the weight and dimensions of the load to be transported are the most critical parameters in the system design. Mechanical tests of prototypes made in this field provide great convenience for the design process, cost, and optimization through simulation programs. Consequently, software programs are capable of conducting analyses of interdisciplinary studies, such as mechanics, structural analysis, computational fluid dynamics, and heat transfer, employing the finite element method [5].

The Finite Element Method (FEM) is a numerical analysis technique used to solve complex engineering problems and predict the behavior of a structure or system when subjected to physical effects. This method is based on the principle of dividing the design into small finite elements and analytically examining each element [9]. FEM allows for the identification of potential weak points in the design, optimization of material usage, and verification of safety factors. Additionally, it simulates the system's stress, deformation, and other mechanical properties before producing physical prototypes, thereby helping to reduce costs and accelerate the design process. Consequently, it ensures that the design can operate reliably even under the most challenging conditions, thus preventing potential design errors.

This paper presents the design of an autonomous mobile robot with load-carrying capability developed in a Computer-Aided Design (CAD) environment. The mechanical system of the designed mobile robot was analyzed using the Finite Element Analysis (FEA) method to assess total deformation and stress. Furthermore, the wheel driving capability of the vehicle and mechanism of the scissor system were tested in a simulation environment. In the rest of the paper, Section 2 describes the system, programs used, general control mechanism, structural characteristics of the designed vehicle, and types of mechanical analysis used. Section 3 presents the analysis set-up and test results. Section 4 discusses the overall conclusion of the paper.

1.1 Related Works

In this section, within the scope of our study on AMRs, we review the literature on the utilization of AMRs in the industrial and social domains, mechanical analysis, and simulations of driving systems. The keywords "AMR," "ANSYS," "Driving Systems," and "Simulation" were employed in the literature search. A summary of the pertinent studies identified using these keywords is presented in Table 1. AMRs utilized for material handling and storage in the industry can be readily integrated with various mapping techniques, providing a significant advantage for transportation operations.

AMRs are employed not only in industrial logistics but also in numerous areas for societal benefits. AMRs have recently become prevalent, particularly in the healthcare sector, where they have been effectively utilized for the transportation of medicines and food within hospitals. Baskoro et al. [10], in their study titled "An Autonomous Mobile Robot Platform for Medical Purpose", asserted that the highly maneuverable AMR named ROM20 can be utilized in various applications such as disinfectant mist spraying and food distribution heating in a hospital environment. This study demonstrates the functionality of AMRs in the healthcare field. In another study by Yan et al. [11] posited that AMRs provide significant advantages in material-handling operations in industrial applications. They also noted that AMRs face flexibility challenges in path alterations but overcome this issue by employing Simultaneous Localization and Mapping (SLAM) techniques.

67

Recent advancements in drive mechanisms for autonomous robots with high maneuverability have led to substantial progress. The work of Dhelika et al. [12] serves as an exemplar, wherein a motorized hospital bed utilizing a swerve drive mechanism was developed to provide holonomic mobility in healthcare environments. The simplicity and cost-effectiveness of the swerve drive system facilitate its integration into existing systems with minimal modifications. Additionally, the work by Ziqi et al. [13] presents significant research on drive mechanisms and mobility systems for autonomous mobile robots. This study thoroughly examines the advantages and challenges of swerve drive systems, proposing novel methods for enhancing maneuverability and mechanical durability. The research strengthens the scientific foundation of the swerve drive system utilized in our vehicle and directly relates to previous studies on drive mechanisms.

The mechanical design and analysis of autonomous mobile robots have been extensively studied using simulation tools such as Ansys, which provides robust capabilities for structural and dynamic evaluations. Demir et al. [14] conducted static and dynamic analyses of a mobile transportation robot with mecanum wheels, utilizing Ansys Workbench to assess the robot's structural integrity under a maximum load of 300 N. The study calculated critical parameters such as maximum stress and deformation to validate the design under extreme operating conditions. In another study, Prabhakaran et al.

[15] focused on a mobile robot designed for material handling, analyzing the structural behavior of the robot's chassis under a 300 N payload. The researchers utilized Ansys to simulate and validate the mechanical integrity of the chassis, ensuring the design could withstand the operational stresses, with maximum stress values of 35.99 MPa and deformation calculated at 0.000248 m.

Simulations of autonomous mobile robots and robotic systems are extensively employed to enhance the accuracy and efficiency of real-time applications. Koca et al. [16] simulated a mobile tank-driving robot in ROS and Gazebo environment. In this study, the physical and inertial properties of the robot were defined, and the motion and control of the robot were simulated. The simulations have made significant contributions in terms of identifying the challenges that mobile robots may encounter in real environments. Specifically, modeling and simulation of tank driving systems increase the reliability of real-time applications and facilitate the development of these systems. Ağralı et al. [17] simulated robot arms with the V-REP (CoppeliaSim) simulator. In the study, MATLAB and V-REP were synchronized to control the robot arm with a PID controller, and trajectory tracking and torque control were simulated with forward and inverse kinematic methods. This approach has been employed to ensure the accurate operation of robot arms, and such simulations are considered an important step towards more precise control of robotic systems.

Table 1. Summary of key studies on AMRs

Study	Focus Area	Techniques Used	Key Findings
Baskoro et al. (2020) [10]	Use of AMRs in healthcare	ROM20 AMR in hospital environments	The developed ROM20 AMR was used in various hospital applications such as disinfectant spray and food distribution, demonstrating the functionality of AMRs in healthcare.
Yan et al. (2023) [11]	Material handling in industrial environment	SLAM (Simultaneous Localization and Mapping)	AMRs provide significant advantages in material handling, overcoming flexibility issues in path changes through SLAM techniques.
Dhelika et al. (2021) [12]	Holonomic mobility and drive mechanism	Swerve drive mechanism	The swerve drive mechanism-equipped motorized hospital bed offers simplicity and cost-effectiveness, enabling easy integration into existing systems.
Zhao et al. (2023) [13]	Drive mechanisms and mobility systems in AMRs	Swerve drive system	The study presents new approaches to enhance the maneuverability and mechanical durability of swerve drive systems in AMRs.
Demir et al. (2021) [14]	Mechanical analysis	Static and dynamic analysis with Ansys Workbench	The Mecanum wheeled mobile robot's ability to safely operate under a load of 300 N was analyzed.
Prabhakaran et al. (2021) [15]	Structural durability analysis	SolidWorks and Ansys	The structural design of a mobile robot capable of carrying 30 kg was analyzed to determine maximum stress and deformation values.
Koca et al. (2020) [16]	AMR simulation	Simulation in ROS and Gazebo	A tank-steer mobile robot's physical and control features were successfully simulated for real-time applications.
Ağralı et al.(2020) [17]	Robot arm simulation	MATLAB and V-REP synchronization, PID controller	The robot arm's torque and trajectory control were successfully simulated using inverse and forward kinematic methods.

2. MATERIAL AND METHOD

The AMR development phase is divided into design, mechanical analysis, hardware, software, and simulations. In this study, the CAD program SolidWorks was used for vehicle design. SolidWorks was chosen because of its user-friendly interface, comprehensive range of tools, and robust simulation capabilities. Among CAD programs, SolidWorks facilitates the modeling of complex geometries and rapid visualization of designs. It is also compatible with analytical methods such as the FEM and

simulations that incorporate strength analysis [18]. The Ansys software utilized in these simulations directly supports SolidWorks file formats, such as. stl, .sldasm, and parasolid, enabling the seamless transfer of designs to the analysis environment. This approach mitigates the potential issues that may arise during file transfer. Driving simulations were conducted in a CoppeliaSim environment to perform the necessary tests, and the AMR behavior in various scenarios was investigated. Figure 1 shows the design stages of the mobile robot with payload-carrying capability.
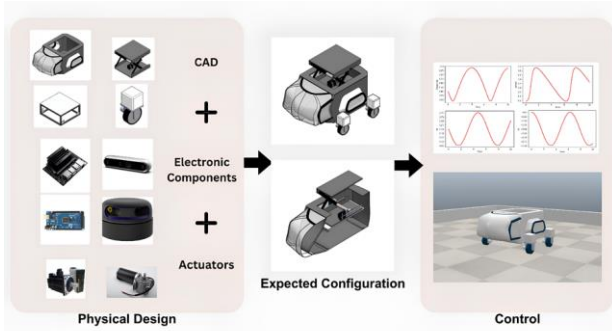
Figure 1. Design stages of a mobile robot with payload-carrying capability

Mechanical analysis is an essential stage in which a model designed with SolidWorks and prepared for analysis must be performed prior to production, particularly when its primary function is load-bearing. Ansys, which is utilized for the mechanical analysis of the vehicle, conducts the analysis using the FEM.

FEM is the process of transforming a finite function into a vector space using numerical methods in the domain of infinite function. [19]. The structure under analysis is divided into a specific number of small parts, termed finite elements, with the objective of mathematically examining the 'behavior' of each part using formulas derived from partial differential equations. The process from a model's real-world state to its discretized state is shown in Figure 2.

Figure 2. The process from a model's real-world state to its discretized state

FEA encompasses specific components such as thermal, electromagnetic, fluid, and structural operating environments. This analytical method provides a detailed visualization of structural deformation and torsion, while simultaneously illustrating the distribution of stresses and displacements. In structural simulations, FEA facilitates the production of stiffness and strength visualizations and contributes to the optimization of weight, materials, and costs. Furthermore, it offers a diverse range of simulation options to regulate the complexity between the modeling and analysis of a system.

In FEA, objects with complex geometries, which are challenging to analyze as a single unit, are subdivided into numerous smaller parts and analyzed separately. These subdivisions are referred to as "mesh". The mesh constitutes an integral component of the model and requires careful control to obtain the optimal results. Elements comprising small shapes are interconnected by points (nodes) that form the geometry of the model. Figure 3 illustrates the node structure that connects the elements [20].
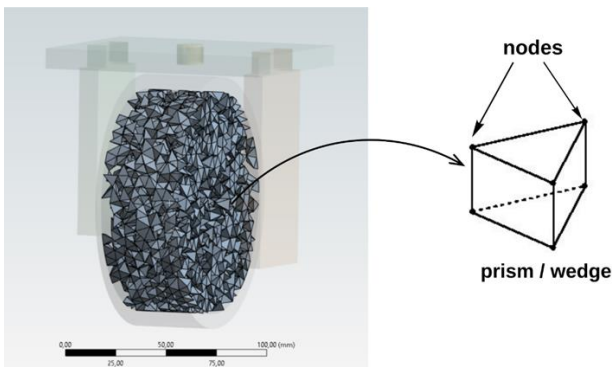

Figure 3. Illustrates the node structure that connects the elements

Mesh quality, element size, and element type are the most critical factors to consider when conducting a mesh analysis. The element size can be reduced in specific regions of the model, which is particularly crucial in critical areas where a high stress or deformation is anticipated. The mesh quality is ensured by through the uniformity of the element shape and optimized size distribution. Optimizing the mesh structure enhances accuracy while maintaining a reasonable solution time. To improve the mesh quality, adjustments are made based on the type and quantity of the elements utilized. Different element types and sizes influence the analysis results [21].

Mesh types are generally categorized as two-dimensional and three-dimensional. Two-dimensional structures are classified as triangular, and quadrilateral meshes. Triangular mesh comprises three-sided elements, and is generally preferred for surface modeling, and is utilized for modeling complex surfaces owing to its flexible structure. A quadrilateral mesh consists of four-sided elements and is often favored to provide more stable results in smooth geometries. Examples of three-dimensional mesh structures include tetrahedral, hexahedral, and wedge meshes. Tetrahedral mesh consists of tetrahedron elements and enables the modeling of complex geometries with high accuracy. Hexahedral mesh comprises hexahedron elements and is suitable for planar structures or regular geometries. Wedge mesh contains prism/wedge elements and is employed in transition zones, complex structures, or when detailed modeling of specific parts is required, which is particularly advantageous in areas that require precise examination.

Selecting appropriate mesh element types for the part reduces the number of elements, thereby decreasing the analysis time and post-analysis processing time. Furthermore, for nonlinear systems and instances in which the arrangement of elements is physically significant, the utilization of hexahedral and quadrilateral

69

shaped elements is more suitable. Consequently, hex20, tet10, and wed15 were predominantly used in the analysis. The mesh types are also formulated according to the combination of the element types. The mesh types vary based on the arrangement and structure of the elements. Each mesh type presents distinct advantages and disadvantages; therefore, a type that aligns with the requirements of the application should be selected. A structured mesh is preferable for simpler geometries and when expeditious solutions are required, whereas a nonstructured mesh offers a more flexible solution for complex geometries. Hybrid mesh is frequently utilized to balance both accuracy and solution efficiency in complex

models. An adaptive mesh is an appropriate method to achieve precise results; however, the processing time and computational cost are higher [21].

The appropriate selection of the mesh structure and type is a critical factor that directly influences the accuracy of the simulation results and the efficiency of the computational process. The determination of which mesh type to employ should be based on consideration of the model geometry and the parameters to be analyzed. Figure 4 shows the Ansys interface of the mesh analyzed part.
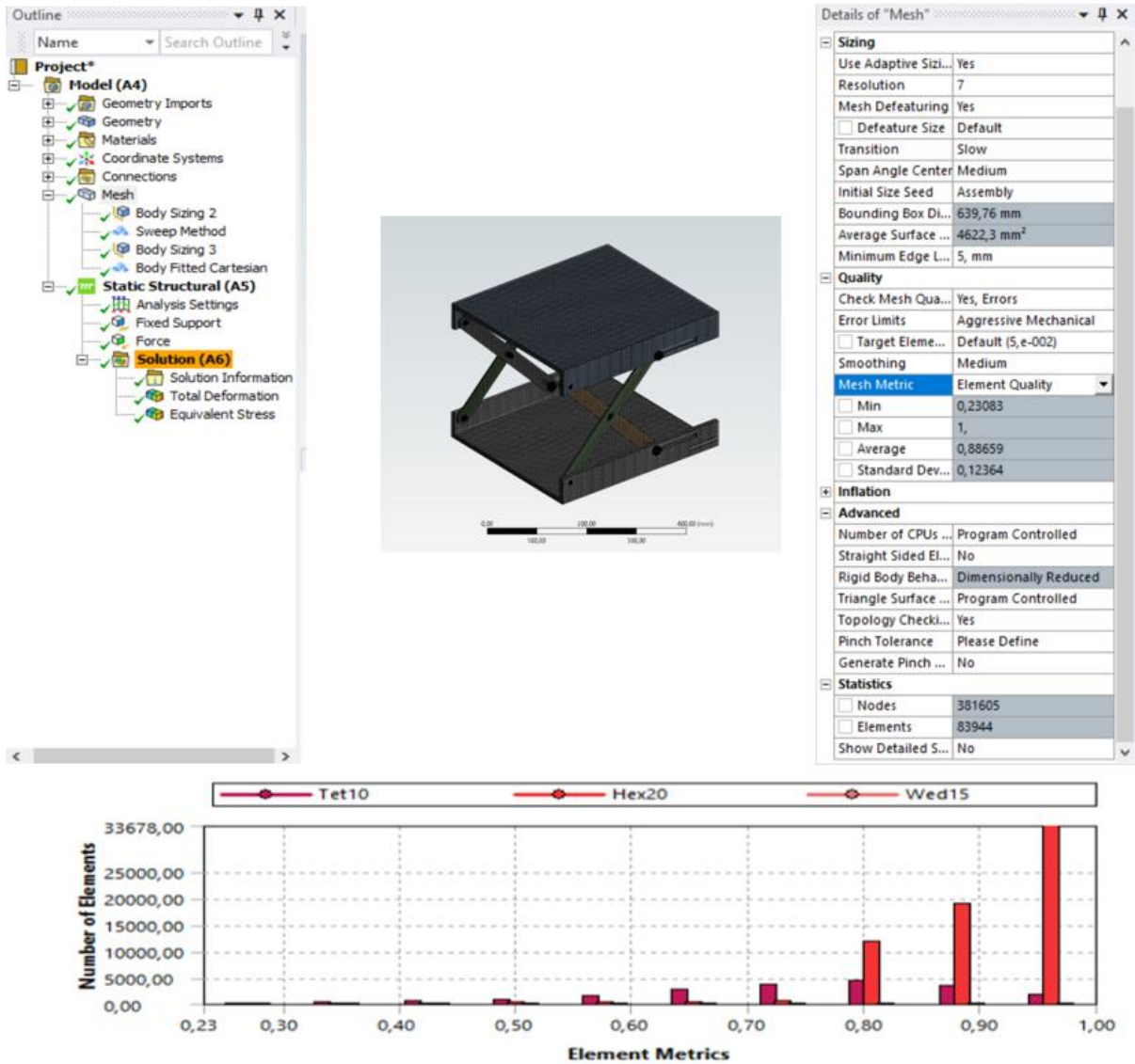
Figure 4. Ansys interface of the mesh analyzed part

Ansys is comprised of various programs for conducting different analyses. In this study, Workbench and Mechanical from the Ansys suite were utilized. Ansys Mechanical, which performs static and dynamic analyses of parts and assemblies in complex structures as well as

torsion, stress, vibration, and heat transfer analyses, simulates this work and enables the observation of their behavior in real-world conditions [22]. The steps of the FEM in Ansys are schematized in flowchart form in Figure 5.
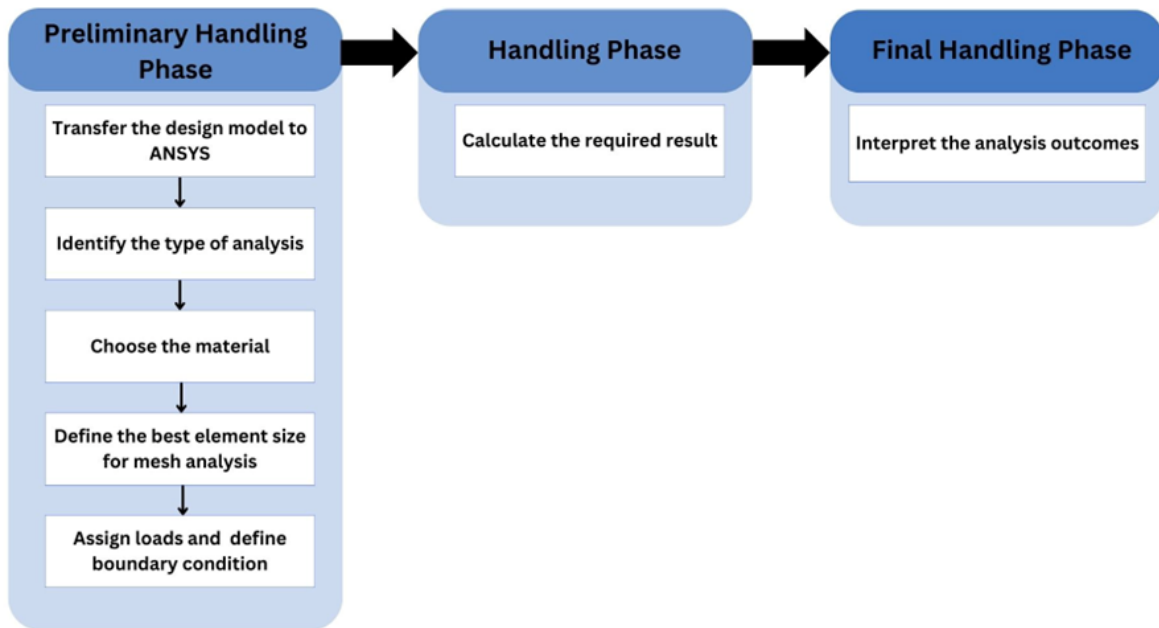
Figure 5. The steps of the FEM in Ansys

In the subsequent phase, simulations are utilized to examine real-time robot system design, modeling, and production, encompassing computer, electronics, mechanics, and control systems, among other interdisciplinary aspects. This process evaluates the performance of the model in the design verification stage prior to initiating production under the specified environmental conditions. Given that simulators are appropriate for conducting necessary tests of a theoretically designed robot or robotic system in a virtual environment, numerous robot simulators such as Gazebo, Webots, and CoppeliaSim have been developed [17]. Among these platforms, CoppeliaSim, which was employed in this study, facilitates the simulation of complex robotic scenarios by creating and manipulating 3D models of robots, sensors, and environments [23]. In the CoppeliaSim environment, the system requires control through code blocks to enable the movement and processing of data received from sensors of the mobile robot. Within the CoppeliaSim simulation environment, Lua Script can be utilized to control the mobile robot's movement via code blocks; alternatively, programming languages such as MATLAB, C/C++, or Python can be employed. Python, a high-level programming language known for its versatility and extensive library support, was selected for the implementation of the motion and deep learning algorithms of the mobile robot [17].
The Spyder integrated development environment (IDE) was employed to develop and manage Python code in conjunction with CoppeliaSim. Spyder provides support for developers and contributes to more effective simulation execution [24].

2.1. Robot Kinematics

Robot kinematics is employed to investigate the motion of robots within a given workspace. By leveraging robot kinematics, the position and orientation of the end effector and the corresponding joint variables can be determined within the robot's operational environment. Robot kinematics is divided into two distinct categories: forward kinematics and inverse kinematics. The forward kinematics of the robot is employed to determine the position of the end effector corresponding to the value of each joint variable, while each joint variable corresponding to the position of the end effector is calculated by inverse kinematics [25].

2.1.1. Wheel kinematics

As the wheel system of the vehicle, as shown in Figure 6, a DC motor was used to rotate the wheel, and a servo motor was used to direct the wheel at certain angles to increase the movement capacity. A total of 8 motors were used in each wheel, one DC motor and one servo motor.
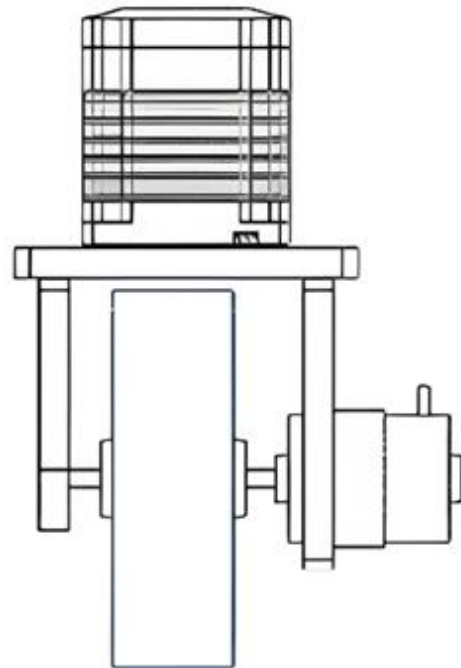

Figure 6. Single wheel structure of the designed vehicle

Vehicle structures with an independent translation and steering module on each wheel are called Wheel Independent Steering or Swerve Drive. Such drive systems are used in weight transportation, agricultural machinery or the Mars Rover. Advantages of the swerve drive system:

- The system provides a high level of mobility. In swerve driving, the direction of movement and orientation are independent, allowing the robot to face forward while moving sideways. Furthermore, the Instantaneous Center of Rotation (ICR) is not fixed in swerve driving, as in ackermann and differential driving. This flexibility allows it to combine linear and rotational movements, which other driving systems cannot do.

- They have wheel structures suitable for payload carrying. Although the degree of freedom is the same as for swerve driving, omni wheels cannot carry the same load due to the lower carrying capacity of the rollers that allow them to move sideways.
- It does not depend on wheel deflections as a multi-wheel differential drive does. This allows the robot to use more motor torque to move forward, consuming less power. While omni and mecanum wheels have movement limitations due to wheel clogging in dust and dirty environments, swerve drive wheels do not have such problems [26]. Figure 7 shows the wheel configurations.
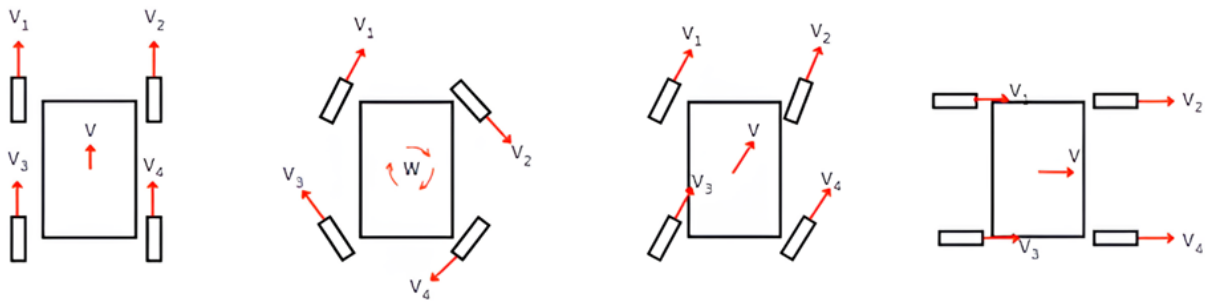
Figure 7. Wheel configurations

In short, in the designed autonomous mobile vehicle, the wheels are controlled independently at different angular speeds. If we consider the single-wheel system, the DC motor performs a rotational motion in the y-axis, which allows the wheel to perform a translational motion in the x-axis. The servomotor adjusts the wheel orientation by rotating in the z-axis. Figure 8 shows the vehicle-wheel axis sets.
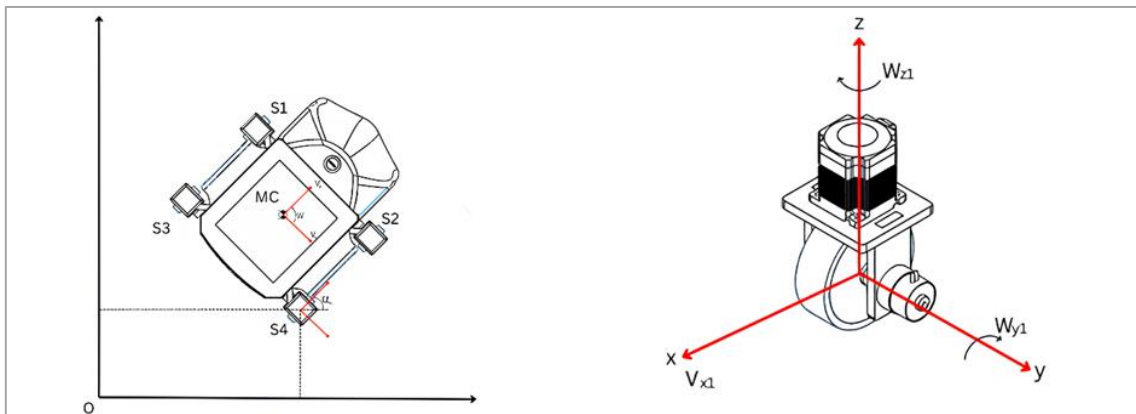
Figure 8. Vehicle-wheel axis sets

The vector sum of the wheel speeds is shown in Equation 1. If the position of the vehicle relative to a fixed set of axes x and y, the direction of our position axis remains constant as the vehicle moves. The position of the single wheel structure relative to the axis of rotation is $\vec{r} = (r_x, r_y, 0)$. When the robot moves with a linear velocity $\vec{v} = (v_x, v_y, 0)$ and an angular $\vec{\omega} = (0, 0, w_x)$ the linear velocity of the wheel is calculated as in Equation 2 [27].

$$\vec{v_1} + \vec{v_2} + \vec{v_3} + \vec{v_4} = \vec{V} \tag{1}$$

$$\vec{V_m} = \vec{V} + \vec{\omega} \times \vec{r} \tag{2}$$

The matrix form of the linear velocity of the wheel is presented in Equation 3. If we assume that the angular velocity of the vehicle is zero, the displacement matrix is as shown in Equation 4. Substituting this equation into Equation 3, Equations 5 and 6 are obtained.

$$\begin{bmatrix} V_{mx} \\ V_{my} \end{bmatrix} = \begin{bmatrix} 1 & 0 & -r_y \\ 0 & 1 & r_x \end{bmatrix} \begin{bmatrix} V_x \\ V_y \\ \omega \end{bmatrix} \qquad (3)$$

(r_{0x}, r_{0y}) : The initial position of the wheel in relation to the center of the robot

$\theta(t)$: Heading over time

t : Duration

$$\begin{bmatrix} r_x \\ r_y \end{bmatrix} = \begin{bmatrix} \cos(\omega t) & -\sin(\omega t) \\ \sin(\omega t) & \cos(\omega t) \end{bmatrix} \begin{bmatrix} r_{0x} \\ r_{0y} \end{bmatrix} \qquad (4)$$

$$V_{mx}(t) = v_x - \omega \times (r_{0x} \times \sin(\omega t) + r_{0y} \times \cos(\omega t)) \qquad (5)$$

$$V_{my}(t) = v_y + \omega \times (r_{0x} \times \cos(\omega t) - r_{0y} \sin(\omega t)) \qquad (6)$$

$$V_{mx}(t) = v_x - \omega x \sqrt{(r_{0x}^2 + r_{0y}^2)} \, x \cos(\omega t - \tan^{-1}(r_{0x}, r_{0y})) \qquad (7)$$

$$V_{my}(t) = v_y + \omega \times \sqrt{(r_{0x}^2 + r_{0y}^2)} \\ \times \cos(\omega t - \arctan(-r_{0y}, r_{0x})) \qquad (8)$$

By applying Equations 7 and 8, the vehicle velocity is calculated sinusoidally according to the origin. The velocity of the wheel:

$$\theta(t) = \arctan\left(v_{my}(t), v_{mx}(t)\right) - \omega t, mod \, 2\pi \qquad (10)$$

2.1.2. Lift system kinematics

Autonomous mobile robots with payload carrying capability require special payload lifting mechanisms to move payloads from one location to another. These mechanisms can operate both manually and automatically. In general, scissor platforms are the preferred option, as they minimize the footprint of the payload lifting mechanism within the mobile robot and avoid the restriction of its mobility. These platforms are composed of scissors fixed to each other by bearings at the joints, and they offer a high payload capacity and durability.

For the movement of the scissors, the shaft of a servo motor is connected to the cylinder between two opposite scissors. With the rotation of this shaft connected to the servo motor, the scissor bases are shifted back and forth. So the upper platform to which the scissors are connected moves simultaneously on the vertical axis. In line with this movement, the height of the platform is adjusted and the load handling operation takes places. Figure 9 shows mechanism of lift system.
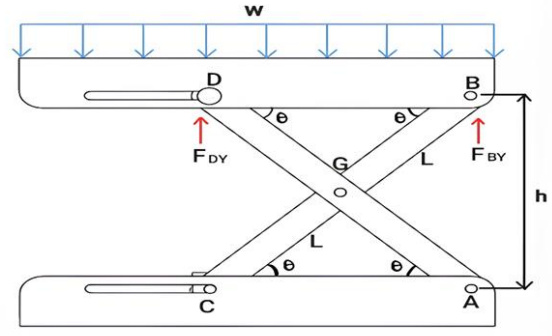
Figure 9. Lift system

W : Distributed load

d_{AC} : Length of AC

L : Length of the scissors

h : Platform height

F_{BY} and F_{DY} : Forces applied by the scissors to the platform

L_w : Distance of the distributed load to the moment point

The vertical height of the scissors system to which the upper platform is connected is h, the angle of the scissors with the horizontal is θ and the connections between h and θ are shown in Equation (11-17).

$$L^2 = \left(\frac{h}{2}\right)^2 + \left(\frac{d_{AC}}{2}\right)^2 \qquad (11)$$

$$\left(\frac{h}{2}\right)^2 = L^2 - \left(\frac{d_{AC}}{2}\right)^2 \qquad (12)$$

$$|\overrightarrow{v_m}(t)| = \sqrt{v_{mx}^2(t) + v_{my}^2(t)} \qquad (9)$$

$$\frac{d_{AC}}{2} = \cos\theta \times L \qquad (13)$$

$$\left(\frac{h}{2}\right)^2 = L^2 - (\cos\theta \times L)^2 \qquad (14)$$

$$\left(\frac{h}{2}\right)^2 = L^2(1 - \cos\theta^2) = L^2 \times \sin\theta^2 \qquad (15)$$

$$\sin\theta = \frac{\frac{h}{2}}{L} \quad , \quad h = 2 \times L \times \sin\theta \qquad (16)$$

$$\frac{d_{AC}}{2} = L \times \cos\theta \qquad (17)$$

Instead of point forces, a distributed load is applied to the scissors system. The applied distributed load must be converted into a single singular force in order to substitute it in the moment and force equations. k represents the area of the upper platform where the distributed load is applied, m represents the total mass of the platform and the distributed load. W represents the total force exerted by the upper platform and the distributed load reduced to a singular force. This transformation is shown in Equation 18.

73

$$W = w \times L \tag{18}$$

During the movement of the scissor system, points A and B remain stationary while points C and D move. Due to this motion, the velocity equations of points C and D are expressed in Equation (19-29) [19].

Velocity equations for point C:

$$V_C = V_G + V_{\frac{C}{G}} \tag{19}$$

$$V_C = V_G + \frac{d}{dt}\left(r_{\frac{C}{G}}\right) \tag{20}$$

$$r_{\frac{C}{G}} = |CG| \times \cos\theta \times i + \sin\theta \times j \tag{21}$$

$$\frac{d}{dt}\left(r_{\frac{C}{G}}\right) = |CG| \times \cos\theta \times \frac{d\theta}{dt} \times i \times \sin\theta \times \frac{d\theta}{dt} \times j \tag{22}$$

$$V_{Cx} = \frac{dG}{dt} - |CG| \times \sin\theta \times \frac{d\theta}{dt} \tag{23}$$

$$V_{Cy} = \frac{dG}{dt} - |CG| \times \cos\theta \times \frac{d\theta}{dt} \tag{24}$$

Velocity equations for point D:

$$V_D = V_G + V_{\frac{D}{G}} \tag{25}$$

$$V_D = V_G + \frac{d}{dt}\left(r_{\frac{D}{G}}\right) \tag{26}$$

$$r_{\frac{D}{G}} = |DG| \times \cos\theta \times i + |DG| \times \sin\theta \times j \tag{27}$$

$$V_{Dx} = \frac{dG}{dt} - |DG| \times \sin\theta \times \frac{d\theta}{dt} \tag{28}$$

$$V_{Dy} = \frac{dG}{dt} - |DG| \times \cos\theta \times \frac{d\theta}{dt} \tag{29}$$

The free body diagram of the scissors used in the lifting system is shown in Figure 10. In this diagram, the connection point of the scissors is called G and the connection points between the scissors and the platform are called A, B, C, D.
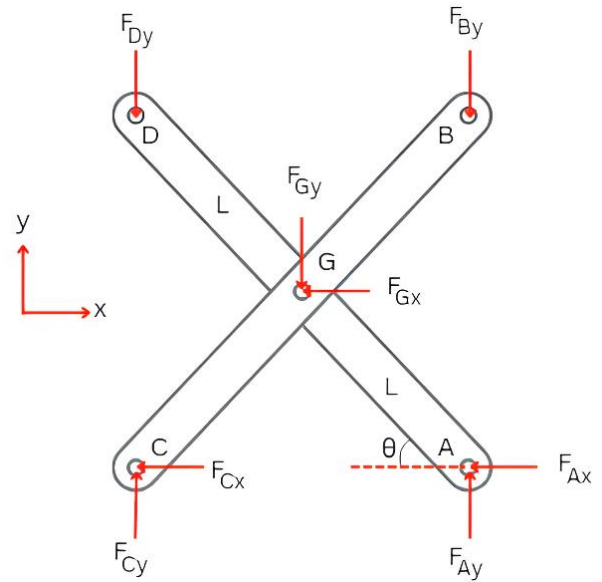
Figure 10. Free body diagram of scissors

The clockwise direction was determined as the direction of rotation of the moment and considered as the positive direction for the whole equation. Then, the total moment and the total force in the x and y axis were calculated for the whole system. These calculations are expressed in Equation below [19].

$$\sum M_D = 0; -W \times |L_w| + 2 \times F_{By} \times |DP| = 0 \tag{30}$$

$$\sum F_y = 0 \; ; \; 2F_{Dy} - W + 2F_{By} = 0 \tag{31}$$

$$\sum F_x = 0; \quad F_{Gx} - F_{Ax} = 0 \tag{32}$$

$$\sum F_y = 0; \quad -F_{Dy} + F_{Gy} + F_{Ay} = 0 \tag{33}$$

$$\sum M_d = 0; \quad -F_{By} \times 2 \times \cos\theta - F_{Gy} \times L \times \sin(90 - \theta) + F_{Gx} \times L \times \sin\theta \tag{34}$$

$$\sum F_x = 0; \quad F_{Cx} - F_{Gx} = 0 \tag{35}$$

$$\sum F_y = 0; \quad -F_{By} - F_{Gy} + F_{Cy} = 0 \tag{36}$$

2.2. Robot Controller

Sensors and simulation environments are often used in robots to obtain the information required for joint handling, such as robot positions, velocities and interaction forces between the load and mobile robots [28]. In order to analyze the motion of the mobile robot in real environment, the URDF file of the vehicle designed in Solidworks is exported to the CoppeliaSim environment. Figure 11 shows the vehicle exported to the CoppeliaSim environment. URDF (United Robotics Description Format) file is a language format written in

accordance with XML (Extensible Markup Language) language structure to describe robots. In this file, "continuous" is used for continuous rotation and "revolute" is used for rotation within a certain angle range.
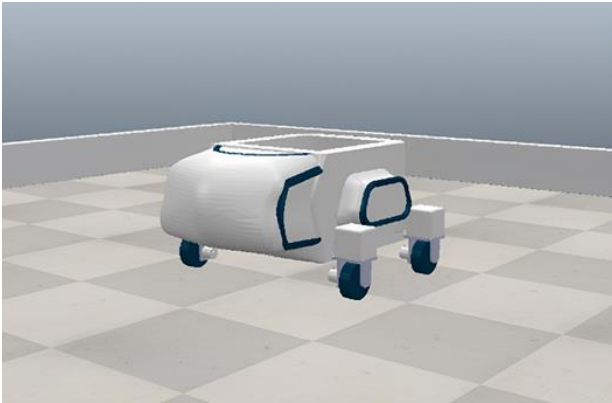
Figure 11. The vehicle exported to CoppeliaSim environment

Python was used to control the parameters of the vehicle exported to the CoppeliaSim environment. To establish a connection between CoppeliaSim and Python language, Spyder IDE, which has an easy and understandable interface and can be easily integrated with CoppeliaSim, was used. In this way, the program is made ready to control the parameters such as velocity, direction and angle of the joint that give the mobile robot the ability to move.

2.3. System design

One of the challenges faced by mobile robots is the problem of localization in an indoor environment. Inaccurate localization can lead to inefficient path planning and inaccurate detection of obstacle locations. Therefore, it is possible to improve the indoor localization of mobile robots by using different sensors. Sensors integrated into the robot include ultrasonic, infrared and laser sensors, as well as LIDAR, depth and stereo vision cameras [29]. Figure 12 shows the system design.
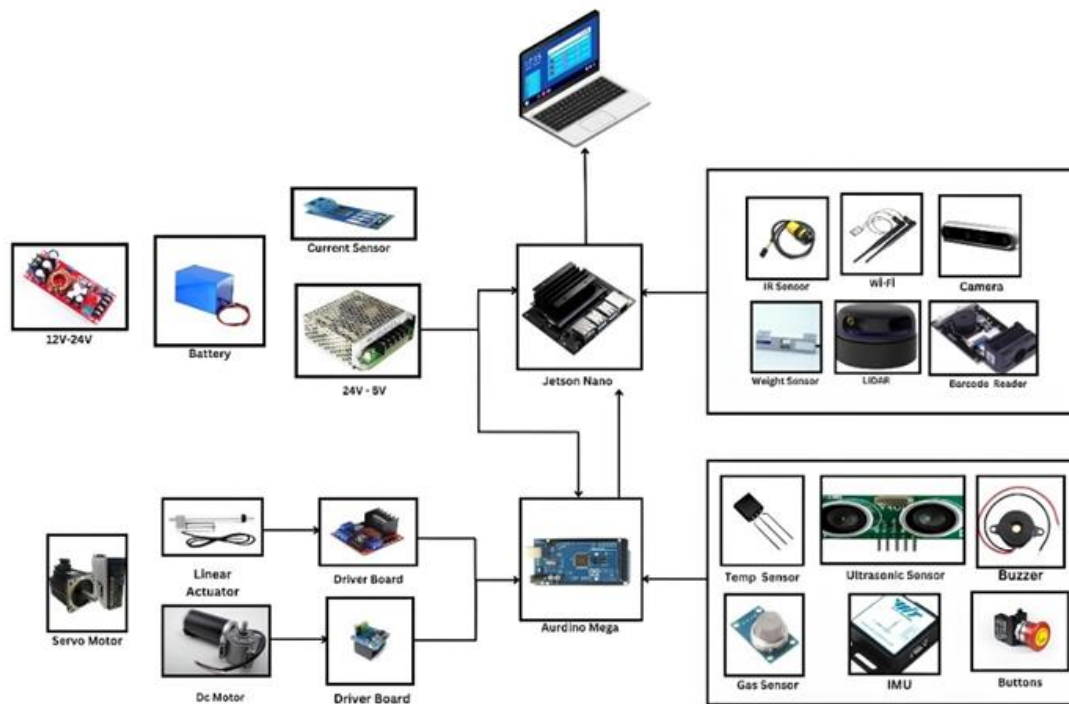
Figure 12. System design

Today, autonomous vehicle technologies are advancing rapidly with the integration of Artificial Intelligence (AI) and deep learning algorithms. These developments require powerful processing capabilities and advanced AI-enabled hardware. NVIDIA Jetson Nano, a platform designed for robotic systems, was used as the main processor board. Jetson Nano manages the processes of collecting and processing data from various sensors in an autonomous vehicle, generating the corresponding control commands, and providing communication between the vehicle and the ground station via a Wi-Fi module. Electronic components connected to the main processor board:

- LIDAR (Laser Imaging Detection and Ranging) is a system that detects the position and distance of objects by sending laser pulses and calculating the return time of signals reflected from objects. In autonomous vehicles, LIDAR sensors continuously scan and map the vehicle's surroundings [30].
- Algorithms that combine camera, depth and image data are used to efficiently perform artificial intelligence tasks such as object recognition, path tracking and mapping.
- The weight sensor is responsible for calculating the weight of an object by measuring the strain on the vehicle. The data obtained from the sensor

is used to determine whether the lift is capable of lifting the load in question.

- Arduino Mega is a coprocessor board used to reduce the processing intensity on the main processor board.

Arduino is an open source physical programming platform that realizes basic input and output applications with peripherals using the processing/wiring language [31].

The Arduino Mega, preferred for its large number of input/output pins and ease of use, sends data from sensors and electronic components to the main processor card. The main processor provides motor control according to the data received from the board. Electronic components connected to the coprocessor board:

- Ultrasonic sensors are detection devices that measure the distance of objects with sound waves. By placing this sensor all around the vehicle, the autonomous vehicle can detect objects and avoid collisions by avoiding objects. This increases the vehicle's ability to maneuver effectively and ensures safe progress.
- IMU is an electronic unit that collects various data such as angular velocity (gyro), acceleration, magnetic field and inclination (inclinometer) in a single sensor. These sensors are needed in areas such as factories where GNSS signals may be insufficient or interrupted [32].
- The motors and driver boards are controlled by Arduino Mega and used to control the motion of DC and servo motors.

2.4. Experimental setup

In the design of AMR, the weight and dimensions of the payload to be transported represent among the most critical factors that directly affect the payload capacity. In order to ensure the safe transportation of the load, it is imperative that the maximum weight does not exceed the capacity of the AMR. The design of the vehicle's transport platform is informed by an understanding of the dimensions of the load. In the process of sizing an AMR the physical characteristics of the area in which it will operate are taken into account. These include the width of roads, narrow passages, and the robot's ability to navigate these environments. Additionally, the design considers the presence of other equipment in the operational environment, such as safety sensors and emergency stop mechanisms. It also ensures that there is sufficient space for batteries and motors, preventing any potential hazards to personnel.

The payload carrying vehicle, which was designed as an original design unlike the current examples, is shown in Figure 14. When designing the vehicle, it was taken as a reference that it can go under a 50x95 cm platform and carry a load of 125 kg. Accordingly, the weight of the vehicle designed in 885×796×464 mm dimensions is approximately 60 kg. According to the dimensions of the

vehicle, which is moved with the swerve driving system, the wheel dimensions were determined as 125x40 mm.

Figure 13. Closed and open state of the scissor system

The scissor system used for load carrying in the mobile robot is 400×360×120 mm in closed state and 400x360x323 in open state and is shown in Figure 13. In addition, the upper platform to which the scissors are connected can be opened to a height of 187 mm from the upper base of the vehicle. The chassis, to which the wheels are attached, and which carries the electronics and the lifting system, has dimensions of 460×500×218 mm. In designing the chassis, several considerations were taken into account, including the ability to safely carry the load and the lifting system, support for the body, dimensions that fit within the body, and sufficient space for electronic components.
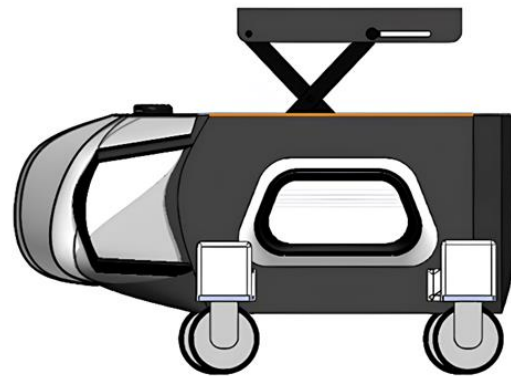
Figure 14. Side view of the designed vehicle

The materials that are scheduled to be utilized in the production of the vehicle are stainless steel and an aluminum alloy. Stainless steel is renowned for its exceptional corrosion and rust resistance in industrial settings, which guarantees the AMR's durability and dependability over an extended period. Furthermore, stainless steel was selected for the scissors, pins, and cylinder due to its superior strength compared to aluminum alloys, which allows for the safe transportation of heavy loads. Aluminum alloy was selected for the body, chassis, wheel joints, and the upper and lower base of the lift due to its lightweight, durable, and easily machinable properties. The reduced weight of aluminum alloys results in decreased energy consumption, which in turn improves the vehicle's driving dynamics and increases maneuverability, thereby extending battery life [33]. The structural properties of the materials used in the mobile vehicle are shown in Table 2.

76

Table 2. Material information

Properties	Stainless Steel	Aluminum Alloy	Unit
Density	7750	2770	Kg m^{-3}
Young's Modulus	193000	71000	MPa
Poisson Ratio	0.31	0.33	MPa
Shear Modulus	73664	26692	MPa
Yield Strength	207	280	MPa
Tensile Strength	586	310	MPa

The strategic selection of mesh sizes in ANSYS analysis is of great importance in terms of providing the appropriate sensitivity to different regions of the analysed structure. In this study, the smallest mesh size of 3 mm was preferred for critical connection points with high stress concentrations, joints of moving parts and areas with complex geometries. More detailed analyses were performed by using this small mesh size, especially in areas that require precise solutions such as connection points in the lever system and wheel connection areas.

Conversely, the largest mesh size employed in the analysis, 6 mm, was utilised in regions where the load density is more homogenously distributed and does not necessitate high precision. This approach was selected in order to optimise the solution time and reduce the computational load. The largest mesh size was employed for the wheel diameter, while the remaining components were modelled with appropriate mesh sizes between these two sizes. Consequently, different mesh sizes were chosen according to the requirements of each region, resulting in an optimal balance between solution time and accuracy.

The mesh, stress, and deformation analyses of the design were transferred to the static structural module of Ansys for analysis. Initially, a static analysis of the mesh was performed, which examined the real-world behavior of the analyzed parts under load. Based on the analysis, a determination was made regarding the suitability of the materials used in the design.

3. RESULTS

To obtain results approximating real-world conditions from finite element analyses conducted using Ansys, it is essential to carefully examine the values of element quality and skewness derived from the mesh analysis. Element quality can be calculated as the ratio of the volume to the sum of the squares of the edge lengths for 2D elements. In another way, for 3D elements, it is calculated as the square root of the cube of the sum of the squares of the side lengths. Element quality represents a composite quality metric ranging from zero to one. When the parameter value is 'one', it indicates an ideal cube or square. When the value is zero, it has a negative volume. [34].

For Mesh, skewness is one of the primary quality measures. Skewness determines the proximity of a face or cell to its ideal (equilateral or equiangular) shape. A skewness value approaching 0 indicates that the element closely approximates its ideal shape (e.g., equilateral shapes for triangular or quadrilateral elements). As the skewness value increases, the elements deviate further from the ideal shape, potentially distorting the analysis results. In Ansys, the skewness value is typically measured on a scale from 0 to 1, with a recommended maximum value of 0.95. Lower skewness values facilitate more accurate analysis results [35].

The results of the analysis show that element quality varies between 0.8 and 1 on average, while skewness is between 0.1 and 0.2. Therefore, it can be concluded that the deformation analysis, which evaluates how much a structure or material changes shape under applied forces and assesses its performance under real-world conditions, and the stress analysis, which determines the internal forces acting within a material and its ability to withstand applied loads, yield results that are close to reality.

The results of the analyses of the body, chassis, wheel mechanism, and lift system are listed in Table (3-6).

3.1. Body

For the outer shell of the vehicle, a body with dimensions of 885×670×355 mm was designed using aluminum alloy, which is a tough material. Figure 16 shows the element metric values of the different mesh types in the car body mesh analysis. It can be seen that element types such as tet10, hex20, wed15, tri3, and quad4 were used. This indicates that a hybrid mesh structure is preferred for representing the complex geometry of the model more accurately. For the outer shell of the vehicle, a body with dimensions of 885×670×355 mm was designed using aluminum alloy, which is a tough material.

The tet10 (tetrahedral) elements used in the analysis are typically preferred for irregular mesh structures and are useful for solving complex geometries. However, they do not provide the same level of accuracy as hexahedral elements do. In contrast, hex20 (hexahedral) elements, which occupy a large space in the model, offer a high solution accuracy and computational efficiency in regular mesh structures. Additionally, wed15 (wedge) elements are used in areas close to the surfaces of the model; these elements are beneficial in regions where triangular-based prismatic structures must align with complex surfaces. The surface elements in the model are represented by tri3 and quad4 elements. tri3 (triangular) elements are preferred for more complex surfaces and irregular areas, while quad4 (quadrilateral) elements are used to convert regular surfaces into a more homogeneous mesh structure [36-37].

In conclusion, the hybrid mesh structure was optimized according to the geometric characteristics by combining both regular and irregular elements. This strategy enhances the solution accuracy while balancing computational costs. In particular, the combined use of hex20 and tet10 elements allows for a denser mesh structure in critical areas, thereby increasing the reliability of the analysis results. The 3D model in Figure 15 illustrates the distribution of these elements over the model, showing the homogeneity of the mesh structure, both on the surface and within the internal structure.
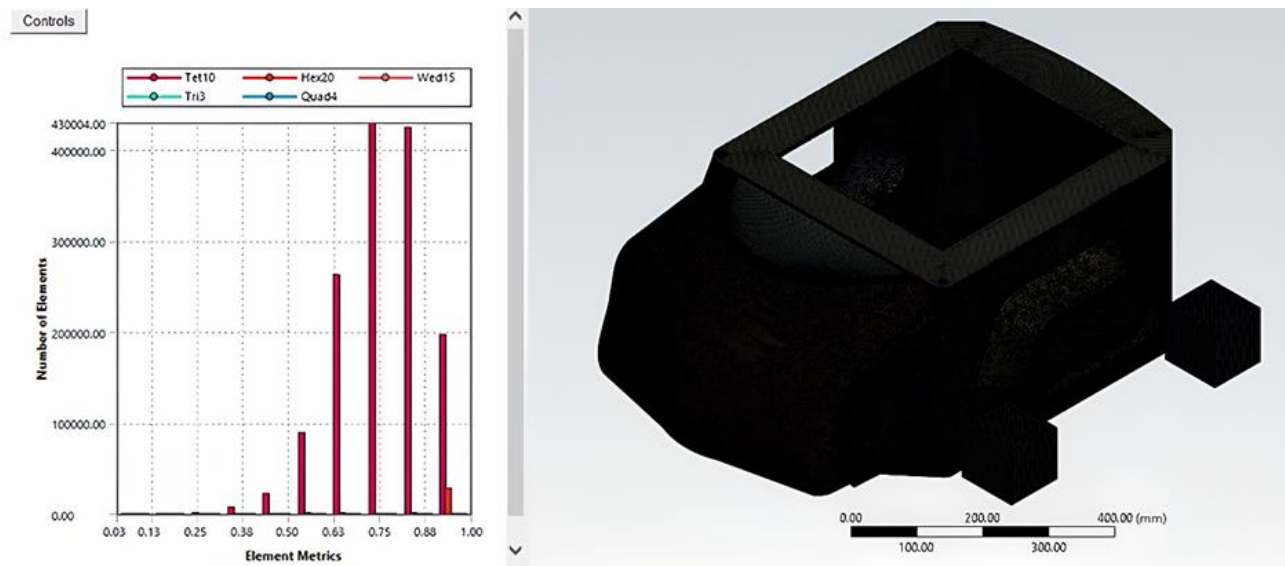
77

Figure 15. Body mesh analysis

Figure 16 and the data presented in Table 3 were used to evaluate the quality of the mesh structure used in the vehicle body design and the geometric accuracy of its elements. The graph examines various quality metrics of the elements with two particularly significant metrics: element quality and skewness values.

The element quality is a critical factor in determining the analytical accuracy of mesh structures. The average element quality value is 0.78, which is considered acceptable, although the ideal value is closer to 1. A value of 0.78 indicates that most elements possess sufficient quality; however, some elements may exhibit reduced quality. The maximum element quality value is 1, indicating that some elements are of excellent quality, while the minimum quality value of 0.0295 suggests that certain elements have very low quality. Nonetheless, the presence of such low-quality elements in the non-load-bearing sections of the body is unlikely to significantly affect the overall accuracy of the results.

The skewness metric reflects the distortion in the shape of the elements. A low skewness value indicates a better element geometry. The maximum skewness value is 0.99, suggesting that some elements are nearly deformed. Such high skewness values can lead to erroneous deformation and stress analysis. The average skewness value of 0.3 is generally acceptable; however, caution may be necessary in regions where elements exhibit high skewness. The minimum skewness value of 1.3×10^{-10} is nearly zero, indicating that some elements have a very regular shape. Owing to the complex structure of the body, 1,463,049 elements and 2,798,461 nodes were utilized. This large number of elements signifies a detailed analysis and appropriate representation of the intricate geometry of the body.

These data suggest that, overall, the body mesh structure is sufficient, although improvements could be made in terms of element quality and skewness in certain areas. In particular, during the deformation and stress analyses, elements with high skewness may result in erroneous outcomes. However, considering that these areas do not

bear loads, their effect on the overall analysis results is expected to be minimal.

Table 3. Body mesh analysis results

Number of Elements	Number of Nodes	Element Quality	Skewness
1463049	2798461	Max: 1 Avg: 0.78 Min: 0.0295	Max: 0.99 Avg: 0.3 Min: 1.3×10^{-10}

The effects of the forces on the vehicle's body are evaluated through deformation analyses, as shown in Figure 16, while the stress analyses are presented in Figure 17. The deformation analysis illustrates the deformations that occur under an applied force of 325 N on the body. This analysis is critical for understanding the mechanical stability and durability of the body.

According to the analysis results, the deformation ranged from 0 to 0.55 mm. This is considered a very small deformation range. Given the dimensions of the vehicle body, this amount of deformation can be deemed insignificant. Considering that the body is not a primary load-bearing component and that a durable material such as aluminum alloy is used, it can be stated that this deformation does not pose a safety concern.

In conclusion, the body exhibits good resistance to the applied forces, and the resulting deformation is not significant enough to affect the structural integrity of the vehicle. This indicates that the body was designed safely, with minimal deformation occurring in sections that did not carry loads.
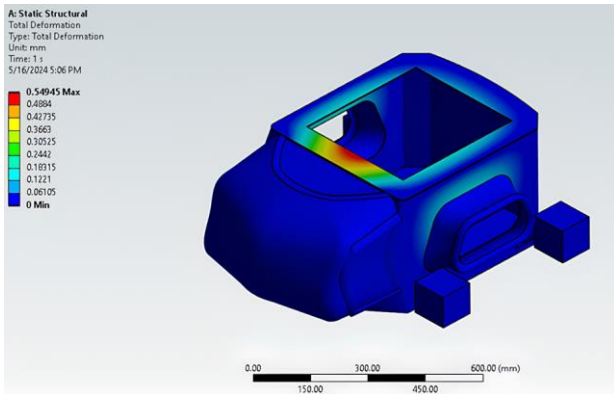
Figure 16. Vehicle body deformation analysis

The stress analysis illustrates the stresses occurring in various regions of the body under the same applied force of 325 N. The stress values range from 0 to 33.6 MPa. Considering the force applied on the body and the mechanical properties of the material, these stress levels are also quite low. Given the mechanical properties of aluminum alloy, these stress levels remain well below the yield limits of the material.

In other words, according to the stress analysis results, the body remained within a safe operating range under the applied forces. No excessive stress occurs in any part of the body, indicating that the design of the body possesses adequate durability against forces and pressures.
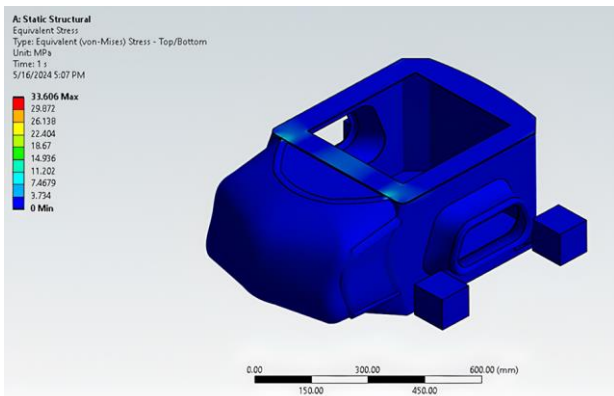
Figure 17. Vehicle body tension analysis

In other words, according to the stress analysis results, the body remained within a safe operating range under the

applied forces. No excessive stress occurs in any part of the body, indicating that the design of the body possesses adequate durability against forces and pressures. Both analyses are critical simulations that examine the mechanical properties of the body. The deformation analysis in Figure 16 demonstrates that the body deforms minimally under applied forces. However, the stress analysis in Figure 17 shows that the stresses occurring in different regions of the body remain within a safe range. These results indicate that the design of the vehicle and the materials used are safe against forces and loads and are unlikely to cause issues in the long term.

3.2. Chassis

The chassis has dimensions of 460×500×218 mm and is generally rectangular. Therefore, the chassis, which carries the entire weight and load of the system, is one of the most critical components for autonomous vehicles. Accordingly, the chassis is designed using aluminum alloy, which is both lightweight and durable. The main reason for this is that aluminum increases the carrying capacity while simultaneously reducing the overall weight of the vehicle. In addition, aluminum alloys offer high strength and corrosion resistance, creating long-lasting and durable structures. This is especially critical for autonomous mobile vehicles that operate under harsh environmental conditions.

The mesh structure used in the analysis of the chassis was determined based on the complexity of the geometry and the accuracy of the analysis. Despite the rectangular structure of the chassis, a more flexible and adaptive mesh structure is required in some curved regions and corners. Therefore, the mesh structure shown in Figure 18 was obtained using tetrahedral (tet10) and hexahedral (hex20) elements together for the mesh element, and mesh analysis of this structure was performed. Tetrahedral elements were used in the geometrically complex and angular regions to capture fine details and model complex areas more precisely. On the other hand, hexahedral elements have a more regular structure, especially when used on flat surfaces and rectangular structures, and are preferred on wider and flatter surfaces. The choice of these mesh elements reduced the analysis time and at the same time increased the accuracy of the chassis analysis.

79

Figure 18. Chassis mesh analysis

The results of the mesh analysis for the chassis are presented in Table 4. According to this table, the chassis contains 43760 elements and 210717 nodes in total. The large number of elements allows the geometry to be modeled in detail and allows better determination of the stress and deformation values at different points of the structure. This is of great importance in the analysis of criti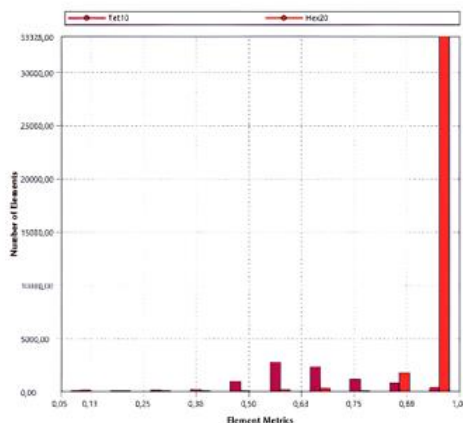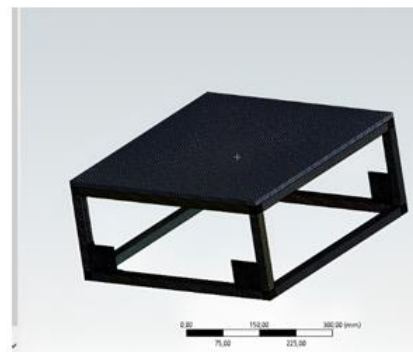cal load-bearing structures such as chassis. The maximum element quality calculated in the analysis is 1, and the average quality is 0.89, indicating that the mesh structure is of very high quality. A high element quality improves the accuracy of the analysis results, allowing the stress distributions on the structure to be accurately calculated. On the other hand, skewness, which is another important parameter that evaluates the deformation of the mesh elements, was found to have a maximum value of 0.93 and an average skewness value of 0.1. A low skewness value indicates that the shape of the elements is close to their ideal geometry; thus, the analysis results are reliable.

Table 4. Chassis mesh analysis results

Number of Elements	Number of Nodes	Element Quality	Skewness
43760	210717	Max: 1 Avg: 0.89 Min: 0.0527	Max: 0.93 Avg: 0.1 Min: 1.3x10⁻¹⁰

The reference force of 1300 N applied to the chassis was calculated according to the lifting capacity of the vehicle and the maximum load it can carry. This force was applied to the chassis, and its durability and deformation capacity were tested. The deformation and stress analyses of the chassis are presented in Figures 19 and 20, respectively. As a result of the analysis, the total deformation values vary between 0 and 0.1878 mm. This deformation range shows that the chassis undergoes minimal deformation under load and, therefore, has sufficient structural strength. In addition, the stress values on the chassis were found between 2.71×10^{-6} MPa and 35.84 MPa. These values indicate that the material is within the safe operating range by maintaining its elastic limits.
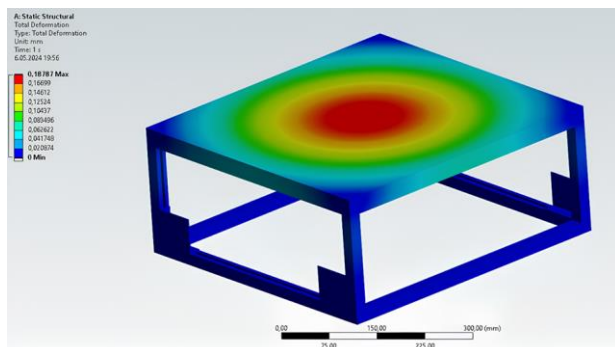
Figure 19. Chassis deformation analysis

Based on the mesh and stress analyses, it is concluded that the chassis design is adequate in terms of both mesh quality and load-carrying capacity. A high-quality mesh structure and low skewness values indicate that the chassis provides reliable analysis results. Considering the stress and deformation results on the chassis, it is concluded that the design is suitable for the production phase.
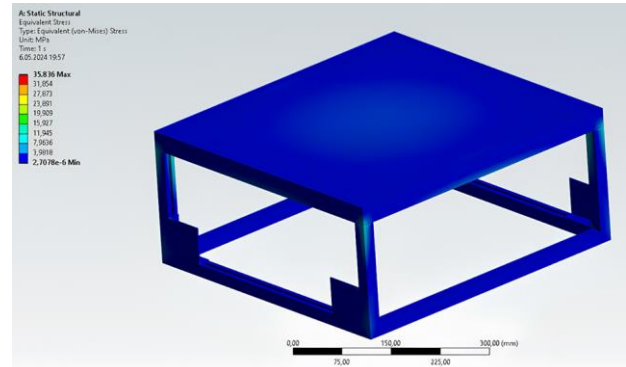
Figure 20. Chassis tension analysis

3.3. Wheel Mechanism

A 125×40 mm drive wheel made of polyurethane material was used in an autonomous mobile vehicle with a Swerve driving system. The polyurethane material wheel, which was selected considering that the autonomous mobile vehicle will be operated in a factory environment, can be under load up to 250 kg; therefore, the wheels were selected as fixed points when performing deformation and stress analysis. The mesh analysis of the aluminum alloy apparatus, which is utilized for the attachment point to the vehicle and the connection of the motors, which are integral to the driving system, to the wheel (the most crucial component), is shown in Figure 21. To enhance the quality of mesh analysis, appropriate element types were selected for the components in question. Cartesian mesh analysis was employed for the rectangular and square parts, whereas the sweep method was used for the cylindrical regions. Additionally, body sizing and face sizing were applied to the remaining parts. Once the requisite mesh types were selected, enhancements were made to the analysis by determining the mesh size according to the overall characteristics of the part.
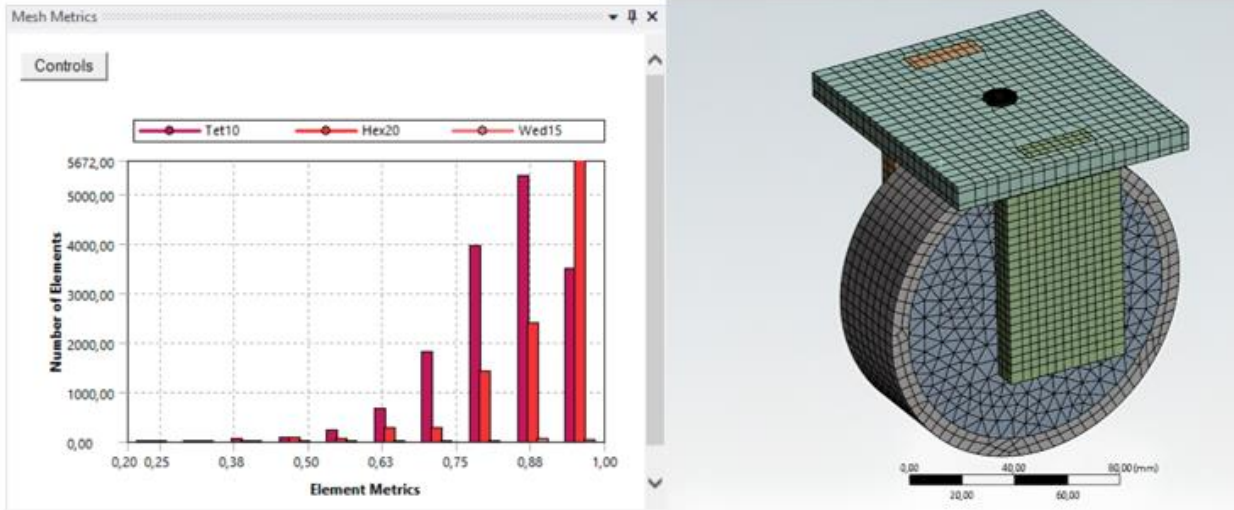
Figure 21. Wheel system mesh analysis

Upon examination of the mesh analysis results for the wheel system illustrated in Table 5, it becomes evident that the skewness and element quality values are calculated using 73,864 nodes and 25,743 elements following the implementation of the aforementioned improvements. Based on these calculations, the maximum skewness value is 0.92 and the average element quality value is 0.87. Because the values obtained were within the desired range, it is concluded that the mesh analysis is sufficient.

Table 5. Wheel system mesh analysis results

Number of Elements	Number of Nodes	Element Quality	Skewness
25743	73864	Max: 1 Avg: 0.87 Min: 0.19	Max: 0.92 Avg: 0.19 Min: 1.3×10^{-10}

Mechanical analysis of the wheel mechanism was conducted under the assumption that the total weight of the vehicle with the maximum load (1800 N) would be borne by the wheels in the absence of friction.

The deformation and stress analyses of the wheel module as a function of the applied force are shown in Figures 22 and 23, respectively. As a result of these analyses, it can be seen that the total deformation value is between 0 and 0.04 mm, while the stress values are between 3.44×10^{-6} MPa and 75.37 MPa. Considering these results, it is observed that the wheel module is sufficiently durable to fulfill the desired task.
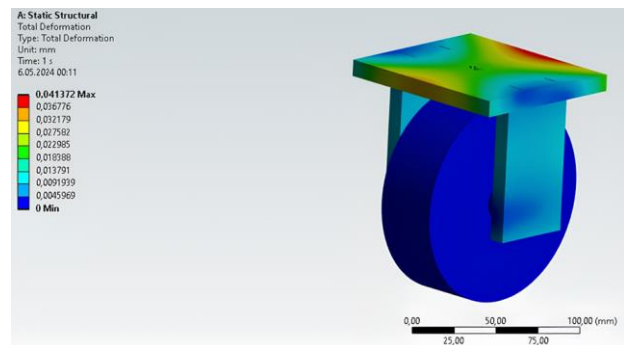
Figure 22. Wheel system deformation analysis

Figure 23. Wheel system stress analysis

3.4. Lift System

The vehicle's lifting system had dimensions of 400×360×323 mm. The upper and lower bases were constructed from aluminum alloys owing to their light weights. The scissors, cylinder, and pins were manufactured from stainless steel, owing to their durability. Analyses were conducted to assess whether these materials would also demonstrate the desired performance in practice. The results of the analysis are in accordance with the expected outcomes based on the calculations performed using the kinematic equations.
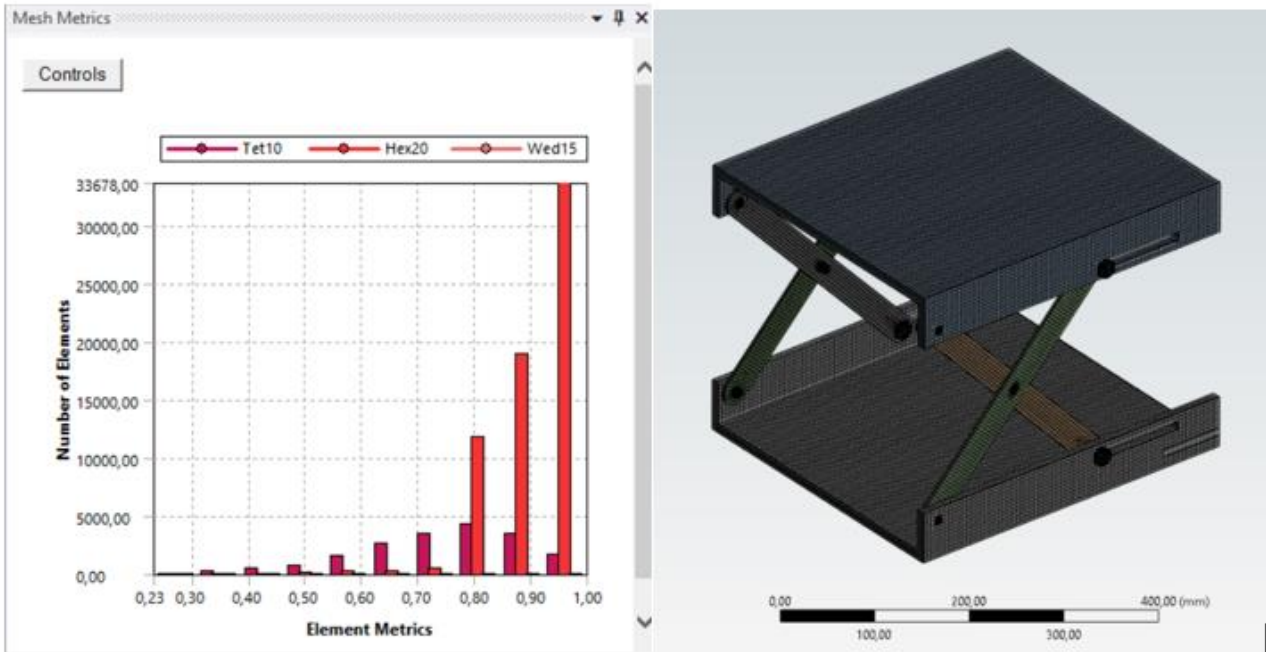
Figure 24. Lift system mesh analysis

Figure 25 illustrates the table of the mesh analysis for the element types, while Table 6 presents the results. As observed in Figure 24, tet10, hex20, and wed15 were utilized in the mesh analysis. As indicated in Table 6, there are 83944 elements and 381605 nodes. The average element quality value obtained from the table is 0.89, which indicates that the geometry is of a high quality and that the analysis can be conducted with confidence. The simplicity of the shape has resulted in the average skewness value coming out low at 0.098644. This indicates that the system is relatively balanced.

Table 6. Lift system mesh analysis results

Number of Elements	Number of Nodes	Element Quality	Skewness
83944	381605	Max: 1 Avg: 0.89 Min: 0.23	Max: 0.99 Avg: 0.0986 Min: 1.3×10^{-10}

Figure 25 presents the results of the deformation analysis. The results indicate that the system is at a minimum deformation level, demonstrating high resistance to deformation. The maximum and minimum deformation values obtained are 0.65 mm and 0 mm. Figure 26 displays the stress analysis results against a 1250 N force applied to the system. The results indicate a maximum value of 58.76 MPa and a minimum value of 1.14×10^{-10} MPa. The choice of materials aluminum alloy and stainless steel confirms the system's outstanding resistance to stress and its capability to comfortably withstand loads up to 127.2 kg. Based on the analyses conducted, it can be concluded that the lift system designed is suitable for operational use.
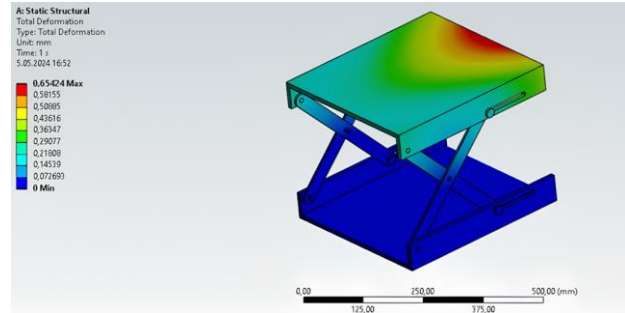
Figure 25. Lift system deformation analysis
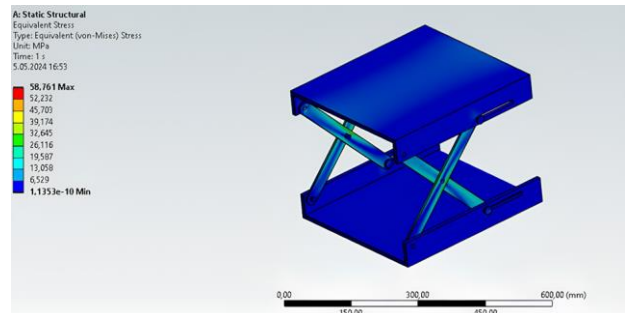
Figure 26. Lift system tension analysis

4. DISCUSSION AND CONCLUSION

This study focuses on the design, kinematic analysis, and mechanical durability of an autonomous mobile robot equipped with a scissor lift mechanism and a swerve drive system. The necessary electronic components for the vehicle's mobility and structural integrity have been identified, and kinematic formulas have been derived through theoretical calculations. The analyses conducted have confirmed that the vehicle can lift loads of the desired weight.

FEA was conducted utilizing Ansys to investigate the stress and deformation distributions of the vehicle under various loads, evaluating the vehicle's structural integrity

in simulated real-world conditions. A maximum deformation of 0.55 mm and a stress of 33.6 MPa were observed under a force of 325 N applied to the body. The chassis exhibited a maximum deformation of 0.1878 mm and a stress of 35.84 MPa under a load of 1300 N. The wheel mechanism demonstrated the capacity to support loads with a deformation of 0.04 mm and a stress of 75.37 MPa under a force of 1800 N. The lifting mechanism was analyzed with a force of 1250 N, resulting in a deformation of 0.65 mm and a stress of 58.76 MPa.

The analyses indicated that the vehicle, constructed of aluminum alloy and stainless steel, possesses the capacity to bear loads of up to 1250 N without significant deformation or stress. The quality of mesh, skewness values, and element types (tet10, hex20 etc.) contributed to the accuracy and reliability of the analyses.

This study focuses on the avoidance system of the mobile robot, neglecting significant factors such as the control of the lever system and frictional forces. However, in practical applications, these omitted factors can substantially impact the vehicle's performance. Notably, temperature variations are critical to the long-term durability of the design. Thermal expansion at elevated temperatures or contraction at low temperatures can result in deformation and loss of precision in mechanical systems. Furthermore, particulate matter, prevalent in industrial environments, can increase frictional forces on wheel steering mechanisms, potentially leading to obstructions or wear. This may affect steering accuracy, particularly in independent wheel control systems. Additionally, while static load tests verify instantaneous structural durability, it is essential to consider that the vehicle will be subject to fatigue and wear effects during prolonged use. Repetitive loads can cause mechanical components to deteriorate over time, increasing the risk of failure. Moreover, the vibrations and sudden impacts that the mobile robot will experience in industrial applications can also negatively affect structural integrity. Considering these factors, it is evident that the elements disregarded in the design process can adversely impact the long-term performance and durability of the robot. Therefore, a more comprehensive analysis and testing against dynamic loads in conjunction with environmental factors could be conducted to obtain results more representative of real-world conditions.

Future research will encompass a more comprehensive analysis that incorporates the simulation of the lift system, as well as the effects of dynamic loads, friction, and dynamic behavior under varying operational conditions. Dynamic analysis—time-dependent assessments—will be conducted following the static analysis, as such analyses are more complex and time-consuming. However, they are essential for evaluating the system's performance under real-time external forces and changing speeds, ensuring reliable operation in real-world scenarios. Additionally, the development of path planning algorithms that enable the robot to navigate safely by sensing its environment is proposed. The application of deep learning methods and camera-based image processing techniques for object recognition will also be considered. Furthermore, techniques for effective mapping will be explored, enabling the robot to create a map of its environment and utilize it efficiently. Research will be conducted on SLAM (Simultaneous Localization and Mapping) algorithms, which allow robots to determine their positions while mapping unknown environments. The Gazebo simulation environment has been selected for these studies. The preference for Gazebo over CoppeliaSim is attributed to Gazebo's broader resources and the availability of numerous ready-made packages that can integrate seamlessly with ROS (Robot Operating System). This will facilitate more efficient and straightforward execution of tasks such as mapping, image processing, and simulation integration.

REFERENCES

[1] Haruna AI, Sankar R, Samaila A. Design and development of an instructional mobile robot for effective learning of material handling in mechanical workshops in universities. Mater Today Proc. 2023.

[2] Corke P. Robotics, Vision and Control: Fundamental Algorithms in MATLAB®. 1st ed. Berlin: Springer-Verlag; 2011.

[3] Tagliavini L, Colucci G, Botta A, Cavallone P, Baglieri L, Quaglia G, et al. Wheeled Mobile Robots: State of the Art Overview and Kinematic Comparison Among Three Omnidirectional Locomotion Strategies. J Intell Robot Syst. 2022;106(3).

[4] Raikwar S, Fehrmann J, Herlitzius T. Navigation and control development for a four-wheel-steered mobile orchard robot using model-based design. Comput Electron Agric. 2022; 202:105432.

[5] Yamaç Hİ, Yılmaz T. Mobil Robotlar için Yük Altındaki Davranış Analizinin İncelenmesi. Fırat Üniversitesi Mühendislik Bilimleri Dergisi. 2022;34(1):433-8.

[6] Roland Siegwart and Illah R. Nourbakhsh, Introduction to Autonomous Mobile Robots, 1st ed. Cambridge, Massachusetts: MIT Press; 2004.

[7] Demir C, Bozdemir M. Swedish tekerlekli mobil robot tasarımı ve 3b yazıcıyla imalatı, 4th International Congress On 3d Printing (Additive Manufacturıng) Technologies and Digital Industry, Antalya: 2019. p. 144-153.

[8] Huang H, Gao J. Backstepping and Novel Sliding Mode Trajectory Tracking Controller for Wheeled Mobile Robots. Mathematics. 2024;12(10):1458.

[9] Nikishkov GP. Introduction To The Finite Element Method. Japan: 2004 Lecture Notes. University of Aizu, Aizu-Wakamatsu 965-8580; 2004

[10] Baskoro CHAHB, Saputra HM, Mirdanies M, Susanti V, Radzi MF, Aziz RIA. An Autonomous Mobile Robot Platform for Medical Purpose. 2020 International Conference on Sustainable Energy Engineering and Application (ICSEEA). Tangerang: IEEE; 2020. p. 41-44.

[11] Yan SYW, Chamniprasart K, Phueakthong P, Pinrath N. Autonomous Mobile Robot for Material Handling in an Industrial Plant. The Annual

Conference on Engineering and Information Technology. Osaka: ACEAIT; 2023.

[12] Dhelika R, Hadi AF, Yusuf PA. Development of a Motorized Hospital Bed with Swerve Drive Modules for Holonomic Mobility. Applied Sciences. 2021;11(23):11356.

[13] Zhao Z, Xie P, Meng MQ-H. ODD: Omni Differential Drive for Simultaneous Reconfiguration and Omnidirectional Mobility of Wheeled Robots. arXiv preprint arXiv:2407.10127 (2024).

[14] Demir N, Sucuoglu HS, Bogrekci I, Demircioglu P. Structural & Dynamic Analyses and Simulation of Mobile Transportation Robot. Int. J. of 3D Printing Tech. Dig. Ind. 2021; 5(3): 587- 595.

[15] Prabhakaran S, Aravinth KT, Adhik N, Vikram R. Design and Analysis of Autonomous Mobile Robot. Nat. Volatiles & Essent. Oils. 2021; 8(5): 3020-3030.

[16] Koca YB, Gökçe B, Aslan Y. ROS/Gazebo Ortamında Tank Sürüş Özellikli Mobil Bir Robotun Similasyonu. Journal of Materials and Mechatronics: A (JournalMM). 202; 1(1), 29-41.

[17] Ağralı E, Çavaş M. V-REP Robotik Simülatör ile Robot Kol Simülasyonu. Fırat Üniversitesi Mühendislik Bilimleri Dergisi. 2020;32(2):435-44.

[18] Akin JE. Finite Element Analysis Concepts via SolidWorks. Rice University. Houston, Texas; 2009.

[19] Aksoy S. Makas Platformlu Mobil Robot Tasarımı ve Analizi [Bitirme Tezi]. Konya: Konya Teknik Üniversitesi Mühendislik ve Doğa Bilimleri Fakültesi; 2023.

[20] Madier D. An Introduction to the Fundamentals of Mesh Generation in Finite Element Analysis. FEA Academy; 2023

[21] Ansys. The Fundamentals of FEA Meshing for Structural Analysis. 2021 April 28 [cited 2024 September 28]. Available from: https://www.ansys.com/blog/fundamentals-of-fea-meshing-for-structural-analysis

[22] Cadsay. Ansys nedir?. [cited 2024 April 28]. Available from: https://cadsay.com/ansys-nedir

[23] Coppelia Robotics. CoppeliaSim. [cited 2024 April 27]. Available from: https://www.mathworks.com/products/connections/product_detail/coppeliasim.html

[24] Büyükarslan P. Spyder Nedir? Nasıl Kurulur?. [cited 2024 April 30]. Available from: https://www.sistemlinux.org/2018/05/spyder-nedir-nasil-kurulur.html

[25] Adar NG. Mobil İnsansı Robot Tasarımı İmalatı ve Kontrolü [Doktora Tezi]. Sakarya: Sakarya Üniversitesi Fen Bilimleri Enstitüsü; 2016.

[26] van der Velde P. Swerve drive introduction. 2022 December 4 [cited 2023 Jun 13]. Available from: https://www.petrikvandervelde.nl/posts/Swerve-drive-introduction

[27] Chiefdelphi, Whitepaper: Swerve Drive Skew and Second Order Kinematics. 2022 November [cited 2023 Jun 10]. Available from: https://www.chiefdelphi.com/t/whitepaper-swerve-drive-skew-and-second-order-kinematics/416964

[28] Gong Z, Nie Z, Liu Q, Liu XJ. Design and control of a multi-mobile-robot cooperative transport system based on a novel six degree-of-freedom connector. ISA Trans. 2023;139:606-20.

[29] Sukop M, Grytsiv M, Jánoš R, Semjon J. Simple Ultrasonic-Based Localization System for Mobile Robots. Applied Science. 2024;14(9):3625.

[30] Akyol S, Uçar A. Rp-Lidar ve Mobil Robot Kullanılarak Eş Zamanlı Konum Belirleme ve Haritalama. Fırat Üniversitesi Mühendislik Bilimleri Dergisi. 2019;31(1):137-43.

[31] Güngör O. Kaçak Elektrik Kullanımının GSM Aracılığıyla Takibi. EMO Bilimsel Dergi. 2015;4(8):29-34.

[32] Nalbantoğlu V, Seymen B. Ataletsel Seyrüsefer Sistemleri. Mühendis ve Makina. 2007;48(566):7-13.

[33] JR Callister WD, Rethwisch DG. Materials Science and Engineering: An Introduction. 10th ed. Hoboken, NJ: Wiley; 2018.

[34] FEATips. ANSYS Mesh Metrics Explained. 2022 November 21 [cited 2024 June 15]. Available from: https://featips.com/2022/11/21/ansys-mesh-metrics-explained/

[35] Simscale. Mesh Quality. 2024 July 30 [cited 2024 September 20]. Available from: https://www.simscale.com/docs/simulation-setup/meshing/mesh-quality/

[36] Bommes D, Lévy B, Pietroni N, Puppo E, Silva C, Tarini M, et al. Quad-Mesh Generation and Processing: A Survey. Computer Graphics Forum. 2013;32(6): 51-76.

[37] Motooka Y, Noguchi S, Igarashi H. Evaluation of Hexahedral Mesh Quality for Finite Element Method in Electromagnetics. Materials Science Forum. 2010;670:318–324.

84

Türk Doğa ve Fen Dergisi
Turkish Journal of Nature and Science
www.dergipark.gov.tr/tdfd

BINGÖL UNIVERSITY

Synthesis and Characterization of 2,4-*di*-methyl-, and 3,4-*di*-methyl-phenol Derivatives of Hexachlorocyclotriphosphazatriene

Saliha BEGEÇ[1*] (iD)

[1] İnönü University, Arts and Sciences Faculty, Chemistry Department, Malatya, Türkiye
Saliha BEGEÇ ORCID No: 0000-0001-5331-6736

Corresponding author: saliha.begec@inonu.edu.tr

Abstract: In this study, the reactions of hexachlorocyclotriphosphazatriene, $N_3P_3Cl_6$ (**1**) with bulky phenols (**2a** and **2b**) have been reported. For this purpose, two different phenols [2,4-*di*-methyl-phenol (**2a**) and 3,4-*di*-methyl-phenol (**2b**)] were selected. Reactions were carried out preparing sodium salts of phenols in tetrahydrofuran (THF) solvent at a 1:1 molar ratio and under argon atmosphere. Two new mono phenoxy-substituted phosphazene compounds [($N_3P_3Cl_5OC_6H_3$-Me-2,4 (**3**) and $N_3P_3Cl_5OC_6H_3$-Me-3,4 (**4**)] were separated and purified from the reaction mixtures using thin layer and column chromatography techniques. The molecular structures of new compounds were characterized by ^1H, ^{13}C, ^{31}P NMR spectroscopy and elemental analyses.

Bulky phenols are widely used as antioxidant. Therefore, it can be expected that the new compounds obtained may show antioxidant activity. Moreover, since the obtained new mono phenoxy-phosphazene derivatives contain five P-Cl bonds, these compounds have potential use in the preparation of new small organocyclophosphazene derivatives.

85

Hekzaklorosiklotrifosfazatrienin 2, 4-*di*-metil ve 3, 4-*di*-metil-fenol Türevlerinin Sentezi ve Karakterizasyonu

Öz: Bu çalışmada hacimli fenoller ile hekzaklorosiklotrifosfazatrienin reaksiyonları rapor edildi. Bu amaç için, iki değişik fenol [2,4-*di*-metil-fenol (**2a**) ve 3,4-*di*-metil-fenol (**2b**)] seçildi. Reaksiyonlar argon atmosferi altında 1:1 mol oranında tetrahidrofuran (THF) çözücüsü içinde fenollerin sodyum tuzları hazırlanarak gerçekleştirildi. İki yeni mono fenoksi-sübstitüe fosfazen bileşiği [$N_3P_3Cl_5OC_6H_3$-Me-2, 4 (**3**) and $N_3P_3Cl_5OC_6H_3$-Me-3, 4 (**4**)] ince tabaka ve kolon kromatografisi teknikleri kullanılarak reaksiyon karışımlarından ayrıldı ve saflaştırıldı. Yeni bileşiklerin moleküler yapıları ^1H, ^{13}C, ^{31}P NMR spektoskopisi ve elemental analiz yöntemleri ile karakterize edildi.

Hacimli fenoller antioksidan olarak yaygın bir şekilde kullanılmaktadır. Bu nedenle elde edilen yeni bileşiklerin antioksidan aktivite göstermesi beklenebilir. Ayrıca elde edilen yeni mono fenoksi-fosfazen türevleri beş tane P-Cl bağı içerdiğinden bu bileşikler yeni küçük organosiklofosfazen türevlerinin hazırlanmasında potansiyel kullanıma sahiptir.

1. INTRODUCTION

One of the most studied and best known heterocyclic compounds are cyclophosphazenes [1-4]. Hexachlorocyclotriphosphazene [$N_3P_3Cl_6$, trimer (**1**)] is a very important compound due to used in synthesis of most halophosphazenes. This compound in the most popular compound in the cyclophosphazene series, and its reactions have been investigated in great detail [5-10]. The physical and chemical properties of cyclotriphosphazene derivatives, depending on of the substituted groups. These derivatives are used in the preparation of functional materials in many fields (science, technology, medical) as antimicrobial, anticancer, antifungal, antibacterial, antitumor, liquid

crystals, organic light emitting diodes (OLEDs), flame retardant properties, electrical conductivity, fluorescent chemosensors [11-28].

A large number of reactions of phenols with hexachlorocyclotriphosphazatriene,[$N_3P_3Cl_6$, (1)] have been investigated [29-31]. Phenoxy derivatives of compound (1) are potentially used in the preparation of many organophosphazene derivatives. These derivatives found variety of applications in science and technology including, nonlinear optical properties, thermal and electrochemical properties, flame retardant, thermal stability [32-35].

In this study, the bulky phenols have been selected as a nucleophile. Bulky phenols are widely used as antioxidants. Because bulky phenols are interested in preparation of stable phenoxyl radicals and biologically active compounds such steric factors of substituents also play a major role in determining the biological activity and effective antioxidant activity of these kind of chemicals via inhibiting lipid peroxidation and lowering the oxidative stress of the organism [36-37].

We have previously reported the reactions of $N_3P_3Cl_6$ with 2, 6-*di-tert*-butylphenoxide, 2, 6-*di-tert*-butyl-4-methylphenoxide, 2, 4, 6-*tri-tert*-butylphenoxide, 2, 4, 6-*tri*-methyl-phenoxide and $N_4P_4Cl_8$ with 2,6-*di-tert*-butyl-4-methylphenoxide [38-42].

In the present work have been reported the reactions of $N_3P_3Cl_6$ with the sodium salts of 2, 4-*di*-methyl-phenol, 3, 4-*di*-methyl-phenol. Two new mono- (2,4-*di*-methyl- and 3,4-*di*-methyl-) phenoxy-substituted phosphazene compounds were obtained as majör products. The structures of these obtained compounds were determined by elemental analysis, ^{1}H, ^{13}C and ^{31}P NMR spectroscopy techniques.

2. MATERIAL AND METHOD

2.1. Experimental

Synthetic steps were carried out under an inert atmosphere by using standard schlenk techniques. Hexachlorocyclotriphosphazatriene, [$N_3P_3Cl_6$], (1), was provided by Aldrich and purified recrystallization from *n*-hexane. 2,4-*Di*-methyl-phenol and 3,4-*di*-methyl-phenol (Aldrich Chemical Co. Ltd.) were used as supplied. The tetrahydrofuran (THF) used as solvent was distilled under argon from sodium benzophenone prior to use. Reactions were observed by using silica gel 60 F$_{254}$ pre-coated Thin Layer Chromatography (TLC) plates (Merck, Kieselgel 60, 0.25 mm thickness) and the separating conditions were determined. The separation of compounds 3 and 4 was achieved by column chromatography using silica gel (Merck, Kieselgel 60,

230–400 mesh, for 3 g crude product, 100 g silica gel in a column, of 3 cm in diameter and 60 cm in lenght).

The structures of 3 and 4 were determined by elemental analyses, ^{1}H, ^{13}C, ^{31}P NMR spectroscopy and purity of the new compounds was checked by TLC. Microanalysis were carried out with a LECO 932 CHNS-O apparatus. Melting points were measured in open capillary tubes with an Elektrothermal-9100 melting point apparatus and were uncorrected.

^{1}H (300.13 MHz), ^{13}C (75.47 MHz), and ^{31}P (121.49 MHz) spectra were recorded in CDCl$_3$ solutions a BRUKER 300 MHz spectrometer using 85% H$_3$PO$_4$ as an external reference for ^{31}P and TMS as internal reference for ^{1}H NMR. All data were recorded for solutions in CDCl$_3$. The ^{1}H- and ^{13}C-NMR chemical shifts were measured using SiMe$_4$ (δ=0) as an internal standard, and the ^{31}P chemical shifts were measured using 85% H$_3$PO$_4$ as an external standard.

2.1.1. Synthesis of 2-(2,4-*di*-methylphenoxy)-2,4,4,6,6-pentachlorocyclo-2λ^5, 4λ^5, 6λ^5-triphosphazatriene (3)

General method for the preparation, of phenoxy substituted phosphazenes derivatives 3 and 4 (Figure 1.).

To a solution of the respective phenol (1.05 g; 8.62 mmol) in THF (15 mL) at 20 °C during 0.5 h, metallic Na (0.99 g; 43 mmol) were added under argon atmosphere. The excess of Na was removed by filtration and the solution of the sodium phenoxide was cooled and then frozen with a liquid nitrogen-acetone mixture. To this mixture N$_3$P$_3$Cl$_6$ (1) (3 g; 8.62 mmol) in 10 mL of THF was added and the resulting mixture was stirred to come to an ambient temperature. The mixture was stirred 48 hour at room temperature, after the precipitated salt (NaCl) was filtered and the solvent was removed with rotary evaporator. Column chromatography was applied to the remaining white solid. The reaction mixture was chromatographed on silica gel: 100 g [eluent: acetone : *n*- hexane 1:3 (for 3); dichloromethane : *n*- hexane 1:10 (for 4)].

2-(2, 4-*di*-methylphenoxy)-2,4,4,6,6-pentachlorocyclo-2λ^5, 4λ^5, 6λ^5-triphosphazatriene (3)

Viscous oil; Yield: 0.856 g (23 %). Found: C, 22.60; H, 2.36; N, 9.23 % Calcd for N$_3$P$_3$Cl$_5$C$_8$ H$_9$O (433.5 g/mol) : C, 22.16; H, 2.07; N, 9.69 %. NMR (CDCl$_3$): ^{1}H, δ 2.12 (s, 3H, C*H$_3$-ortho*), 2.33 (s, 3H, C*H$_3$-para*), 7.00-7.28 (m, 3H, Ar-*H*) (Figure 3.); ^{13}C, δ 16.55 (s, 1C, *CH$_3$-ortho*), 20.82 (s, 1C, *CH$_3$-para*), 120.63; (s, C(6), phenyl), 127.68; (s, C(2), phenyl), 129.91; (s, C(5), phenyl), 132.38; (s, C(4), phenyl), 136.28; (s, C(3), phenyl), 146.24 (s, 1C, C-ipso) (Figure 4.); ^{31}P, AB$_2$ pattern, δ_A=12.43, δ_B=22.53, $^2J_{AB}$ =59.9 Hz. (Figure 2.).
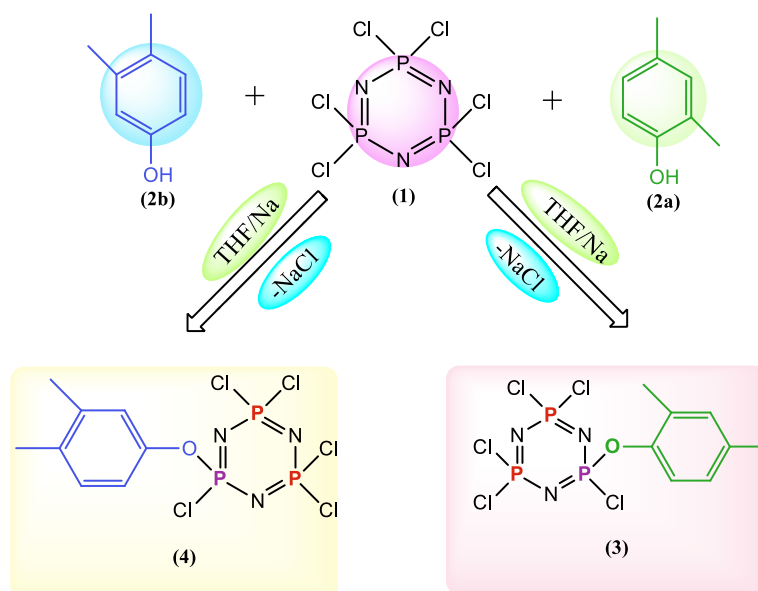
Figure 1. Synthesis of compounds **3** and **4**
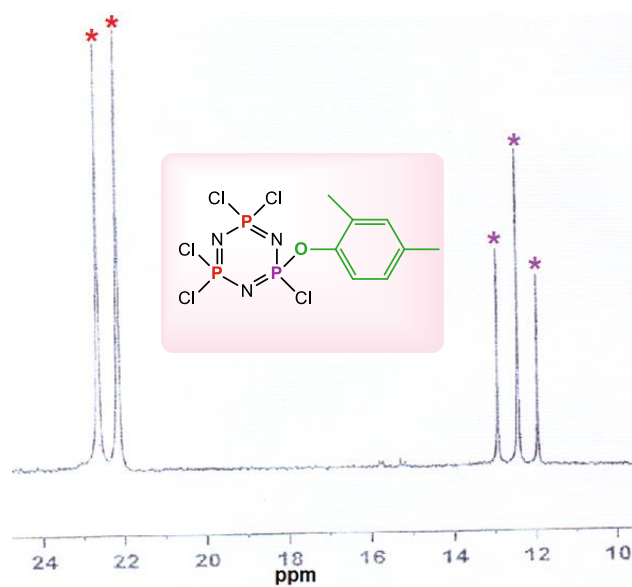
Figure 2. ³¹P NMR spectra of compound (**3**)
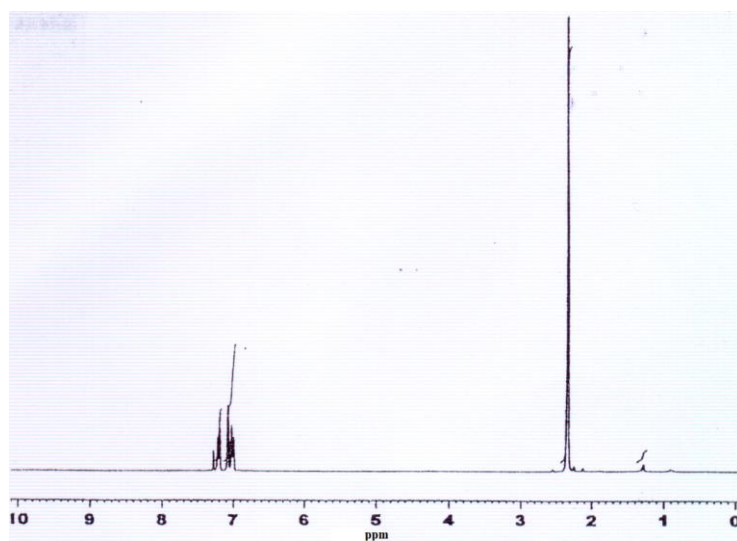
Figure 3. ¹H NMR spectra of compound (**3**)
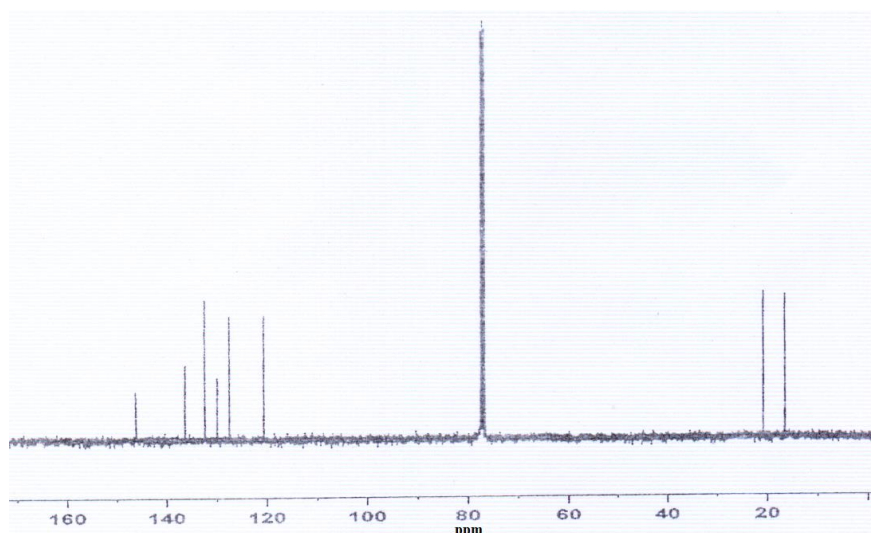
Figure 4. ^{13}C NMR spectra of compound (**3**)

2-(3, 4-*di*-methylphenoxy)-2,4,4,6,6-pentachlorocyclo-2λ^5, 4λ^5, 6λ^5-triphosphazatriene (4)

Viscous oil; Yield: 0,969 g (26 %). Found: C, 22.72; H, 2.54; N, 9.33 % Calcd for

N$_3$P$_3$Cl$_5$C$_8$ H$_9$O (433.5 g/mol) : C, 22.16; H, 2.07; N, 9.69 %. NMR (CDCl$_3$): ^{1}H, δ 2.25 (s, 3H, C*H$_3$-para*), 2.28 (s, 3H, C*H$_3$-meta*), 6.92-7.28 (m, 3H, Ar-*H*); ^{13}C, δ 19.21 (s, 1C, *CH$_3$-meta*), 19.89 (s, 1C, *CH$_3$-para*), 118.14 (s, C(6), phenyl), 118.21 (s, C(2), phenyl) , 122.18 (s, C(5), phenyl) , 134.44 (s, C(4), phenyl) , 138,27 (s, C(3), phenyl), 147.87 (s, 1C, C-ipso); ^{31}P, AB$_2$ pattern, δ_A = 12.46, δ_B = 22.43, $^2J_{AB}$ = 59.9 Hz.

3. RESULTS

The reacions of **1** with an equimolar amount of **2a** and **2b** in THF gave the mono-substituted products **3** and **4.** New compounds were isolated as a highly viscous oil from the reaction mixtures by column chromatography. The structures of compounds **3** and **4** were identified by using elemental analyses; ^{1}H-, ^{13}C-, and ^{31}P- NMR spectroscopy. The elemental analyses and NMR results are consisted with the predicted structures as explained in the experimental section. The results of elemental analyses of compounds **3** and **4** showed that one chlorine atoms in phosphazene was replaced by an phenol reactive.

^{1}H NMR spectra of compounds **3** and **4** are relatively simple, but informative. The methyl protons resonate at δ =2.12 (s, 3H, C*H$_3$-para*) and 2.33 (s, 3H, C*H$_3$-ortho*) (in a 1:1 ratio), 7.00-7.28 (m, 3H, Ar-H) for **3**. For **4**, the protons of methyl group at the meta position and methyl group at the para position gave singlets at δ =2.25 (s, 3H, C*H$_3$-para*) and 2.28 (s, 3H, C*H$_3$-ortho*) (in a 1:1 ratio), 6.92-7.28 (m, 3H, Ar-H) respectively. The ^{13}C NMR signals for **3**, (*CH$_3$-orto*), (*CH$_3$-para*), (*C*(6)-phenyl, *C*(2)-phenyl, *C*(5)-phenyl, *C*(4)-phenyl, *C*(3)-phenyl and *C*-ipso are observed at 16.55, 20.82, 120.63, 127.68, 129.91, 132.38, 136.28, and 146.24 respectively.

The ^{13}C NMR signals for **4**, (*CH$_3$-meta*), (*CH$_3$-para*), (*C*(6)-phenyl, *C*(2)-phenyl, *C*(5)-phenyl, *C*(4)-phenyl, *C*(3)-phenyl and *C*-ipso are observed at 19.21, 19.89, 118.14, 118.21, 122.18, 134.44, 138.27, and 147.87 respectively.

The ^{31}P NMR spectra of the compounds **3** and **4** showed an AB$_2$ type spin system because of two differernt phosphorus environments within the molecules. The proton-decoupled ^{31}P NMR spectral data of compounds **3** and **4** were very similar. Chemical shifts were δ PCl(OPh) = 12.43, δ PCl$_2$= 22.53 in **3**, δ PCl(OPh) = 12.46, δ PCl$_2$ = 22.43 in **4**. Two bond-coupling constants $^2J_{pp}$ of compounds are the same. This value is 59.9 Hz. All these data are in good agreement with the literature values [43-46].

4. DISCUSSION AND CONCLUSION

In this study, reactions of hexachlorocyclotriphosphazatriene (**1**) with bulky phenols were investigated. The reaction of **1** with an equimolar amount of sodium salts of **2a-b** in THF gave the monosubstituted products (**3** and **4**). Products were isolated by column chromatography.

The structures of two mono-phenoxy-substituted phosphazene derivative compounds (**3** and **4**) are described by ^{1}H, ^{13}C, ^{31}P NMR spectroscopy, and elemental analyses.
The compounds prepared are important. Because bulky phenols have effective antioxidant properties. Therefore, the antioxidant effect of these compounds (**3** and **4**) can be examined in the future.

Additionally, since these compounds contain five P-Cl bonds, they can be used in the synthesis of new phosphazene derivative compounds by interacting with different nucleophiles.

Ethic

There are no ethical issues with the publication of this article.

Conflict of interest

The authors declare that they have no known competing financial interests or personal relationships that could have appeared to influence the work reported in this paper.

REFERENCES

[1] Begeç S. Synthesis and characterization of new spiro cyclotriphosphazene derivatives. *Inorganic Chemistry Communications.* 2022;140;109457.

[2] Bilge S, Demiriz S, Okumus A, Kilic Z, Tercan B, Hokelek T, Buyukgungor O.Phosphorus−Nitrogen Compounds. Part 13. Syntheses, Crystal Structures, Spectroscopic, Stereogenic, and Anisochronic Properties of Novel Spiro-Ansa-Spiro-, Spiro-Bino-Spiro-, and Spiro- Crypta Phosphazene Derivatives. *Inorganic Chemistry.* 2006;45(21):8755-8767.

[3] Tümer Y. Synthesis, structural, and stereogenic characterizations of new trispirocyclotriphosphazenes. *Journal of the Chinese Chemical Society.* 2022;69(11):1897-1907.

[4] Yenilmez Çiftçi G, Şenkuytu E, Yuksel F, Kılıç A. Investigation of the structural properties of 2-naphthylamine substituted cyclotetraphosphazenes. *Polyhedron.* 2014;77:1-9.

[5] Görgülü AO, Koran K, Özen F, Tekin S, Sandal S. Synthesis, structural characterization and anti-carcinogenic activity of new cyclotriphosphazenes containing dioxybiphenyl and chalcone groups, *Journal of Molecular Structure.* 2015; 1087 (5): 1-10. Ibişoğlu H, Erdemir E, Atilla D, Şahin Ün Ş, Topçu, S, Şeker MG. Synthesis, characterization and antimicrobial properties of cyclotriphosphazenes bearing benzimidazolyl rings. *Inorganica Chimica Acta.* 2020; 509(1): 119679.

[6] Karthikeyan S, Krishnamurty SS. Reaction of Hexachlorocyclotriphosphazene with Sodiump-Cresoxide. *Zeitschrift für Anorganische und Allgemeine Chemie.* 1984;*513(6)*:231-240.

[7] Kumar D, Fohlen GM, Parker, JA. Bis-, tris-, and tetrakis-maleimido phenoxy-triphenoxy cyclotriphosphazene resins for fire- and heat-resistant applications. *Journal of Polymer Science: Polymer Chemistry Edition.* 1983; 21(11):3155-3167.

[8] Kumaraswamy S, Vijjulatha M, Muthiah C, Kumara Swamy KC, Engelhardt U. Synthesis, reactivity and structures of spirocyclic products derived from octachlorocyclotetraphosphazene: comparison with spirocyclic cyclotriphosphazenes and linear phosphazenes. *Journal of the Chemical Society, Dalton transactions.* 1999;6:891-900.

[9] Li X, Jiang F, Chen L, Wu M, Chen Q, Bu Y, Hong M. Three novel 3D coordination polymers based on a flexible multisite cyclotetraphosphazene ligand. *Dalton Transactions.* 2012;41:14038-14041.

[10] Ture S, Darcan C, Türkyılmaz O, Kaygusuz Ö. Synthesis, structural characterization and antimicrobial activities of cyclochlorotriphosphazene derivatives derived from N-(1-Naphthyl)- ethylenediamine. *Phosphorus, Sulfur, and Silicon and the Related-Elements.* 2020; 195(6): 507-515.

[11] Akbas H, Okumus A, Kılıç Z, Hökelek T, Süzen Y, Koç ZB, et al. Phosphorus–nitrogen compounds part 27. Syntheses, structural characterizations, antimicrobial and cytotoxic activities, and DNA interactions of new phosphazenes bearing secondary amino and pendant (4-fluorobenzyl)spiro groups. *European Journal of Medicinal Chemistry.* 2013;70:294–307.

[12] Yenilmez Çiftçi G, Tanrıverdi Eçik E, Yıldırım T, Bilgin K, Şenkuytu K, Yuksel F, et al. Synthesis and characterization of new cyclotriphosphazene compounds. *Tetrahedron.* 2013;69(5):1454–1461.

[13] Eker Y, Şenkuytu E, Ölçer Z, Yıldırım T, Yenilmez Çiftçi G. Novel coumarin cyclotriphosphazene derivatives: Synthesis, characterization, DNA binding analysis with automated biosensor and cytotoxicity. *Journal of Molecular Structure* . 2020; 1209; 127971.

[14] Yıldırım T, Bilgin K, Yenilmez Çiftçi G, Tanrıverdi Eçik E, Şenkuytu E, Uludağ Y, et al. Synthesis, cytotoxicity and apoptosis of cyclotriphosphazene compounds as anti- cancer agents. *European Journal of Medicinal Chemistry.* 2012; 52: 213–220.

[15] Okumuş A, Elmas G, Cemaloğlu R, Aydın B, Binici B, Şimşek H, et al. Phosphorus–nitrogen compounds. Part 35. Syntheses, spectroscopic and electrochemical properties, and antituberculosis, antimicrobial and cytotoxic activities of mono-ferrocenyl-spirocyclotetraphosphazenes. *New Journal of Chemistry.* 40, 5588-5603.

[16] Brandt K, Kruszynski R, Bartczak TJ, Czomperlik IP. AIDS-related lymphoma screen results and molecular structure determination of a new crown ether bearing aziridinylcyclophosphazene, potentially capable of ion-regulated DNA cleavage action. *Inorganica Chimica Acta.* 2001; 322: 138-144.

[17] Song SC, Lee SB, Lee BH, Ha HW, Lee KT, Sohn, YS. Synthesis and antitumor activity of novel thermosensitive platinum(II)-cyclotriphosphazene conjugates, *Journal of Controlled Release.* 2003;90(3):303-311.

[18] Barbera J, Bardaj M, Jimnez J, Laguna A, Martnez J, Serrano L, et al. Columnar mesomorphic organizations in cyclotriphosphazenes. *Journal of the American Chemical Society.* 2005;127(5):8994-9002.

[19] Davarcı D, Beşli S, Demirbaş E. Synthesis of a series of triple-bridged cyclotriphosphazene hexa-alkoxy derivatives and investigation of their structural and mesomorphic properties. *Liquid Crystals.* 2013;40(5):624-631.

[20] He Q, Dai H, Tan X, Cheng X, Liu F, Tschierske C. Synthesis and characterization of room temperature columnar mesogens of

cyclotriphosphazene with shiff base units. *Journal of Materials Chemistry C*. 2013;1(43): 7148-7154.

[21] Moriya K, Suzuki T, Yano S, Miyajima S. ^{31}P and ^{13}C NMR studies of a liquide crystallinecyclotriphosphazene derivative: orientational characteristics and contrasting shielding anisotropies for inorganic and organic moieties. *The Journal of Physical Chemistry B*. 2001; 105 (33): 7920-7927.

[22] Schrögel P, Hoping M, Kowalsky W, Hunze A. Wagenblast G. Wagenblast C. Phosphazene-Based Host Materials for the Use in Blue Phosphorescent Organic Light-Emitting Diodes. *Chemistry of Materials*. 2011;23 (22): 4947-4953.

[23] Jian S, Xiaodong W, Dezhen W. Novel spirocyclic phosphazene-based epoxy resin for halogen-free fire resistance: synthesis, curing behaviors, and flammability characteristics. *ACS Applied Materials & Interfaces*. 2012;4 (8):4047-4061.

[24] Sun J, Yu Z, Wang X, Wu D. Synthesis and Performance of CyclomatrixPolyphosphazene Derived from Trispiro-Cyclotriphosphazene as a Halogen-Free Nonflammable Material, *ACS Sustainable Chemistry & Engineering*. 2014;2(2): 231-238.

[25] Inoue K, Yamauchi T, Itoh T, Ihara E. Ionic Conductivity of Cross-linked Polymethacrylate Derivatives/Cyclophosphazenes/Li+ Salt Complexes. *Journal of Inorganic and Organometallic Polymers and Materials*. 2007; 17(2): 367-375.

[26] Yenilmez Çiftçi G, Yılmaz S, Bayık N, Şenkuytu E, Kaya EN, Durmuş M, Bulut M. Chemosensor properties of 7-hydroxycoumarin substituted cyclotriphosphazenes. *Turkish Journal of Chemistry*, 2020; 44(1): 64-73.

[27] Şenkuytu, E. A high selective "*Turn-Off*" aminopyrene based cyclotriphosphazene fluorescent chemosensors for Fe^{3+}/Cu^{2+} ions. *Inorganica Chimica Acta*. 2018; 479(1): 58-65.

[28] Dell D, Fitzsimmons BW, Shaw R A. Phosphorus-nitrogen compounds. Part XIII. Phenoxy- and p-bromophenoxy-chlorocyclotriphosphazatrienes. *Journal of the Chemical Society*. (1965); 752: 4070-4073.

[29] Allcock HR, Dembek AA, Mang MN, Riding GH, Parvez M, Visscher KB. Synthesis and structure of small-molecule cyclic phosphazenes bearing ortho-substituted aryloxy and phenoxy substituents. *Inorganic Chemistry*, 1992;31(13): 2734-2739.

[30] Abou-Donia, M. B. (2008). Organophosphorus Ester-Induced Chronic Neurotoxicity, *Archives of Environmental & Occupational Health,* 2003;*58 (8)*: 484-497.

[31] Rojo G, Agulló-López F, Carriedo G. A. , GarcíA Alonso F. J. , Fidalgo Martinez J. I, Nonlinear optical properties of high glass-transition temperature polyphosphazene, *Synthetic Metals,* 2000; 115: 241-244.

[32] Çoşut B, Topaloğlu Aksoy B, Tümay S. O, Şenocak A, Yeşilot S, , Synthesis, optical, and structural properties of bisphenol-bridged aromatic cyclic phosphazenes, *Turkish Journal of Chemistry,* 2020; 44 (1): 48-63.

[33] Mu X, Yuan B, Hu, W, Qiu S, Lei Song L. Hu Y, Flame retardant and anti-dripping properties of polylactic acid/poly(bis(phenoxy)phosphazene)/expandable graphite composite and its flame retardant mechanism, 2015; 93(5): 760-68-760-78.

[34] Cui Y, Ma X, Tang X, Luo Y. Synthesis, characterization, and thermal stability of star-shaped poly(e-caprolactone) with phosphazene core, European Polymer Journal, 2004; 40(2) 299-305.

[35] Nonhebel, D. C., J. M. Tedder, J. M., & J. C. Walton, J. C. (1979). Cambridge Radicals (Cambridge: Cambridge University Press).

[36] Denisov, E. (1995), Handbook of Antioxidants (Boca Raton, FL: CRC Press).

[37] Kılıç A, Begec S, Çetinkaya B, Hökelek T, Kılıc Z, Gündüz N. et al. Unusual Products in the Reactions of Hexachlorocyclotriphosphazatriene with Sodium Aryloxides. *Heteroatom Chemistry*, 1996; 7(4) 249-256.

[38] Hökelek T, Kılıc A, Begeç S, Kılıc Z, Yıldız M. 2-(2,6-*Di-tert*-butyl-4-methylphenoxy)-2,4,4,6,6,8,8-heptachlorocyclo-2λ^5,4λ^5,6λ^5,8λ^5-tetraphosphazatetraene. *Acta Crystallographica Section C: Crystal Structure Communications*. 1996; *C52*: 3243-3246.

[39] Hökelek T, Kılıc A, Begeç S, Kılıc Z. 2,4,4,6,6-Pentachloro-2-(2,6-di-*tert*-butyl-4-methylphenoxy)cyclo-2λ^5,4λ^5,6λ^5-triphosphazatriene. *Acta Crystallographica Section C: Crystal Structure Communications,* 1999;*C55*: 783-785.

[40] Hökelek T, Akduran N, Kılıc A, Begeç S, Kılıc, Z. Crystal Structure of 2,4,4,6,6-Pentachloro-2-(2,4,6-trimethylphenoxy)cyclo-2λ^5,4λ^5,6λ^5-triphosphazatriene, *Analytical Sciences*. 2000;16: 101-102.

[41] Begeç S, Kılıç A. Phenolysis of Hexachlorocyclotriphosphazatriene,. *Heteroatom Chemistry*. 2005;16(4):308-310.

90

Türk Doğa ve Fen Dergisi
Turkish Journal of Nature and Science
www.dergipark.gov.tr/tdfd

Assessment and improvement of thermal comfort conditions in educational buildings: an example of a secondary school

Gonca ÖZER YAMAN[1] , **Perihan ÇULUN[2]** , **Fatma KÜRÜM VAROLGÜNEŞ[1]***

[1] Bingöl University, Engineering and Architecture Faculty, Architecture Department, Bingöl, Türkiye
[2] Bingöl University, Engineering and Architecture Faculty, Mechanical Engineering Department, Bingöl, Türkiye
Gonca ÖZER YAMAN ORCID No: 0000-0002-0156-3994
Perihan ÇULUN ORCID No: 0000-0002-1797-9695
Fatma KÜRÜM VAROLGÜNEŞ ORCID No: 0000-0002-3214-4274

Corresponding author: fkvarolgunes@bingol.edu.tr

Abstract: This study, conducted at a secondary school in the cold winter-hot summer climate type of Bingöl, Turkey, measured temperature, air velocity, and relative humidity, while collecting satisfaction surveys. The findings indicate that while winter indoor temperatures generally remain within comfort ranges, some classrooms have indoor radiation temperatures below 17℃. In summer, indoor temperatures often exceed the 26 ℃ comfort threshold, reaching 30-35℃ in August. Air velocity assessments reveal that speeds above 0.4 m/s in summer provide relief from high temperatures, while speeds below 0.2 m/s in winter are adequate. Children show greater sensitivity to high temperatures than adults, adapting by adjusting windows or clothing. The PMV/PPD model inaccurately predicts students' thermal sensations, showing higher dissatisfaction rates in summer (40.4%) compared to winter (6.8%). The study emphasizes the importance of both natural and mechanical ventilation, advocating for natural ventilation due to its energy efficiency and health benefits. The findings suggest that optimizing thermal conditions through sustainable design practices can significantly enhance health, comfort, and learning outcomes in educational settings.

91

Eğitim Binalarında Termal Konfor Koşullarının Değerlendirilmesi ve İyileştirilmesi: Bir Ortaokul Örneği

Öz: Bu çalışma, Bingöl, Türkiye'deki soğuk kış-sıcak yaz iklim tipinde bulunan bir ortaokulda gerçekleştirilmiştir. Çalışmada sıcaklık, hava hızı ve bağıl nem ölçümleri yapılırken, memnuniyet anketleri de toplanmıştır. Bulgular, kış aylarında iç mekân sıcaklıklarının genellikle konfor aralıklarında kaldığını, ancak bazı sınıflarda iç mekân radyasyon sıcaklıklarının 17℃'nin altında olduğunu göstermektedir. Yaz aylarında ise iç mekân sıcaklıkları genellikle 26℃ konfor eşiğini aşarak, ağustos ayında 30-35℃'ye ulaşmaktadır. Hava hızı değerlendirmeleri, yaz aylarında 0.4 m/s'nin üzerindeki hızların yüksek sıcaklıklardan rahatlama sağladığını, kış aylarında ise 0.2 m/s'nin altındaki hızların yeterli olduğunu ortaya koymaktadır. Çocuklar, yüksek sıcaklıklara karşı yetişkinlere göre daha duyarlıdır ve pencere açma veya giyimlerini ayarlama yoluyla uyum sağlamaktadırlar. PMV/PPD modeli, öğrencilerin termal hislerini doğru bir şekilde tahmin edememekte ve yaz aylarında (%40.4) kış aylarına göre (%6.8) daha yüksek memnuniyetsizlik oranları göstermektedir. Çalışma, doğal ve mekanik havalandırmanın önemini vurgulamakta ve enerji verimliliği ve sağlık yararları nedeniyle doğal havalandırmayı desteklemektedir. Bulgular, sürdürülebilir tasarım uygulamalarıyla termal koşulların optimize edilmesinin eğitim ortamlarında sağlık, konfor ve öğrenme sonuçlarını önemli ölçüde iyileştirebileceğini göstermektedir.

1. INTRODUCTION

The educational environment plays a significant role in influencing students' academic success. Students' awareness of this environment is crucial for learning efficiency and the comfort conditions of the learning area [1-5]. During the school period, students typically spend approximately one-third of their days inside school buildings [6,7]. The comfort conditions of the environment have a direct impact on users' physiological and psychological well-being, which in turn affects their performance of activities [8,9]. Unfavourable comfort conditions in schools, including high temperatures, excessive noise, inadequate lighting, student density, and inadequate equipment for age groups, can negatively affect students' academic performance and cause health problems. Additionally, poor thermal comfort conditions in classrooms can lead to increased energy consumption [10]. The first scientific studies on the effects of thermal comfort conditions in classrooms on students' performance began in the mid-1950s. In recent years, there has been a resurgence of interest in thermal comfort theory, leading to renewed efforts to characterise the thermal environment in a way that is both objective (through measurement) and subjective (through the opinions of users).

In order to achieve optimal comfort conditions, it is essential to consider the individual user's behaviour and spontaneous adaptation to the surrounding environment [11,12]. Further investigation into the relationship between performance and environmental conditions could lead to improvements in comfort levels [13]. A number of studies have demonstrated that the comfort conditions experienced in different types of buildings and climates can vary considerably [14-17]. Consequently, research conducted in different climatic regions is of great importance in terms of comparison and evaluation. Recent studies have revealed that children's metabolic rates, clothing and behaviour differ from adults, and this also creates differences in their feelings of thermal comfort [18-20]. Data on children's thermal comfort are not determined in the standards. Consequently, Yun et al. and Teli et al. have conducted several studies, including those by Teli et al. [19] and Yun et al. [21], which have employed adult PMV models to compare the thermal comfort of children with that of adults. Ter Mors [22] found that the PMV–PPD method underestimated children's thermal sensation by up to 1.5 points in three free-running primary schools in the Netherlands, highlighting children's greater sensitivity to high temperatures and distinct thermal comfort characteristics compared to adults [22]. Furthermore, a study conducted in classrooms in different climates demonstrated that children feel more comfortable at lower temperatures than adults. Yang et al. [23] observed that studies focusing on primary schools where children are located are limited in the literature.

Although recent studies have investigated the thermal comfort and sensations experienced by schoolchildren in cold climate regions [14], it is evident that further research is required in order to achieve more accurate findings. In this study, indoor temperature, relative humidity, air velocity, predicted percentage of dissatisfied (PPD), and the sensation scale for the predicted mean vote (PMV) were examined using both subjective and objective measurements. The study commenced with a comprehensive literature review, during which the scope of the study was delineated. Subsequently, measurements were conducted at the selected school, which is a public institution that caters to students from low- and middle-income backgrounds. The study observed the adaptation of students in the 11-14 age group to indoor thermal environments in naturally ventilated classrooms. The primary objective of the field study is to examine students' feelings and preferences during cooling and heating periods in classrooms within a school building, with the specific aim of determining existing thermal comfort levels to create an environment conducive to studying and intellectual development. The specific aims are to:

- Determine the existing thermal comfort levels for each of the places studied in order to provide a suitable environment for studying and the development of intellectual activities.
- Investigate differences in students' subjective votes regarding the preferred temperature for their best academic performance, taking into account their local context and climatic situation.

The study structure is presented in Figure 1.
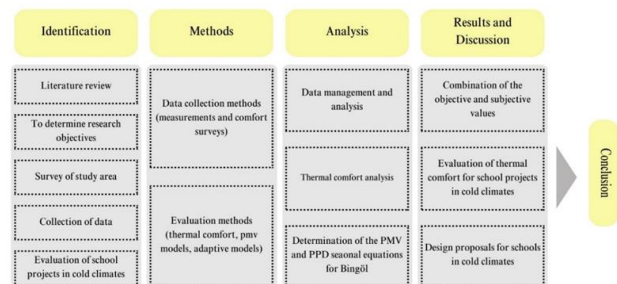
Figure 1. The structure of the study

1.1. Previous Studies

It can be observed that personal factors exert a significant influence on indoor comfort, to a degree that is comparable to that of environmental factors [24]. While environmental factors are defined as indoor air temperature, relative humidity, air velocity and average radiation temperature, personal factors are divided into the individual's clothing thermal resistance and activity level. The Predicted Mean Vote (PMV) thermal sensation index, developed by Fanger [25], is used to express whether an environment is perceived as thermally comfortable by a large group of people. The Predicted Percentage of Dissatisfaction (PPD) index is a metric developed based on the PMV index and used to estimate the percentage of users who are dissatisfied with thermal comfort conditions [26]. The PMV-PPD and adaptive models have been widely used by researchers [27].

The estimation of the PMV and PPD degree in the environment to which standard people are exposed is

investigated on a scale in line with the model created by Fanger and enables the determination of acceptable thermal environmental conditions. In an environment with a high number of people; With the help of this scale, environmental conditions are estimated with the response levels of users in the range of ±3 (warm/warm/slightly warm/neutral/slightly cool/cool/cold). The scope of standards can be divided into three categories: indoor environment in general (ISO 17772, EN 15251, EN 16798), thermal environment (ISO EN 7730, ASHRAE 55, GB/T 50785, SS 553), and indoor air quality (ASHRAE 62.1, ASHRAE 62.2, AS 1668- 2, SS 554) [28]. On the other hand, in Europe, ISO 7730 and in North America, ASHRAE Standard 55 are widely accepted for thermal comfort standards [28,29]. Since our study is on indoor thermal environment ISO (International Organization for Standardization) EN (European Norm) 7730, ASHRAE (American Society of Heating, Refrigerating and Air-Conditioning Engineers) 55 standards are necessary and sufficient to evaluate the results. The ISO EN 7730 thermal comfort standard, based on the PMV model developed by Fanger in 1970, is widely used to evaluate moderate thermal environments in HVAC systems. While its validity in unconditioned environments has been criticized, Fanger suggested the use of PMV in naturally ventilated spaces could be effective with an expectation factor [30]. The PMV model is frequently applied in school thermal comfort assessments.

Kwok and Chun [31] examined thermal comfort in naturally ventilated and air-conditioned classrooms in Japan. Havenith [18] measured the metabolic rates and clothing insulation of school children, highlighting age and activity-specific climate control needs. Studies by Zhang et al. [32] and Hwang et al. [33] assessed the applicability of ASHRAE specifications in tropical and subtropical schools. Hussein and Rahman [34] found higher heat tolerance among Malaysian school participants due to the regional climate. Sanders [35] developed indoor air quality standards for primary schools in Texas, finding that location, orientation, material selection, and ventilation system design significantly impact indoor air quality. Poor ventilation was linked to reduced learning performance, health risks, and economic costs.

Yıldırım [36] emphasized the importance of heat and sound control in educational buildings for student health and learning performance, highlighting the role of insulation. The study proposed solutions for heat and sound comfort issues in Turkish schools, noting that thermal comfort improves teacher and student performance. Proper heating in insulated environments can enhance energy efficiency and reduce pollution, with insulation materials impacting indoor air quality. Kocahakimoğlu [37] found daily variations in indoor environmental quality in primary schools, with higher pollutant levels on weekends and indoor ozone levels linked to outdoor conditions [26]. Teli et al. [29] and Humphreys [38] revealed that children's thermal perceptions differ from those of adults, with children being less sensitive to temperature changes. Studies by

Hwang et al. [33], Kwok and Chun [31], and Zhang et al. [32] assessed the applicability of ASHRAE specifications in tropical schools. Heracleous and Michael [39] found high thermal tolerance among students in Cyprus during both winter and summer. Rodríguez et al. [15] emphasized behavioural, contextual, and age-related influences on thermal comfort in Bogota schools.

2. MATERIAL AND METHOD

2.1. Location and description of the building and the classrooms

The city of Bingöl is located in the Upper Euphrates Section of the Eastern Anatolia Region in Turkey, at 41º 20' and 39º 56' east longitudes and 39º 31' and 36º 28' north latitudes (Figure 2a). According to the Trewartha climate classification, Bingöl province has a climate type that is cold in winters and hot in summers. According to the universal temperature scale, the average temperature in January is -2.6 °C, while the average temperature in July is 26.7 °C. The research was conducted in a school that provides education to students aged 11-14. The school was built in 2003 and is located among residential settlements (Figure 2b-c). The school has an indoor space of 7400 square meters. Figures 3a-b show the floor plan and entrance facade of the school.
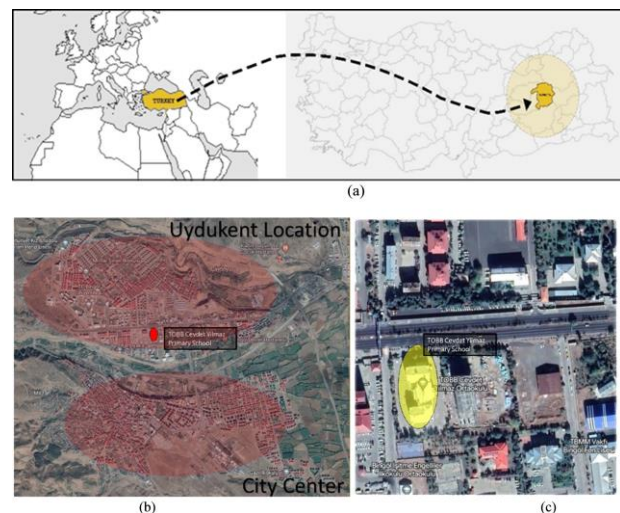
Figure 1.a. The location of Bingöl province on the map of Turkey [40], b,c. The location of the examined school in the city (taken from google earth and edited by the authors)

The school building consists of a U-shaped layout with a basement, ground floor, and three upper floors. Classrooms are primarily located in the north-south oriented side branches, while social activities and common areas are situated in the main middle arm and east-west direction (Figure 3a,3b).

Figure 3.a. The floor plan of the school, b. The view of the entrance facade

The school has a total of 32 classrooms, averaging 53 m² in size with an average of 1.39 m² per student. Window areas in the classrooms where the study was conducted are presented in Table 2. The walls were insulated using the sheathing technique, and the roof design featured a hipped roof system with wide eaves for rain and sun protection. Measurements and evaluations were conducted for the eight classrooms located on the top floor (Figure 4).
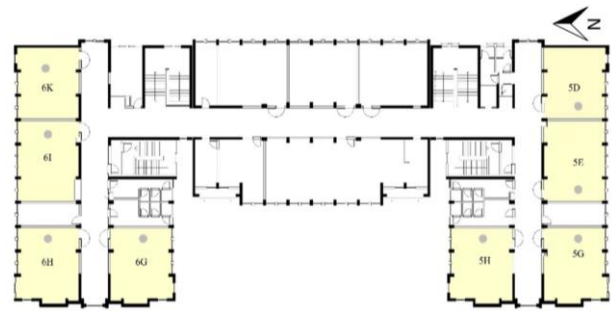
Figure 4. Locations of the classes on the plan

Figure 4 illustrates the distribution of classes within the architectural plan. Four classes (5D, 5E, 5G, 6G) face south, while the remaining four classes (6K, 6I, 6H, 5H) face north. The spatial characteristics of the school and the classrooms where measurements were taken are described in Table 1.

Table 1. Characteristics of the selected classrooms

Class	5G	5H	5E	5D	6G	6H	6K	6I
Width(m)	6.80	6.80	6.80	6.80	6.80	6.80	6.80	6.80
Length (m)	7.60	7.55	7.80	7.60	7.80	7.88	8.60	7.60
Height (m)	3.90	3.90	3.90	3.90	3.90	3.90	3.90	3.90
Volume (m³)	208.22	207.64	224.48	200.66	209.43	208.85	219.77	200.46
Floor area (m²)	53.39	53.24	57.56	51.45	53.70	53.55	56.35	51.34
Total door area (m²)	2.90	2.90	2.90	2.90	2.90	2.90	2.90	2.90
Total windows area (m²)	11.55	11.55	9.90	8.25	11.55	11.55	9.90	8.25
The ratio of window area to the floor area	0.21	0.21	0.17	0.16	0.21	0.21	0.17	0.16
Number of students in the class	45	40	40	35	42	40	45	40
Wall material	Water-based paint + gypsum plaster + brick wall + eps insulation (8 cm.)							
Floor material	Artificial glossy granite + reinforced concrete							
Ceiling material	Water-based paint + reinforced concrete + eps insulation (10cm) + wooden roof cover							
Lighting type	Fluorescent lamp							
Heating type	Natural gas							

During the preparation phase, several visits were made to the school to obtain building plans, gather operational information, and take photographs of each area. Prior to the commencement of the experiments, teachers were provided with a thermal comfort information form, which outlined the parameters of the study and informed them of the importance of thermal comfort. Students were also given a brief overview of the measurements that would be conducted by the teachers and researchers. Technical equipment was installed in the middle of the classroom for the duration of the study (Figure 5c and Table 1).

2.1. Thermal comfort surveys and Data analysis method

Based on the adaptive approach, which suggests people influence their thermal environment consciously or unconsciously [41], we measured conditions in eight north-south oriented top-floor classrooms, expecting them to experience the greatest heat loss. The first stage of the study involved the evaluation of thermal comfort parameters through measurements. Thermal comfort is defined as "a state of mind that expresses satisfaction with the thermal environment and is evaluated through subjective evaluation" [42]. This was analysed through field measurement studies. The measured and investigated thermal comfort objective parameters are as follows [43,38,44,45]:

- Indoor air temperature : Ti (°C)
- Indoor radiation temperature : TR (°C)
- Relative humidity : RH (%)
- Indoor air velocity : Va (m/s)

The temperature on the surface of the walls surrounding the environment may be higher or lower than that inside the space. For example, while the wall temperatures are below the indoor temperature in winter, they are above the indoor temperature in summer. Heat transfer by radiation occurs between these walls and the human body, causing discomfort to users. Therefore, it is necessary to consider the temperatures taken from the walls surrounding the interior space and to evaluate the radiation temperatures of the space. The radiation temperatures of the space can be calculated using different methods. If the instantaneous indoor temperatures (Ti) are known, the Indoor radiation temperature (TR) value can be calculated with equation 1, depending on the indoor temperature (Ti) [46,47].

$$TR = 0.99 \times T_i - 0.01, \qquad R^2 = 0.99 \qquad (1)$$

In this study, indoor comfort conditions were examined during the summer and winter periods at an educational institution in Turkey, where the academic year is divided into two semesters - Fall and Spring. Fall semester starts in September and ends in February, while spring starts in February and ends in June, and summer courses are held during the summer months when there is no regular

education. The winter period (cold months) is when education is in session and students are present at school. The measurements used in this study included data from October to March for the winter period and data from June, August, and September for the summer period. Measurements were taken three times a month, once a week during the summer and winter periods in 2021-2023, as well as in August during summer school, at secondary school in Bingöl. During measurement, the probes were positioned 1.1 meters above the ground to replicate the seated position of students and were placed at least 1.5 meters away from external walls and doors. Instruments were shielded from direct sunlight, cleaned,

and regularly calibrated [14]. The devices used in the study are listed in Table 2 and images taken during the measurements of the schools and classrooms where the measurements were made are shown in Figure 5 (a, b, c). These testing devices were pre-calibrated before starting the tests, and the measurement time took an average of 45-60 minutes in each classroom. The measurement arrangement was positioned equidistantly according to the sitting position of the students. Throughout the study, classroom windows were closed in winter and opened in summer to facilitate natural ventilation, with consideration given to the students' seating positions.

Table 2. Characteristics of the selected classrooms

Parameters	Instrument	Range	Accuracy
Outdoor Temp.	Testo 480 CMI	0 to 60 °C	±0.5
Comfort Temp.	Testo 480 CMI	0 to 60 °C	±0.5
Relative Humidity (RH)	Testo 480 CMI	0 to 100%	± (1.0% RH + 0.7% Reading)
Air flow rate	Hot Wire Anemometer DT8880	0.1 to 25.0 m/s	± %5 ± 0.1m/s
Globe Temperature	Cool-Us CU-IT InfraRed Thermometer	0 to 50 °C	± 0.4 °C
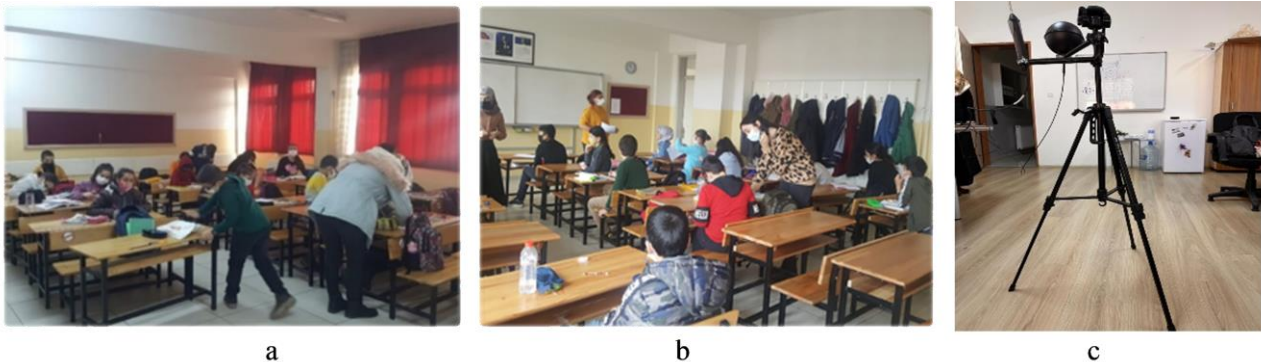
Figure 5. a,b. Images from classes during measurement, c. Measurement set views

Thermal comfort ranges, given in ASHRAE Standard 55 and ISO 7730 international standards [48,49,42], were considered for evaluation using tables and graphics. The recorded data were analysed in detail to evaluate Fanger's indices, PMV and PPD, for thermal comfort according to International ASHRAE Standard 55 and ISO 7730 standard [50,25].

In the study, a survey was administered to the students during the measurements in the classes where measurements were made. The scope of this study encompassed a total of 264 individuals aged 11-14, surveyed in eight classrooms. In alignment with the methodology employed in this study, Teli et al. [29] surveyed an average of 230 pupils aged 7-11 in all eight classrooms of the school during the heating season. Additionally, the suitability of the school where the research was conducted for the study was also taken into consideration. However, it was selected as it had the highest number of students among the schools that were rebuilt following the 2003 Bingöl earthquake. In line with the research objectives, a study was conducted with secondary school students. In determining the schools to be studied, conditions such as suitability, ease of accessibility, voluntariness in participation, and obtaining a sufficient number of participants were taken into consideration in terms of researchers, school administrators and teachers. A total of 124 male (42%)

and 170 female (58%) students participated in the study. Although there is a uniform, which is an official dress code determined by the school, wearing a uniform is not mandatory. Some students wore loose clothing, but it was observed that most students came to school in the form determined by the administration. Consequently, average clothing insulation values for children were calculated (ISO 7730). In addition, the questionnaire administered to all classes at the beginning of the lesson during the measurements. They were in class for about 60 minutes. During the process of conducting objective measurements, students were requested to complete a questionnaire. Participants were given the questionnaires 30 minutes after entering the classroom to ensure they had sufficient time to acclimate to the environment (Duration of one lesson 45-60 min.). Teachers were asked to assist in making the questionnaire understandable. The survey questions briefly included the following topics:

- Respondent's thermal sensation rating for the indoor thermal environment, based on the 7-point ASHRAE thermal sensation scale (cold, cool, slightly cool, neutral, slightly warm, warm, hot).
- Feeling of comfort.
- Dress information.
- Feeling of tiredness.
- Students' activities during the survey.

As a result of the study, evaluations were made by comparing the results of the surveys and measurements.

3. RESULTS AND DISCUSSION

In this study, indoor comfort conditions were examined during the summer and winter periods at an educational institution in Turkey, where the academic year is divided into two semesters - Fall and Spring. The measurements used in this study included data from October to March for the winter period and data from June, August, and September for the summer period. Measurements were taken three times a month, once a week in 2020-2022.

In this study, indoor air temperature (Ti), indoor radiation temperature (TR), relative humidity (RH), and air velocities (Va) were measured, and graphs based on instantaneous and periodic average data were created. As mentioned before since our study is on an indoor thermal environment ISO EN 7730, and ASHRAE 55 standards are necessary and sufficient to evaluate the results. According to ISO 7730, the winter comfort temperature for 50% relative humidity is 20-24°C, while it is known to be 23-26°C in the summer period [51,26]. In the Khovalyg et al. [29] study, the winter temperature range is 19-25°C according to the ISO7730 standard, while it is 20.5-24.5°C according to Ashrae 55. Again, according to the ISO7730 standard, the summer temperature range is 22-27°C; According to Ashrae 55 it is 24-27°C. As can be seen, ISO 7730 keeps the comfort range wider, while Ashrae 55 narrows the comfort range by 2-3°C. While ISO 7730 has different categories, Ashrae does not have any categories and determines the acceptable values of the thermal environment. In this regard, ASHRAE 55 summer and winter comfort temperatures were taken as reference in the range of 23-26°C and 20-24°C, respectively, and relative humidity was taken as reference in the range of 30-60% for both summer and winter periods.

3.1. Indoor Air Temperature Measurement Results of Spaces

Figure 6 presents graphs illustrating the temporal evolution of indoor air temperatures in classrooms during the winter months. To facilitate comparison, the lower and upper limits (20-24°C) of the ASHRAE 55 standard for winter are also included in the same graphs. The data in the graphs indicates that indoor temperatures in the classrooms from October to March range between 20-25°C. It can be observed that the indoor temperature values for these months remain within the standard value range. In March, the indoor temperature in the 5D and 5G classrooms falls slightly below the standard minimum value of 19°C. However, the overall indoor temperature in March ranges from 19-22°C, which is close to the standard values.

96
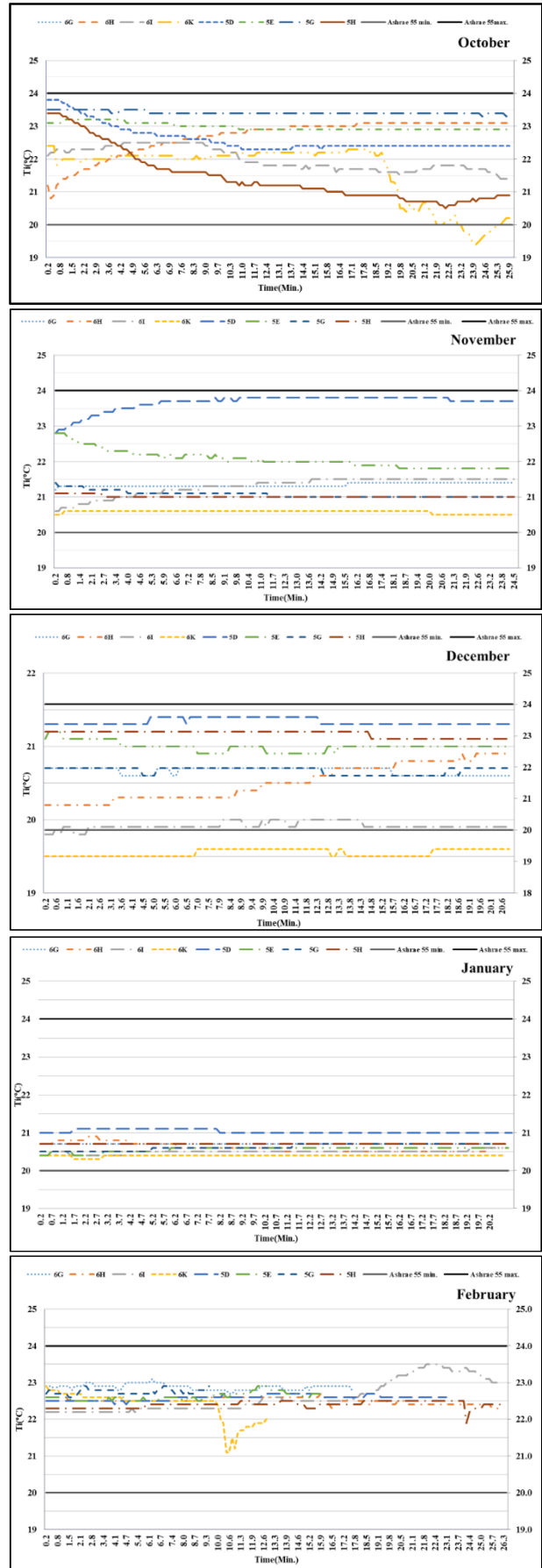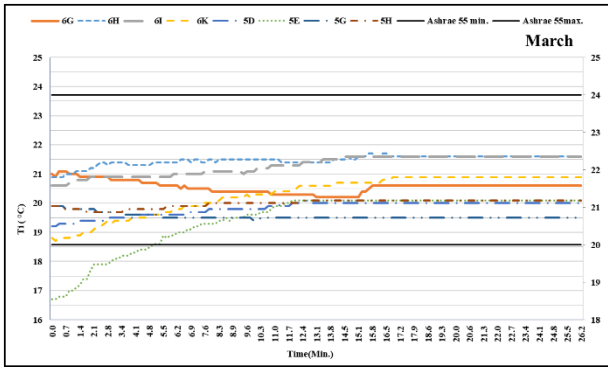
Figure 6. The temperature of indoor classrooms during the winter period

Figure 7 presents the instantaneous indoor air temperatures of the classes during the summer period. In order to facilitate comparison, the summer temperature lower and upper limits (23-26°C) of the ASHRAE 55 standard are also provided. The results in Figure 7 indicate that the temperature values for June, August and September are in the range of 25-28°C, 30-37°C and 23-26°C, respectively. Therefore, the values of June and September are within the standard range. However, for August, which is the hottest and driest month of the year, it is observed that the comfort value is significantly exceeded. Consequently, it can be concluded that indoor temperatures in educational institutions exceed the upper limit of the comfort standard, particularly during the hottest months of the year in this region, namely July and August. It is therefore necessary to implement measures to reduce temperatures to the standard value range.
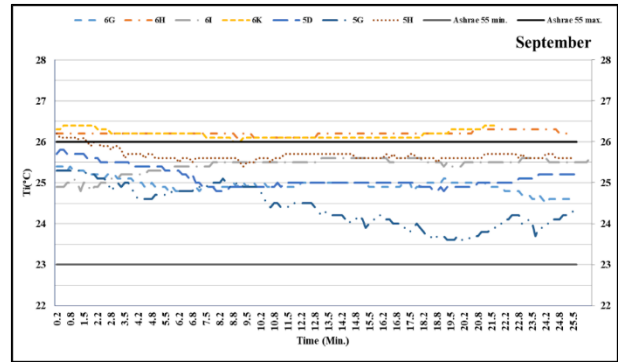
Figure 7. The mean indoor air temperature of the classrooms during the summer period

3.2. The Results of the Indoor Radiation Temperatures Measurements of the Spaces

Indoors radiation temperatures play a crucial role in providing suitable comfort conditions and ensuring appropriate insulation in buildings. Proper insulation can help maintain appropriate radiation temperatures, preventing wall temperatures from dropping too low in winter and rising too high in summer. For example, during the winter months, outdoor temperatures can be very cold, causing wall temperature values to be slightly lower than indoor temperatures. However, to ensure comfort, a maximum difference of 3°C is required between the wall temperature and the indoor temperature. If the temperature difference is greater than 3°C, radiation heat transfer between the body and the cold wall can cause discomfort, even if the environment is heated. Therefore, according to TS 825 (standard in Turkey) insulation standards, the wall temperature value should be at least 17°C. Similarly, during the summer months, air temperatures in various regions can reach very high temperatures such as 40°C. However, the indoor temperature will be lower than this value. Walls facing the warm environment will be warmer than the interior, and even if the interior is ventilated with a device such as an air conditioner, discomfort can occur due to radiation from the high-temperature outer wall to the person's body. Therefore, the insulation properties of the building should be designed so that the interior surface temperature is no more than 3°C lower than the indoor temperature values (for all surfaces such as roof, wall, etc.) Appropriate thermal insulation must be used in the building to provide summer and winter comfort conditions (TS 825). With proper thermal insulation, heat losses from inside to outside are prevented in winter, and heat transfer from outside to inside is prevented in summer. Comparisons of indoor temperature and indoor radiation temperature values of classrooms in winter and summer seasons are given in table 3 and Figure 8 (a, b).

97
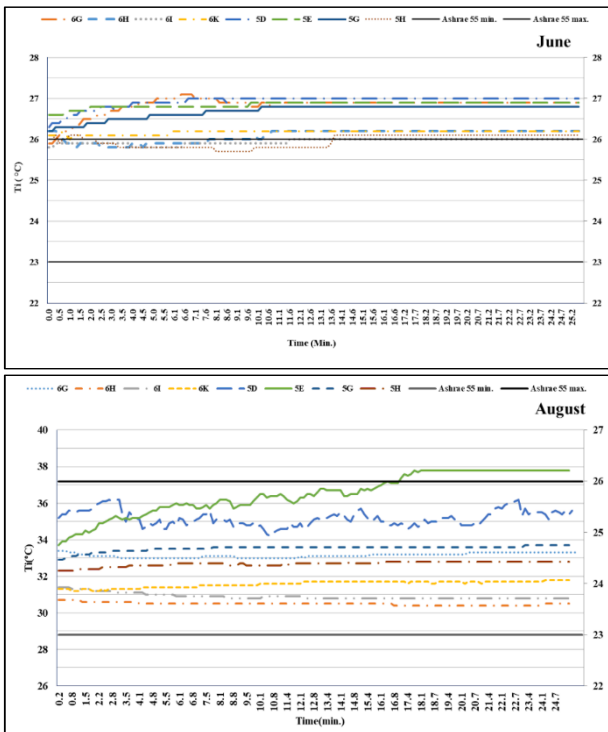
Table 3. A comparison of the mean indoor temperature during the winter and summer seasons, along with the indoor radiation temperature values

Average parameters	5G	5H	5E	5D	6G	6H	6K	6I
	Winter period							
T_i	19.6	19.9	18.8	19.6	20.6	21	20	21.1
RH (%)	36.6	35.6	38.6	36.4	40.1	40	48.9	39.7
T_R	16.1	15.3	12.8	18.3	18.3	17.6	18.3	16.62
	Summer period							
T_i	30.5	29	31	31	30	28	28	28
RH (%)	23	23	21	22	25	25	23	25
T_R	27	28	29	28	28	26	27	27
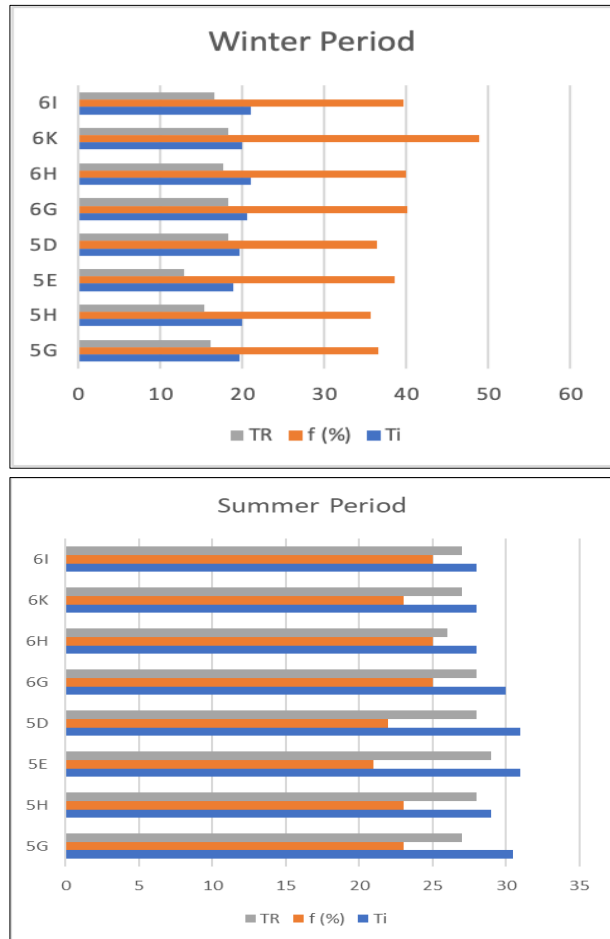
Figure 8.a. Comparison of winter indoor temperature, indoor radiation temperature values, b. Comparison of summer indoor temperature, indoor radiation temperature values

The instantaneous indoor radiation temperatures, calculated using equation 1 as a function of the indoor temperature, are shown in Figures 9 and Figure 10 for the winter and summer periods, respectively. Figure 9 indicates that, during the winter period, the indoor radiation temperatures generally fall below the lower limit of the ASHRAE 55 standard, with the exception of October, November, and December. The indoor temperature graphs presented earlier indicate that the indoor temperatures range between 20 and 25 degrees Celsius in October and November, 20 and 22 degrees Celsius in December and January, and decrease slightly to 19 and 22 degrees Celsius in March. It is evident that the indoor radiation temperatures for these months decreased by 1-2°C and fell below the lower limit of the comfort conditions in some classes in October and November, and

below the lower limit for all classes in December and January.

As can be observed, while the indoor temperatures are within the comfort range in winter, the indoor radiation temperatures are at the lower limit of TS 825. It is evident from Table 3 and Figure 8 that the wall temperature value drops to 12°C in March, which is below the 17°C threshold set out in the TS 825 standard. While proper heating can be achieved, it cannot be said that proper insulation has been provided. This is problematic, as the wall temperature has dropped to 12°C even in March. The indoor radiation temperatures will be lower due to the wall temperatures in February and January when the cold is more severe. This will cause condensation on the walls and, subsequently, mould growth.
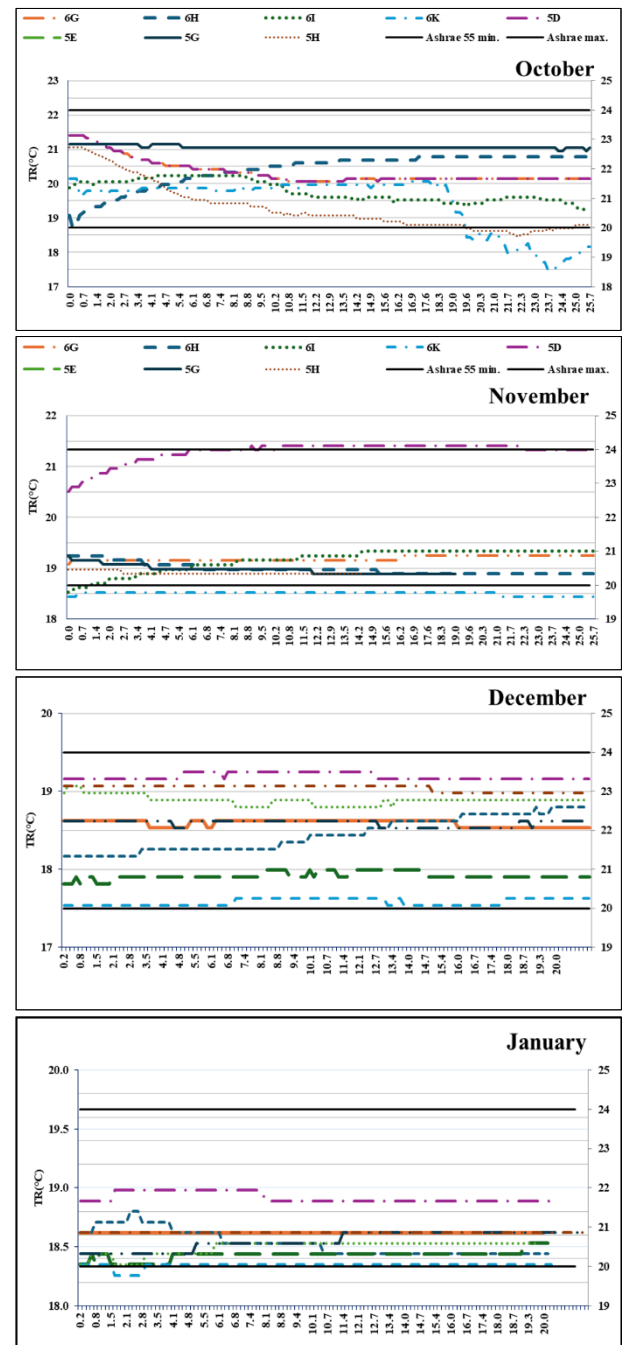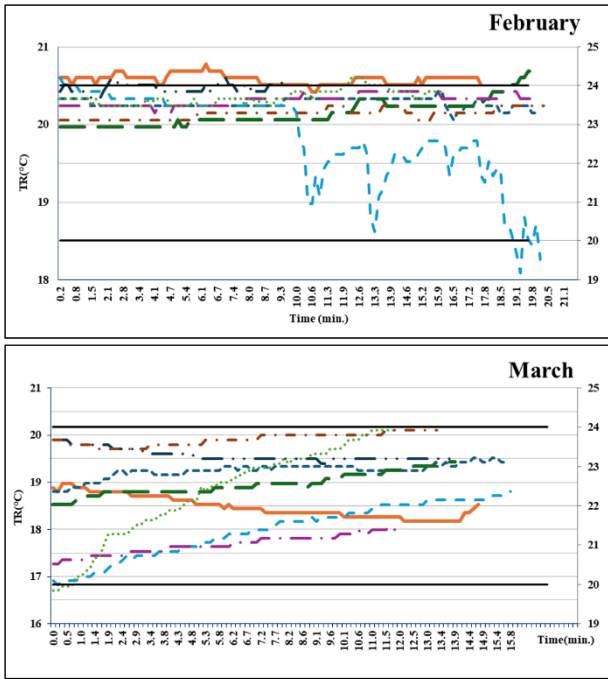
Figure 9. Indoor radiation temperatures in the winter period

Figure 10 presents the instantaneous indoor radiation temperatures during the summer months. The data indicates that the values in June fall within the ASHRAE standard limits and are therefore suitable for comfort conditions. However, the temperature values in August exceed the standards by approximately 30℃, with maximum values observed. In contrast, temperatures in September are below the standard. As with the overall conclusion drawn from the indoor temperature results presented in these graphs, it is evident that necessary precautions should be taken to manage high temperatures when these spaces are used in July and August, which are the hottest and driest months of the summer.
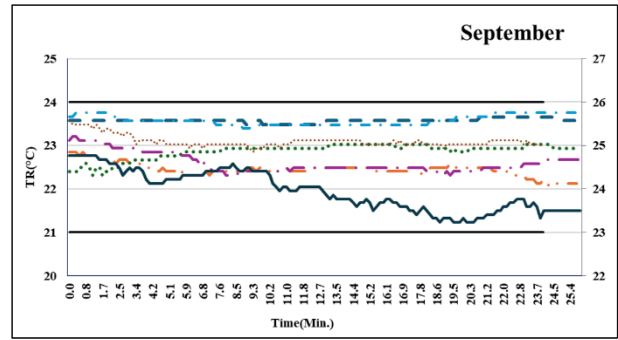
Figure 10. Summer Indoor radiation temperatures

3.3. The results of the relative humidity measurements of the spaces

Relative humidity is another important parameter that affects thermal comfort. It is defined as the ratio of the amount of water vapour in the air to the maximum amount of water vapor it can hold at the same temperature, expressed as a percentage. As shown in Equation 2, it is calculated by dividing the absolute pressure of the air by the saturation pressure at the same temperature. According to the ASHRAE 55 standard, the recommended relative humidity range for comfort is between 30-65%. However, some sources suggest that a range of relative humidity of 35-60% would be more suitable [51]. It is useful to evaluate the relative humidity discomfort in cases where it is below the lower limit and above the upper limit. If the relative humidity value falls below the lower limit (below 30-40%), it causes health problems such as dryness and itching on the skin and lips. On the other hand, in cases of over 65%, it will cause discomfort such as difficulty in breathing, excessive sweating, and feeling of suffocation. These conditions can have a significant impact on human work and productivity. The World Health Organization reports that there is a possibility of airborne transmission as well as human-to-human transmission of viruses. It has also been determined by many studies that contamination and viruses are frequently transmitted through the air. This situation is closely related to the amount of humidity in the air. The rate of spread of influenza (flu) virus is higher when the relative humidity is below 40% (Metz, 2015). This is why low relative humidity is a major contributing factor to seasonal flu outbreaks, especially during the winter months [52].

99
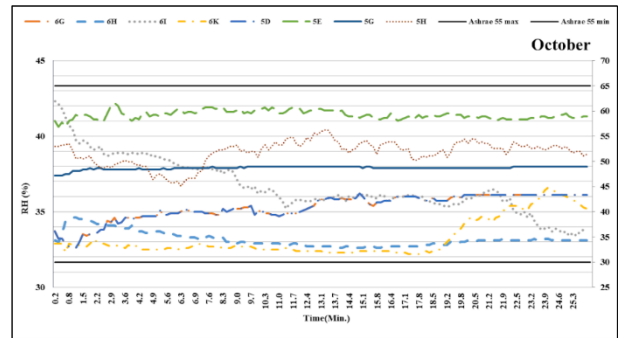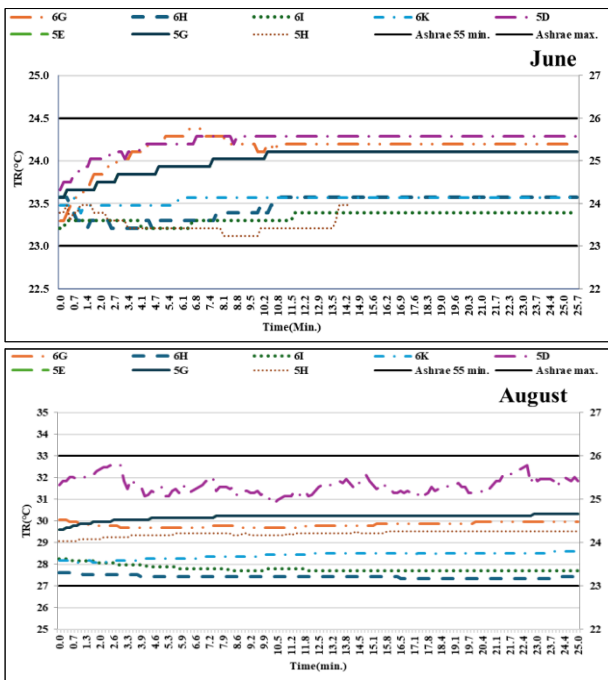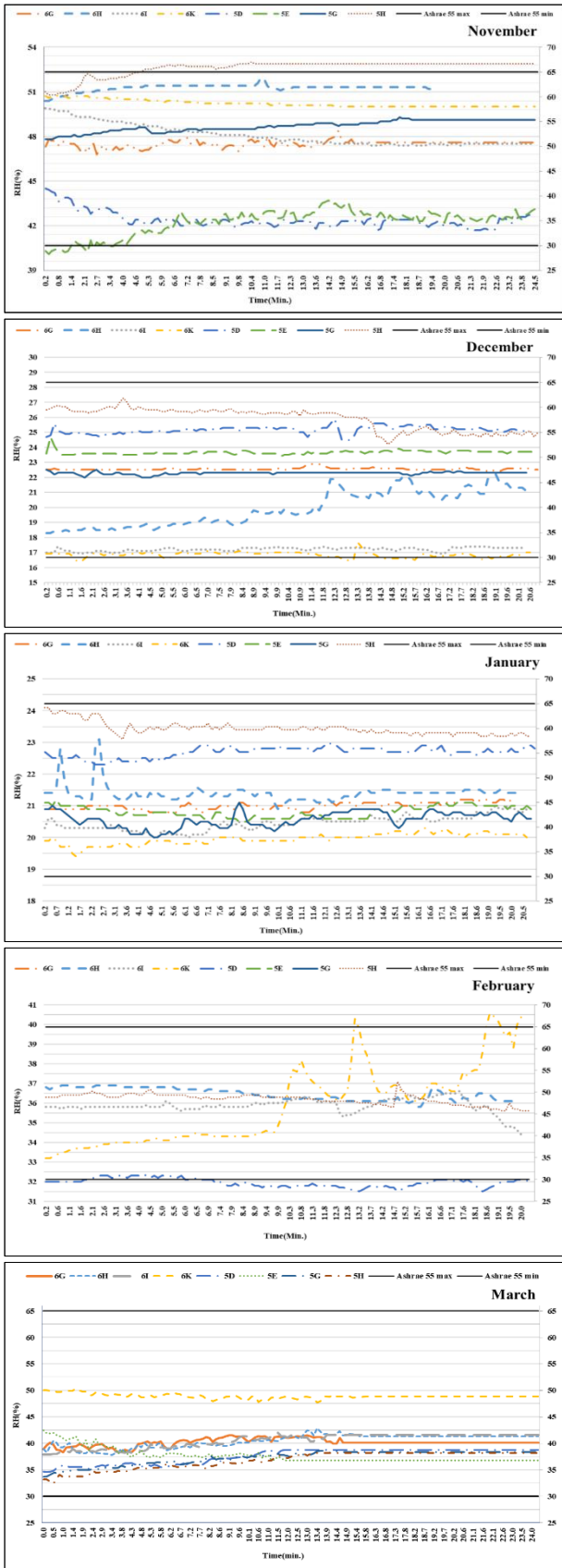
Figure 11. Relative humidity values in winter period

Figure 11 presents instantaneous relative humidity graphs for different spaces during the winter months. Based on these graphs for the winter period in Figure 10, it can be seen that relative humidity rates fall within the standard range except December and January months. However, in December and January, relative humidity rates are

between 15-25%, indicating discomfort. This extreme drop in relative humidity can be attributed to the hot and dry weather during these months in 2022-2023. As a matter of fact, according to Turkey's meteorological data, 2022 December has been recorded as 15 sunny days and 8 rainy days. In summary, the months of December and January were quite dry in the related year. As for the summer period, the relative humidity values for most classes are close to the lower limit of 30-35% (as shown in Figure 12). Therefore, it can be concluded that these classes are generally uncomfortable, especially in August when humidity levels are lowest. Table 3 also provides similar results for relative humidity values. The average humidity level during the winter period is above 35%, while the average values during the summer are at around 30%, dropping to 12% in August, which is the hottest and driest month of the summer.
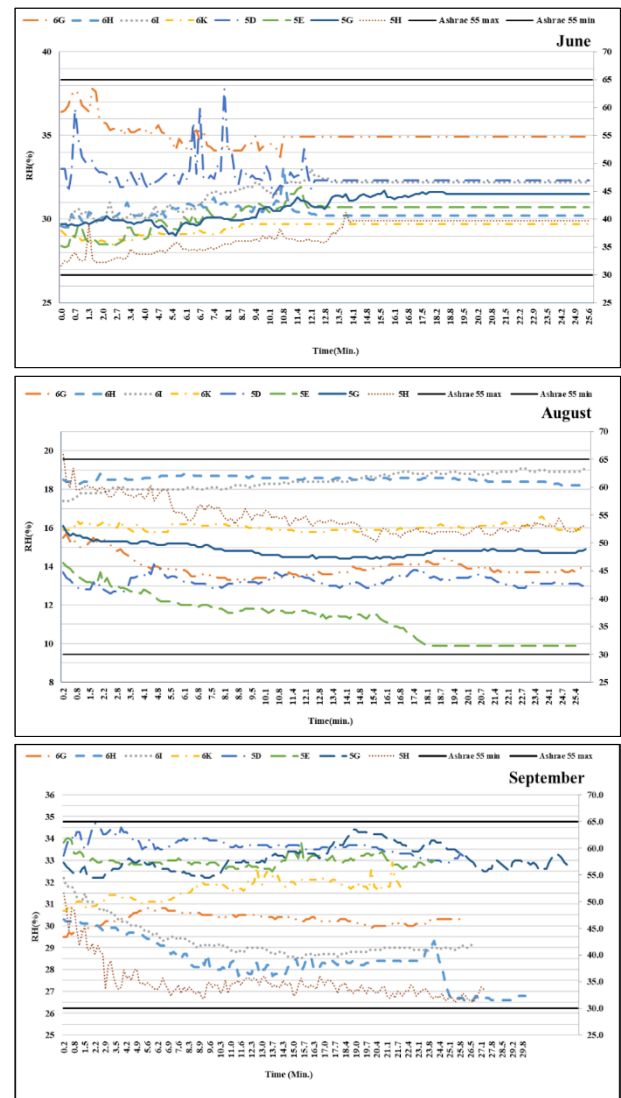
Figure 12. Relative humidity values in the summer period

3.4. The results of the air velocity measurements of the spaces

Measurements were made in naturally ventilated classrooms with air circulation through windows and doors. Lee and Zakaria (2024) state in their study that classroom ventilation is very important when it comes to

creating a successful learning environment, with several advantages in terms of comfort and productivity for both students and teachers [58].

The comfort conditions of an environment are closely related to the air velocity, as well as the temperature and humidity of the ambient air. While stagnant air at low temperatures does not cause discomfort, it can become suffocating in high temperatures. For instance, at an ambient temperature of 20 °C, a comfortable air velocity is 0.15 m/s, whereas at an ambient temperature of 24 °C, an air velocity of 0.22 m/s is more suitable for comfort [53]. Therefore, buildings should be designed to make the most of natural ventilation, taking into account the climatic conditions of the region and the orientation of the building. In this regard, it is recommended that buildings be designed in a manner that optimises the utilisation of natural ventilation, taking into account the climatic conditions of the region and the orientation of the building. The air velocities of the classes for the winter and summer periods are presented in Figures 13 and 14. From the winter period graph, it can be seen that the air velocities of the classes are at the standard value in December. However, the data for October is mostly above 0.2 m/s, which is uncomfortable. In some classes, the data for January exceeds 0.2 m/s. In February, the air velocities in the 5H and 5D classes increased to 1 m/s at certain moments due to door or window openings. However, when considering all other classes, the velocity values were consistently below 0.2 m/s throughout the measurement period. It is evident that the velocity value exceeded 0.2 m/s during the measurement period in almost all classes in October. This can be attributed to the fact that October is a transitional month between the summer and winter periods, with doors and windows not generally kept closed during this time. It is understood that the values in December, January, and February, which are the other months of the winter period, are generally below 0.2 m/s (Figure 13).
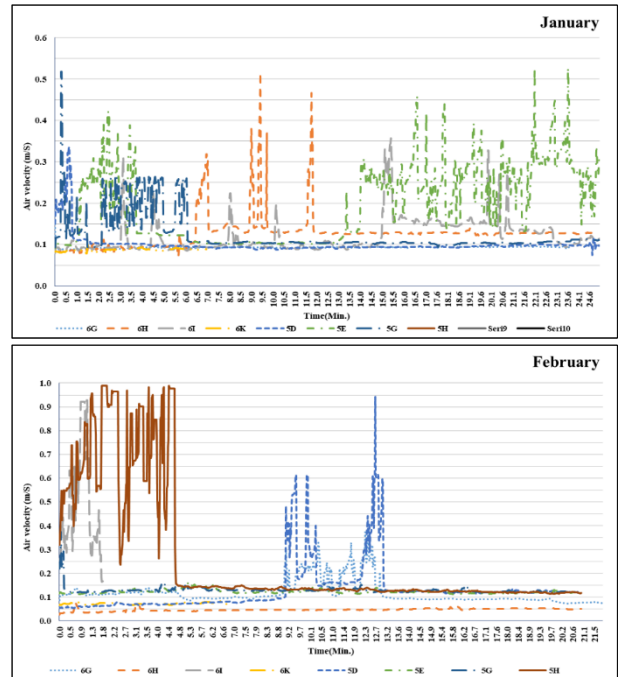
Figure 13. Air velocities of the winter period

Figure 14 presents summer air velocities. The August graph shows that only classes 5H and 5G have air velocities close to the standard value (approximately 0.2 m/s), while the other classes have much higher air velocities. The optimal air velocity for comfort during summer is 0.22 m/s at an ambient temperature of 24 °C (Halıcı 2019). Given that the average ambient temperature in August is 33 °C, an ambient air velocity of around 0.4 m/s is not considered uncomfortable, as it will mitigate the effect of the sweltering heat. Since ventilation is achieved through window openings in the summer period and measurements are taken while the windows are open, it is apparent that the air velocities are higher (around 0.4 m/s) compared to the winter months. Nevertheless, prolonged exposure to air velocities of 0.6 or 0.8, as illustrated in Figure 14, may have detrimental effects on one's health, even during the summer months.

101
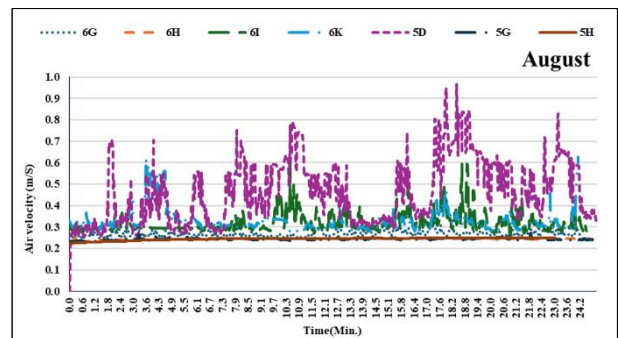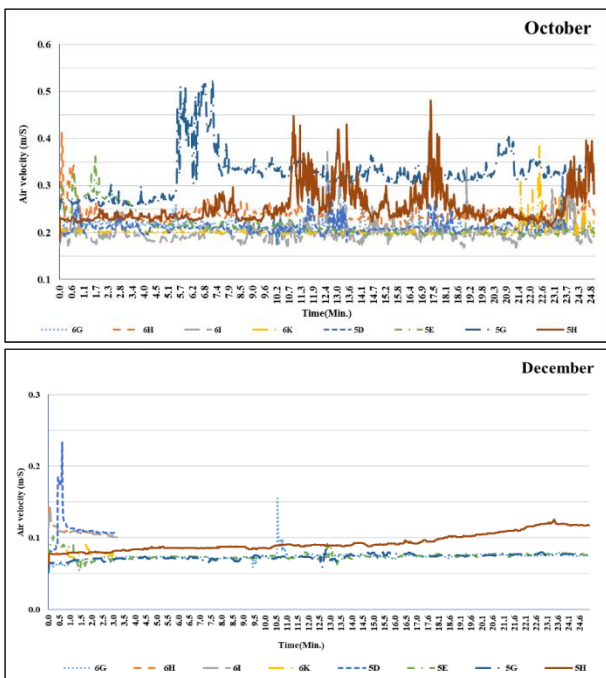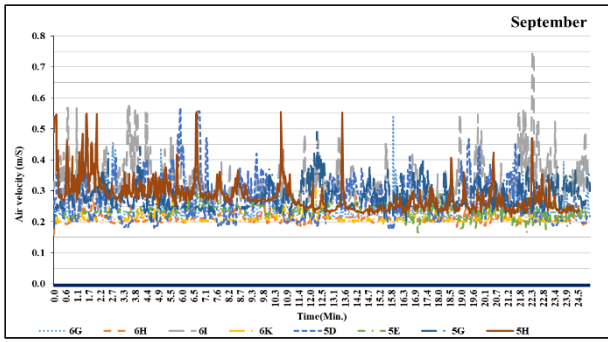
Figure 14. Air velocities of the summer period

3.5. Thermal responses: thermal sensation and thermal preference votes

The evaluation of the survey data applied during measurements in the classrooms is included in this section. According to the survey data applied during the study, students expressed a preference for additional insulation layers, such as school jackets, coats, or thermal underwear, to prevent heat loss from the body during the winter months. Consequently, the "clo" values of average clothing insulation for children are employed in ISO 7730. The clothing thermal resistance was calculated as 0.35 for the summer period and 0.70 for the heating period, providing an "error band" for PMV estimation. As there was no significant difference in the values of the thermal parameters, each class was characterised by a single PMV and PPD value. A total of 3% of the collected responses were excluded from the data analysis. This approach of excluding inconsistent responses from the analyses was adopted in line with previous studies [29,54]. The PPD values derived from the measured data were contrasted with the percentage of dissatisfied individuals estimated by evaluating the questionnaires. The thermal sensations of the users were gauged using the ASHRAE scale, with thermal sensation values (TSV) ranging from cold (TSV = -3) to hot (TSV = +3) (Table 4).

Table 4. The thermal sensation scale (TSV)

Cold	Cool	Slightly cool	Neutral	Slightly warm	Warm	Hot
-3	-2	-1	0	+1	+2	+3

In the PMV formula (ISO 7730), the metabolic rate is factored in two ways. The metabolic rate of an average adult at rest (RMR) is integrated into the empirical equation with a resting value of 58.15 W/m². This is described as the ratio of the metabolic rate during physical activity to the resting metabolic rate, commonly referred to as "MET." According to ASHRAE [29], 1 MET is defined as "the metabolic rate of a sedentary person (seated, quiet): 1 MET = 58.15 W/m² = 50 kcal/(h·m²)." By its design, the PMV equation is tailored to adult physiology. Additionally, the metabolic rates per unit skin surface area for various activities provided by frequently used standards reflect typical values for an average adult. These values are derived from experiments involving adult subjects and may not directly apply to children. Children have a higher resting metabolic rate per kilogram of body weight compared to adults, which gradually decreases as they grow. Furthermore, children's school

day activities differ significantly from those of adults. Consequently, there is a pressing need for a thermal comfort model that specifically addresses the physiological characteristics of children.

Table 5. Survey results according to the thermal sensation scale

Period		T_i	Thermal Sensation scale (TSV)							Total
			-3	-2	-1	0	1	2	3	
Winter Period	5G	19.6	0	0	0	0	3	5	2	10
	5H	19.9	0	0	3	5	10	6	0	26
	5E	18.8	0	0	0	2	3	3	0	8
	5D	19.6	0	0	1	3	2	4	0	10
	6G	20.6	0	1	2	4	11	15	2	34
	6H	21	0	0	3	5	14	12	0	34
	6K	20	0	0	0	2	8	6	0	18
	6I	21.1	0	0	2	8	9	11	0	30
	Total		0	1	11	29	60	64	5	170
	%		0	0.6	6.5	17.1	35.2	37.6	3.0	
Summer Period	5G	26.7	0	0	0	7	5	6	0	18
	5H	25.8	0	0	0	1	4	2	0	8
	5E	26.8	0	0	0	8	6	2	0	16
	5D	26.9	0	0	2	6	5	5	0	18
	6G	26.8	0	0	0	6	7	9	8	30
	6H	26	0	0	2	2	5	5	0	16
	6K	26.1	0	0	0	0	4	4	0	8
	6I	25.9	0	0	0	2	4	4	0	10
	Total		0	0	4	32	40	37	11	124
	%		0	0	3.2	25.8	32.3	29.9	8.9	
Cumulative total			0	1	15	61	100	101	16	
%			0	0.4	5.1	20.7	34.0	34.4	5.4	

Several previous thermal comfort studies with children used calculations in the PMV model to address the difference in metabolic rates. Havenith [18] determined that metabolic rates for school activities are in the range of 52-64 W/m2. This value is approximately 10% lower than the adult's sedentary activities (office work) (70 W/m2) equivalent. Children's RMR has been measured in numerous studies over the past 20 years, but there is no standard value that can be used to calculate the "MET" for the "average" child. For this reason, the metabolic rate used in the literature was calculated as 1.2 MET (58/48.8) (sedentary activity) [24,29,55]. The survey results according to the thermal sensation scale are shown in Table 5 and Figure 15 (a, b). According to the related table survey results of the thermal sensation scale, 124 surveys were collected in this period due to the winter period coinciding with the Covid epidemic, and 170 surveys were collected in the summer period due to the decrease in the effect of the epidemic and normalization of the process.
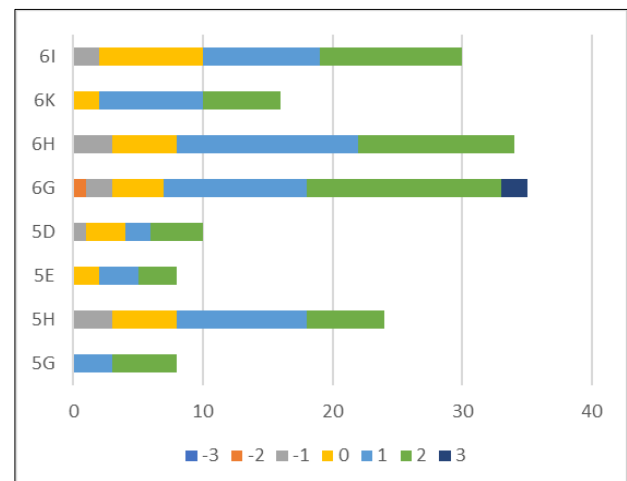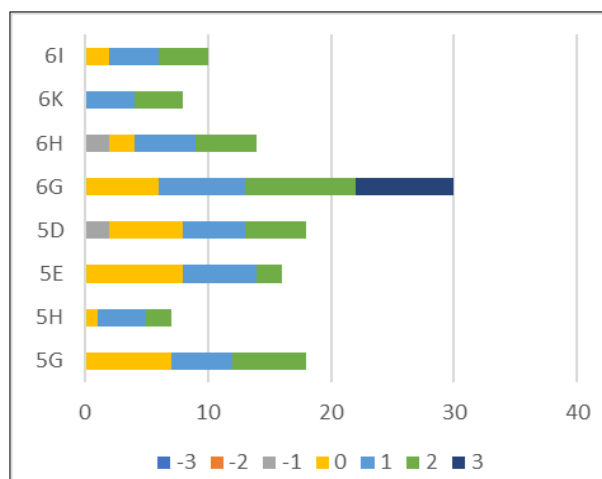
Figure 15. a. Graph of winter period survey results according to ASHRAE Thermal Sensation Scale, b. Graph of summer period survey results according to ASHRAE Thermal Sensation Scaled

In the winter period, 17.1% of students voted 'neutral,' while 58.8% voted within the comfort range (-1 to +1). During the summer period, 25.8% voted 'neutral,' and 61.3% voted within the comfort range (-1 to +1). Overall, it was found that students generally fell within the comfort range in both seasons. Some students felt the classrooms were too cool in winter, but this was due to their clothing choices, as many wore coats and thermal underwear. The majority of students (89.9%) voted within the range of 0 to +2, indicating their comfort level. Factors contributing to this comfort level included high-temperature natural gas heating, double-glazed windows, and crowded classrooms. During the summer period, even with windows open, 88% of students voted within the range of 0 to +2, while nearly 78% expressed a desire for cooler classrooms in summer. The measurements showed that the thermal comfort level was generally within the standard range, except for August. The PMV average was 0.34 with a PPD index of 36.2%. According to surveys, 6.8% of students were dissatisfied during the winter period, while 40.4% were dissatisfied during the summer period. This indicates that students' thermal comfort aligns with the measurements but differs slightly from the PMV model, highlighting the unique thermal sensations of children. Factors such as limited control over windows and clothing adjustments in classrooms may contribute to these differences.

Mustapha et al. (2024) state that, in general, the reliability and validity of different methods used in thermal comfort studies depend on the specific context and purpose of the assessment. In addition, the combination of different methods, such as the use of field measurement methods to measure actual thermal conditions and the use of subjective assessments to capture the individual experiences and preferences of building occupants, can provide a more comprehensive and reliable assessment of thermal comfort in classrooms and emphasises the importance of future research in different climate zones [59]. In this context, the results of this study conducted in a cold climate region provide reliable, original and valuable data.

4. CONCLUSION AND RECOMMENDATIONS

In this study, thermal comfort research was conducted during the summer and winter periods from 2021 to 2023, as well as in August during the summer school session, at a secondary school in Bingöl. This school has the highest number of students among the secondary schools built after the 2003 earthquake in Bingöl. The research was conducted using both qualitative and quantitative research techniques, with questionnaires used for the qualitative aspect and devices used for the quantitative aspect. The study involved evaluating the responses of 264 students, aged 11 to 14, who each completed a questionnaire containing 28 questions. Simultaneously, climatic variables were also measured to correspond with the students' thermal perception. The analytical study includes a comparison between the students' thermal sensation and preference, the derivation of thermal neutrality and comfort range, and a comparison of results with national and international thermal comfort standards. Uncomfortable temperatures directly or indirectly affect the comfort status of individuals. So, this can harm student's health, work efficiency, and energy savings. According to the measurement results, although the indoor temperatures are in the comfort range in the winter period, it has been observed that the indoor radiation temperatures of some classrooms are below 17°C in the winter months. During summer, the indoor temperature is generally above the comfort upper value ($T_i > 26°C$), reaching high temperatures of 30-35°C, especially in August, the hottest month.

Comfort conditions are closely related to the relative humidity and air velocity as well as the temperature of the indoor air. The relative humidity of the ambient air is also adversely affected in case of hot or cold conditions of outside. It has been determined from the results that both summer and winter relative humidity values are generally low. The shift of relative humidity to the uncomfortable range brings along various diseases and disorders, especially viruses such as influenza virus in winter. Low relative humidity also increases the risk of contamination. It is known that virus transmission is less, especially at high temperature and relative humidity values [56]. Uncomfortable relative humidity will also cause an increase in upper respiratory tract infections, as well as cause dryness, irritation, and itching on the skin. In this regard, it is essential to have devices that control humidity and temperature in places such as schools, universities, student dormitories, factories, and work workshops where many people gather. However, it is useful to inform people about situations where these parameters are in the uncomfortable zone. Accordingly, it is necessary to take measures such as automatic activation of the heater or air conditioner when necessary, operating the device that humidifies the environment in case of low humidity, or lowering high humidity through the air conditioner.

Apart from temperature and relative humidity, air velocity is also a parameter to be considered. In transition months between the summer and winter periods (like October and November), doors and windows are not kept closed generally. So, in these months, the air velocity has

103

exceeded 0.2 m/s. The values for the winter (December, January, and February) period, when the doors and windows are kept closed, are generally below 0.2 m/s and are in the standard range. The air speeds of the summer season were generally around 0.4 m/s, and it cannot be said to be uncomfortable as it will reduce the overwhelming effect of the extremely high-temperature values in the relevant months. As well-known stagnant air at low temperatures does not disturb; In case of high temperatures, the stagnant air will be suffocating. For example, while the airspeed is 0.15 m/s at an ambient temperature of 20 °C, 0.22 m/s at an ambient temperature of 24 °C is more suitable for comfort [53]. In this regard, natural or mechanical ventilation of the environment is even more important. Although some studies say that mechanical ventilation is more suitable for Thermal comfort in Schools [57], natural ventilation should be preferred more since mechanical ventilation includes both energy consumption and negative conditions such as sick building syndrome. Therefore, it should be designed to make maximum use of natural ventilation, taking into account the climatic characteristics of the region where the buildings will be constructed and the location of the building according to the directions.

The study revealed that children are more sensitive to high temperatures compared to adults, and thus prefer lower temperatures in classrooms. Children tend to adapt to thermal sensations by opening and closing windows and doors, as well as wearing light clothing during the summer period in classrooms where they spend most of their day. During the winter period, it was observed that they tend to wear thicker clothing to maintain thermal comfort. The PMV/PPD model does not provide full success in predicting the thermal sensations of students in naturally ventilated classrooms. While it shows the maximum percentage (31.6%) of the students who are not satisfied with the indoor conditions, the thermal sense of 89.1% of the students falls within the comfort range (-1 to +1). According to the surveys, only 6.8% of the students were dissatisfied during the winter period, while 40.4% were dissatisfied during the summer period. So, it was determined that the thermal comfort of the students was compatible with the measurements and slightly different from the PMV model. The extremely high temperature and dryness of the summer months, in which it is seen, caused the dissatisfaction rate to be higher. Insufficient ventilation also affects this situation negatively. This result also shows that children's thermal sensations are different from adults. Children's behaviour in adapting to the environment by opening and closing windows or adjusting their clothes in classrooms may explain such differences. A lot of work has been and continues to be done on the indoor thermal comfort of educational buildings. These studies carried out in different climatic regions, are of great importance for comparison and evaluation. It is expected that this study will lead to further research for schools in the region. Considering the relationship between energy efficiency, physical comfort conditions, and learning in school buildings, it would be beneficial to include passive features in school buildings to make them thermally comfortable throughout the year

while using minimal energy, and thus make them sustainable.

Finally, although this study was conducted in Bingöl, further research is needed in schools located in different climate regions to assess thermal comfort conditions more broadly. To enhance the generalizability of the findings, conducting similar studies in other climates will provide a more comprehensive understanding. Implementing sustainable design practices in school buildings can significantly improve health, comfort, and learning outcomes in educational environments.

REFERENCES

[1] Corgnati S P, Filippi M. and Viazzo S. Perception of the thermal environment in high school and university classrooms. Subjective preferences and thermal comfort. Building and Environment. 2007; 42: 951-959.

[2] Şensoy S and Sağsöz A. Öğrenci Başarısının Sınıfların Fiziksel Koşulları İle İlişkisi. Ahi Evran Üniversitesi Kırşehir Eğitim Fakültesi Dergisi. 2015; 16: 87-104.

[3] Earthman G I. School facility conditions and student academic achievement. 2002.

[4] Ali H H, Almomani H M and Hindeih M. Evaluating indoor environmental quality of public-school buildings in Jordan. Indoor and Built Environment. 2009; 18: 66-76.

[5] Suleman Q and Hussain I. Effects of classroom physical environment on the academic achievement scores of secondary school students in kohat division, Pakistan. International Journal of Learning & Development 4: 71-82. (2014).

[6] Almeida RM, Ramos N M and De Freitas V P. Thermal comfort models and pupils' perception in free-running school buildings of a mild climate country. Energy and Buildings. 2016; 111: 64-75.

[7] Aparicio-Ruiz P, Barbadilla-Martin E, Guadix J. A field study on adaptive thermal comfort in Spanish primary classrooms during summer season. Building and Environment. 2021; 203: 108089.

[8] Zomorodian Z S, Tahsildoost M and Hafezi M. Thermal comfort in educational buildings: A review article. Renewable and Sustainable Energy Reviews. 2016; 59: 895-906.

[9] Hassanain M A and Iftikhar A. Framework model for post-occupancy evaluation of school facilities. Structural Survey. 2015; 33: 322-336.

[10] Saraiva T S, De Almeida M, Bragança L. Environmental comfort indicators for school buildings in sustainability assessment tools. Sustainability. 2018; 10: 1849.

[11] Bernardi N and Kowaltowski D C. Environmental comfort in school buildings: A case study of

awareness and participation of users. Environment and behavior. 2006; 38: 155-172.

[12] Kowaltowski D C, Muianga E A D, Granja A D. A critical analysis of research of a mass-housing programme. Building Research & Information. 2019; 47: 716-733.

[13] Jindal A. Thermal comfort study in naturally ventilated school classrooms in composite climate of India. Building and Environment. 2018; 142: 34-46.

[14] Torriani G, Lamberti G, Salvadori G, et al. Thermal comfort and adaptive capacities: Differences among students at various school stages. Building and Environment. 2023; 237: 110340.

[15] Rodríguez C M, Coronado M C and Medina J M. Thermal comfort in educational buildings: The Classroom-Comfort-Data method applied to schools in Bogotá, Colombia. Building and Environment. 2021; 194: 107682.

[16] Kwong Q J, Adam N M and Sahari B. Thermal comfort assessment and potential for energy efficiency enhancement in modern tropical buildings: A review. Energy and Buildings. 2014; 68: 547-557.

[17] De Dear R and Schiller Brager G. The adaptive model of thermal comfort and energy conservation in the built environment. International journal of biometeorology. 2001; 45: 100-108.

[18] Havenith G. Metabolic rate and clothing insulation data of children and adolescents during various school activities. Ergonomics. 2007; 50 (10): 1689-1701.

[19] Teli D, Jentsch M F and James P A. The role of a building's thermal properties on pupils' thermal comfort in junior school classrooms as determined in field studies. Building and Environment. 2014; 82: 640-654.

[20] Nam I, Yang J, Lee D, Park E and Sohn J R. A study on the thermal comfort and clothing insulation characteristics of preschool children in Korea. Building and Environment. 2015; 92: 724-733.

[21] Yun H, Nam I, Kim J, Yang J, Lee K and Sohn J. A field study of thermal comfort for kindergarten children in Korea: An assessment of existing models and preferences of children. Building and Environment. 2014; 75: 182-189.

[22] Ter Mors S, Hensen J L, Loomans M G. Adaptive thermal comfort in primary school classrooms: Creating and validating PMV-based comfort charts. Building and Environment. 2011; 46: 2454-2461.

[23] Yang B, Olofsson T, Wang F. Thermal comfort in primary school classrooms: A case study under subarctic climate area of Sweden. Building and Environment. 2018; 135: 237-245.

[24] Havenith G, Holmér I. and Parsons K. Personal factors in thermal comfort assessment: clothing properties and metabolic heat production. Energy and Buildings. 2002; 34: 581-591.

[25] Fanger P O. Thermal comfort. Analysis and applications in environmental engineering. Thermal comfort. Analysis and applications in environmental engineering. 1970.

[26] Özdamar M and Umaroğulları F. Bir Ofis Yapısı Örneğinde Isıl Konfor ve İç Hava Kalitesinin İncelenmesi. Megaron. 2017; 12.

[27] Guevara G, Soriano G and Mino-Rodriguez I. Thermal comfort in university classrooms: An experimental study in the tropics. Building and Environment. 2021; 187, 107430.

[28] Khovalyg D, Kazanci O B, Halvorsen H, Gundlach I, Bahnfleth W P, Toftum J, and Olesen B W. Critical review of standards for indoor thermal environment and air quality. Energy and Buildings. 2020; 213, 109819.

[29] Teli D, Jentsch M F and James, P A. Naturally ventilated classrooms: An assessment of existing comfort models for predicting the thermal sensation and preference of primary school children. Energy and Buildings. 2012; 53: 166-182.

[30] AAlfano F R D A, Ianniello E and Palella B I. PMV–PPD and acceptability in naturally ventilated schools. Building and Environment. 2013; 67: 129-137.

[31] Kwok A G and Chun C. Thermal comfort in Japanese schools. Solar energy. 2003; 74: 245-252.

[32] Zhang G, Zheng C and Yang W. Thermal comfort investigation of naturally ventilated classrooms in a subtropical region. Indoor and Built Environment. 2007; 16: 148-158.

[33] Hwang R L, Lin T P, Chen C P. Investigating the adaptive model of thermal comfort for naturally ventilated school buildings in Taiwan. International journal of biometeorology. 2009; 53: 189-200.

[34] Hussein I and M. Hazrin A Rahman. Field study on thermal comfort in Malaysia. European Journal of Scientific Research. 2009); 37(1): 134-152.

[35] Sanders M D. Assessment of Indoor Aır Qualıty in Texas Elementary Schools. The University of Texas at Austin. PhD Thesis. 2008. The University of Texas at Austin.

[36] Yıldırım S T. Eğitim Yapılarında Isı ve Ses Konforu Sorunlarını Değerlendirilmesi. İzolasyon Dünyası Dergisi. 2008; 72: 70-74.

[37] Kocahakimoğlu C, Turan D, Özeren F, Sofuoğlu A and Sofuoğlu S C. İlköğretim Okullarında Bina İçi Hava Ozon Derişimleri. IX. Ulusal Tesisat Mühendisleri Kongresi ve Sergisi. TESKON, İzmir. 2009; 697-703.

[38] Humphreys M A, Nicol J F and Raja I A. Field studies of indoor thermal comfort and the progress of the adaptive approach. Advances in building energy research. 2007; 1: 55-88.

[39] Heracleous C and Michael A. Thermal comfort models and perception of users in free-running school buildings of East-Mediterranean region. Energy and Buildings. 2020; 215: 109912.

[40] Çulun P, Kürüm Varolgüneş F, Özer G and Kılınç C. Thermal Comfort Comparison of Different Dwelling Typologies. İDEALKENT. 2022; 13 (38): 2677-2701.

[41] Choi J-H. ve Yeom D. (2019) Development of the data-driven thermal satisfaction prediction model as a function of human physiological responses in a built environment. Building and Environment 150: 206-218.

105

[42] ASHRAE-Handbook. Physiological Principles. Comfort and Health. 1989.

[43] Chen X, Yang H and Sun K. A holistic passive design approach to optimize indoor environmental quality of a typical residential building in Hong Kong. Energy. 2016; 113: 267-281.

[44] Yilmaz Z. Akilli binalar ve yenilenebilir enerji. Tesisat Muhendisligi Dergisi. 2006; (91): 7-15.

[45] Wang Z. A field study of the thermal comfort in residential buildings in Harbin. Building and Environment. 2006; 41: 1034-1039.

[46] Djongyang N and Tchinda R. An investigation into thermal comfort and residential thermal environment in an intertropical sub-Saharan Africa region: Field study report during the Harmattan season in Cameroon. Energy Conversion and Management. 2010; 51: 1391-1397.

[47] Nagano K and Mochida T. Experiments on thermal environmental design of ceiling radiant cooling for supine human subjects. Building and Environment. 2004; 39: 267-275.

[48] Peeters L, De Dear R and Hensen J. Thermal comfort in residential buildings: Comfort values and scales for building energy simulation. Applied Energy. 2009; 86: 772-780.

[49] ASHRAE Standard 55. Thermal Environmental Conditions for Human Occupancy. (2017). https://www.cibse.org/knowledge-research/knowledge-portal/ashraestandard-55-thermal-environmental-conditions-for-human-occupancy.

[50] De Oliveira C C, Rupp R F and Ghisi E. Influence of Air Movement and Air Humidity on Thermal Comfort in Office Buildings in Florianópolis, Brazil. 35th PLEA Conference-Sustainable Architecture and urban Design: Planning Post Carbon Cities. 2020.

[51] Yamankaradeniz R, Horuz İ, Coşkun S, Kaynaklı Ö, Yamankaradeniz N. iklimlendirme esasları ve uygulamaları. 2015; 3. Baskı, Bursa.

[52] Shaman J, Pitzer Virginia E, Viboud Cecile, Grenfell B T, Lipsitch M. Absolute humidity and the seasonal onset of ınfluenza in the continental United States. 2010; 8 (2): e1000316

[53] Halıcı F. kalorifer ve havalandırma tesisatı ısı yalıtımı ve örnek proje. Birsen yayınevi. 2019. İstanbul.

[54] Corgnati S P, Ansaldi R and Filippi M. Thermal comfort in Italian classrooms under free running conditions during mid seasons: Assessment through objective and subjective approaches. Building and Environment. 2009; 44: 785-792.

[55] Amorim PRdS. Energy expenditure and physical activity patterns in children: applicability of simultaneous methods. Queensland University of Technology. 2007.

[56] Ahlawat A, Wiedensohler A and Mishra S K. An Overview on the Role of Relative Humidity in Airborne Transmission of SARS-CoV-2 in Indoor Environments. Aerosol Air Qual. Res. 2020; 20: 1856–1861. https://doi.org/10.4209/aaqr.2020.06.0302

[57] Toftum J et. al. Association between classroom ventilation mode and learning outcome in Danish schools/ Building and Environment. 2015; 92. 494e503.

[58] Lee, Y. H., & Zakaria, M. A. (2024). The Investigation of Ventilation Strategies on Indoor Thermal Comfort for a Classroom. Recent Trends in Civil Engineering and Built Environment, 5(1), 262-271.

[59] Mustapha, T. D., Hassan, A. S., Nasir, M. H. A., Khozaei, F., & Arab, Y. (2024). From perception to prediction: A comparative study of thermal comfort assessment techniques in school facilities. Energy and Buildings, 313, 114233.3.

Türk Doğa ve Fen Dergisi
Turkish Journal of Nature and Science

Comparative Analysis of LSTM Architectures for Wind Speed Prediction: A Case Study in Muş, Türkiye

İhsan TUĞAL[1*] iD

[1] Muş Alparslan University, Engineering and Architecture Faculty, Software Department, Muş, Türkiye
İhsan TUĞAL ORCID No: 0000-0003-1898-9438

Corresponding author: i.tugal@alparslan.edu.tr

Abstract: Accurate wind speed prediction is critical for energy planning and sustainable development, particularly in regions like Muş, Turkey, where renewable energy potential remains underexplored. While many studies focus on wind speed forecasting using conventional methods, there is a research gap in evaluating the comparative effectiveness of advanced Long Short-Term Memory (LSTM) architectures for this purpose. This study aims to assess the predictive performance of five LSTM models (Vanilla LSTM, Stacked LSTM, Bidirectional LSTM, Attention LSTM, and Residual LSTM) on daily wind speed data from Muş. The dataset, obtained from the Muş Meteorological Office, consists of 20,088 daily wind speed measurements from 1969 to 2023. The results demonstrated that the Vanilla LSTM achieved the lowest MSE and MAE, indicating its superior overall accuracy, while the Attention LSTM achieved the lowest MAPE, showcasing better percentage-based accuracy. These findings suggest that Vanilla LSTM and Attention LSTM are the most effective models for wind speed forecasting in Muş. The choice between these models depends on prioritizing either absolute error minimization or percentage error accuracy, providing a strategic framework for model selection in similar renewable energy forecasting applications.

107

Rüzgar Hızı Tahmini için LSTM Mimarilerinin Karşılaştırmalı Analizi: Türkiye, Muş'ta Bir Vaka Çalışması

Öz: Rüzgar hızı tahmini, enerji planlaması ve sürdürülebilir kalkınma için kritik bir öneme sahiptir. Yenilenebilir enerji potansiyelinin yeterince araştırılmadığı Türkiye'nin Muş gibi bölgelerinde özellikle daha önemlidir. Pek çok çalışma rüzgar hızı tahmini için geleneksel yöntemlere odaklanmış olsa da, gelişmiş Uzun Kısa Süreli Bellek (LSTM) mimarilerinin karşılaştırmalı etkinliğini değerlendirme konusunda bir araştırma eksikliği bulunmaktadır. Bu çalışma, Muş bölgesindeki günlük rüzgar hızı verilerinde beş farklı LSTM modelinin (Vanilla LSTM, Stacked LSTM, Bidirectional LSTM, Attention LSTM ve Residual LSTM) tahmin performansını değerlendirmeyi amaçlamaktadır. Muş Meteoroloji Müdürlüğü'nden elde edilen veri seti, 1969-2023 yıllarını kapsayan 20.088 günlük rüzgar hızı ölçümünden oluşmaktadır. Sonuçlar, Vanilla LSTM'in en düşük MSE ve MAE değerleri ile genel doğrulukta üstün performans gösterdiğini, Attention LSTM'in ise en düşük MAPE ile yüzdesel doğruluk açısından daha başarılı olduğunu göstermektedir. Bu bulgular, Vanilla LSTM ve Attention LSTM modellerinin Muş veri setinde rüzgar hızı tahmini için en etkili modeller olduğunu ortaya koymaktadır. Bu modeller arasındaki seçim, toplam hata veya yüzdesel hata önceliklendirilmesine bağlı olarak stratejik bir çerçeve sunmaktadır.

1. INTRODUCTION

In today's world, climate change and environmental impacts have made the use of sustainable and renewable resources in energy production imperative. Wind energy is recognized as one of the most crucial renewable energy sources. Precise wind speed prediction is essential for maximizing the efficiency of wind energy utilization. These predictions are used in various fields, including energy production forecasts, turbine placement, and energy grid management.

Wind energy is essentially a byproduct of the sun. The uneven heating of the atmosphere by the sun, the irregular surfaces of the Earth (such as mountains and valleys), and the planet's rotation around the sun all combine to create wind. Because wind is abundant and will persist as long as the sun heats the Earth, it is a sustainable resource. Wind energy is a clean and renewable power source. Wind turbines use the power of the wind to drive a generator and produce electricity. Wind generates electricity without burning fuel or creating air pollution.

Land-based, large-scale wind turbines are among the most cost-effective energy sources available today. Moreover, the cost efficiency of wind energy continues to improve with advancements in wind energy science and technology. Wind energy can be seamlessly incorporated into rural or isolated areas, including farms, mountainous regions, or coastal and island areas, where strong wind resources are frequently present. These prime wind locations are usually found in regions with sparse populations.

Wind farms impact the environment differently than traditional power plants, but there are still concerns about the noise from turbine blades and the visual impact on the scenery. There are also impacts on wildlife.

Turkey plans to significantly increase its renewable energy capacity by 2035, with substantial growth in solar, wind, and hydroelectric energy. Given the growing preference for renewable sources in new installations, it is anticipated that renewable energy will account for 64.7% of the total installed capacity. Turkey aims to achieve net zero emissions by 2053. By 2035, the installed capacity of wind energy is projected to reach 29.6 GW (24.6 GW onshore, 5 GW offshore). Wind and solar are considered intermittent renewable energy sources. (Turkey National Energy Plan (2020-2035), 2022)

Energy production and consumption require extensive planning skills. The greatest support for this planning comes from advancing technology. The increase in data and the development of artificial intelligence technologies have significantly aided this planning. Long-term recorded meteorological data serve as a guide in predicting energy production and consumption. Some of this data consists of a series of data points or observations recorded at different or regular intervals. Defined as time series data, this information can be analyzed using artificial intelligence techniques, and it can be used for future predictions.

Time series forecasting is a method that predicts future events based on historical data. Recent advancements in this field have been substantial, particularly with the rise of deep learning techniques. Long Short-Term Memory (LSTM) networks have gained significant attention for their effectiveness in time series forecasting. LSTM networks have demonstrated remarkable success in predicting meteorological time series data due to their capacity to capture long-term dependencies, distinguishing them from other forecasting models [1].

This study was conducted to analyze regional wind energy and predict wind energy using machine learning methods, utilizing long-term daily average wind speed data from Muş Province. For this study, 54 years of daily average wind speed time series data, spanning from 1969 to 2023, were obtained from the Muş Central Meteorology Measurement Station (38°45'03.3"N 41°30'08.1"E). The dataset comprises a total of 20,089 daily records. Each record in our dataset includes the day, month, year, and average wind speed. Wind measurements were taken at a height of 10 meters above ground level. The central region of Muş does not experience strong winds. However, certain areas of Muş hold potential for wind energy production. Consequently, various projects have been initiated to harness wind energy in Muş, and it is anticipated that the number of such projects will increase over time[2].

The primary objective of this study is to predict future wind speeds using wind speed data from Muş Province spanning from 1969 to 2023. The aim is to provide analyses to support decision-makers in showcasing the regional wind energy potential. Additionally, the study seeks to evaluate the performance of the Long Short-Term Memory (LSTM) model and examine the impact of different LSTM model selections on performance. For this purpose, forecasts will be made using various LSTM models. Efforts have been undertaken to boost the use of wind energy, a clean and renewable source, for generating electricity, in support of the goal to achieve a zero-carbon footprint.

108

2. LITERATURE REVIEW

Studies on wind speed forecasting typically focus on physical models, statistical methods, machine learning and deep learning techniques, as well as combined and hybrid models [3].

Physical methods rely on data such as terrain, topography, obstacles, atmospheric pressure, and ambient temperature for predictions. These models, however, demand significant computational resources and require detailed information about various weather variables, which may not always be available [4].

Statistical methods include techniques such as Kalman filtering, ARIMA, and wavelet transform [5]. Autoregressive Integrated Moving Average (ARIMA) models are commonly used [6]. However, the accuracy of these models depends on the characteristics of the dataset and model parameters, and they often fall short in complex and variable datasets. Statistical methods are particularly less favored when data is nonlinear.

Machine learning techniques offer more flexible and powerful forecasting capabilities compared to statistical methods. Techniques such as Support Vector Machines (SVM) [7] and Decision Trees [8] are commonly used for wind speed prediction. However, the performance of these techniques often varies depending on the size and complexity of the dataset.

Deep learning techniques, particularly in large and complex datasets, exhibit strong performance. Recurrent Neural Networks (RNNs) are commonly used for forecasting temporal dependencies [9]. However, RNNs face challenges in learning long data sequences. Long Short-Term Memory (LSTM) networks address these issues. LSTM networks play a significant role, especially in predicting time series data. Studies have demonstrated that LSTM networks perform exceptionally well in wind speed forecasting [10].

Köse and Güneşer [11] evaluated the annual wind speed distribution and wind power density at seven stations in the Western Black Sea Region of Turkey for the period 2010–2014. The results indicate that, with the exception of Sinop, the region does not have sufficient wind energy potential for investment in wind energy.

Wadi et al. [12] carried out a technical evaluation of Turkey's wind energy potential. They conducted a feasibility study using hourly wind speed data recorded at a height of 30 meters in the Çatalca district from 2008 to 2010, aiming to assess the potential use of wind energy in Turkey. The Weibull two-parameter probability function was employed to estimate monthly and annual wind potential and power density, utilizing three different calculation methods. The simulation outcomes indicated that the studied area is appropriate for establishing large-scale wind farms.

Onat and Ersoz [13] examined the wind climate characteristics and energy potentials of three regions in Turkey. They used a five-layer Sugeno-type ANFIS model to identify the relationship between wind speed and other climatic variables to determine the wind characteristics in these regions. In the second phase, they employed WASP software to analyze the wind energy potential using wind speed data. Finally, the study calculated the technical electricity output and capacity utilization rates of installed turbines if wind farms were to be established in the selected regions.

Arslan et al. [14] analyzed the wind speed variability across Turkey and its influence on electricity production from 1980 to 2013. The study utilized reliable data from 77 stations. Hourly average wind speeds of 3.80 m/s or higher were recorded at the Gökçeada, Çanakkale, and Mardin stations, located in the Aegean, Southeastern, and Marmara regions of Turkey, respectively. Wind energy potential was assessed using the Weibull distribution. The findings reveal that Çatalca boasts the highest wind energy potential in Turkey, not only due to its high wind speeds but also because of its vast rural areas suitable for wind farm development.

Sırdaş [15] used harmonic analysis to model daily wind speed data collected from ten stations in Turkey's Marmara region between 1993 and 1997, accounting for various meteorological conditions. Notable differences in wind patterns were found between the western and eastern parts of the Marmara region. The study involved calculating the contribution of each harmonic component to the total variance, which led to the creation of regional variance maps.

Shao et al. [16] introduced a wind speed forecasting model utilizing LSTM neural networks, optimized with the Firework Algorithm (FWA) for tuning hyperparameters. The performance of this optimized model was assessed against other deep learning and regression-based wind speed prediction methods. The findings revealed that the LSTM model enhanced with FWA achieved lower prediction errors compared to alternative wind speed forecasting models.

Pradhan et al. [17] created a hybrid model for forecasting wind speed, consisting of two phases. The first phase involves breaking down wind speed sample data using wavelet techniques, while the second phase uses this decomposed data for predictions with a Recurrent Wavelet Neural Network (RWNN). To evaluate the model's performance, it was compared with traditional Recurrent Neural Network (RNN) forecasting approaches. The results from real-world data highlighted the model's effectiveness in terms of average absolute error and convergence rate.

Lu et al. [18] performed an extensive review of metaheuristic optimization techniques for forecasting wind energy. They created a detailed classification system for these algorithms to enhance the optimization of wind energy forecasting model parameters. The algorithms are designed to discover optimal solutions within constraints, which are essential for fine-tuning the primary parameters of forecasting models. They also proposed a thorough and scientific multi-error evaluation framework for analyzing wind energy forecasting errors. This review covers various error evaluation methods, including deterministic, uncertainty, and testing approaches. Additionally, it offers a quantitative analysis of the strengths, weaknesses, accuracy, and computational costs associated with these methods.

Hu et al. [19] aimed to enhance wind speed forecasting accuracy with their LSTMDE-HELM approach. This method combines LSTM networks, Hysteretic Extreme Learning Machine (HELM), Differential Evolution (DE) algorithm, and nonlinear hybrid mechanisms. To improve the Extreme Learning Machine (ELM) performance, they integrated a hysteretic biological neural feature into the ELM's neuron activation function. Furthermore, because the ideal number of hidden layers and neurons per layer in the LSTM was not initially clear, the DE algorithm was used to optimize these parameters. This approach aims to strike a balance between learning accuracy and model complexity. The hybrid model was evaluated using data from a wind farm in Inner Mongolia, China, with two forecasting intervals: ten minutes (short-term) and one hour (medium-term). The findings reveal that this hybrid method outperforms other models across four performance metrics and in statistical assessments.

Chen et al. [20] developed a new two-layer nonlinear combination method called EEL-ELM for short-term wind speed forecasting problems, such as ten minutes and

109

one hour ahead predictions. To demonstrate the effectiveness of the proposed EEL-ELM method, two real-world case studies from a wind farm in Inner Mongolia, China, were applied. Simulation results reveal that EEL-ELM achieved better forecasting performance compared to eight other wind speed forecasting methods, based on three evaluation metrics and three statistical tests.

Alhussan et al. [21] proposed an improved model for enhancing wind speed forecasting accuracy. They utilized a novel optimization algorithm known as Generalized Adaptive Differential Evolution (GADTO), which integrates Dipper-Throated Optimization (DTO) with Genetic Algorithm (GA). This optimization technique was applied to fine-tune the parameters of a Bidirectional LSTM (BiLSTM) forecasting model. To assess the statistical significance of their approach compared to existing methods, they employed variance analysis (ANOVA) and Wilcoxon signed-rank tests. The findings confirmed the statistical significance and reliability of their method, achieving a mean root mean square error (RMSE) of 0.00046, which outperforms the accuracy of other new forecasting methods.

Subramani et al.'s [27] study reviews advancements in renewable energy, focusing on solid oxide fuel cells and electrolysers for green hydrogen production. Highlighting the significance of wind energy, it emphasizes accurate forecasting for efficient energy management. Machine learning methods like Support Vector Regression (SVR) and Random Forest have improved prediction accuracy. The paper also explores challenges like uncertainty in renewable energy production, data availability, and model interpretability, aiming to enhance grid integration and support a sustainable future.

A key challenge in wind energy utilization is its variability across seasonal and interannual timescales due to atmospheric changes. Yang et al.'s study [28] highlights a model's ability to provide skillful seasonal wind energy predictions in the U.S. Great Plains, particularly during peak energy seasons (winter and spring). The model leverages year-to-year variations in the El Niño-Southern Oscillation, which influence large-scale wind and storm patterns. In the Southern Great Plains, it predicts

significant wind energy changes months in advance with high accuracy. This capability supports optimizing wind energy use during peak production periods.

In wind forecasting, different time intervals are used in the literature (long term: >3 days, medium term: a few hours - 3 days, short term: a few minutes - a few hours). However, these time periods are not fixed and vary according to researchers and needs [22, 23]. Some studies have divided the time intervals into four categories as "very short", "short", "medium" and "long", each of which has been aimed at different areas of use [24]. In addition, some other studies have determined intervals of a few hours for the short term, a few hours to 3 days for the medium term and >6 days for the long term [25, 26]. This study, which makes daily forecasts, can be accepted as medium term when evaluated according to different studies.

3. MATERIAL AND METHOD

3.1. Data and Wind in Muş

Data obtained from the Muş Provincial Directorate of Meteorology were preprocessed and prepared for application to the LSTM model. Due to technical reasons, dates with missing measurements were identified, and the missing values for these dates were replaced with the averages of corresponding days and months from 1969 to 2023. The dataset includes 20,088 daily wind speed measurements. Measurement values for the specified time interval are shown in Figure 1. 80% of the data was used for training, while the remaining data was used for testing. Additionally, 20% of the training data was reserved for validation. The data was normalized to a scale between 0 and 1.

In Muş, summers are characterized by hot, dry, and clear weather, while winters are known for being freezing, snowy, and partly cloudy. Annual temperatures generally vary between -20°C and +30°C [29]. Wind patterns in any area are strongly affected by local topography and other environmental factors, resulting in more pronounced variations in wind speed and direction at any given moment compared to average conditions.
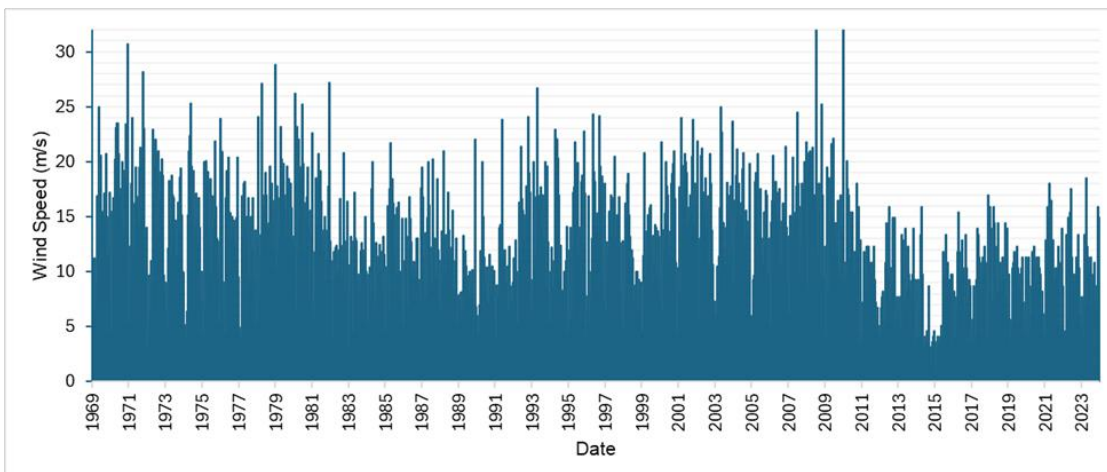
Figure 1. Average Daily Wind Speed of Muş

Figure 2 provides information on the wind speed distribution in Muş Province. It is observed that the most common daily average wind speed range is between 10 and 20 m/s. The average wind speed in the dataset is approximately 6.31 m/s, with a standard deviation of around 3.88 m/s. This standard deviation of 3.88 m/s indicates a wide dispersion of wind speed values around the mean in the dataset.
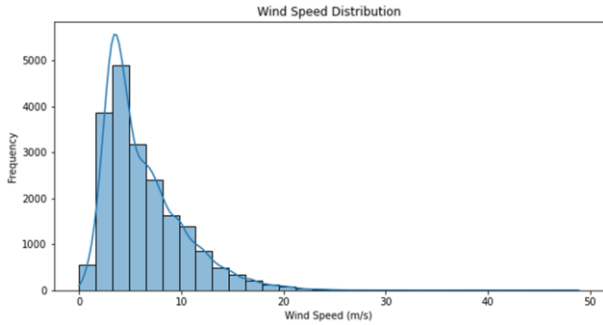
Figure 2. Wind Speed Distribution in Muş

Examining the boxplot in Figure 3, the minimum wind speed is 0 m/s, indicating that there were some days with no wind. This could potentially be a measurement error. It is observed that 25% of the wind speed values in the dataset are below 3.5 m/s, which is the first quartile. The median wind speed, which is the 50th percentile, is below 5.1 m/s. While the annual average wind speed is 6.31 m/s, the median is 5.1 m/s. The fact that the mean is slightly higher than the median suggests that a few high wind speed values (outliers) are raising the average. Additionally, 75% of the wind speed values are below 8.2 m/s, indicating that a large portion of the dataset has moderate wind speeds. The wide distribution of the data is an important factor to consider in the modeling process. The highest recorded wind speed is 48.9 m/s, which suggests the presence of very strong winds.
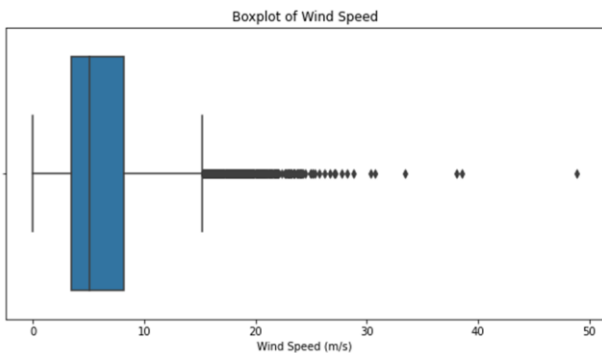
Figure 3. Boxplot of Wind Speed in Muş

For Muş, considering the hourly average wind vector (speed and direction), the average daily wind speed shows slight seasonal variations throughout the year. Figure 4 presents the monthly average wind speeds for the years 1969-2023. The windiest period of the year, characterized by an average wind speed exceeding 7 m/s, lasts from April to September. May is the windiest month in Muş, with an hourly average wind speed of around 8.57 m/s. Conversely, January is the calmest month, with an hourly average wind speed of approximately 4 m/s.
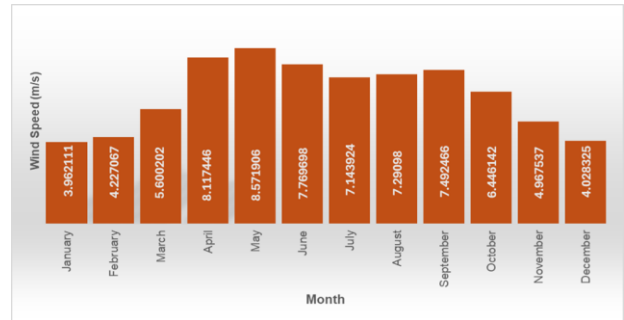
Figure 4. Monthly average wind speed

Examining the monthly and annual average wind speeds in Figure 5, some years show noticeable increases or decreases. The year with the highest annual average wind speed was 1979, with an average speed of 9.33 m/s. In contrast, 2014 had the lowest average wind speed at 2.27 m/s.
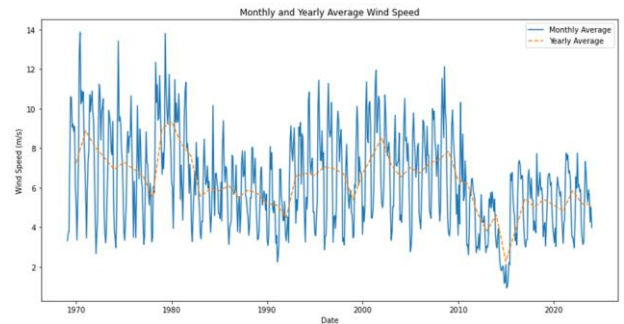
Figure 5. Monthly and Yearly Average Wind Speed in Muş

In Figure 6, the "Observed" section represents our original time series data, encompassing all changes in wind speed over time. This data includes seasonal variations, long-term trends, and random fluctuations. The "Trend" component illustrates long-term trends over time, showing whether wind speed generally increases or decreases. In Muş, we can observe both long-term increases and decreases in wind speed. The "Seasonal" component represents regular, repeating changes occurring at specific times of the year. The "Residual" component refers to random fluctuations that the model does not explain. It represents what remains after removing the trend and seasonal components from the observed data. This component indicates irregular and unpredictable changes in the dataset. Significant fluctuations in the residual component may suggest that the model does not fully capture all the dynamics of the data. Variations can be observed in certain time intervals.

111
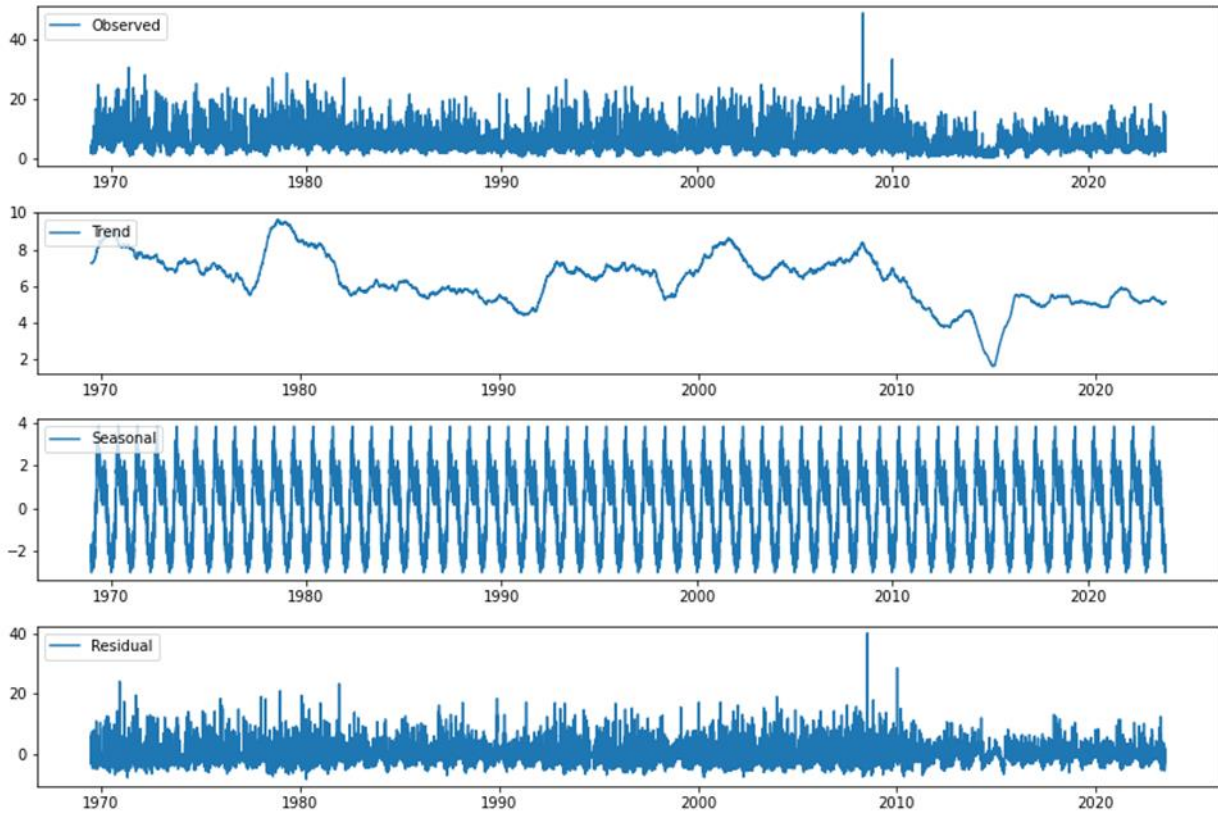
Figure 6. Observed, Trend, Seasonal, Residual behavior of wind speed in Muş

3.2. Long-Short Term Memory

LSTM networks are a type of artificial neural network commonly used for modeling time series data. They are designed to address the long-term dependency problems encountered by traditional Recurrent Neural Networks (RNNs). LSTMs are highly effective for sequence prediction tasks because they can retain information over long periods. The architecture of an LSTM can be visualized as a series of repeating "blocks" or "cells". An LSTM network consists of five fundamental components: hidden state (h_t), cell state (c_t), forget gate (f_t), input gate (i_t) and output gate (o_t). These components work together to control how information is stored, updated, and retrieved, enabling LSTMs to handle complex time series and sequence data effectively.
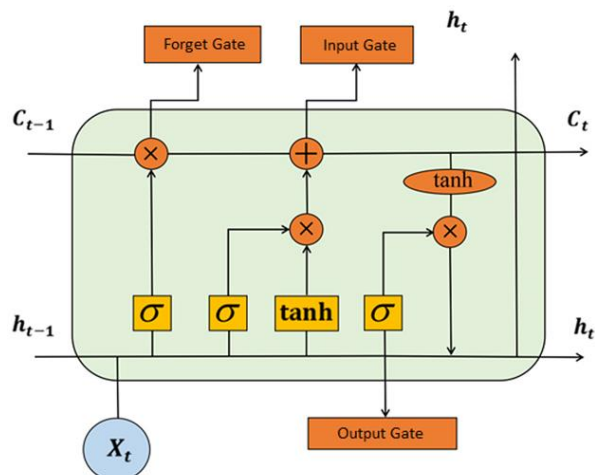
Figure 7. The architecture of an LSTM

Forget Gate

The forget gate determines which information from the cell state should be discarded. The output of the forget gate is computed using the sigmoid activation function.

$$f_t = \sigma(W_f \cdot [h_{t-1}, x_t] + b_f) \tag{1}$$

σ is the sigmoid function. W_f is the weight matrix for the forget gate. b_f is the bias vector for the forget gate. h_{t-1}, is the hidden state from the previous time step. x_t is the input vector at the current time step. The forget gate's output, f_t, is a vector with values between 0 and 1, indicating how much of each component of the cell state should be retained or forgotten [30].

Input Gate

The input gate controls how new information is added to the cell state. This process occurs in two stages: first, it determines how much of the new information should be updated; second, it generates candidate values for the cell state.
The input gate's output and the candidate values for the cell state are determined through the following calculations:

$$i_t = \sigma(W_f \cdot [h_{t-1}, x_t] + b_f) \tag{2}$$

$$\tilde{c}_t = \tanh(W_c \cdot [h_{t-1}, x_t] + b_c) \tag{3}$$

In summary, the input gate determines which portions of the new information will be incorporated into the cell

112

state, while the candidate cell state offers the potential new information for addition [31].

Updating the Cell State

The cell state is updated using the outputs from the forget gate and the input gate:

$$c_t = f_t \cdot c_{t-1} + i_t \cdot \tilde{c}_t \tag{4}$$

c_t is the updated cell state. c_{t-1} is the cell state from the previous time step. $f_t \cdot c_{t-1}$ represents the amount of information retained from the previous cell state. $i_t \cdot \tilde{c}_t$ represents the amount of new information added to the cell state. This mechanism allows the LSTM to maintain long-term dependencies by effectively managing and updating the cell state over time.

Output Gate

The output gate determines which information from the cell state will be outputted. The output gate's output is calculated as follows:

$$i_o = \sigma(W_o \cdot [h_{t-1}, x_t] + b_o) \tag{5}$$

The hidden state (h_t) is then calculated using the output gate's output and the updated cell state:

$$h_t = o_t \cdot \tanh(c_t) \tag{6}$$

Through these equations and gates, the LSTM model effectively manages long-term dependencies and overcomes the long-term dependency problems faced by traditional RNNs.

3.3. Performance Evaluation

Five different LSTM architectures were employed to make predictions, and their performance was compared. Each model's predictions were assessed against the actual values using various error metrics. The training process was conducted over 100 epochs, and minibatches consisting of 32 samples were utilized. The prediction performance was evaluated using the following three loss function metrics:

Mean Squared Error (MSE): It calculates the mean of the squared differences between predicted and observed values. MSE assigns greater weight to larger errors compared to smaller ones, which makes it effective for evaluating the extent of prediction errors. Smaller MSE values suggest that the model's predictions are more accurate.

$$MSE = \frac{1}{n} \sum_{i=1}^{n} (y_i - \hat{y}_i)^2 \tag{7}$$

Mean Absolute Error (MAE): It assesses the mean of the absolute differences between predicted and actual values. MAE gives equal weight to all errors, without

emphasizing larger errors over smaller ones. Lower MAE values indicate a higher overall accuracy of the model's predictions.

$$MAE = \frac{1}{n} \sum_{i=1}^{n} |y_i - \hat{y}_i| \tag{8}$$

Mean Absolute Percentage Error (MAPE): It calculates the average of the absolute differences between predicted and actual values, expressed as a percentage of the actual values. MAPE offers a percentage-based evaluation of prediction errors, with lower MAPE values reflecting a smaller percentage of error in the predictions.

$$MAPE = \frac{1}{n} \sum_{i=1}^{n} \left| \frac{(y_i - \hat{y}_i)}{y_i} \right| x100 \tag{9}$$

In all models, the LSTM layer contained a default of 50 neurons. The dropout rate was set at the default value of 0.2, the learning rate was maintained at 0.001, and the Adam optimization algorithm was used. These parameters are significant factors influencing each model's training and prediction performance. The evaluation determined which model demonstrated superior performance.

3.4. LSTM Models

Vanilla LSTM

The Vanilla LSTM is a single-layer, straightforward LSTM network. Initially proposed by Hochreiter and Schmidhuber (1997), this model is commonly used for processing time series and sequential data [1]. LSTM cells are capable of storing and updating information over time, making them effective for learning long-term dependencies. However, the disadvantage of the Vanilla LSTM is that its performance can be limited, especially on very deep and complex data. The model may tend to forget the information it has learned over time, making it less effective at learning more complex relationships. Its advantages include its ability to learn long-term dependencies and its generally easy implementation [32]. A Vanilla LSTM model typically consists of an input layer, an LSTM layer, and an output layer. Input Layer receives a sequence containing time steps and features. LSTM Layer processes the data by updating the cell state and hidden state. The output layer is usually a dense layer and produces the final predictions. Vanilla LSTM networks are utilized in various domains, including time series forecasting, language modeling, machine translation, and speech recognition. In this study, the model comprises a single LSTM layer, a dropout layer, and an output layer as seen in Figure 8.

113
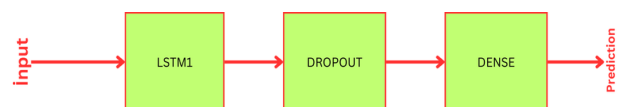
Figure 8. Vanilla LSTM

Stacked LSTM

The Stacked LSTM network consists of multiple LSTM layers stacked on top of each other. The advantage of this structure is that it increases the capacity to learn more complex and abstract features. Deeper structures generally provide stronger model performance. However, the disadvantage of Stacked LSTM is that it carries the risk of overfitting, as the model requires larger parameter sets and more computational power [33].

A Stacked LSTM model typically includes an input layer, multiple LSTM layers, and an output layer. Stacked LSTM networks are used for handling complex sequential data tasks, including natural language processing (NLP) and sophisticated time series forecasting [33]. In this study, the model architecture stacks two LSTM layers as seen in Figure 9. The first LSTM layer generates outputs for all time steps, which are then fed into the second LSTM layer. A dropout layer follows each LSTM layer.

Figure 9. Stacked LSTM

Bidirectional LSTM

The Bidirectional LSTM network analyzes input data in both forward and backward directions, enabling the model to capture contextual information from both past and future time steps at each stage. However, the disadvantage of this model is the increased computational cost due to bidirectional learning [34].

Typically, a Bidirectional LSTM model includes an input layer, a bidirectional LSTM layer, and an output layer. The Bidirectional LSTM layer comprises two distinct

LSTM layers: one processes data in the forward direction and the other in the backward direction. This architecture is particularly useful for tasks that benefit from understanding context from both directions, such as natural language processing (NLP), bioinformatics, speech recognition, and sentiment analysis. [10, 35]. In this study, the model includes two bidirectional LSTM layers, each followed by a dropout layer as seen in Figure 10. Each LSTM layer is configured to operate in both forward and backward directions.

114

Figure 10. Bidirectional LSTM

Attention LSTM

The attention mechanism enables the model to prioritize different input time steps differently, particularly in noisy and fluctuating data. When integrated into LSTM networks, known as Attention LSTM, this mechanism allows the model to concentrate on key time steps, improving its overall performance. The attention mechanism allows the model to focus on important information, so it can go beyond the limited memory capacity of LSTM. The advantage of this model is that it can make more accurate predictions, especially in data with long-term dependencies. The disadvantage is that it

requires additional computational load and more time to train the model [36].

An Attention LSTM model typically includes an input layer, an LSTM layer, an attention layer, and an output layer. Attention LSTM networks are particularly effective for tasks that require emphasis on specific segments of the input, such as machine translation, image captioning, speech recognition, and text summarization [37, 38]. In this study, the model includes the attention mechanism in addition to LSTM layers as seen in Figure 11. The first LSTM layer generates outputs for all time steps, which are then processed by the attention layer
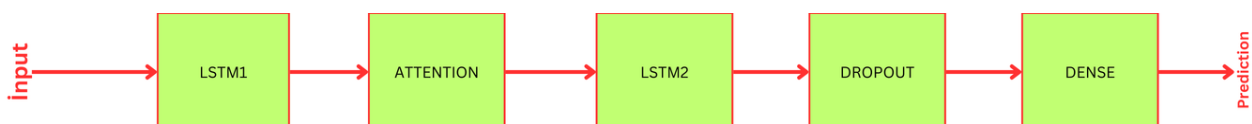
Figure 11. Attention LSTM

Residual LSTM

Residual LSTM networks use residual connections to overcome the vanishing gradient problem commonly found in deep networks. These connections help preserve

the flow of information between LSTM layers, making it possible to train deeper models more effectively. Its advantages are that it provides a more efficient learning process and is resistant to the vanishing gradient problem. However, the disadvantage of Residual LSTM is that the

model becomes more complex with additional layers and parameters, and therefore carries the risk of overfitting [39].

A Residual LSTM model generally includes input layer, multiple LSTM layers, residual connections and output layer. Residual connections facilitate information flow between LSTM layers by bypassing some layers, thus mitigating the vanishing gradient problem. Residual LSTMs are used in tasks requiring very deep networks, such as advanced time series analysis and complex sequence modeling [40, 41]. In this study, the residual model comprises three LSTM layers connected with residual connection as seen in Figure 12. The first two LSTM layers generate outputs for all time steps. The third LSTM layer integrates with the last time step of the first LSTM layer via an Add layer to form a residual connection. The model is completed with a dropout layer and an output layer.
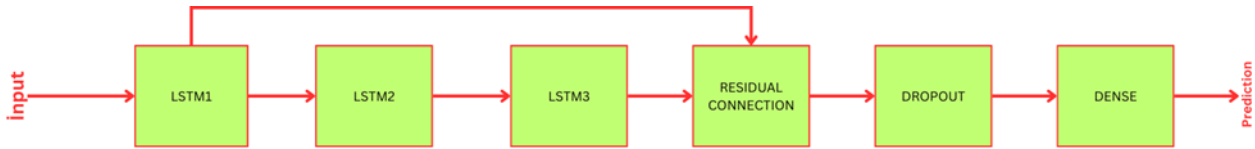
Figure 12. Residual LSTM

4. RESULTS

When evaluating LSTM models, it is crucial to consider both their performance and training time to determine which model is most appropriate for a given application scenario. In this study, various LSTM models have been compared specifically for wind speed forecasting. This comparison helps identify the model that best balances prediction accuracy and computational efficiency for the task at hand. This comparison does not mean that these models always give similar ranking results. Comparing models with the same hyperparameters (learning rate, dropout rate, number of LSTM units) allows you to assume that the performance differences are due solely to the model architectures. This approach provides a good starting point to see the relative differences between the models. It makes the results more methodologically meaningful. However, different structures of LSTM architectures may give different responses to the same hyperparameter set. Since Stacked and Residual LSTM contain more parameters, they may need different learning rate or dropout rate values to reach optimum performance. Attention and Bidirectional LSTM have more information processing capacity and therefore may work better with a different number of units (number of LSTM cells). Rather than comparing the models, it would be healthier to perform hyperparameter optimization to obtain better results and fully evaluate the potential of each model. This study did not focus on suitable hyperparameters.

Table 1. Performance Evaluation of LSTM models

Model	MSE	Time	MAE	Time	MAPE	Time
Vanilla LSTM	**4.218**	2s 9ms/step	**1.410**	1s 8ms/step	0.299	1s 6ms/step
Stacked LSTM	4.258	3s 15ms/step	1.441	2s 13ms/step	0.305	2s 11ms/step
Bidirectional LSTM	4.384	4s 18ms/step	1.470	4s 21ms/step	0.299	3s 15ms/step
Attention LSTM	4.256	3s 14ms/step	1.505	3s 15ms/step	**0.288**	1s 8ms/step
Residual LSTM	4.373	2s 10ms/step	1.425	3s 18ms/step	0.302	2s 12ms/step

Table 1 offers a comparison of performance metrics to determine the most effective LSTM model for wind speed forecasting for Muş dataset. Mean Squared Error (MSE), Mean Absolute Error (MAE), and Mean Absolute Percentage Error (MAPE) are metrics. These metrics allow for a comprehensive assessment of the models' prediction accuracy from different perspectives. Additionally, training times help evaluate the model's complexity and computational efficiency.

The Vanilla LSTM model shows the lowest MSE and MAE values, demonstrating its superior overall performance. It can be seen in Figure 13 and Figure 14. Its MAPE value is also moderate compared to other models, suggesting a reasonable level of percentage error in predictions. Given its simpler architecture, the Vanilla LSTM has the shortest training time, making it a favorable option for scenarios that require rapid model training.
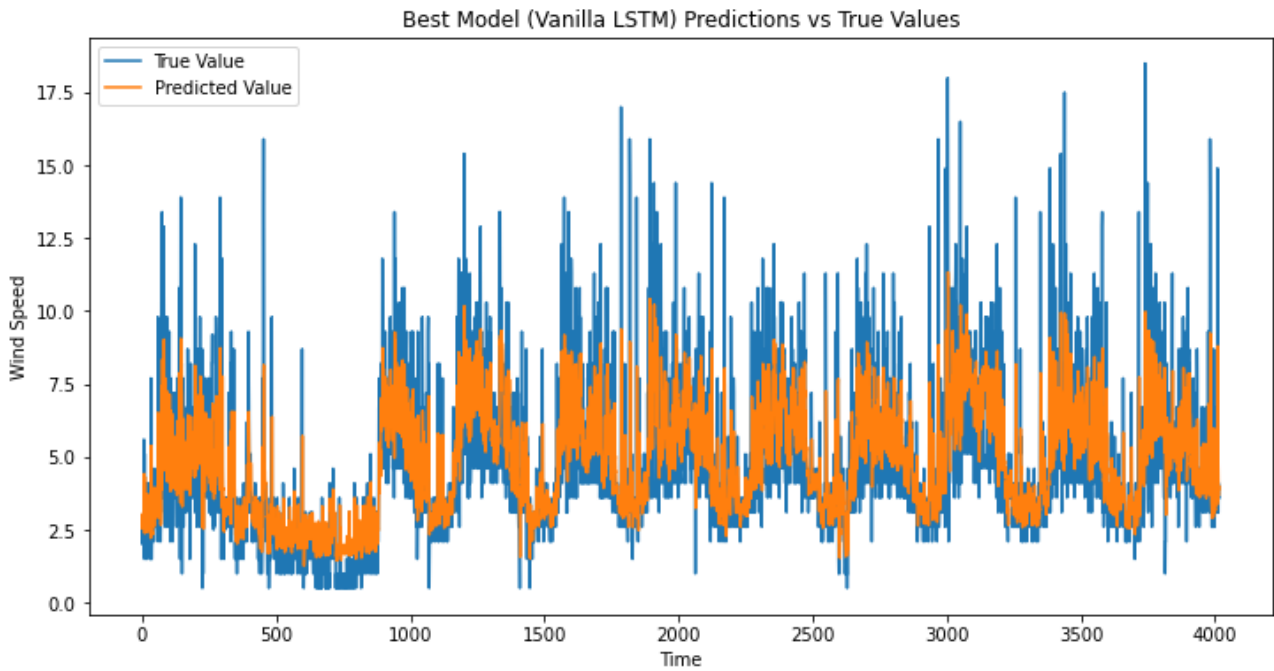
Figure 13. Vanilla LSTM predictions with MSE loss function
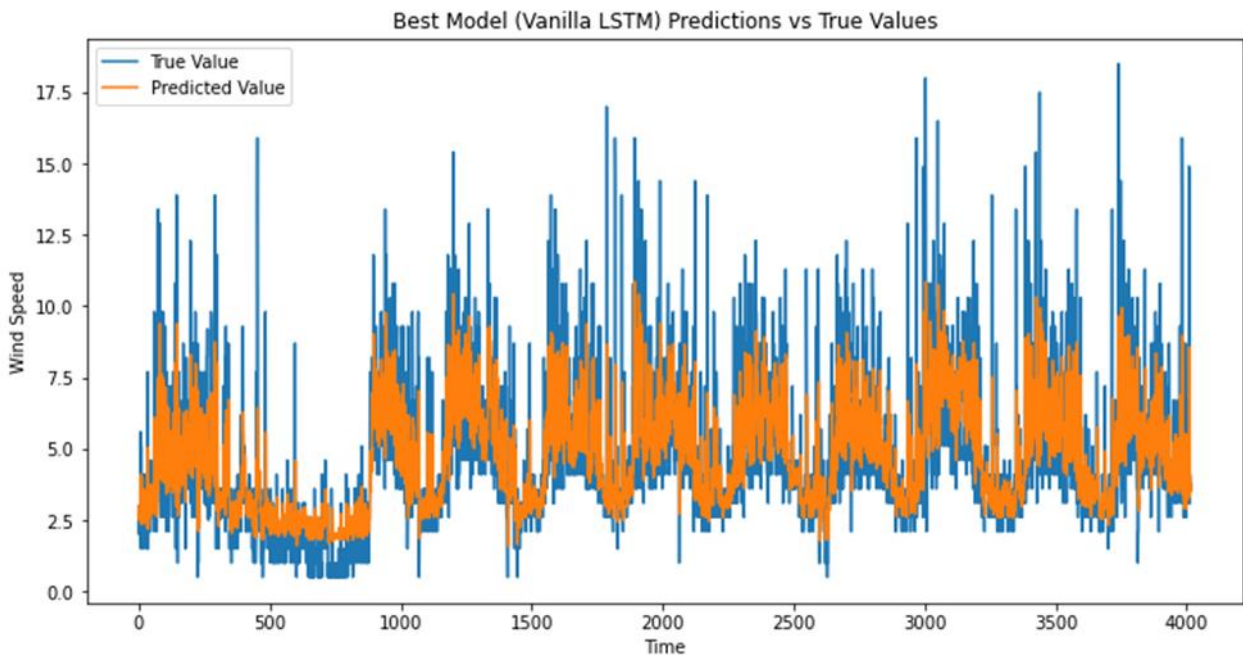
Figure 14. Vanilla LSTM predictions with MAE loss function

The Attention LSTM model has a moderate MSE value but achieves the lowest MAPE, indicating that it makes the least percentage error in predictions. Despite having a somewhat higher MAE value, the model's ability to focus on significant time steps has reduced the overall percentage error rate. The inclusion of the attention mechanism has not significantly increased the training time, suggesting that the Attention LSTM can provide rapid training even with the addition of this mechanism. Due to the nature of time series such as wind, Attention models are better able to capture trends and sudden changes.

The Residual LSTM model shows higher error rates than other models for both MSE and MAE. Its MAPE value is average. The residual connections have not significantly improved the model's performance on this dataset. In terms of training time, the model shows an average performance.

Overall, the Attention LSTM model demonstrates the best performance in terms of MAPE as seen in Figure 15. This indicates that the model is more consistent and accurate in percentage terms. However, the Vanilla LSTM model has the lowest MSE and MAE values, showing the best performance in terms of total error amount.
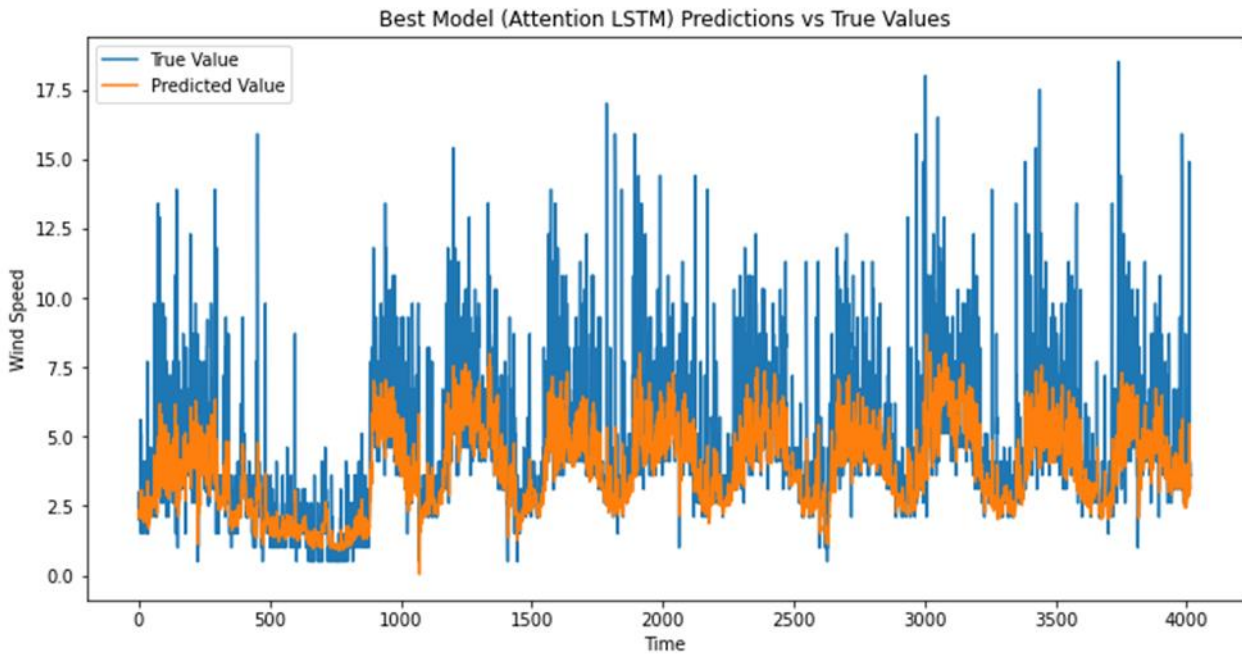
Figure 15. Attention LSTM predictions with MAPE loss function

Based on the results, it would be beneficial to focus on optimizing and fine-tuning the better-performing Vanilla and Attention LSTM models. If the percentage error rate is higher, the Attention LSTM model should be preferred. However, if minimizing the total error amount is the goal, the Vanilla LSTM model is a more suitable option.

Table 2. Total parameters of Models

Model	Total Parameter Numbers
Vanilla	10,451
Stacked	30,651
Attention	30,651
Residual	50,851
Bidirectional	81,301

Table 2 shows the total numbers of parameters for each model. Total parameter numbers reflect the complexity and computational requirements of each model. Vanilla LSTM (10,451 parameters) is suitable for small data sets due to its simplicity and fast training. Stacked and Attention LSTM models (30,651 parameters) can learn more complex dependencies; Attention provides a more focused context between time steps, while Stacked provides a broader perspective. Residual LSTM (50,851 parameters) is advantageous in cases that require deep structures and aim to reduce gradient loss. Bidirectional LSTM (81,301 parameters) can provide the strongest results by learning the past and future simultaneously, but it carries the highest computational cost and overfitting risk. If there is no significant difference between the results, models with fewer parameters may be preferred.

The difference between the models is higher in comparison in terms of time. It is seen that there is no extreme difference in the results in terms of error metrics. Since there is no significant difference between error metrics, simpler or faster models may be preferred. If your application requires real-time prediction, models that require less computation time (e.g. Vanilla LSTM) should be preferred. Attention and Bidirectional LSTM models

generally learn more information, but in time series such as wind this can create an unnecessary time cost if this extra information is not useful. Therefore, the model to be chosen also depends on the dataset.

5. CONCLUSION

This study compared the performance of five distinct LSTM architectures for wind speed prediction in Muş, Turkey. The findings indicate that both Vanilla and Attention LSTM models are effective for wind speed prediction in Muş, with the Vanilla LSTM model excelling in total error minimization and the Attention LSTM model excelling in percentage error accuracy.

Overall, the study's findings underscore the efficacy of LSTM techniques in predicting wind speed and emphasize their potential for real-world applications. The success of LSTM models in predicting wind speed is a significant step for wind energy production and management. Accurate predictions can improve energy production planning and grid management processes.

In this study, an initial comparison was made with the same hyperparameters for all models, in a subsequent study, individual hyperparameter settings for each model should be optimized using Grid Search or Bayesian Optimization methods to get the best results. This makes it better for us to reveal the true potential of the models. Future work could involve further optimization and fine-tuning of these models to enhance their predictive capabilities. To further enhance the performance of the Vanilla and Attention LSTM models, hyperparameter optimization and additional data preprocessing techniques can be applied. The effects of different learning rates and dropout rates can also be explored.

117

Acknowledgement

REFERENCES

[1] Hochreiter S, Schmidhuber J. Long Short-Term Memory. Neural Comput 1997; 9: 1735–1780.

[2] Governorship of Muş, www.mus.gov.tr.

[3] Shang Z, He Z, Chen Y, et al. Short-term wind speed forecasting system based on multivariate time series and multi-objective optimization. Energy 2022; 238: 122024.

[4] Wu C, Wang J, Chen X, et al. A novel hybrid system based on multi-objective optimization for wind speed forecasting. Renew Energy 2020; 146: 149–165.

[5] Aly HHH. An intelligent hybrid model of neuro Wavelet, time series and Recurrent Kalman Filter for wind speed forecasting. Sustain Energy Technol Assessments 2020; 41: 100802.

[6] Liu X, Lin Z, Feng Z. Short-term offshore wind speed forecast by seasonal ARIMA - A comparison against GRU and LSTM. Energy 2021; 227: 120492.

[7] He J, Xu J. Ultra-short-term wind speed forecasting based on support vector machine with combined kernel function and similar data. EURASIP J Wirel Commun Netw 2019; 2019: 248.

[8] Xu W, Ning L, Luo Y. Wind Speed Forecast Based on Post-Processing of Numerical Weather Predictions Using a Gradient Boosting Decision Tree Algorithm. Atmosphere (Basel) 2020; 11: 738.

[9] Wang Y, Zou R, Liu F, et al. A review of wind speed and wind power forecasting with deep neural networks. Appl Energy 2021; 304: 117766.

[10] Joseph LP, Deo RC, Prasad R, et al. Near real-time wind speed forecast model with bidirectional LSTM networks. Renew Energy 2023; 204: 39–58.

[11] Köse B, Güneser MT. Assessment of Wind Characteristics and Wind Energy Potential in West Black Sea Region Of Turkey. Eskişehir Tech Univ J Sci Technol A - Appl Sci Eng 2019; 20: 227–237.

[12] Wadi M, Kekezoglu B, Baysal M, et al. Feasibility Study of Wind Energy Potential in Turkey: Case Study of Catalca District in Istanbul. In: 2019 2nd International Conference on Smart Grid and Renewable Energy (SGRE). IEEE, pp. 1–6.

[13] Onat N, Ersoz S. Analysis of wind climate and wind energy potential of regions in Turkey. Energy 2011; 36: 148–156.

[14] Arslan H, Baltaci H, Akkoyunlu BO, et al. Wind speed variability and wind power potential over Turkey: Case studies for Çanakkale and İstanbul. Renew Energy 2020; 145: 1020–1032.

[15] Sirdaş S. Daily wind speed harmonic analysis for Marmara region in Turkey. Energy Convers Manag 2005; 46: 1267–1277.

[16] Shao B, Song D, Bian G, et al. Wind Speed Forecast Based on the LSTM Neural Network Optimized by the Firework Algorithm. Adv Mater Sci Eng 2021; 2021: 1–13.

[17] Pradhan PP, Subudhi B. Wind speed forecasting based on wavelet transformation and recurrent neural network. Int J Numer Model Electron Networks, Devices Fields; 33. Epub ahead of print 12 January 2020. DOI: 10.1002/jnm.2670.

[18] Lu P, Ye L, Zhao Y, et al. Review of meta-heuristic algorithms for wind power prediction: Methodologies, applications and challenges. Appl Energy 2021; 301: 117446.

[19] Hu Y-L, Chen L. A nonlinear hybrid wind speed forecasting model using LSTM network, hysteretic ELM and Differential Evolution algorithm. Energy Convers Manag 2018; 173: 123–142.

[20] Chen M-R, Zeng G-Q, Lu K-D, et al. A Two-Layer Nonlinear Combination Method for Short-Term Wind Speed Prediction Based on ELM, ENN, and LSTM. IEEE Internet Things J 2019; 6: 6997–7010.

[21] Alhussan AA, M. El-Kenawy E-S, Abdelhamid AA, et al. Wind speed forecasting using optimized bidirectional LSTM based on dipper throated and genetic optimization algorithms. Front Energy Res; 11. Epub ahead of print 1 June 2023. DOI: 10.3389/fenrg.2023.1172176.

[22] Chandra DR, Kumari MS, Sydulu M. A detailed literature review on wind forecasting. In: 2013 International Conference on Power, Energy and Control (ICPEC). 2013, pp. 630–634.

[23] Keren B., Sabitha K. Probabilistic forecasting of wind power generation using extreme learning machineinvolving bootstrap method. ITECH 2016; 04: 729–736.

[24] Azad HB, Mekhilef S, Ganapathy VG. Long-Term Wind Speed Forecasting and General Pattern Recognition Using Neural Networks. IEEE Trans Sustain Energy 2014; 5: 546–553.

[25] Wang X, Guo P, Huang X. A Review of Wind Power Forecasting Models. Energy Procedia 2011; 12: 770–778.

[26] Sharma N, Deo R. Wind speed forecasting in Nepal using self-organizing map-based online sequential extreme learning machine. In: Predictive Modelling for Energy Management and Power Systems Engineering. Elsevier, pp. 437–484.

[27] Subramani K, J SS, Habelalmateen MI, et al. Predicting Wind Energy: Machine Learning from Daily Wind Data. E3S Web Conf 2024; 540: 03009.

[28] Yang X, Delworth TL, Jia L, et al. Skillful seasonal prediction of wind energy resources in the contiguous United States. Commun Earth Environ 2024; 5: 313.

[29] Tugal I, Sevgin F. Analysis and forecasting of temperature using time series forecasting methods a case study of Mus. Therm Sci 2023; 27: 3081–3088.

[30] Lu J, Wang Y, Zhu Y, et al. DACLnet: A Dual-Attention-Mechanism CNN-LSTM Network for the Accurate Prediction of Nonlinear InSAR Deformation. Remote Sens 2024; 16: 2474.

[31] Lattari F, Rucci A, Matteucci M. A Deep Learning Approach for Change Points Detection in InSAR Time Series. IEEE Trans Geosci Remote Sens 2022; 60: 1–16.

[32] Wu Y, Yuan M, Dong S, et al. Remaining useful life estimation of engineered systems using vanilla LSTM neural networks. Neurocomputing 2018; 275: 167–179.

[33] Ma M, Liu C, Wei R, et al. Predicting machine's performance record using the stacked long short-term memory (LSTM) neural networks. J Appl Clin Med Phys; 23. Epub ahead of print 16 March 2022. DOI: 10.1002/acm2.13558.

[34] da Silva DG, Meneses AA de M. Comparing Long Short-Term Memory (LSTM) and bidirectional LSTM deep neural networks for power consumption prediction. Energy Reports 2023; 10: 3315–3334.

[35] Ghosh S, Ekbal A, Bhattacharyya P. Natural language processing and sentiment analysis: perspectives from computational intelligence. In: Computational Intelligence Applications for Text and Sentiment Data Analysis. Elsevier, pp. 17–47.

[36] Muhammad K, Mustaqeem, Ullah A, et al. Human action recognition using attention based LSTM network with dilated CNN features. Futur Gener Comput Syst 2021; 125: 820–830.

[37] Kang Q, Chen EJ, Li Z-C, et al. Attention-based LSTM predictive model for the attitude and position of shield machine in tunneling. Undergr Sp 2023; 13: 335–350.

[38] Wen X, Li W. Time Series Prediction Based on LSTM-Attention-LSTM Model. IEEE Access 2023; 11: 48322–48331.

[39] Yue B, Fu J, Liang J. Residual Recurrent Neural Networks for Learning Sequential Representations. Information 2018; 9: 56.

[40] Vatsa A, Hati AS, Kumar P, et al. Residual LSTM-based short duration forecasting of polarization current for effective assessment of transformers insulation. Sci Rep 2024; 14: 1369.

[41] Fu S, Zhang Y, Lin L, et al. Deep residual LSTM with domain-invariance for remaining useful life prediction across domains. Reliab Eng Syst Saf 2021; 216: 108012.

Türk Doğa ve Fen Dergisi
Turkish Journal of Nature and Science
www.dergipark.gov.tr/tdfd

BINGÖL UNIVERSITY

Antioxidant Potential and Phytochemical Profile of Althaea (Hatmi) and Hibiscus Flower Extracts: A Comprehensive Analysis

Hafize DİLEK TEPE[1*] iD **, Fatma DOYUK[1]** iD

[1,] Manisa Celal Bayar University, Application Science and Research Center (ASRC), Manisa

Hafize DİLEK TEPE ORCID No: 0000-0002-6035-6901
Fatma DOYUK ORCID No: 0000-0002-3448-9540

Corresponding author: hafize.dilek@hotmail.com

Abstract: In this study, the bioactive components and antioxidant properties of Althaea (Hatmi) and Hibiscus plants were assessed using various methods. Both aqueous and ethanol extracts of these plants yielded distinct and effective results. Antioxidant activity was evaluated using 2,2-diphenyl-1-picrylhydrazyl (DPPH), 2,2'-azino-bis (3-ethylbenzothiazoline-6-sulfonic acid) (ABTS), and Ferric Reducing Antioxidant Power (FRAP) assay at concentrations of 25, 50, 75, and 100 mg/mL. Hatmi extracts, both ethanol and aqueous, exhibited high DPPH activity, particularly at 75 and 100 mg/mL, while Hibiscus showed a linear increase in DPPH activity with concentration, reaching 2000 μM Trolox Equivalent (TE) /g dry weight (DW) at 100 mg/mL. In ABTS assays, lower concentrations of ethanol extracts were more effective, but higher aqueous concentrations showed greater activity. FRAP results indicated high antioxidant activity in Hatmi ethanol extracts, with activity reaching 2700 μM TE/g DW at higher concentrations. Phenolic analysis revealed high levels of apigenin 7-glucoside, hesperidin, and caffeic acid in Hatmi, while Hibiscus extracts contained significant amounts of chlorogenic acid and quercetin. Gas Chromatography-Mass Spectrometry (GC-MS) analysis showed that Hatmi had a higher abundance of volatile organic compounds compared to Hibiscus.

Althaea (Hatmi) ve Hibiscus Çiçek Ekstrelerinin Antioksidan Potansiyeli ve Fitokimyasal Profili: Kapsamlı Bir Analiz

Öz: Bu çalışmada, Althaea (Hatmi) ve Hibiscus bitkilerinin biyoaktif bileşenleri ile antioksidan özellikleri çeşitli yöntemlerle değerlendirildi. Her iki bitkinin sulu ve etanol ekstrelerinden farklı ve etkili sonuçlar elde edildi. Antioksidan aktiviteler, 25, 50, 75 ve 100 mg/mL konsantrasyonlarında 2,2-diphenyl-1-picrylhydrazyl (DPPH), 2,2'-azino-bis (3-ethylbenzothiazoline-6-sulfonic acid) (ABTS) ve Ferric Reducing Antioxidant Power (FRAP) testleri kullanılarak ölçüldü. Hatmi ekstreleri, hem etanol hem de sulu ekstraktlarda, özellikle 75 ve 100 mg/mL konsantrasyonlarında yüksek DPPH aktivitesi gösterdi. Hibiscus ekstrelerinde ise DPPH aktivitesi, konsantrasyon arttıkça doğrusal bir şekilde yükseldi ve 100 mg/mL'de 2000 μM Trolox Eşdeğeri (TE) /g kuru ağırlık (DW) seviyesine ulaştı. ABTS testlerinde, düşük konsantrasyonlardaki etanol düşük konsantrasyonlarda bile etki gösterirken (25, 50 mg/mL), sulu ekstraksiyonlarının yüksek konsantrasyonları (75, 100 mg/mL) daha fazla aktivite gösterdi. FRAP testlerinde, Hatmi etanol ekstrelerinde yüksek antioksidan aktivite gözlemlendi ve yüksek konsantrasyonlarda 2700 μM TE/g DW seviyelerine ulaşıldı. Hatmi çiçeklerinde yüksek miktarda apigenin 7-glukozid, hesperidin ve kafeik asit gibi fenolikler elde edilirken, Hibiscus ekstrelerinde ise önemli miktarda klorojenik asit ve kuersetin fenolik bileşenleri elde edildi. Gaz Kromatografisi-Kütle Spektrometrisi (GC-MS) analizi, Hatmi çiçeklerinin uçucu organik bileşen çeşitliliği ve miktarı açısından Hibiscus çiçeklerinden daha zengin olduğunu göstermiştir.

1. INTRODUCTION

Consumers are becoming increasingly health-conscious and prefer foods with high nutritional value [1,2]. Many consumers prefer products derived from natural sources over those containing synthetic chemicals due to potential negative health impacts [2,3]. Therefore, many researchers have focused on the potential benefits and importance of wild medicinal plants for food and human health, showing growing interest in this field [2–5]. Some studies have indicated that a quarter of the world's medicines and drugs are produced from medicinal plants [6,7]. Research on the chemical and pharmacological aspects of wild plants has played a significant role in increasing the use of medicinal plants by revealing the presence of bioactive compounds and their beneficial effects on human and animal health systems[8–10].

The Malvaceae family is represented worldwide by over 80 genera and more than 1000 species. Most commonly found in South America, members of this family are present nearly everywhere except for the coldest regions of the world [11,12]. The plants of this family are herbs or shrubs, usually with stellate hairs. The Malvaceae family has medicinal uses thanks to mucilage, fixed oils and essential oils. Some of the most commonly used species in folk medicine are as follows: Althaea officinalis, Malva sylvestris, Alcea biennis, Abelmoschus esculentus, Hibiscus [13–17].

Figure 1. *Althaea officinalis L.*

Althaea officinalis Linn (AO), known as marshmallow (Hatmi in Türkiye), is a hairy herb, annual and perennial plant belonging to the family Malvaceae (Figure 1) [18]. AO parts have been traditionally utilized in the treatment of various ailments such as coughs, colds, stomach ulcers, kidney stones, enteritis, and mucous membrane irritation [19,20]. Multiple studies have indicated the diverse therapeutic properties of AO extracts, including antitussive, anti-inflammatory, anti-estrogenic, antimicrobial, immunomodulatory, and antioxidant effects [19–22] Analytical investigations have revealed the predominant composition of AO, which comprises starch (25%-35%), pectin (11%), sucrose (10%), mucilage (5%), and saccharides [18–21,23]. Despite its extensive traditional use and therapeutic potential, the chemical profile of AO remains relatively understudied, with only 46 compounds identified thus far, encompassing 17 flavonoids, 3 coumarins, 1 steroid, 1 triterpenoid, and 24 other miscellaneous compounds [24].

Figure 2. *Hibiscus sabdariffa*

Hibiscus sabdariffa (HS) is a tropical shrub belonging to the Malvaceae family with red or green edible calyxes (Figure 2). These parts are rich in protein, calcium, niacin, riboflavin, iron, phenols, amino acids, carotene, and vitamin C [25]. Due to its high content of polyphenolic acid, triterpenoids, polysaccharides, organic acids (citric, malic acids, etc. , and flavonoids, HS is widely known as a medicinal plant in tropical countries [26]. The calyces contain high levels of anthocyanins, such as delphinidin-3-sambubioside, cyanidin-3-sambubioside, cyanidin-3-glucoside, and delphinidin-3-glucoside, which make them a promising natural colorant for various food industrial purposes, including the production of juices, wines, and carbonated soft drinks [27]. Additionally, studies have shown that beers supplemented with Hibiscus sabdariffa or sea buckthorn have higher levels of bioactive compounds and antioxidant activity compared to control samples [28,29].

The purpose of this study is to compare the phytochemical compositions and antioxidant properties of Hibiscus sabdariffa (HS) and Althaea officinalis Linn (Hatmi), emphasizing their medicinal and industrial potentials. Both plants have significant potential in these areas, but they exhibit important differences. HS is notable for its nutrient-rich calyces and potential as a natural colorant, while AO is recognized for its versatile therapeutic properties. This review underscores the necessity for further research into the chemical constituents and pharmacological effects of HS and AO, offering insights that could lead to expanding applications in both medicine and industry.

2. MATERIAL and METHOD

2.1. Extraction methods

Dried *Hibiscus sabdariffa* (Hibiscus) and *Althaea officinalis L.* (Hatmi) flowers were obtained from a local market in Manisa, Türkiye (**Figure 3**). A sample of 1 gram was taken, and 40 mL of ethanol (100%) was added. Extraction was carried out using Ultra-turrax (IKA T25, Staufen, Germany) at 5000×g for 3 min at room temperature for 30 min. The resulting extract solution was filtered and stored in amber glass bottles at +4 ^{0}C until further analysis. In the experiments, the abbreviations used are as follows: HA: Althaea ethanol extract, HA AQ: Althaea aqueous extract, HIBIS ETOH: Hibiscus ethanol extract, and HIBIS AQ: Hibiscus aqueous extract.

Figure 3. a) Dried Hatmi flowers, b) Dried Hibiscus flowers.

2.2. Antioxidant activity assays

The FRAP analysis was performed according to the following procedure with some modifications [30]. The stock solutions included 300 mM acetate buffer (3.1 g C2H3NaO2.3H2O and 16 mL C2H4O2), pH 3.6, 10 mM TPTZ (2, 4, 6-tripyridyl-s-triazine) solution in 40 mM HCl, and 20 mM FeCl3.6H2O solution. The fresh working solution mix was prepared as follows: 25 mL acetate buffer, 2.5 mL TPTZ solution, and 2.5 mL FeCl3.6H2O solution and then warmed at 37 0C before use. Leaves extracts (150 µL) were allowed to react with 2850 µL of the FRAP solution for 30 min in a dark condition. Then, absorbance was taken at 593 nm using the spectrophotometer (TECAN, Männedorf, Switzerland). The standard curve was linear between 25 and 600 mM Trolox. Results were expressed in mM Trolox equivalents (TE)/g dry mass (DM).

The DPPH analysis was performed according to the following procedure with minor modifications [31]. The stock solution was freshly prepared by dissolving 24 mg of DPPH in 100 mL of methanol, and then 10 mL of this solution was taken and diluted with 45 mL of methanol. Leaves extracts (150 µL) were allowed to react with 2850 µL of the DPPH solution for 2 h in a dark condition. Then, absorbance was taken at 515 nm using the spectrophotometer (TECAN, Männedorf, Switzerland). The standard curve was linear between 25 and 800 mM Trolox. Results are expressed in mM Trolox equivalents (TE)/g dry mass. In all measurements, additional dilution was needed if the analysis value measured was over the linear range of the standard curve.

For ABTS assay of leaf extracts was performed according to the following method with some modifications [32]. A stock solution containing 7.4 mM ABTS and 2.6 mM potassium persulfate was prepared. The prepared stock solution was kept at room temperature for 12 h and then 1 mL was taken and diluted with 60 mL of methanol before the analysis. Leaves extracts (150 µL) were allowed to react with 2850 µL of the ABTS solution for 2 h in a dark condition. Then, absorbance was taken at 734 nm using the spectrophotometer (TECAN, Männedorf, Switzerland). The standard curve was linear between 25 and 600 mM Trolox. Results were expressed in mM Trolox equivalents (TE)/g dry mass).

2.3. Determination of phenolic compounds by LC-MS/MS

Determination of phenolic profiles of leaves extracts, high-performance liquid chromatography-mass spectrometer - mass spectrometer (Agilent 1260 Triple Quadrupole MS/MS) were used. Each analysis was performed with three replications. HPLC column C18 ODS used in the analyses (25x4.6 mmx5 µm) was used. Injection volume for analysis: 2 µL. Water/0.1% formic acid (A), and methyl alcohol (99.9%) (B) were used as a carrier phase. The gradient method is as follows: 3 min 2% B, 6 min 25% B, 10 min 50% B, 14 min 95% B, 17.5 min 2% B. Flow rate: 0.4 mL/min. The identification of compounds was performed in positive and negative modes [33].

2.4. Determination of volatile organic molecules by GC-MS

Volatile molecules in the extract were qualitatively analyzed in electron ionization (EI) mode with Agilent Technology 7890A Gas Chromatography (GC) Mass spectrometer (MS). Chromatographic column Agilent HP-5 MS, capillary column (30 m x 0.25 mm, the film thickness of 0.25 mm). The furnace temperature was started at 40°C, followed by standing for 5 min, then at 5°C min-1 at 280°C and held for 5 min. Helium gas (99.999%) was used as the carrier gas. The constant flow rate is 1.5 mL min-1 and the injector temperature is 250°C. The extract was injected in splitless mode with 1.0 mL. Interpretation of the mass spectrum was performed according to the National Institute of Standards and Technology (NIST) database.

122

3. RESULTS and DISCUSSION

3.1. Antioxidant activity results

Antioxidant activity was evaluated using DPPH, ABTS, and FRAP parameters. The ethanol and aqueous extracts of Hatmi and Hibiscus plants were compared at concentrations of 25, 50, 75, and 100 mg/mL. In the DPPH activity assays, both the ethanol and aqueous extracts of Hatmi flowers exhibited high levels of activity, particularly at concentrations of 75 and 100 mg/mL. In contrast, for the Hibiscus flowers, a linear increase in DPPH activity was observed with increasing concentrations in both extracts. At a concentration of 100 mg/mL, the activity reached up to 2000 µM TE/g DW. Consequently, it was determined that Hibiscus flowers provided a more significant response in DPPH activity (Figure 4a). In ABTS assays, low-dose ethanol extractions of Hatmi and Hibiscus plants have proven more effective (25, 50 mg/mL). Antioxidants are essential for maintaining overall health because they protect the body from oxidative stress, which is caused by free radicals. Free radicals are unstable molecules that can damage cells, proteins, and DNA, potentially leading to aging and various diseases, including cancer, heart disease, and neurodegenerative disorders [34-36].
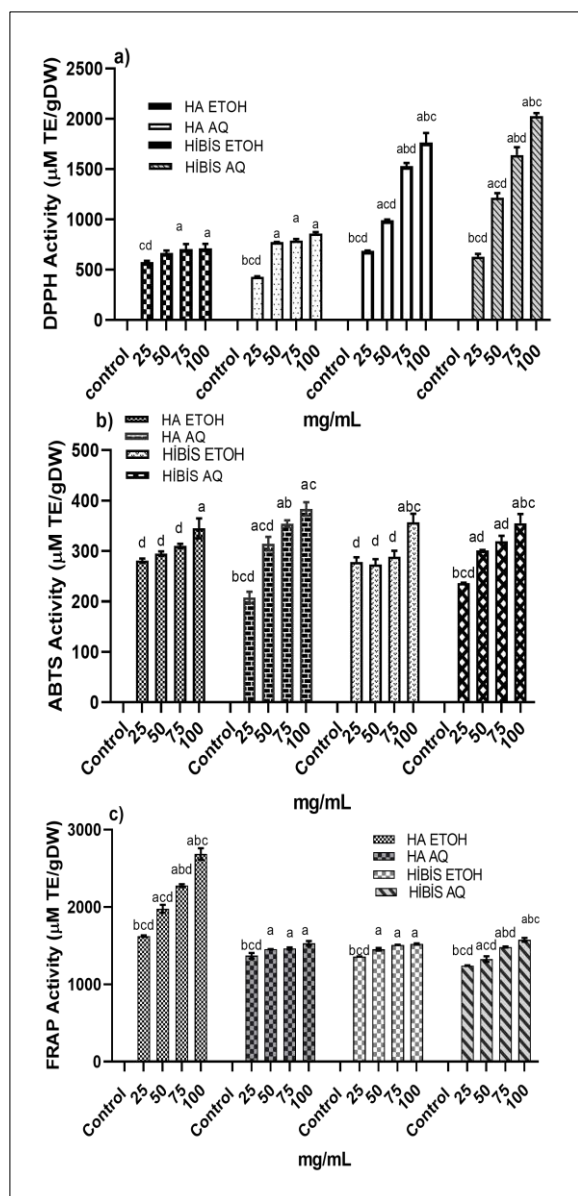
Figure 4. a) DPPH activity, b) ABTS activity, c) FRAP activity results of extracts. a: compared to 25 mg/mL, b: compared to 50 mg/mL, c: compared to 75 mg/mL, d: compared to 100 mg/mL. P<0.05.

The ABTS activity results at these concentrations range between 220 and 280 µM TE/g DW. However, in the aqueous extractions of both plants, higher concentrations demonstrated even greater activity (75, 100 mg/mL). At these concentrations, the ABTS activity levels reach the range of 350-400 µM TE/g DW (Figure 4b). According to the FRAP results, the ethanol extract of Hatmi flower exhibited high antioxidant activity. Specifically, at concentrations of 75 and 100 mg/mL, activity results of 2400 and 2700 µM TE/g DW were obtained, respectively. Additionally, the aqueous extract of the Hibiscus flower also demonstrated significant antioxidant activity. It was observed that as the concentration increased, the FRAP activity also showed a linear and significant increase (Figure 4c). Farhat et al. found that the capacity of Althaea officinalis water extract to scavenge DPPH free radicals increased with higher concentrations, achieving a strong antioxidant activity of 75% at 6.0 mg/mL [37]. The findings of Farhat et al. show a significant similarity to our study. Their research indicates that the capacity of

plant extracts to scavenge free radicals increases with higher concentrations. This aligns with our results, which also demonstrate that higher concentrations tend to enhance antioxidant activity. In particular, the ethanol extract of the Hatmi flower exhibits strong antioxidant activity, paralleling the findings of Farhat et al. Similarly, the increase in activity observed in the aqueous extract of the Hibiscus flower highlights the critical impact of concentration on antioxidant effectiveness. These findings suggest that concentration plays a crucial role in enhancing the antioxidant potential of plant sources [37] .

3.2. Phenolic compounds results by LCMSMS

Table 1. Phenolic compounds of Hatmi plant extracts.

Compound Name	HA ETOH (µg/g)	HA AQ (µg/g)
(-)-Epicatechin	0.680±0.03	0.658±0.08
(+)-Catechin	ns	0.549±0.054
2.5-Dihydroxybenzoic acid	1.535±0.10	4.309±.005
3,4-Dihydroxyphenylacetic acid	0.194±0.01	0.237±0.163
3-Hydroxybenzoic acid	9.420±0.28	29.490±1.07
3-hydroxytyrosol	0.708±0.01	1.409±0.037
4-Hydroxybenzoic acid	8.729±0.21	25.995±0.12
Apigenin 7-glucoside	884.195±2.8	30.005±1.53
Apigenin	53.522±0.11	75.292±1.81
Caffeic acid	34.211±0.02	85.764±4.38
Chlorogenic acid	0.912±0.07	11.935±0.10
Eriodictyol	0.671±0.06	3.207±0.04
Ferulic acid	16.254±0.32	80.174±1.34
Gallic acid	1.144±0.01	6.242±0.39
Hesperidin	200.592±5.04	199.320±6.51
Hyperoside	0.402±2.544	113.594±1.27
Kaempferol	29.354±0.05	26.310±1.04
Luteolin	1.635±0.202	2.837±0.134
oleuropein	0.043±0.002	0.032±0.001
p-Coumaric acid	14.983±0.280	61.565±0.54
Pinoresinol	0.375±0.100	131.416±12.6
Protocatechuic acid	1.502±0.045	4.211±0.02
Pyrocatechol	0.611±1.31	0.168±0.05
Quercetin	2.90±0.10	7.849±0.52
Rosmarinic acid	0.073±0.008	0.010±0.001
Sinapic acid	0.438±0.04	2.387±0.16
Syringic acid	4.804±0.14	13.709±0.93
Taxifolin	12.417±0.07	264.049±15.92
Verbascoside	0.077±0.07	0.820±0.155

According to the results obtained from the analysis of phenolic components, different compounds were obtained from the ethanol and aqueous extractions of Hatmi flowers. Specifically, apigenin 7-glucoside was found in high amounts in the ethanol extract at 884.19 µg/g.

123

Subsequently, hesperidin (200.592 μg/g), apigenin (53,52 μg/g), and caffeic acid (34.21 μg/g) were determined to be present in high amounts. In the aqueous extracts of Hatmi flowers, phenolic components such as hesperidin (199.32 μg/g), pinoresinol (131.41 μg/g), and taxifolin (264.04 μg/g) were found in high amounts (Table 1). Farhat et al. identified the following phytochemicals in the extraction of the Athena plant using LC-MS analysis: 5 phenolic acids (syringic acid, gallic acid, caffeic acid, p-coumaric acid, and trans-ferulic acid) and 8 flavonoids (catechin, apigenin, chrysin, quercetin, kaempferol, genistein, rutin trihydrate, and galangin) [37]. The anti-cancer effects observed in the water extract can be attributed to its major constituents, including polysaccharides, flavonoids, phenolic acids, and coumarins [38,39]. Especially, Quercetin exhibits strong antioxidant and anti-inflammatory properties that are closely related to the prevention and treatment of cardiovascular diseases and cancer [40].

Table 2. Phenolic compounds of Hibiscus plant extracts.

Compound Name	HİB ETOH (μg/g)	HİB AQ (μg/g)
2,5-Dihydroxybenzoic acid	8.01±0.31	27.39±0.71
3,4-Dihydroxyphenylacetic acid	0.11±0.03	0.01±0.002
3-Hydroxybenzoic acid	1.20±0.16	3.54±0.21
3-hydroxytyrosol	0.07±0.001	0.11±0.01
4-Hydroxybenzoic acid	0.94±0.01	2.80±0.26
Apigenin 7-glucoside	0.32±0.016	ns
Apigenin	1.49±0.012	ns
Caffeic acid	18.64±0.08	28.41±0.30
Chlorogenic acid	452.50±4.14	942.34±6.06
Ferulic acid	2.77±0.10	3.75±0.16
Gallic acid	13.29±0.12	203.45±3.12
Hesperidin	32.18±0.31	8.09±0.30
Hyperoside	24.53±0.45	56.96±0.04
Kaempferol	6.51±0.19	1.94±0.36
p-Coumaric acid	1.92±0.13	3.51±0.18
Pinoresinol	0.80±0.02	24.18±0.38
Protocatechuic acid	8.12±0.08	28.63±0.06
Pyrocatechol	5.81±0.27	25.53±0.22
Quercetin	69.72±0.06	49.69±0.15
Sinapic acid	3.52±0.08	4.79±0.11
Syringic acid	25.11±0.53	38.09±0.65
Taxifolin	0.55±0.07	0.74±0.02
Verbascoside	0.01±0.001	0.23±0.01

In the ethanol and aqueous extracts of hibiscus flowers, common phenolic compounds such as chlorogenic acid, quercetin, syringic acid, caffeic acid, and hyperoside were obtained in high amounts. However, some were found predominantly in ethanol extracts, while others were more abundant in aqueous extracts. For instance, chlorogenic acid (942.34 μg/g), hyperoside (56.96 μg/g), and caffeic (28.41 μg/g) acid were found in higher quantities in the aqueous extracts, whereas quercetin (69.72 μg/g) and hesperidin (32.18 μg/g) were obtained in higher amounts in the ethanol extract (Table 2). Plant phenolic compounds possess strong free radical scavenging activity and high antioxidant capacities, making them more antimicrobial and effective against various diseases and infections [41]. Therefore, the high phenolic content found in this study suggests that consuming H. sabdariffa plants and their products could enhance human health by neutralizing free radicals, which may help prevent neurodegenerative diseases and cancer development [9]. The findings regarding the phenolic compounds in both ethanol and aqueous extracts of hibiscus flowers highlight the complexity and variability of these bioactive compounds. The presence of significant amounts of chlorogenic acid, hyperoside, and caffeic acid in the aqueous extracts suggests that these compounds may be particularly effective in enhancing the antioxidant properties of the plant when extracted with water. Conversely, the higher levels of quercetin and hesperidin in the ethanol extracts indicate that certain phenolic compounds are more soluble in organic solvents, potentially enhancing their bioavailability.

Given that plant phenolic compounds are known for their strong free radical scavenging activity and high antioxidant capacities, the findings imply that the consumption of H. sabdariffa and its products could provide substantial health benefits. The ability of these compounds to neutralize free radicals may contribute to the prevention of oxidative stress-related conditions, such as neurodegenerative diseases and cancer.

3.3. Volatile organic molecules result by GC-MS
In GC-MS analysis of volatile organic compounds from extracts of Hatmi and Hibiscus flowers, it was found that Hatmi flowers contained a greater abundance of organic compounds than Hibiscus. The results were determined by scanning against the device library, accepting matches above 80%. Tricosane, linoleic acid ethyl ester, ethyl oleate, nonanoic acid, p-vinylguaiacol, 9,12-octadecadienoic acid (Z, Z), cis-vaccenic acid, and other organic volatile compounds were obtained from the extract of Hatmi flowers (Table 3). In a study, it was demonstrated that the hexane extract of A. officinalis flowers is rich in both saturated fatty acids (including palmitic acid, nonacosane, heptacosane, and pentacosane) and unsaturated fatty acids (such as omega-3 α-linolenic acid and omega-6 linoleic acid) [42]. Flavonoids are a class of heterocyclic natural compounds that are widely distributed in plants, occurring as glycosides and free aglycones. Consistent with the authors' findings, A. officinalis was found to be rich in quercetin, rutin, apigenin, coumarins, and kaempferol [43]. These compounds exhibited cytotoxic activities against cancer cells by interacting with various molecules involved in apoptosis and proliferation pathways [44,45].

124

Table 3. Volatile organic molecules of Hatmi plant extracts.

CAS	Label	Mass (DB)	Formula (DB)	m/z	Library	Score (Lib)
5906-76-3	Dimethylsilanol; Silanol, dimethyl	76	C2H8OSi	45.1	Wiley7Nist05.L	84.12
1464-53-5	2,2-Bioxirane	86	C4H6O2	55.1	Wiley7Nist05.L	84.58
600-22-6	Propanoic acid, 2-oxo, methyl ester	102	C4H6O3	43.1	Wiley7Nist05.L	85.68
42403-25-8	Pyrrolidine- Alpha, Alpha, Alpha, Alpha- D4	75.1	C4H5D4N	43.1	Wiley7Nist05.L	85.38
98-00-0	2-furanmethanol	98.1	C5H6O2	81.1	NIST11.L	93.6
10230-62-3	2,4-dihydroxy-2,5-dimethyl-3(2H)-furan-3-one	144	C6H8O4	101	NIST11.L	88.74
33325-40-5	Propanoic acid,3- (acetylthio)-2-methyl	162	C6H10O3S	43.1	Wiley7Nist05.L	80.81
65-71-4	Thymine	126	C5H6N2O2	43.1	Wiley7Nist05.L	83.47
30533-08-5	2-propanamine, N-methyl-N-nitroso	102	C4H10N2O	43.1	Wiley7Nist05.L	80.15
28564-83-2	4H-pyran-4-one, 2,3-dihdyro-3,5-dihydroxy-6-methyl	144	C6H8O4	43.1	NIST11.L	95.68
25395-31-7	1,2,3-propanetriol, diacetate	143.9	C7H12O5	43.1	Wiley7Nist05.L	82.1
112-05-0	Nonanoic acid	158	C9H18O2	43.1	Wiley7Nist05.L	88.75
7786-61-0	p-vinylguaiacol	150.1	C9H10O2	135	Wiley7Nist05.L	93.36
1000130-99-3	Z-10-Tetradecen-1-ol acetate	254	C16H30O2	43.1	NIST11.L	84.77
1000130-14-3	d-glycero-d-ido-heptose	210	C7H14O7	57.1	NIST11.L	82.02
0-00-0	3-deoxy-d-mannoic acid lactone	141.9	C6H10O5	57.1	Wiley7Nist05.L	83.39
502-69-2	2-pentadecanone,6,10,14-trimethyl	268	C18H36O	43.1	NIST11.L	87.98
57-10-3	Hexadecanoic acid	256.2	C16H32O2	73	Wiley7Nist05.L	96.06
628-97-7	Hexadecanoic acid, ethyl ester	284.3	C18H36O2	88.1	Wiley7Nist05.L	96.13
60-33-3	9,12-Octadecadienoic acid (Z,Z)	280.2	C18H32O2	67.1	NIST11.L	85.07
506-17-2	Cis-Vaccenic acid	281.1	C18H34O2	55.1	NIST11.L	87.99
544-35-4	Linoleic acid ethyl ester	308.3	C20H36O2	55.1	NIST11.L	82.69
111-62-6	Ethyl oleate	310.3	C20H38O2	55.1	Wiley7Nist05.L	88.75
111-61-5	Octadecanoic acid, ethyl ester	312.3	C20H40O2	88.1	NIST11.L	87.35
638-67-5	Tricosane	324.4	C23H48	57.1	NIST11.L	95.95
301-02-0	9-Octadecenamide, (Z)	281.1	C18H35NO	59.1	NIST11.L	81.72
629-99-2	Pentacosane	352.4	C25H52	57.1	NIST11.L	90.91
593-49-7	Heptacosane	380.4	C27H56	57.1	NIST11.L	90.75
621-61-4	Octadecanoic acid, 2-hydroxy-1-(hydroxymethyl) ethyl ester	358.2	C21H42O4	98.1	NIST11.L	89.89

Table 4. Volatile organic molecules of Hibiscus plant extracts.

CAS	Label	Mass (DB)	Formula (DB)	m/z	Library	Score (Lib)
1112-39-6	Silane, dimethoxydimethyl	120.1	C4H12O2Si	105	Wiley7Nist05.L	81,23
497-23-4	2 (5H)- Furanone	84	C4H4O2	55.1	NIST11.L	90.22
98-01-1	Furfural	96	C5H4O2	39.1	NIST11.L	99.15
8.03.2170	2,5 - Furandione, d	112	C5H4O3	68.1	NIST11.L	93.53
620-02-0	2-Furancarboxaldehyde, 5-methyl	110	C6H6O2	53.1	NIST11.L	97.76
161500-43-2	Oxazolidine, 2,2-diethyl-3-methyl	140.2	C8H17NO	114	NIST11.L	83.96
932-85-4	2 (3H)- Furanone, 5-ethoxydihydro	129.1	C6H10O3	85	NIST11.L	91.29
28564-83-2	4H-Pyran-4-one,2,3-dihydro-3,5-dihydroxy-6-methyl	144	C6H8O4	43.1	NIST11.L	95.21
67-47-0	5-hydroxymethylfurfural	126	C6H6O3	97	NIST11.L	97.92
498-07-7	beta-D-Glucopyranose ,1,6,anhydro	161.8	C6H10O5	60.1	NIST11.L	91.96
80286-58-4	Arteannuic acid	234.2	C15H22O2	121.1	NIST11.L	82.4
112-39-0	Hexadecanoic acid, methyl ester	270.2	C17H34O2	74.1	NIST11.L	86.12
57-10-3	Hexadecanoic acid	256.2	C16H32O2	73.1	Wiley7Nist05.L	94.89
60-33-3	9,12-Octadecadienoic acid (Z,Z)	280.2	C18H32O2	67.1	NIST11.L	93
301-02-0	9-Octadecenamide, (Z)	281.1	C18H35NO	59.1	Wiley7Nist05.L	87.08

Volatile organic molecules such as furfural, arteannuic acid, hexadecanoic acid methyl ester, hexadecanoic acid, and 9-octadecenamide (Z) were obtained in extracts of Hibiscus flowers. The gas chromatography-mass chromatography (GC–MS) analysis of oil from H. sabdariffa flower obtained from Nigeria showed the presence of linoleic acid (22.7%) and hexadecenoic acids of 64.3% [46]; the seed oil from Austria showed oleic acid (24.7%), linoleic acid (43.2%) and palmitic acid (17.3%) as the major chemical compositions [6]. However, α-terpineol and linalool dominated the seed oil from Cuba [47]. It can be observed that there is no uniformity in the chemical compositions of the oil; it varies based on geographical locations [48].

These findings suggest that environmental factors, such as soil composition, climate, and agricultural practices, play a crucial role in determining the chemical profiles of Hibiscus oils. This lack of uniformity highlights the importance of considering geographic variations when evaluating the potential applications of these oils in food, cosmetics, or medicinal uses. Further studies could explore the implications of these differences for the antioxidant and therapeutic properties of Hibiscus extracts, potentially leading to more targeted applications based on specific regional profiles.

4. CONCLUSION

The findings of this study indicate that aqueous and ethanol extractions produce different effects on the bioactive components and antioxidant properties of the plants. Notably, the aqueous extract of the Hibiscus flower exhibited high DPPH radical scavenging activity, while the ethanol extract of the Hatmi flower was found to be more effective in FRAP assays. This suggests that the choice of solvent significantly influences the profile of active compounds and their corresponding activities. Aqueous extractions typically tend to extract polar compounds, particularly phenolic compounds and antioxidants that are soluble in water. The richness of such compounds in the Hibiscus flower may be one of the key reasons for its high antioxidant activity. In contrast, ethanol and other less polar solvents are more effective at extracting phenolic compounds and fatty acids.

The high activity observed in the ethanol extract of the Hatmi flower may therefore result from ethanol's ability to solubilize these compounds more effectively. These differences highlight the critical role that the extraction methods play in determining the active components obtained and, ultimately, their potential health benefits. Thus, further investigation into these plants, particularly using various extraction methods, is essential to better understand their health benefits and enhance their potential in pharmaceutical applications.

REFERENCES

[1] Li H Bin, Cheng KW, Wong CC, Fan KW, Chen F, Jiang Y. Evaluation of antioxidant capacity and total phenolic content of different fractions of selected microalgae. Food Chemistry 2007;102:771–6. https://doi.org/10.1016/J.FOODCHEM.2006.06.022.

[2] Awolu OO, Oladeji OA. (PDF) Natural Plant Pigments and Derivatives in Functional Foods Development n.d. https://www.researchgate.net/publication/352787718_Natural_Plant_Pigments_and_Derivatives_in_Functional_Foods_Developments (accessed May 10, 2024).

[3] Aberoumand A. A Review Article on Edible Pigments Properties and Sources as Natural Biocolorants in Foodstuff and Food Industry 2011:71–8. https://www.researchgate.net/publication/228492881_A_Review_Article_on_Edible_Pigments_Properties_and_Sources_as_Natural_Biocolorants_in_Foodstuff_and_Food_Industry (accessed May 10, 2024).

[4] Collins AR. Antioxidant intervention as a route to cancer prevention. European Journal of Cancer (Oxford, England: 1990) 2005;41:1923–30. https://doi.org/10.1016/J.EJCA.2005.06.004.

[5] Seal T, Pillai B, Chaudhuri K. Evaluation of Nutritional Potential of Five Unexplored Wild Edible Plants Consumed by the Tribal People of Arunachal Pradesh State in India. Journal of Food and Nutrition Research, Vol 5, 2016, Pages 1-5 2016;5:1–5. https://doi.org/10.12691/JFNR-5-1-1.

[6] Malik RN, Husain SZ, Nazir I. Heavy metal contamination and accumulation in soil and wild plant species from industrial area of Islamabad, Pakistan. Pakistan Journal of Botany 2010;42:291–301.

[7] Cragg GM, Newman DJ. Natural product drug discovery in the next millennium. Pharmaceutical Biology 2001;39:8–17. https://doi.org/10.1076/PHBI.39.7.8.5868.

[8] Maganha EG, Halmenschlager R da C, Rosa RM, Henriques JAP, Ramos ALL de P, Saffi J. Pharmacological evidences for the extracts and secondary metabolites from plants of the genus Hibiscus. Food Chemistry 2010;118:1–10. https://doi.org/10.1016/J.FOODCHEM.2009.04.005.

[9] Fraga CG, Croft KD, Kennedy DO, Tomás-Barberán FA. The effects of polyphenols and other bioactives on human health. Food & Function 2019;10:514–28. https://doi.org/10.1039/C8FO01997E.

[10] Prosper An C, Esiaba I, Ajbaye O, Adesuyi AO. Polyphenolic Content and Antioxidant Activity of Hibiscus sabdariffa Calyx. Research Journal of Medicinal Plant 2011;5:557–66. https://doi.org/10.3923/rjmp.2011.557.566.

[11] Goldberg A, Hutchinson J. Hutchinson's Families: Third Edition. Taxon 1974;23:627. https://doi.org/10.2307/1218791.

[12] Heywood VH (Vernon H. Flowering plants of the world 1979:335.

[13] Türkan Ş, Malyer H, Öz Aydin S. Ordu İli ve Çevresinde Yetişen Bazı Bitkilerin Etnobotanik Özellikleri. Fen Bilimleri Enstitüsü Dergisi 2006;10:162–6.

[14] Rouhi H, Ganji F. Effect of althaea officinalis on cough associated with ACE inhibitors. Pakistan Journal of Nutrition 2007;6:256–8. https://doi.org/10.3923/PJN.2007.256.258.

[15] Kültür Ş. Medicinal plants used in Kırklareli Province (Turkey). Journal of Ethnopharmacology 2007;111:341–64. https://doi.org/10.1016/j.jep.2006.11.035.

[16] Kara AA, Algur ÖF, Köseoğlu MŞ. Bazı Şifalı Bitkilerin Helicobacter pylori üzerindeki Antimikrobiyal Aktiviteleri. Cumhuriyet Science Journal 2016;1. https://doi.org/10.17776/csj.32537.

[17] Baytop T. Türkiye'de Bitkiler ile Tedavi (Geçmişte ve Bugün) Türkiye'de Kullanılan Tıbbi Bitkiler. 40th ed. İstanbul: İ.Ü.Eczacılık Fak..; 1984.

[18] Al-Snafi AE. The Pharmaceutical importance of Althaea officinalis and Althaea rosea: A review. International Journal of PharmTech Research 2013;5:1378–85.

[19] Fahamiya N, Shiffa M, Aslam M, Nazeem Fahamiya C, Muzn F. Unani perspective of Khatmi (Althaea officinalis). Journal of Pharmacognosy and Phytochemistry 2016;5:357–60.

[20] Reinelt N, Melzig MF. Der Echte Eibisch Althaea officinalis L. Zeitschrift Fur Phytotherapie 2017;38:91–6. https://doi.org/10.1055/S-0043-103256/ID/R04-17-PORT-REINELT-0029/BIB.

[21] Satish Kumar S, Sudhakar S, Kapil S, Snigdha T. Ethnopharmacological Review on Althaea Officinalis. WwwWjppsCom 2016;5:425. https://doi.org/10.20959/wjpps20167-7095.

[22] Singh A, Idris M. A brief review on a Unani Drug: Khatmi (Althaea officinalis). Asian Journal of Pharmacy and Pharmacology 2018;4:394–8. https://doi.org/10.31024/ajpp.2018.4.4.3.

[23] Mousavi SF, Razavi SMA, Koocheki A. Marshmallow (Althaea officinalis) flower gum. Emerging Natural Hydrocolloids: Rheology and Functions 2019:397–423. https://doi.org/10.1002/9781119418511.CH16.

[24] Xue T-T, Xu H-B, Tang Z-S, Duana J-A, Liu H-B, Shi X-B, et al. Progress in Chemical Compositions and Pharmacological Activities of Althaea officinalis. Med Res 2021;5:210002–210002. https://doi.org/10.21127/yaoyimr20210002.

[25] Shruthi VH, Ramachandra CT, Nidoni U, Hiregoudar S, Naik N, Kurubar AR. Physico-Chemical, Nutritional and Functional Properties of Roselle (Hibiscus sabdariffa L.). International Journal of Current Microbiology and Applied Sciences 2017;6:2976–82. https://doi.org/10.20546/ijcmas.2017.612.347.

[26] Amaya-Cruz D, Peréz-Ramírez IF, Pérez-Jiménez J, Nava GM, Reynoso-Camacho R. Comparison of the bioactive potential of Roselle (Hibiscus sabdariffa L.) calyx and its by-product: Phenolic characterization by UPLC-QTOF MSE and their

anti-obesity effect in vivo. Food Research International 2019;126:108589. https://doi.org/10.1016/j.foodres.2019.108589.

[27] Cn O, Mo C, Fc I, Chukwuma Mo. Phytochemical analysis and medicinal uses of Hibiscus sabdariffa. International Journal of Herbal Medicine 2015;2:16–9.

[28] Adadi P, Kovaleva EG, Glukhareva T V., Shatunova SA, Petrov AS. Production and analysis of non-traditional beer supplemented with sea buckthorn. Agronomy Research 2017;15:1831–45. https://doi.org/10.15159/AR.17.060.

[29] Essiedu JA, Adadi P, Kovaleva EG. Production and characterization of beer supplemented with Hibiscus sabdariffa (Malvaceae). Food Frontiers 2022;3:328–38. https://doi.org/10.1002/fft2.127.

[30] Benzie IFF, Strain JJ. The Ferric Reducing Ability of Plasma (FRAP) as a Measure of "Antioxidant Power": The FRAP Assay. Analytical Biochemistry 1996;239:70–6. https://doi.org/10.1006/ABIO.1996.0292.

[31] Brand-Williams W, Cuvelier ME, Berset C. Use of a free radical method to evaluate antioxidant activity. LWT - Food Science and Technology 1995;28:25–30. https://doi.org/10.1016/S0023-6438(95)80008-5.

[32] Arnao MB, Cano A, Acosta M. The hydrophilic and lipophilic contribution to total antioxidant activity. Food Chemistry 2001;73:239–44. https://doi.org/10.1016/S0308-8146(00)00324-1.

[33] Gören AC, Çikrikçi S, Çergel M, Bilsel G. Rapid quantitation of curcumin in turmeric via NMR and LC-tandem mass spectrometry. Food Chemistry 2009;113:1239–42. https://doi.org/10.1016/j.foodchem.2008.08.014.

[34] Varışlı B, Caglayan C, Kandemir FM, Gür C, Ayna A, Genç A, et al. Chrysin mitigates diclofenac-induced hepatotoxicity by modulating oxidative stress, apoptosis, autophagy and endoplasmic reticulum stress in rats. Molecular Biology Reports 2023;50:433–42. https://doi.org/10.1007/S11033-022-07928-7/FIGURES/4.

[35] Eriten B, Kucukler S, Gur C, Ayna A, Diril H, Caglayan C. Protective Effects of Carvacrol on Mercuric Chloride-Induced Lung Toxicity Through Modulating Oxidative Stress, Apoptosis, Inflammation, and Autophagy. Environmental Toxicology 2024. https://doi.org/10.1002/TOX.24397.

[36] Kucukler S, Benzer F, Yildirim S, Gur C, Kandemir FM, Bengu AS, et al. Protective Effects of Chrysin Against Oxidative Stress and Inflammation Induced by Lead Acetate in Rat Kidneys: a Biochemical and Histopathological Approach. Biological Trace Element Research 2021;199:1501–14. https://doi.org/10.1007/S12011-020-02268-8/TABLES/5.

[37] Farhat C, Younes H, Alyamani OA, Mrad M, Hourani N, Khalifeh H, et al. Chemical characterization and in vitro biological evaluation of aqueous extract of Althaea officinalis L. flower grown in Lebanon. Journal of Herbal Medicine 2022;34:100575.

127

https://doi.org/10.1016/j.hermed.2022.100575.

[38] Böker I, Sendker J, Stark T, Kelber O, Fink C, Hensel A. Cytoprotective effects of aqueous extracts from marshmallow roots (Althaea officinalis L.). Zeitschrift Für Phytotherapie 2012;33. https://doi.org/10.1055/S-0032-1313246.

[39] Tobyn G, Denham A, Whitelegg M. Althaea officinalis, marshmallow; Malva sylvestris, common mallow; Alcea rosea, hollyhock. Medical Herbs 2011:67–78. https://doi.org/10.1016/B978-0-443-10344-5.00013-6.

[40] Formica J V., Regelson W. Review of the biology of quercetin and related bioflavonoids. Food and Chemical Toxicology 1995;33:1061–80. https://doi.org/10.1016/0278-6915(95)00077-1.

[41] Panche AN, Diwan AD, Chandra SR. Flavonoids: An overview. Journal of Nutritional Science 2016;5. https://doi.org/10.1017/JNS.2016.41.

[42] Mahdi Valiei. Chemical composition and antimicrobial activity of the flower and root hexane extracts of Althaea officinalis in Northwest Iran. Journal of Medicinal Plants Research 2011;5. https://doi.org/10.5897/JMPR11.963.

[43] Kadhum HH, Abd AH, Al-Shammari AM. HPLC analysis and chemical composition identification of isolated flavonoid fraction of Althaea officinalis from Iraq. AIP Conference Proceedings 2019;2123. https://doi.org/10.1063/1.5116972.

[44] Kuntz S, Wenzel U, Daniel H. Comparative analysis of the effects of flavonoids on proliferation, cytotoxicity, and apoptosis in human colon cancer cell lines. European Journal of Nutrition 1999;38:133–42.
https://doi.org/10.1007/S003940050054.

[45] Ramos S. Effects of dietary flavonoids on apoptotic pathways related to cancer chemoprevention. The Journal of Nutritional Biochemistry 2007;18:427–42.
https://doi.org/10.1016/J.JNUTBIO.2006.11.004.

[46] Inikpi E, Lawal OA, Ogunmoye AO, Ogunwande IA. Volatile composition of the floral essential oil of Hibiscus sabdariffa L. from Nigeria. ~ 4 ~ American Journal of Essential Oils and Natural Products 2014;2:4–07.

[47] Pino C, Olmo-Mira F, Cabello P, Martínez-Luque M, Castillo F, Roldán MD, et al. The assimilatory nitrate reduction system of the phototrophic bacterium Rhodobacter capsulatus E1F1. Biochemical Society Transactions 2006;34:127–9. https://doi.org/10.1042/BST0340127.

[48] Alara OR, Abdurahman NH. GC–MS and FTIR analyses of oils from Hibiscus sabdariffa, Stigma maydis and Chromolaena odorata leaf obtained from Malaysia: Potential sources of fatty acids. Chemical Data Collections 2019;20:100200. https://doi.org/10.1016/j.cdc.2019.100200.

Bioactive component analysis and *in vitro* antioxidant activities of *Plantago Major* L.

Berna ŞAHİN[1] ID **, Ahmet SAVCI[2*]** ID

[1]Department of Molecular Biology and Genetics, Faculty of Arts and Sciences, Mus Alparslan University, 49250 Mus, Türkiye
Berna ŞAHİN ORCID No: 0009-0008-7176-539X
Ahmet SAVCI ORCID No: 0000-0002-9609-785X

*Corresponding author: a.savci@alparslan.edu.tr

Abstract: *Plantago major* L. (*P. major*) is a plant used by people for medicinal purposes. This study prepared ethanol extract after species identification of *P. major* plant growing in Varto district of Muş. Phenolic content and amount were determined by high pressure liquid chromatography (HPLC). Four different methods were used for antioxidant activities. As a result of the chemical content analysis of the plant, the highest amount of trans-p-cumaric acid (89.0 ng/μL), abscisic acid (11.4 ng/μL) and salicylic acid (8.20 ng/μL) were detected. When the antioxidant results were evaluated, it was observed that the extract scavenged DPPH and ABTS radicals with a power close to that of standard antioxidants. At the same time, the extract significantly reduced Fe^{3+} and Cu^{2+} ions. It was found that the activity of the samples generally increased with increasing absorbance. The fact that there are few studies on the antioxidant activity of *P. major* in the literature makes this study even more important. We hope that this study will shed light on future research on this species.

129

Plantago Major L.'nin biyoaktif bileşen analizi ve *in vitro* antioksidan aktiviteleri

Öz: *Plantago major* L. (*P. major*) halk arasında tıbbi amaçlarla kullanılan bir bitkidir. Bu çalışmada, Muş'un Varto ilçesinde yetişen *P. major* bitkisinin tür tanımlaması yapıldıktan sonra etanol ekstraktı hazırlanmıştır. Fenolik içeriği ve miktarı HPLC ile belirlendi. Antioksidan aktiviteler için dört farklı yöntem kullanıldı. Bitkinin kimyasal içerik analizi sonucunda sırasıyla en yüksek miktarda Trans-p kumarik asit (89.0 ng/μL), Absisik asit (11.4 ng/μL), Salisilik asit (8.20 ng/μL) tespit edildi. Antioksidan sonuçlar değerlendirildiğinde, ekstraktın DPPH ve ABTS radikallerini standart antioksidanlara yakın bir güçle temizlediği gözlenmiştir. Aynı zamanda ekstrakt Fe^{3+} ve Cu^{2+} iyonlarını önemli ölçüde azaltmıştır. Örneklerin aktivitesinin genel olarak absorbans artışıyla birlikte arttığı tespit edilmiştir. Literatürde *P. major*'un antioksidan aktivitesi üzerine sınırlı sayıda çalışma olması bu çalışmayı daha da önemli kılmaktadır. Bu çalışmanın, bu türle ilgili gelecekte yapılacak araştırmalara ışık tutacağını umuyoruz.

1. INTRODUCTION

Molecules with unoccupied electrons in their terminal orbitals are defined as free radicals. An excess of these radicals, which are constantly produced in the body, causes oxidative damage. As a result of oxidative damage, various diseases occur in the body, including cancer, cardiovascular diseases, neurodegenerative diseases, Alzheimer's and immune diseases. Therefore, free radicals must be neutralised by antioxidants [1,2].

Enzymes, the glutathione molecule and hormones, which are endogenous antioxidants, are the molecules responsible for establishing the basic antioxidant balance. However, in addition to these molecules, exogenous molecules may also need to be ingested to scavenge free radicals. Plants, which contain important bioactive components, are the most important members of the exogenous antioxidants [3-5].

Plantago, which belongs to the Plantaginaceae family, is a plant used by the public for medicinal purposes. It is known that this plant, whose leaves, roots, seeds and aerial parts are consumed, is used as a wound healer and in the treatment of skin diseases. This genus, which is represented by about 275 species worldwide, has been

reported to have 22 species in Turkey, two of which are endemic [6,7].

P. major L., whose benefits as a folk medicine have been recognised worldwide for many years, is known to contain a variety of bioactive constituents, including phenolic acid derivatives, flavonoids, terpenoids fatty acids, and, alkaloids, which contribute to its specific healing sides [8]. Various studies have reported that *P. Major* has antioxidant, antibacterial, anti-inflammatory and wound healing properties [9-11]. In this study, we determined the phenolic content of *P.Major* using high pressure liquid chromatography (HPLC). In this research we determined the phenolics of *P. major* using high pressure liquid chromatography (HPLC). We used various *in vitro* methods to determine its antioxidant properties. We believe that this study will guide future studies and make a significant contribution to the literature.

2. MATERIAL AND METHOD

2.1. Plant collection and species identification

P. Major L. was collected in East Anatolia, Muş, Varto district, and the species was determined by Murat Aydın ŞANDA of the Molecular Biology and Genetics Department of Muş Alparslan University. The chemical processes were carried out in the laboratories of Muş Alparslan University.

2.2. Preparation of Extracts

The plants were collected during the growing season (May, 2024) and dried. After species identification, the ethanol extract of the plant was obtained using a Soxhlet apparatus. For the extracts, about 50 g of plant samples were dissolved in 300 mL of ethanol. The extracts were filtered and lyophilised in the laboratories of the Molecular Biology and Genetics Department of Muş Alparslan University.

2.3. Phenolic Compound Analysis by HPLC

Agilent Technologies 1260 Infinity II HPLC device (Agilent, USA) was used to determine the phenolic substance content. Ascorbic acid, gallic acid, 3,4-dihydroxybenzoic acid, 4-hydroxybenzoic acid, trans-p-coumaric acid, myricetin, abscisic acid, quercetin, apigenin, kaempferol, curcumin, catechol, vanillin, caffeic acid, cinnamic acid, rosmarinic acid and salicylic acid (Dr. Ehrenstofer GmbH, Germany) standards were used. The final concentrations of the standards were weighed to be 10 mg/mL and placed in 50 mL volumetric flasks. The prepared standards were prepared by adding 1% acetic acid and 1/9 acetonitrile to the prepared standards. The stock solution required to dissolve the standards was prepared by adding 1/1 methanol to the solution. Stock standards were prepared in 5 different dilutions (100 mM, 75 mM, 50 mM, 25 mM and 10 mM) and loaded onto the HPLC device [12]. For HPLC analysis, 1 mL of the previously prepared ethanol extract was taken, 4 mL of stock solution was added and

vortexed. The mixture was passed through filters with a pore diameter of 0.45 µm and approximately 0.5 mL was transferred into vials. Samples were loaded onto the HPLC device to determine the phenolics in the resulting mixture. As mobile phases, 1% acetic acid was used for solvent A and acetonitrile was used for B. The HPLC configuration consists of 1260 DAD WR detector (272, 280 and 310 nm), 1260 Quat Pump VL pump (1 mL/min flow rate), 1260 Vialsampler (20 µl injected) and G7130A column oven (28 °C). The analytical column used for analysis is ACE 5 C18 (250x4.6 mm id). The necessary procedure and information to load the homogenates we prepared before into HPLC were performed according to our previous study [13].

2.4. Antioxidant Assays

2.4.1. Reducing Power of Fe^{3+} Ions

The reducing power of Fe^{3+} ions to Fe^{2+} ions was determined by Oyaizu method [14]. The volume of the samples (25, 50 and 100 µg/mL) taken in tubes was completed to 200 µL with distilled water. After adding 500 µL each of buffer solution (pH: 6.6) and $K_3Fe(CN)_6$ to each tube, it was incubated for twenty minutes (50 °C). Then 500 µL of trichloroacetic acid (TCA) was added to the mixture. After centrifugation, 500 µL of the supernatant was taken and the same amount of distilled water and 100 µL of $FeCl_3$ were added. Absorbances were measured at 700 nm in a micro-volume spectrophotometer.

2.4.2. Cu^{2+} Ions Reduction Power By CUPRAC Method

After taking different concentrations of extracts and standards into test tubes, their total volumes were made up to 1 mL with distilled water. 0.25 mL each of $CuCl_2$, ethanolic neocuprin and acetate buffer were added. After thirty minutes of incubation, the absorbance values of the samples at 450 nm were recorded [15].

2.4.3. DPPH Radical Scavenging Assay

Ethanol was added to the extracts (25 µg/µL, 50 µg/µL and 100 µg/µL) in test tubes to a final volume of 600 µL. After 200 µL of 1,1-diphenyl-2-picrylhydrazyl (DPPH) solution was added, the reaction was allowed to incubate for about 30 minutes to complete the reaction. Absorbance values at 517 nm were measured with the help of a spectrophotometer [16].

2.4.4. ABTS Radical Scavenging Assay

(2,2′-Azino-bis(3-ethylbenzthiazoline-6-sulfonic acid) (ABTS) solution was diluted with phosphate buffer until the absorbance of the solution reached 0.750 ± 0.025 at 734 nm. After the total volume of the samples was made up to 200 mL with water, 1 mL of $ABTS^{+\cdot}$ solution was added. After 30 minutes of incubation, the absorbance values of the extracts were measured at 734 nm [17].

3. RESULTS

3.1. Phenolic Substance Analysis

The phenolic compound composition of *P. major* analysed by HPLC device was evaluated with the phenolics introduced as standard. The results showed that the extract contained significant amounts of phenolic compounds (**Table 1**). According to the results, the highest amounts of trans-p-cumaric acid (89.0ng/μL), abscisic acid (11.4 ng/μL), salicylic acid (8.20 ng/μL), rosemarinic acid (3.32 ng/μL), ascorbic acid (2.48 ng/μL), myricetin (2.05ng/μL) and cinnamic acid (0.79 ng/μL) were detected in the extract. Chromatograms of the standards and ethanol extract used in HPLC analysis are shown in **Figure 1 and Figure 2.**
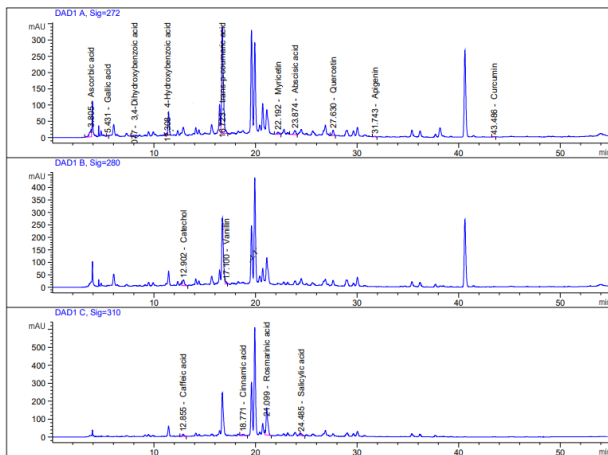
Figure 1. Chromatogram curves of the standards used in HPLC analysis
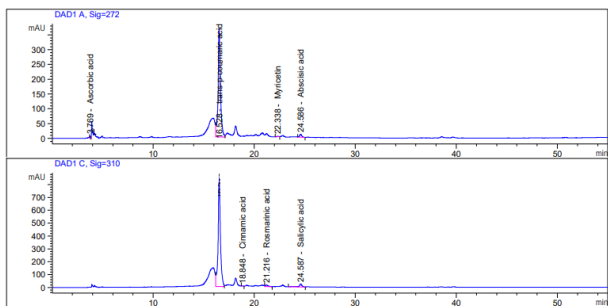
Figure 2. Chromatogram curves of the *P.major* ethanol extract used in HPLC analysis

Table 1. Phenolic substance amounts (ng/μL) by the HPLC analysis results of *P.major* ethanol extract

Phenolics	Amounts
Ascorbic acid	2,483
Gallic acid	-
3, 4-dihydroxybenzoic acid	-
4- hydroxybenzoic acid	-
Trans-p coumaric acid	**89.085**
Myricetin	2.058
Abscisic acid	**11.416**
Quercetin	-
Apigenin	-
Kaemferol	-
Curcumin	-
Catechol	-
Vanillin	-
Caffeic acid	-
Cinnamic acid	0,791
Rosemarinic acid	3.322
Salicylic acid	**8.209**

3.2. Antioxidant Activities

Four different *in vitro* methods were used to determine the antioxidant properties of the extracts. The data obtained as a result of the research showed that *P. major* has strong antioxidant properties. The % activities of extract and standard antioxidants at the highest concentration, FRAP, CUPRAC, DPPH and ABTS are shown in **Table 2**. The FRAP method was preferred to determine the reducing power of ferric ions. According to the experimental results, the extract was found to have lower activity than standard antioxidants (BHA, BHT and AA). However, it was observed that the extract had significant activity and its activities increased as the concentration of the samples increased (**Figure 3**).

Excess iron, one of the most important metals for the organism, can cause several undesirable side effects. Excess Fe^{2+} ions in the environment can be converted to hydroxyl radical, a very dangerous free radical, by the Fenton reaction [21]. Therefore, FRAP is one of the most preferred methods for researchers. In our research, we found that studies on the reducing power of the genus *Plantago* were quite limited. Beara et al. found that extracts of *P. altissima* and *P. lanceolata* strongly reduced ferric ions [18]. Huan et al. reported that polysaccharides from *Plantago asiatica* L. have significant reducing power, but lower than the antioxidant power of BHT [22]. In another study, *P. albicans* ethanol extract was found to have stronger reducing activity than hexane, dichloromethane and acetone extracts and weaker reducing activity than ascorbic acid (AA) [23]. The results of this study generally support previous studies.

Figure 3. Comparison of ferric ion reduction capacities of ethanol extract of *P. major* with standard antioxidants (BHA, BHT and AA)

According to the CUPRAC results of this study, the extract strongly reduced Cu^{2+} ions and had similar performance with standard antioxidants. The activities of all samples were found to increase with increasing concentration (**Figure 4**). In previous studies, no study was found on the reducing power of cupric ions in this plant genus. Therefore, this study may be the first in this area.

131
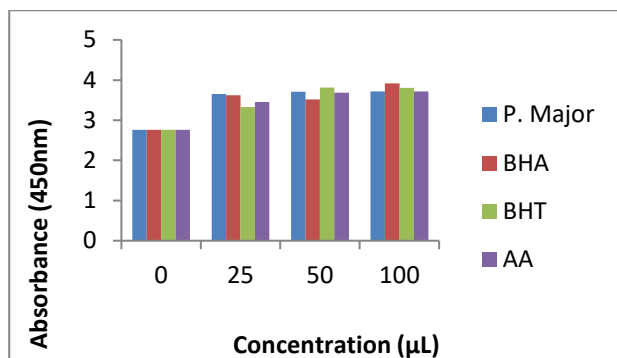
Figure 4. Comparison of cupric ion reduction capacities of ethanol extract of *P. major* with standard antioxidants (BHA, BHT and AA)

According to the results of DPPH radical scavenging activity, it was observed that the extract scavenged radicals very strongly. At the highest concentration (100μg/mL), the DPPH radical scavenging percentages of the samples were as follows: BHA (88.57%) > AA (84.89%) > *P. major* (81.72%) > BHT (64.61%). Furthermore, the activities of the samples increased with increasing concentration (**Figure 5**).
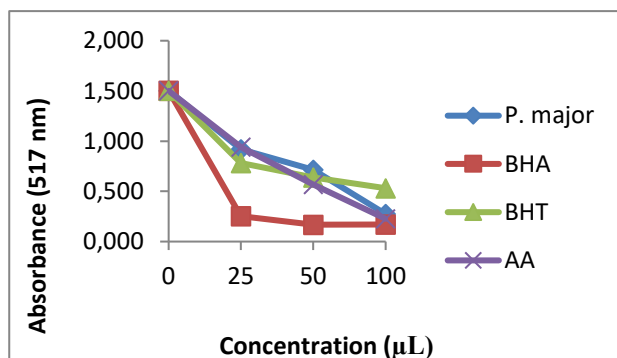
Figure 5. Comparison of DPPH radical scavenging activity of *P. major* extract with standard antioxidants

The ABTS radical scavenging results showed similar data to the DPPH results. It was observed that the activities generally increased with increasing concentration (**Figure 6**). The ABTS radical scavenging percentages of the samples at the highest concentration were ranked as follows: AA (93.10) > BHA (92.50) > P.major (91.05) > BHT (84.52).
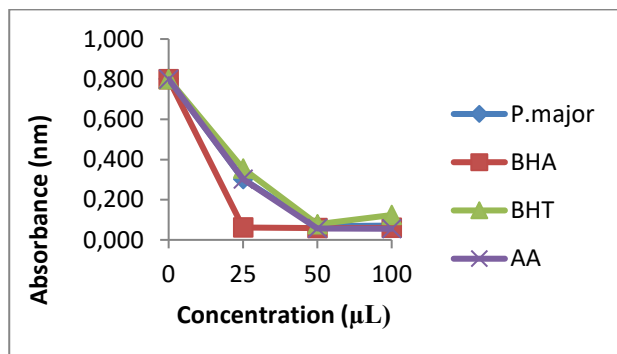
Figure 6. Comparison of ABTS radical scavenging activity of P. major extract with standard antioxidants

Table 2. Antioxidant activities of extract and standart antioxidants at 100μL

Samples (100μL)	Ferric ion reduction capacities (%)	Cupric ion reduction capacities (%)	DPPH radical scavenging activity (%)	ABTS radical scavenging activity (%)
P.major	77.01±0.3	25.61±0.2	81.72±0.1	91.05±0.4
BHA	85.63±0.11	29.36±0.5	88.57±0.3	92.50±0.1
BHT	85.96±0.7	27.43±0.2	64.61±0.3	84.52±0.2
AA	82.60±0.2	25.62±0.8	84.90±0.1	93.10±0.2

4. DISCUSSION AND CONCLUSION

In the literature review, it was observed that the genus *Plantago* contains various bioactive components such as phenolics, flavonoids, terpenes, alkaloids and polysaccharides. According to the research results of Beara et al. it was found that *P. altissima* and *P. lanceolata* extracts were rich in phenolic acids [18]. Significant amounts of p-hydroxybenzoic acid, gallic acid, chlorogenic acid, vanillic acid, luteolin, cinnamic acid and apigenin were detected. Another study reported that *P. major* leaf and seed extracts contained significant amounts of phenolic and flavonoids [19]. Kartini et al. reported that the methanol extract of P. *major* contained significant amounts of chlorogenic acid, caffeic acid, vanillin and p-coumaric acid [20]. Although this study is similar to studies in the literature, there are differences in the content and amounts of phenolic compounds. This could be due to different species, geographical differences, climate change and different solvent usage.

Excess iron, one of the most important metals for the organism, can cause several undesirable side effects. Excess Fe^{2+} ions in the environment can be converted to hydroxyl radical, a very dangerous free radical, by the Fenton reaction [21]. Therefore, FRAP is one of the most preferred methods for researchers. In our research, we found that studies on the reducing power of the genus *Plantago* were quite limited. Beara et al. found that extracts of *P. altissima* and *P. lanceolata* strongly reduced ferric ions [18]. Huan et al. reported that polysaccharides from *Plantago asiatica* L. have significant reducing power, but lower than the antioxidant power of BHT [22]. In another study, *P. albicans* ethanol extract was found to have stronger reducing activity than hexane, dichloromethane and acetone extracts and weaker reducing activity than ascorbic acid (AA) [23]. The results of this study generally support previous studies.
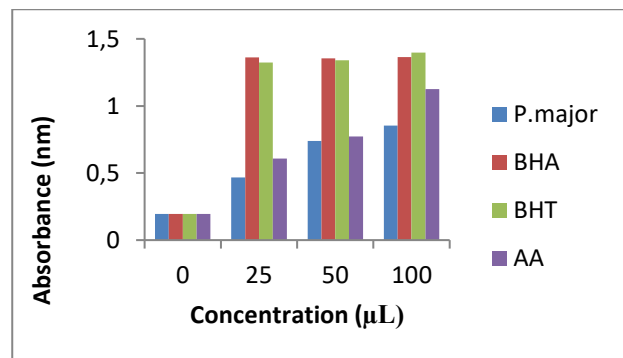
Several studies on the DPPH radical scavenging activity of the genus *Plantago* were found in the literature. Kadri reported that *P. albicans* ethanol extract scavenged DPPH radicals more than other extracts and standard antioxidants. The results of the study were as follows Ethanol (IC50: 19.17) > Acetone (IC50: 21.33) > Aqueous (IC50: 64.33) > Ascorbic acid (IC50: 102.00) > Dichloromethane (IC50: 169.00) > Hexane (IC50: 515.33) [21]. In another study it was reported that *P. ovata* Forssk polysaccharides were very effective in scavenging DPPH radicals [24]. According to the results of the study by Kartini et al., methanol extract of *P. major* scavenged DPPH radicals very strongly [20]. In another study, Bahadori et al. found that methanol extract of *P.*

lanceolata scavenged DPPH radicals strongly according to the results of their study [6]. When the results of this study are compared with previous studies, they are found to be mutually supportive.

In the study by Huan et al. the ABTS radical scavenging activity of *P. asiatica* L. polysaccharides was found to increase with increasing concentration [22]. In another study, water and ethanol extracts of *P. albicans* were found to be more effective in scavenging ABTS radicals than hexane, dichloromethane and acetone extracts [23]. There is no study on the ABTS radical scavenging activity of *P. major*. However, our study is in parallel with studies on other plant species.

Plants rich in phenolic compounds, which are commonly used for medicinal purposes, are antioxidant organisms that act as electron donors to scavenge free radicals. In this study, ethanol extract of *P. major* collected in Muş province was prepared after species identification. Phenolic content and amount were determined by HPLC apparatus. Four different *in vitro* methods were used to determine the antioxidant capacity of the extract. As a result of the chemical content analysis of the plant, the highest amount of trans-p-cumaric acid (89.0 ng/μL), abscisic acid (11.4 ng/μL) and salicylic acid (8.20 ng/μL) were detected. When the antioxidant results were evaluated, it was observed that the extract scavenged DPPH and ABTS radicals with a power close to that of standard antioxidants. At the same time, the extract significantly reduced Fe^{3+} and Cu^{2+} ions. It was found that the activity of the samples generally increased with increasing absorbance. The fact that there are few studies on the antioxidant activity of *P. major* in the literature makes this study even more important. We hope that this study will shed light on future research on this species.

Acknowledgement

REFERENCES

[1] Savcı A, Dicle S. Phenolic Characterization and in vitro Biological Activities of Ranunculus Cornutus DC. Bitlis Eren Üniversitesi Fen Bilimleri Dergisi. 2023, 12: 4, 969–977.

[2] Savcı A, Buldurun K, Kırkpantur G. A new Schiff base containing 5-FU and its metal Complexes: Synthesis, Characterization, and biological activities. Inorg. Chem. Commun., Volume 134, 2021, 109060.

[3] Gonul Baltaci N, Guler C, Ceylan H,, Kalin SN, Adem S, Kocpinar EF et al. In vitro and in vivo effects of iron on the expression andactivity of glucose 6-phosphate dehydrogenase,6-phosphogluconate dehydrogenase, and glutathionereductase in rat spleen. J Biochem Mol Toxicol. 2019, 33: e22229.

[4] Koçpınar EF. Association of the phenolic content, DNA protective activity and some antioxidant properties in the Achillea arabica Kotschy Flower. Bitlis Eren Üniversitesi Fen Bilimleri Dergisi, 2021, 10: 3, 773–783.

[5] Alminderej F, Bakari S, Almundarij TI, Snoussi M, Aouadi K, Kadri A. Antimicrobial and wound healing potential of a new chemotype from Piper cubeba L. Essential oil and in silico study on S. aureus tyrosyl-tRNA synthetase protein. Plants, 2021, 10, 205–224.

[6] Bahadori MB, Sarikurkcu C, Kocak MS, Calapoglu M, Uren MC, Ceylan O. Plantago lanceolata as a source of health-beneficial phytochemicals: Phenolics profile and antioxidant capacity. Food Biosci., 2020, Volume 34, 100536.

[7] Wingren AG, Faik RZ, Holefors A, Filecovic E, Gustafsson A. In vitro effects of undifferentiated callus extracts from Plantago major L, Rhodiola rosea L and Silybum marianum L in normal and malignant human skin cells. Heliyon, 2023, 9: 6, e16480.

[8] Sukweenadhi J, Setiawan KI, Avanti C, Kartini K, Rupa EJ, Yang DC. Scale-up of green synthesis and characterization of silver nanoparticles using ethanol extract of Plantago major L. leaf and its antibacterial potential. S. Afr. J. Chem. Eng., 2021, 38, 1-8.

[9] Zubair M, Wid´en C, Renvert S, Rumpunen K. Water and ethanol extracts of Plantago major leaves show anti-inflammatory activity on oral epithelial cells. J. Tradit. Complement. Med. 2019, 9 (3), 169–171.

[10] Gonçalves S, Romano A. The medicinal potential of plants from the genus Plantago (Plantaginaceae). Ind. Crops Prod. 2016, 83, 213–226.

[11] Zubair M, Nybom H, Lindholm C, Brandner JM, Rumpunen K. Promotion of wound healing by Plantago major L. leaf extracts- Ex-vivo experiments confirm experiences from traditional medicine. Nat. Prod. Res., 2016, 30 (5), 622–624.

[12] Tapan S. Quantitative Hplc Analysis of Phenolic Acids, Flavonoids and Ascorbic Acid in Four Different Solvent Extracts of Two Wild Edible Leaves, Sonchus Arvensis and Oenanthe Linearis of North-Eastern Region in India. Journal of Applied Pharmaceutical Science. 6:2 157-166, 2016.

[13] Savcı, A., E. Koçpınar, Y. Alan, and M. Kurşat. 2020. Antioxidant, antimicrobial, and DNA protection activities of some Tanacetum species and phenolic richness in their ethanolic extracts. International Food Research Journal, 27(1).

[14] Oyaizu M. Studies on Products of Browning Reaction Prepared From Glucose Amin. Jpn. J. Nutr. Diet., 1986, 44:6, 307-315.

[15] Malhi R, Singh I, Carmieli R, Savci A, Sharma R. Copper(II) complexes of fused ring selenosemicarbazones: Synthesis, structure elucidation, biological activity and molecular modeling. Polyhedron, 2023, 233, 116319.

[16] Blois MS. Antioxidant Determinations by the Use of a Stable Free Radical. Nature, 1958, 181:4617, 1199-1200.

[17] Re R, Pellegrini N, Proteggente A, Pannala A, Yang M, Rice-Evans C. Antioxidant activity applying an improved ABTS radical cation decolorization assay. Free Radic. Biol. Med., 1999, 26:9-10, 1231-1237.

[18] Beara IN, Lesjak MM, Orčić DZ, Simin ND, Četojević-Simin DD, Božin BN et al. Comparative analysis of phenolic profile, antioxidant, anti-inflammatory and cytotoxic activity of two closely-related Plantain species: Plantago altissima L. and Plantago lanceolata L. LWT- FOOD SCI TECHNOL, 2012, 47:1, 64-70.

[19] Farid A, Sheibani M, Shojaii A, Noori M, Motevalian M. Evaluation of anti-inflammatory effects of leaf and seed extracts of Plantago major on acetic acid-induced ulcerative colitis in rats. J. Ethnopharmacol., 2022, 298, 115595.

[20] Kartini S, Piyaviriyakul P, Siripong O, Vallisuta. HPTLC simultaneous quantification of triterpene acids for quality control of Plantago major L. and evaluation of their cytotoxic and antioxidant activities, Ind Crops Prod, 2014, 60, 239-246.

[21] Alhafez A, Savci A, Alan Y, Söylemez R, Kilic A. Preparation of Cu(II), Ni(II), Ti(IV), VO(IV), and Zn(II) metal complexes derived from novel vic-dioxime and investigation of their antioxidant and antibacterial activities. Chem. Biodiversity, 2022, 19:3, e202100768.

[22] Huan C, Zhang R, Xie L, Wang X, Wang X, Wang X et al. Plantago asiatica L. polysaccharides: Physiochemical properties, structural characteristics, biological activity and application prospects: A review. Int. J. Biol. Macromol., 2024, 258: 2, 128990.

[23] Kadri A. Comprehensive phytochemical analysis of various Plantago albicans solvent extracts and their potential antioxidant and antimicrobial effects. Biocatal Agric Biotechnol., 2023, 53, 102886.

[24] Nuerxiati R, Mutailifu P, Lu C, Abuduwaili A, Aierken A, Yang Z et al. Optimization of alkali extraction, structure, and antioxidant activity of protein-bound polysaccharide from seeds of Plantago ovata Forssk. Ind Crops Prod, 2022, 183, 114920.

134

Türk Doğa ve Fen Dergisi
Turkish Journal of Nature and Science

BINGÖL UNIVERSITY

Optimizing Weight in Gear Wheels with Different Filling Geometries

Hanife KARA[1*] iD **, Mahir UZUN** iD

[1]Inonu University, Engineering Faculty, Mechanical Engineering Department, Malatya, Türkiye
[2] Inonu University, Engineering Faculty, Mechanical Engineering Department, Malatya, Türkiye
Hanife KARA ORCID No: 0000-0003-3087-748X
Mahir UZUN ORCID No 0000-0002-0907-6875

Corresponding author: mahir.uzun@inonu.edu.tr

Abstract: Gears are important machine elements widely used in industry. A mechanism can consist of only two gears, while in more complex systems, gears of different sizes and numbers are used. However, the use of a large number of gears can increase the weight and cost of the machine. The production methods developed with today's technology allow for the easy production of all kinds of geometries. In this study, in order to minimize the weight of spur gears, triangular, square and hexagonal shaped infill geometries were applied to the gear body. Designs with different edge lengths and infill thicknesses were modeled with SolidWorks software and finite element analysis was performed in ANSYS software. As a result of the analyses, it was determined that the square profile design offered the lightest solution. When compared to the unfilled design, a 63.65% reduction in weight was achieved.

Farklı Dolgu Geometrilerine Sahip Dişli Çarklarda Ağırlığın Optimize Edilmesi

Öz: Dişli çarklar, endüstride yaygın olarak kullanılan önemli makine elemanlarıdır. Bir mekanizma yalnızca iki dişli çarktan oluşabileceği gibi, daha karmaşık sistemlerde farklı boyutlarda ve sayılarda dişliler kullanılmaktadır. Ancak, fazla sayıda dişli çarkın kullanımı makine ağırlığını ve maliyetini artırabilmektedir. Günümüz teknolojisiyle gelişen üretim yöntemleri, her türlü geometrinin kolayca üretilmesine olanak tanımaktadır. Bu çalışmada, düz dişli çarkların ağırlığını minimuma indirmek amacıyla, çark gövdesine üçgen, kare ve altıgen şekillerinde dolgu geometrileri uygulanmıştır. Farklı kenar uzunlukları ve dolgu kalınlıklarına sahip tasarımlar, SolidWorks yazılımı ile modellenmiş ve ANSYS yazılımında sonlu elemanlar analizi gerçekleştirilmiştir. Analizler sonucunda, kare profilli tasarımın en hafif çözüm sunduğu belirlenmiştir. Dolgusuz tasarımla karşılaştırıldığında, ağırlıkta %63,65 oranında bir azalma elde edilmiştir.

1. INTRODUCTION

Gear systems play a crucial role in power transmission and regulating mechanical motion. Widely used across industries such as manufacturing, automotive, and aerospace, these systems are continuously optimized for performance, durability, and energy efficiency. In recent years, topology optimization has emerged as a prominent method in gear design. This approach is recognized as a powerful tool for reducing structural weight and enhancing mechanical performance [1-3].

Studies on the potential of topology optimization in gear design demonstrate its ability to balance lightweight and durability. Ramadani et al. [4] explored the feasibility of using this method to design low-vibration, lightweight gear bodies. Patel and colleagues [5] highlighted that topology optimization could significantly reduce weight while improving energy efficiency in automotive applications.

Asymmetric tooth designs in gear systems have gained attention as an alternative method to enhance mechanical performance. Kapelevich [6] emphasized that such designs increase tooth strength, thereby extending

operational life. Similarly, Song and Kim [7] investigated the impact of asymmetric tooth geometries on vibration reduction.

Material selection and heat treatment techniques have also been comprehensively examined for their effects on the performance of gear systems. Sharma et al. [8] demonstrated the positive impact of heat treatment on durability, while Doğan and Kamer [9] emphasized that additive manufacturing methods enable the production of optimized gear designs with reduced material usage. Additive manufacturing also facilitates the creation of complex geometries.

The integration of lattice structures has been identified as a significant innovation for lightweight and high-strength gear designs. Kara and Altun [10] noted that these structures are effective in reducing weight. Additionally, Maiti et al. [11] examined the impact of composite materials on lightweight gear systems, highlighting their advantages in vibration control and durability, which support modern design approaches.

Understanding and controlling the vibration behavior of gear systems is crucial for overall performance. Li et al. [12] analyzed how vibration characteristics can be optimized through material choices. Furthermore, studies on lubrication techniques to minimize energy losses in gear systems are noteworthy. Xu and Zhang [13] reported the positive effects of innovative lubrication solutions on energy efficiency.

Moreover, artificial intelligence and machine learning methods have ushered in a new era in gear design. Wang and Chen [14] demonstrated how these methods could be employed to rapidly generate optimized designs. It is anticipated that these technologies will play a significant role in the design of more complex systems in the future.

2. MATERIAL AND METHOD

In the study, the material to be used in gear designs was first determined. For this purpose, Polyamide (PA), a polymer material frequently used in engineering applications and easily producible through additive manufacturing, was selected. To obtain the mechanical properties of the material, a Type IV tensile test specimen was designed according to the ASTM D638 (ASTM, 2014) standard [9].
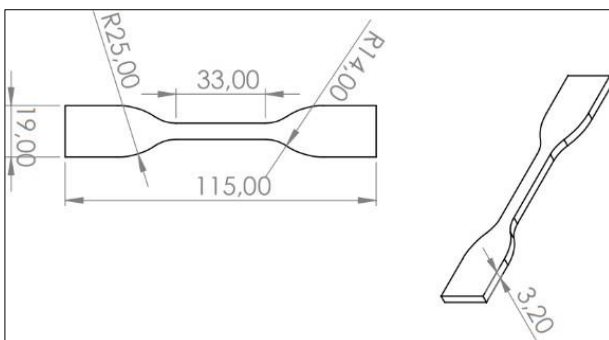
Figure 1. Tensile test specimens

To obtain the mechanical properties of the Polyamide material, a Polyamide filament from Flashforge was procured. The designed test specimen was produced using the FDM method. An industrial 3D printer, the CoreMax600 Pro, was used for the production of the test specimens. The specimens were tested using the Shimadzu AGS-X tensile testing machine available at our university. The tensile test was conducted on the specimens using the Shimadzu AGS-X tensile testing machine with a 10 kN load capacity, maintaining a grip distance of 65 mm. The tests were carried out at a tensile speed of 5 mm/min until the specimens experienced failure. Five Polyamide (PA-Nylon) specimens were subjected to testing, and their mechanical properties were compared after the tensile tests.

Figure 2. Tensile testing setup

Table1. Test results

Number	Yield Strength (Mpa)	Young's Modulus (Mpa)
1	87,621	2540,129
2	93,503	2744,989
3	83,899	2459,031
4	79,552	2502,065
5	85,166	2635,595
Average	**85,9482**	**2576,3618**

2.1. Modeling of Gear Wheels

In the subsequent phase of the study, individual gear models were created using SolidWorks. The solid models were then analyzed using the finite element analysis (FEA) software ANSYS Workbench. The CAD model of the spur gear involved in this study was created with the following design parameters:

- *Module (m): 4 mm*
- *Number of teeth (z): 25*
- *Pressure angle (α): 20°*
- *Gear width: 20 mm*
- *Shaft diameter: 20 mm*

During the design process of the gear wheels, the Equations dialog box in SolidWorks was used. The equations that define the geometric dimensions of the gear were imported into SolidWorks, and these parameters were applied to model the gear accurately.

The gear's tooth profile was designed as an involute profile. To generate this profile, involute profile equations were entered into the curve drawing command in SolidWorks, enabling the creation of the precise tooth profile.
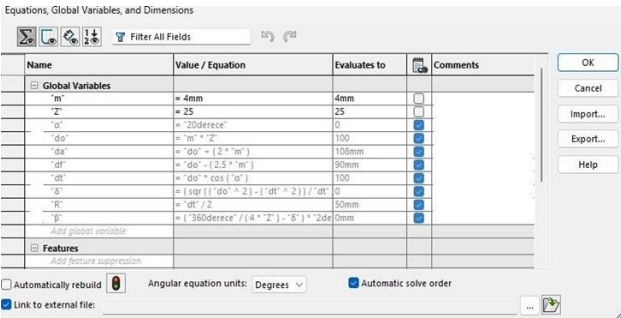
Figure 3. Equation Used in Solidworks

Subsequently, the gear model was created in SolidWorks using these equations throughout all stages of the design.
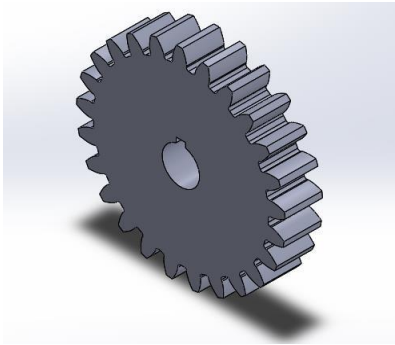
Figure 4. Model of Spur Gear

In the study, triangular, hexagonal, and square geometries were utilized for the gear designs. The designs were made in such a way that there were no gaps in the gear body, with 4 different edge lengths and 4 different fill thicknesses for each geometry. For the hexagonal geometry, a total of 16 gear designs were created using edge lengths of 6 mm, 8 mm, 10 mm, and 12 mm, and fill thicknesses of 1.5 mm, 2 mm, 2.5 mm, and 3 mm. As an example, visual representations of gears with the same thicknesses but different edge lengths are provided.
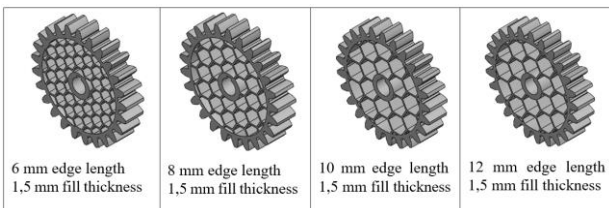
Figure 5. Hexagonally Geared Designs

For the square geometry, a total of 16 gear designs were created using edge lengths of 10, 12, 14, and 16 mm, and fill thicknesses of 1.5, 2, 2.5, and 3 mm. Visual representations of gears with the same thicknesses but different edge lengths are provided as examples.
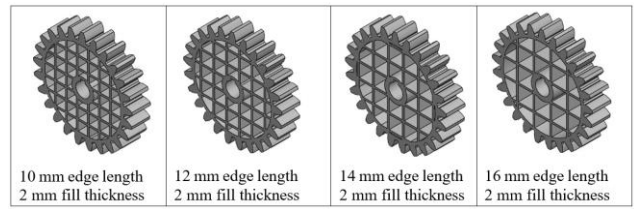
Figure 6. Square Geometry Gear Designs

For the triangular geometry, a total of 16 gear designs were created using edge lengths of 12, 14, 16, and 18 mm, and fill thicknesses of 1.5, 2, 2.5, and 3 mm.
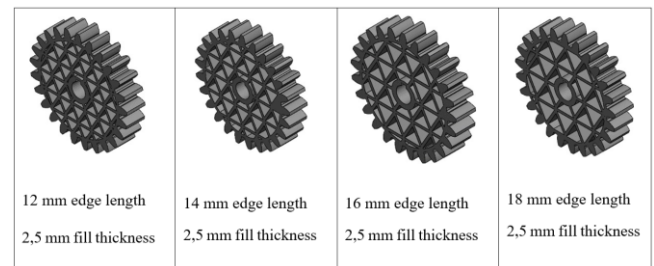
Figure 7. Triangle Geometry Gear Designs

2.2. Finite Elements Analysis

In the analysis phase, the analysis of a standard spur gear, which had not undergone any material removal, was first performed. Subsequently, analyses of the specially designed spur gear models were conducted in the static-structural mode of ANSYS Workbench 2020 R1.

Initially, the designs were created in SolidWorks. The designed gear models were then imported into ANSYS. For the solid models introduced into ANSYS, Polyamide (PA), the most commonly used material in gear manufacturing, was assigned, taking into account both cost considerations and material preference.

As another step in the finite element analysis, meshing was performed. The mesh applied to the gear models significantly impacts the analysis results. Initially, a default mesh was applied, and the sizing command was used to improve the mesh quality. After completing the meshing process, boundary conditions were defined. The gear wheels were fixed at the shaft hole, and loading was applied to the tooth profile, as shown in Figure 8.
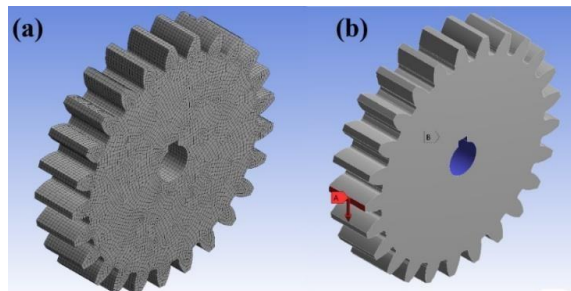
Figure 8. Finite Element Model of the Gear: (a) Mesh Structure and (b) Boundary Conditions

137

In the analyses performed, forces of 250N, 500N, 750N, 1000N, and 1250N were applied incrementally to the samples. The force at which yield stress was reached was considered as the failure load.
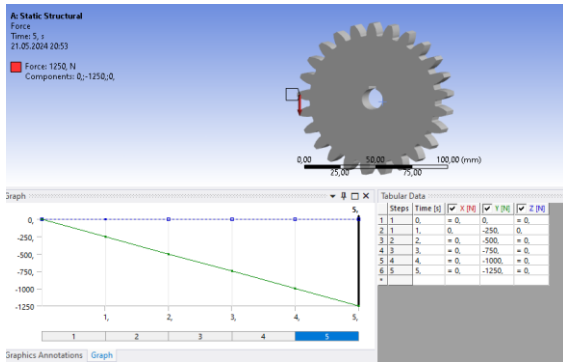
Figure 9. Applied Loads in the Finite Element Model

The same boundary conditions were applied to all gear models, and stress analyses under load were performed. The Von-Mises maximum stress values from the stress analyses were used as the basis for evaluation.
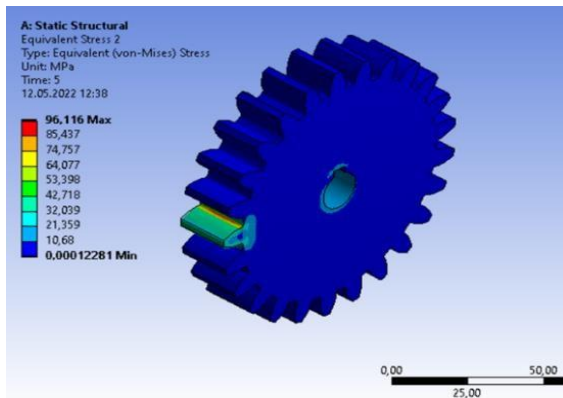
Figure 10. Von-Mises Stress Distribution of the Untreated Spur Gear

In Figure 10, the stresses resulting from the applied loads on the spur gear are shown step by step. As expected, the yield stress was reached at the tooth root and along the line. The force at which yield stress was achieved was considered the failure load. Yield stress was reached at step 4.5, with the applied force being 1125 N. Thus, the untreated spur gear reached yield stress at 1125 N.
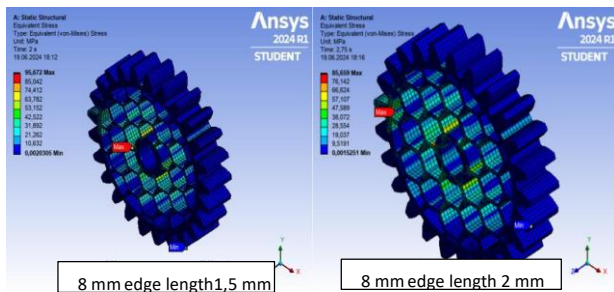
Figure 11. Von-Mises Stress Distribution of Hexagonal Geometry Gears with 8 mm Edge Length and 1.5 mm and 2 mm Fill Thicknesses
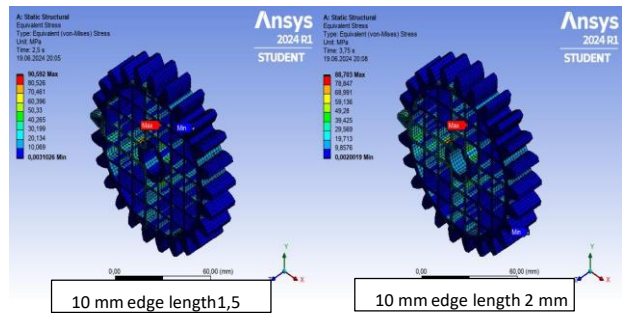
Figure 12. Von-Mises Stress Distribution of the Square Geometry Gear with 10 mm Edge Length and 1.5 mm and 2 mm Fill Thicknesses
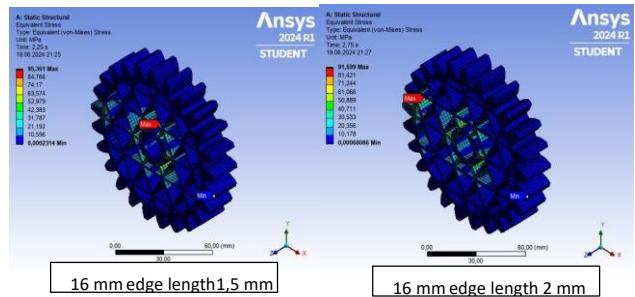
Figure 13. Von-Mises Stress Distribution of the Triangular Geometry Gear with 16 mm Edge Length and 1.5 mm and 2 mm Fill Thicknesses

In the designed gears, it is desired that the maximum stress always occurs at the tooth root for each loading condition. For the triangular geometry, this condition is achieved with a fill thickness between 1.5 mm and 2 mm. At 1.5 mm thickness, the maximum stress appears on the body and in different regions of the geometry and edge lengths. This stress distribution indicates that these areas may fail under operating conditions. However, when the thickness is increased to 2 mm, it is observed that the body is safe, and the maximum stress shifts to the tooth root (Figures 11-13).

3. RESULTS AND DISCUSSION

Initially, designs were created for gears with triangular, square, and hexagonal geometries on the gear body, using 4 different edge lengths and 4 different fill thicknesses. Stress analyses of the designed gears were conducted using the ANSYS program to evaluate their performance under load.

The analysis showed that in fully filled spur gears, the maximum stress occurred at the tooth **root**, which is typical for spur gear designs. For gears where material was removed from the body, it was observed that the stresses increased as the material was removed toward the **center** of the gear. The material removal process continued until the stresses were reduced to a level below the yield stress, thus achieving the goal of reaching the optimal weight without compromising the strength of the gear. The weights of the designs were obtained using SolidWorks and compared with the weight of the untreated spur gear to assess the effectiveness of the material reduction.

During the gear selection process, the gears where the maximum stresses were concentrated at the tooth root under loading conditions were considered optimal. Gears where maximum stresses appeared on the gear body were excluded from consideration, as these areas would likely be more prone to failure or damage during operation. This careful approach ensured that only the designs with the most reliable stress distribution and optimal performance were chosen for further evaluation.

10 mm edge length 3 mm fill thickness   14 mm edge length 1,5 mm fill thickness   16 mm edge length 1,5 mm fill thickness
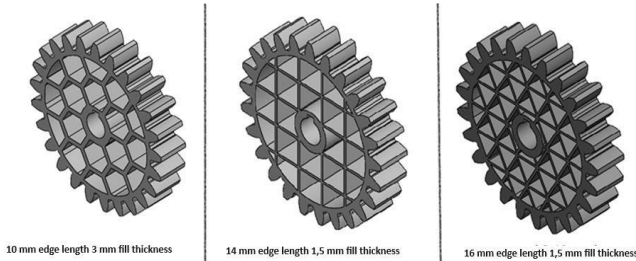
Figure 14. Optimum Gears for All Geometries

Among all the designs and weights, the lightest gear was achieved with the square geometry. This gear represented a significant weight reduction of 63.65%, marking a groundbreaking achievement in the literature for such a substantial weight reduction.

The use of lightweight gears offers several advantages in mechanical systems. First, reducing the weight of the gears helps decrease the overall weight of the system, leading to improved energy efficiency. As the weight decreases, the friction and energy losses in the system are also minimized. This not only leads to energy savings but also improves the balance and stability of mechanical systems, enabling machines to operate with greater precision and efficiency. Additionally, lightweight gears are easier to handle and assemble, simplifying the logistics and labor involved in manufacturing and maintaining the system.

With the continuous advancement in technology, further reductions in gear weight can be achieved by exploring different gear geometries and incorporating artificial neural networks into the design process. These innovations hold great potential for optimizing gear performance, enhancing energy savings, and reducing material usage, contributing to the development of more sustainable and efficient mechanical systems.

Acknowledgements

5. REFERENCES

[1] Ramadani, R., Belsak, A., Kegl, M., Predan, J., & Pehan, S. (2018). Topology Optimization Based Design of Lightweight and Low Vibration Gear Bodies. International Journal of Simulation Modelling, 17(1), 92-104.

[2] Karpat, F., Çavdar, K., & Babalık, F. C. (2002). Bilgisayar Yardımıyla Düz, Helisel, Konik ve Sonsuz Vida Dişli Mekanizmalarının Boyutlandırılması ve Analizi. Mühendis ve Makine Dergisi, 510.

[3] Akpolat, A. (2020). Analysis of Contact Stresses in Spur Gears by Finite Element Method. Avrupa Bilim ve Teknoloji Dergisi, (17), 539-545.

[4] Patel, M., Valiulla, H., Khatod, V., Chaudhary, B., & Gondalia, V. (2019). Topology Optimization of Automotive Gear Using FEA. International Journal of Recent Technology and Engineering, 8(4), 1079-1084.

[5] Ayyıldız, M., Çiçek, A., & Fuat, K. (2010). Bilgisayar Destekli Tasarımda Parametrik Dişli Çark Uygulamaları. Gazi Üniversitesi Mühendislik Mimarlık Fakültesi Dergisi, 25(3).

[6] Kapelevich, A. (2000). Geometry and Design of Involute Spur Gears with Asymmetric Teeth. Mechanism and Machine Theory, 35(1), 117-130.

[7] Doğan, O., & Kamer, M. S. (2022). Eklemeli İmalat Yöntemi ile Optimum Düz Dişli Çark Tasarımı ve Üretimi. Bitlis Eren Üniversitesi Fen Bilimleri Dergisi, 10(3), 1093-1103.

[8] Kramberger, J., Šraml, M., Glodež, S., Flašker, J., & Potrč, I. (2004). Computational Model for the Analysis of Bending Fatigue in Gears. Computers & Structures, 82(23–26), 2261-2269.

[9] ASTM. (2014). D638. Standard Test Method for Tensile Properties of Plastics. American Society for Testing and Materials Standard.

[10] Sharma, A., Gupta, R., & Mehta, P. (2017). Effect of Heat Treatment on Weight Reduction and Performance of Spur Gears. Materials Today: Proceedings, 4(8), 7657-7663.

[11] Maiti, S., Singh, K., & Das, S. (2019). Composite Materials in Spur Gear Applications: A Weight Reduction Perspective. Journal of Composite Materials, 53(4), 453-465.

[12] Sharma, P., Singh, R., & Gupta, M. (2020). Topology Optimization for Lightweight Gear Design. Advances in Mechanical Engineering, 12(6), 113-122.

[13] Tiwari, D., Mishra, A., & Verma, V. (2021). Combined Material Removal and Surface Treatment for Weight Reduction in Helical Gears. International Journal of Precision Engineering and Manufacturing, 22(3), 345-355.

[14] Singh, R., Kaur, H., & Sandhu, K. (2019). Geometric Design Optimization of Spur Gears with Advanced Filling Techniques. Mechanics and Design Journal, 6(2), 231-242.

139

[15] Kara, S., & Altun, M. (2022). The Impact of Lattice Structures on Weight Reduction of Gears. Mechanical Systems and Signal Processing, 35(8), 101234.

Türk Doğa ve Fen Dergisi
Turkish Journal of Nature and Science

www.dergipark.gov.tr/tdfd

BINGÖL UNIVERSITY

Color Response of Turfgrass Cultivars to Gibberellic Acid under Mediterranean Climate Conditions

Emre KARA[1]* (iD) **, Mustafa SÜRMEN[1]** (iD) **, Türkan METİN[1]** (iD) **Bekir Sami GÜNGÖR[1]** (iD)

[1] Aydın Adnan Menderes University, Faculty of Agriculture, Department of Field Crops, Aydın, Türkiye
Emre KARA ORCID No: 0000-0002-5535-8398
Mustafa SÜRMEN ORCID No: 0000-0001-9748-618X
Türkan METİN ORCID No: 0009-0000-0073-3990
Bekri Sami GÜNGÖR ORCID No: 0009-0005-6597-1937

*Corresponding author: emre.kara@adu.edu.tr

Keywords
Color,
Turfgrass,
Plant growth regulator,
Turfgrass quality

Abstract: Plant growth regulators (PGRs) are broadly used in turfgrass management. Gibberellic acid is also applied in many plants due to its positive effects on plant growth and development. However, some studies have indicated that these applications may have a negative effect on color. The study aimed to find out the effect of different doses of gibberellic acid applications on visual quality in different turfgrass species. Gibberellic acid was applied as control, 0.05 and 0.1 kg ha^{-1}. Among the turfgrass species, twenty different cultivars of four different species were used as material in the experiment. Although studies have demonstrated that this plant growth regulator enhances stress tolerance, it has been observed to diminish color values (L, a*, b*). Visual quality is a crucial aspect of lawns. The study also revealed that grass varieties exhibited differential responses to gibberellic acid with respect to visual quality and color properties.

141

Akdeniz İkliminde Renk Bakımından Çim Çeşitlerinin Giberellik Aside Tepkisi

Anahtar Kelimeler
Renk,
Çim,
Bitki büyüme düzenleyicisi
Çim kalitesi

Öz: Bitki büyüme düzenleyicileri çim alan yönetiminde yaygın olarak kullanılmaktadır. Giberellik asit de bitki büyümesi ve gelişimi üzerindeki olumlu etkileri nedeniyle birçok bitkide uygulanmaktadır. Ancak, bazı çalışmalar bu uygulamaların renk üzerinde olumsuz bir etkiye sahip olabileceğini göstermiştir. Bu çalışma, farklı çim türlerinde farklı dozlarda giberellik asit uygulamalarının görsel ve renk kalitesi üzerindeki etkisini bulmayı amaçlamıştır. Giberellik asit kontrol, 0.05 ve 0.1 kg ha^{-1} olarak uygulanmıştır. Çim türleri arasında 4 farklı türün 20 farklı çeşidi denemede materyal olarak kullanılmıştır. Görsel kalite, görsel derecelendirme sistemi kullanılarak değerlendirilmiştir. Renk kalitesi spektrofotometre kullanılarak incelenmiştir. Genel olarak, giberellik asit kullanımının görsel kalite üzerinde olumsuz etkileri olduğu gözlenmiştir. Bu bitki büyüme düzenleyicisinin stres koşullarına karşı direnci artırdığını gösteren çalışmalar olmasına rağmen renk değerleri (L, a*, b*) açısından düşüşlere neden olduğu gözlenmiştir. Görsel kalite çim alanlar için çok önemlidir. Çalışma neticesinde ayrıca çim çeşitlerinin görsel kalite ve renk özellikleri bakımından giberellik aside farklı tepkiler verdiği gözlemlenmiştir.

1. INTRODUCTION

Turfgrass is a vital component of urban and suburban landscapes, offering functional, environmental, and aesthetic advantages. Studies have shown that turfgrasses play a role in reducing soil erosion, surface runoff, and safeguarding water quality [1]. Additionally, they aid in carbon sequestration, nutrient cycling, and maintaining water quality [2]. Turfgrass also helps mitigate the impacts of urban sprawl in rapidly urbanizing societies [3] and it is good for menthal health. The economic significance of the turfgrass industry is substantial, driven by factors such as property development, environmental

benefits, and the aesthetic appeal of turfgrass in urban environments [4].

Turfgrass color is a critical aspect of turfgrass quality due to its aesthetic significance. Studies have emphasized the importance of turfgrass color in enhancing the visual quality of turfgrass [5]. The color of turfgrass is a key characteristic that significantly influences its overall quality and appeal to consumers [6]. Maintaining an intense green color in turfgrass is essential for improving its aesthetic value and increasing consumer acceptance [6]. Additionally, turfgrass color is commonly used as a primary indicator of its quality conditions [7].

The color of turfgrass is influenced by various factors such as fertilization, genetic characteristics, and environmental conditions. Nitrogen is crucial for maintaining turfgrass density and color, as well as enhancing its resistance and recovery from stress [8]. Studies have shown that the application of colorants can enhance turfgrass color and quality, especially during stressful and dormant periods [9,10]. Moreover, the genetic color of turfgrass cultivars plays a significant role in achieving the desired aesthetic value of turfgrass [11]. Furthermore, research has underscored the significance of color differentiation in turfgrass studies, as it has ramifications for a multitude of facets of turfgrass research, including the utilization of pesticides, fertilizers and cultivars. [12]. Digital image analysis is a valuable method for quantifying turfgrass color and evaluating turfgrass quality in research studies [13].

Gibberellic acid (GA) has been identified as a key regulator affecting various aspects of plant growth and development, including turfgrass. Gibberellin application resulted usually in the yellowing of grass leaves. This effect can be reduced by higher nitrogen fertilization. Gibberellic Acid is used in sports facilities to extend the period of exploitation from early spring to late autumn. Research has shown that GA application can enhance growth rates in turfgrass, potentially aiding in the recovery of injured areas by promoting growth in the surrounding turf [14]. Moreover, GA has been linked to regulating shoot elongation in higher plants, which is crucial for managing turfgrass effectively [15]. However, it is thought that it may have a negative effect on the color quality of grass. In this study conducted for this purpose, the effects of different doses of gibberellic acid on the color quality of twenty different grass species in the Mediterranean climate were examined.

2. MATERIAL AND METHOD

2.1. Study site

The field study was established at Aydın Adnan Menderes University (Aydın, Türkiye) Research and experimental fields (37° 45' 51" N, 27° 45' 32" E, 27 m altitude) as a split-plot experiment in randomized block design with three replications in 2023-2024. The soil in which the experiment was conducted had an alkaline, sandy-loamy texture, low organic matter content, and an adequate amount of mineral matter, based on samples taken before to the experiment (Table 1.).

Table 1. Soil traits of the experiment field (0-30 cm)

P ppm	K ppm	Ca ppm	Mg ppm	Na ppm	Fe ppm	pH	Total Salt (%)	Organic Matter (%)
19	903	2740	1164	46	8.32	8.16	0.0093	1.20

When the climate data taken during the turfgrass vegetation period in the area where the experiment was carried out were compared with the long-term means, it was observed that the experimental year was warmer and drier in terms of average temperatures. Especially high winter temperatures caused a faster growth in all turfgrass species (Table 2.).

Table 2. Some climate variables for the years 2023, 2024 and long-term mean*

	Mean Temperature (°C)		Total Precipitation (mm)	
Months	2023/24	LTM	2023/24	LTM
September	24.8	23.9	22.1	43.8
October	19.7	18.8	2.2	79.9
November	15.9	13.4	151.4	40.9
December	11.7	9.4	95.1	50.9
January	9.5	8.2	74.2	27.8
February	10.4	9.4	6.1	13.4
March	12.7	12.1	5	17.9
April	19.1	16.2	21.9	10.0
Total	15.4	13.9	378	573.7

LTM: Long term mean: 1985-2022.

2.2. Field management

A total of 20 cultivars of four different species were used in the experiment. These cultivars are generally the ones that can be evaluated in mixtures and used intensively in turfgrass areas. Information about the varieties is given in Table 3.

Table 3. Cultivars of the experiment

Lolium perenne L.	*Festuca arundinacea* L.	*Poa pratensis* L.	*Festuca rubra rubra*
Belida	Sergei	Zeptor	Kolossos
Sox Fan	Greenfront	Geisha	
Blackstone	Eye Candy		
Troya	Tomcat-1		
Monsieur	Brockton		
Stravinsky	Jaguar AG		
Spark	Meister		
Ankyra	Starlett		
Essence			

The experiment was conducted with three replications, with 75 grams of grass seed applied per square meter. Irrigation was performed on a daily basis until germination, utilizing an oscillating garden lawn irrigation nozzle that allowed for the precise control of its width. The first mowing process took place when the plants reached a height of 15 cm. The mowing operations were carried out with AL-KO HIGHLINE 46.5 P-A gasoline lawnmower from a height of 7-8 cm in order not to affect any kind of development. No herbicide was applied for weed control in the trial, and Fiskars® Stand-up Weed Puller (4-claw) was used to remove weeds. Turfgrasses were fertilized with mineral fertilizers at rates: 180 kg N ha^{-1}, 60 kg P$_2$O$_5$ ha^{-1}, and 120 kg K$_2$O ha^{-1} before sowing. From March onwards, a fertilization rate of 50 kg N ha^{-1} was applied following each mowing, marking the onset of active growth. Gibberellic acids were applied in March 2024 at three rates (control, 0.05, 0.1 kg PGR ha^{-1}) with knapsack sprayer. Irrigation was done with sprinkler irrigation systems according to the water capacity of the field only when the plant needs it.

2.3. Measurements

The color parameters such as L* (Lightness), a* (Red to green), and b* (yellow to blue) of the samples were determined by using a colorimeter (Hunter lab, Color flex EZ model: 45°/0°). Then, the CIE L*a*b* values related to each sample were recorded separately. The chroma was assessed following the methodology outlined by Rezah et al. [16]. The Commission Internationale de l'Eclairage (CIE) Lab color system was used to compute color parameters in relation to the D65 illuminant standard. The projection of color components is represented by this CIELab system on the axes L, a, and b. Lightness is represented by the L value, which is 100 for white and 0 for black. The chromatic coordinates that are described by the values a and b are green-red and blue-yellow, respectively. A hue of green or blue is represented by a negative an or b, and a hue of red or yellow by a positive an or b, respectively. In accordance with the National Turfgrass Evaluation Program (NTEP) in the United States [17,18] turfgrass quality was measured on a scale of 1 to 9, with the lowest score indicating broad leaf, very poor appearance, and light green turfgrass, and the highest score indicating thin

leaves, a very good appearance, and dark green turfgrass. Three turfgrass characteristics were assessed: leaf texture, overall appearance, and turfgrass color. Green canopy cover measured by Canopeo was maesured at after gibberellic acid application. Canopeo is a tool developed for measuring fractional green canopy cover in various vegetation types, including turfgrass. It utilizes color ratios of red to green (R/G) and blue to green (B/G) along with an excess green index to assess canopy cover [19]. Research has shown that Canopeo is effective in estimating green coverage of living turfgrasses, although additional calibration may be necessary for colorant-treated turfgrasses [20]. Measurements were carried out 30 days after the application of the treatments.

2.4. Statistical analysis

Statistical analyses were performed using R Studio (v4.1.2) [21]. The Shapiro–Wilk test was used to determine the distribution of normality. The relationships between the traits were analyzed at $p < 0.01$ level of significance by using analysis of variance and LSD test in randomized completely block design as split plots.

3. RESULTS AND DISCUSSION

Turfgrass cultivars had significantly different color characteristics. However, they all had in common their response to gibberellic acid application doses. Yellowish and lighter leaves appeared as gibberellic acid application increased. For L* values, the interaction was significantly different. Higher gibberellic acid doses resulted in lighter leaves (L = 38.46). Among the cultivars, *Festuca arundinacea* cv. Greenfront had the lightest character (L= 42.39). However, the control treatment of this variety was also lightest. The darkest (L= 31.34) turfgrass cultivar was *Lolium perenne* cv. Blackstone. The stunning result was that the increase in gibberellic acid dose in this turfgrass cultivar did not increase the lighter properties of the turfgrass color much. Since the cultivars had their genetic characteristics, the changes in all of them were at different levels (Table 4.).

143

Table 4. Effect of gibberellic acid application on turfgrass color CIELab (L*) parameter.

Cultivar/Doses	L*			Mean**
	Control	0.05 kg ha⁻¹	0.1 kg ha⁻¹	
Lp-Belida	38.90	39.98	42.95	40.61 c
Fa- Sergei	39.13	39.17	41.94	40.08 d
Pp-Zeptor	38.46	39.62	40.34	39.47 e
Fa-Greenfront	41.77	42.07	43.33	42.39 a
Fa-Eye Candy	29.10	34.81	35.94	33.28 k
Lp-Sox Fan	29.04	35.18	36.44	33.55 jk
Lp-Blackstone	30.81	31.46	31.76	31.34 m
Lp-Truva	30.12	31.90	34.40	32.14 l
Fa-Tomcat	32.24	32.13	36.32	33.56 jk
Lp-Monsieur	31.10	33.48	36.81	33.79 ıj
Fa-Brockton	34.66	37.90	37.98	36.84 h
Pp-Geisha	38.09	38.98	39.04	38.70 f
Lp-Stravinsky	38.17	41.32	41.73	40.40 cd
Frr-Kolossos	39.69	41.46	42.31	41.15 b
Lp-Spark	32.02	38.73	41.26	37.34 g
Fa-Jaguar AG	33.74	37.92	40.62	37.43 g
Fa-Meister	31.03	32.56	36.78	33.46 jk
Lp-Ankyra	31.88	33.60	34.72	33.40 jk
Fa-Starlett	32.73	33.55	35.94	34.07 l
Lp-Essence	29.96	32.05	38.63	33.54 jk
Mean**	34.13 c	36.39 b	38.46 a	

cv:1.28 LSDcul: 0.43, LSDdoses: 0.17; **mean values with different letters are significantly different ($p < 0.01$).

In terms of a* mean values, significantly different characteristics were observed for both varieties and doses. Higher green (a*= -8.668) was observed with the increase in dose. However, the increase in green color does not show a characteristic alone. At the same time, b* averages should also be examined together. The increase in b* characteristic leads to an increase in the yellowish characteristic. The b* values, which we will explain after expressing the differences between grass varieties, also increased with the increase in gibberellic acid dose. Among the turfgrass cultivars, the highest green (a*=-9.317) was obtained with *Festuca arundinacea* cv. Brockton. The lowest was obtained with *Lolium perenne* cv. Spark and *Festuca arundinacea* cv. Sergei. As observed in Lightness values, the averages of this character also showed different results according to genetic differences (Table 5.).

Table 5. Effect of gibberellic acid application on turfgrass color CIELab (a*) parameter.

Cultivar/Doses	a*			Mean**
	Control	0.05 kg ha⁻¹	0.1 kg ha⁻¹	
Lp-Belida	-8.256	-8.670	-8.760	-8.562 j
Fa- Sergei	-5.943	-7.603	-8.320	-7.288 a
Pp-Zeptor	-6.503	-9.513	-9.700	-8.572 j
Fa-Greenfront	-7.353	-8.690	-9.270	-8.437 j
Fa-Eye Candy	-6.673	-9.050	-9.350	-8.357 hj
Lp-Sox Fan	-6.960	-9.040	-9.666	-8.555 j
Lp-Blackstone	-7.280	-8.193	-8.706	-8.060 fg
Lp-Truva	-7.696	-7.893	-8.283	-7.957 eg
Fa-Tomcat	-7.473	-7.636	-9.403	-8.171 gı
Lp-Monsieur	-7.476	-7.686	-8.600	-7.921 eg
Fa-Brockton	-8.736	-9.553	-9.663	-9.317 l
Pp-Geisha	-8.626	-8.783	-9.153	-8.854 k
Lp-Stravinsky	-7.546	-7.636	-7.753	-7.645 bd
Frr-Kolossos	-8.026	-8.053	-8.263	-8.114 gh
Lp-Spark	-7.083	-7.290	-7.673	-7.348 a
Fa-Jaguar AG	-6.763	-7.920	-7.593	-7.425 ab
Fa-Meister	-7.390	-7.573	-8.226	-7.730 ce
Lp-Ankyra	-8.076	-8.266	-8.850	-8.397 ıj
Fa-Starlett	-6.720	-8.343	-8.453	-7.838 df
Lp-Essence	-7.183	-7.576	-7.683	-7.481 ac
Mean**	-7.388 a	-8.248 b	-8.668 c	

cv:3.52 LSDcul:0.266 LSDdoses:0.103; **mean values with different letters are significantly different ($p < 0.01$).

Significantly different traits were observed for the b* character in relation to the a* parameter. Likewise, the interaction was significant as in all traits. This character, in which yellowish was observed in a certain way, had higher values with the increase in dose. In this respect, the highest result (b*= 18.26) was obtained with 0.1 kg ha⁻¹. Although it was observed that *Poa pratensis* cv. Zeptor was the yellowest among the varieties (b*=24.68), when the control group was controlled, it was observed that this variety was more yellow than the other varieties before the plant growth regulator application. In this respect, the most striking yellowing was observed in *Festuca arundinacea* cv. Eye Candy. The variety average with the lowest yellow color pigment was *Lolium perenne* cv. Sox Fan, cv. Blackstone (Table 6.).

Table 6. Effect of gibberellic acid application on turfgrass color CIELab (b*) parameter.

Cultivar/Doses	b* Control	0.05 kg ha^{-1}	0.1 kg ha^{-1}	Mean**
Lp-Belida	17.78	18.80	19.03	18.53 d
Fa- Sergei	17.88	21.30	21.75	20.31 c
Pp-Zeptor	23.65	24.99	25.40	24.68 a
Fa-Greenfront	12.96	18.79	19.76	17.17 fg
Fa-Eye Candy	12.46	17.03	17.50	15.66 ı
Lp-Sox Fan	11.89	13.86	14.84	13.53 l
Lp-Blackstone	11.76	14.03	14.33	13.37 l
Lp-Truva	14.78	18.27	19.05	17.37 ef
Fa-Tomcat	13.55	14.81	22.41	16.92 g
Lp-Monsieur	13.41	13.94	17.02	14.79 jk
Fa-Brockton	21.57	23.39	23.68	22.88 c
Pp-Geisha	15.86	16.87	17.88	16.87 g
Lp-Stravinsky	14.04	15.13	15.53	14.90 j
Frr-Kolossos	16.41	16.75	17.10	16.75 g
Lp-Spark	14.04	14.37	14.87	14.43 k
Fa-Jaguar AG	14.88	15.57	16.41	15.62 ı
Fa-Meister	13.06	17.07	17.53	15.89 hı
Lp-Ankyra	16.76	17.87	18.34	17.66 e
Fa-Starlett	14.66	16.86	17.00	16.17 h
Lp-Essence	14.00	15.22	15.83	15.01 j
Mean**	15.27 c	17.24 b	18.26 a	

cv:2.64 LSDcul: 0.41 LSDdoses: 0.16; **mean values with different letters are significantly different ($p < 0.01$).

It was observed that gibberellic acid treatments caused statistical differences at the level of ($p < 0.01$) in terms of canopy cover and visual quality among turfgrass species. The changes observed in terms of color characteristics were in the same direction in terms of canopy cover and visual quality characters. It was determined that gibberellic acid treatments decreased the canopy cover as well as the color quality. Compared to the control treatment, all but three varieties were observed above 90% cover. *Lolium perenne* cv. Stravinsky was the cultivar that was observed to be more affected by canopy cover with gibberellic acid application. *Lolium perenne* cv. Essence was the least affected variety and had the highest average value (97.49%). The effect of gibberellic acid on visual quality was determined by visual rating. Decreases in visual quality were observed due to yellowish. The highest visual quality value was obtained from the control with 6.75. Although there were different visual values among the varieties, *Festuca arundinacea* cv. Starlett had a higher visual quality (6.33). The rapid decline in visual quality was observed with *Lolium perenne* cv. Truva (Table 7.).

145

Table 7. Effect of gibberellic acid application on turfgrass canopy cover and visual quality

Cultivar/Doses	Canopeo (Canopy Cover%)** Control	0.05 kg ha^{-1}	0.1 kg ha^{-1}	Mean	Visual Quality(1-9)** Control	0.05 kg ha^{-1}	0.1 kg ha^{-1}	Mean
Lp-Belida	92.70	87.66	87.37	89.24 f	6.00	4.33	3.33	4.55 hı
Fa- Sergei	98.37	95.69	94.68	96.24bc	6.33	5.33	4.00	5.22 dg
Pp-Zeptor	97.41	97.58	91.41	95.47cd	6.33	4.66	3.33	4.77 gı
Fa-Greenfront	90.37	87.25	86.52	88.05 f	5.66	5.00	4.00	4.88 fh
Fa-Eye Candy	98.69	92.51	92.16	94.45de	7.00	5.33	4.33	5.55 be
Lp-Sox Fan	98.40	95.44	92.22	95.35cd	6.66	6.00	5.00	5.88 ab
Lp-Blackstone	96.05	98.49	95.92	96.82ab	7.00	5.00	3.33	5.11 eg
Lp-Truva	86.48	79.81	77.53	81.27 ı	8.00	4.00	2.66	4.88 fh
Fa-Tomcat	95.14	87.76	83.98	88.96 f	7.00	5.33	3.00	5.11 eg
Lp-Monsieur	98.98	96.89	96.34	97.40ab	8.00	5.33	4.33	5.88 ab
Fa-Brockton	85.09	84.15	81.77	83.67 h	6.00	5.00	3.33	4.77 gı
Pp-Geisha	97.92	97.28	93.61	96.27ac	6.00	5.00	3.33	4.77 gı
Lp-Stravinsky	98.37	80.95	80.56	86.62 g	6.00	5.00	4.00	5.00 fh
Frr-Kolossos	97.47	95.03	90.90	94.47de	5.66	4.33	3.00	4.33 ı
Lp-Spark	95.99	95.66	92.36	94.67de	7.66	5.66	4.00	5.77 bc
Fa-Jaguar AG	97.70	97.22	87.02	93.98 e	6.33	6.00	4.66	5.66 bd
Fa-Meister	96.05	92.87	92.96	93.96 e	8.00	4.66	3.33	5.33 cf
Lp-Ankyra	94.54	89.43	80.67	88.21 f	7.00	5.00	2.66	4.88 fh
Fa-Starlett	87.19	80.89	77.03	81.70 ı	7.33	5.66	6.00	6.33 a
Lp-Essence	98.14	97.76	96.56	97.49 a	7.00	5.00	3.00	5.00 fh
Mean**	95.05 a	91.51 b	88.58 c		6.75 a	5.08 b	3.73 c	

cv:1.44 LSDcul: 1.23, LSDdoses:0.47, cv:10.74 LSDcul:0.52 LSDdoses:0.20 ; **mean values with different letters are significantly different ($p < 0.01$).

Gibberellic acid, a plant growth regulator, has been extensively studied for its effects on plant pigments. While gibberellic acid is known to positively influence various aspects of plant growth and development, such as stem elongation, germination, and flowering [22], there is evidence suggesting that it can have negative effects on plant coloration. Research has shown that gibberellic acid can alter the contents of pigments in plants. For instance, a study on the application of gibberellic acid on Asarum europaeum L. cut leaves found that gibberellic acid affects the biosynthesis of photosynthetic pigments [23]. Additionally, the application of gibberellic acid, along with other phytohormones, was found to increase pigment content in salinized wheat plants [24]. Gibberellic acid is reported to have very positive effects on tillering, growth and root characteristics in plants [25]. However, there is also striking information that gibberellic acid applications in particular yellowish turfgrass species [26]. In a study on this subject, the effect of different plant growth regulators on turfgrass species was examined. The results clearly indicated that gibberellic acid caused color loss in turfgrass species [17]. Despite its positive properties, this study aimed to examine the effects on color loss, canopy cover and visual quality in different turfgrass species. The fact that the studies on this subject are in different species and there are not enough studies on this subject has revealed the necessity of this study for turf areas where color quality is very important. It is also stated that the color loss problem that will occur in turf color and quality can be reduced by using higher nitrogen fertilizer [27].

4. CONCLUSION

Gibberellic acid (GA) is a plant growth regulator widely used in agriculture and turfgrass areas to enhance plant growth and development. GA promotes cell elongation and division, resulting in increased shoot growth and overall turf vigor. This can be particularly advantageous during the early growing season or in cool climates where turfgrass might otherwise be slow to green up. Additionally, the application of GA can improve the grass's stress tolerance. It aids in strengthening the turf against environmental stresses such as drought, salinity, and extreme temperatures, making it more resilient and maintaining its aesthetic appeal under challenging conditions. However, there are some considerations to keep in mind when using GA on turfgrass. Different turfgrass species respond differently to GA, so understanding the specific needs and responses of the turfgrass being managed is essential. At the same time, striking results were obtained in this study based on the potential that gibberellic acid applications may cause yellowing of turfgrass color and changes in visual quality for these and similar reasons. In the study conducted on different species varieties, the negative effects of gibberellic acid applications on canopy coverage, especially in the establishment year, were revealed. In terms of color values, decreases in green color quality were detected especially with increasing dose. Different responses were observed among species.

REFERENCES

[1] Philocles S, Torres A, Patton A, Watkins E. The adoption of low-input turfgrasses in the midwestern us: the case of fine fescues and tall fescue. Horticulturae. 2023;9(5):550.

[2] Bauer S, Lloyd D, Horgan B, Soldat D. Agronomic and physiological responses of cool-season turfgrass to fall-applied nitrogen. Crop Science. 2012;52(1):1-10.

[3] Brosnan JT, Chandra A, Gaussoin RE, Kowalewski A, Leinauer B, Rossi FS, et al. A justification for continued management of turfgrass during economic contraction. Agricultural & Env Letters. 2020;5(1).

[4] Haydu JJ, Hodges AW, Hall CR. Economic Impacts of the Turfgrass and Lawncare Industry in the United States. EDIS. 2006;(7).

[5] Salehi H, Khosh-Khui M. Turfgrass Monoculture, Cool-Cool, and Cool-Warm Season Seed Mixture Establishment and Growth Responses. HortSci. 2004;39(7):1732-5.

[6] Santos PLFd, Silva PST, Matos AMS, Alves ML, Nascimento MVLd, Castilho RMMd. Aesthetic and sensory quality of Emerald grass (Zoysia japonica) as a function of substrate cultivation and mineral fertilization. Ornam Hortic. 2020;26(3):381-9.

[7] Kazemi F, Golzarian MR, Rabbani Kheir Khah SM. Quality and Establishment of Some Water-Conserving Turfgrass Species for Sustainable Development and Some Ecosystem Services in Arid Urban Environments. Land. 2024 May 21;13(6):721.

[8] Baldwin CM, Brede AD. Quantifying Nitrogen Requirement for Creeping Bentgrass Putting-Green Cultivars. Agronomy Journal. 2012 Sep;104(5):1208-16.

[9] Shearman R, Wit L, Severmutlu S, Budak H, Gaussoin R. Colorant Effects on Dormant Buffalograss Turf Performance. horttech. 2005;15(2):244-6.

[10] Pinnix GD, McCauley RK, Miller GL. Air Temperature Effects on Turfgrass Colorant Transfer. Crop Forage & Turfgrass Mgmt. 2018;4(1):1-6.

[11] Serba DD, Hejl RW, Burayu W, Umeda K, Bushman BS, Williams CF. Pertinent Water-Saving Management Strategies for Sustainable Turfgrass in the Desert U.S. Southwest. Sustainability. 2022;14(19):12722.

[12] Berndt WL, Karcher DE, Richardson MD. Color-distance modeling improves differentiation of colors in digital images of hybrid bermudagrass. Crop Science. 2020;60(4):2138-48.

[13] Karcher DE, Richardson MD. Quantifying Turfgrass Color Using Digital Image Analysis. Crop Science. 2003;43(3):943-51.

[14] Barker WL, Beam JB, Askew SD. Effects of Rimsulfuron Lateral Relocation on Creeping Bentgrass (Agrostis stolonifera). Weed technol. 2005;19(3):647-52.

[15] Tan Z, Qian Y. Light Intensity Affects Gibberellic Acid Content in Kentucky Bluegrass. HortSci. 2003;38(1):113-6.

[16] Rezaei S, Ghobadian B, Ebadi M, Jangi F, Ghomi H. Effects of cold plasma on the color parameters of Hyssop (Hyssopus officinalis L.) using color imaging instrumentation and spectrophotometer. Color Research & Application. 2020;45(1):29-39.

[17] Głąb T, Szewczyk W, Gondek K. Response of Kentucky Bluegrass Turfgrass to Plant Growth Regulators. Agronomy. 2023;13(3):799.

[18] Whitman B, Iannone BV, Kruse JK, Unruh JB, Dale AG. Cultivar blends: A strategy for creating more resilient warm season turfgrass lawns. Urban Ecosyst. 2022;25(3):797-810.

[19] Patrignani A, Ochsner TE. Canopeo: A Powerful New Tool for Measuring Fractional Green Canopy Cover. Agronomy Journal. 2015;107(6):2312-20.

[20] Chhetri M, Fontanier C. Use of Canopeo for Estimating Green Coverage of Bermudagrass during Postdormancy Regrowth. hortte. 2021;31(6):817-9.

[21] R Core Team, R language and environment for statistical computing. R Foundation for Statistical. Computing, 2020.

[22] El-Sheikh MA, Rajaselvam J, Abdel-Salam EM, Vijayaraghavan P, Alatar AA, Devadhasan Biji G. Paecilomyces sp. ZB is a cell factory for the production of gibberellic acid using a cheap substrate in solid state fermentation. Saudi Journal of Biological Sciences. 2020;27(9):2431-8.

[23] Pogroszewska E, Joniec M, Rubinowska K, Najda A. Effect of pre-harvest application of gibberellic acid on the contents of pigments in cut leaves of Asarum europaeum L.. Acta Agrobot. 2014;67(2):77-84.

[24] Aldesuquy H. Synergistic effect of phytohormones on pigment and fine structure of chloroplasts in flag leaf of wheat plants irrigated by seawater. Egyptian Journal of Basic and Applied Sciences. 2015;2(4):310-7.

[25] Abdullah BS, Abdulrahman YA. Effect of different concentrations of gibberellic acid on seeds germination and growth in different turf grass genera. Kufa Jour. Agri. Sci. 2017;9(2):226-247.

[26] Christians NE, Patton AJ, Law QD. Fundamentals of Turfgrass Management. John Wiley & Sons: Hoboken, NJ, USA, p. 480, 2017.

[27] Matthew C, Hofmann WA, Osborne MA. Pasture response to gibberellins: A review and recommendations. New Zealand Journal of Agricultural Research. 2009;52(2):213-25.

Türk Doğa ve Fen Dergisi
Turkish Journal of Nature and Science
www.dergipark.gov.tr/tdfd

BINGÖL UNIVERSITY

Retrospective Analysis of Extremity Fractures in Cats: 288 Cases (2018-2023)

Ali GÜLAYDIN[1*] , Nihat ŞINDAK[1] , Mustafa Barış AKGÜL[1] , Müzzemil Hattap SOYSAL[2] ,
Onur YILDIRIM[1] , Sevdet KILIÇ[1] , Maruf YILMAZ[1] , Bahar ERDEN[1]

[1] Siirt University, Faculty of Veterinary Medicine, Department of Surgery, Siirt, Türkiye
[2] Siirt University, Institute of Health Sciences, Department of Veterinary Surgery, Siirt, Türkiye

Ali GÜLAYDIN ORCID No: 0000-0002-7200-1040
Nihat ŞINDAK ORCID No: 0000-0003-0431-8940
Mustafa Barış AKGÜL ORCID No: 0000-0002-9365-9925
Müzzemil Hattap SOYSAL ORCID No: 0009-0002-6760-8494
Onur YILDIRIM ORCID No: 0000-0002-5462-6100
Sevdet KILIÇ ORCID No: 0000-0003-1033-658X
Maruf YILMAZ ORCID No: 0009-0009-6757-7457
Bahar ERDEN ORCID No: 0000-0002-8775-6673

*Corresponding author: a.gulaydin@siirt.edu.tr

Abstract: This retrospective study analyzed the prevalence, etiology, and treatment methods of limb fractures in 288 cats that were admitted to the Siirt University Animal Health Application and Research Hospital between 2018 and 2023 with trauma-related fractures. The findings revealed that the most common fractures occurred in the femur (47.91%), tibia-fibula (22.56%), and humerus (11.45%). It was determined that 56.25% of the fractures were caused by unknown traumas, 23.95% by fall from heights, and 19.79% by traffic accidents. In terms of treatment approaches, surgical intervention was preferred in complex cases, while cage rest and medical treatment [(0.3 mg/kg for 3 days meloksikam (Meloxicam, Bavet, Tuzla, İstanbul, Türkiye)] were chosen for simpler fractures. Surgical treatment was applied in 54.3% of femur fractures and 67.6% of tibia-fibula fractures. These findings highlight that the fracture type and severity of trauma are key factors in determining the appropriate treatment strategy for feline limb fractures. The research findings will contribute to future studies on the most frequently broken bones in cats, the rates of surgical or conservative treatment of these fractures, and various factors that may affect treatment choices. Conducting more comprehensive studies on the subject will make significant contributions to the literature and to veterinary clinicians.

Kedilerde Ekstremite Kırıklarının Retrospektif Analizi: 288 Olgu (2018-2023)

Anahtar Kelimeler
Kedi,
Kırık,
Medikal tedavi,
Retrospektif,
Cerrahi tedavi

Öz: Bu retrospektif çalışmada, 2018-2023 yılları arasında Siirt Üniversitesi Hayvan Sağlığı Uygulama ve Araştırma Hastanesi'ne getirilen ve travmaya bağlı ekstremite kırığı tespit edilen 288 kedide kırıkların prevalansı, etiyolojisi ve tedavi yöntemleri analiz edildi. Bulgular, en sık görülen kırıkların femur (%47,91), tibia-fibula (%22,56) ve humerus (%11,45) kemiklerinde meydana geldiğini gösterdi. Olguların %56,25'inin sebebi bilinmeyen travmalar, %23,95'inin yüksekten düşme ve %19,79'unun da trafik kazası nedeniyle meydana geldiği belirlendi. Tedavi yaklaşımlarında, kompleks vakalarda operatif müdahale ön plana çıkarken, daha basit kırıklarda ise kafes istirahati ve medikal tedavi tercih edildi. Femur kırıklarının %54,3 ve tibia-fibula kırıklarının ise %67,6'sında operatif tedavi yöntemi uygulandı. Çalışmadan elde edilen veriler kedilerde ekstremite kırıklarının tedavisinde doğru tedavi stratejisinin belirlenmesinde kırık türü ve travma şiddetinin önemli faktörler olduğunu gösterdi. Araştırma bulguları, kedilerde en sık kırılan kemikler, bu kırıkların cerrahi veya konservatif yöntemlerle sağaltım oranları ve tedavi seçimlerini etkileyebilecek çeşitli faktörler üzerine ileride yapılacak olan çalışmalara katkı sağlayacak nitelikte olup, konuyla ilgili daha kapsamlı çalışmaların yapılması literatür bilgiye ve klinisyen veteriner hekimlere önemli katkılar sunacaktır.

148

1. INTRODUCTION

A fracture is defined as the complete or partial disruption of bone integrity. The clinical signs of fractures include lameness, swelling, abnormal mobility, and crepitus, and these signs vary depending on the affected bone, the fracture's location, and type (transverse, oblique, comminuted, spiral, etc.) [1, 2]. In cats, limb fractures are more common than other types of fractures [3]. Studies report that femur fractures are the most frequently observed, with hind limb fractures occurring more often than forelimb fractures [2, 4-7].

The etiology of fractures in cats and dogs includes fall from heights, traffic accidents, human-induced injuries, animal bites, and unknown traumas [1, 7-10]. The incidence of fractures in cats varies depending on factors such as age, gender and activity level. Younger, more active cats are at higher risk of fractures due to fall from heights, traffic accidents, fights, or pathological conditions that weaken the bones [2].

Understanding fracture biomechanics and classification is critical for effective treatment, as these factors guide surgical techniques and postoperative care strategies [2, 11]. According to Farghali et al. [2], fracture classification should consider the cause of the fracture, whether it is open or closed, the severity of bone damage, the number of fragments, the direction of the fracture line, the location, bone stabilization, the severity of soft tissue damage, and the time of occurrence.

Bone fractures in cats can be treated using various operative and conservative treatment methods (cage rest+medical treatment). Treatment options include external and internal fixation, supportive bandaging, cage rest, and limb amputation. The choice of appropriate treatment depends on the type of fracture, availability of necessary orthopedic implants, and the owner's consent [6, 12, 13].

This retrospective study aims to provide descriptive data on the prevalence, etiology, and types of fractures in cats presented to Siirt University Animal Health Application and Research Hospital between 2018 and 2023, with an emphasis on the demographic characteristics of the affected cats, including age, gender and breed.

2. MATERIAL AND METHOD

In this retrospective study, data from 288 cats of various breeds, ages, and genders, admitted to Siirt University Animal Health Application and Research Hospital between 2018 and 2023 with limb fractures confirmed by clinical and radiological examinations, were analyzed.

The cats were classified by age into three groups: 0-1 year (excluding one-year-olds), 1-2 years (including one- and two-year-olds), and >2 years (excluding two-year-olds). They were also categorized by breed as mixed breed, British Shorthair, Scottish Fold, Van cat, Ankara cat, Siamese, and Persian cat.

Affected bone was assessed based on the anatomical position of the fracture line. In addition, the etiology of the fractures was classified into categories such as unknown trauma, traffic accidents, and fall from heights. The treatment options applied were evaluated as surgical interventions and conservative tratments.

Ethical Approvment: This study is not subject to the permission of HADYEK in accordance with the "Regulation on Working Procedures and Principles of Animal Experiments Ethics Committees" 8 (k). The data, information and documents presented in this article were obtained within the framework of academic and ethical rules.

3. RESULTS

This study evaluated 288 cases of limb fractures diagnosed among 1,524 cats admitted to Siirt University Animal Health Application and Research Hospital between 2018 and 2023, representing 18.89% of the total cases. The annual distribution of cases was recorded as 10.7% (n=31) in 2018, 19.7% (n=57) in 2019, 27% (n=78) in 2020, 18% (n=52) in 2021, 12.8% (n=37) in 2022, and 11.4% (n=33) in 2023. The highest incidence of fractures was observed in 2020, followed by a decline in cases after 2021.

Of the 288 cats evaluated, 50.69% (n=146) were male and 49.30% (n=142) were female. In terms of age distribution, 46.87% (n=135) were in the 0-1 year group, 43.05% (n=124) in the 1-2 year group, and 10.06% (n=29) were 2 years or older. Breed distribution showed that 79.51% (n=229) of the cats were mixed breed, 6.59% (n=19) were British Shorthair, 5.55% (n=16) were Scottish Fold, 3.81% (n=11) were Van cats, 2.08% (n=6) were Ankara cats, 1.38% (n=4) were Siamese cats, and 1.04% (n=3) were Persian cats (Table 1).

In terms of etiology, 56.25% (n=162) of the fractures were caused by unknown trauma, 23.95% (n=69) were due to fall from heights, and 19.79% (n=57) resulted from traffic accidents. The anatomical distribution of fracture etiology is shown in Table 2.

The treatment methods applied to the cases are presented in Table 3. The findings indicate that both cage rest combined with conservative treatment and surgical intervention combined with medical treatment [(0.3 mg/kg for 3 days meloksikam (Meloxicam, Bavet, Tuzla, İstanbul, Türkiye)] were utilized. All cases received medical treatment, and femur and tibia-fibula fractures were the most common fracture types requiring surgical intervention.

Table 1. Distribution of signalment information for the cases included in the study, along with the etiology and anatomical localization of the fractures identified.

Signalement	n	%
Male	146	50.69
Female	142	49.30
0-1 Age	135	46.87
1-2 Age	124	43.05
>2 Age	29	10.06
Mixed Breed	229	79.51
British Shorthair	19	6.59
Scottish Fold	16	5.55
Van Cat	11	3.81
Ankara Cat	6	2.08
Siamese cats	4	1.38
Persian Cat	3	1.04
Etiology of Fractures		
Fall From Heights	69	23.95
Unknown Traumas	162	56.25
Traffic Accidents	57	19.79
Affected Bones		
Femur	138	47.91
Tibia- Fibula	65	22.56
Humerus	33	11.45
Radius-Ulna	20	6.94
Metacarpus	19	6.59
Metatarsus	13	4.51
Total	**288**	**100**

Table 2. Distribution of fractures according to their etiological data in the cases.

Fractures	Unknown Traumas	Fall From Heights	Traffic Accidents	Total
Femur	73 (52.89%)	33 (23.91%)	32 (23.18%)	138 (47.91%)
Tibia- Fibula	36 (55.38%)	15 (23.07%)	14 (20.53%)	65 (22.56%)
Humerus	15 (45.45%)	11 (33.33%)	7 (21.21%)	33 (11.45%)
Radius-Ulna	17 (85%)	3 (15%)	0	20 (6.94%)
Metacarpus	12 (63.15%)	4 (21.05%)	3 (15.78%)	19 (6.59%)
Metatarsus	9 (69.23%)	3 (23.07%)	1 (7.69%)	13 (4.51%)
Total	162 (%56.25)	69 (23.95%)	57 (19.79%)	288 (100%)

Table 3. Distribution of treatment methods applied for the diagnosed fractures.

Fractures	Cage Rest + Medical Treatment	Surgical Treatment + Medical Treatment	Total
Femur	63 (45.6%)	75 (54.3%)	138 (100%)
Tibia- Fibula	21 (32.3%)	44 (67.6%)	65 (100%)
Humerus	13 (39.3%)	20 (60.6%)	33 (100%)
Radius-Ulna	7 (35%)	13 (65%)	20 (100%)
Metacarpus	8 (42.1%)	11 (57.8%)	19 (100%)
Metatarsus	6 (46.1%)	7 (53.8%)	13 (100%)
Total	118 (40.9%)	170 (59%)	288 (100%)

4. DISCUSSION AND CONCLUSION

This study provides a retrospective evaluation of feline limb fractures diagnosed over the past five years at Siirt University Animal Health Application and Research Hospital. It differs from previous studies by focusing solely on cats and comprehensively evaluating fractures in all limb regions.

Previous research has shown that hind limb fractures, particularly femoral fractures, are the most common in cats [2, 4, 7, 8]. The finding in our study that femur fractures were the most prevalent is consistent with these prior findings. In our study, fractures were most frequently observed in the femur, followed by the tibia-fibula, humerus, radius-ulna, metacarpal, and metatarsal bones. These results align with other studies in the literature. For instance, Farghali et al. [2] found that femur fractures were the most common, followed by tibia-fibula, humerus, radius-ulna, and other bones. Similarly, Ali [8] also reported femur as the most frequently fractured bone, but found radius-ulna fractures to be more prevalent than tibia-fibula fractures.

Thus, the affected bones in our study shows similarities with Farghali et al. [2] and partial agreement with Ali [8].

The etiology of feline limb fractures shows significant variability. Studies by Scott and McLaughlin [14] and Piermattei et al. [15] have identified traffic accidents and fall from heights as the leading causes of fractures in cats. However, our study revealed a different distribution of trauma etiology. In our findings, the most common cause of fractures was unknown trauma (56.25%), followed by fall from heights (23.95%) and traffic accidents (19.79%). The high incidence of unknown trauma is likely due to the fact that many of the patients were stray cats, and the history provided by municipal workers or animal welfare volunteers may have been incomplete. Additionally, environmental factors, living conditions, and regional traffic patterns may have influenced this distribution. Stray cats, living without control and exposed to the external environment, are more susceptible to trauma, and the exact cause of their injuries may often remain undetermined.

When examining age and gender distribution, our study produced results both similar to and different from previous research. In a study conducted by Farghali et al. [2] of 149 cats, 60.83% were female and 39.17% were male, contrasting with our results, where no significant difference was observed between the genders. Farghali et al. [2] also found that the majority of fracture cases occurred in younger cats, a finding consistent with our study. Hill [16] reported that 75% of fractures occurred in cats aged 2 years or younger, and Phillips [17] found that 80% of fractures were in cats under 3 years of age. Our study showed a slight male predominance, in line with previous research, with 46.87% of fractures occurring in cats aged 0-1 years and 43.05% in the 1-2 year age group. These findings suggest that the small differences in gender distribution are negligible, while young cats remain at higher risk of fractures.

Various surgical and conservatif treatment (cage rest+medical treatment) options are available for managing feline limb fractures [7, 12, 18]. Studies indicate that surgical methods are typically preferred in more complex cases, while cage rest and medical treatment are often suitable for simpler fractures with high healing potential [12, 18]. In our study, cage rest combined with medical treatment was employed in 45.6% of femur fractures, 32.3% of tibia-fibula fractures, 39.3% of humerus fractures, 35% of radius-ulna fractures, 42.1% of metacarpal fractures, and 46.1% of metatarsal fractures. Surgical intervention combined with medical treatment was applied in 54.3% of femur fractures, 67.6% of tibia-fibula fractures, 60.6% of humerus fractures, 65% of radius-ulna fractures, 57.8% of metacarpal fractures, and 53.8% of metatarsal fractures. Despite the higher number of femur fractures, the relatively lower rate of surgical intervention may be due to factors such as the patient's overall condition or the pet owner refusing the operation. Ultimately, fracture type, location, and owner preferences play crucial roles in determining the treatment strategy [12, 19].

The results of this study revealed that the most common fractures in cats occur in the femur, with the majority of these fractures being attributed to unknown traumas. Additionally, the data showed a higher incidence of fractures in younger and inexperienced cats, with femur and tibia-fibula fractures often requiring surgical intervention. The frequent occurrence of unknown traumas in stray cats highlights this as a significant etiological factor in clinical practice, emphasizing the need for more detailed evaluations of such cases. This study has the potential to serve as a significant reference for future research regarding the types of bones that are most frequently fractured in cats, the proportion of these fractures that are treated surgically versus conservatively, and the factors that may influence treatment options. Future investigations should address these topics more comprehensively in order to deepen the knowledge base in this field and provide guidance for clinical practice.

151

REFERENCES

[1] Keosengthong A, Kampa N, Jitpean S, Seesupa S, Kunkitti P, Hoisang S. Incidence and classification of bone fracture in dogs and cats: a retrospective study at a Veterinary Teaching Hospital, Khon Kaen University, Thailand (2013-2016). Vet Integr Sci. 2019;17(2):127-39.

[2] Abo-Soliman A, Ahmed A, Farghali H. Incidence of appendicular bone fracture in dogs and cats: retrospective study at Veterinary Hospital of Cairo University and some private clinics in Egypt. World Vet J. 2020;10:77.

[3] Rochlitz I. Clinical study of cats injured and killed in road traffic accidents in Cambridgeshire. J Small Anim Pract. 2004;45(8):390-4.

[4] Cardoso CB, Rahal SC, Agostinho FS, Mamprim MJ, Santos RR, Ednaldo Filho S, et al. Long bone fractures in cats: a retrospective study. Vet Zootec. 2016;23(3):504-9.

[5] El-shafey S, El-Mezyen AEM, Behery A, Abd El Raouf M. Tibial and fibular fractures in dogs and cats: retrospective study. Zagazig Vet J. 2022;50(1):52-61.

[6] Canlı R, Çatalkaya E, Kanay BE, Saylak N, Kilinç M, Altan S, et al. A retrospective study on the evaluation of hind limb bone fractures in cats. Int J Vet Anim Res. 2024;7(1):7-11.

[7] Gülaydın A, Alkan İ. Evaluation of distal femur fractures in cats by hybrid external fixator. Ankara Univ Vet Fak Derg. 2024;71(1):89-100.

[8] Ali LMB. Incidence, occurrence, classification and outcome of small animal fractures: a retrospective study (2005-2010). Int J Anim Vet Sci. 2013;7(3):191-6.

[9] Uwagie-Ero EA, Abiaezute CN, Okorie-Kanu OJ, Odigie EA, & Asemota OD. Retrospective evaluation of canine fractures in southern Nigeria. Comp Clin Path, 2018;27:1127-32.

[10] Libardoni RDN, Serafini GMC, Oliveira CD, Schimites PI, Chaves RO, Feranti JPS, et al. Appendicular fractures of traumatic etiology in dogs: 955 cases (2004-2013). Cienc Rural. 2016;46:542-6.

[11] Vidane AS, Elias MZJ, Cardoso JMM, Come JASS, Harun M, Ambrósio CE. Incidência de fraturas em cães e gatos da cidade de Maputo (Moçambique) no período de 1998-2008. Cienc Anim Bras. 2014;15:490-4.

[12] Harari J. Treatments for feline long bone fractures. Vet Clin North Am Small Anim Pract. 2002;32(4):927-47.

[13] Zurita M, Craig A. Feline diaphyseal fractures: management and treatment options. J Feline Med Surg. 2022;24(7):662-74.

[14] Scott HW, McLaughlin R. Introduction to feline orthopedic surgery. In: Scott HW, McLaughlin R, editors. Feline orthopedics. London: Manson Publishing; 2007. p. 9-16.

[15] Piermattei DL, Flo GL, DeCamp CE. Handbook of small animal orthopedics and fracture repair. 3rd ed. Missouri: Saunders; 2006.

[16] Hill FWG. A survey of bone fractures in the cat. J Small Anim Pract. 1977;18(7):457-63.

[17] Phillips IR. A survey of bone fractures in the dog and cat. J Small Anim Pract. 1979;20(11):661-74.

[18] Shales C. Fracture management in small animal practice: 2. Assessment and planning. In Pract. 2008;30(7):374-84.

[19] Denny HR. A guide to canine and feline orthopedic surgery. 3rd ed. Oxford: Blackwell Science; 1993.

Ensemble and Non-Ensemble Machine Learning-Based Classification of Liver Cirrhosis Stages

Zeinab Mahdi MOUMIN[1] , İrem Nur ECEMİŞ[2*] , Mustafa KARHAN[3]

[1]Çankırı Karatekin University, Institute of Science, Department of Electronics and Computer Science, Çankırı, Türkiye
[2*]Çankırı Karatekin University, Faculty of Engineering, Department of Computer Engineering, Çankırı, Türkiye
[3]Çankırı Karatekin University, Institute of Science, Department of Electronics and Computer Science, Çankırı, Türkiye

Zeinab Mahdi MOUMIN ORCID No: 0009-0003-8889-9160
İrem Nur ECEMİŞ ORCID No: 0000-0001-9535-2209
Mustafa KARHAN ORCID No: 0000-0001-6747-8971

Corresponding author: iremnurecemis@karatekin.edu.tr

Abstract: Cirrhosis is a chronic liver condition characterized by gradual scarring of the tissue in the liver, which then leads to one of the more serious health problems. Early diagnosis and detection of this condition are critical to managing the patient's situation and planning his treatment. Machine learning is a computer science field in which many complex issues have otherwise been successfully resolved, especially in medicine. This work focuses on constructing an artificial intelligence system, assisted by machine learning algorithms, to help professionals diagnose liver cirrhosis at its early stage. In this paper, four different models have been constructed with the aid of clinical parameters of patients and machine learning techniques: Random Forest, KNN, histogram-based Gradient Boosting, and Soft Voting. Two feature selection methods (Chi-Square and mutual information) have been combined to select the most relevant features in the dataset. Then non-ensemble and ensemble methods are applied to detect the liver disease. The random forest model achieved the highest score among other model with 97.4 % accuracy with a 10-fold cross-validation method.

153

Topluluk ve Topluluk Olmayan Makine Öğrenmesine Dayalı Karaciğer Sirozu Evrelerinin Sınıflandırılması

Öz: Siroz, karaciğerdeki dokunun kademeli olarak yaralanmasıyla karakterize kronik bir karaciğer rahatsızlığıdır. Bu rahatsızlık ilerleyen dönemde daha ciddi sağlık sorunlarına yol açar. Bu rahatsızlığın erken teşhisi ve tespiti, hastanın durumunu yönetmek ve tedavisini planlamak için kritik öneme sahiptir. Makine öğrenimi, özellikle tıpta birçok karmaşık sorunun başarıyla çözüldüğü bir bilgisayar bilimi alanıdır. Bu çalışma, profesyonellerin karaciğer sirozunu erken aşamada teşhis etmelerine yardımcı olmak için makine öğrenimi algoritmalarıyla desteklenen bir yapay zeka sistemi oluşturmaya odaklanmaktadır. Bu makalede, hastaların klinik parametreleri ve makine öğrenimi tekniklerinin yardımıyla dört farklı model oluşturulmuştur: Rastgele Orman, KNN, Histogram Tabanlı Gradyan Artırma ve Yumuşak Oylama. Veri kümesindeki en alakalı özellikleri seçmek için iki özellik seçme yöntemi (Chi-square ve karşılıklı bilgi) birleştirilmiştir. Ardından karaciğer hastalığını tespit etmek için topluluk dışı ve topluluk yöntemleri kullanılmıştır. Rastgele orman modeli, 10 katlı çapraz doğrulama yöntemi ile %97,4 doğrulukla diğer modeller arasında en yüksek puanı elde etmiştir.

1. INTRODUCTION

The body's largest organ is the liver, which is important in digestion and detoxification. However, factors such as viral infections and alcohol consumption can damage the liver, leading to life-threatening conditions [1]. Liver conditions, including hepatitis, cirrhosis, liver tumors, and cancer, are significant contributors to mortality worldwide. Cirrhosis alone is responsible for hundreds of thousands of death annually. There are approximately 71 million people worldwide who have liver cirrhosis and other chronic liver diseases, and it resulted in an estimated 1.3 million deaths in 2021 [2]. The World Health Organization has considered liver cirrhosis to be one of the major concerns to global health, adding about 3–4 million new cases yearly. The highest frequency is in the developing countries in Asia and Africa, in contrast to Western nations in Europe and North America [3]. Symptoms of liver cirrhosis frequently appear only in the later stages of the disease. Most infected patients, however are asymptomatic at the initial stages thus resulting in a more significant damage of the liver and rise in mortality rates [4]. The vaccination is not an option for individuals with severely damaged livers. Thus, establishing the extent of damage to the liver is very necessary to ensure that doctors can quickly identify and provide treatment for chronic infections. Full treatment ensures that the illness does not pass from one individual to another [5]. Machine learning, as a subset of artificial intelligence, has been an emerging avenue that potentially diagnoses and classifies cirrhosis. Based on large datasets and algorithms, machine learning models could analyze a variety of factors and patterns in a patient to predict the likeliness of cirrhosis [6]. Machine learning may have the potential to improve diagnosis for diseases that have made an interest in the biomedical field while bringing down diagnostic costs simultaneously [7].

Several machine learning algorithms have been executed for identifying liver conditions. Meng et al. [8] applied a dataset of ROI ultrasound images consisting of 79 images of healthy liver ROIs, 89 images of early-stage liver fibrosis ROIs, and 111 images of late-stage liver fibrosis ROIs. They pose a liver fibrosis classification method employing transfer learning (TL) with VGGNet, and a deep classifier called FCNet. Huang et al. [9], discover how features such as gender and weight could impact the commonness of liver cirrhosis in different populations. The study states that all of the above-mentioned criteria should be taken into consideration while developing any manual or AI-driven system to get the desired results for the most appropriate treatment solutions from health experts. In simple research Cheng et al. [10], the contribution of attributes by patients was considerably different in terms of sex, body mass index, bilirubin, alanine aminotransferase, and so on. The study has shown that the mean BMI value for male patients over 60 is lower than for female patients under 60. Higher BMI values are also linked to an increased risk. Using Regression Logistic, and RF, Bedeir and Hadi [11] developed a machine learning model to predict cirrhosis liver. Every model was assessed based on performance measures such as accuracy and test error. The results obtained from employing the feature selection method were compared with those obtained without feature selection. The results highlighted that the Random Forest model gives the best accuracy at 96.59 %. The authors suggest future studies to measure the performance of the proposed framework in different patient populations and healthcare settings. The data set used in [12] is the northeast Andhra Pradesh, India dataset obtained from the UCI Machine Learning Repository In this study, they employed six concepts of machine learning like Logistic Regression, KNN, Decision Tree, Support Vector Naive Bayes and Random Forest. In another paper, ensemble methods that give high results on different data sets were examined [13]. Additional metrics evaluated the performance of models based on different performance measures like accuracy, precision, recall and F1-score. Topcu et al. [14] employed Logistic Regression (LR), K-Nearest Neighbors (KNN), Random Forest (RF), AdaBoost, and Bernoulli Naive Bayes (BernoulliNB). The Random Forest algorithm achieved the highest score, approximately 98%. The paper employed a "Cirrhosis Patient Survival Prediction" dataset from the UCI. This dataset contained 418 patients with liver conditions and 17 clinical features to predict the state of patients with liver cirrhosis. In another study, Zhang et al. [15] built a machine learning-based model to identify and predict the different fibrosis stages. They employed clinical data from 618 chronic hepatitis patients treated at Zhejiang Provincial People's Hospital between February 2017 and September 2021. Six different learning algorithms (Logistic Regression, Support vector machine, Bayes, K-Nearest Neighbor, Decision Tree (DT), and Random Forest) were used to build the predictive model. The researchers identified the most relevant features from the data with maximum relevance, minimum redundancy (mRMR), and gradient boosting decision tree (GBDT) methods. The Decision Tre model showed strong performance in detecting liver fibrosis stages with high Area under the Curve (AUC) values in both the training cohort (0.898 to 0.944) and the external validation cohort (0.876 to 0.933). Choi and Oh [16] built a machine learning-based approach to detect and predict liver cirrhosis. They employed a dataset of 6980 patients treated between January 2021 and December 2018. Machine learning (Gaussian Naive Bayes, Extreme Gradient Boosting (XGBoost), Random Forest, and Least Absolute Shrinkage and Selection Operator Regression) was applied to identify significant risk factors for cirrhosis. The XGBoost model performed best, with AUC values of 0.832 in the training set and 0.829 in external validation, proving the most effective for cirrhosis prediction. In another paper, Hirano et al. [17] used image data from 75 patients who had undergone liver biopsy and contacted CT scans. The model's performance was evaluated using recall, accuracy, and specificity metrics. They utilized logistic regression with L2 norm regularization to combine multiple texture features from CT images into single combined features. The combined feature showed the highest performance with an accuracy of 76%.

Devikanniga et al. [18] assessed models' performance through precision, recall, and accuracy. They employed an optimized support vector to predict liver disease

accurately. The support vector was optimized using the crow search Algorithm (CSA). The optimized support vector model outperformed traditional SVM and State-of-the-art classification models. The SVM showed an accuracy of 99.49 %. In another paper, Md et al. [19] leverage ensemble learning algorithms to predict liver disease. The dataset in this study is the Indian liver patient dataset. The most relevant features were selected through univariate selection, feature importance, and correlation matrix. Among the six ensemble methods (Gradient Boosting, XGBoost, Bagging, Random Forest, Extra Trees, Stacking), the Extra tree method achieved the highest accuracy score of 91.82%.

In this paper, the proposed approach is using Random Forest and KNN, Histogram-Based Gradient Boosting, Soft Voting to classify the patients with different stages of cirrhosis. The performance of these algorithms was compared in terms of accuracy, precision, recall and F1-score. The remainder of the paper is structured as follows:

Section 1 reviews related work in machine learning for cirrhosis classification and prediction, while Section 2 presents our approach. The findings are presented in Section 3 and a few avenues for future work follow the conclusion.

2. MATERIAL AND METHOD

The proposed method comprises different sections that work simultaneously to achieve the study objective. To start, the dataset is collected then the preprocessing step occurs. The datasets are split into tests and training sets following the preprocessing step. The classification algorithms like Random Forest, KNN, and histogram-based Gradient Boosting and Soft Voting are trained and tested using the K-fold cross-validation method on the Cirrhosis Patient Survival Prediction dataset. And liver disease dataset. Figure 1 displays the block diagram of the proposed method, beginning with the initial step of sourcing the datasets from the UCI repository.

Figure 1. Approach for liver cirrhosis detection

2.1. Datasets

The paper employed a "Cirrhosis Patient Survival Prediction" dataset acquired from the UCI repository. The original data originated from a Mayo Clinic study on primary biliary cirrhosis (PBC) of the liver, conducted

between the years 1974 and 1984. This dataset contained 418 patients with liver conditions and 20 clinical features to predict the state of patients with liver cirrhosis. Among these, 10.53% are male patients, and 89.47% are female patients. Table 1 contains a brief description of the attributes and their data types.

Table 1. Cirrhosis dataset attribute description (Dataset 1) [20]

S.No.	Attribute	Description	Data type
1	ID	Unique identifier	Integer
2	N-Days	Number of days between registration and the earlier of death, transplantation, or study analysis time in July 1986	Integer
3	Status	Status of the patient C (censored), CL (censored due to liver tx), or D (death)	Categorical
4	Drug	Type of drug D-penicillamine or placebo	Categorical
5	Age	Age	Integer
6	Sex	M (male) or F (female)	Categorical
7	Ascites	Presence of ascites N (No) or Y (Yes)	Categorical
8	Hepatomegaly	Presence of hepatomegaly N (No) or Y (Yes)	Categorical
9	Spiders	Presence of spiders N (No) or Y (Yes)	Categorical
10	Edema	N (no edema and no diuretic therapy for edema), S (edema present without diuretics), or Y (edema despite diuretic therapy)	Categorical
11	Bilirubin	Serum bilirubin	Continuous
12	Cholesterol	Serum cholesterol	Integer
13	Albumin	Albumin	Continuous
14	Copper	Urine copper	Integer
15	Alk_Phos	Alkaline phosphatase	Continuous
16	SGOT	SGOT	Continuous
17	Tryglicerides	Tryglicerides	Integer
18	Platelets	Platelets per cubic	Integer
19	Prothrombin	Prothrombin time	Continuous
20	Stage	Histologic stage of disease (1, 2, 3, or 4)	Categorical

Another dataset was used to expand the research. The second dataset was collected from a hospital in the Northeast of Andhra Pradesh, India. The Data contains 584 patients' records; 416 patients were diagnosed with liver disease, and 167 patients were healthy individuals, highlighting an imbalance between the two classes. The dataset's attributes comprise aspects related to patient demographics and different biomarkers affiliated with liver disease. In Table 2, there is a brief description of all features of the liver disease dataset.

Table 2. Liver disease dataset attribute description (Dataset 2) [21]

S.No.	Attribute	Description	Data type
1	Age	Age	Integer
2	Gender	Gender of the patient	Binary
3	TB	Total Bilirubin	Continuous
4	DB	Direct Bilirubin	Continuous
5	Alkphos	Alkaline Phosphotase	Integer
6	Sgpt	Alamine Aminotransferase	Integer
7	Sgot	Aspartate Aminotransferase	Integer
8	TP	Total Proteins	Continuous
9	ALB	Albumin	Continuous
10	A/G Ratio	Albumin and Globulin Ratio	Continuous
11	Selector	It is the target variable, 1 means patient is suffering from liver disease, and 0 means the patient is heathy.	Binary

2.1.1. Dataset pre-processing

Data pre-processing is a fundamental process in the field of data analysis. It entails preparing raw data, which includes cleaning and organizing, to render it suitable for machine learning models. Depending on the dataset, different pre-processing techniques can be used [22]. Data cleaning is the step that deals with the handling of missing and noisy data to achieve data consistency. For the Cirrhosis Patient Survival Prediction dataset, the missing values have been handled using two methods. Median imputation replaces missing values in numeric columns with the median value of that column. The mode imputation method replaces the missing values of nonnumeric columns with the most frequent value in the respective column [23]. Traditional machine learning algorithms are driven by mathematical models and hence require numeric computations and statistical operations. Since these algorithms are searching for meaningful patterns or relationships in the data, it becomes a necessity that the data has to be in a numerical representation format. Categorical variables were converted by a label encoding method. Scaling is one of the fundamental stages of preprocessing in machine learning workflows aimed at improving performance. The attributes will be scaled with the StandardScaler technique. In the dataset, the target value Stage is imbalanced. The imbalance of such a target variable was stabilized before the methods of classification were applied, followed by the application of SMOTE-Tomek Link [24]. This method is a technique for handling imbalanced datasets. The SMOTE method generates synthetic samples for the minority class rather than simply duplicating existing minority samples. This approach is employed because it eliminates the risk of overfitting when the same data points are duplicated.

Here is a brief description of how the SMOTE method works:

- For every instance in the minority class, SMOTE determined its K-Nearest Neighbors within the same class. Then, it chooses one of the nearest neighbors at random.
- A new synthetic sample is created by interpolating between the original sample and the selected neighbor. The formula to create a synthetic sample is below:

$$\text{synthetic sample} = \text{sample} + \text{gap}(\text{neighbor} - \text{sample})$$

Where gap is a random value between 0 and 1 this process repeats until the minority class has the same number of observations as the majority class, balancing the overall class distribution.

The synthetic sample allows the models to learn observations of minority class patterns, enhancing classification results across all classes and, foremost more generalized performance.

Figure 2 presents the bar chart of the outcome variable before and after SMOTE.
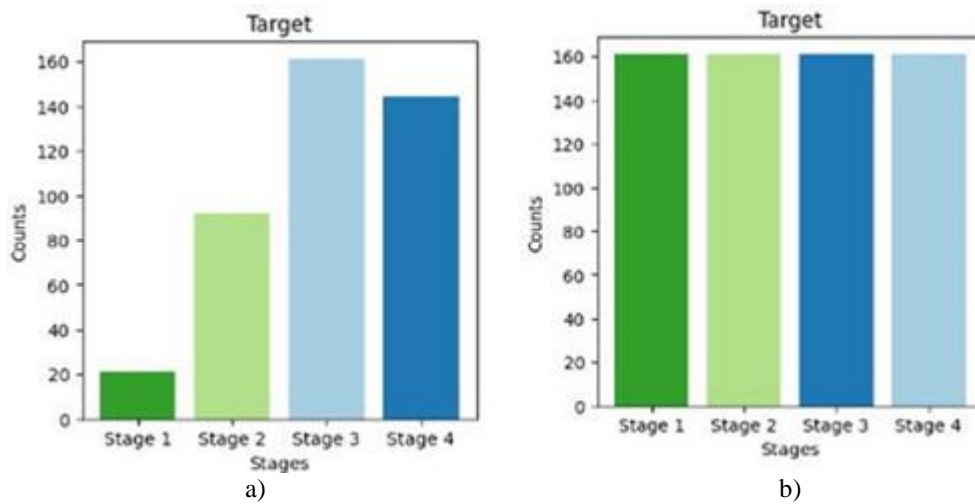
Figure 2. (a) Bar plot of outcome variable before SMOTE, (b) Bar plot of outcome variable after SMOTE.

2.2. Feature Selection

Feature Selection methods are techniques employed to reduce the features in the dataset to improve the performance machine learning models. Therefore the less relevant and redundant features are removed from the dataset Over the past few decades, several algorithms have been elaborated to pinpoint the most relevant attributes. In this study, two methods have been combined to select the most significant features.

2.2.1. Chi-square test

Chi-Square test is a statistical method that does not form hypotheses regarding the distribution pattern of the dataset. Chi-Square method measures the obtained results experimentally with expected results theoretically. It analyzes the relationship between the target and the categorical variables. Chi-square tests use the same formula to calculate the statistic. The formula is shown in Equation 1. Chi-square (X^2):

$$X^2 = \sum \frac{(O - E)^2}{E} \qquad (1)$$

Where:
- X^2 is the chi-square test statistic
- Σ is the summation operator
- O is the obtained frequency
- *E* is the expected frequency

2.2.2. Mutual information

Mutual Information is a statistical measure employed to scale the information obtained about the target variable through random variables. Mutual information between two variables, X and Y, spelled as I(X;Y), describe how much knowing the value of X dismisses ambiguity about Y. If X and Y are independent, I(X;Y)=0 means X contributes any information about Y. If X and Y are entirely dependent, then I(X;Y) is maximized. The formula is shown in Equation 2. Mutual Information:

$$I(X;Y) = \sum_{x \epsilon X} \sum_{y \epsilon Y} p(x,y) \log \left(\frac{p(x,y)}{p(x)p(y)} \right) \qquad (2)$$

Where:

p(x,y) = the joint probability distribution of X and Y

p(x) and p(y) = the marginal distribution of X and Y

Higher Mutual information score indicates that the random variable has useful information about the target variable.

Unlike other feature selection methods, mutual information does not assume a specific distribution and selects features with no linear relevance to the target. The features chosen for this statistical measure are Platelets, Spiders, Trylicerides, Bilerubin, SGOT, Sex, Ascites, Chotesterol, Drug, Copper, Alk-Phos, Status, N-Days and Age.

2.3. Brief Description of Machine Learning Techniques

2.3.1. Random forest

Random Forest is a supervised machine learning method for regression and classification problems. The Random Forest model combines the output of several decision trees to attain one result. Every tree in the ensemble is constructed of a data slice drawn from a training set with replacement [25]. The performance it gives is better than that of other models. This classifier is able to manage large datasets.

Here is a brief description of how the Random Forest technique works:

- Preparation Data: The dataset is split into train and test sets. Random Forest can handle categorical and numerical datasets.
- Random Sampling and bootstrapping: Random forest builds every tree on various random samples of the training dataset. Each sample is drawn with

157

bootstrapping, meaning that some samples will repeat while others will not.

- Growing each decision tree: Random forest selects a random sample of feature sets at every split. Random feature selection enhances generalization. After selecting a subset, the model determines the best split by evaluating different thresholds. Every tree grows until it grows fully.
- Aggregating Predictions: After all trees grow to the maximum depth, prediction are made individually for each input sample. The class with the most votes from the individual trees is chosen as the final output for classification tasks.

Random Forest model sets the default number of trees at 100 and the gini criterion for splitting nodes. These parameters allow the trees to grow with no limit on the depth of the trees.

2.3.2. K-Nearest neighbor

K-Nearest Neighbor algorithm is one of the simplest supervised learning machines. The KNN technique is employed for the classification and regression tasks. The KNN algorithm registered all the available data and groups to make a new data point based on similarity.

Here is a brief description of how the K-Nearest Neighbors (KNN) technique functions [26]:

- Data Representation and Initialization: Every data point is illustrated in multi-dimensional space. Each dimension corresponds to the feature of dataset. KNN technique does not learn from the training phase as the other algorithms. Instead, it memorizes the training dataset.
- Distance Calculation: KNN calculates the distance between a new data point and other points to predict the class of the data point. Common distance metrics exclude Euclidean, Manhattan and Murkowski distances.
- Finding Neighbors: Following the distance calculation step, KNN selects the nearest data points to the new data points.
- Majority Voting: To classify the new data point, the class that occurs the most among the neighbors is assigned to it.

The KNN model is set with the default Euclidean distance to extend the proximity between data points. By default, the number of neighbors was set to 5, and the leaf size was assessed to 30.

2.3.3. Histogram-based gradient boosting

HistGradientBoosting short for Histogram-Based Gradient Boosting is powerful supervised machine learning method designed for both regression and classification tasks. This algorithm is an ensemble machine learning that creates an accurate predictive model by sequentially combining several weaker models, typically decision trees. It is another gradient boosting

algorithm, that utilizes histogram-based techniques to speed up the training phase and improve memory efficiency. In the Histogram-Based Gradient Boosting classifier, the default learning rate was set to 0.1, and the default number of boosting iterations to 100. The default value for the minimum number of samples required in a leaf node is 20.

2.3.4. Soft voting

Voting is an ensemble machine learning technique that merges predictions from several models to enhance model performance beyond what a single model could achieve alone. This ensemble method helps individual model weaknesses and enhances overall performance. There are different types of ensemble techniques. Soft voting, or weighted voting, considers the probability scores assigned by each base model for each class. It calculates the weighted average of these probabilities to make the final prediction. The voting classifier employs a soft voting by default; each classifier is included in the voting classifier with no weighting. Figure 3 illustrates the soft voting.
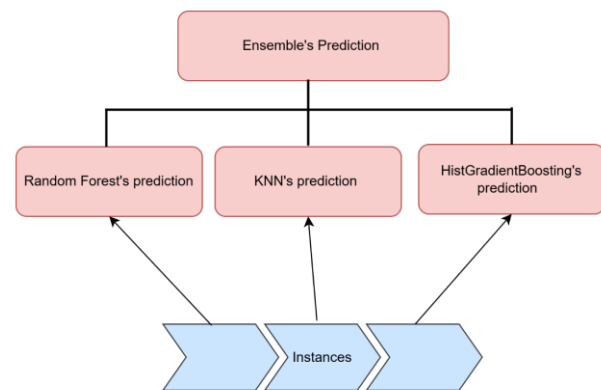
Figure 3. Working process of soft voting

2.4. Performance Measurement Metric

Random Forest, histogram-based Gradient Boosting, KNN and Soft Voting algorithms are used in this study. Experiments are performed using hold out method. Accuracy, F-Measure, Recall and Precision measures are used for the classification of observations. Confusion matrix is a tabular representation of prediction outcomes of any binary. The form of the confusion matrix is given in Figure 4.
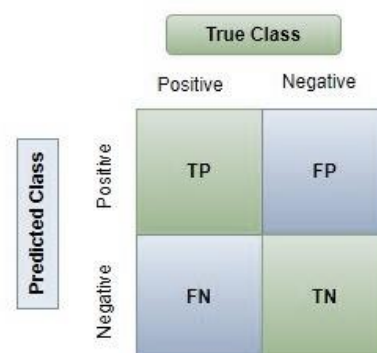
Figure 4. Confusion matrix elements

158

- TP refers to True Positive. True, it can be understood as the model expected to show positive class.
- False Positive is FP. Though it is False, it can be understood as the model projected positive class.
- False Negative refers to FN. Though it is False, one can understand it as the model expected negative class.
- TN, or True Negative, is It is True and can be seen as the model expected negative class.

The accuracy metric refers as the number of correct predictions to the total number of predictions. The accuracy formula is shown in Equation 3.

$$Accuracy = \frac{\sum(TP + TN)}{\sum(TP + FN + TN + FP)} \quad (3)$$

The precision metric is used to overcome the limitation of accuracy. The precision determines the proportion of positive prediction that was actually correct and is shown in Equation 4.

$$Precision = \frac{\sum TP}{\sum(TP + FP)} \quad (4)$$

The Recall metric calculate the proportion of actual positive that was identified incorrectly. The metric formula is given in Equation 5.

$$Recall = \frac{\sum TP}{\sum(TP + FN)} \quad (5)$$

3. RESULTS AND DISCUSSION

Table 3 presents the results of different machine models with cross-validation method. Different performance metrics were used to assess the performance of four machine learning classifiers on a cirrhosis dataset. The outcomes reveal that Random Forest classifier exhibit the highest accuracy score (96.6%), recall (86.7%), precision (97.7%), and F1-score (86.7%). This method is succeeded by the soft voting and hist gradient boosting methods, which achieve a commendable 95.2% and 94.7% accuracy score respectively. KNN has the lowest accuracy score (76.6%).

Table 3. Performance of classification algorithms on various measures (5-fold cross-validation)

Model	Accuracy	Precision	Recall	F1-score
Random Forest	0.966	0.967	0.842	0.867
KNN	0.890	0.920	0.836	0.864
HistGradientBoosting	0.947	0.792	0.772	0.767
Soft Voting	0.952	0.790	0.777	0.769

Table 4. Performance of classification algorithms on various measures (10-fold cross-validation) with Dataset 1

| Model	Accuracy	Precision	Recall	F1-score
Random Forest	0.974	0.878	0.875	0.900
KNN	0.895	0.879	0.839	0.850
HistGradientBoosting	0.940	0.742	0.754	0.745
Soft Voting	0.959	0.811	0.796	0.791

Table 5. Performance of classification algorithms on various measures (10-fold cross-validation) with Dataset 2

Model	Accuracy	Precision	Recall	F1-score
Random Forest	0.8092	0.8139	0.8090	0.8083
KNN	0.7381	0.7328	0.7378	0.7563
HistGradientBoosting	0.7959	0.8010	0.7956	0.7947
Soft Voting	0.8032	0.8108	0.8030	0.8018

Regarding F1-score, Random Forest performed the best with a score of 86.7%, whereas HistGradientBoosting had the lowest F1-score at 76.7%. Based on these evaluation metrics, Random Forest emerged as the most effective classifier to classifying the stage of cirrhosis.

Looking at Table 4 in terms of accuracy values, The Random Forest algorithm is concluded to perform better than the four algorithms in comparison. It gives higher accuracy in respective to other classification algorithms with an accuracy of (97.4 % for 10-fold cross-validation). The remaining three methods have achieved acceptable scores on the various performance classifications. However, a rise in the accuracy score is seen in this table compared to when the 10-fold cross-validation method is applied.

Table 5 presents the results of different machine models with 10-fold validation. Different performance metrics were used to assess the performance of four machine learning classifiers on the liver disease dataset. The Random Forest model achieved the highest accuracy, precision, recall and F1-score. Then, the HistGradientBoosting and soft voting model achieved a score slightly lower than the score achieved by the Random Forest. The KNN model showed the lowest accuracy score. The KNN is only a non-ensemble model, so it tends to be biased toward the majority class in imbalanced datasets since it is likely to have more nearby points from the dominant class. Random Forest is an ensemble of decision trees that fuses several decision boundaries. Random Forest model minimizes overfitting and accomplishes high accuracy. By bootstrapping and selecting a sample of the features at every split, random forest prevents any single tree from dominating the decision-making process. The model is more robust and less sensitive to the noise in the dataset. Compared to the two other ensemble models, Random Forest's performance changes depending on the dataset. Furthermore Random Forest model reduces the false

positives and negatives. Random Forest can handle non-linear data and performs well with default parameters. Unlike KNN, it struggles when the decision boundary is complex. Compared to the KNN model, ensemble models like Random Forest, HistGradientBoosting, and Soft Voting produce superior accuracy, precision, recall, and F1-score. Reducing bias and variance enhances stability and captures complex patterns.

4. CONCLUSION

Liver disease, including cirrhosis, is a significant contributor to mortality in today's world. The application of machine learning techniques holds promise in reducing mortality rates by facilitating early disease detection. This study evaluated the cirrhosis dataset using four classification algorithms: Random Forest, histogram-based Gradient Boosting, KNN, and Soft Voting algorithms. In the experiment, two feature selections have been employed to drop the redundant attributes. Random Forest achieved the highest accuracy with the cross-validation method and was superior to other machine learning algorithms in two datasets. The work can be extended and improved employing a more suitable dataset can give more in-depth information on the variables that can help predict classifying the disease in a better way. In order to achieve this, hyperparameters can be employed to optimize the performance of ensemble and non-ensemble methods.

REFERENCES

[1] The Digestive Process: The Liver and its Many Functions. Johns Hopkins Medicine. 2019 Nov 19. Available from: https://www.hopkinsmedicine.org/health/conditions-and-diseases/the-digestive-process-the-liver-and-its-many-functions.

[2] H. Devarbhavi, S. K. Asrani, J. P. Arab, Y. A. Nartey, E. Pose, and P. S. Kamath, "Global Burden of Liver Disease: 2023 Update," Journal of Hepatology, vol. 79, no. 2, Mar. 2023, doi: https://doi.org/10.1016/j.jhep.2023.03.017.

[3] Mohamed AA, Elbedewy TA, El-Serafy M, El-Toukhy N, Ahmed W, et al. Liver cirrhosis virus: A global view. World Journal of Hepatology. 2015;7(26):2676-80.

[4] Cirrhosis of the Liver. American Liver Foundation. 2023 Mar 16. Available from: https://liverfoundation.org/liver-diseases/complications-of-liver-disease/cirrhosis/.

[5] Buechter M, Gerken G. Liver Function—How to Screen and to Diagnose: Insights from Personal Experiences, Controlled Clinical Studies and Future Perspectives. J Pers Med. 2022;12(10):1657.

[6] Hanif I, Khan MM. Liver Cirrhosis Prediction using Machine Learning Approaches. 2022 IEEE 13th Annual Ubiquitous Computing, Electronics & Mobile Communication Conference (UEMCON). 2022.

[7] Ahsan MM, Luna SA, Siddique Z. Machine-Learning-Based Disease Diagnosis: A Comprehensive Review. Healthcare (Basel). 2022;10(3):541.

[8] Meng D, Zhang L, Cao G, Cao W, Zhang G, Hu B. Liver Fibrosis Classification Based on Transfer Learning and FCNet for Ultrasound Images. IEEE Access. 2017;5:2169-3536.

[9] Huang R, Rao H, Yang M, Gao Y, Wang J, et al. Noninvasive measurements predict liver fibrosis well in liver cirrhosis virus patients after direct-acting antiviral therapy. Dig Dis Sci. 2020;65(5):1491-500.

[10] Cheng Z, Zhang Y, Zhou C. QSAR models for phosphoramidate prodrugs of 2'-methylcytidine as inhibitors of Liver cirrhosis virus based on PSO boosting. Chem Biol Drug Des. 2011;78(6):948-59.

[11] Bedeir A, El-Hadi M. A Proposed Framework for Predictive Analytics for Cirrhosis of the Liver Using Machine Learning. Maǧallaẗ Al-Ǧamʿiyyaẗ Al-Miṣriyyaẗ Li Nuẓum Al-Maʿlūmāt wa Tiknūlūǧyā Al-Ḥāsibāt. 2023;31(31):114-23.

[12] Rahman AKMS, Javed M, Tasnim Z, Roy J, Hossain SA. A Comparative Study On Liver Disease Prediction Using Supervised Machine Learning Algorithms. 2019;8(11):419-22.

[13] Sürücü S, Diri B. Transferemble: a classification method for the detection of fake satellite images created with deep convolutional generative adversarial network. J Electron Imaging. 2023;32(4):043004.

[14] Topcu AE, Elbasi E, Alzoubi YI. Machine Learning-Based Analysis and Prediction of Liver Cirrhosis. In: Proceedings of the 2024 47th International Conference on Telecommunications and Signal Processing (TSP); 2024; Prague, Czech Republic. p. 191-194.

[15] Zhang C, Shu Z, Chen S, et al. A machine learning-based model analysis for serum markers of liver fibrosis in chronic hepatitis B patients. Sci Rep. 2024;14:12081.

[16] Choi YS, Oh E. Investigating of Machine Learning Based Algorithms for Liver Cirrhosis Prediction. Adv Eng Intell Syst. 2024;3(1):115-130.

[17] Hirano R, Rogalla P, Farrell C, et al. Development of a classification method for mild liver fibrosis using non-contrast CT image. Int J Comput Assist Radiol Surg. 2022;17:2041-2049.

[18] Devikanniga D, Ramu A, Haldorai A. Efficient Diagnosis of Liver Disease using Support Vector Machine Optimized with Crow Search Algorithm. EAI Endorsed Trans Energy Web. 2020;7(29):e10.

[19] Md AQ, Kulkarni S, Joshua CJ, Vaichole T, Mohan S, Iwendi C. Enhanced preprocessing approach using ensemble machine learning algorithms for detecting liver disease. Biomedicines. 2023;11(2):581.

[20] Dickson ER, Grambsch PM, Fleming TR, Fisher LD, Langworthy A. Prognosis in primary biliary cirrhosis: model for decision making. Hepatology. 1989;10(1):1-7.

[21] Straw I, Wu H. Investigating for bias in healthcare algorithms: a sex-stratified analysis of supervised machine learning models in liver disease prediction. BMJ Health Care Inform. 2022;29(1).

[22] Lee GY, Alzamil L, Doskenov B, Termehchy A. A survey on data cleaning methods for improved

machine learning model performance. arXiv preprint arXiv:2109.07127. 2021.

[23] Kwak SK, Kim JH. Statistical data preparation: management of missing values and outliers. Korean J Anesthesiol. 2017;70(4):407-411.

[24] Batista GEAPA, Prati RC, Monard MC. A study of the behavior of several methods for balancing machine learning training data. SIGKDD Explor Newsl. 2004;6(1):20-29.

[25] Chen X, Ishwaran H. Random forests for genomic data analysis. Genomics. 2012;99(6):323-329.

[26] Tembusai ZR, Mawengkang H, Zarlis M. K-nearest neighbor with K-fold cross validation and analytic hierarchy process on data classification. Int J Adv Data Inf Syst. 2021;2(1):45-52.

BINGÖL UNIVERSITY

Investigation of the Effects of Acetylsalicylic Acid Administration at Different Doses on Behavioral Disorders in Rats

Hasan ŞİMŞEK[1*] iD , **Özge KANDEMİR[2]** iD , **Nurhan AKARAS [3]** iD

[1] Aksaray University, Faculty of Medicine, Department of Physiology, Aksaray, Türkiye
[2] Aksaray University, Vocational School of Technical Sciences, Department of Food Processing, Aksaray, Türkiye
[3] Aksaray University, Faculty of Medicine, Department of Histology and Embryology, Aksaray, Türkiye
Hasan ŞİMŞEK ORCID No: 0000-0001-5573-4923
Özge KANDEMİR ORCID No: 0000-0001-8884-4168
Nurhan AKARAS ORCID No: 0000-0002-8457-9448

Corresponding author: hasansimsek@aksaray.edu.tr

Abstract: Aspirin is one of the most widely used non-steroidal anti-inflammatory drugs worldwide. Neurodegenerative diseases adversely affect the central nervous system, leading to cognitive decline. Aspirin has different pharmacological activities at different doses. Therefore, this study aimed to determine the effects of acetylsalicylic acid (ASA), the active ingredient of aspirin, administered at different doses on the parameters that play a role in cognitive function using molecular and histological methods and behavioral tests. For this purpose, 28 Wistar rats were divided into 4 groups. Control, ASA-low dose (1mg/kg), ASA-moderate dose (10mg/kg) and ASA-high dose (100mg/kg). ASA was intragastrically administered as a single dose, and an open field test was performed 3 hours later. Subsequently, hippocampus tissues were obtained, and the hippocampus tissue structure was analyzed by analyzing the parameters involved in antioxidant capacity, inflammation, apoptosis, and memory. ASA, especially at moderate doses, increased antioxidant capacity and partially reduced inflammation and apoptotic damage. At high doses, the opposite effect was observed, and the damage levels. Similar effects were detected by histological examination. Although there were no structural defects at low or moderate doses, structural defects were observed at high doses. Although there was no difference in the open field test findings between the groups, the time spent in the center, distance traveled, and speed were slightly higher in the ASA moderate-dose group. In conclusion, ASA may contribute to the improvement of cognitive function at low and moderate doses. However, high doses may cause cognitive impairment.

162

Farklı Dozlarda Asetilsalisilik Asit Uygulamasının Sıçanlarda Davranış Bozuklukları Üzerindeki Etkilerinin Araştırılması

Öz: Aspirin, dünya genelinde en yaygın kullanılan non-steroid anti-inflamatuvar ilaçlardan biridir. Norodejeneratif hastalıklar merkezi sinir sistemini olumsuz etkileyerek bilişsel fonksiyonların gerilemesine neden olur. Aspirin farklı dozlarda farklı farmakolojik aktiviteye sahiptir. Bu nedenle bu çalışmadaki amaç, farklı dozlarda uygulanan aspirin etken maddesi asetilsalisilik asitin (ASA) bilişsel fonksiyonlarda rol oynayan parametreler üzerindeki etkilerinin moleküler ve histolojik yöntemlerle ve davranış testleri ile belirlenmesidir. Bu amaç doğrultusunda 28 Wistar rat 4 gruba ayrılmıştır. Kontrol, ASA-düşük doz (1mg/kg), ASA-orta doz (10mg/kg) ve ASA-yüksek doz (100mg/kg). ASA tek doz intragastrik olarak uygulandı ve 3 saat sonrasında açık alan testi uygulandı. Ardından hipokampüs dokuları alınarak antioksidan kapasite, inflamasyon, apoptozis ve hafızada rol oynayan parametrelerin analizi ile hipokampüs doku yapısı incelendi. ASA özellikle orta dozda antioksidan kapasiteyi arttırıp, inflamasyon ve apoptotik hasarı kısmı olarak azaltmıştır. Yüksek dozda ise tersi etki göstererek hasar düzeylerini arttırmıştır. Benzer etkiler histolojik incelemede de tespit edilmiş olup düşük ve orta dozda yapısal bozulmalar yok iken yüksek dozda yapısal bozukluklar görülmüştür. Açık alan testi bulgularında gruplar arası fark yok iken merkezde geçirilen süre, kat edilen mesafe ve hız ASA orta doz uygulanan grupta kısmen daha yüksektir. Sonuç olarak, ASA düşük ve orta düzeyde bilişsel fonksiyonların iyileşmesine katkı sağlayabilir ancak yüksek dozda bilişsel fonksiyonların bozulmasına neden olabilir.

1. INTRODUCTION

Neurodegenerative diseases affecting the central nervous system (CNS) cause damage to nerve cells and neurological problems, placing significant burdens on patients, their relatives, and the healthcare sector. Cognitive impairment caused by Alzheimer's disease (AD) has a significant negative impact on the quality of life of middle-aged and older individuals worldwide [1]. Neurodegenerative diseases, such as AD, begin with the gradual onset of memory loss. Over time, they manifest themselves with cognitive and behavioral problems, such as impairments in language, planning ability, and visuospatial skills [2].

Antibiotics and salicylates are the drugs of choice in both outpatients and inpatients; common side effects include diarrhea and gastrointestinal irritation, while toxic effects on the CNS are less well documented [3]. Acetylsalicylic acid (ASA, aspirin) is a non-steroidal anti-inflammatory drug (NSAIDs) commonly used to relieve pain, fever, and inflammation [4]. ASA is consumed globally at an average of 30 grams per person per year, with daily consumption reaching 35,000 kilograms in the United States alone; it is prescribed as secondary prophylaxis after heart attack in both Asian and Western societies for its antiplatelet effects; and low-dose long-term ASA is also used to reduce the risk of heart attack and stroke in individuals without a history of cardiovascular disease [5].

Some correlative studies indicate an unclear relationship between aspirin treatment and memory [6]. There is no evidence that low-dose aspirin improves cognitive performance in healthy women aged 65 years and older. Higher doses that inhibit COX enzymes may be more effective than the low doses of 75 mg used in the AD2000 study, but they also carry a higher risk of toxicity. In addition, these higher doses were found to have similar properties to NSAIDs [7]. Neuroinflammation is a major driver of many neurodegenerative diseases, such as multiple sclerosis, AD, and Parkinson's disease. While cytokines, growth factors, and reactive oxygen species (ROS) are released to aid neuronal repair, these substances can damage healthy tissues in chronic conditions, and oxidative stress is manifested in many of these diseases by an imbalance between ROS production and antioxidant defense [8] High doses of aspirin lead to increased levels of malondialdehyde (MDA), a product of lipid peroxidation (LPO), which can cause serious changes in the brain. LPO affects cell functions involving polyunsaturated fatty acids, impairing the activity of membrane-bound enzymes and can lead to atrophy or death of neurons. MDA level is used to assess ROS-induced brain damage in aging and neurodegenerative diseases and may affect learning and memory functions in the hippocampus [7]. Brain damage and neuronal loss are also associated with activation of microglia, astrocytes and invasive macrophages that overproduce toxic substances such as tumor necrosis factor (TNF)-α, and interleukin (IL)-1β [9]. The reasons for adverse effects of aspirin may be due to variations in experimental models or specifically to the concentrations of aspirin administered. It is well-established that low, moderate, and high doses of aspirin target different molecules [10]. This suggests that ASA may have different pharmacological and biological effects at different doses.

The aim of this study was to compare the effects of ASA, which is recommended for use in CNS-related diseases, on cognitive functions and brain memory markers at different doses. For this purpose, biochemical, molecular, and histological methods were used.

2. MATERIAL AND METHOD

2.1. Chemicals

ASA (≥99.0%, CAS Number: 50-78-2) and other chemicals were obtained from Sigma (St. Louis, USA).

2.2. Ethics Committee Aprproval

Ethical approval was obtained from Necmettin Erbakan University Local Animal Experiments Ethics Committee (25.09.2024, 2024-87).

2.3. Experimental Groups and Procedures

In the experiment, 28 *Wistar albino* rats weighing 220-250 g and aged 10-12 weeks were used. Animals were kept in cages in a controlled room with a constant temperature of 24-25ºC and a twelve (12 h) hour dark-light cycle (07:00-19:00 light; 19:00-07:00 dark). They were given unlimited access to water and standard chow. All animal experiments were performed at the KONÜDAM Experimental Medicine Application and Research Center (Konya / Türkiye). Rats were randomly divided into 4 groups with 7 rats in each group.

1: Control Group: 1 ml of physiologic saline was administered via intragastric gavage.
2: ASA - low dose (ASA-L): ASA 1 mg/kg was administered via intragastric gavage.
3: ASA - moderate dose (ASA-M): ASA 10 mg/kg was administered via intragastric gavage.
4: ASA - high dose (ASA-H): ASA 100 mg/kg was administered via intragastric gavage.

The protocol for ASA administration and tissue collection time was determined from the study by Senol et al. [7] and the doses were determined based on the study of Espiridiao et al. [11].

2.4. Open Field Test

The open field apparatus was made of water-resistant material and had a square shape with a base size of 80 × 80 cm and a height of 40 cm. The base was marked with 16 equal squares, and the 4 squares in the center were classified as the "center area" and the 12 squares on the edges as the "peripheral area". During the experiment, rats were placed in the center of the area and allowed to explore the area freely for 5 min; video recording was performed during this time. The time spent in the center, the number of transitions to the center, the distance moved

163

in the center, and the velocity were recorded in the four squares in the center area to assess anxiety levels. After the experiment, the open field apparatus was cleaned with ethanol in each rat to eliminate any remaining odors [12].

2.5. Tissue Collection

Three hours after ASA administration, the animals were decapitated under light sevoflurane anesthesia, and brain tissue samples were collected. Then, some brain tissue samples were stored at -80°C until genetic analyses were performed. The other part was left in 10% formaldehyde solution for use in histological analyses.

2.5. RT-PCR

At the end of the experiment, relative mRNA transcript levels of the gene regions listed in Table 1 were determined in hippocampus tissue samples using qRT–PCR. A QIAzol Lysis Reagent (79306; Qiagen) was used for total RNA isolation from hippocampus tissue samples. cDNA synthesis from the obtained total RNA was performed using the OneScript Plus cDNA Synthesis Kit (ABM, G236, Richmond, Canada). The prepared cDNAs were combined with primer sequences and BlasTaq™ 2X qPCR MasterMix (ABM, G891, Richmond, Canada) to form a reaction mixture. This mixture was run on a Rotor-Gene Q (Qiagen) device in the cycle and temperature program described according to the manufacturer's instructions. After the completion of the cycles, gene expression was normalized to β-Actin and evaluated by the $2^{-\Delta\Delta CT}$ method [13].

Table 1. Primer sequences

Gene	Sequences (5'-3')	Product length
Cu-Zn SOD	F: AGTCCCGCCCCTTCTAAAAC R: CAATGGCCTCTGTGTAGCCC	387
CAT	F: ATGGCAACTGTCCCTGAACT R: AGTGACACTGCCTTCCTGAA	670
GPx	F: CTCGAGTGACAAGCCCGTAG R: ATCTGCTGGTACCACCAGTT	290
NF-κB	F: AGTCCCGCCCCTTCTAAAAC R: CAATGGCCTCTGTGTAGCCC	106
IL-1β	F: ATGGCAACTGTCCCTGAACT R: AGTGACACTGCCTTCCTGAA	197
TNF-α	F: CTCGAGTGACAAGCCCGTAG R: ATCTGCTGGTACCACCAGTT	139
Caspase-3	F: ACTGGAATGTCAGCTCGCAA R: GCAGTAGTCGCCTCTGAAGA	270
Bax	F: TTTCATCCAGGATCGAGCAG R: AATCATCCTCTGCAGCTCCA	154
Bcl-2	F: GACTTTGCAGAGATGTCCAG R: TCAGGTACTCAGTCATCCAC	214
Glutamat	F: ACAGCAGAGTTCCAGGACAG R: GTCTATGTGAAGGTCACGCC	212
NMDA-R	F: TAGTTAGCCACCCGCCTACT R: GTCCGCGCTTGTTGTCATAG	357
CREB	F: TGCACAGACCACTGATGGAC R: CTGTGTAGGAAGTGCTGGGG	160
HSP27	F: GTCAACCACTTCGCTCCTGA R: CGACTCTGGGCCTCCAATTT	288
β-Actin	F: CAGCCTTCCTTCCTGGGTATG R: AGCTCAGTAACAGTCCGCCT	360

2.6. Histopathological Examination

Hippocampus tissue samples were fixed in 10% neutral formalin buffer for 24 h. After tissue tracking was completed, 5 μm thick sections were prepared from the paraffin blocks using a microtome. These sections were placed on slides, stained with hematoxylin and eosin (H&E), examined, and photographed using an Olympus Cx 43 microscope (Japan).

2.6. Statistical Analysis

One-way ANOVA followed by Tukey's post hoc test (SPSS 20.0; Chicago, USA) was applied to analyze the differences and significance levels between the groups.

All results are presented as mean ± SE. $p < 0.05$ was taken as the significance level.

3. RESULTS

3.1. Open Field Test Findings

In the open-field test (Figure 1), the distance moved in the center (A), velocity (B), time spent in the center (C), and the number of transitions from the edge to the center (D) were determined. For all these parameters, the highest level was observed in the ASA-M group, and the lowest level was observed in the ASA-H group. The differences between the groups were not significant ($p > 0.05$).

164
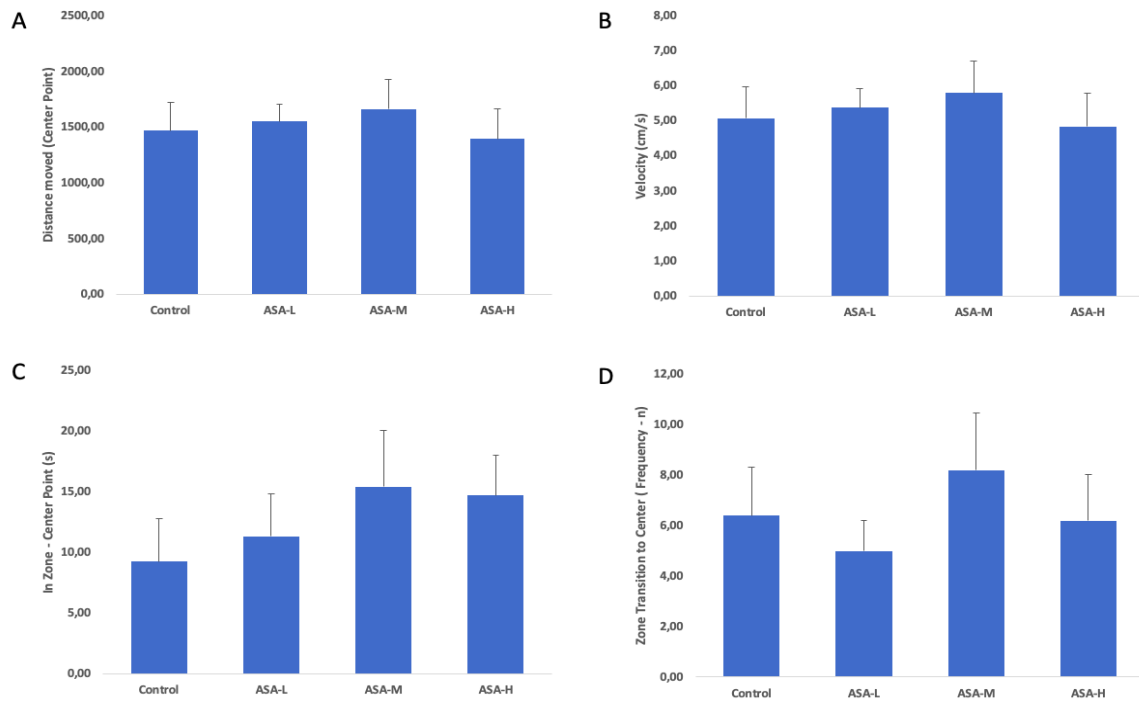
Figure 1. Open field test results

3.2. Antioxidant Capacity Findings

Superoxide dismutase (SOD), catalase (CAT), and glutathione peroxidase (GPx) activities were determined to determine the level of antioxidant capacity in hippocampus tissues (Figure 2). The highest activities of SOD, CAT, and GPx were detected in the ASA-M group, whereas the lowest activities were detected in the ASA-H group ($p < 0.05$).

Figure 2. Effects of different doses of ASA on antioxidant enzymes in rat hippocampus tissues. Values are given as mean ± SE. Different letters indicate statistical difference: *$p < 0.05$

3.3. Apoptosis Findings

To determine the extent of apoptotic damage in hippocampus tissues, apoptotic cysteine-aspartic acid protease-3 (Casp-3) and BCL2-associated X (Bax) and antiapoptotic B-cell lymphoma 2 (Bcl-2) levels were determined (Figure 3). The highest levels of Casp-3 and Bax and the lowest levels of Bcl-2 were detected in the

ASA-M group, whereas the lowest levels of Casp-3, Bax, and Bcl-2 were detected in the ASA-H group (p<0.05).

Figure 3. Effects of different doses of ASA on apoptotic and antiapoptotic markers in rat hippocampus tissues. Values are given as mean ± SE. Different letters indicate statistical difference: *p<0.05

3.4. Inflammation Findings

Nuclear factor kappa B (NF-κB), TNF-α, and IL-1β mRNA transcription levels were determined to determine inflammation damage in hippocampus tissues (Figure 4).

The lowest NF-κB, TNF-α, and IL-1β levels were detected in the ASA-M group (p>0.05), whereas the highest NF-κB, TNF-α, and IL-1β mRNA transcription levels were detected in the ASA-H group (p<0.05).
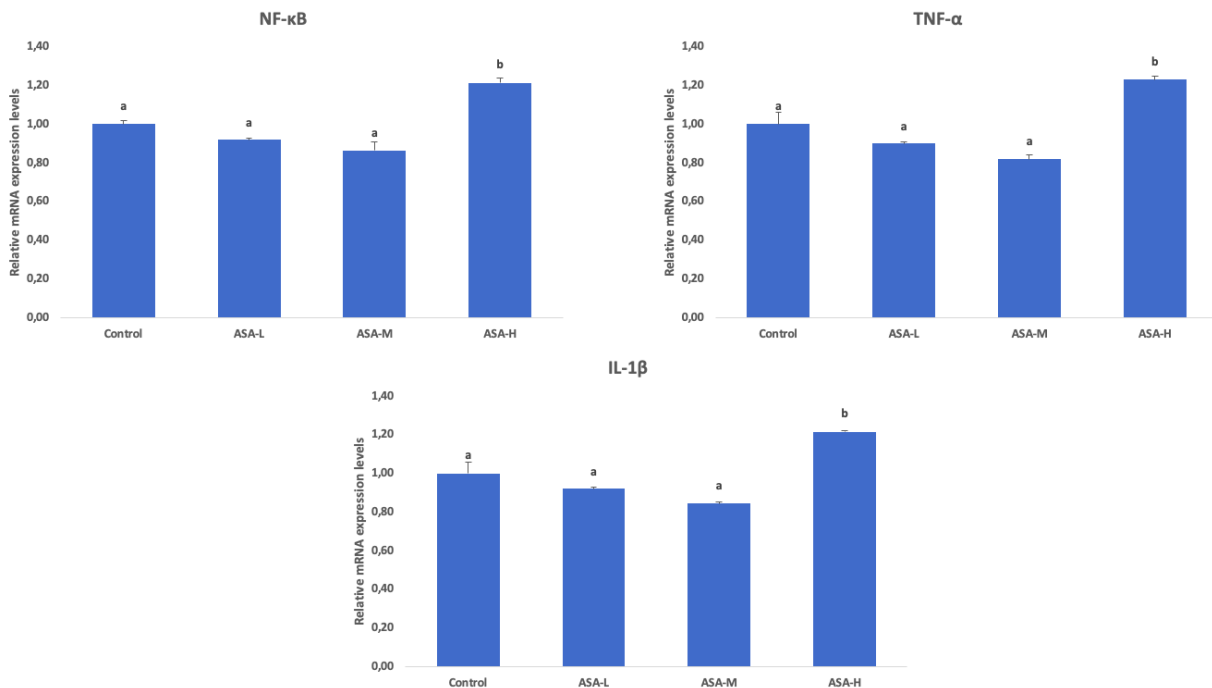
Figure 4. Effects of different doses of ASA on inflammatory markers in rat hippocampus tissues. Values are given as mean ± SE. Different letters indicate statistical difference: *p<0.05

3.5. Memory markers expressions

Glutamate, cAMP-response element binding protein (CREB), and N-methyl-D-aspartate (NMDA) mRNA transcription levels associated with memory were analyzed (Figure 5). The highest glutamate and CREB levels were observed in the ASA-M group, whereas the lowest levels were observed in the ASA-H group ($p < 0.05$). The highest level of NMDA was observed in the ASA-H group, whereas the lowest level was observed in the ASA-M group ($p < 0.05$).
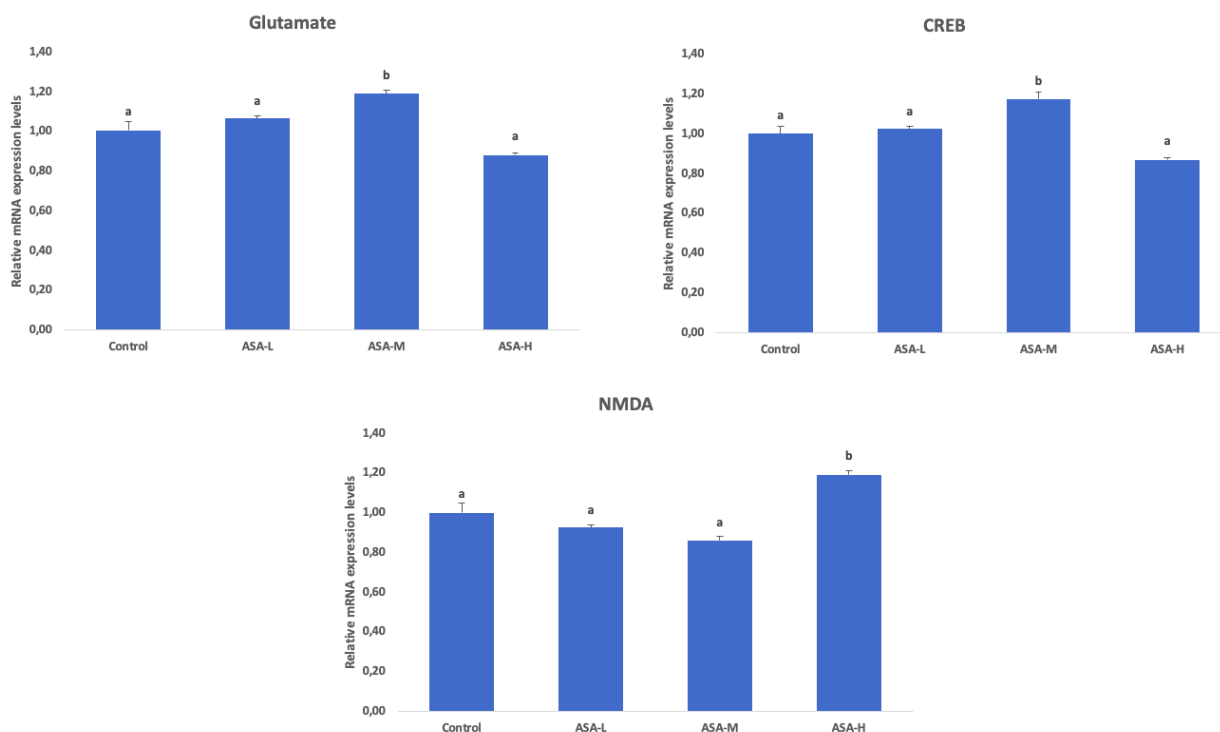
Figure 5. Effects of different doses of ASA on glutamate, CREB and NMDA mRNA transcription levels in rat hippocampus tissues. Values are given as mean ± SE. Different letters indicate statistical difference: *$p < 0.05$

3.6. HSP27 exprenssions

HSP27 mRNA transcription, which protects against apoptotic damage in hippocampus tissues, was also determined (Figure 6). HSP27 levels increased in the ASA-L and ASA-M groups, with the highest level in the ASA-M group and the lowest level in the ASA-H group ($p < 0.05$).
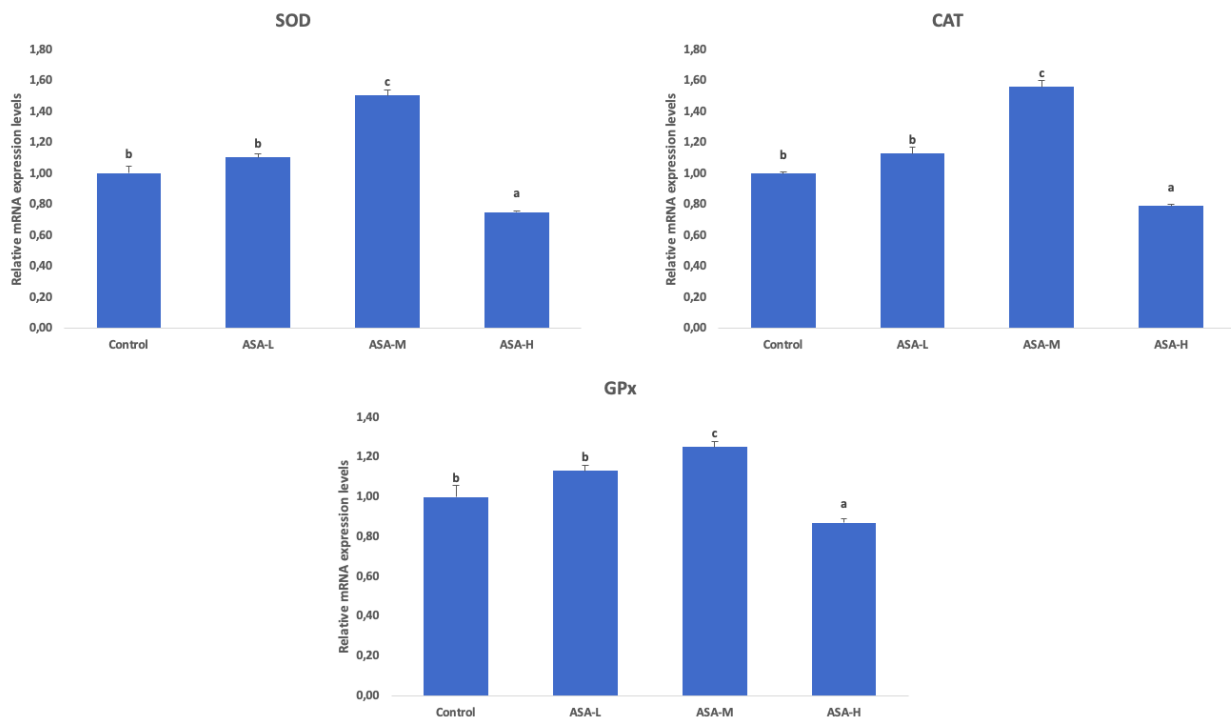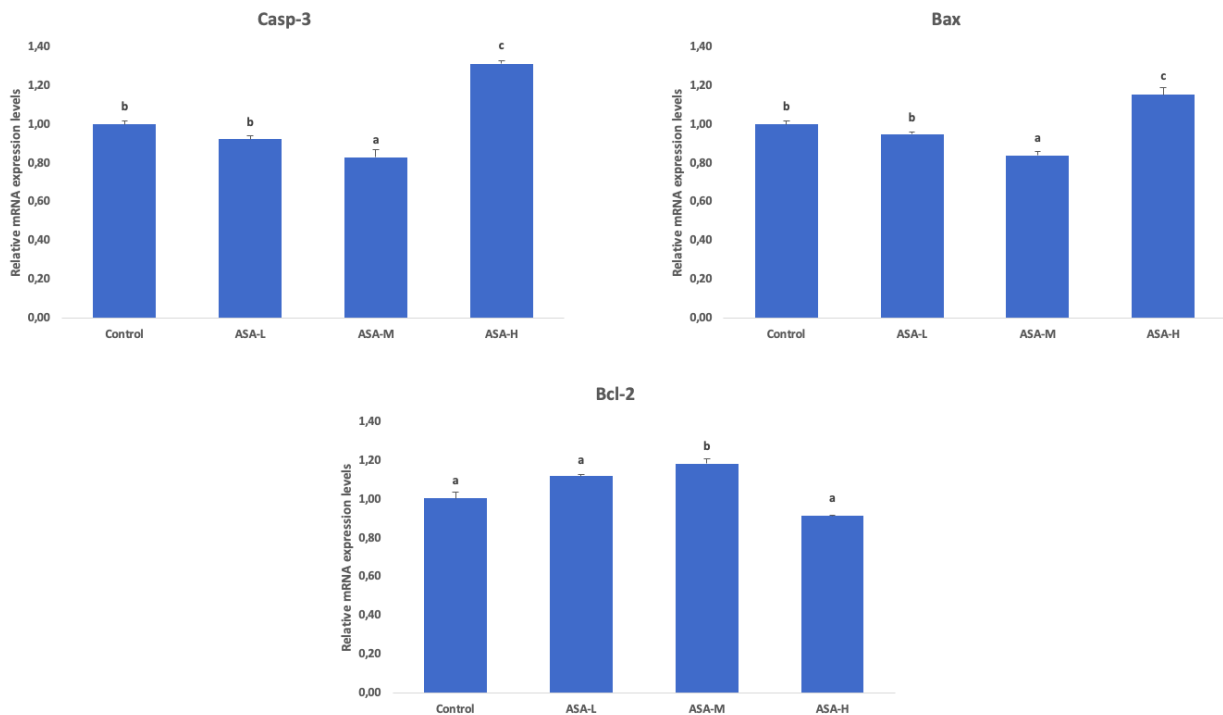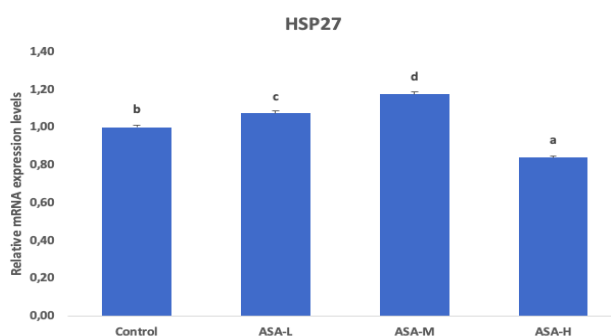
Figure 6. Effects of different doses of ASA on HSP27 mRNA transcription levels in rat hippocampus tissues. Values are given as mean ± SE. Different letters indicate statistical difference: *$p < 0.05$

3.7. Histopathological examinations

In the histopathological study, the morphological findings of the hippocampus were examined at high magnification (200x) according to the hematoxylin and eosin (H&E) staining results and are presented in Figure 7. When hippocampus samples obtained from rats in the control group were examined, it was observed that they had a normal histological structure. In addition, the CA1, CA2, CA3, and CA4 regions and the dental gyrus region could be easily distinguished. To standardize our comparisons, the CA1 and dental gyrus regions were defined and examined at high magnification (Figure 7a, 7a1). In the low- and moderate-dose images of the ASA-treated groups, the regular, dense, and regular arrangement of neurons in the CA1 regions of the hippocampi was striking. In addition, neurons in the CA1 region had clear, dark nuclei and a light cytoplasm. In the dental gyrus region, the molecular, granular, and polymorphic cell

layers were regular; in particular, the cells in the granular layer were quite compactly arranged and had characteristic cell bodies (Figure 7b, 7b1, 7c, 7c1). High-dose ASA treatment had undesirable effects, such as irregular neuronal arrangement and decreased neuronal density, compared with the control. There were also vacuoles and degenerative changes in the pericellular areas of the cells. In addition, nuclei became unclear and smaller, and cytoplasmic borders lost their normal structure (Figure 7d, 7d1).
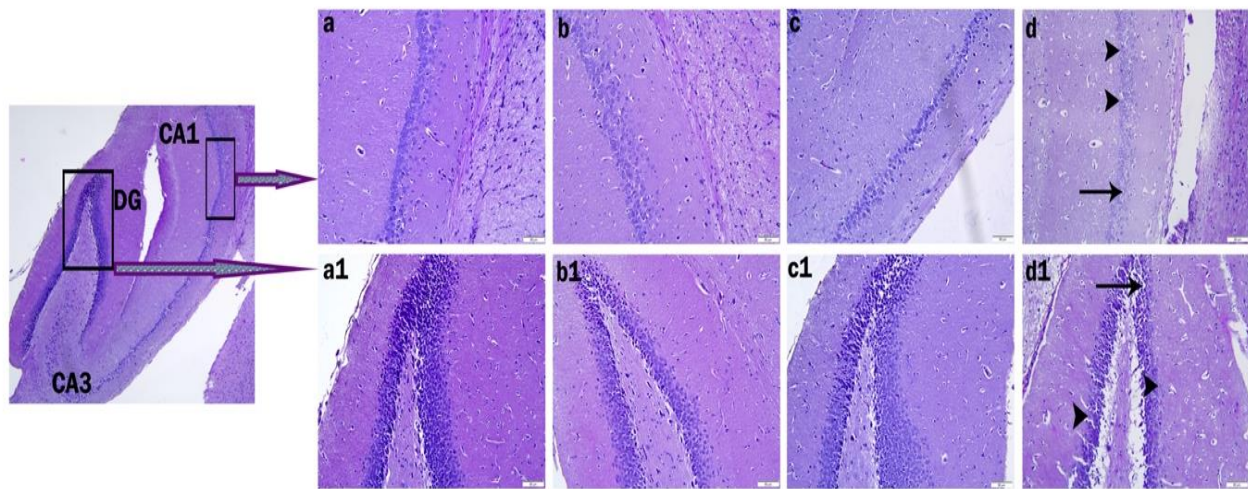
Figure 7. Representative photomicrographs of CA1 and dental gyrus regions of the hippocampus in all experimental groups. A,a1: Normal morphology of CA1 and dental gyrus regions in control group, b,b1: ASA-L group, c,c1: ASA-M group, d,d1: ASA-H group. Arrowheads: degenerating neurons, arrows: pericellular vacuolization. Hematoxylin and Eosin (H&E) staining, Original magnification: X200.

4. DISCUSSION AND CONCLUSION

NSAIDs are widely used worldwide to control pain and inflammation, with approximately 70 million prescriptions written each year in the US alone; these drugs usually have mild side effects at normal doses but can cause serious toxicity at excessive doses [14]. ASA is also an NSAID, and it can exert different pharmacological effects at different doses. Therefore, the effects of acute ASA administration at different doses on behavioral disorders were investigated using molecular, histological, and cognitive tests.

Inflammation and neutrophil migration are critical in the pathogenesis of NSAIDs [15]. Inflammation is the initial response of an organism to injury, which, when uncontrolled with the release of inflammatory mediators, can lead to inflammatory diseases and organ dysfunction [16]. NF-κB upregulation plays an important role in triggering inflammation [17]. NF-κB is involved in the stimulation of proinflammatory cytokines [18]. In the inflammatory process, NF-κB undergoes rapid phosphorylation by IkBα and IkB kinase-β (IKKβ), leading to the release of pro-inflammatory cytokines [19]. TNF-α and IL-1β, which are among these proinflammatory cytokines, are effective in the development of inflammation [20,21]. TNF-α leukocyte migration to the inflamed area in the tissues [22,23]. IL-1β triggers acute inflammatory responses by increasing the expression of adhesion molecules on endothelial cells, mobilizing inflammatory cells, and leading to the proliferation of circulating leukocytes [24]. In this study, the mRNA transcription levels of NF-κB, TNF-α, and IL-1β, which are effective against inflammation, were highest in the ASA-H group. In contrast, NF-κB, TNF-α, and IL-1β mRNA transcription levels were lower in the ASA-L and ASA-M groups than in the control group. These findings suggest that ASA can effectively alleviate inflammation at low and moderate doses and neuroinflammatory at high doses.

Oxidative stress is defined as the disruption of the balance between ROS and antioxidants in the presence of ROS [25,26]. In addition to neuroinflammation, oxidative stress has been suggested to contribute to the pathophysiological processes leading to neuronal loss in individuals with aging and neurological diseases, such as Alzheimer's disease and Parkinson's disease [27]. Oxidative stress activates different damage pathways [28–30]. The body has a defense system against the damage caused by free radicals [31]. Antioxidants are enzymatic and nonenzymatic agents [32]. Antioxidant enzymes such as SOD, CAT, and GPx are actively involved in scavenging oxygen-derived free radicals from oxidative stress to prevent further cell damage [33–35]. SOD, which converts superoxide to hydrogen peroxide (H_2O_2), is an important antioxidant enzyme involved in oxidative stress, whereas CAT, which converts H_2O_2 to oxygen and water, also plays an important role. Furthermore, GPx neutralizes the effects of cytotoxic lipid peroxides and H_2O_2 as a defense mechanism [36,37]. ROS, which are known as free radicals, cause oxidative damage by affecting macromolecules such as carbohydrates, proteins, nucleic acids, and lipids [38]. Increased ROS can cause cell death through proteolysis and lipid oxidation [39,40]. Owing to these properties, oxidative stress causes neuronal damage in brain tissue, which has at low defense against oxidative stress [41]. Potentially toxic drugs and their metabolites directly affect the biochemistry of the cell, firstly through increased oxidative stress and secondly through altered intracellular signaling pathways associated with apoptotic or necrotic

cell death [42]. According to the antioxidant capacity findings obtained in our study; ASA tried to resist neuronal damage by increasing antioxidant capacity at low and moderate doses, but at high doses it reduced antioxidant capacity and left the tissue vulnerable to neuronal damage.

Apoptosis, which protects the body by eliminating damaged or dangerous cells, can also cause stress or damage to healthy cells [43,44]. A relationship between intracellular ROS levels and apoptosis has also been reported [45]. Apoptosis pathways are activated by DNA or protein damage following excessive ROS production [46]. Apoptosis can also be induced by various stimuli such as cytokines, hormones, toxic insults, and viruses [47]. The mitochondrial pathway plays critical roles in apoptosis and is regulated by members of the Bcl-2 protein family, such as Bax and Bcl-2 [48,49]. Disruption of the balance between Bax and Bcl-2 in favor of Bax leads to the release of cytochrome C from mitochondria into the cytoplasm [50]. After cytochrome C passes into the cytoplasm, it combines with Apaf-1 to activate apoptotic caspase [51]. Caspases are inactive inside the cell; when a caspase becomes active, a chain reaction activates other pro-caspases [52]. Caspase-3, an important caspase, is also known as executioner caspase and is pro-apoptotic [53,54]. In this study, it was found that apoptotic activity in the ASA-H group was triggered by increased Casp-3 and Bax levels and a decrease in Bcl-2. On the other hand, in the ASA-L and ASA-M groups, apoptotic Casp-3 and Bax levels decreased while antiapoptotic Bcl-2 levels increased. When the apoptotic findings are evaluated together, ASA has ameliorative properties against apoptosis at low and moderate doses and increases at high doses.

Glutamate is an excitatory neurotransmitter in the brain that plays an important role in neuronal functions such as learning and memory. The activation of NMDA receptors leads to the formation of reactive oxygen and nitrogen species, which contribute to neuronal death [7]. Phosphorylation activation of CREB exhibits protective properties against apoptosis by accelerating Bcl-2 activation [55]. CREB is also one of the factors involved in memory and learning [56]. Glutamate and CREB mRNA transcription levels were increased in the ASA-M group, which may have contributed to the increase in neuronal and cognitive activity. The lowest NMDA level was detected in the ASA-M group. According to these findings, moderate-dose ASA may have a positive effect on cognitive function. High doses showed the opposite effect.

The open field test is commonly used to measure general locomotor activity and willingness to explore in rats [12]. Data on the effect of aspirin on cognitive functions are inconsistent; some studies suggest that ASA does not affect memory, while others argue that it positively affects neurocognitive behaviors. Furthermore, few placebo-controlled studies have failed to confirm the positive effects of aspirin on cognitive decline [57]. Increasing evidence suggests that aspirin may slow the progression of vascular pathology and cognitive loss in AD. However,

even at low doses, there is a risk of serious side effects, especially in elderly patients [7]. Although there was no difference between the groups in the findings of the open field test, the time spent, distance moved, and velocity in the center area were observed in the ASA-M group.

A similar picture was observed in hippocampus tissue. In ASA-L and ASA-M groups, histologic features close to the control group were found. However, in the ASA-H group, the adverse effects caused irregular arrangement and decreased density of neurons. In this group, there were signs of vacuolization and degeneration in the areas around the cells. Cell nuclei became smaller and indistinct and the boundaries of the cytoplasm were disrupted. Decreased antioxidant capacity and increased inflammation and apoptotic damages detected especially in the ASA-H group may have played a role in the formation of these structural defects.

As a conclusion, ASA may be effective in the prevention of behavioral disorders at low and moderate doses, whereas, at high doses, it may have the opposite effect and contribute to the progression of behavioral disorders.

REFERENCES

[1] Yan Z, Shi X, Wang H, Si C, Liu Q, Du Y. Neurotrophin-3 Promotes the Neuronal Differentiation of BMSCs and Improves Cognitive Function in a Rat Model of Alzheimer's Disease. Front Cell Neurosci 2021;15:629356.

[2] Mohammadbaghban E, Taravati A, Najafzadehvarzi H, Khaleghzadeh-Ahangar H, Tohidi F. Oral administration of encapsulated catechin in chitosan-alginate nanoparticles improves cognitive function and neurodegeneration in an aluminum chloride-induced rat model of Alzheimer's disease. Physiol Rep 2024;12:e16095.

[3] Abd-Elhakim YM, Abdel-Motal SM, Malhat SM, Mostafa HI, Moselhy AAA, Beheiry RR, et al. Curcumin mitigates neurotoxic and neurobehavioral changes of gentamicin and sodium salicylate in rats by adjusting oxidative stress and apoptosis. Life Sci 2021;265:118824.

[4] Mohamed DI, El-Din A, El-Waseef A, Nabih D;, El-Kharashi ES;, Abd El-Kareem OA;, et al. Acetylsalicylic Acid Suppresses Alcoholism-Induced Cognitive Impairment Associated with Atorvastatin Intake by Targeting Cerebral miRNA155 and NLRP3: In Vivo, and In Silico Study. Pharmaceutics 2022, Vol 14, Page 529 2022;14:529.

[5] Gholami M, Sadegh M, Koroush-arami M, Norouzi S, Arismani RJ, Asadi E, et al. Targeting memory loss with aspirin, a molecular mechanism perspective for future therapeutic approaches. Inflammopharmacology 2023 31:6 2023;31:2827–42.

[6] Vergil Andrews JF, Selvaraj DB, Kumar A, Roshan SA, Anusuyadevi M, Kandasamy M. A Mild Dose of Aspirin Promotes Hippocampal Neurogenesis and Working Memory in Experimental Ageing Mice. Brain Sciences 2023, Vol 13, Page 1108 2023;13:1108.

[7] Senol N, Ceyhan BM, Ersoy IH, Senol A, Acarturk G, Sutcu R. Aspirin increases NMDA receptor subunit 2A concentrations in rat hippocampus. Journal of Receptors and Signal Transduction 2012;32:17–21.

[8] de S. Moreira D, Figueiró PW, Siebert C, Prezzi CA, Rohden F, Guma FCR, et al. Chronic Mild Hyperhomocysteinemia Alters Inflammatory and Oxidative/Nitrative Status and Causes Protein/DNA Damage, as well as Ultrastructural Changes in Cerebral Cortex: Is Acetylsalicylic Acid Neuroprotective? Neurotox Res 2018;33:580–92.

[9] Blanchard HC, Taha AY, Rapoport SI, Yuan ZX. Low-dose aspirin (acetylsalicylate) prevents increases in brain PGE2, 15-epi-lipoxin A4 and 8-isoprostane concentrations in 9 month-old HIV-1 transgenic rats, a model for HIV-1 associated neurocognitive disorders. Prostaglandins Leukot Essent Fatty Acids 2015;96:25–30.

[10] Crisanti P, Laplace O, Lecain E, Jonet L, Jeanny JC, Omri B. The role of PKCζ in NMDA-induced retinal ganglion cell death: Prevention by aspirin. Apoptosis 2006;11:983–91.

[11] Espiridião S, Oliveira-Filho R, Simões M, Mamede J, L Kulay J. Liver and kidney ultrastructural changes caused by acetylsalicylic acid treatment during pregnancy in rats. Clin Exp Obstet Gynecol 2002;29:37–9.

[12] Wang J ying, Zhang Y, Chen Y, Wang Y, Li S yuan, Wang Y fei, et al. Mechanisms underlying antidepressant effect of transcutaneous auricular vagus nerve stimulation on CUMS model rats based on hippocampal α7nAchR/NF-κB signal pathway. J Neuroinflammation 2021;18.

[13] Livak KJ, Schmittgen TD. Analysis of Relative Gene Expression Data Using Real-Time Quantitative PCR and the 2−ΔΔCT Method. Methods 2001;25:402–8.

[14] Gür C, Kandemir Ö, Kandemir FM. Ratlarda diklofenak ile indüklenen kardiyotoksisite üzerine krisinin etkilerinin oksidatif stres, endoplazmik retikulum stresi ve apoptoz belirteçleri ile değerlendirilmesi. Kocatepe Veterinary Journal 2022;15:151–60.

[15] Simsek H, Akaras N. Acacetin ameliorates acetylsalicylic acid-induced gastric ulcer in rats by interfering with oxidative stress, inflammation, and apoptosis. Int J Med Biochem 2023;6:96–103.

[16] Semis HS, Gur C, Ileriturk M, Kaynar O, Kandemir FM. Investigation of the anti-inflammatory effects of caffeic acid phenethyl ester in a model of λ-Carrageenan–induced paw edema in rats. Hum Exp Toxicol 2021;40:S721–38.

[17] Semis HS, Gur C, Ileriturk M, Kandemir FM, Kaynar O. Evaluation of Therapeutic Effects of Quercetin Against Achilles Tendinopathy in Rats via Oxidative Stress, Inflammation, Apoptosis, Autophagy, and Metalloproteinases 2021;50:486–98.

[18] Semis HS, Kandemir FM, Kaynar O, Dogan T, Arikan SM. The protective effects of hesperidin against paclitaxel-induced peripheral neuropathy in rats. Life Sci 2021;287:120104.

[19] Kankılıç NA, Şimşek H, Akaras N, Gür C, Küçükler S, İleritürk M, et al. The ameliorative effects of chrysin on bortezomib-induced nephrotoxicity in rats: Reduces oxidative stress, endoplasmic reticulum stress, inflammation damage, apoptotic and autophagic death. Food and Chemical Toxicology 2024;190:114791.

[20] Ileriturk M, Ileriturk D, Kandemir O, Akaras N, Simsek H, Erdogan E, et al. Naringin attenuates oxaliplatin-induced nephrotoxicity and hepatotoxicity: A molecular, biochemical, and histopathological approach in a rat model. J Biochem Mol Toxicol 2024;38:e23604.

[21] Temel Y, Kucukler S, Yıldırım S, Caglayan C, Kandemir FM. Protective effect of chrysin on cyclophosphamide-induced hepatotoxicity and nephrotoxicity via the inhibition of oxidative stress, inflammation, and apoptosis. Naunyn Schmiedebergs Arch Pharmacol 2020;393:325–37.

[22] Kandemir Ö, Aksu EH. The Effects of Vancomycin on Sperm Motility and Testicular Inflammation in Rats. Veterinary Sciences and Practices 2022;17:41–4.

[23] Caglayan C, Temel Y, Kandemir FM, Yildirim S, Kucukler S. Naringin protects against cyclophosphamide-induced hepatotoxicity and nephrotoxicity through modulation of oxidative stress, inflammation, apoptosis, autophagy, and DNA damage. Environmental Science and Pollution Research 2018;25:20968–84.

[24] Kankılıç NA, Şimşek H, Akaras N, Gür C, İleritürk M, Küçükler S, et al. Protective effects of naringin on colistin-induced damage in rat testicular tissue: Modulating the levels of Nrf-2/HO-1, AKT-2/FOXO1A, Bax/Bcl2/Caspase-3, and Beclin-1/LC3A/LC3B signaling pathways. J Biochem Mol Toxicol 2024;38:e23643.

[25] Şimşek H, Küçükler S, Gür C, Akaras N, Kandemir FM. Protective effects of sinapic acid against lead acetate-induced nephrotoxicity: a multi-biomarker approach. Environmental Science and Pollution Research 2023;30:101208–22.

[26] Ozyigit F, Deger AN, Kocak FE, Ekici MF, Simsek H, Arık O. Protective effects of hesperidin in gastric damage caused by experimental ischemia-reperfusion injury model in rats. Acta Cir Bras 2024;39:e391124.

[27] Kara Y, Doguc DK, Kulac E, Gultekin F. Acetylsalicylic acid and ascorbic acid combination improves cognition; Via antioxidant effect or increased expression of NMDARs and nAChRs? Environ Toxicol Pharmacol 2014;37:916–27.

[28] Taştan TB, Akaras N, Demir Ö, Ugan RA. Protective effect of astaxanthin and metformin in the liver of rats in which the polycystic ovary syndrome model was formed by giving letrozole. Iran J Basic Med Sci 2023;26:688.

[29] Çomaklı S, Kandemir FM, Küçükler S, Özdemir S. Morin mitigates ifosfamide induced nephrotoxicity by regulation of NF-kappaB/p53 and Bcl-2 expression. Biotechnic & Histochemistry 2022;97:423–32.

[30] Cakmak F, Kucukler S, Gur C, Comakli S, Ileriturk M, Kandemir FM. Morin provides therapeutic effect by attenuating oxidative stress, inflammation, endoplasmic reticulum stress, autophagy, apoptosis, and oxidative DNA damage in testicular toxicity caused by ifosfamide in rats. Iran J Basic Med Sci 2023;26:1227.

[31] Erisir M, Kandemir FM, Yüksel M. The effects of Caesarean section on lipid peroxidation and some antioxidants in the blood of newborn calves. Vet Arh 2013;83:153–9.

[32] Kandemir FM, Ileriturk M, Gur C. Rutin protects rat liver and kidney from sodium valproate-induce damage by attenuating oxidative stress, ER stress, inflammation, apoptosis and autophagy. Mol Biol Rep 2022;49:6063–74.

[33] Ekinci Akdemir FN, Yildirim S, Kandemir FM, Aksu EH, Guler MC, Kiziltunc Ozmen H, et al. The antiapoptotic and antioxidant effects of eugenol against cisplatin-induced testicular damage in the experimental model. Andrologia 2019;51:e13353.

[34] Aksu EH, Kandemir FM, Yıldırım S, Küçükler S, Dörtbudak MB, Çağlayan C, et al. Palliative effect of curcumin on doxorubicin-induced testicular damage in male rats. J Biochem Mol Toxicol 2019;33:e22384.

[35] Akaras N, Toktay E, Celep NA, Yuce N, Simsek H, Ozkan HI. Antioxidant Effects of Bromelain on Paracetamol-Induced Renal Injury in Rats. Archives of Basic and Clinical Research 2023;5:364–71.

[36] Şimşek H, Gür C, Küçükler S, İleritürk M, Akaras N, Öz M, et al. Carvacrol Reduces Mercuric Chloride-Induced Testicular Toxicity by Regulating Oxidative Stress, Inflammation, Apoptosis, Autophagy, and Histopathological Changes. Biol Trace Elem Res 2024;202:4605–17.

[37] Akaras N, Abuc OO, Koc K, Bal T, Geyikoglu F, Atilay H, et al. (1 → 3)-β-d-glucan enhances the toxicity induced by Bortezomib in rat testis. J Food Biochem 2020;44:e13155.

[38] Aktas MS, Mehmet Kandemir F, Kirbas A, Hanedan B, Aydin MA. G Evaluation of oxidative stress in sheep infected with Psoroptes ovis using total antioxidant capacity, total oxidant status, and malondialdehyde level. J Vet Res 2017;61(2):197-201.

[39] Akarsu SA, Gür C, İleritürk M, Akaras N, Küçükler S, Kandemir FM. Effect of syringic acid on oxidative stress, autophagy, apoptosis, inflammation pathways against testicular damage induced by lead acetate. Journal of Trace Elements in Medicine and Biology 2023;80:127315.

[40] Çomaklı S, Özdemir S, Küçükler S, Kandemir FM. Beneficial effects of quercetin on vincristine-induced liver injury in rats: Modulating the levels of Nrf2/HO-1, NF-kB/STAT3, and SIRT1/PGC-1α. J Biochem Mol Toxicol 2023;37:e23326.

[41] Yıldız MO, Çelik H, Caglayan C, Kandemir FM, Gür C, Bayav İ, et al. Neuromodulatory effects of hesperidin against sodium fluoride-induced neurotoxicity in rats: Involvement of neuroinflammation, endoplasmic reticulum stress, apoptosis and autophagy. Neurotoxicology 2022;90:197–204.

[42] Keleş ON, Can S, Çiğşar G, Çolak S, Erol HS, Akaras N, et al. Hepatoprotective Effects of B-1,3-(D)-Glucan on Bortezomib-Induced Liver Damage in Rats. Kafkas Univ Vet Fak Derg 2014;20:929–38.

[43] Akaras N, Kucukler S, Gur C, Ileriturk M, Kandemir FM. Sinapic acid protects against lead acetate-induced lung toxicity by reducing oxidative stress, apoptosis, inflammation, and endoplasmic reticulum stress damage. Environ Toxicol 2024;39:3820–32.

[44] Akaras N, Gür C, Caglayan C, Kandemir FM. Protective effects of naringin against oxaliplatin-induced testicular damage in rats: Involvement of oxidative stress, inflammation, endoplasmic reticulum stress, apoptosis, and histopathology. Iran J Basic Med Sci 2024;27:466.

[45] Aksu EH, Kandemir FM, Küçükler S, Mahamadu A. Improvement in colistin-induced reproductive damage, apoptosis, and autophagy in testes via reducing oxidative stress by chrysin. J Biochem Mol Toxicol 2018;32(11):e22201.

[46] Şimşek H, Küçükler S, Gür C, İleritürk M, Aygörmez S, Kandemir FM. Protective effects of zingerone against sodium arsenite-induced lung toxicity: A multi-biomarker approach. Iran J Basic Med Sci 2023;26:1098.

[47] Akaras N, Gür C, Şimşek H, Tuncer SÇ. Effects of Quercetin on Cypermethrin-Induced Stomach Injury: The Role of Oxidative Stress, Inflammation, and Apoptosis. Gümüşhane Üniversitesi Sağlık Bilimleri Dergisi 2023;12:556–66.

[48] Akaras N, Kandemir FM, Şimşek H, Gür C, Aygörmez S. Antioxidant, Antiinflammatory, and Antiapoptotic Effects of Rutin in Spleen Toxicity Induced by Sodium Valproate in Rats. Türk Doğa ve Fen Dergisi 2023;12:138–44.

[49] Akaras N, Bal T, Atilay H, Selli J, Halici MB. Protective effects of agomelatine on testicular damage caused by bortezomib. Biotechnic & Histochemistry 2017;92:552–9.

[50] Kankılıç NA, Küçükler S, Gür C, Akarsu SA, Akaras N, Şimşek H, et al. Naringin protects against paclitaxel-induced toxicity in rat testicular tissues by regulating genes in pro-inflammatory cytokines, oxidative stress, apoptosis, and JNK/MAPK signaling pathways. J Biochem Mol Toxicol 2024;38:e23751.

[51] Gencer S, Gür C, İleritürk M, Küçükler S, Akaras N, Şimşek H, et al. The ameliorative effect of carvacrol on sodium arsenite-induced hepatotoxicity in rats: Possible role of Nrf2/HO-1, RAGE/NLRP3, Bax/Bcl-2/Caspase-3, and Beclin-1 pathways. J Biochem Mol Toxicol 2024;38:e23863.

[52] Şimşek H, Demiryürek Ş, Demir T, Atabay HD, Çeribasi AO, Bayraktar R, et al. Assessment of expressions of Bcl-XL, b-FGF, Bmp-2, Caspase-3, PDGFR-α, Smad1 and TGF-β1 genes in a rat model of lung ischemia/reperfusion. Iran J Basic Med Sci 2016;19:209.

[53] Yılmaz S, Küçükler S, Şimşek H, Aygörmez S, Kandemir FM. Naringin protects against colistin-induced sciatic nerve damage by reducing oxidative

171

stress, apoptosis and inflammation damage. J Exp Clin Med 2024;41:53–9.

[54] Tanyeli A, Eraslan E, Güler MC, Kurt N, Akaras N. Gossypin Protects Against Renal Ischemia-Reperfusion Injury in Rats. Kafkas Univ Vet Fak Derg 2020;26:89–96.

[55] Guo KM, Li W, Wang ZH, He LC, Feng Y, Liu HS. Low-dose aspirin inhibits trophoblast cell apoptosis by activating the CREB/Bcl-2 pathway in pre-eclampsia. Cell Cycle 2022;21:2223–38.

[56] Rangasamy SB, Dasarathi S, Pahan P, Jana M, Pahan K. Low-Dose Aspirin Upregulates Tyrosine Hydroxylase and Increases Dopamine Production in Dopaminergic Neurons: Implications for Parkinson's Disease. Journal of Neuroimmune Pharmacology 2019;14:173–87.

[57] Vergil Andrews JF, Selvaraj DB, Kumar A, Roshan SA, Anusuyadevi M, Kandasamy M. A Mild Dose of Aspirin Promotes Hippocampal Neurogenesis and Working Memory in Experimental Ageing Mice. Brain Sciences 2023, Vol 13, Page 1108 2023;13:1108.

Türk Doğa ve Fen Dergisi
Turkish Journal of Nature and Science
www.dergipark.gov.tr/tdfd

The Effect of Sodıum Hypochlorite and Hydrogen Peroxide on the Vase life of Cut Rose Flowers

Ezgi DOĞAN MERAL[1*] iD **, Çiçek ARMAN[2]** iD **Zahide SÜSLÜOĞLU[3]**, iD **Serda ARSLAN[4]** iD

[1,3]Bingöl University, Agriculture Faculty, Horticulture Department, Bingöl, Türkiye
[2,4] Bingöl University, Agriculture Faculty, Landscape Architecture Department, Bingöl, Türkiye
Ezgi DOĞAN MERAL ORCID No: 0000-0003-0854-7134
Çiçek ARMAN ORCID No: 0009-0008-5304-8290
Zahide SÜSLÜOĞLU ORCID No: 0000-0002-3958-6374
Serda ARSLAN ORCID No: 0009-0008-8792-2847

Corresponding Author: ezgidgn23@gmail.com

Abstract: Cut roses are a popular choice for bouquets and floral arrangements, but their short vase life can be a significant drawback. This study investigated the use of hydrogen peroxide (H_2O_2) and sodium hypochlorite as potential treatments to extend the vase life of cut roses. Cut flowers (*R. hybrida* cv 'Samourai') were placed in glass containing solutions in six different treatments: Hydrogen peroxide (H_2O_2, 400, 600, 800 μM); Sodium hypochlorite (NaOCl, 50, 100, 200 mg L^{-1}) and distilled water as a control. Vase life, relative fresh weight, water uptake, color change of flower, flower open rate, pH and EC changes of solutions were among the parameters recorded over 15 days. According to the results, the solution containing 600 μM of H_2O_2 resulted in the highest values for vase life, relative fresh weight, water uptake, and least color change of the flowers. This was followed by the solution containing 400 μM of H_2O_2. The 50 mg L^{-1} sodium hypochlorite treatment, along with the control, resulted in the lowest outcomes in terms of vase life, water uptake, and overall flower quality preservation during the vase life period. The quality and postharvest performance of cut rose flowers were found to be significantly affected by the use of 400 μM and 600 μM H_2O_2 in preservation solutions.

173

Sodyum Hipoklorit ve Hidrojen Peroksidin Kesme Gül Çiçeklerinin Vazo Ömrü Üzerine Etkisi

Öz: Kesme güller, buketler ve çiçek aranjmanlarında kullanılan önemli süs bitkilerindendir ancak kısa vazo ömürleri bu kullanımları için dezavantaj oluşturmaktadır. Bu çalışmada, farklı dozlarda hidrojen peroksit (H_2O_2) ve sodyum hipoklorit (NaOCl) kullanılarak kesme güllerin vazo ömrü üzerine etkileri araştırılmıştır. Çalışmada *R. hybrida* cv. 'Samourai' kesme çiçekleri 6 faklı uygulama içerisindeki solüsyonlara yerleştirilmiştir. Hidrojen peroksit, 400, 600, 800 μM dozları ile Sodyum hipoklorit 50, 100, 200 mg L^{-1} dozları kullanılan araştırmada kontrol grubu olarak ise distile su kullanılmıştır. Vazo ömrü, oransal taze ağırlık, toplam su alımı, goncaların renk değişimi, çiçek açılım oranı, solüsyonların pH ve EC değişimleri 15 gün boyunca izlenmiştir. Sonuçlara göre, 600 μM H_2O_2 uygulaması vazo ömrü, taze ağırlık, su alımı ve en az çiçek renk değişimi bakımından en yüksek değerlere sahipti. Bunu 400 μM H_2O_2 içeren uygulama takip etmiştir. Vazo ömrü boyunca kontrol ile birlikte 50 mg L^{-1} sodyum hipoklorit uygulaması hem vazo ömrü, su alımı bakımından hem de çiçeklerin kalitelerinin korunmasında iyi bir sonuç vermemiştir. 400 μM ve 600 μM H_2O_2 içeren vazo solüsyonlarının kullanılması kesme gül çiçeklerinin kalitesinin ve vazo ömrünün önemli ölçüde etkilendiği bulunmuştur. 400 ve 600 μM H_2O_2 uygulamalarının kesme gül çiçeklerinde vazo ömrünü uzattığı ve çiçek kalitesini koruduğu belirlenmiştir

1. INTRODUCTION

Extending the vase life and maintaining the quality of cut flowers is a crucial aspect of the floriculture industry. Factors such as water loss, ethylene exposure, microbial growth, and physiological changes can significantly impact the postharvest longevity of cut flowers [1]. Many variables affect cut flower vase life and postharvest performance [2,3]. Numerous elements influence it, such as ethylene, the atmosphere's makeup, flower handling, growing conditions, carbohydrates, blockage of the xylem channel, and chemical preservation solutions [4, 5] states that the most prevalent microorganisms in vase solutions, foliage, and stems of cut flowers are filamentous fungus, bacteria, and yeasts [6]. In the case of cut rose flowers, a common practice is to use chemical preservatives to prolong their vase life [6,7,8].

The post-harvest longevity of cut flowers is a critical factor in their successful commercialization and consumer satisfaction. Among the various flower varieties, roses are particularly susceptible to early senescence, leading to significant postharvest losses. [9]. To address this challenge, researchers have explored the use of treatments to prolong the vase life of cut roses. One potential approach is the application of sanitizing agents, such as sodium hypochlorite (NaClO) and hydrogen peroxide (H_2O_2), which have been shown to have antimicrobial properties and the ability to regulate physiological processes in cut flowers [1]. Sodium hypochlorite is a widely used disinfectant that can effectively suppress the growth of harmful bacteria and fungi, thereby reducing the risk of pathogen-induced deterioration in cut flowers [1]. Hydrogen peroxide, on the other hand, is a potent oxidizing agent that can directly impact the biochemical and physiological processes involved in flower senescence. [10]. Some studies have demonstrated that the treatment of these chemicals can significantly enhance the vase life of various cut flower species, including gladiolus and potted plants. However, there is a lack of comprehensive research on the specific effects of sodium hypochlorite and hydrogen peroxide on the vase life of cut rose flowers. The present study aims to investigate the efficacy of sodium hypochlorite and hydrogen peroxide, as cost-effective and readily available alternatives, on the vase life of cut roses.

2. MATERIAL AND METHOD

2.1. Material
Cut roses of *Rosa x hybrida* cv. 'Samourai' were used in the experiments. Early in the morning, flowering stems were taken at the tight (loose pointed bud) stage (commercial harvest stage) from a commercial grower in Şanlıurfa. In line with commercial procedures, stems were graded for consistent quality, bundled into bunches of several stems, and then recut to 35 cm in length. Within four to five hours, the bouquets were packed dry and delivered from the cultivation field to the refrigeration laboratory in commercial flower

boxes. The study was carried out in the vase life room of Bingöl University, Department of Horticulture.

In order to prevent air embolism, flowering stems were trimmed to a uniform length of 35 cm under distilled water upon arrival at the laboratory. Before being used, knives were surface sterilized by being rinsed in 95% (v/v) ethanol. Hands were used to remove leaves from the lowest 20 centimeters of stems that would have otherwise been submerged in vase water. The stems were arranged at random in glass vases holding 1000 ml of test solutions at different concentrations 1000 ml of distilled water (control). As mentioned previously for cutters, ethanol was used to surface sterilize glass vases. Various concentrations of Hydrogen Peroxide (H_2O_2, 400, 600, 800 μM; Sigma) and sodium hypochlorite (NaOCl, 50, 100, 200 mg L^{-1}; Sigma) were the test solutions. Flowers were put in a controlled environment room at 12 h photoperiod (08:00–20:00 h), 60±5%, 20±1∘C, relative humidity, and provided by 15 mol photons m^{-2} s^{-1} irradiance of fluorescent lamps On the day of the vase life experiment, the solutions were prepared freshly.

2.2. Method

2.2.1. Vase life

Each flower's vase life was determined by counting the days from the day the flowers were placed to the test solutions until they lost their decorative value (color altered, wilted, and lost turgidity). The maximum width of each blossom was used to establish the flower diameter, which was then measured using a vernier caliper. Fifteen flowers were chosen for each treatment, and vase life averages were calculated.

2.2.2. Relative fresh weight (RFW;%), Total solution uptake (g stem^{-1})

The average daily amount of vase solution absorbed by cut roses, vases, and flower stems was measured by independently weighing every three days. The results of subtraction were expressed in milliliters (mL). Fresh weight of flower stems was measured individually and every three days; the findings were reported as a percentage of the initial fresh weight (RFW).

Every three days the weights of the flowers and vases without flowers were measured separately. The average daily water uptake (Equality 1.) was calculated as follows:

$$\text{Daily water uptake (g stem}^{-1}\text{ day}^{-1}) = (S_{t-1} - S_t) \qquad (1)$$

where St is the weight (g) of the vase solution on day t = 1, 2, 3, etc. and S_{t-1} is the weight (g) of the vase solution on the previous day. The daily water intakes were then summed to determine the total solution uptake.

2.2.3. Colour change of flowers through the vase life

Color variations were recorded from the first to the last day, and CIELAB values were calculated using a colorimeter (Lovibond; Spectrophotometer a sphere, Serie SP60).

The CIE L*, a*, and b* color space system was used to gather measurements, and the a* and b* values were used to determine the hue angle ($h°$) ((Equality 2.) and chroma values ($C*$) (Equality 3.)

$$[h° = 180 + \tan^{-1}(b*/a*)] \qquad (2)$$
$$[C* = (a*^2 + b*^2)1/2] \qquad (3)$$

2.2.4. Flower opening rate (FOR)

The bud diameter was measured every three days from day 0 for up to 9 days in order to determine the flower opening rate. An equation of [11] was adjusted to estimate the ratio of flower opening (Equality 4.)

FOR (%) =
$$\frac{\text{Flower diameter on the dn} - \text{Flower diameter on the d0}}{\text{Flower diameter on the d0}} \times 100$$
(4)

n: 0,3,6,9 the end of the measurement

2.2.5. pH and EC of solutions through the vase life

Days 0 through 15th day were used to measure the pH of the solutions using a pH/ORP meter (HI 2211 HANNA Instruments RI/USA) and a Conductivity Benchtop (Orion 3-Star, Thermo Scientific) to estimate the electrical conductivity (EC).

2.3. Statistical Analysis

The experiment was established according to the randomised plots design with 5 replications and 3 plants in each replicate. Using SPSS software, the data were analyzed using analysis of variance (ANOVA), and differences between means were examined using the Duncan multiple test (P≤0.05).

3. RESULTS

3.1. Vase Life

Although statistically significant differences were observed between the treatments in terms of vase life, Hydrogen peroxide 600 μM and Hydrogen peroxide 400 μM were in the same statistical group (P≤ 0.05). The longest vase life was determined in Hydrogen peroxide 600 μM with 12.0 days, followed by Hydrogen peroxide 400 μM with 11.60 days and Sodium hypochlorite 200 mg L^{-1} with 10.0 days. The shortest vase life was obtained from the control group with 8.0 days (Figure 1).

175

Figure 1. Effect of different vase solutions on the vase life of cut roses (SH 50; sodium hypochlorite 50 mg L^{-1}, SH 100; sodium hypochlorite 100 mg L^{-1}, SH 200; sodium hypochlorite 200 mg L^{-1}, HP 400: Hydrogen peroxide 400 μM, HP 600: Hydrogen peroxide 600 μM, HP 800: Hydrogen peroxide 800 μM).

3.2. Relative Fresh Weight (RFW;%), Total Solution Uptake (g stem^{-1}),

The relative fresh weight of cut roses was found to grow in all treatments (except from SH 100 treatment)

until the third day, at which point it steadily dropped in all treatments (Figure 2).
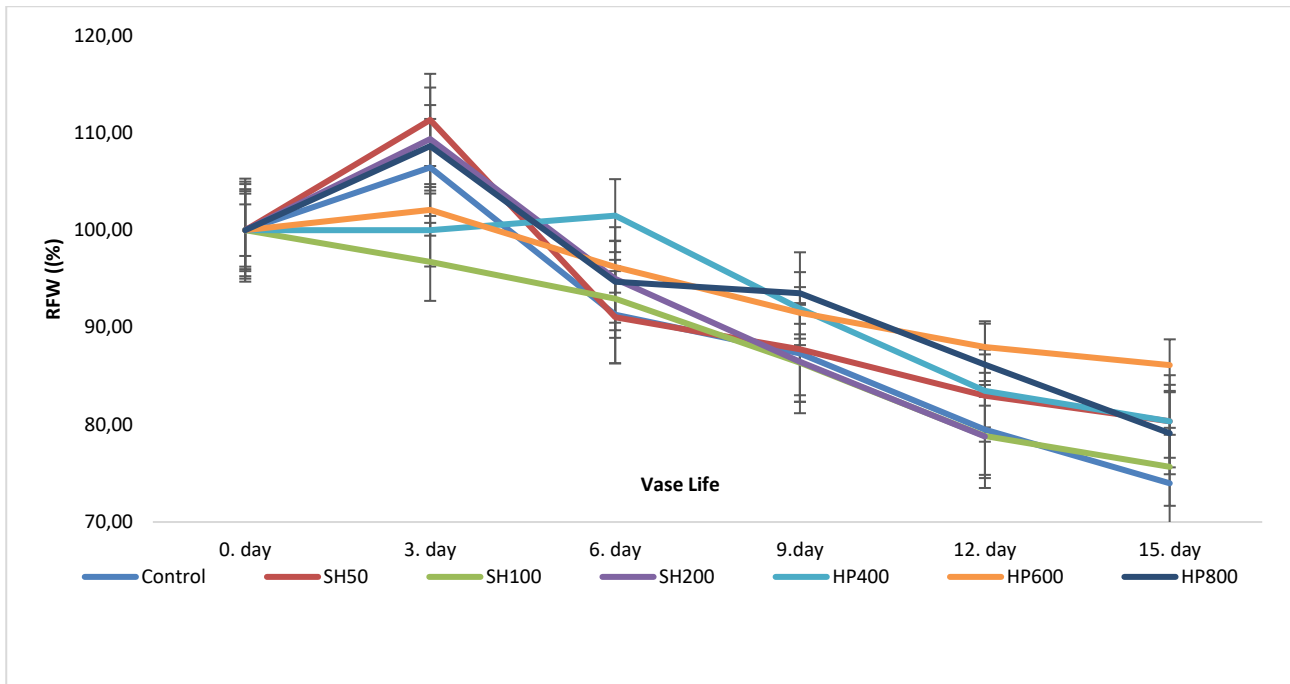
Figure 2. Effect of different vase solutions on relative fresh weight change in cut roses (SH 50; sodium hypochlorite 50 mg L^{-1}, SH 100; sodium hypochlorite 100 mg L^{-1}, SH 200; sodium hypochlorite 200 mg L^{-1}, HP 400: Hydrogen peroxide 400 μM, HP 600: Hydrogen peroxide 600 μM, HP 800: Hydrogen peroxide 800 μM).

Similar findings were obtained for solution uptake in terms of vase life results and statistically significant differences were observed between treatments in terms of total solution uptake (P≤ 0.05). The highest total solution uptake was determined in HP 600 treatment (58.61 g stem^{-1}), followed by HP 400 treatment (49.11 g stem^{-1}). The lowest solution uptake was realised in the control group (Figure 3).
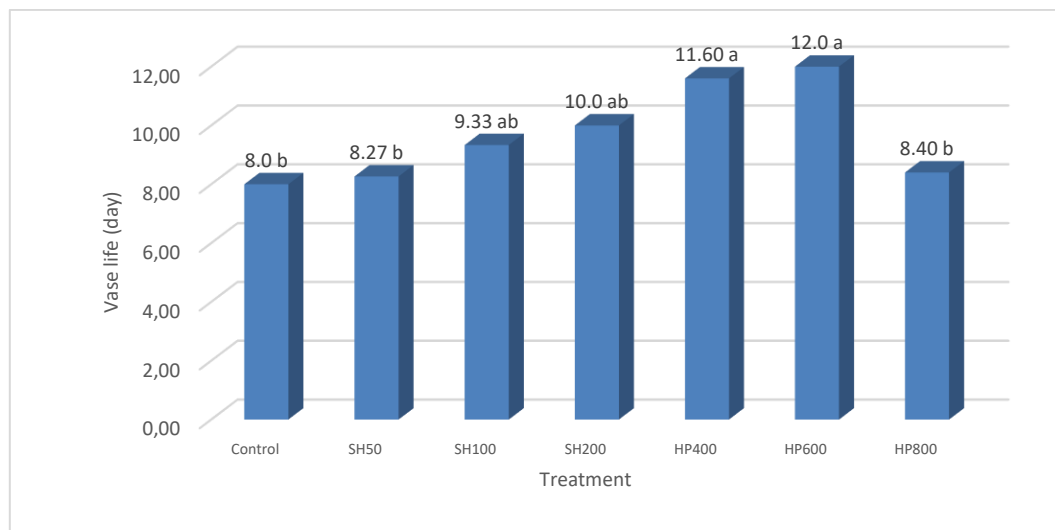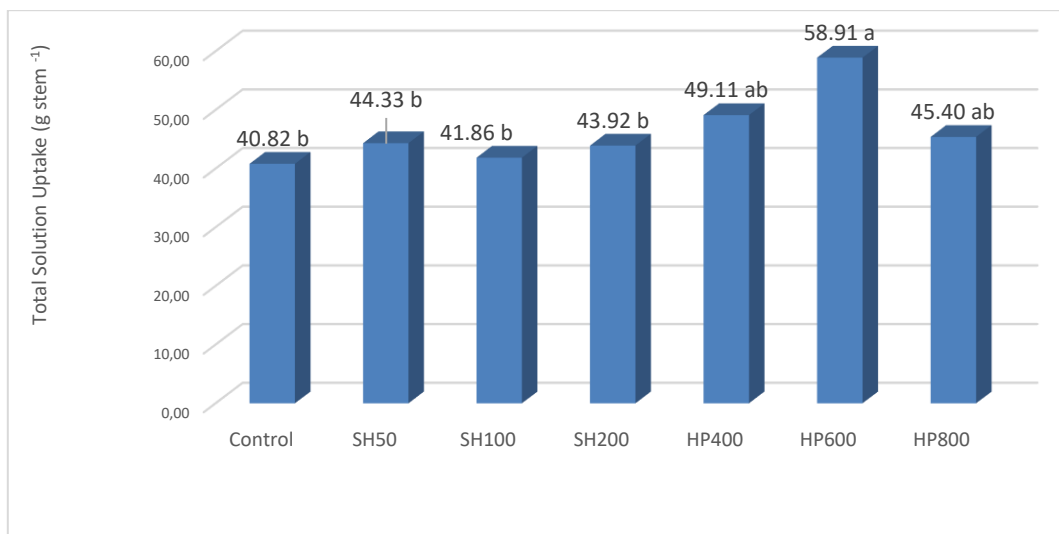
176

Figure 3. Effect of different vase solutions on total solution uptake in cut roses (SH 50; sodium hypochlorite 50 mg L^{-1}, SH 100; sodium hypochlorite 100 mg L^{-1}, SH 200; sodium hypochlorite 200 mg L^{-1}, HP 400: Hydrogen peroxide 400 μM, HP 600: Hydrogen peroxide 600 μM, HP 800: Hydrogen peroxide 800 μM).

3.3. Flower Opening Rate (%)

The fastest rate of flower opening was observed using sodium hypochlorite 100 mg L^{-1}, though the lowest ratio of flower opening was hydrogen peroxide 600 μM treatment. (Fig. 4).
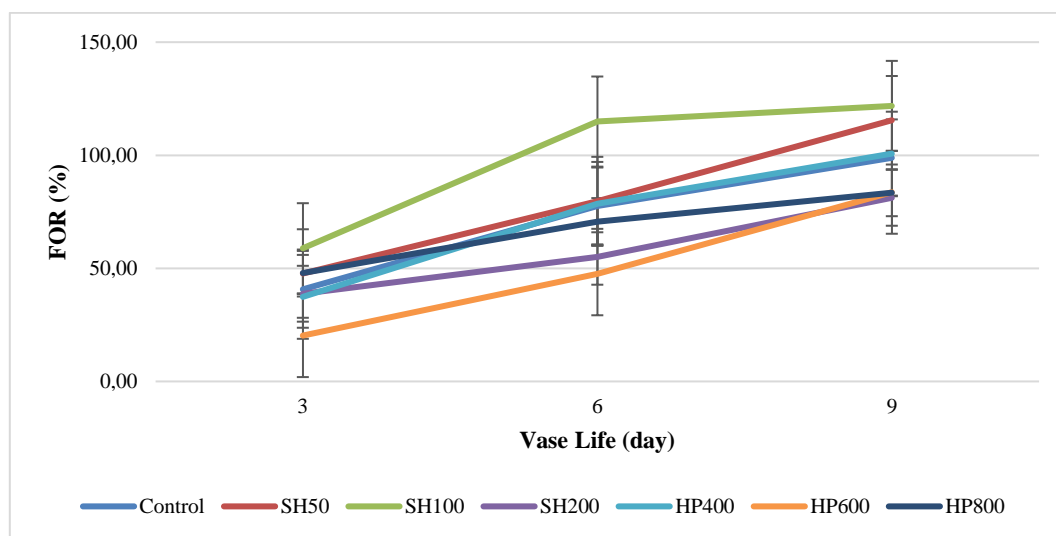

Figure 4. Flower Opening Rate (FOR) in cut roses (SH 50; sodium hypochlorite 50 mg L^{-1}, SH 100; sodium hypochlorite 100 mg L^{-1}, SH 200; sodium hypochlorite 200 mg L^{-1}, HP 400: Hydrogen peroxide 400 μM, HP 600: Hydrogen peroxide 600 μM, HP 800: Hydrogen peroxide 800 μM).

3.4. Colour Change of Flowers

Using a colorimeter, the adaxial side of each fresh petal measured during the vase life (day 0, day 6, day 12, day 15) was used to quantify each cultivar's color. The petal color was measured using the CIE $L*a*b*$ color space: The values of a* are red (positive) and green (negative); b* are yellow (positive) and blue (negative); $C*$, color chroma (higher values denoting increased brightness); $h*$, the color's hue angle between 0 and 360 [12]. $L*$, the color's lightness, falls between 0 (black) and 100 (white). As each rose was viewed through a different solution, the colors were perceived differently. Brightness values ($L*$) of most roses changed during the vase life (Table 1). Other variations in $L*$ $a*$ $b*$ values were seen in the study throughout the vase life of cut red roses. The fresh rose color exhibits high luminosity, or brightness, which is why the 'Samourai' cultivar of rose flowers had a high $L*$ value rating on the 0. day. The color turned dull and the $L*$ *value* decreased in all treatments—including the control—when the blossom had fully faded. In general, the value of the some treatment and control increased as the flower withered and turned brown, orange, pink, or yellow in the latter days of its vase life. The $b*$-*value* of cut rose is positive during the vase life. Aging may cause a modest browning or yellowing of the plants. Hue angles ($h°$ angle) and $C*$ values for red roses changed significantly during the vase life for all treatments (Table 1). The maximum color change was determined at 200 mg L^{-1} sodium hypochlorite the minimum color change was determined in 600 μM H_2O_2 (HP 600) (Table 1).

177

Table 1. The impact of different vase solutions on the hue angle ($h°$), chroma (C*), CIE $L*a*b*$ color values of cut roses throughout their vase life

Treatment	Day 0					Day 6					Day 12					Day 15				
	$L*$	$a*$	$b*$	$h°$	$C*$	$L*$	$a*$	$b*$	$h°$	$C*$	$L*$	$a*$	$b*$	$h°$	$C*$	$L*$	$a*$	$b*$	$h°$	$C*$
Control	36.5	36.5	36.5	21.87	55.6	34.3	48.5	20.64	23.0	52.8	25.0	30.79	19.2	31.9	36.3	18.4	29.5	15.0	27.0	33.1
SH50	32.5	46.7	19.7	22.86	50.6	31.8	45.9	18.4	21.8	49.6	28.1	41.39	15.0	19.8	44.0	27.4	41.3	12.5	16.9	43.7
SH100	32.8	46.4	17.1	20.20	49.4	31.1	44.5	15.84	19.6	47.4	23.9	33.01	6.72	11.5	33.7	15.7	18.1	0.99	3.13	18.1
SH200	32.7	45.9	19.7	23.26	49.9	31.5	44.3	17.32	21.4	47.5	16.2	29.29	2.79	5.4	29.4	15.8	20.4	2.5	6.98	20.6
HP400	34.1	51.9	20.4	21.43	55.7	33.7	48.7	18.9	21.2	52.2	31.9	46.63	16.8	19.8	49.6	29.9	44.7	15.9	19.7	47.5
HP600	35.7	49.7	19.7	21.65	53.4	35.2	43.7	17.88	22.3	47.2	33.6	41.8	15.3	20.1	44.5	30.8	40.7	14.9	20.1	43.3
HP800	35.6	50.4	20.5	22.10	54.4	29.6	49.3	19.45	21.6	53.0	29.3	47.47	11.5	13.6	48.8	28.7	45.3	11.1	13.8	46.7

SH 50; sodium hypochlorite 50 mg L^{-1}, SH 100; sodium hypochlorite 100 mg L^{-1}, SH 200; sodium hypochlorite 200 mg L^{-1}, HP 400: Hydrogen peroxide 400 μM, HP 600: Hydrogen peroxide 600 μM, HP 800: Hydrogen peroxide 800 μM.

4. DISCUSSION AND CONCLUSION

Cut roses are highly susceptible to water stress as the water balance in the petals is easily disturbed after harvesting and cut roses can also be affected by biotic stress causing microbiological vascular occlusion [12]. Our study reveals not only the water uptake of 'Samourai' cut roses after harvest, but also that the water relations of cut roses can be improved by adding additives to the vase solution. Placing the flowers in Hydrogen peroxide solution at a dose of 600 μM increased the vase life by 50% (Table 1), whereas H_2O_2 treatment at a dose of 800 μM caused a decrease in vase life. It is well known that H_2O_2 can cause oxidative stress at high concentrations [13, 14]. On the other hand, low H_2O_2 levels can improve resistance to a number of abiotic stressors, such as heat, drought, cold, and UV radiation. [15]. It has been found that H_2O_2 can positively regulate cut flower senescence at optimal concentrations. An essential signaling molecule, H_2O_2, is involved in many areas of plant development.[15]. Hydrogen peroxide has been shown in several scientific studies to help extend the vase life of cut flowers. In parallel with our study, a study on cut Oriental x Trumpet hybrid lilies revealed that hydrogen peroxide at a concentration of 600 μM increased the vase life of flowers from approximately 9.8 days to 12.8 days. This dose also delayed the opening time of flowers and helped to maintain chlorophyll and water content in the leaves. However, higher concentrations (800 and 1200 μM) showed negative effects. Similarly, in cut peony and gladiolus flowers, hydrogen peroxide treatments have been reported to be associated with oxidative stress and delay the vase life of flowers under the right conditions [16, 17]. A lack of study has been done on the benefits of H_2O_2 for cut flower preservation, despite the fact that it has been discovered to regulate a number of plant growth processes [18, 19, 20]. The pigments in petals showed less change in Hydrogen peroxide 400 μM, and 600 μM treatments during the vase life. Hydrogen peroxide may be an effective agent against bacterial or fungal pathogens due to its antimicrobial action, effectively limiting pathogens while maintaining water transmission and the stability of pigments in the bud. In addition, low doses of C_2H_2 oxidate may cause activation of antioxidant systems without causing damage. This may have limited the oxidation and degradation of pigments by triggering protective responses of cells against harmful effects.

Cut flowers are complicated plant organs; if the postharvest quality of the blooms is lost, the market may reject the product. This study analyzed the visual keeping quality of cut roses using flower opening and senescence. When flowering stems were immersed in 600 μM H_2O_2, they exhibited reduced flower opening and senescence in comparison to the control. This supports the earlier finding that 600 μM H_2O_2 prolonged vase life and parallels thestudy [17]. Many physiological and biochemical processes, including disruption of the water balance, deterioration of photosynthetic pigment, decrease of metabolic components, and loss of membrane integrity, are linked to the senescence of cut flowers [21, 22]. In this study,

there was a significant decrease in the RFW of flowers during the vase life (Figure 2), which has also been reported by some researchers [23, 24]. Compared to the control, 600 μM H_2O_2 significantly reduced the RFW decline of the flowers placed in the vase and the relative fresh weight of the flowers was the highest in the study (Figure 2). This indicates that H_2O_2 in the vase solution reduces the water loss of flowers. In addition, studies have proved that H_2O_2 plays a role in ABA-induced stomatal closure [25, 26]. Stomatal closure is known to be associated with an increase in RFW [27]. Our results also show that the loss of fresh weight was significantly suppressed by 600 μM H_2O_2This suggests that H_2O_2 can improve the water balance of cut flowers. According to Isbashi et al. [28], H_2O_2 spraying enabled *Glycine max* L. to avoid drought stress also through the maintenance of leaf water content. The control group in the study had the greatest pH, while the SH 50 treatment on day 0 had the lowest pH. During the vase life, pH changes varied in all treatments (Table 1). The pH fluctuations observed during the vase life can potentially be attributed to the composition of the fluids inside, the transport physiology of the plant and the amount of microorganisms involved in its metabolism. Shanan [29] and Paul et al. [30] also obtained similar results in their studies. EC values increased throughout the vase life including of the control. This may be due to an increase in the amount of dissolved ions in the water, deterioration in the quality of the vase solution or increased growth of microorganisms. Cell fluids released from plant stems may also increase the EC value. In addition, as bacteria grow in the vase solution, organic and inorganic substances may be released as a result of the metabolic activities of these microorganisms, which may increase the EC value of the water.

In conclusion, the vase life and preservation quality of cut flowers were enhanced by the vase solution's ideal H_2O_2 concentrations. Among all the ageing parameters evaluated, 400 μM and 600 μM H_2O_2 treatments maintained water uptake and reduced the proportional fresh weight loss of flowers, thus increasing the vase life of flowers. This study showed that H_2O_2 at 600 μM dose can be effective in extending the vase life of cut flowers and can be used as a potential floral preservative at the end of harvest of cut roses.

Acknowledgement

REFERENCES

[1] Thakur N. A review on the effect of storage methods and packaging material on the post-harvest longevity of cut flowers. Int J Chem Stud. 2020; 1;8(3):2375–9.

[2] Mayak S, Halevy AH, Sagie S, Bar-Yoseph A, Bravdo B. The water balance of cut rose flowers. Physiol Plan. 1974;31:15–22.

178

[3] Ichimura K, Kawabata Y, Kishimoto M, Goto R, Yamada K. Variation with the cultivar in the vase life of cut rose flowers. Bull Natl Inst Flor Sci. 2002;2:9–20.

[4] Pizano M. Research shows the way for postharvest treatment roses. Flower Technol. 2009;12(6):1–13.

[5] van Doorn WG. Water relations of cut flowers. Hort Rev. 1997;18:1–85.

[6] Meral DE. Increasing the vase life of cut carnation (*Dianthus caryophyllus* L. 'Baltico') by reducing xylem congestion with some solutions. ISPEC J Agric Sci. 2024;8(3):698–708.

[7] Kazaz S, Doğan E, Kılıç T, Ergür EG, Seyhan S. Influence of Holding Solutions on vase life of cut Hydrangea Flowers (*Hydrangea macrophylla* Thunb.). Fresenius Environ Bull. 2019;28(4A):3554–2559.

[8] Kazaz S, Kılıç T, Doğan E, Sekmen Ş. Vase life extension of cut hydrangea (*Hydrangea macrophylla*) flowers. J Hortic Sci Biotechnol. 2020;95(3):325–30.

[9] Reid MS, Jiang C. Postharvest Biology and Technology of Cut Flowers and Potted Plants. In: Horticultural Reviews. Wiley; 2012; p. 1–54.

[10] Akhtar G, Rajwana IA, Sajjad Y, Shehzad MA, Amin M, Razzaq K, et al. Do natural leaf extracts involve regulation at physiological and biochemical levels to extend vase life of gladiolus cut flowers? Sci Hortic. 2021;282:110042.

[11] Li Z, Zhou W, Wang P, Chen Y, Huo S, Wang J, et al. Transcriptome Analysis Reveals the Senescence Process Controlling the Flower Opening and Closure Rhythm in the Waterlilies (*Nymphaea* L.). Front Plant Sci. 2021; 4;12.

[12] van Doorn WG, Schurer K, de Witte Y. Role of Endogenous Bacteria in Vascular Blockage of Cut Rose Flowers. J Plant Physiol. 1989;134(3):375–81.

[13] Prochazkova D, Sairam RK, Srivastava GC, Singh DV. Oxidative stress and antioxidant activity as the basis of senescence in maize leaves. Plant Sci. 2001;161(4):765–71.

[14] Uchida A, Jagendorf AT, Hibino T, Takabe T, Takabe T. Effects of hydrogen peroxide and nitric oxide on both salt and heat stress tolerance in rice. Plant Sci. 2002;163(3):515–23.

[15] Neill S. Hydrogen peroxide signalling. Curr Opin Plant Biol. 2002 ;5(5):388–95.

[16] Skutnik E, Lukaszewska A, Serek M, Rabiza J. Effect of growth regulators on postharvest characteristics of *Zantedeschia aethiopica*. Postharvest Biol Technol. 2001;21(2):241–6.

[17] Liao W, Zhang ML, Huang GB, Yu J. Hydrogen peroxide in the vase solution increases vase life and keeping quality of cut Oriental×Trumpet hybrid lily "Manissa." Sci Hortic 2012;139:32–8.

[18] Fath A, Bethke PC, Jones RL. Enzymes That Scavenge Reactive Oxygen Species Are Down-Regulated Prior to Gibberellic Acid-Induced Programmed Cell Death in Barley Aleurone. Plant Physiol. 2001;126(1):156–66.

[19] Potocký M, Jones MA, Bezvoda R, Smirnoff N, Žárský V. Reactive oxygen species produced by NADPH oxidase are involved in pollen tube growth. New Phytol. 2007; 21;174(4):742–51.

[20] Liao W, Huang G, Yu J, Zhang M, Shi X. Nitric oxide and hydrogen peroxide are involved in indole-3-butyric acid-induced adventitious root development in marigold. J Hortic Sci Biotechnol. 2011 7;86(2):159–65.

[21] Langston BJ, Bai S, Jones ML. Increases in DNA fragmentation and induction of a senescence-specific nuclease are delayed during corolla senescence in ethylene-insensitive (etr1-1) transgenic petunias. J Exp Bot. 2005;56(409):15–23.

[22] Singh A, Kumar J, Kumar P. Effects of plant growth regulators and sucrose on post harvest physiology, membrane stability and vase life of cut spikes of gladiolus. Plant Growth Regul. 2008;55(3):221–9.

[23] Ferrante A, Vernieri P, Serra G, Tognoni F. Changes in abscisic acid during leaf yellowing of cut stock flowers. Plant Growth Regul. 2004;43(2):127–34.

[24] Mutui TM, Emongor VE, Hutchinson M. No The effects of gibberellin $_{4+7}$ on the vase life and flower quality of Alstroemeria cut flowers. Plant Growth Regul. 2006;48:207–14.

[25] Zhang F, Wang Y, Yang Y, Wu H, Wang D, Liu J. Involvement of hydrogen peroxide and nitric oxide in salt resistance in the calluses from *Populus euphratica*. Plant Cell Environ. 2007 Jul 23;30(7):775–85.

[26] Bright J, Desikan R, Hancock JT, Weir IS, Neill SJ. ABA-induced NO generation and stomatal closure in Arabidopsis are dependent on H_2O_2 synthesis. Plant J. 2006 Jan 6;45(1):113–22.

[27] García-Mata C, Lamattina L. Nitric Oxide Induces Stomatal Closure and Enhances the Adaptive Plant Responses against Drought Stress. Plant Physiol. 2001 Jul 1;126(3):1196–204.

[28] Ishibashi Y, Yamaguchi H, Yuasa T, Iwaya-Inoue M, Arima S, Zheng SH. Hydrogen peroxide spraying alleviates drought stress in soybean plants. J Plant Physiol. 2011 Sep;168(13):1562–7.

[29] Shanan N. Optimum pH Value for Improving Postharvest Characteristics and Extending Vase Life of *Rosa hybrida* cv. Tereasa Cut Flowers. Asian J Adv Agric Res. 2017;1(3):1–11.

[30] Paul D, Jannat A, Mahmud A, Akhter MJ, Mahmood S. Preservative solutions on vase life and quality of cut *Polianthes tuberosa* L. Ornam Hortic. 2021 Sep;27(3):417–24.

179

BİNGÖL UNIVERSITY

Carvacrol Ameliorates Cisplatin-Induced Cardiotoxicity By Regulating Notch/Hes1 Signaling Pathway, Oxidative Stress and Cell Death In Rat Cardiac Tissue

Nurhan AKARAS[1*] ID **, Özge KANDEMİR[2]** ID **, Hasan ŞİMŞEK[3]** ID

[1] Aksaray University, Faculty of Medicine, Department of Histology and Embryology, Aksaray, Türkiye
[2] Aksaray University, Vocational School of Technical Sciences, Department of Food Processing, Aksaray, Türkiye
[3] Aksaray University, Faculty of Medicine, Department of Physiology, Aksaray, Türkiye
Nurhan AKARAS ORCID No: 0000-0002-8457-9448
Özge KANDEMİR ORCID No: 0000-0001-8884-4168
Hasan ŞİMŞEK ORCID No: 0000-0001-5573-4923

Corresponding author: nurhanakaras@aksaray.edu.tr

Abstract: Cisplatin is one of the most active cytotoxic agents used mainly in the treatment of solid tumors. High doses and long-term use of Cisplatin are known to cause cardiotoxicity. In recent years, the antiapoptotic and antioxidant effects of Carvacrol in cardiovascular diseases have attracted attention. In this study, the effects of Carvacrol on Cisplatin-induced cardiotoxicity in a rat model were investigated using biochemical and histological methods. Twenty-eight rats were divided into 4 groups: 1. Control group, 2. Carvacrol group, 3. Cisplatin group, 4. Cisplatin + Carvacrol group. The expression of antioxidant enzymes, proinflammatory cytokines, apoptotic, and autophagic proteins was examined in heart tissue obtained from rats sacrificed after the last drug administration. Additionally, heart tissue was evaluated histopathologically. Cisplatin has been observed to cause oxidative stress and inflammatory damage in animal heart tissue. Carvacrol administration significantly increased antioxidant enzyme (superoxide dismutase and glutathione peroxidase) activities while suppressing inflammatory markers (NF-κB, TNF-α, IL-1β). Additionally, Cisplatin induced apoptotic (caspase-3, Bax, Bcl-2) and autophagic (Beclin-1, LC3A, LC3B) markers. It has been determined that carvacrol can protect heart tissues from the destructive effects of cisplatin by exerting anti-apoptotic and anti-autophagic effects. The expression levels of Notch1 and Hes1, which were decreased by cisplatin administration, were upregulated after administration of Carvacrol. H&E staining results showed that Carvacrol preserved myocardial tissue integrity. In conclusion, Carvacrol showed a cardioprotective effect against cisplatin-induced cardiotoxicity.

180

Karvakrol Sıçan Kalp Dokusunda Notch/Hes1 Sinyal Yolunu, Oksidatif Stresi ve Hücre Ölümünü Düzenleyerek Sisplatin Kaynaklı Kardiyotoksisiteyi İyileştirir

Öz: Sisplatin esas olarak katı tümörlerin tedavisinde kullanılan en aktif sitotoksik ajanlardan biridir. Sisplatin'in yüksek doz ve uzun süreli kullanımı kardiyotoksisiteye neden olduğu bilinmektedir. Son yıllarda kardiyovasküler hastalıklarda Karvakrol'ün antiapoptotik ve antioksidan etkileri ilgi görmüştür. Bu çalışmada, bir sıçan modelinde Karvakrol'ün Sisplatin kaynaklı kardiyotoksisite üzerindeki etkileri biyokimyasal ve histolojik yöntemler kullanılarak araştırılmıştır. Yirmi sekiz sıçan 4 gruba ayrıldı: 1. kontrol grubu, 2. Karvakrol grubu, 3. Sisplatin grubu, 4. Sisplatin + Karvakrol grubu. Son ilaç uygulamasından sonra öldürülen sıçanlardan elde edilen kalp dokusunda antioksidan enzimlerin, proinflamatuar sitokinlerin, apoptotik ve otofajik proteinlerin ekspresyonu incelenmiştir. Ayrıca kalp dokusu histopatolojik olarak değerlendirilmiştir. Sisplatin'in hayvanların kalp dokusunda oksidatif strese ve inflamatuar hasara neden olduğu gözlenmiştir. Karvakrol uygulamasının antioksidan enzim (süperoksit dismutaz ve glutatyon peroksidaz) aktivitelerini önemli ölçüde artırırken, inflamatuar belirteçleri (NF-κB, TNF-α, IL-1β) baskıladı. Ayrıca Sisplatin'in apoptotik (caspase-3, Bax, Bcl-2) ve otofajik (Beclin-1, LC3A, LC3B) belirteçleri indükledi. Karvakrol'ün ise anti-apoptotik ve anti-otofajik etki

göstererek kalp dokularını Sisplatin'in yıkıcı etkisinden koruyabildiği belirlenmiştir. Sisplatin uygulaması ile azalmış Notch1 ve Hes1 ekspresyon seviyeleri Karvakrol uygulamasından sonra düzenlenmiştir. H&E boyama sonuçları Karvakrol'ün miyokardiyal doku bütünlüğünü koruduğunu göstermiştir. Sonuç olarak, Karvakrol Sisplatin kaynaklı kardiyotoksisiteye karşı kardiyoprotektif bir etki gösterdi.

1. INTRODUCTION

Cancer, which is expected to increase in the future and poses a major health risk worldwide, is a major cause of disease-related morbidity and mortality. Cancer-related morbidity is not only caused by the disease but also includes the effects of chemotherapy [1-3]. Anti-cancer drugs must be prescribed to treat the disease, and the outcome is hoped to be successful. However, this hope is soon disappointed due to the effects of harmful chemicals that cause multi-organ toxicity and disruption of DNA structure and/or function [4,5]. Cisplatin (CIS, cis-dichlorodiamine platinum II), an anticancer drug, is an inorganic platinum widely used for treating many solid cancers [6,7]. Because CIS cannot distinguish between normal and cancer cells, toxic effects that occur during its use may result in a reduction in the dose or discontinuation of treatment. CIS causes various dose-dependent acute and cumulative side effects, including nephrotoxicity, cardiotoxicity, neurotoxicity, ototoxicity, myelosuppression, and gastrointestinal toxicity [8,9]. There is evidence that CIS can cause acute or chronic cardiotoxicity in the form of electrocardiographic changes and arrhythmias (ventricular arrhythmias, supraventricular tachycardia, atrial fibrillation, atrioventricular block), myocarditis, pericarditis, acute myocardial infarction, hypertension, and coronary vasospasm [8-11]. Recent studies have suggested that oxidative stress plays a significant role in the aforementioned CIS-induced side effects [6,9].

CIS treatment stimulates oxidative stress, apoptosis, and autophagy, and these adverse effects are attributed to its side effects in the body [6,8,9]. Because the oxidant/antioxidant balance is disrupted by excessive production of reactive oxygen species (ROS), increased oxidative stress affects macromolecules, such as membrane lipids, proteins, and DNA, in body cells and thus damages cell integrity [12,13]. Despite this information, the mechanisms involved in cardiotoxicity are still not well characterized. Researchers are constantly searching for ways to prevent the side effects of CIS, increase chemotherapy effects, and reduce costs [7].

Many antioxidants and drugs have been used to completely or partially protect vital organs and cells against CIS damage. However, hope lies in the combination of herbal medicines with targeted drugs. Medicinal plants and their active ingredients are widely used to treat diseases [7,14]. Several medicinal plants have been reported to reduce the toxicity of CIS [7,15-17].

Carvacrol (CRV) is the major monoterpene phenol isomeric with thymol, and it is found in various essential oils in plant species such as Origanum, Thymus, and Corydothymus. Essential oils containing high CRV levels have strong antioxidant properties comparable to those of ascorbic acid, butylated hydroxytoluene, and vitamin E [6,18]. CRV possesses various pharmacological properties, including antioxidant, antimicrobial, antibacterial, and antiapoptotic properties, through its inhibition of proapoptotic effects [7,19,20].

Preventing and/or reducing the side effects of cancer drugs are among the main concerns for patients who must take medications for a long time or permanently. This study describes a novel method for achieving success without exposing these treatments to new drug toxicity. Therefore, this study investigated the efficacy of CRV in improving the toxic effects by inhibiting CIS-induced oxidative damage and apoptosis in rat cardiac tissues.

2. MATERIAL AND METHOD

2.1. Chemicals and Reagents

CIS (CDDP, 25 mg/50 mL) was purchased from Koçak Farma (Istanbul, Turkey). CRV (CAS No. 499-75-2, purity: 98%) was obtained from Sigma-Aldrich Co. (St. Louis, MO, USA). Other chemicals (analytical grade) used in this study were purchased from Sigma and Merck.

2.2. Animals and Experimental Design

In this study, 28 *Wistar albino* rats, weighing 200-250 g and aged 10-12 weeks, were used. The animals were kept in cages in a controlled room with a constant temperature of 24-25°C and a twelve (12 h) hour light-dark cycle (07:00-19:00 light; 19:00-07:00 dark). Rats were fed unlimited amounts of water and standard chow. All animal experiments were performed at the KONÜDAM Experimental Medicine Application and Research Center. The procedures were approved by the local Animal Experiments Ethics Committee (Date: 25.09.2024, meeting no: 2024-080). Previous studies were used to determine the drug and active ingredient doses in this study [4,21,22].

Wistar albino rats were randomly divided into 4 groups with 7 rats in each group.
- Control group: Physiological serum was administered intraperitoneally on the first day.
- Carvacrol group: 50 mg/kg CRV was given orally for 4 days.
- Cisplatin group: On day 1, a single 7 mg/kg dose of CIS was administered intraperitoneally.
- Cisplatin + Carvacrol 50: On the first day, 7 mg/kg CIS was administered intraperitoneally as a single dose, and 50 mg/kg CRV was administered orally for 4 days.

181

24 hours after the last drug administration (day 5), the animals were decapitated under light sevoflurane anesthesia, and heart tissue and blood samples were collected. Blood samples were transferred to vacuum tubes without anticoagulant for biochemical analyses, centrifuged at 3000 rpm at +4 °C for 10 min, and the serum was separated and stored in a deep freezer at -20°C until biochemical analyses were performed.

2.3. Real Time PCR (RT-PCR)

The relative mRNA transcript levels of the gene regions listed in Table 1 were examined in the heart tissues of rats with CIS injury and CRV administration using qRT–PCR technique. First, total RNA was isolated from tissues using QIAzol Lysis Reagent (79306; Qiagen). Then, cDNA synthesis was performed from these RNA samples using the OneScript Plus cDNA Synthesis Kit (ABM, G236, Richmond, Canada). The prepared cDNAs were mixed with primer sequences and BlasTaq™ 2X qPCR MasterMix (ABM, G891, Richmond, Canada) to form a reaction mixture. The mixture was run on a Rotor-Gene Q (Qiagen) instrument for specified time and temperature cycles according to the manufacturer's instructions. After completion of the cycles, gene expressions were normalized to β-Actin and evaluated using the 2-ΔΔCT method [23].

Table 1. Primer sequences

Gene	Sequences (5'-3')	Product length
Cu-Zn SOD	F: AGTCCCGCCCCTTCTAAAAC R: CAATGGCCTCTGTGTAGCCC	387
CAT	F: ATGGCAACTGTCCCTGAACT R: AGTGACACTGCCTTCCTGAA	670
GPx	F: CTCGAGTGACAAGCCCGTAG R: ATCTGCTGGTACCACCAGTT	290
NF-κB	F: AGTCCCGCCCCTTCTAAAAC R: CAATGGCCTCTGTGTAGCCC	106
IL-1β	F: ATGGCAACTGTCCCTGAACT R: AGTGACACTGCCTTCCTGAA	197
TNF-α	F: CTCGAGTGACAAGCCCGTAG R: ATCTGCTGGTACCACCAGTT	139
Caspase-3	F: ACTGGAATGTCAGCTCGCAA R: GCAGTAGTCGCCTCTGAAGA	270
Bax	F: TTTCATCCAGGATCGAGCAG R: AATCATCCTCTGCAGCTCCA	154
Bcl-2	F: GACTTTGCAGAGATGTCCAG R: TCAGGTACTCAGTCATCCAC	214
Beclin-1	F: TCTCGTCAAGGCGTCACTTC R: CCATTCTTTAGGCCCCGACG	198
LC3A	F: GACCATGTTAACATGAGCGA R: CCTGTTCATAGATGTCAGCG	139
LC3B	F: GAGCTTCGAACAAAGAGTGG R: CGCTCATATTCACGTGATCA	152
Notch1	F: GTGGGATGGACTGGACTGTG R: GCGCAGGAAGTGGAAGGAGTT	117
Hes1	F: CGCCGGGCAAGAATAAATGA R: ATGTCTGCCTTCTCCAGCTT	104
β-Actin	F: CAGCCTTCCTTCCTGGGTATG R: AGCTCAGTAACAGTCCGCCT	360

2.4. Histopathological Analysis

Tissue specimens were kept in 10% formalin solution for 48 h for fixative purposes. Fixed tissues were first passed through increasing grades of alcohol (70-100%) and then cleared in xylene. As the last step in the tissue tracking phase, 5 μm thick sections were prepared from the prepared paraffin blocks using a microtome. The prepared sections were stained with hematoxylin and eosin (H&E) for general histological evaluation. Stained sections of cardiac tissues were examined under a light microscope (Olympus Cx43; Japan) and photographed.

2.5. Statistical Analysis

Statistical analysis of biochemical findings was performed using one-way ANOVA and Tukey HSD test was used to determine the relationship between the groups. Results are presented as Mean ± Standard Error Mean. The results of histological examination were analyzed using the nonparametric Kruskal-Wallis test and Mann–Whitney U test for comparison of paired groups. The statistical significance level was set as $p < 0.05$.

3. RESULTS

3.1. Anti-Oxidant Effect of Carvacrol on Cisplatin-Induced Oxidative Stress

The antioxidant effects of CRV on CIS-induced oxidative stress in rat heart tissue are presented in Figure 1. In the CIS alone group, there was a significant decrease in the expression of SOD, CAT, and GPx compared with the control group. In contrast, combined treatment with CIS and CRV triggered an increase in the levels of antioxidants (SOD, GPx) compared with the CIS group. These results demonstrate that CRV partially reduces the CIS effect by decreasing total antioxidant activation in rat cardiac tissue.

Figure 1. Effect of Carvacrol and Cisplatin treatments on SOD, CAT, GPx mRNA expression levels in heart tissue. Values are given as mean ± SD. Control vs others: *p < .05, **p < .01, ***p < .001, CIS vs others: #p < .05, ##p < .01, ###p < .001

3.2. Anti-Inflammatory Effect of Carvacrol on Cisplatin-Induced Inflammation

The expressions of inflammation markers in rat heart tissue are presented in Figure 2. In this study, CIS administration induced a series of inflammatory changes that mediated cardiac tissue damage. The levels of NF-kB, TNF-α and IL-1β, which are important markers involved in inflammation, were higher in the CIS group than in the control (p <0.001). Combined treatment with CIS and CRV reduced the levels of these markers by attenuating CIS-induced inflammation. However, there was no significant difference in NF-kB, TNF-α and IL-1β levels between the control and CRV groups.

183

Figure 2. Effect of Carvacrol and Cisplatin treatments on NF-κB, TNF-α, IL-1β mRNA expression levels in heart tissue. Values are given as mean ± SD. Control vs others: *p < .05, **p < .01, ***p < .001, CIS vs others: #p < .05, ##p < .01, ###p < .001

3.3. Anti-Apoptotic Effect of Carvacrol on Cisplatin-Induced Apoptosis

The anti-apoptotic effect of CRV against CIS-induced apoptosis in rat cardiac tissue is presented in Figure 3. The expression levels of pro-apoptotic Bax, anti-apoptotic Bcl-2, and caspase-3 (Casp-3) proteins were examined, and no significant differences were found between control and CRV. While there was a decrease in Bcl-2 expression in the CIS group, there was a significant increase in Bax and Casp-3 protein levels. In the CIS+CRV group, there was an increase in Bcl-2 expression and a significant decrease in Bax and Casp-3 protein expressions, unlike the group given only CIS.
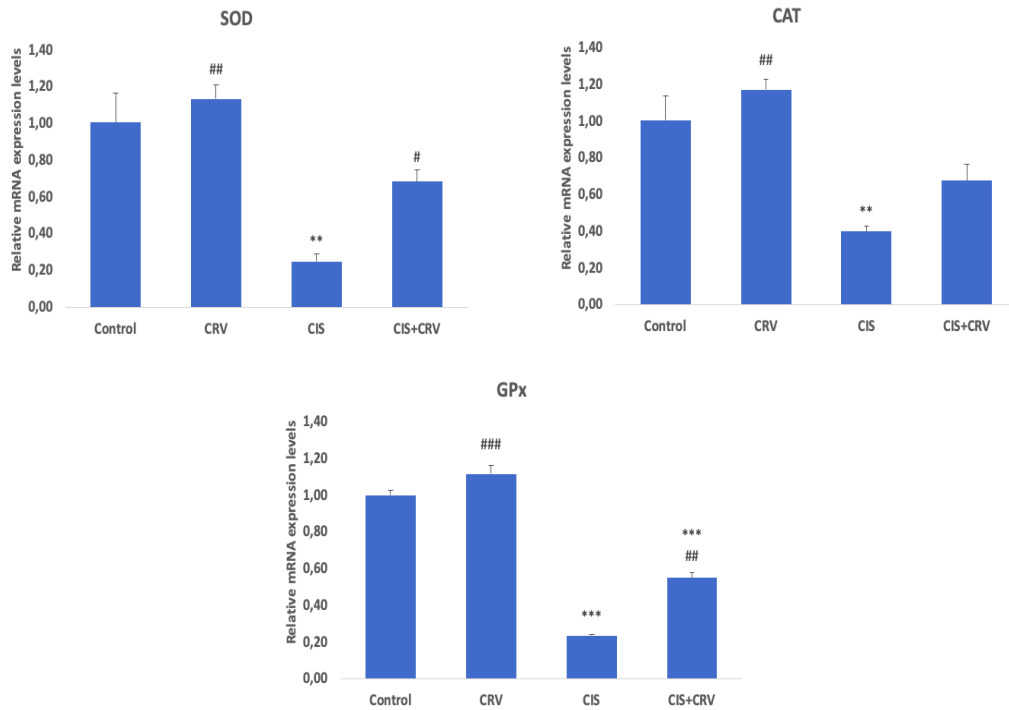

Figure 3. Effect of Carvacrol and Cisplatin treatments on Bax, Bcl-2, Casp-3 mRNA expression levels in heart tissue. Values are given as mean ± SD. Control vs others: *$p < .05$, **$p < .01$, ***$p < .001$, CIS vs others: #$p < .05$, ##$p < .01$, ###$p < .001$

3.4. Anti-Autophagic Effect of Carvacrol on Cisplatin-Induced Autophagy

Autophagic protein levels using the PCR method are presented in Figure 4. In the CIS group, Beclin-1, LC3A, and LC3B expression levels increased significantly compared with the control group ($p<0.001$). On the contrary, there was a significant decrease in autophagic parameters in the CIS+CRV group.
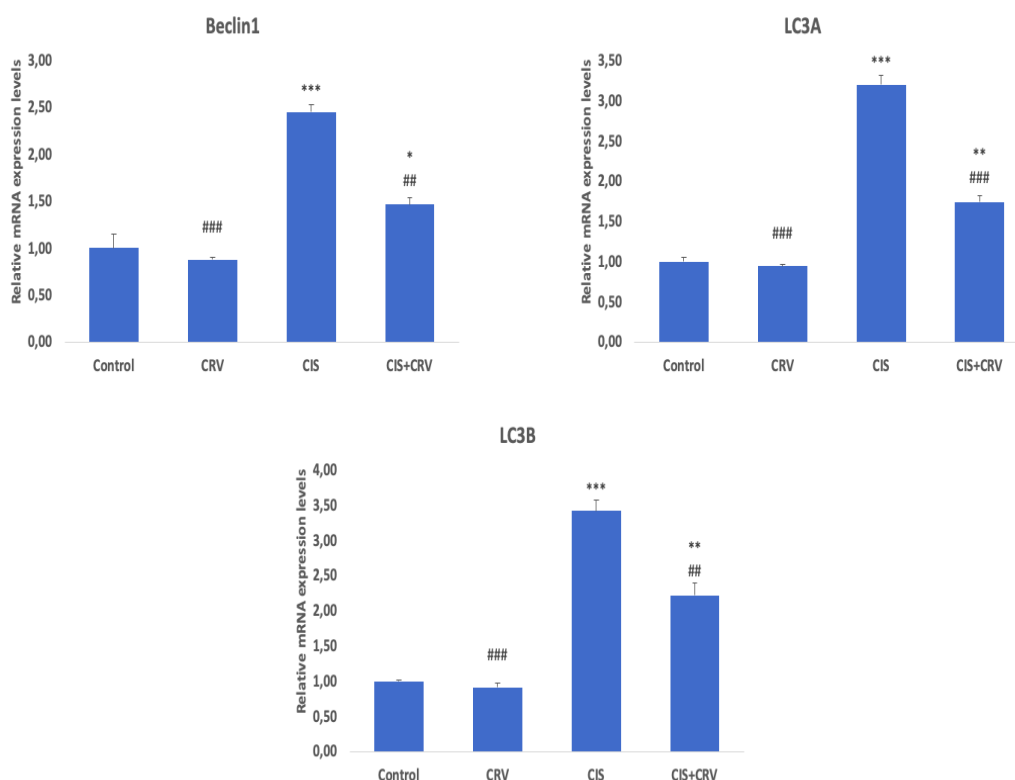
Figure 4. Effect of Carvacrol and Cisplatin treatments on Beclin-1, LC3A, LC3B mRNA expression levels in heart tissue. Values are given as mean ± SD. Control vs others: *p < .05, **p < .01, ***p < .001, CIS vs others: #p < .05, ##p < .01, ###p < .001

3.5. Effect of Carvacrol on Cisplatin-Induced Decreased Notch1 and Hes1 Protein Expressions

In this study, the Notch1/Hes1 pathway was examined using RT-PCR, and the results are presented in Figure 5.

The results show that CIS treatment downregulates the Notch1/Hes1 pathway. However, CRV application significantly increased Notch1 and Hes1 levels compared with the CIS group (p <0.05).
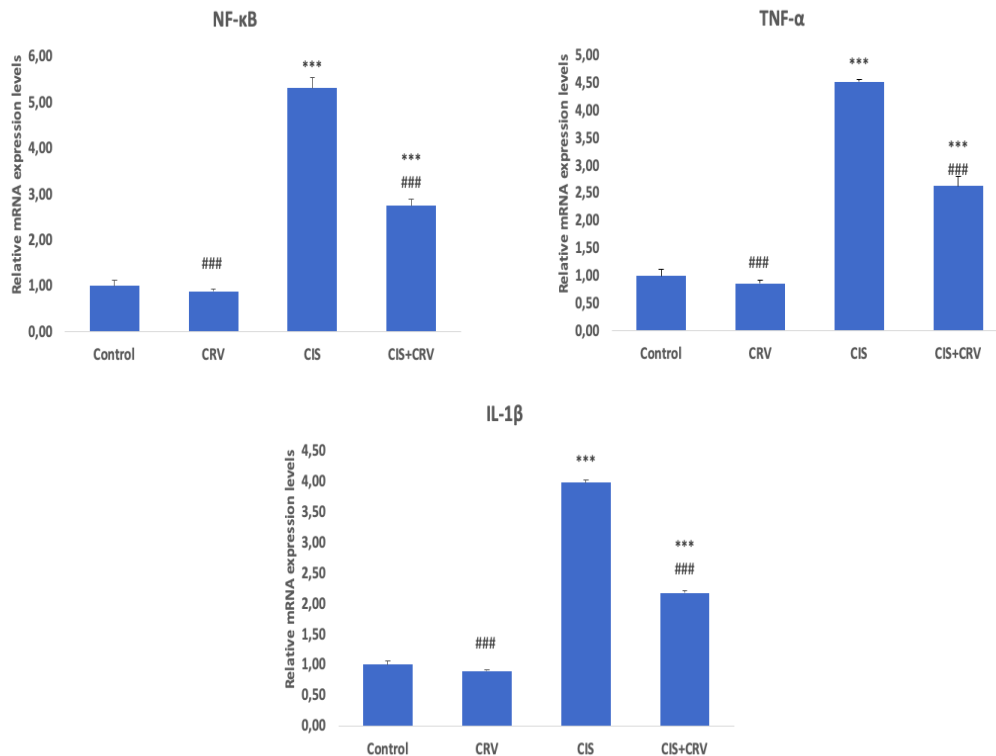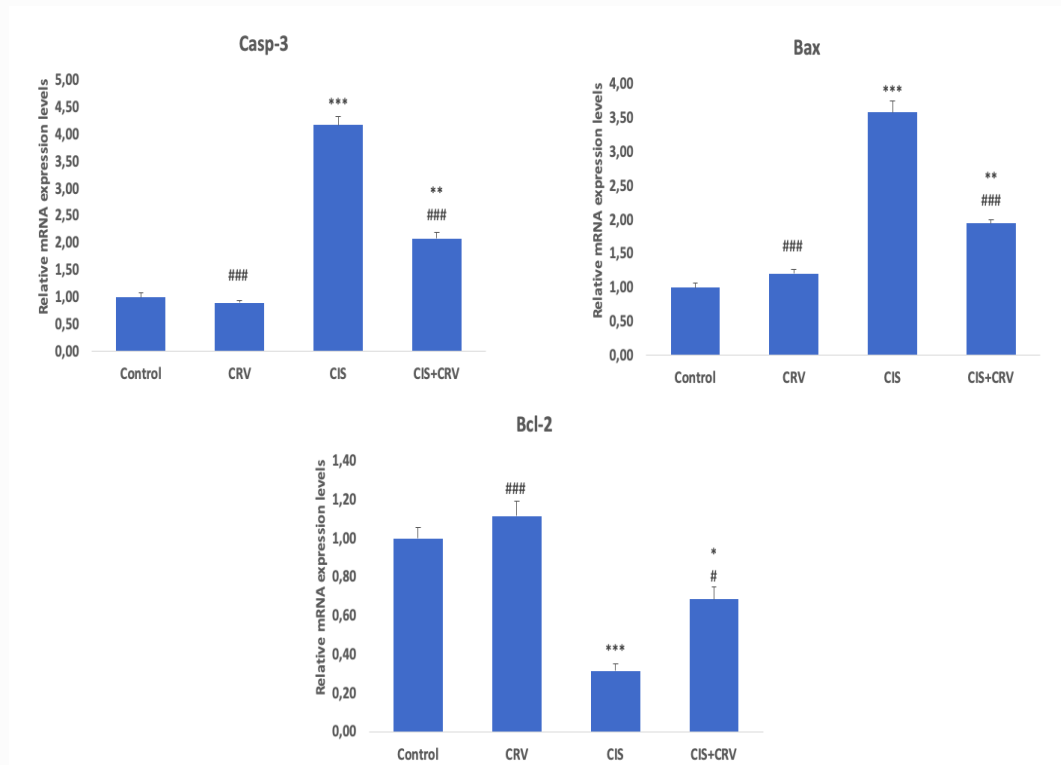
185
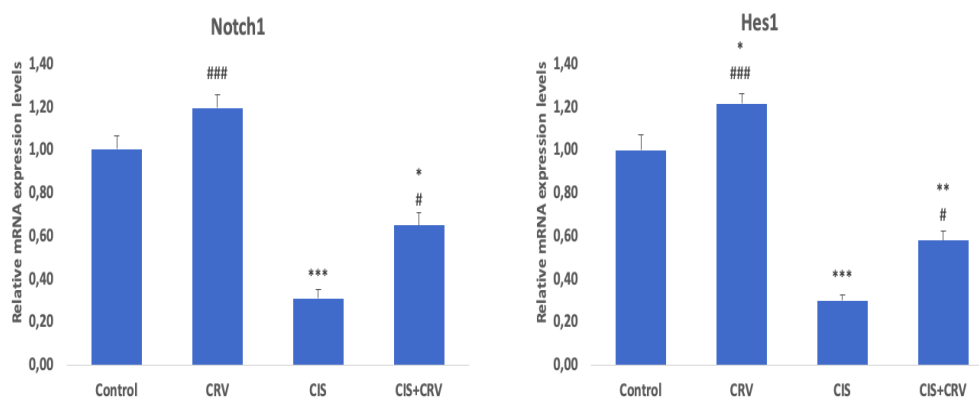
Figure 5. Effect of Carvacrol and Cisplatin treatments on Notch 1, Hes1 mRNA expression levels in heart tissue. Values are given as mean ± SD. Control vs others: *p < .05, **p < .01, ***p < .001, CIS vs others: #p < .05, ##p < .01, ###p < .001

3.6. Effect of Carvacrol on Cisplatin-Induced Morphological Changes

To evaluate the effects of CIS and CRV on the heart, histopathological analysis was performed using H&E staining. The results are presented in Figure 6. When the cardiac histological structure of the control group was examined, the myocardial layer was normal. The muscles in this layer were regularly arranged, the cytoplasm was slightly acidophilic, and the nucleus was single, oval, and central. There were vessels in the connective tissue

between the muscles (Figure 6A). No histopathological lesions were observed in the group that received only CRV (Figure 6B). In the CIS administration group, there were degenerative changes in the myocardial layer. Specifically, these events primarily disturbed cardiac myofibril organization and eosinophilic changes in the cytoplasm of cardiocytes. Additionally, pyknotic nuclei and vacuolization in the cytoplasm were observed. When the connective tissue was examined, there was vascular congestion, hemorrhage, and inflammatory cell infiltration consisting of lymphocytes (Figure 6C). The

combination of CIS and CRV caused mild edema in the interstitial area, decreased bleeding, and vascular congestion. Except for mild vacuolar degeneration in a few cardiocytes, almost all cardiocytes exhibited an appearance close to that of the control. The histopathological findings show that the model was successfully established and that CVR treatment had a protective effect (Figure 6D). Histopathological results are summarized in Table 2.

Table 2. Scoring of histopathological changes

Histopathological changes	Control	CRV	CIS	CIS + CRV
Disruption of cardiac muscle architecture	-	-	+++	+
Vascular congestion	-	-	+++	+
Interstitial hemorrhage	-	-	++	+
Inflammatory cell infiltration	-	-	+++	+
Necrosis	-	-	++	+

The severity of the lesions was graded as follows: score (–) was considered normal, score (+) was considered mild, score (++) was considered moderate, and score (+++) was considered severe.
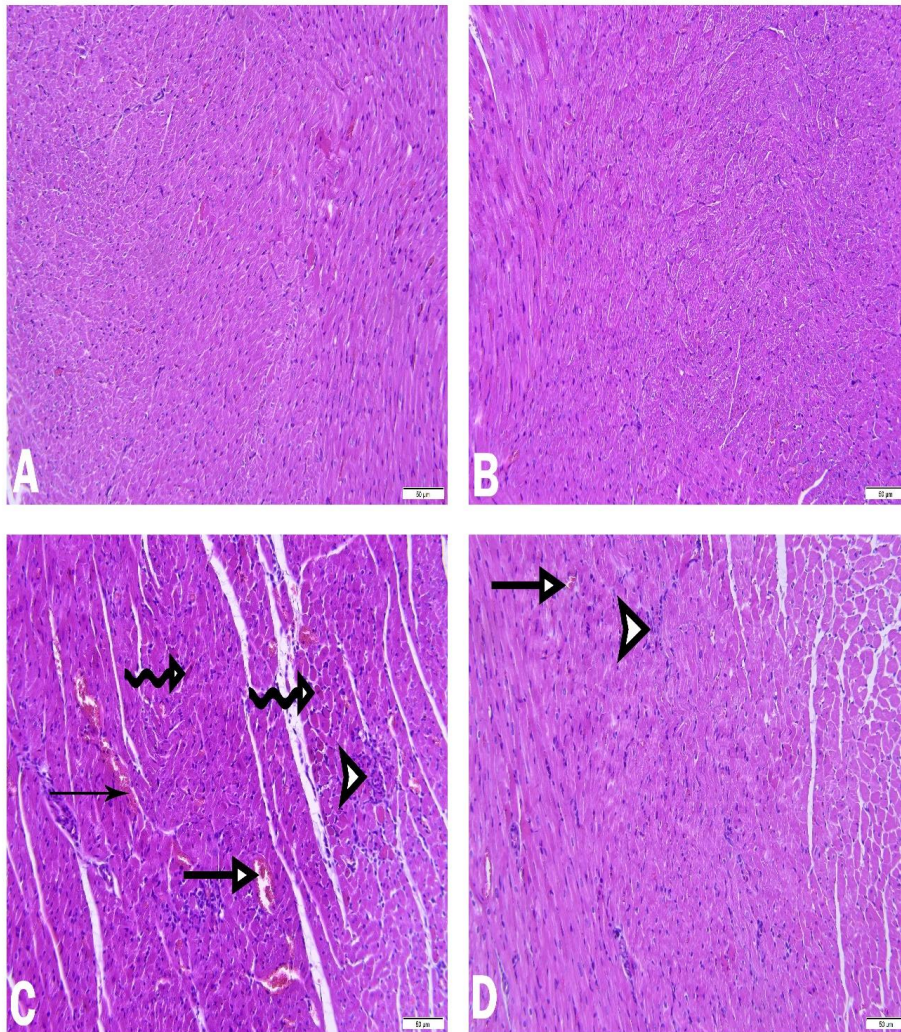
Figure 6. Histopathological evaluation results of rat cardiac tissues treated with Cisplatin (CIS) and Carvacrol (CRV). Heart sections of control (A) and CRV only group (B) show typical histological architecture. CIS only group (C) shows severe histological changes with general loss of normal architecture including disorganized cardiac myofibrils, vascular congestion (thick arrow) and hemorrhage (thin arrow), inflammatory cell infiltration (arrowhead), necrotic cardiomyocytes (curved arrow). CIS+CRV (D) shows mild myocardial degenerative changes such as almost regular cardiac myofibrils, decreased inflammatory cells (arrowhead), rare areas of vascular congestion (thick arrow). Hematoxylin and Eosin (H&E) staining, (Bar: 50 μm)

4. DISCUSSION AND CONCLUSION

Despite its healing effects of CIS, which has a very important place in the fight against cancer, CIS has many side effects. In particular, ventricular dysfunction, impaired cardiomyocyte contractility, and bradycardia due to cisplatin distribution in the sinoatrial node area are of great concern [10, 11]. The first step underlying these hemodynamic abnormalities in the heart is oxidative stress, as presented in this study. Others include effects on inflammation, apoptosis, autophagy, and the Notch signaling pathway [11, 24-26].

Chemotherapeutic drugs generally damage the cell membrane and release intracellular proteins. This may be due to cell membrane lipid peroxidation, which may impair the integrity and function of cardiocytes [14, 27, 28]. Due to these effects, CIS increases reactive molecules in heart tissue and causes depletion of antioxidant molecules [29]. GSH, an antioxidant, plays an important role in maintaining cell security and scavenging ROS. SOD, CAT, and GPx are antioxidant enzymes necessary for improving heart function. While CAT and GPx dissociate H2O2, SOD dismutates the superoxide anion [30-36]. The use of antioxidant treatment in chemotherapy is an important area of research because of the potential of antioxidants to mitigate the harmful side effects of chemotherapeutic agents while maintaining or enhancing their efficacy. Chemotherapeutic agents produce excess amounts of reactive oxygen species as part of their mechanism of action against cancer cells. Oxidative damage may also affect the integrity of healthy tissues and has side effects, such as cardiotoxicity, nephrotoxicity, hepatotoxicity, and neurotoxicity. Antioxidants can counteract this damage by neutralizing ROS and reducing tissue damage in healthy cells [37-39]. In this study, it was determined that acute administration of CIS probably induced lipid peroxidation in the heart tissue and thus reduced SOD, CAT, and GPx activities. This result is likely due to inhibition of the breakdown of O2- into molecular oxygen and water. CRV administration regulated antioxidant levels (SOD, GPx) similar to the control.

Oxidative stress and inflammation are closely related biologically and play common roles in the pathogenesis of organ damage [40-42]. Increased ROS contributes to disease pathogenesis by mediating the expression of the redox-sensitive transcription factor NF-κB and inducing excessive release of proinflammatory cytokines [43-46]. Previous in vitro rat studies have shown that CIS triggers NF-B and inflammatory cytokine mRNA expression in different tissues and causes damage to multiple organs [17, 47]. The current study revealed that Cisplatin causes an increase in the expression levels of NF-kB, TNF-α and IL-1β and this increase is a strong trigger for the inflammatory cascade. In conclusion, CIS induces inflammatory cell infiltration into cardiac tissue. When cisplatin and CRV combined treatment was compared with CIS treatment alone, a decrease in NF-kB, TNF-α and IL-1β expressions was observed. This result was found to be consistent with recent studies showing that CRV has anti-inflammatory properties [6,19].

Another important consequence of CIS-induced ROS increase is the apoptosis process [20]. Bax protein plays an important role in apoptosis and is a proapoptotic factor found in the cytosol that belongs to the Bcl-2 family. When apoptosis is triggered, Bax is transported to the mitochondria, and cytochrome c release is induced [48, 49]. Cytochrome c released into the cytosol also initiates the activation of cysteine proteases. Among cysteine proteases, caspase 3 is the main apoptotic effector, leading to cytoskeletal disassembly, nuclear destruction, and other changes associated with apoptosis [50-53]. All mechanisms involved in inducing caspase-3 activity play a role in CIS-induced apoptosis [54].

In the present study, it was found that the ratio of the proapoptotic Bax gene to the antiapoptotic Bcl-2 gene shifted toward proapoptosis in pathological processes such as ischemic heart disease, dilated cardiomyopathy, and myocardial infarction [16, 17]. In another study, following CIS administration, a significant increase in caspase-3 activity and nuclear DNA fragmentation was observed in heart tissue, which was reported to indicate apoptotic cell death [55]. This study showed that CIS treatment was associated with Bax overexpression and low expression of the antiapoptotic Bcl-2 gene. Therefore, the Bax/Bcl-2 ratio increased; it was shown that it acts as a regulator determining the sensitivity of cells to apoptosis as a proapoptotic index. In addition, CIS has been shown to activate all these apoptotic pathways and trigger caspase 3. These results can be explained by the fact that CIS significantly promotes the release of large amounts of reactive oxygen species, which is considered a direct trigger for the apoptosis process. CRV treatment showed its effect by suppressing the expression of the proapoptotic Bax protein, reducing the expression of the apoptotic mediator Casp-3, and increasing the expression of the antiapoptotic Bcl-2 molecule. In conclusion, CRV's regulation of the mitochondrial pathway may be due to its strong antioxidant properties that potentially prevent apoptosis.

Another consequence of CIS-induced oxidative stress is cardiac cell death, which involves autophagy and apoptosis [56]. Autophagy is an important mechanism for controlling cell homeostasis. It is a critical biological process involved in catabolic processes, such as the elimination of damaged and misfolded proteins [57]. However, excessive autophagy stimulates functional and structural disorders in cells [58, 59]. The autophagy process is regulated by specific genes such as Beclin-1, LC3A, and LC3B [60]. Beclin-1 is an indispensable protein for cell-related processes such as development, immunity, and tumor suppression. LC3 activates autophagosome formation, and LC3A is converted to LC3B form via conjugation with phosphatidylethanolamine. LC3B protein is triggered by oxidative stress and contributes to the formation of autophagosome [42, 61, 62]. In the current study, it was found that CIS increased Beclin-1, LC3A, and LC3B expression in rat heart tissue, whereas CRV treatment decreased autophagy protein expression. In the present study, the increase in autophagy with CIS drug

187

administration caused cell damage, which can also be explained in histopathological images.

The discovery of new pathways that may play a role in CIS-induced cardiac tissue damage is a promising therapeutic approach. In recent years, the possible role of the notch pathway in CIS-induced organ toxicities has been investigated, and it has been emphasized that this pathway should also be investigated. The notch signaling pathway is conserved throughout evolution and plays a critical role in determining cell fate during development. The notch gene family encodes a single-pass transmembrane receptor that participates in the signaling pathway [26, 63]. Mammals have four notch genes (Notch 1-4). JAG1, JAG2, DLL1, DLL3, and DLL4. Notch1 and Notch2 are widely expressed in mammals and play an important role in embryonic development. One of the best-known notch target genes is the Hairy-Enhancer of Split (HES)1 protein, which acts as a transcriptional repressor [63, 64]. In this study, the mRNA levels of Notch1 and Hes1 were significantly decreased in the CIS group, and CRV treatment significantly increased the decrease in translational levels of the evaluated Notch1 and Hes1 pathway molecules.

Studies have emphasized that oxidative stress, inflammation, and cell death contribute to the pathophysiology of acute CIS-induced cardiotoxicity, with pathological changes being involved in the process [14, 24, 29].

The biochemical and molecular findings in the present study were confirmed by histopathological examination of heart tissues showing fiber degeneration, vascular congestion, hemorrhage, inflammatory cell infiltration, and necrosis in the CIS group. In addition, in the histopathological evaluation performed in the group given CRV together with CIS, CRV protected the myocardial structure. In summary, the antioxidant potential of CRV reduced histopathological changes, supporting our hypothesis that it could protect against CIS-induced cardiotoxicity.

In conclusion, the findings show that CRV has promising cardioprotective effects against CIS-induced cardiotoxicity and improves cardiac damage markers. The healing effect of CRV was achieved by reducing oxidative stress, inflammation, apoptosis, and autophagy. Additionally, the Notch signaling pathway was impaired in CIS but was reversed by CRV. This study revealed a possible role for the Notch pathway in the pathogenesis of cisplatin-induced cardiotoxicity. This strategy also paves the way for further investigation of the Notch pathway and makes it promising to test other Notch inhibitors for their possible cardioprotective properties in future studies.

188

REFERENCES

[1] Gur C, Kandemir FM, Caglayan C, Satıcı, E. Chemopreventive effects of hesperidin against paclitaxel-induced hepatotoxicity and nephrotoxicity via amendment of Nrf2/HO-1 and caspase-3/Bax/Bcl-2 signaling pathways. Chemico-biological interactions.2022; 365:110073.

[2] Aksu EH, Kandemir FM, Yıldırım S, Küçükler S, Dörtbudak MB, Çağlayan C, et al. Palliative effect of curcumin on doxorubicin-induced testicular damage in male rats. Journal of biochemical and molecular toxicology. 2019; 33(10):e22384.

[3] Erkaya N, Parlak SN. Effects of beta-1, 3-D glucan on systemic bortezomib treated rat pancreas Journal of Experimental and Clinical Medicine.2022; 39 (3):743-748

[4] Dehghani MA, Shakiba Maram N, Moghimipour E, Khorsandi L, Atefi Khah M, Mahdavinia M. Protective effect of gallic acid and gallic acid-loaded Eudragit-RS 100 nanoparticles on cisplatin-induced mitochondrial dysfunction and inflammation in rat kidney. Biochimica et biophysica acta. Molecular basis of disease, 2020;1866(12):165911.

[5] Ileriturk M, Ileriturk D, Kandemir O, Akaras N, Simsek H, Erdogan E, et al. Naringin attenuates oxaliplatin-induced nephrotoxicity and hepatotoxicity: A molecular, biochemical, and histopathological approach in a rat model. Journal of biochemical and molecular toxicology. 2024;38(1):e23604.

[6] Dinc K, Ozyurt R, Coban TA, Yazici GN, Suleyman Z, Yavuzer B, et al. The effect of carvacrol on the proinflammatory cytokines, histology, and fertility outcome of cisplatin-related ovarian change in a rat model. Taiwanese journal of obstetrics & gynecology. 2023; 62(2):256–263.

[7] Ragab TIM, Zoheir KMA, Mohamed NA, El Gendy AEG, Abd-ElGawad AM, Abdelhameed MF, et al. Cytoprotective potentialities of carvacrol and its nanoemulsion against cisplatin-induced nephrotoxicity in rats: development of nano-encasulation form. Heliyon. 2022;8(3):e09198.

[8] Stojic IM, Zivkovic VI, Srejovic IM, Nikolic TR, Jeremic NS, Jeremic JN, et al. Cisplatin and cisplatin analogues perfusion through isolated rat heart: the effects of acute application on oxidative stress biomarkers. Molecular and cellular biochemistry. 2028;439(1-2), 19–33.

[9] Lash LH. Unexpected Enhancement of Cytotoxicity of Cisplatin in a Rat Kidney Proximal Tubular Cell Line Overexpressing Mitochondrial Glutathione Transport Activity. International journal of molecular sciences. 2022; 23(4), 1993.

[10] Rosic G, Srejovic I, Zivkovic V, Selakovic D, Joksimovic J, Jakovljevic V. The effects of N-acetylcysteine on cisplatin-induced cardiotoxicity on isolated rat hearts after short-term global ischemia. Toxicology reports. 2015; 2: 996–1006.

[11] El-Shoura EAM, Hassanein EHM, Taha HH, Shalkami AS, Hassanein MMH, Ali FEM, et al. Edaravone and obeticholic acid protect against cisplatin-induced heart toxicity by suppressing

oxidative stress and inflammation and modulating Nrf2, TLR4/p38MAPK, and JAK1/STAT3/NF-κB signals. Naunyn-Schmiedeberg's archives of pharmacology. 2024;397(8):5649–

[12] El-Sawalhi MM, Ahmed LA. Exploring the protective role of apocynin, a specific NADPH oxidase inhibitor, in cisplatin-induced cardiotoxicity in rats. Chemico-biological interactions. 2014; 207:58–66.

[13] Tanyeli A, Eraslan E, Güler M, Kurt N, Akaras N. Gossypin Protects Against Renal Ischemia-Reperfusion Injury in Rats. Kafkas Univ Vet Fak Derg. 2010; 26 (1): 89-96.

[14] Yildirim C, Cangi S, Orkmez M, Yilmaz SG, Bozdayı MA, Yamaner H, et al. Sinapic acid attenuated cisplatin-induced cardiotoxicity by inhibiting oxidative stress and inflammation with GPX4-mediated NF-kB modulation. Cardiovascular Toxicology. 2013; 23(1):10-22.

[15] Zhao L. Protective effects of trimetazidine and coenzyme Q10 on cisplatin-induced cardiotoxicity by alleviating oxidative stress and mitochondrial dysfunction. Anatolian journal of cardiology. 2019; 22(5):232–239.

[16] Saleh DO, Mansour DF, Mostafa RE. Rosuvastatin and simvastatin attenuate cisplatin-induced cardiotoxicity via disruption of endoplasmic reticulum stress-mediated apoptotic death in rats: targeting ER-Chaperone GRP78 and Calpain-1 pathways. Toxicology reports. 2020;7:1178–1186.

[17] Soliman AF, Anees LM, Ibrahim DM. (2018). Cardioprotective effect of zingerone against oxidative stress, inflammation, and apoptosis induced by cisplatin or gamma radiation in rats. Naunyn-Schmiedeberg's archives of pharmacology. 2018; 391(8):819–832.

[18] El-Sayed EM, Abd-Allah AR, Mansour AM, El-Arabey AA. Thymol and carvacrol prevent cisplatin-induced nephrotoxicity by abrogation of oxidative stress, inflammation, and apoptosis in rats. Journal of biochemical and molecular toxicology. 2015; 29(4):165–172.

[19] Aksu EH, Kandemir FM, Altun S, Küçükler S, Çomaklı S, Ömür AD. Ameliorative Effect of Carvacrol on Cisplatin-Induced Reproductive Damage in Male Rats. Journal of biochemical and molecular toxicology. 2016; 30(10):513–520.

[20] Hassanshahi A, Kaeedi A, Rahmani MR, Hassanshahi J. The Effects of ThymusCaramanicus Jalas Extract and Its Main Constituent Carvacrol Against Cisplatin-Induced Nephrotoxicity in Mice. Iranian journal of pharmaceutical research IJPR. 2024;23(1): e140212.

[21] Gencer S, Gür C, İleritürk M, Küçükler S, Akaras N, Şimşek H, et al. The ameliorative effect of carvacrol on sodium arsenite-induced hepatotoxicity in rats: Possible role of Nrf2/HO-1, RAGE/NLRP3, Bax/Bcl-2/Caspase-3, and Beclin-1 pathways. Journal of biochemical and molecular toxicology. 2024; 38(10):e23863.

[22] Şimşek H, Gür C, Küçükler S, Ileritürk M, Akaras N, Oz M, et al. Carvacrol Reduces Mercuric Chloride-Induced Testicular Toxicity by Regulating Oxidative Stress, Inflammation, Apoptosis, Autophagy, and Histopathological Changes. Biol Trace Elem Res. 2024;202(10):4605-4617.

[23] Livak KJ, Schmittgen TD. Analysis of relative gene expression data using real-time quantitative PCR and the 2(-Delta Delta C(T)) Method. Methods. 2001; 25 (4):402–408.

[24] Bukhari IA, Mohamed OY, Alhowikan AM, Lateef R, Hagar H, Assiri RA, et al. Protective Effect of Rutin Trihydrate Against Dose-Dependent, Cisplatin-Induced Cardiac Toxicity in Isolated Perfused Rat's Heart. Cureus. 2022;14(1):e21572.

[25] Coskun R, Turan MI, Turan IS, Gulapoglu M. The protective effect of thiamine pyrophosphate, but not thiamine, against cardiotoxicity induced with cisplatin in rats. Drug and chemical toxicology. 2014; 37(3):290–294.

[26] Abd El-Rhman RH, El-Naga RN, Gad AM, Tadros MG, Hassaneen SK. Dibenzazepine Attenuates Against Cisplatin-Induced Nephrotoxicity in Rats: Involvement of NOTCH Pathway. Front Pharmacol. 2020; 11:567852.

[27] Semis HS, Kandemir FM, Kaynar O, Dogan T, Arikan SM. The protective effects of hesperidin against paclitaxel-induced peripheral neuropathy in rats. Life sciences. 2021; 287:120104.

[28] Ağğül AG, Kuzu M, Kandemir FM, Küçükler S, Çağlayan C. Alterations in Enzyme Activity of Carbonic Anhydrase, 6-phosphogluconate Dehydrogenase and Thioredoxin Reductase in Rats Exposed to Doxorubicin and Morin. Clinical and Experimental Health Sciences. 2020;10 (3), 228-234

[29] Başak Türkmen N, Aşkın Özek D, Taşlıdere A, Çiftçi O, Saral Ö, Gül CC. Protective Role of Diospyros lotus L. in Cisplatin-Induced Cardiotoxicity: Cardiac Damage and Oxidative Stress in Rats. Turk J Pharm Sci. 2022;19(2):132-137.

[30] Keleş O, Can S, Cigsar G, Colak S, Erol H, Akaras N, et al. Hepatoprotective effects of B-1, 3-(D)-glucan on bortezomib-induced liver damage in rats. Kafkas Universitesi Veteriner Fakultesi Dergisi, 2014;20(6):929-38.

[31] Ekinci-Akdemir FN, Yildirim S, Kandemir FM, Gülçin İ, Küçükler S, Sağlam YS, et al. The effects of casticin and myricetin on liver damage induced by methotrexate in rats. Iran J Basic Med Sci. 2018;21(12):1281-1288.

[32] FM Kandemir, M Ozkaraca, S Küçükler, C Caglayan, B Hanedan. Preventive effects of hesperidin on diabetic nephropathy induced by streptozotocin via modulating TGF-β1 and oxidative DNA damage. Toxin reviews. 2018;37 (4):287-293

[33] Aydin M, Cevik A, Kandemir FM, Yuksel M, Apaydin AM. Evaluation of hormonal change, biochemical parameters, and histopathological status of uterus in rats exposed to 50-Hz electromagnetic field. Toxicology and industrial health. 2009;25(3):153–158.

[34] Semis HS, Gur C, Ileriturk M, Kaynar O, Kandemir FM. (2021). Investigation of the anti-inflammatory effects of caffeic acid phenethyl ester in a model of

189

λ-Carrageenan-induced paw edema in rats. Human & experimental toxicology. 2021; 40: S721–S738.

[35] Erisir M, Kandemir FM, Yüksel M. The effects of Caesarean section on lipid peroxidation and some antioxidants in the blood of newborn calves. Veterinarski arhiv. 2013; 83 (2):153-159

[36] Akaras N, Toktay E, Celep NA, Yüce N, Şimşek H, Özkan Hİ. Antioxidant Effects of Bromelain on Paracetamol-Induced Renal Injury in Rats. Arch Basic Clin Res. 2023; 10: 1-8

[37] Varışlı B, Caglayan C, Kandemir FM, Gür C, Ayna A, Genç A, et al. Chrysin mitigates diclofenac-induced hepatotoxicity by modulating oxidative stress, apoptosis, autophagy and endoplasmic reticulum stress in rats. Molecular Biology Reports. 2023; 50(1): 433-442.

[38] Ayna A, Özbolat S. N, Darendelioglu E. Quercetin, chrysin, caffeic acid and ferulic acid ameliorate cyclophosphamide-induced toxicities in SH-SY5Y cells. Molecular Biology Reports. 2020; 47:8535-8543

[39] Kızıl HE, Caglayan C, Darendelioğlu E, Ayna A, Gür C, Kandemir FM, et al. Morin ameliorates methotrexate-induced hepatotoxicity via targeting Nrf2/HO-1 and Bax/Bcl2/Caspase-3 signaling pathways. Molecular Biology Reports. 2023; 50(4):3479-3488.

[40] Taştan Bal T, Akaras N, Demir Ö, Ugan RA. Protective effect of astaxanthin and metformin in the liver of rats in which the polycystic ovary syndrome model was formed by giving letrozole. Iran J Basic Med Sci. 2023;26(6):688-694.

[41] Şimşek H, Küçükler S, Gür C, Akaras N, Kandemir FM. Protective effects of sinapic acid against lead acetate-induced nephrotoxicity: a multi-biomarker approach. Environ Sci Pollut Res Int. 2023;30(45):101208-101222.

[42] Şimşek H, Küçükler S, Gür C, İleritürk M, Aygörmez S, Kandemir FM. Protective effects of zingerone against sodium arsenite-induced lung toxicity: A multi-biomarker approach. Iran J Basic Med Sci. 2023;26(9):1098-1106.

[43] Akaras N, Ileriturk M, Gur C, Kucukler S, Oz M, Kandemir FM. The protective effects of chrysin on cadmium-induced pulmonary toxicity; a multi-biomarker approach. Environ Sci Pollut Res Int. 2023;30(38):89479-89494.

[44] Akaras N, FM Kandemir, H Şimşek, C Gür, S Aygörmez. Antioxidant, Antiinflammatory, and Antiapoptotic Effects of Rutin in Spleen Toxicity Induced by Sodium Valproate in Rats. Türk Doğa ve Fen Dergisi. 2023; 12 (2):138-144

[45] Akaras N, Simsek H, Ordu M. A histological and biochemical study of the protective role of hesperidin in testicular ischemia-reperfusion injury. Int J Med Biochem 2023;6(1):21-27

[46] Akaras N, Gür C, Şimşek H, Tuncer SÇ. Effects of Quercetin on Cypermethrin-Induced Stomach Injury: The Role of Oxidative Stress, Inflammation, and Apoptosis. Gümüşhane Üniversitesi Sağlık Bilimleri Dergisi. 2023;12 (2):556-566

[47] Khadrawy YA, Hosny EN, El-Gizawy MM, Sawie HG, Aboul Ezz HS. The Effect of Curcumin Nanoparticles on Cisplatin-Induced Cardiotoxicity in Male Wistar Albino Rats. Cardiovasc Toxicol. 2021;21(6):433-443.

[48] Akarsu SA, Gür C, İleritürk M, Akaras N, Küçükler S, Kandemir FM. Effect of syringic acid on oxidative stress, autophagy, apoptosis, inflammation pathways against testicular damage induced by lead acetate. J Trace Elem Med Biol. 2023;80:127315.

[49] Akaras N, Kucukler S, Gur C, Ileriturk M, Kandemir FM. Sinapic acid protects against lead acetate-induced lung toxicity by reducing oxidative stress, apoptosis, inflammation, and endoplasmic reticulum stress damage. Environ Toxicol. 2024;39(7):3820-3832.

[50] Akaras N, Gür C, Caglayan C, Kandemir FM. Protective effects of naringin against oxaliplatin-induced testicular damage in rats: Involvement of oxidative stress, inflammation, endoplasmic reticulum stress, apoptosis, and histopathology. Iran J Basic Med Sci. 2024;27(4):466-474.

[51] Akarsu SA, İleritürk M, Küçükler S, Akaras N, Gür C, Kandemir FM. Ameliorative effects of sinapic acid against vancomycin-induced testicular oxidative damage, apoptosis, inflammation, testicular histopathologic disorders and decreased epididymal sperm quality. Reprod Toxicol. 2024;129:108666.

[52] Akarsu SA, Gür C, Küçükler S, Akaras N, İleritürk M, Kandemir FM. Protective Effects of Syringic Acid Against Oxidative Damage, Apoptosis, Autophagy, Inflammation, Testicular Histopathologic Disorders, and Impaired Sperm Quality in the Testicular Tissue of Rats Induced by Mercuric Chloride. Environ Toxicol. Published online August 3, 2024.

[53] Yilmaz S, Gur C, Kucukler S, Akaras N, Kandemir FM. Zingerone attenuates sciatic nerve damage caused by sodium arsenite by inhibiting NF-κB, caspase-3, and ATF-6/CHOP pathways and activating the Akt2/FOXO1 pathway. Iran J Basic Med Sci. 2024;27(4):485-491.

[54] Ekinci Akdemir FN, Yildirim S, Kandemir FM, Aksu EH, Guler MC, Kiziltunc Ozmen H, et al. The antiapoptotic and antioxidant effects of eugenol against cisplatin-induced testicular damage in the experimental model. Andrologia. 2019;51(9):e13353.

[55] Xing JJ, Mi XJ, Hou JG, Cai EB, Zheng SW, Wang SH,et al. (2022). Maltol mitigates cisplatin-evoked cardiotoxicity via inhibiting the PI3K/Akt signaling pathway in rodents in vivo and in vitro. Phytotherapy research: PTR. 2022;36(4):1724–1735.

[56] Ma W, Wei S, Zhang B, Li W. Molecular Mechanisms of Cardiomyocyte Death in Drug-Induced Cardiotoxicity. Front Cell Dev Biol. 2020;8:434.

[57] Semis HS, Gur C, Ileriturk M, Kandemir FM, Kaynar O. Evaluation of Therapeutic Effects of Quercetin Against Achilles Tendinopathy in Rats via Oxidative Stress, Inflammation, Apoptosis, Autophagy, and Metalloproteinases. Am J Sports Med.

[58] Kandemir FM, Ileriturk M, Gur C. Rutin protects rat liver and kidney from sodium valproate-induce damage by attenuating oxidative stress, ER stress, inflammation, apoptosis and autophagy. Mol Biol Rep. 2022;49(7):6063-6074.

[59] Çomaklı S, Özdemir S, Küçükler S, Kandemir FM. Beneficial effects of quercetin on vincristine-induced liver injury in rats: Modulating the levels of Nrf2/HO-1, NF-kB/STAT3, and SIRT1/PGC-1α. J Biochem Mol Toxicol. 2023;37(5):e23326.

[60] Kankılıç NA, Şimşek H, Akaras N, Gür C, Ileritürk M, Küçükler S, et al. Protective effects of naringin on colistin-induced damage in rat testicular tissue: Modulating the levels of Nrf-2/HO-1, AKT-2/FOXO1A, Bax/Bcl2/Caspase-3, and Beclin-1/LC3A/LC3B signaling pathways. J Biochem Mol Toxicol. 2024;38(2):e23643.

[61] Tuncer SÇ, Küçükler S, Gür C, Aygörmez S, Kandemir FM. Effects of chrysin in cadmium-induced testicular toxicity in the rat; role of multi-pathway regulation. Mol Biol Rep. 2023;50(10):8305-8318.

[62] Kankılıç NA, Küçükler S, Gür C, Akarsu SA, Akaras N, Şimşek H, et al. Naringin protects against paclitaxel-induced toxicity in rat testicular tissues by regulating genes in pro-inflammatory cytokines, oxidative stress, apoptosis, and JNK/MAPK signaling pathways. Journal of biochemical and molecular toxicology. 2024; 38(7):e23751.

[63] Zhou B, Lin W, Long Y, Yang Y, Zhang H, Wu K, et al. Notch signaling pathway: architecture, disease, and therapeutics. Signal Transduct Target Ther. 2022;7(1):95.

[64] Luo X, Zhang L, Han GD, Lu P, Zhang Y. MDM2 inhibition improves cisplatin-induced renal injury in mice via inactivation of Notch/hes1 signaling pathway. Hum Exp Toxicol. 2021;40(2):369-379.

191

Türk Doğa ve Fen Dergisi
Turkish Journal of Nature and Science

www.dergipark.gov.tr/tdfd

BINGÖL UNIVERSITY

Investigation of Waste Mineral Wool in Geopolymer Production

Mehrzad MOHABBI[1]* , Mehmet Nuri KOLAK[2]

[1] Bingöl University, Faculty of Engineering and Architecture, Civil Engineering Department, Bingöl, Türkiye
[2] Bingöl University, Vocational School of Technical Sciences, Department of Construction, Bingöl, Türkiye
Mehrzad MOHABBI ORCID No: 0000-0001-8584-1658
Mehmet Nuri KOLAK ORCID No: 0000-0003-3533-3422

*Corresponding author: mnkolak@bingol.edu.tr

Abstract: Mineral wools are widely used insulation materials in the construction industry; however, their non-recyclable nature poses an environmental challenge. In this study, mineral wool wastes were sustainably utilized by grinding them into powder and activating them with Na_2SiO_3 and $NaOH$ solutions. During the production process, different silica modulus ratios of Na_2SiO_3 (2.0, 2.5, and 3.0) were examined, and the optimal ratio was determined to be 2.5. The mechanical properties of the samples were evaluated after curing at various temperatures (25°C, 50°C, 75°C, and 100°C), with the maximum compressive strength of 59.2 MPa observed in glass wool samples. Thermal curing enhanced compressive strength, particularly at 75°C, for glass wool-based samples. Additionally, the compressive strengths of the samples stabilized after a curing period of 90 days. These findings demonstrate the feasibility of recycling mineral wool wastes into high-performance materials and highlight the significant role of thermal curing in enhancing mechanical properties.

192

Atık Mineral Yünlerin Jeopolimer Üretiminde Kullanımının İncelenmesi

Öz: Mineral yünler inşaat sektöründe yaygın olarak kullanılan yalıtım malzemeleridir; ancak geri dönüştürülemeyen yapıları çevresel bir sorun teşkil etmektedir. Bu çalışmada, mineral yün atıkları toz haline getirilip Na_2SiO_3 ve $NaOH$ çözeltileri ile aktifleştirilerek sürdürülebilir bir şekilde değerlendirilmiştir. Üretim sürecinde farklı Na_2SiO_3 silika modülü oranları (2.0, 2.5 ve 3.0) incelenmiş ve optimum oran 2.5 olarak belirlenmiştir. Numunelerin mekanik özellikleri çeşitli sıcaklıklarda (25°C, 50°C, 75°C ve 100°C) kürlendikten sonra değerlendirilmiş ve en yüksek basınç dayanımı 59,2 MPa ile cam yünü numunelerinde gözlenmiştir. Termal kürleme, cam yünü bazlı numuneler için özellikle 75°C'de basınç dayanımını artırmıştır. Ayrıca, numunelerin basınç dayanımları 90 günlük bir kürleme süresinden sonra stabilize olmuştur. Bu bulgular, mineral yün atıklarının yüksek performanslı malzemelere geri dönüştürülmesinin uygulanabilirliğini göstermekte ve termal kürlemenin mekanik özelliklerin geliştirilmesindeki önemli rolünü vurgulamaktadır.

1. INTRODUCTION

Ordinary cement production is a main contributor to CO_2 [1]. An alternative activity to reduce CO_2 emission from ordinary Portland cement production is geopolymer-based binder materials development [2]. Geopolymerization is the dissolution of aluminosilicate in an alkaline condition, and result a three-dimensional network between amorphous and semi-crystalline [3]. Sources of aluminosilicate can be natural [2-4] or industrial by product [5-7]. NaOH, Na_2SiO_3, KOH and

K_2SiO_3 are mainly used as alkaline solutions. In general, geopolymers show better mechanical performance [8, 9]. Buildings account for about 33% of global energy consumption and about 30% of CO_2 gas, in addition approximately than 1/2 of buildings' energy consumption is by building heating and cooling [10]. So there are an interest in finding and production of new binding materials containing Phase Change Materials to improving and decreasing energy consumption. There are some studies on these topics [11-13]. The conversion of waste and byproduct materials to cementing materials

helps conserving the environment and existing resources. Geopolymers considered as principal alternative to ordinary cement and can significantly reduce harmful gas emissions and greatly reduce the high energy consumption in cement industry [3, 14, 15]. Geopolymers can be prepared from aluminosilicate-based or kaolinite-rich industrial waste materials with an alkaline solution [16, 17]. Geopolymers show better mechanical performance [18-20]. In cold countries, structures are exposed to frost. This is a major problem in terms of durability [21, 22]. The effect of freeze-thaw cycles on the mechanical properties of cementitious and some geopolymer binders has been studied in many investigations [23-27]. Rock and glass wools are the most used insulation materials in the building industry [28]. These wastes are produced by demolition. European countries produced 2.3 million tons waste mineral wool and will increase to 2.5 million tons by 2020 [29]. Rock and glass wool wastes are non-recyclable material. Since these natural or industrial geopolymer base materials can be used in many industrial by-product materials, CO_2 emission reductions of up to 80% compared to Portland cement can be achieved [30]. Mineral wools have acceptable chemical composition for geopolymerization (Table 1).

Table 1. Rock and glass wool Chemical composition [31]

Component	SW New [%]	SW Old [%]	GW New [%]	GW Old [%]
CaO	18.2	16.6	7.9	7.3
SiO_2	39.4	44.1	61.3	61.9
Al_2O_3	15.9	14.3	2	3.3
Fe_2O_3	9.8	5.5	1.4	1.2
Na_2O	1.3	1.2	16.3	16
K_2O	0.5	0.3	1	0.8
MgO	11.4	14.7	2	2.9
P_2O_5	0.1	0	0.2	0
TiO_2	1	0.2	0.1	0
SO_3	0.1	0	2	0.3
Cl	0	0	0.1	0.1
LOI 550°C	4.3	2.6	9.4	8.8

In terms of amorphous feature which increases their reactivity, they are completely amorphous and this is seen with the help of X-ray and XRD results [32, 33]. This study justifies the feasibility of rock and glass wool as geopolymer base material. UPV and compressive strength tests results provided main measurement for this feasibility.
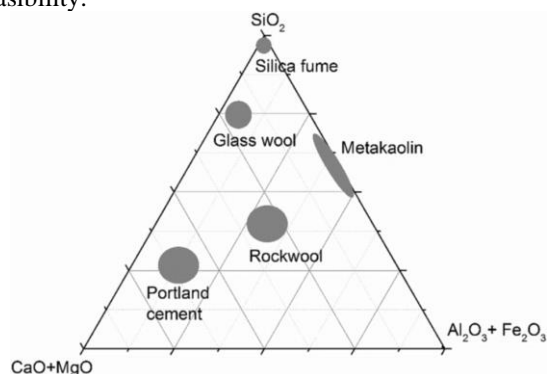

Figure 1. Comparison of chemical compositions of various alkali binder based materials [34]

The chemical compositions of mineral wool compared to other alkali active binders are shown in Figure 1.

In the study by Weil et al. two geopolymer mixtures were prepared to examine the CO_2 emissions that cause global warming. At the end of this study, they stated that geopolymers derived from fly ash and slag emitted less CO_2 than normal cement [35]. Energy consumption in geopolymer cements production is approximately 40% less than normal Portland cement [36]. It is stated that the amount of Si/Al is important factor in the geopolymer production [37]. Torgal et al. [38] reported that the main materials that can be activated with alumina and silicate based alkalis are kaolinite clay, metakaolin, combining of fly ash and metakaolin in different ratios, combining of slag and metakaolin in different ratios and mixtures of slag and red mud. They conducted Ca-Si and Ca-Al based experiments on these materials and measured the hydration development with XRD and infrared rays. Kong et al [39] exposed metakaolin and fly ash to high temperatures together and made them more active. They stated that this was due to the high amount of alumina and silica in fly ash. They determined that metakaolin had an amorphous structure at high temperatures (approximately 800°C) and transformed into an activated aluminosilicate. The effects of aggregate, plasticizer and temperature on geopolymer cement were investigated in the study. It was stated that as the sample sizes increased, the compressive strength decreased due to thermal cracks. If the aggregate grain diameters were smaller than 10 mm, the shelling was more common. It was thought that this phenomenon could be prevented if it was larger than 10 mm. It was stated that the superplasticizer additive reduced the strength in geopolymer concretes and did not have a significant contribution to the total workability.

In the study conducted by Malolepszy 2009, it was stated that Na_2CO_3 is suitable for activating slags containing large amounts of C_2MS (M: alkali metal). It was stated that NaOH is a good activator for slags containing large amounts of C2AS. The activation of different systems with NaOH, Na_2CO_3 and Na_2OSiO_2 was investigated by Krivenko (1992). It was stated that Na_2SiO_3 (sodium silicate or glass water) is a very effective activator [40]. Allahverdi et al., [41] prepared geopolymer cement using pumice type natural pozzolan around Taftan Mountain and combinations of NaOH and Na_2SiO_3 as activators. Three different silica moduls were prepared by adding sodium hydroxide to sodium silicates. Three different geopolymer cement systems were formed with sodium oxide contents weight. Water/cement ratio was taken as 0.36, 0.40 and 0.44. As a result of the study; they stated that Taftan pozzolan can be activated by using NaOH and Na_2SiO_3 in appropriate proportions; it can be converted into geopolymer cement formation providing appropriate workability and 28-day compressive strength of 63 MPa. It was explained that natural pozzolans can be activated and geopolymer cement can be produced by using a mixture of sodium silicate and sodium hydroxide in certain proportions as alkali activators. In the literature, early strength, acid resistance, sulfate behavior, shrinkage of geopolymers has been investigated, especially on fly ash. [42-46]. Energy consumption in the

geopolymerization is almost 40% less than the energy needed ordinary Portland cement [36].

Atiş et al. [47] investigated the use of a new binder that would activate slag without using Portland cement in their studies. Compressive strengths, flexural tensile strengths were measured and drying shrinkage in a 6-month period was examined. At the same time, the hydration development of the samples was examined. It was stated that the setting start and end times were earlier in liquid sodium silicate and sodium hydroxide-activated cements compared to normal Portland cement, and the cements activated with sodium carbonate were the same as normal Portland cement. It was stated that with the increase in the silica modulus, the effect of liquid sodium silicate on gaining final strength and flexural tensile strength was higher. It was stated that the mortars produced with sodium silicate and sodium hydroxide-activated slags were more brittle, and the behavior of the mortars produced with sodium carbonate was similar to normal Portland cement.

Komljenovic et al [48] investigated the microstructure properties of fly ash (Class F) geopolymers. They stated that the most important parameters in the alkali activation method are activator properties and density, while the important parameter in fly ash is fineness. They stated that the compressive strength of fly ash geopolymers (<43μm) is generally high. The best results were obtained by using sodium silicate solution. It was stated that the compressive strength is largely dependent on the Si/Al ratio. Anuar et al [49] used NaOH and Na_2SiO_3 mixed as alkaline liquid in their studies. In this study, geopolymer concrete samples were used in two different molars (8M and 14M sodium hydroxide NaOH). 3, 7, 14, 21 and 28 day compressive strengths were tested in laboratory conditions. They stated that the best result for compressive strength was obtained by 14M NaOH.

A major environmental challenge for the construction industry is the non-recyclability of mineral wool waste. In recent years, efforts have focused on recycling these wastes and developing environmentally friendly binder systems. This study aims to transform mineral wool waste (glass wool and rock wool) into sustainable materials. The waste materials were processed using the alkaline activation method and investigated at different silica modulus ratios (2.0, 2.5, and 3.0). Additionally, the effects of thermal curing conditions (25°C, 50°C, 75°C, and 100°C) on the mechanical properties were examined. The primary objective of the study is to identify the optimal parameters for converting mineral wool waste into high-performance materials. The findings not only contribute to sustainable material design but also provide an environmentally friendly solution for addressing the issue of mineral wool waste.

2. MATERIAL AND METHOD

2.1. Material

Mineral wools were obtained from waste mineral wools that had completed their service life at Bingöl University

education facilities. These mineral wools were ground in the Los Angeles Device (Figure 2) and then made ready for use with the help of a ring grinder.

Figure 2. Grinding stages of mineral wool

Mineral wools consisting of rock wool and glass wool were ground and made ready for use in geopolymer production (Figure 2).

2.2. Alkaline Solution Production Method

According to the results obtained from the preliminary experiments, different mixtures of glass water and sodium hydroxide solutions were used for alkaline solution production in this study and project. In alkaline solution production, Na_2SiO_3/NaOH mixtures were prepared at 3 different ratios. Compressive strength and UPV tests were carried out for geopolymers produced at three different ratios. Our Na_2SiO_3/NaOH ratios were selected as 3, 2.5 and 2 (Figure 3).

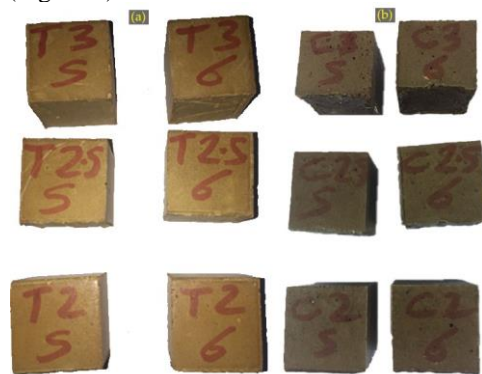**Figure 3.** Produced samples (a) rock wool, (b) glass wool

2.3. Experimental Procedure

The compressive strength of the geopolymer composites after curing was determined according to ASTM C109. UPV was performed according to the principles specified in ASTM C597-16. Experiments were carried out with three specimens from each mixture group. The average of 3 sample results for each mixture group was used.

194

3. RESULT AND DISCUSSION

3.1. Compressive Strength and Ultrasonic Pulse Velocity Tests

Compressive strength and ultra sound tests were performed on samples produced from glass wool and rock wool. The material and molarity used were taken into account when coding the sample. For example, when coding for C3, the first letter of the glass wool in the mixture and the molarity ratio were used. Our samples were produced in 3x3x3 cm³ molds and their 3, 7, 14, 28 and 90 day compressive strengths and UPV values were measured. The 1-day compressive strength of our samples was determined to be very high. According to the results, it was determined that the samples produced from glass wool were more advantageous in geopolymer production. In other words, higher strength geopolymer samples can be produced by using glass wool. Considering this situation, the experiments were continued on glass wool. The compressive strength and UPV test results related to glass wool are presented in Figures 7, 8. In all three molarity cases, the one-day compressive strengths of the samples were higher than 60 MPa. However, in the 3 Molarity and 2 Molarity usage cases, the compressive strengths decreased to 30.04 MPa and 25.80 MPa, respectively.
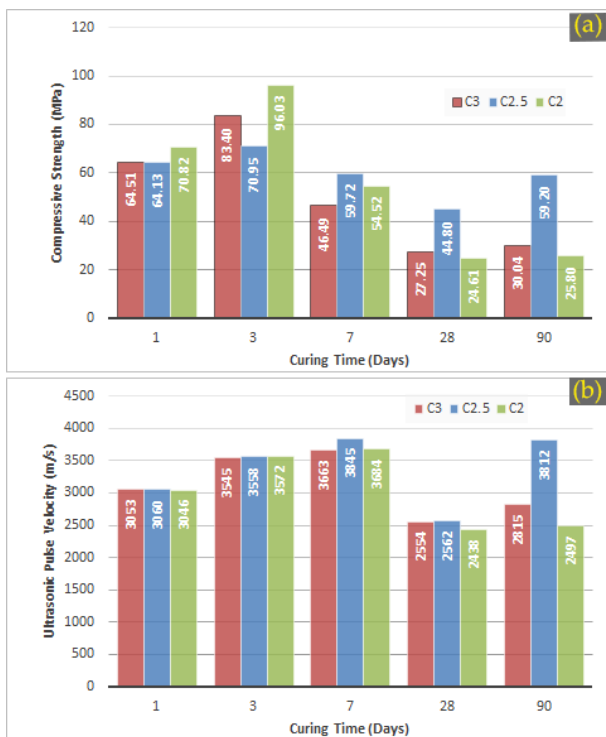

Figure 4. Results of glass wool based samples (a) compressive strengths and (b) UPV

In the 2.5 molarity case, the compressive strength was obtained as 59.20 MPa. The 90-day compressive strengths in the C2 and C3 coded samples decreased by approximately 65% and 50%, respectively (compared to the one-day compressive strengths). Compared to the change in the C2 and C3 coded samples, the compressive strength in C2.5 was less than 10% (Figure 4a). When the UPV test results are examined; In the 90-day

measurements, there was an approximately 25% increase in the UPV value in the C2.5 coded sample, while there was a decrease of approximately 15% and 10% in the C2 and C3 coded samples, respectively (compared to the one-day UPV values). In the first 7-day measurements, an increase in UPV values is observed for all molarity conditions. However, there was a decrease in the UPV value of the 28-day sample (Figure 4b).

Compressive strength and UPV test results for rock wool are presented in Figures 5. In all three molarity cases, there was a decrease in the compressive strength of the samples up to the 7-day curing period. The 90-day compressive strengths for T3, T2.5 and T2 were determined as 21.70 MPa, 20.01 MPa and 23.40 MPa, respectively. The decrease in 90-day compressive strengths for T3 and T2.5 was approximately 40%, while it was approximately 50% for T2 (Figure 5a). When the UPV test results are examined; In the 90-day measurements, there was an approximately 3% increase in the UPV value in the T2 coded sample, while there was a smaller decrease of less than 1% in the C2 and C3 coded samples (compared to the one-day UPV values). In the first 7-day measurements, a decrease in UPV values is observed for all molarity conditions (Figure 5b).
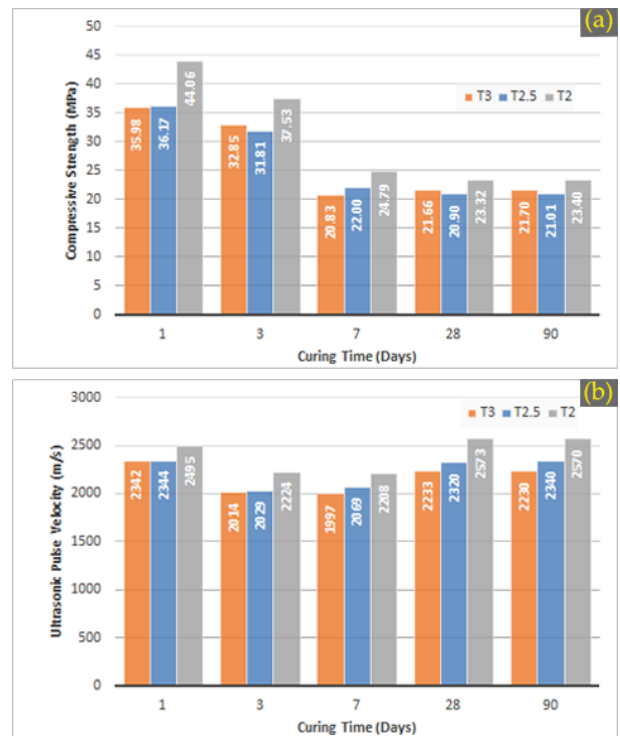
Figure 5. Results of rock wool based samples (a) compressive strengths and (b) UPV

It is clearly seen in Figure 4a and Figure 5a that the 7 and 28-day compressive strengths of the samples did not become stable. On the other hand, when Figure 4a and Figure 5a are examined, it is seen that the compressive strengths of the samples became stable at the end of 90 days. Therefore, in the study, the 90-day compressive strengths were taken into account when determining the molarity ratio with the rock wool and glass wool to be used. When the 90-day compressive strengths are taken into account, the sample using the C2.5 coded glass wool

with 2.5 molarity gives the best compressive strength. In the continuation of the study, 2.5-molarity mixtures were prepared under three different curing temperatures (25 ºC, 50 ºC and 100 ºC) to determine the effect of the curing temperature on the compressive strength.

In the study of Yadollahi et al. [50] it was stated that the increase in silica modulus increases the compressive strength. Similarly, in our study, it was observed that the compressive strength values obtained for 2.5 silica modulus were higher than 2 silica modulus in the samples using glass wool. However, a reverse situation was detected in the samples where stone wool was used.

3.2 Compressive Tests at Different Curing Temperatures

In the continuation of the studies, the compressive strengths of the 2.5 molarity samples produced from glass wool at 25 ºC, 50 ºC and 100 ºC cure temperature conditions were determined. In addition, the experiments conducted at 75 ºC were repeated against any doubts. The results are presented graphically in Figures 11-13. Since the necessary hardening did not occur in the samples kept in the mold at 25 ºC for 24 hours, their 1-day strengths did not yield results. For this reason, their 3, 7, 14, 28 and 90-day compressive strengths were examined. However, since there was no problem in the initial cure conditions of 50 ºC and 100 ºC, their 1, 3, 7, 28 and 90-day compressive strengths were examined.

Figure 6. Compressive strengths of 2.5 molarity samples produced from glass wool (a) at 25-50ºC and (b) at 75-100ºC curing conditions
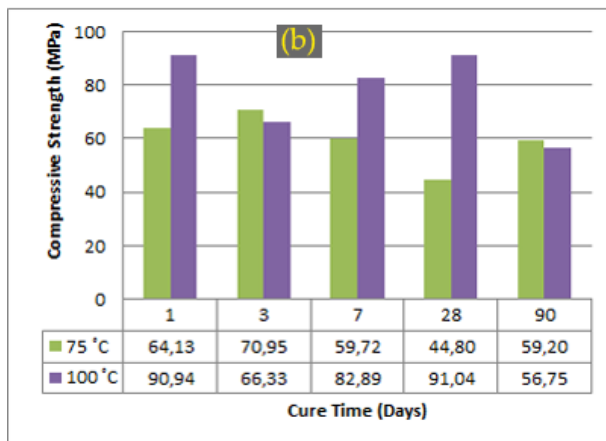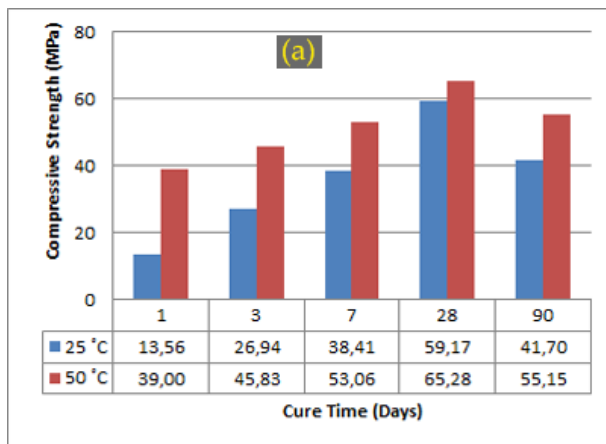
When the compressive strengths of the samples produced from glass wool under 75 ºC curing conditions were examined, the highest compressive strength was reached in the 3-day samples. However, there was a decrease in the compressive strength in the 7 and 28-day samples (Figure 6b).

When the compressive strengths of the samples produced from glass wool were examined under 25 ºC curing conditions, the highest compressive strength was reached in the 28-day samples. The compressive strength took its lowest value in the 3-day samples. There was an increase in compressive strength in direct proportion to the curing time (Figure 6a).

In samples produced from glass wool under 50 ºC and 100 ºC cure conditions, compressive strengths increased in direct proportion to the cure time. While the first day compressive strength of samples produced at 50 ºC was 39 MPa, the 28-day compressive strength was determined as 65.278 MPa. While the first day compressive strength of samples produced at 100 ºC was 90.945 MPa, the 28-day compressive strength was determined as 91.037 MPa. When the results were examined, it was seen that the samples produced under the initial cure conditions of 100 ºC reached the best compressive strength. However, as the cure time increased, it was seen that the compressive strength of samples produced at 75 ºC cure temperature was better.

Figures 6a and 6b show that curing temperature and curing time have a significant effect on compressive strength. At low temperatures (25 °C and 50 °C), the compressive strength increased up to 28 days, while a decreasing trend was observed after 28 days. At higher temperatures (75 °C and 100 °C), although the strength was high on the first day, fluctuations occurred depending on the curing time. Especially at 75 °C, the strength increased again at the end of 90 days, while at 100 °C, the strength decreased on the 3rd day and then recovered. This shows that both temperature and time-dependent chemical processes have complex effects on material properties.

4. CONCLUSION

This study demonstrated that mineral wool waste, including glass wool and rock wool, can be effectively utilized as raw materials for alkali-activated materials. The results revealed that the chemical and mineralogical composition of these wastes makes them highly suitable for alkali activation. The results are listed below:

- The mechanical properties of the specimens were significantly improved by thermal curing. The highest compressive strength (59.2 MPa) was obtained in glass wool specimens cured at 75°C. This shows that a suitable curing temperature improves the strength by increasing the density of the binder matrix.
- The effect of silica modulus ratios (2.0, 2.5 and 3.0) on mechanical properties was investigated and the optimum silica modulus ratio was determined as 2.5. This ratio balanced the amount of silica

196

dissolved, ensuring adequate polymerisation and increasing the homogeneity of the binder matrix.

- Glass wool samples exhibited higher mechanical properties compared to stone wool. This was attributed to the higher SiO_2 content in glass wool and a structural composition more favourable to alkali activation.

- It was observed that the compressive strength values stabilised at the end of the 90-day curing period. This shows that the long-term mechanical performance is reliable and the effects of curing time decrease with time.

- This study has shown that mineral wool waste can be utilised to produce sustainable materials for the construction industry. The recovery of wastes both reduces the environmental burden and provides an opportunity for the development of new binder systems.

Although the findings of the study prove that mineral wool wastes are applicable in the production of construction materials, their long-term durability and performance under different environmental conditions need to be investigated. Additionally, the effects of chemical and structural properties of different waste sources (e.g. old mineral wool and new mineral wool) on performance should be investigated in detail.

Acknowledgement

REFERENCES

[1] Benhelal E, Zahedi G, Shamsaei E, Bahadori A. Global strategies and potentials to curb CO2 emissions in cement industry. J Clean Prod. 2013;51:142–61.

[2] Davidovits J. Geopolymers: inorganic polymeric new materials. *J Therm Anal Calorim.* 1991;37(8):1633–56.

[3] Davidovits J. *Geopolymer Chemistry and Applications*. Saint-Quentin, France: Geopolymer Institute; 2011.

[4] Yip CK, Lukey GC, Provis JL, van Deventer JSJ. Effect of calcium silicate sources on geopolymerisation. *Cem Concr Res.* 2008;38(4):554–64.

[5] Diaz E, Allouche E, Eklund S. Factors affecting the suitability of fly ash as source material for geopolymers. *Fuel.* 2010;89(5):992–6.

[6] Nath P, Sarker PK. Effect of GGBFS on setting, workability and early strength properties of fly ash geopolymer concrete cured in ambient condition. *Constr Build Mater.* 2014;66:163–71.

[7] Thokchom S, Dutta D, Ghosh S. Effect of incorporating silica fume in fly ash geopolymers. *World Acad Sci Eng Technol.* 2011;60:243–7.

[8] Ryu GS, Lee YB, Koh KT, Chung YS. The mechanical properties of fly ash-based geopolymer concrete with alkaline activators. *Constr Build Mater.* 2013;47:409–18.

[9] Fu Y, Cai L, Wang Y. Freeze–thaw cycle test and damage mechanics models of alkali-activated slag concrete. *Constr Build Mater.* 2011;25(7):3144–8.

[10] Pilehvar S, Sanfelix SG, Szczotok AM, Rodríguez JF, Valentini L, Lanzón M, et al. Effect of temperature on geopolymer and Portland cement composites modified with micro-encapsulated phase change materials. *Constr Build Mater.* 2020;252:119055.

[11] Giro-Paloma J, Martínez M, Cabeza LF, Fernández AI. Types, methods, techniques, and applications for microencapsulated phase change materials (MPCM): A review. *Renew Sustain Energy Rev.* 2016;53:1059–75.

[12] Khudhair AM, Farid MM. A review on energy conservation in building applications with thermal storage by latent heat using phase change materials. *Energy Convers Manag.* 2004;45(2):263–75.

[13] Tyagi VV, Buddhi D. PCM thermal storage in buildings: a state of art. *Renew Sustain Energy Rev.* 2007;11(6):1146–66.

[14] Duxson P, Provis JL, Lukey GC, Van Deventer JSJ. The role of inorganic polymer technology in the development of 'green concrete'. *Cem Concr Res.* 2007;37(12):1590–7.

[15] Schneider M, Romer M, Tschudin M, Bolio H. Sustainable cement production—present and future. *Cem Concr Res.* 2011;41(7):642–50.

[16] Part WK, Ramli M, Cheah CB. An overview on the influence of various factors on the properties of geopolymer concrete derived from industrial by-products. *Constr Build Mater.* 2015;77:370–95.

[17] Singh B, Ishwarya G, Gupta M, Bhattacharyya S. Geopolymer concrete: A review of some recent developments. *Constr Build Mater.* 2015;85:78–90.

[18] Karakoç MB, Türkmen İ, Maraş MM, Kantarci F, Demirboğa R, Toprak MU, et al. Mechanical properties and setting time of ferrochrome slag based geopolymer paste and mortar. *Constr Build Mater.* 2014;72:283–92.

[19] Karthik A, Sudalaimani K, Kumar CV. Investigation on mechanical properties of fly ash-ground granulated blast furnace slag based self-curing bio-geopolymer concrete. *Constr Build Mater.* 2017;149:338–49.

[20] Yaseri S, Hajiaghaei G, Mohammadi F, Mahdikhani M, Farokhzad R. The role of synthesis parameters on the workability, setting and strength properties of binary binder based geopolymer paste. *Constr Build Mater.* 2017;157:534–45.

[21] Cao J, Chung D. Damage evolution during freeze–thaw cycling of cement mortar, studied by electrical resistivity measurement. *Cem Concr Res.* 2002;32(10):1657–61.

[22] Marzouk H, Jiang D. Effects of freezing and thawing on the tension properties of high-strength concrete. *ACI Mater J.* 1994;91(6):577–86.

[23] Jacobsen S, Sellevold EJ. Self-healing of high-strength concrete after deterioration by freeze/thaw. *Cem Concr Res.* 1996;26(1):55–62.

197

[24] Yazıcı H. The effect of silica fume and high-volume Class C fly ash on mechanical properties, chloride penetration and freeze–thaw resistance of self-compacting concrete. *Constr Build Mater.* 2008;22(4):456–62.

[25] Allahverdi A, Abadi MM, Hossain KMA, Lachemi M. Resistance of chemically-activated high phosphorous slag content cement against freeze–thaw cycles. *Cem Concr Res Technol.* 2014;103:107–14.

[26] Slavik R, Bednarik V, Vondruska M, Nemec A. Preparation of geopolymer from fluidized bed combustion bottom ash. *J Mater Process Technol.* 2008;200(1-3):265–70.

[27] Jo B-W, Park S-K, Park J-B. Properties of concrete made with alkali-activated fly ash lightweight aggregate (AFLA). *Cem Concr Compos.* 2007;29(2):128–35.

[28] Müller A, Leydolph B, Stanelle K. Recycling mineral wool waste: technologies for the conversion of the fiber structure, Part 1. *Int J Miner Process.* 2009;58(6):378–81.

[29] Väntsi O, Kärki T. Mineral wool waste in Europe: a review of mineral wool waste quantity, quality, and current recycling methods. *J Mater Cycles Waste Manag.* 2014;16(1):62–72.

[30] Luukkonen T, Abdollahnejad Z, Yliniemi J, Kinnunen P, Illikainen M. One-part alkali-activated materials: A review. *Cem Concr Res.* 2018;103:21–34.

[31] Yliniemi J, Luukkonen T, Kaiser A, Illikainen M, editors. Mineral wool waste-based geopolymers. *IOP Conference Series: Earth and Environmental Science.* IOP Publishing; 2019.

[32] Yliniemi J, Kinnunen P, Karinkanta P, Illikainen M. Utilization of mineral wools as alkali-activated material precursor. *Materials.* 2016;9(5):312.

[33] Yliniemi J, Laitinen O, Kinnunen P, Illikainen M. Pulverization of fibrous mineral wool waste. *J Mater Cycles Waste Manag.* 2018;20(2):1248–56.

[34] Kinnunen P, Yliniemi J, Talling B, Illikainen M. Rockwool waste in fly ash geopolymer composites. *J Mater Cycles Waste Manag.* 2017;19(3):1220–7.

[35] Weil M, Dombrowski K, Buchwald A. Life-cycle analysis of geopolymers. In: *Geopolymers.* Elsevier; 2009. p. 194–210.

[36] Li Z, Ding Z, Zhang Y, editors. Development of sustainable cementitious materials. Proceedings of International Workshop on Sustainable Development and Concrete Technology; Beijing, China; 2004.

[37] Komnitsas KA. Potential of geopolymer technology towards green buildings and sustainable cities. *Procedia Eng.* 2011;21:1023–32.

[38] Pacheco-Torgal F, Castro-Gomes J, Jalali S. Alkali-activated binders: A review. Part 2. About materials and binders manufacture. *Constr Build Mater.* 2008;22(7):1315–22.

[39] Kong DL, Sanjayan JG. Effect of elevated temperatures on geopolymer paste, mortar and concrete. *Cem Concr Res.* 2010;40(2):334–9.

[40] Ünsal Sağlık A. Alkali-silica reactivity and activation of ground perlite-containing cementitious mixtures [dissertation]. Middle East Technical University; 2009.

[41] Alahverdi A, Mehrpour K, Najafikani E. Taftan pozzolan-based geopolymer cement. *Cem Concr Res.* 2008.

[42] Bakharev T. Geopolymeric materials prepared using Class F fly ash and elevated temperature curing. *Cem Concr Res.* 2005;35(6):1224–32.

[43] Bakharev T. Resistance of geopolymer materials to acid attack. *Cem Concr Res.* 2005;35(4):658–73.

[44] Bakharev T. Durability of geopolymer materials in sodium and magnesium sulfate solutions. *Cem Concr Res.* 2005;35(6):1233–46.

[45] Thokchom S, Ghosh P, Ghosh S. Acid resistance of fly ash based geopolymer mortars. *Int J Recent Trends Eng.* 2009;1(6):36–40.

[46] Thokchom S, Ghosh P, Ghosh S. Resistance of fly ash based geopolymer mortars in sulfuric acid. *ARPN J Eng Appl Sci.* 2009;4(1):65–70.

[47] Atiş CD, Bilim C, Çelik Ö, Karahan O. Influence of activator on the strength and drying shrinkage of alkali-activated slag mortar. *Constr Build Mater.* 2009;23(1):548–55.

[48] Komljenović M, Baščarević Z, Bradić V. Mechanical and microstructural properties of alkali-activated fly ash geopolymers. *J Hazard Mater.* 2010;181(1-3):35–42.

[49] Anuar K, Ridzuan A, Ismail S. Strength characteristic of geopolymer concrete containing recycled concrete aggregate. *Int J Civ Environ Eng.* 2011;11(1):59–62.

[50] Yadollahi MM, Benli A, Demirboğa R. The effects of silica modulus and aging on compressive strength of pumice-based geopolymer composites. *Construction and Building Materials.* 2015;94:767–74.

Investigation of Leishmaniasis Seroprevalence in Dogs in Bingöl Province of Turkey

Murat UZTİMÜR [1*] 🆔 , **Hakan KEÇECİ** [1] 🆔 , **Taylan TURAN** [2] 🆔 , **Cennet Nur ÜNAL** [1] 🆔

[1]Bingöl University, Faculty of Veterinary Medicine, Department of Internal Medicine, 12000, Bingöl, Turkey
[2] Gazi University, Faculty of Pharmacy, Department of Biochemistry, 06330, Ankara, Turkey.
Murat UZTİMÜR, ORCID No:0000-0001-9294-1825
Hakan KEÇECİ, ORCID No: 0000-0001-5654-0581
Taylan TURAN, ORCID No:0000-0001-7335-1213
Cennet Nur ÜNAL, ORCID No:0000-0002-8676-6490

Corresponding author: cnaltunboga@gmail.com

(Received: 23.10.2024, Accepted: 04.12.2024, Online Publication: 30.12.2024)

Keywords	
Dog, ELISA, *Leishmania*, Prevalence	**Abstract:** Canine leishmaniasis is a lethal zoonotic disease caused by *Leishmania infantum* (*L. infantum*) and seen in Asia, Europe, America, and Africa. Dogs play an important role in the spread of the disease as they can be infected clinically and are reservoirs for other mammals and humans. The aim of the present study was to investigate the prevalence of leishmaniasis in asymptomatic dogs in Bingöl province. In this study, a total of 84 dogs of different breeds, ages, and sexes (male/female) were used. Leishmania antibody IgG levels in the serum of the dogs were measured using an ELISA Kit. It was determined that 5 (19.2%) of the dogs aged <2 years and 7 (12.1%) of the dogs aged ≥2 years were Leishmania seropositive. 7 (17.9%) of the female dogs and 5 (11.1%) of the male dogs were detected Leishmania seropositive. The prevalence of Leishmania seropositive was determined as 14.2% in this study. The effect of gender (p=0.562) and age (p=0.501) factors on the occurrence of Leishmania infection was not determined. In conclusion, in this study, the prevalence of leishmaniasis in asymptomatic dogs in Bingöl province, which is not an endemic region, was determined. This finding shows the presence of Leishmania infection in the region and poses a significant risk to public health.

199

Türkiye'nin Bingöl İli Köpeklerinde Leishmaniasis Seroprevalansının Araştırılması

Anahtar Kelimeler	
Köpek, ELISA, *Leishmania*, Prevalans	**Öz:** Köpek leishmaniasisi, *Leishmania infantum*'un (*L. infantum*) yol açtığı Asya, Avrupa, Amerika ve Afrika kıtalarında görülen öldürücü zoonotik bir hastalıktır. Köpekler hem klinik olarak enfekte olabildikleri hem de diğer memelilere ve insanlara rezervuarları oldukları için hastalığın yayılmasında önemli bir rol oynamaktadır. Mevcut çalışma ile Bingöl ilindeki asemptomatik köpeklerde leishmaniasis prevalansının araştırılması amaçlanmıştır. Bu çalışmada farklı ırk, yaş ve cinsiyetten (erkek/dişi) oluşan toplam 84 adet köpek kullanıldı. Köpeklerin serumunda *leishmania* antikoru IgG seviyeleri bir ELISA Kiti kullanılarak ölçüldü. Yaşı <2 olanlardan 5 (%19.2), 2≥ olanlardan 7 (%12.1) adet köpeğin *leishmania* seropozitif olduğu belirlendi. Dişi köpeklerin 7 (%17.9), erkek köpeklerin 5 (%11.1) tanesinin *leishmania* seropozitif olduğu tespit edildi. Çalışmada *leishmania* prevalansı %14.2 olarak belirlendi. *Leishmania* enfeksiyonunun görülmesinde cinsiyet (p=0.562) ve yaş (p=0.501) faktörlerinin etkisi tespit edilmedi. Sonuç olarak, bu çalışmada endemik bölge olmayan Bingöl ilinde asemptomatik köpeklerde Leishmaniasis prevalansı tespit edilmiştir. Bu bulgu, bölgede *leishmania* enfeksiyonunun varlığını göstererek, halk sağlığı açısından önemli bir risk teşkil ettiğini ortaya koymaktadır.

1. INTRODUCTION

Canine leishmaniasis is a lethal zoonotic disease caused by *Leishmania infantum* (*L. infantum*) and seen in Asia, Europe, America and Africa. Domestic dogs are known to be the main reservoir of human infection and phlebothumus sand flies are known to be the vectors of the disease [1]. Dogs play an important role in the spread of the disease as they can both be clinically infected and act as reservoirs for other mammals and humans [2]. In

addition, it can be transmitted non-vectorally between dogs through blood transfusion, placenta, and mating [3]. *Leishmania* species are defined as diheteroxenous parasites because they complete their life cycle in the bodies of both a vertebral and an invertebral vector [1]. *Leishmania* parasites exist in two main morphological forms, amastigote and promastigote. Sand flies ingest infected macrophages containing the amastigote form while sucking blood from infected animals [1]. In the vector's organism, it turns into a promastigote form within 4–25 days and multiplies by simple division. Then, this form is transferred to the host while the vector sucks blood. In the host, the parasite infects macrophages and initiates the disease with the amastigote form [3]. Leishmaniasis disease is seen in four main clinical forms: visceral, cutaneous, mucocutaneous, and diffuse cutaneous forms. In Turkey, two forms caused by different *leishmania* species are seen as cutaneous leishmaniasis (CL) and visceral leishmaniasis (VL) [3, 4]. Although the most common form of the disease is the cutaneous form, the visceral form is the most serious as it clinically affects vital organs [3]. In dogs affected by the disease, showing more than three clinical signs are classified as symptomatic, dogs showing one to three clinical signs are classified as oligosymptomatic, and dogs showing no clinical signs are classified as asymptomatic [4, 5]. Common clinical symptoms of leishmaniasis include local or generalized lymphadenopathy, weight loss, anorexia, dermatological lesions, swelling in the joints and legs, and onychogryposis, while less common clinical symptoms include eye lesions, epistaxis, renal failure, lameness, diarrhea, and meningitis [1, 4]. Although the prevalence of leishmaniasis may vary depending on the diagnostic method used, it is reported to be between 0% and 27.5% in Turkey [3, 6, 7], percent 16.6 in the Mediterranean basin with 2.5 million infected dogs, and 15.2% globally [8]. The prevalence of leishmaniasis in asymptomatic dogs in Bingöl province is unknown. Based on this, the aim of the present study was to investigate the prevalence of leishmaniasis in asymptomatic dogs in Bingöl province.

2. MATERIAL AND METHOD

The study was conducted with the approval of the Bingöl University Animal Experiments Local Ethics Committee (B.Ü HADYEK Date: 2024/01 Decision No:01/08).

2.1. Collection of Blood Samples

In this study, a total of 84 dogs of different breeds, ages and genders were used. Breeds, ages and genders of dogs are presented in Table 1. The study was conducted in Bingöl province, which is located between 41º 20 and 39º - 56º east longitudes and 39º - 31 and 36º - 28º north latitudes of Turkey. The animals were brought to the Internal Medicine Department of the Animal Hospital of the Faculty of Veterinary Medicine of Bingol University. As a result of the systematic clinical examination, age, gender and clinical examination findings were recorded. Five ml blood samples were taken from the vena cephalica antebrachi of the animals into gel serum tubes (BD Vacutainer, Plymouth, UK). Blood samples were

centrifuged at 5000 rpm for 5 minutes and the sera were transferred to Eppendorf tubes and stored at -20 oC for up to 3 months until analyzed.

2.2. ELISA Analysis

Leishmania antibody IgG levels in the serum of dogs were measured using a commercially available ELISA Kit (Shanghai Coon Koon Biotech Co., Ltd, China, CK-bio-24415) according to the manufacturer's instructions. The method relies on the ability of biotinylated detection antibodies to capture the *leishmania* antibody IgG present in serum. Before 50 µL of positive and negative control were placed into the positive and negative wells, while 10 µL serum samples were diluted with 40 µL sample diluent and added to the remaining wells. Next, 100 µL HRP conjugate reagent was added to each well and incubated at 37 oC for 60 min. After the incubation step, the plate was inverted to empty all contents and were washed 5 times with 400 µL of wash solution. Subsequently, 50 µL of chromogen solution A and then 50 µL of chromogen solution B were added to each well respectively and incubated at 37 oC for 15 min. After that, 50 µL stop solution was added to each well. Absorbances were measured in the microplate reader at a wavelength of 450 nm within 15 min after having added the stop solution. The ELISA test was considered valid, if the mean absorbance of the positive control was greater than 1.00 and the mean absorbance of the negative control was less than 0.15. The evaluation of the test result was based on the critical cut off value. The critical cut off value was calculated by adding 0.15 to the average absorbance value obtained in the negative control wells. The absorbance of the sample was considered negative if less than this cut-off value and positive if greater than or equal to this cut-off value.

2.3. Statistical Analysis

Statistical analysis of the data was performed using SPSS 26 (IBM SPSS Statistics for Windows, Version 22.0. Armonk, NY: IBM Corp.). Gender and age variables were compared using the Chi-square test. Differences with a value of <0.05 were considered statistically significant as a result of the analysis.

3. RESULTS

In the study, 84 dogs consisting of Kangal, Golden Retriever, Malinois, and mixed breeds were used. Information was obtained from the patient owners that all of the dogs lived in a home and went outside at certain times of the day. When the dogs were categorized according to age, 26 were <2 years old, 58 were 2≥ years old, and when classified according to gender, 45 dogs were male and 39 dogs were female. It was determined that 5 (19.2%) dogs aged <2 years and 7 (12.1%) dogs aged ≥2 years were seropositive for *leishmania*. 7 (17.9%) female dogs and 5 (11.1%) male dogs were found to be seropositive for *leishmania*. The prevalence of *leishmania* seropositive was found to be 14.2% in the study. Gender (p = 0.562) and age (p = 0.501) factors had no effect on the occurrence of *leishmania* infection. The obtained

epidemiological data, animal number information, percentage expressions, and Chi-square test results are presented in Table 1.

Table 1. Prevalence of *leishmania* infection and epidemiological data based on sex, age and race and Chi-square test results

Epidemiological Data	Number and Rate of Dogs Tested	Number and Rate of Positive Dogs	Chi-square test P values
Breed			
Kangal	15 (%17.8)	5 (%33.3)	
Golden Retreiver	2 (%2.3)	-	
Malinois	23 (%27.3)	1 (%4.3)	
Mix Breed	44 (%52.3)	6 (%13.6)	
Sex			0.562
Male	45 (%53.5)	5 (%11.1)	
Female	39 (%46.4)	7 (%17.9)	
Age			0.501
<2	26 (%30.9)	5 (%19.2)	
2≥	58 (%69.04)	7 (%12.1)	
Total	84	12(%14.2)	

4. DISCUSSION AND CONCLUSION

Leishmaniasis is considered a neglected tropical zoonotic disease that poses a potentially fatal risk to humans and causes serious public health problems in developing countries. Dogs that show clinical signs of disease can be diagnosed and managed. However, asymptomatic dogs are potential sources of *leishmania* vector infection and facilitate the transmission cycle of the disease [9]. In order to adequately implement the necessary control measures for *leishmania* disease and reduce transmission, its prevalence in a region must be known. In this study, the prevalence of *leishmania* in asymptomatic dogs in Bingöl province is reported for the first time.

Various serological diagnostic tests, including indirect immunofluorescence tests, direct agglutination tests, ELISA tests, and cross immunoelectrophoresis, are used in the diagnosis of leishmaniasis [10]. Molecular tests can go beyond the limitations found in serological tests, but it is stated that they are not fully applicable in field studies due to high cost and laboratory environment requirements [11]. Immunochromatographic tests and direct agglutination tests are frequently used in the field and their confirmation is done with ELISA tests that allow the evaluation of more animals [12]. In this direction, in the presented study, it was preferred to investigate the prevalence of leishmaniasis in dogs in Bingöl province with the ELISA method, similar to the studies conducted by Zerpa et al. [13] and Arslan et al. [14].

Leishmaniasis is more common seen in Mediterranean regions with tropical and subtropical climates due to the long lifespan and breeding season of sandflies and is considered endemic in these areas [15]. Among the regions of Turkey considered endemic for leishmaniasis, seropositivity rates have been reported as 14.1% in Aydın/Kuşadası, 4.6% in İzmir/Selçuk, 3.8% in Manisa/Turgutlu, 22% in Muğla/Bodrum [5], 27.18% in Adana [16], and 18.5% in Mersin [17]. Similarly, high prevalence rates have been detected abroad, including 18.6% in South America [8] and 33.1% in Venezuela [13] where it is considered endemic. However, as a result of changing climatic conditions and animal movements, the disease is also encountered in non-endemic regions. When the prevalence in non-endemic regions is evaluated, it has been detected as 58.1% in Germany [18], 2.72% in valley villages and 11.32% in villages on the foothills of mountains in France [19], 4.7% in northern Spain, 3% [20], in Çankırı province in Turkey [21], 2.92% in Istanbul province [22], and 0% in Diyarbakır province [7]. In this study, it was determined that the seroprevalence of leishmaniasis in dogs in the non-endemic Bingöl province was 14.2%, and this finding was higher than in the non-endemic regions of Çankırı, İstanbul, Diyarbakır, France, and lower than in the non-endemic region of Germany. The differences in the seropositivity prevalence rates of leishmaniasis in non-endemic regions may be related to the results of climate conditions, animal movements, types of analysis, and variable protective measures.

Age is considered a risk factor for leishmaniasis, for which no consensus has been reached [20,23]. Dantas-Torres et al. [24] and Gálvez et al. [25] reported higher *leishmania* seropositivity rates in young dogs, while Miró et al. [20] and Selim et al. [26] reported higher seropositivity rates in older dogs. In contrast to these, in the study conducted by Miranda et al. [23] and Almeida et al. [27], age was not seen as a risk factor, while in the study conducted by Gálvez et al. [28], it was reported that a bimodal age distribution could be formed, with one peak in young dogs (1-2 years old) and the second peak in old dogs (7-8 years old). The reason for the variability in the age factor among leishmaniasis seropositive studies is explained as the immaturity of the immune system in young people or the fact that resistant animals are infected at a young age and the immune system weakens in older ages and as a result of various diseases [23]. In this study, according to the Chi-square test result, age factor was found to be a factor that did not affect leishmaniasis seropositivity (p = 0.501). The results obtained in the present study are consistent with those determined by Almeida et al. [27] and Miró et al. [20]. It is thought that this variability between studies is related to race, categorization of age range, environmental factors, and population size.

The gender factor is considered a risk factor in some studies [5, 28], while it is considered insignificant in some studies [14, 29]. While a study by Dantas Torres et al. [24] reported higher seropositivity in male dogs, studies by Almeida et al. [27] and Cortes et al. [30] found no difference between the genders. In studies with higher prevalence in males, this was attributed to the fact that male dogs exhibit more roaming behaviour [26]. Although the number of male dogs was relatively higher in this study, the Chi-square test between male and female dogs did not reveal a significant difference in leishmaniasis seropositivity (p=0.562). The results obtained in the present study are similar to those of Almeida et al. [27], Selim et al. [26], and Cortes et al. [30]

but not in agreement with those found by Dantas-Torres et al. [24].

In conclusion, in this study, the prevalence of leishmaniasis was detected in %14.2 asymptomatic dogs in Bingöl province, which is not an endemic region. This finding shows the presence of *leishmania* infection in the region and poses a significant risk to public health. The data obtained may form an important basis for the development of effective control strategies and public health measures in our country. In further studies, it will be useful to evaluate different risk factors in the prevalence of *leishmania*, to test various diagnostic methods and to conduct research in a larger study population.

REFERENCES

[1] Bañuls AL, Hide M, Prugnolle F. *Leishmania* and the leishmaniases: a parasite genetic update and advances in taxonomy, epidemiology and pathogenicity in humans. Adv Parasitol. 2007;64:455-458.

[2] Bolukbas CS, Pekmezci GZ, Gurler AT, Pekmezci D, Guzel M, Hokelek M, et al. Evidence of *Leishmania spp*. antibodies and DNA in dogs in the Middle Black Sea Region of Turkey. Ankara Üniv Vet Fak Derg. 2016;63(2):111-114.

[3] Çelik BA, Çelik ÖY, Şahin T. Retrospective Evaluation of Canine Leishmaniasis in Turkey. FÜ Sağ Bil Vet Derg. 2019;33(2):123-130.

[4] Bilgin Z, Turan N, Yilmaz H, Ferroglio E, Tuzer E. Prevalence of leishmaniosis in dogs in Istanbul, Turkey determined by using PCR. J Hellenic Vet Med Soc. 2015;66(2):106-112.

[5] Atasoy A, Pasa S, Ertabaklar H. Seroprevalence of canine visceral leishmaniasis around the Aegean cost of Turkey. Kafkas Üniv Vet Fak Derg. 2010:16(1);1-6.

[6] Dogan N, Ozbel Y, Ozensoy Toz S, Dinleyici EÇ, Bor O. Sero-epidemological survey on canine visceral leishmaniasis and the distribution of sandfly vectors in Northwestern Turkey: Prevention strategies for childhood visceral leishmaniasis. J Trop Pediatr. 2006;52(3):212-217.

[7] İçen H, Babür C, Bademkıran S, Çelebi B, Şimşek A, Özyurtlu N, et al. Diyarbakır bölgesindeki sahipsiz köpeklerde toxoplasmosis, leishmaniasis ve listeriozisin seroprevalansı. Türkiye Parazitol Derg. 2010;34(1):6-10.

[8] Priolo V, Ippolito D, Rivas-Estanga K, De Waure C, Martínez-Orellana P. Canine leishmaniosis global prevalence over the last three decades: a meta-analysis and systematic review. Comp Immunol Microbiol Infect Dis. 2024;112;102211.

[9] Lopes JV, Michalsky ÉM, Pereira NCL, Paula AJVD, Souza AGM, Pinheiro LC, et al. Canine visceral leishmaniasis in area with recent *Leishmania* transmission: prevalence, diagnosis, and molecular identification of the infecting species. Rev Soc Bras Med Trop. 2020;53:e20200141.

[10] Pozio E, Gradoni L, Bettini S, Gramiccia M. Leishmaniasis in Tuscany (Italy): VI. Canine leishmaniasis in the focus of Monte Argentario (Grosseto). Acta Trop. 1981;38(4):383-393.

[11] Pessoa-e-Silva R, Vaitkevicius-Antão V, de Andrade, TAS, de Oliveira Silva, AC, de Oliveira GA, Trajano-Silva LAM, et al. The diagnosis of canine visceral leishmaniasis in Brazil: Confronting old problems. Exp Parasitol. 2019;199:9-16.

[12] Travi BL, Cordeiro-da-Silva A, Dantas-Torres F, Miró G. Canine visceral leishmaniasis: Diagnosis and management of the reservoir living among us. PLOS Negl Trop Dis. 2018;12(1);e0006082.

[13] Zerpa O, Ulrich M, Negrón E, Rodríguez N, Centeno M, Rodríguez V. Canine visceral leishmaniasis on Margarita Island (Nueva Esparta, Venezuela). Trans R Soc Trop Med Hyg. 2000;94(5), 484-487.

[14] Arslan S, Öncel T, Yenilmez K, Turan N. Detection of *Leishmania* infantum seropositivity in dogs by ELISA technique in Thrace region of Turkey. Eurasian J Vet Sci. 2019;35(3);165-169.

[15] Espejo LA, Costard S, Zagmutt FJ. Modelling canine leishmaniasis spread to non-endemic areas of Europe. Epidemiol Infect. 2015;143(9):1936-1949.

[16] Karakuş M, Töz S, Ertabaklar H, Paşa S, Atasoy A, Arserim SK, et al. Evaluation of conjunctival swab sampling in the diagnosis of canine leishmaniasis: A two-year follow-up study in Çukurova Plain, Turkey. Vet Parasitol. 2015;214(3-4):295-302.

[17] Utuk A, Gokmen G, Bolacalı M, Balkaya I, Simsek S. A serologic survey on canine leishmaniasis in Kocaeli, Sakarya, Mersin and Elazığ provinces of Turkey. Isr J Vet Med. 2018; 4: 3-7.

[18] Geisweid K, Weber K, Sauter-Louis C, Hartmann K. Evaluation of a conjunctival swab polymerase chain reaction for the detection of *Leishmania* infantum in dogs in a non-endemic area. Vet J. 2013;198(1):187-192.

[19] Dereure J, Vanwambeke SO, Malé P, Martinez S, Pratlong F, Balard Y, et al. The potential effects of global warming on changes in canine leishmaniasis in a focus outside the classical area of the disease in southern France. Vector Borne Zoonotic Dis. 2009;9(6):687-694.

[20] Miró G, Checa R, Montoya A, Hernández L, Dado D, Gálvez R. Current situation of *Leishmania* infantum infection in shelter dogs in northern Spain. Parasit Vectors. 2012;5:1-7.

[21] Yucesan B, Ozkan O, Tuncer S, Ocal Z. Molecular Detectıon of Canine Leishmaniasis in Northern Anatolia, Turkiye. Iran J Parasitol. 2023;18(4);483.

[22] Koenhemsi L, Fabrizio V, Mariella P, Antonella M, Or E. Seroprevalence of leishmaniosis among healthy dogs in Istanbul. Isr J Vet Med. 2020;75(1):31-34.

[23] Miranda S, Roura X, Picado A, Ferrer L, Ramis A. Characterization of sex, age, and breed for a population of canine leishmaniosis diseased dogs. Res Vet Sci. 2008;85(1):35-38.

[24] Dantas-Torres F, de Brito MEF, Brandão-Filho SP. Seroepidemiological survey on canine leishmaniasis among dogs from an urban area of Brazil. Vet Parasitol. 2006;140(1-2):54-60.

[25] Gálvez, R., Montoya, A., Cruz, I., Fernández, C., Martín, O., Checa, R., et al. Latest trends in

Leishmania infantum infection in dogs in Spain, Part I: Mapped seroprevalence and sand fly distributions. Parasit Vectors, 2020;13:1-12.

[26] Selim A, Shoulah S, Abdelhady A, Alouffi A, Alraey Y, Al-Salem WS. Seroprevalence and risk factors associated with canine leishmaniasis in Egypt Vet Sci. 2021;8(10):236.

[27] Almeida ADBPFD, Sousa VRF, Cruz FACSD, Dahroug MAA, Figueiredo FB, Madeira MDF. Canine visceral leishmaniasis: seroprevalence and risk factors in Cuiabá, Mato Grosso, Brazil. Rev Bras Parasitol Vet. 2012;21:359-365.

[28] Gálvez R, Miró G, Descalzo MA, Nieto J, Dado D, Martín, O, et al. Emerging trends in the seroprevalence of canine leishmaniosis in the Madrid region (central Spain). Vet Parasitol. 2010;169(3-4):327-334.

[29] Bakirci S, Bilgiç HB, Köse O, Aksulu A, Hacılarlıoğlu S, Erdoğan H, et al. Molecular and seroprevalence of canine visceral leishmaniasis in West Anatolia, Turkey. Turk J Vet Anim Sci. 2016;40(5):637-644.

[30] Cortes S, Vaz Y, Neves R, Maia C, Cardoso L, Campino L. Risk factors for canine leishmaniasis in an endemic Mediterranean region. Vet Parasitol. 2012;189(2-4):189-196.

Türk Doğa ve Fen Dergisi
Turkish Journal of Nature and Science

www.dergipark.gov.tr/tdfd

Silent Treasures of Nature: The Awakening of Bingöl Lakes With Ecotourism

Alperen MERAL[1*] [iD] , Yeşim KABAY[1] [iD] , Sefa BAYRAM[1] [iD] , Rozelin KAYALI[1] [iD] ,

Ahmet USLU[2] [iD]

[1] Bingöl University, Agriculture Faculty, Landscape Architecture Department, Bingöl, Türkiye
[2] Bingol University, Vocational School of Social Sciences, Office Services and Secretarial Department, Bingöl, Türkiye

Alperen MERAL ORCID No: 0000-0001-6714-7187
Yeşim KABAY ORCID No: 0009-0006-3403-7671
Sefa Bayram ORCID No: 0009-0007-7282-557X
Rozelin KAYALI ORCID No: 0009-0000-5852-266X
Ahmet USLU ORCID No: 0000-0001-8745-423X

*Corresponding author: alperenmeral@bingol.edu.tr

Abstract: With its abundant natural beauty and pristine ecosystems, Bingöl is one of Turkey's best-kept natural secrets. One of the most remarkable elements of these beauties is the natural lakes in the region. However, for many years, both security and carelessness have prevented these lakes' tourism potential from being realised. Ecotourism, which aims to sustainably protect natural and cultural resources, offers an important opportunity for the development of tourism in these regions. This study examined the ecotourism potential of four natural lakes in the province of Bingöl with the goal of promoting tourism in these areas.

Within the scope of the research, firstly, a survey was conducted with 192 people to determine the perspectives of Bingöl people on ecotourism and the potential in the province where they live. SWOT studies were conducted for four designated natural lakes (Balpınar Lake, Gerindal Lake, Natural Thermal Water Situated in Ilıcalar, Sarıçiçek Lake) in collaboration with professionals, including academics and students from the landscape architecture department. Based on the collected data, the research concluded with the creation of landscape designs for the chosen lakes. The primary objective of this project is to serve as a model for ecotourism design of concealed natural attractions.

204

Doğanın Sessiz Hazineleri: Bingöl Göllerinin Ekoturizm İle Uyanışı

Öz: Bingöl, zengin doğal güzellikleri ve bozulmamış ekosistemleriyle Türkiye'nin gizli kalmış doğa hazinelerinden biridir. Bu güzelliklerin en dikkat çekici unsurlarından biri de bölgedeki doğal göllerdir. Ancak, bu göllerin turizm potansiyeli uzun yıllar boyunca gerek güvenlik gerekse ihmalkarlık nedeniyle göz ardı edilmiştir. Doğal ve kültürel kaynakların sürdürülebilir şekilde korunmasını amaçlayan ekoturizm, bu bölgelerdeki turizmin gelişmesi için önemli bir fırsat sunmaktadır. Bu bağlamda, Bingöl ilindeki dört doğal göl, ekoturizm potansiyeli açısından incelenmiş ve bu bölgelerin turizme kazandırılması hedeflenmiştir.

Araştırma kapsamında ilk olarak Bingöl halkının ekoturizme ve yaşadıkları ildeki potansiyele bakış açılarını belirlemek için 192 kişi ile anket çalışması yapılmıştır. Seçilen dört doğal göl için (Balpınar Gölü, Gerindal Gölü, Ilıcalar Beldesi Doğal Termal Su Yatağı, Sarıçiçek Gölü) uzman kişiler ile (öğretim elemanları ve peyzaj mimarlığı bölümü öğrencileri) SWOT analizleri yapılmıştır. Elde edilen veriler doğrultusunda son olarak seçilen göllerin peyzaj tasarımları yapılarak araştırma sonuçlandırılmıştır. Yapılan bu çalışmanın saklı kalmış doğal güzelliklerin ekoturizm planlamasında örnek olması araştırmanın temel amacıdır.

1. INTRODUCTION

Anatolia is abundant in natural and cultural resources, as it is a region where numerous civilisations thrived thousands of years ago, leaving behind their remnants. Consequently, it accommodates many forms of tourist [1], [2]. In 2019, global tourism revenue was estimated at 2 trillion dollars [3], [4]. Ecotourism activities, expanding at an average annual rate of 10%, are among the most rapidly increasing sectors in the global tourism market. Ecotourism activities represent 1-2% of the overall tourism market [3], [4], [5]. The Turkey Tourism Strategy 2023 document indicates that Turkey possesses distinctive opportunities in various forms of tourism beyond coastal tourism; however, this potential remains underexploited. It also highlights the overconcentration in the Mediterranean-Aegean coastal region, unregulated construction, inadequate infrastructure, and environmental issues in the coastal hinterlands and adjacent areas. The paper aims to leverage the natural, cultural, historical, and geographical assets of our country while maintaining a balance between preservation and utilisation, and to enhance tourism by offering alternative options [3], [6]. The potential of Turkey, coupled with the diminishing rural population and the escalating demand for rural development, renders ecotourism an optimal tourism strategy for the nation, necessitating the promotion of ecotourism to economically invigorate rural regions [3].

Ecotourism encompasses all tourism activities occurring in natural and cultural settings, with the objective of fostering the social and economic advancement of local communities through environmental conservation. These activities emphasise the acknowledgement and advancement of the local culture, geology, flora, and fauna of a certain place [7]. Ecotourism, as defined by the International Ecotourism Society, refers to responsible travel to natural regions that conserves the environment, supports the welfare of local communities, and incorporates interpretation and education. Training must encompass both personnel and guests [8]. The rise in this form of travel poses a concern, including the depletion of natural resources. Consequently, in addressing the demand for diversity, it is equally crucial to cultivate environmental consciousness in regions where ecotourism operations occur [9]. The Turkey Tourism Strategy 2023 asserts that ecotourism will facilitate economic stabilisation in its implementation regions, generate employment opportunities, foster business growth, enhance infrastructure investments, offer recreational and touristic prospects, augment public revenues, and elevate local awareness regarding environmental conservation and development [10].

Ecotourism endeavours seek to offer guests enlightening and enriching experiences while safeguarding natural and cultural heritage [11]. The sustainable utilisation of natural resources in ecotourism is achievable through multidisciplinary planning that safeguards existing habitats while preserving the biological integrity of the region [12].

Numerous initiatives categorised as rural tourism, ecotourism, and agrotourism are designed and executed within various rural and regional development programs in our country. These activities have the capacity to augment the family income of the residents in the region and generate new employment opportunities [13], [14]. Bingöl signifies the area of lakes and a multitude of lakes. Subsequently, Bingöl was referred to as Çevlik. Çevlik denotes a vineyard-garden. Çevlik is a designation currently employed by the inhabitants of Bingöl [15]. The province of Bingöl contains lakes that are remarkable natural phenomena. These natural ecosystems have gone unexamined for numerous years, their aesthetic appeal and ecological importance obscured. The increasing interest in ecotourism has illuminated these 'silent jewels,' offering a significant chance to preserve and highlight their distinctive attributes. This article examines the integration of natural lakes in Bingöl province into ecotourism, the local populace's attitudes towards tourism, and landscape design methodologies. The findings of this study regarding the awakening of nature's quiet treasures through ecotourism and the future of sustainable tourism may be pertinent to both planners and practitioners.

2. MATERIAL AND METHOD

2.1. Study Areas

The research region selected comprises Balpinar, Gerindal, Sarıçiçek lakes, and the Ilıcalar Town Natural Thermal Water, which have gained significant popularity among users in Bingöl Province and have had considerable growth in drawing domestic tourists in recent years. The primary rationale for selecting these areas is their recognition within Bingöl province, although they fail to garner adequate attention due to insufficient advertising (Figure 1).
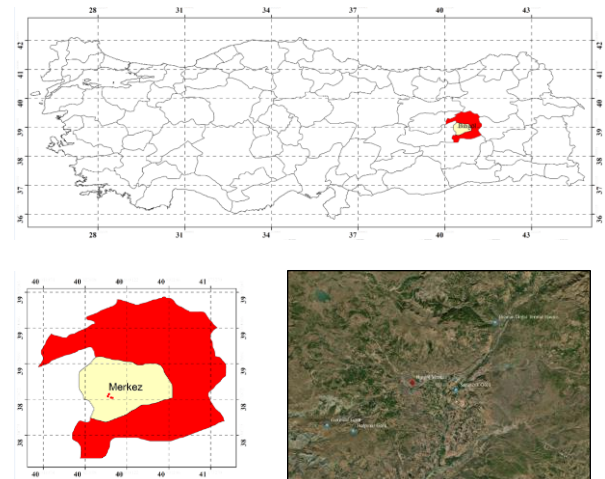
Figure 1. Location of designated lakes

Balpınar Lake, designated as a study area, is also referred to as Metan and Kız Lake in the region. The lake encompasses a surface area of roughly 2000 square meters. The lake is situated at an elevation of roughly 2000 m, 21.5 km from the town of Bingöl. It is rumoured that a young girl took her own life by leaping into this lake

after being denied her beloved. Subsequent to this event, the lake was designated as Girl Lake in the area [16] (Figure 2).

Figure 2. Balpınar Lake

Gerindal Lake, another lake, is situated inside the confines of Şaban village, 18 km from the city of Bingöl. Academic investigations indicate that the lake environs harbour new floristic records [17], [18]. Furthermore, the lake's position at the confluence of the Elazığ and Bingöl provincial borders has resulted in a direct confrontation between the two provinces. The lake, possessing significant ecotourism potential, will attract numerous tourists following strategic planning and promotion [19]. The interviews revealed that the location is intriguing due to the belief among the populace that its water possesses therapeutic properties (Figure 3).

Figure 3. Gerindal Lake

Another lake chosen for the study was Sarıçiçek Lake, also referred to as Sülüklü Lake. Sarıçiçek Lake is about 17.5 km from the town of Bingöl (Figure 4). The user interviews revealed that the region is notable for its natural beauty and bike paths.

Figure 4. Sarıçiçek Lake

The final region chosen for the investigation is the natural thermal water situated in Ilıcalar, Bingöl province. The pond, much frequented by visitors, is situated 21.1 km from the town of Bingöl (Figure 5). The demand for thermal centres has recently surged as individuals have begun to choose healthy lifestyles and eschew synthetic medications [20]. Consequently, the promotion of regions with these characteristics has become significantly important for tourism. This location was chosen for the research to promote the natural water supply for ecotourism.

Figure 5. Natural thermal water situated in Ilıcalar

2.2. Executing Surveys and SWOT Analyses

Public engagement is seen as a fundamental element of local tourist development [21]. During the execution of integrated planning, the populace assumes stewardship of the region and readily supports planners and implementers [22]. The natural lakes of Bingöl present a significant possibility for ecotourism due to their ecological diversity and aesthetic appeal. Nonetheless, tourist endeavours in the region cannot achieve sustainability without the backing of the local populace, as indicated in the research. The objective of conducting surveys is to ascertain how user demands will vary by incorporating diverse user profiles into the research [23].

This research performed 192 surveys to elucidate the perspectives of various user profiles from the population of Bingöl towards tourism and to illuminate shortcomings in present tourist activities.

SWOT analysis is applicable in the phases of strategic planning, problem identification, and solution creation. This strategy is often employed when numerical data is inadequate and the information is in the memory of specialised individuals or consumers [7], [24], [25]. To assess the strengths, weaknesses, opportunities, and threats of the chosen places, SWOT analyses were conducted with the expert group and the students from the Department of Landscape Architecture (Figure 6).

Figure 6. Survey, SWOT analysis, and research trips

2.2. Development of Landscape Designs

A respectful approach to environment in landscape design constitutes a fundamental principle of ecotourism [26]. Ecotourism and landscape design are crucial for the conservation of natural resources and the implementation of sustainable environmental planning. Landscape design in ecotourism initiatives aims to conserve natural aesthetics and bolster the ecology. In this instance, landscape design offers tourists an aesthetically pleasing

and informative experience by maintaining the area's natural integrity, whilst mitigating environmental degradation and fostering regional growth. Ecotourism planning seeks to conserve the region's unique ecological structure [27].

Ecotourism-oriented landscape designs were implemented around the chosen lakes following the collection of user feedback during the project phase. These designers sought to establish spaces that harmonise with the natural surroundings, prioritise ecological sustainability, and provide both aesthetic and utilitarian experiences for visitors. The research seek to both restore Bingöl's natural lakes and promote them as ecotourism destinations.

Landscape designs were developed utilising AutoCAD, ArchiCAD, and Lumion software, with distinct 3D visualisations created for each lake included in the research, as given in the article.

3. RESULTS AND DISCUSSION

3.1. Survey Questions and Responses Obtained

The surveys indicated that most participants stressed the necessity of developing alternative tourism products in Bingöl to enhance ecotourism. The surveys conducted in the province indicate that the ecotourism potential remains undiscovered due to inadequate promotion and advertising, that the assessments of touristic supply are insufficient, yet the development of ecotourism is expected to continue to rise.

The research articulates that Bingöl province possesses year-round ecotourism potential, is geographically proximate to regions with established ecotourism, is less renowned than competing provinces, has a sufficient young population available for ecotourism initiatives, and can diversify tourism activities due to its rich folkloric culture.

Analysis of another survey question reveals that awareness of ecotourism in Bingöl is inadequate, there are infrastructural deficiencies in ecotourism services, unplanned development is leading to the degradation of natural and cultural resources, and there are shortcomings in financing and support for tourism.

It was found that ecotourism regions are expanding due to advancements in communication and transportation infrastructure, and that interest in tourism activities in Bingöl province is steadily rising. Upon enquiring about the participants' perspectives and recommendations for the advancement of ecotourism initiatives in Bingöl province, they expressed a desire to enhance transit infrastructure, elevate public awareness, and offer training on the sustainability of environment and natural resources. Participants highlighted several issues, including the inadequate advertising and marketing in Bingöl, which possesses significant ecotourism potential year-round due to its natural lakes, waterfalls, plateaus, ski centres, and thermal springs. Consequently, it fails to capture a substantial share of tourism compared to neighbouring provinces. Additionally, social facilities in

current tourism areas are lacking, and there is insufficient financial and incentive support for the restoration and rehabilitation of these regions. Management systems require enhancement, and tourism activities must be diversified (Table 1).

Table 1. Survey questions and responses obtained

Question	Criteria	N	Frequance
Job	Other	7	3.60
	Officer	45	23.40
	Student	107	55.70
	Private sector	33	17.20
Study Area	Balpınar	50	26.00
	Gerindal	49	25.50
	Sarıçiçek	50	26.00
	Ilıcalar	43	22.40
Alternative tourism products should be developed for the development of ecotourism	Totally agree	101	52.60
	Agree	66	34.40
	Undecided	13	6.80
	Disagree	9	4.70
	Totally disagree	3	1.60
How do you evaluate the ecotourism potential of Bingöl province?	Very high	20	10.40
	High	26	13.50
	Normal	47	24.50
	Low	87	45.30
	Very Low	12	6.30
What do you think is the level of effectiveness of the activities for diversification of touristic supply in Bingöl province?	Very high	20	10.40
	High	20	10.40
	Normal	47	24.50
	Low	70	36.50
	Very Low	35	18.20
When the consumption trends in the tourism sector are observed, the development of ecotourism will continue to increase	Totally agree	50	26.00
	Agree	77	40.10
	Undecided	52	52.00
	Disagree	9	9.00
	Totally disagree	4	4.00
The abundance of diverse tourism resources and the possibility for year-round tourism in Bingöl province 1(Weak/Strong)5	1	34	17.70
	2	49	25.50
	3	57	29.70
	4	34	17.70
	5	18	9.40
Proximity to developed regions in terms of ecotourism due to its geographical location 1(Weak/Strong)5	1	35	18.20
	2	51	26.60
	3	63	32.80
	4	31	16.10
	5	12	6.30
Lower demand for alternative activities of equivalent quality compared to rival provinces 1(Weak/Strong)5	1	44	22.90
	2	42	21.90
	3	45	23.40
	4	31	16.10
	5	30	15.60
Young and dynamic population that can be utilised in ecotourism supply 1(Weak/Strong)5	1	18	9.40
	2	38	19.80
	3	51	26.60
	4	43	22.40
	5	42	21.90
Exotic culture with rich folkloric and cultural elements and an emphasis on hospitality 1(Weak/Strong)5	1	18	9.40
	2	19	9.90
	3	45	26.40
	4	49	24.10
	5	58	30.20
	1	41	21.40
	2	51	26.60

Question	Criteria	N	Frequance
Proximity of the selected areas to settlements 1(Weak/Strong)5	3	69	35.90
	4	20	10.40
	5	11	5.70
Awareness of ecotourism is at an adequate level 1(Weak/Strong)5	1	30	15.60
	2	42	21.90
	3	62	32.30
	4	26	12.50
	5	32	16.70
Inadequacies in the infrastructure utilised for ecotourism services 1(Weak/Strong)5	1	5	7.80
	2	38	19.80
	3	68	35.40
	4	32	16.70
	5	39	20.30
Destruction of natural, cultural and historical resources due to unplanned development and utilisation 1(Weak/Strong)5	1	31	16.10
	2	35	18.20
	3	56	29.20
	4	28	14.60
	5	42	21.90
Financing difficulties and inadequacy of support mechanisms for ecotourism 1(Weak/Strong)5	1	35	18.20
	2	28	14.60
	3	52	27.10
	4	37	19.30
	5	40	20.80
Development of green consumer movement based on environmental sensitivity 1(Not important / Important)5	1	32	16.70
	2	23	12.00
	3	46	24.00
	4	28	14.60
	5	63	32.80
Expansion of ecotourism coverage area thanks to developing communication and transportation facilities 1(Not important /Important)5	1	28	14.60
	2	35	18.20
	3	38	19.80
	4	38	19.80
	5	53	27.60
Intensification of interest in ecotourism, culture and special interest tourism, which have potential within the borders of Bingöl province 1(Not important /Important)5	1	19	9.90
	2	27	14.10
	3	43	22.40
	4	58	30.20
	5	45	23.40
The ageing Bingöl population has a high potential in terms of ecotourism 1(Not important /Important)5	1	14	7.30
	2	23	12.00
	3	70	36.50
	4	45	23.40
	5	40	20.80
Ecotourism activities in locations close to Bingöl province 1(Not important /Important)5	1	30	15.60
	2	39	20.30
	3	65	33.90
	4	28	14.60
	5	30	15.60
Increasing the competitiveness of rival provinces 1(Not important /Important)5	1	32	16.70
	2	35	18.20
	3	57	29.70
	4	33	17.20
	5	35	18.20
Risk of destruction of sensitive	1	19	9.90
	2	42	21.90
	3	47	24.50

Question	Criteria	N	Frequance
ecosystems subject to ecotourism 1(Not important /Important)5	4	34	17.70
	5	50	26.00
Standardisation of alternative tourism products by losing their local characteristics 1(Not important /Important)5	1	27	14.10
	2	39	20.30
	3	61	31.80
	4	42	21.90
	5	23	12.00
The most problematic areas for ecotourism development	Marketing	75	39.10
	Management and business administration	93	48.40
	Protection of the ecological environment	80	41.70
	Financing	79	41.10
	Infrastructure and transport	81	42.20
	Education and employment	92	47.90
Additional opinions and suggestions on diversification of tourism in Bingöl province	No idea	49	25.50
	Easy transport	15	7.80
	Education	26	13.50
	Marketing/Advertising	32	16.70
	Social facilities	15	7.80
	Financial supports	20	10.40
	Improvement of management systems	16	8.30
	Diversification of tourism activities	19	9.90

The outcomes of the survey indicate that nearly all participants recognise the ecotourism potential of Bingöl province. It has been concluded that it fails to garner the requisite attention in the province owing to insufficient investments resulting from both promotional shortcomings and economic challenges.

3.2. Outcomes of SWOT Analysis

SWOT analyses were performed independently for four distinct locations by specialists and students from the Bingöl University Department of Landscape Architecture (Table 2). Within the scope of the project, the experts were selected among the academicians of landscape architecture, faculty of agriculture, faculty of veterinary medicine and vocational school of social sciences who are familiar with Bingöl province. All of the students are undergraduate students of landscape architecture department.

Table 2. Outcomes of SWOT Analysis

	Internal analysis		External analysis	
	Strengths	**Weaknesses**	**Opportunities**	**Threats**
Balpınar Lake	Supported by natural resources and has an adequate supply of water throughout all seasons	Insufficient transport infrastructure Inadequate advertising and promotion	Significant tourism potential	Contamination of the lake and its environs by visitors
	Numerous endemic plant species can thrive in the vicinity of the lake.	Insufficient understanding on tourism No facilities are available surrounding the lake.	It possesses the potential to enhance regional development via tourism.	The lake's considerable depth poses a drowning risk for anybody who enter it.
Gerindal Lake	Adequate water levels in the lake during all seasons. The lake possesses a legendary narrative.	Insufficient transport infrastructure	Exhibiting significant potential for tourism Facilitating rural advancement	
	Visually appealing (heart) aspect of the lake	Inadequate promotion and advertising	Additional natural attractions in the area are observable during excursions to the lake.	Contamination of the lake and its vicinity by visitors
	Functioning as a crater lake The lake and its environs host diverse vegetation and animals.	No facilities are available surrounding the lake.	The lake is suitable for summer activities.	
Sarıçiçek Lake	Utilising natural water resources for nourishment	Intermittent reduction in water volume	Enhancing tourism potential via promotional and advertising initiatives	During the winter months, the thick ice covering that forms on the surface diminishes oxygen levels, potentially harming the aquatic organisms residing in the lake.
	Proximal to the urban core		Possessing ecotourism potential	
	Facilitated roadway transportation	Lack of awareness regarding the lake's tourism potential	Initiation of reverse migration in the region through the promotion of tourism	Unconscious water usage might diminish water availability.
	Contribution to the region with agricultural and livestock management		Contribution to rural advancement	

	Sufficient amount and thermal quality of the subterranean water resources	Insufficient advertising and promotion	Utilisation of geothermal energy resources for applications such as heating, among others.	Elevated seismic hazard in areas with geothermal springs
Natural thermal water situated in Ilıcalar	Thermal water resources can be utilised for therapeutic purposes.	Inability to attract investors who will convert thermal resources into economic investments	Facilitating regional development through the conversion of thermal resources into investments	Economic fluctuations may postpone the intended investments.
	The province is recognised in the region for thermal tourism and attracts visitors for this reason.	Insufficient transport infrastructure	Execution of investments utilising EU grant funding and contracted projects	In the long term, global warming may pose a significant issue.

3.3. Landscape Designs

During the design process, people familiar with the lakes were questioned to identify the problems they observed, which informed the subsequent designs. Satellite and drone imagery were utilised during the planning phase to measure the lake areas and serve as a foundational reference.

3.3.1. Balpınar Lake

The region's name clearly indicates its extensive utilisation by beekeepers in Bingöl province. Balpinar Lake, a popular destination for individuals seeking to gather mushrooms and the edible plant known as rhubarb (*Rheum ribes*), attracts numerous visitors. Designs were developed in accordance with the requirements gathered from the designated nature path and picnic area and included into the project.

The user interviews indicated a heightened desire for walking pathways and picnic spaces surrounding the lake. Landscape designs were also influenced in this manner (Figure 7).
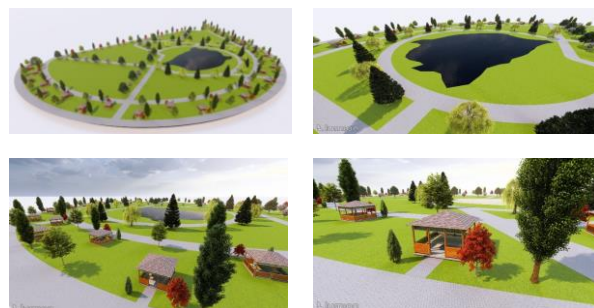

Figure 7. Balpınar Lake landscape design

3.3.2. Gerindal Lake

Gerindal Lake is notable for its heart-shaped surrounding landscape. Due to the proximity of the lake to the city, the presence of plateaus on the road leading to the lake in the summer months, which are intensively used by the people engaged in nomadic animal husbandry, the stabilised roads, the fact that important destinations in terms of beekeeping are on the route, and the fact that it offers beautiful mountain views for Bingöl province, which is famous for its mountains, the region is especially frequented by nature walks and motocross trips. During the summer months, it accommodates beekeepers, animal breeders, and researchers on its indigenous plant species diversity. In accordance with the gathered requirements, the design of walking trails, picnic places, a facility for basic necessities, and appropriate zones for water activities has emerged as a priority. Subsequently, landscape designs were created and incorporated into the research (Figure 8).
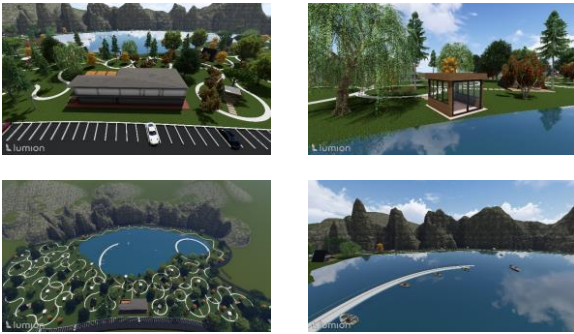

Figure 8. Gerindal Lake landscape design

3.3.3. Sarıçiçek Lake

Sarıçiçek Lake is a popular destination for visitors who engage in walking and picnicking, owing to its close vicinity to Bingöl city core. Consequent to the user interviews, the design of the area as a picnic space and the incorporation of water sports facilities emerged as primary considerations. The concepts that evolved informed the designs, which were incorporated into the research (Figure 9).

Figure 9. Sarıçiçek Lake landscape design

3.3.4. Natural thermal water situated in Ilıcalar

The interviews yielded requests for the lake, characterised by its natural open pool structure, to be developed for winter tourism, to construct social amenities in the vicinity, and to promote ecotourism. Designs were developed in accordance with the obtained demands and incorporated into the research (Figure 10).

Figure 10. Natural Thermal Water Situated in Ilıcalar

Ecotourism is a sustainable tourism model that emphasises the conservation of the natural environment and the cultural history of a location. It constitutes a response to mass tourism and serves as an appropriate alternative for ecologically sensitive regions, as it is not confined to a particular season and incorporates components of rural and cultural tourism [28]. This research aims to establish an ecotourism route in Bingöl province that accommodates year-round tourism by transcending seasonal limitations.

The correlation between ecotourism and landscape design is crucial for the preservation of natural regions, sustainable tourism, and the support of local communities. Landscape design is essential for reducing ecological degradation and improving tourist experiences by maintaining the natural integrity of ecotourism locations. Ecological establishments like Feynan Ecolodge provide visitors with an experience that enhances environmental consciousness through sustainable designs utilising local materials. Furthermore, visitors are afforded the opportunity to engage with nature through environmentally integrated design, so enhancing the role of ecotourism in sustainable development. Ecological resorts like Elewana Tarangire Treetops in Tanzania offer tourists an immersive experience in nature through environmentally integrated architecture and efficient water management systems. These projects help the local economy while preserving the natural scenery. Conversely, institutions like the Oregon Zoo Education Centre enhance environmental awareness and promote sustainability through their educational initiatives [29].

Designs that ensure the protection of natural habitats and biodiversity support nature-based tourism and contribute economically to local communities [27]. Sustainable landscaping strategies in these projects encompass the preservation of indigenous flora and water resources while honouring the natural ecosystem. Simultaneously, features such as ecological paths, observation points, and informational signage facilitate ecotourism's contribution to enhancing environmental consciousness while acquainting visitors with the region's natural splendour.

4. DISCUSSION AND CONCLUSION

Ecotourism, an expanding sector of the tourism industry, has garnered significant interest in recent years for its capacity to foster environmental conservation, cultural preservation, and sustainable economic growth. An increasingly significant feature of ecotourism is its correlation with landscape design.

Landscape design seeks to uphold ecological and cultural values grounded in sustainable principles. Consequently, landscape architects may conserve natural ecosystems while simultaneously developing tourist attractions. Such designs assist the primary objectives of ecotourism: enhancing environmental awareness and bolstering the local economy [30].

The interplay between ecotourism and landscape design is intricate and multifarious. Ecotourism offers a concrete economic motivation for conservation, as it is an industry that significantly relies on the natural resources of numerous sites. Nonetheless, the same business may present considerable risks to the environment if not meticulously controlled and engineered.

Landscape design is essential for the advancement and efficacy of ecotourism projects. Landscape design may improve visitor experiences, promote the preservation of natural settings, and foster a stronger link between tourists and the local ecology. A poorly planned area will lack a conceptual framework to direct tourism development and destination management, adversely affecting actual ecotourism benefits [31].

Bingöl possesses significant potential for ecotourism because to its natural landscapes and lakes. Landscape design initiatives can save and enhance these natural regions while economically benefiting local populations. Landscaping focused on ecotourism around water resources will enhance visitor experiences and foster ecological sustainability. Consequently, enhancing Bingöl's ecotourism potential can safeguard the region's natural resources and elevate the living standards of its inhabitants. It will also promote ecotourism by offering an educational experience to visitors.

As a result of the surveys conducted within the scope of the research, it was concluded that the people of Bingöl are conscious about ecotourism, that they cannot receive sufficient investment compared to the neighbouring provinces, and that they will support the activities to be carried out since they think that they will prevent migration as they can create employment. They also stated that they will contribute to the construction of settlement and necessary equipment applications as both local and provincial people.

Upon evaluating the answers derived from the questionnaires, the objective is to advance ecotourism in Bingöl province;
- Formulating strategies to guarantee sustainable utilisation in the regions,
- Creating marketing and promotions to attract visitors to regions that are secure and remain unspoiled,
- The formulation and execution of ecotourism initiatives ought to have financial backing from both governmental and commercial entities,
- Promoting tourism variety in the province, which possesses significant folkloric and gastronomic attributes,
- Local governments ought to promote ecotourism to the public via social and economic awareness initiatives,
- The importance of teaching and creating awareness among local communities regarding this subject should be underscored.

Considering the lakes in the study area and the activities that can be done;

Balpinar Lake stands out as an area frequently visited by users due to its proximity to the centre, the well-maintained road on which transportation is provided and the collection of plants with income-generating value. When we look at the disadvantages of the lake, the small surface area of the lake, the fact that it does not provide living opportunities for living creatures in the lake, and the infrastructure (electricity, sewerage) do not provide opportunities for activities such as water sports, fishing and accommodation.

Gerindal Lake stands out with its natural beauties. Especially the presence of endemic plants in the region causes the region to be visited frequently due to scientific studies. The surface area of Lake Gerindal is large enough to allow water sports. However, as in Balpınar Lake, it does not allow activities such as accommodation in the region due to the insufficiency of infrastructure facilities and the difficulty of transportation and the difficulty of access by road in case of any emergency.

Sarıçiçek Lake is among the regions frequently visited by local people due to its natural beauty, proximity to the centre and proximity to Sarıçiçek village. The lake in question also provides water sports as a surface area. Here, the establishment of a facility will be problematic due to the fact that the lands around the lake are private parcels.

Ilıcalar natural hot water spring is foreseen to be an area where accommodation facilities are planned in line with the request of the people of the region due to its proximity to the town centre, the richness of infrastructure facilities, and the fact that it is a place that can be reached by public transport.

As a result of the research conducted based on all these situations, when the potentials of the 4 lakes subject to the research are evaluated, it is seen that all of them have their own unique characteristics. If ecotourism planning is to be made, it has been concluded that the priority ranking should be Ilıcalar-Balpınar-Gerindal and Sarıçiçek Lake.

Furthermore, based on the observations, interviews, and surveys, it can be stated that the residents of Bingöl endorse ecotourism, desire its development in the region

211

as a source of employment and income, and possess the requisite awareness. Ecotourism undeniably serves as a spur for the social and economic development of local populations in today's more popularised globe. This research has been conducted to advance ecotourism planning in Bingöl province and to motivate institutions and organisations towards this objective.

Acknowledgement

REFERENCES

[1] T. Arslan and M. Kiper, "Anadolu'da doğa turizmi kapsamında doğa yürüyüşü güzergâhlarının belirlemesinde örnek bir çalışma," Tekirdağ Ziraat Fakültesi Dergisi, vol. 4, no. 2, pp. 165–174, 2007.

[2] Ü. Kement and F. Öztürk, "Bingöl ili doğa ve kültür varlıklarının turistik açıdan değerlendirilmesi," Journal of Recreation and Tourism Research, vol. 3, no. 4, pp. 13–22, 2016.

[3] BAKA, "Ekoturizm sektör raporu," Isparta, 2020.

[4] UNWTO, "World tourism barometer and statistical annex, August/September 2020," https://www.e-unwto.org/doi/abs/10.18111/wtobarometereng.2020.18.1.5?role=tab.

[5] R. Buckley, Ecotourism: Principles and practices. Cambridge: CAB International, 2009.

[6] Kültür ve Turizm Bakanlığı, "Türkiye turizm stratejisi," Ankara, 2007.

[7] H. Vural, "Ekoturizm ve rekreasyona yönelik yerel halk talepleri; 'Bingöl Ilıcalar örneği,'" Batman Üniversitesi Yaşam Bilimleri Dergisi, vol. 9, no. 1, pp. 39–52, 2019.

[8] TIeS, "What is ecotourism?," https://ecotourism.org/what-is-ecotourism/.

[9] Ü. Kement, "Ekoturizm faaliyetlerine katılan bireylerin değer inanç form teorisi kapsamında çevre dostu davranışların açıklanması," Elektronik Sosyal Bilimler Dergisi, vol. 18, no. 72, pp. 2182–2195, 2019.

[10] Ü. Kement, S. Çavuşoğlu, and B. Başar, "Ekolojik tutumun demografik özellikler açısından incelenmesi: Bingöl Yüzen Adalar örneği," Journal of Recreation an Tourism Research, vol. 4, no. 4, pp. 154–161, 2017.

[11] M. Honey, Ecotourism and sustainable development: Who owns paradise? Island Press, 1999.

[12] A. Yüksel, A. Meral, Y. Demir, and E. Eroğlu, "Çapakçur Mikrohavzası'nda (Bingöl) mikrohavza ölçekli peyzaj değerlendirmesi," Türk Tarım ve Doğa Bilimleri Dergisi, vol. 7, no. 1, pp. 16–26, 2020, doi: 10.30910/turkjans.679893.

[13] F. Pezikoğlu, "Sürdürülebilir tarım ve kırsal kalkınma kavramı içerisinde tarım-turizm-kırsal alan ilişkisi ve sonuçları," KMÜ Sosyal ve Ekonomik Araştırmalar Dergisi, vol. 14, no. 22, pp. 83–92, 2012.

[14] A. Yüksel, A. Meral, Y. Demir, and E. Eroğlu, "Yamaç mikrohavzası'nda (Bingöl) arazi kullanımı durumunun CBS ile belirlenmesi ve agro-turizm potansiyelinin değerlendirilmesi," Türk Tarım ve Doğa Bilimleri Dergisi, vol. 5, no. 3, pp. 236–244, 2018, doi: 10.30910/turkjans.448340.

[15] K. Tatlıoğlu, "Kentleşme ve sürdürülebilir kalkınma sürecinde Bingöl ilinin sosyo-kültürel ve ekonomik durumu üzerine genel bir değerlendirme," The Journal of Bingöl Studies, vol. 2, no. 1, pp. 29–54, 2015.

[16] Y. Atar, "Doğa harikası kız gölü keşfedilmeyi bekliyor," İHA, Bingöl, 2013.

[17] L. Behçet and Y. Yapar, "Asteraceae, Fabaceae ve Lamiaceae Familyalarına ait B8 karesi için yeni floristik kayıtlar," Iğdır Üniversitesi Fen Bilimleri Enstitüsü Dergisi, vol. 11, no. 3, pp. 1792–1802, 2021, doi: 10.21597/jist.876831.

[18] L. Behçet and Y. Yapar, "Türkiye'den bazı kareler için yeni floristik kayıtlar," BEÜ Fen Bilimleri Dergisi, vol. 9, no. 4, pp. 1482–1495, 2020.

[19] Z. Gürbüz and O. Gürbüz, Turizme kaynak oluşturan değerler: TRB1 Bölgesi. Ankara: IKSAD Publishing House, 2022.

[20] A. Uslu, "Bingöl ili termal kaynaklarına yönelik pazarlama çalışmalarının incelenmesi," Journal of Recreaction and Tourism Research, vol. 3, no. 4, pp. 32–40, 2016.

[21] D. J. Timothy and S. W. Boyds, Heritage tourism. Harlow: Prentice Hall, 2003.

[22] A. Meral, "Peyzaj karakterleri çalışmalarının entegre havza yönetim modellerinde değerlendirilmesi; Bingöl Çapakçur, Yeşilköy, Yamaç mikrohavzaları örneği," Doktora Tezi, Düzce Üniversitesi, 2021.

[23] A. Meral, R. Kayalı, Y. Kabay, and Y. E. Avcı, "Bingöl kenti açık yeşil alanlarının doğal afetlere hazırlık durumları ve leke senaryoları," Bozok Tarım ve Doğa Bilimleri Dergisi, vol. 2, no. 1, pp. 58–72, 2023.

[24] H. Vural, A. Meral, and S. Ş. Doğan, "Üniversite Kampüs Peyzaj Planlaması Üzerine Kullanıcı Değerlendirmesi: Bingöl Üniversitesi Örneği," Türk Tarım ve Doğa Bilimleri Dergisi, vol. 6, no. 1, pp. 106–117, 2019, doi: 10.30910/turkjans.515363.

[25] M. Yurtcan, A. Meral, and B. Ç. Kurdoğlu, "Yaya kullanımını destekleyen stratejilerin geliştirilmesine yönelik bir durum değerlendirme çalışması: Bingöl Çapakçur Vadisi, Eski Saray Caddesi," Bozok Tarım ve Doğa Bilimleri Dergisi, vol. 3, no. 1, pp. 16–26, 2024.

[26] J. Fan, "Tourism landscape design based on sustainable development," in 7th International Conference on Education, Management, Computer and Medicine, 2016, pp. 1002–1004.

[27] T. Kiper, O. Uzun, and O. Ateş, "Kırsal kalkınma, ekoturizm planlaması, kırsal planlama çalışmalarının niceliksel analizi," Akademia Doğa ve İnsan Bilimleri Dergisi, vol. 8, no. 1, pp. 1–18, 2022.

[28] S. Öztürk, "Determining management strategies for the Sarikum Nature Protection Area," Environ Monit Assess, vol. 187, no. 3, p. 113, 2015, doi: 10.1007/s10661-015-4302-3.

[29] S. Putran, "20 examples of sustainable ecotourism architecture in the world," Rethinking the Future.

[30] İ. Tazebay and N. Akpıbar, "Türk kültüründe bahçe," Bilgi Dergisi, vol. 54, pp. 243–253, 2010.

[31] C. M. Libosada, "Business or leisure? Economic development and resource protection—Concepts and practices in sustainable ecotourism," Ocean Coast Manag, vol. 52, no. 7, pp. 390–394, 2009, doi: 10.1016/j.ocecoaman.2009.04.004.

213